1

FEASIBILITY ANALYSIS FOR PREDICTING
A KINETIC KILL ZONE
FOR AIRCRAFT HOMING MISSILE DEFENSE

THESIS

Mark E. Ennis, Captain, USAF

AFIT/GE/GEO/94M-01

DEPARTMENT OF THE AIR FORCE
AIR UNIVERSITY
AIR FORCE INSTITUTE OF TECHNOLOGY

Wright-Patterson Air Force Base, Ohio

REPORT DOCUMENTATION PAGE

Form Approved
OMB No. 0704-0188

1. AGENCY USE ONLY *(Leave blank)*

2. REPORT DATE
March 1994

3. REPORT TYPE AND DATES COVERED
Masters Thesis

4. TITLE AND SUBTITLE

FEASIBILITY ANALYSIS FOR PREDICTING A KINETIC KILL ZONE FOR AIRCRAFT HOMING MISSILE DEFENSE

5. FUNDING NUMBERS

6. AUTHOR(S)

Mark E. Ennis, Capt USAF

7. PERFORMING ORGANIZATION NAME(S) AND ADDRESS(ES)

Air Force Institute of Technology
Wright-Patterson AFB, OH 45433

8. PERFORMING ORGANIZATION REPORT NUMBER

9. SPONSORING/MONITORING AGENCY NAME(S) AND ADDRESS(ES)

Dr Duane Warner
WL/AAWD-2,
Wright-Patterson AFB, OH 45433

10. SPONSORING/MONITORING AGENCY REPORT NUMBER

11. SUPPLEMENTARY NOTES

12a. DISTRIBUTION / AVAILABILITY STATEMENT

APPROVED FOR PUBLIC RELEASE; DISTRIBUTION UNLIMITED.

12b. DISTRIBUTION CODE

13. ABSTRACT *(Maximum 200 words)*

An extended Kalman filter is used to predict a kinetic kill zone for use in aircraft self-defense versus homing missiles. The analysis is limited to an in-the-plane analysis and focuses on finding the model parameters which have the largest impact on the predicted kill zone. No attempt is made to optimize the design of the filter model itself. The analysis computes the kill zone relatitve to an assumed aircraft trajectory using strictly filter computed statistics. No Monte-Carlo simulations are used throughout the thesis. The filter assumed to be on the evading aircraft, uses an onboard laser radar (ladar) to provide measurements of aircraft-to-missile relative range, range-rate, line-of-sight and line-of-sight rate. The missile is assumed to be in a post burnout coast-to-intercept phase of flight.

14. SUBJECT TERMS

Kinetic Kill Zone, Aircraft Self Defense

15. NUMBER OF PAGES
367

16. PRICE CODE

17. SECURITY CLASSIFICATION OF REPORT	18. SECURITY CLASSIFICATION OF THIS PAGE	19. SECURITY CLASSIFICATION OF ABSTRACT	20. LIMITATION OF ABSTRACT
unclassified	unclassified	unclassified	UL

Vita

Mark Edward Ennis was born on July 17th 1966 in Pittsburgh Pennsylvania. After graduating from South Park High School in 1984, he received an AFROTC scholarship at the University of Pittsburgh, to study electrical engineering. He was commissioned upon graduation in May 1988 and entered active duty on January 15th 1989. His first assignment was to the Air Force Acquisition Logistics Center at Wright Patterson AFB, where he worked in support of Wright Laboratory's Electronic Countermeasures Advanced Development Branch. He remained at this assignment until entering AFIT in June 1992. Upon graduation he will be assigned to WR-ALC/LYLE to work on engineering support for the F-15 radar.

AFIT/GE/GEO94M-01

FEASIBILITY ANALYSIS FOR PREDICTING
A KINETIC KILL ZONE
FOR AIRCRAFT HOMING MISSILE DEFENSE

THESIS

Mark E. Ennis, Captain, USAF

AFIT/GE/GEO/94M-01

AFIT/GE/GEO/94M-01

FEASIBILITY ANALYSIS FOR PREDICTING A KINETIC KILL ZONE FOR AIRCRAFT HOMING MISSILE DEFENSE

THESIS

Presented to the Faculty of the School of Engineering

of the Air Force Institute of Technology

Air University

In Partial Fulfillment of the

Requirements for the Degree of

Master of Science in Electrical Engineering

Mark E. Ennis, B.S.

Captain, USAF

March 1994

Approved for public release; distribution unlimited

Acknowledgements

This thesis is the culmination of many months of effort, and much hard work not all of which is my own. As such I would like to take this opportunity to sincerely thank those individuals whose help and guidance made this thesis possible.

The thesis topic was sponsored by Dr Duane Warner of the Electronic Warfare Division within Wright Laboratories. His clear definition of the problem at hand, willingness to spend the time to provide assistance as needed, and pointed editing comments all contributed to the success of this project.

Most of my limited understanding of missile dynamics came from Dr George Vogel of the Electronic Warfare Division within Wright Laboratories. His time and effort in making this thesis a success is certainly deserving of thanks.

Mr Stanton Musick was an invaluable asset in providing MSOFE assistance (the software package used for the thesis simulations). He took many hours often late in the evening to help me with this massive undertaking. Without his continuous support I doubt I could have ever accomplished the simulation work this thesis entailed.

A special word of thanks goes out to Major Randall Paschall who willingly took up this massive effort as my thesis advisor. He provided encouragement when needed, and kept me on track. Without his constant support I don't know if I could ever have found the light at the end of the tunnel.

I am greatly indebted to my committee members for all their assistance on this project. Everything I didn't learn about missiles from Dr Vogel, I learned from Dr Mier Pachter. Dr Peter Maybeck provided the tough editing critiques which really pulled the final document together, but the toughest critics produce the best results. Lt Col Robert Riggins spent lots of valuable time assisting me with troubleshooting and especially with understanding INS's.

A special note of love goes out to my parents, William E. Ennis and Barbara J. Macurak. You sacrificed so much of yourselves to raise nine children. I owe everything I've accomplished in life to what you've provided me.

Finally a note of thanks goes out to the one who at times was my strongest ally - God. To quote from one of my favorite poems - *FOOTPRINTS* (author unknown) - "During your times of trial and suffering when you see only one set of footprints, it was then that I carried you." You certainly carried me through this one. No matter where my accomplishments take me, or my life path leads, let me never forget that it is the love of God and neighbor that makes a man the most successful.

I thank you all sincerely for the time and effort you spent in making this project the success that it was. May God bless all of you and provide you with a happy and rich life.

Mark Edward Ennis

Table of Contents

List of Figures

List of Tables

List of Symbols

Symbol	Definition	Page
$\int$	Integration	1-4
$\varnothing$	Line-of-Sight Angle	1-4
$\Re$	Scenario Range	1-4
σ	RMS Value	1-5
T_{TG}	Time-to-Go	1-6
T_{TI}	Time-to-Intercept	1-6
T_p	Processing Time	1-6
T_d	Deployment Time	1-6
T_e	Estimation Time	1-6
T_s	State Propagation Time	1-6
T_{ps}	Complete Filter Cycle Time	1-7
δ	delta	1-7
π	angle (radians)	2-2
β_t	Target Heading	2-3
β_m	Missile Heading	2-3
v_t	Target Velocity	2-3
v_{tn}	Target North Velocity	2-3
v_{te}	Target East Velocity	2-3
v_m	Missile Velocity	2-3
v_{mn}	Missile North Velocity	2-3
v_{me}	Missile East Velocity	2-3
a_r	Radial Acceleration	2-4
$a_\varnothing$	Angular Acceleration	2-4
$\partial(sym)/\partial t$	First Derivative	2-4
$\partial^2(sym)/\partial t^2$	Second Derivative	2-4

r_i	Residue	2-6
p_i	Laplace Domain Pole	2-6
s	Laplace Transform Variable	2-6
$H(s)$	Transfer Function (Laplace-Domain)	2-6
z_i	Laplace Domain Zero	2-7
τ_i	Lag Time Constant	2-7
n	Proportional Navigation Constant	2-7
A_L	Generated Missile Lateral Acceleration	2-9
A_{Lcomd}	Commanded Missile Lateral Acceleration	2-9
C_D	Coefficient of Drag	2-9
C_L	Coefficient of Lift	2-10
ρ	Air Density	2-10
γ	Speed of Sound in Air	2-10
h	Altitude	2-10
S/M	Missile Surface to Mass Ratio	2-10
C_{DO}	Zero Lift Drag	2-10
C_{DL}	Lift Induced Drag	2-10
R_{turn}	Radius of Aircraft Turn	2-11
ω	Angular Turn Rate	2-11
G_{level}	Aircraft Turn Acceleration in g Units	2-11
θ	Initial Aircraft Turn Phase Angle	2-11
X_{te}, Y_{tn}	Aircraft Position	2-11
J_{te}, J_{tn}	Aircraft Jerk	2-11
Σ	Summation	2-14
$\Leftrightarrow$	From-To	2-14
$x_s(t)$	Truth State	2-14
$x_f(t)$	Filter State	2-15
$(\underline{sym})$	Vector	2-16

$\underline{x}(t)$	State Vector	2-16
$w(t)$	White Noise	2-16
$f\{sym\}$	Function of	2-16
$G\{sym\}$	Noise Shaping Function	2-16
$Q(t)$	Noise Strength	2-17
g	Acceleration in Gravity Units	2-17
θ_i	Missile Seeker Reference Angles	2-18
k	Gain Constant	2-18
$C_n{}^2$	Refractive Index Structure Parameter	2-23
$<\theta^2>$	Mean Squared Beam Wander	2-23
D_o	Optics Diameter	2-23
$\alpha_L{}^{1/2}$	Ladar Field-of-View	2-25
$\alpha_d{}^{1/2}$	Detector Field-of-View	2-25
k_{scan}	Ladar Frames per Measurement	2-25
n_d	Number of Detectors in Array	2-25
n_{air}	Index of Refraction for Air	2-27
c	Speed of Light in Vacuum	2-27
T_{OA}	Time-of-Arrival	2-27
T_{OL}	Time-of-Launch	2-27
T_{clock}	Receiver Clock Time	2-27
T	Temperature	2-27
P	Pressure	2-27
λ	Laser Wavelength	2-27
Δf	Doppler Shift	2-29
$z(t_i)$	Measurement	2-32

Abstract

An extended Kalman filter is used to predict a kinetic kill zone for use in aircraft self-defense versus homing missiles. The analysis is limited to an in-the-plane analysis and focuses on finding the model parameters which have the largest impact on the predicted kill zone. No attempt is made to optimize the design of the filter model itself. The analysis computes the kill zone relatitve to an assumed aircraft trajectory using strictly filter computed statistics. No Monte-Carlo simulations are used throughout the thesis. The filter assumed to be on the evading aircraft, uses an onboard laser radar (ladar) to provide measurements of aircraft-to-missile relative range, range-rate, line-of-sight and line-of-sight rate. The missile is assumed to be in a post burnout coast-to-intercept phase of flight.

FEASIBILITY ANALYSIS FOR PREDICTING A KINETIC KILL ZONE

FOR AIRCRAFT HOMING MISSILE DEFENSE

I Introduction

1.1 Background

The class of munitions called "expendables", chaff and flares has always been a primary source of endgame aircraft self defense, primarily because they are economical. The economic advantage comes from being able to defend against a large class of missile types with only a few standard expendables.

Due to increasing complexities in missile seeker Electronic Counter-Countermeasure (ECCM) technologies, self defense expendables used for Electronic Countermeasures (ECM) purposes have become increasingly more diverse and specialized, limiting the expendables' generic usefulness. Optical and electro-optical missile seekers have become common, and their sophistication is demanding new expendable technology in the visual and Infrared (IR) spectrums. For example, IR missile seekers are using spectral color discrimination and source rise times to help reject IR flares. Radar based seekers employ home-on-jam, special frequency filtering and pulse coding techniques to defeat radar ECM techniques. The spread of ECCM technologies forces ECM technologies to diversify to provide adequate multispectral coverage, thus reducing the economy of using expendable munitions for aircraft self defense.

An expendable mini-ball shot cannister might potentially restore the generic usefulness inherent in expendable munitions [20]. Conceptually, such a kinetic kill cannister would allow one expendable package to be deployed in virtually any endgame missile scenario because the kinetic kill cannister does not defeat the missile by jamming the missile's seeker head, but rather by hitting the missile as depicted in Figure 1-1. The successful employment of a kinetic energy impact device would negate current seeker ECCM capabilities provided by the proliferation of missile seeker technologies. However, in order to use such a defense mechanism, one must accurately predict the future flight path of the hostile tracking missile. This prediction is made using noise-corrupted and incomplete measurements from the evading aircraft's sensors. The predicted final time of the kinetic intercept, must exceed the sum of the kill zone estimation processing time and the kill cannister deployment time, and must still allow enough remaining missile flight time to prevent the disabled missile from entering into a lethal fusing range.

1.2 Problem Statement

This thesis explores the use of an extended Kalman Filter to estimate the future flight path of a homing missile tracking a friendly aircraft. The missile's predicted flight path is estimated using noise corrupted measurements available from an onboard Laser Radar (ladar), and the aircraft's Inertial Navigation Subsystem (INS), and the estimated flight path is used to define a kill zone volume. The ladar provides range, range-rate, angle and angle-rate measurements of the missile relative to the aircraft. The INS provides aircraft velocity measurements. Acceleration measurements are also assumed to be available from a g-meter or other source. Aircraft maneuvers are restricted to readily predictable constant speed, constant angle-rate turns (see Section 1.4). The calculated kill zone volume

1. The missile at B is tracking the Aircraft at A to an intercept point E.

2. The aircraft is taking measurements of the tracking missile and has reached steady-state in the error estimation.

3. While at A, the aircraft estimates that the missile will be contained within D, when the aircraft reaches C.

4. The aircraft deploys the countermeasure from A, to intercept D while the aircraft flies the assumed trajectory to C.

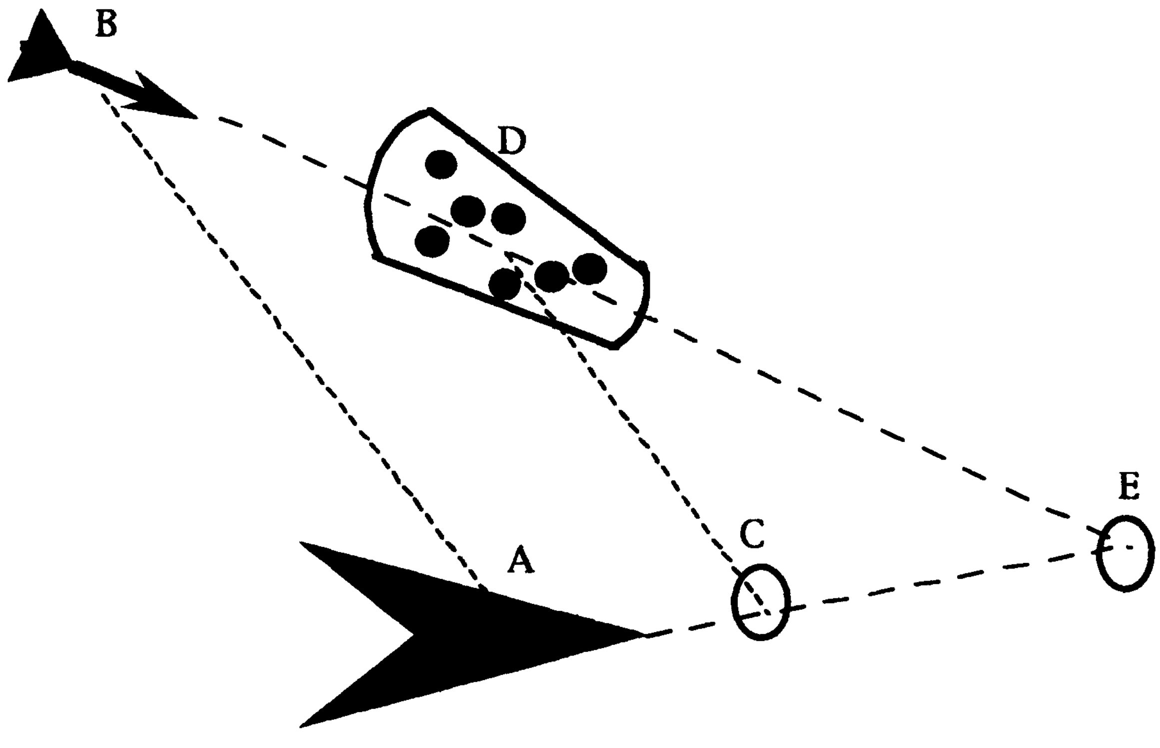

Figure 1-1 Illustration of Hard Kinetic Kill Zone

is determined by propagating the filter estimated range and angle covariance errors forward to the desired intercept time.

The boundaries of the kill zone are estimated through a three step process. First, during the missile acquisition phase, missile detection and filter initial conditions are provided to the filter from a Missile Warning Receiver (MWR). Second, during the estimation phase, the filter uses the measurement updates provided by the aircraft sensors to determine the errors in MWR-provided states. Finally, during the prediction phase, the filter propagates the states forward to the desired intercept time. Because the filter is predicting forward in time, no measurement updates are provided during the prediction phase, causing the filter covariances to diverge.

The kinetic kill zone is given as a horizontal plane volume cross-section throughout this study, since all models and analysis techniques used in this thesis are defined in the horizontal plane. Actual calculation of the kill zone volume proceeds as follows. The desired future intercept time is chosen. The filter states are propagated forward to the desired intercept time. A from the filter states, a new aircraft position is estimated for the desired intercept time. The missile's position is then calculated from the filter's range, $\Re(t)$, and angle, $\varnothing(t)$ estimates defined relative to the new aircraft position at the desired intercept time, and the filter's estimated 1σ bounds, $\Re_e(t_f)$ and $\varnothing_e(t_f)$, at the desired intercept time. These parameters determine the two dimensional intercept cross-section shown in Figure 1-2. The volume cross-section representing the final kill zone shown in Figure 1-2 is calculated as

$$\text{Volume Cross-Section} = \int_{\Re}\int_{\varnothing} \Re(t_f)\, \delta\Re(t_f)\, \delta\varnothing(t_f) \tag{1-1}$$

where the limits of integration, $\Re$ and $\varnothing$, are defined by

$\Re$ over the interval $\Re(t_f) \pm \eta\, \Re_e(t_f)$,

$\varnothing$ over the interval $\varnothing(t_f) \pm \eta\, \varnothing_e(t_f)$, and

$\Re(t_f)$ is the estimated range at the final time,

$\varnothing(t_f)$ is the estimated Line-of-Sight (LOS) angle at the final time,

$\Re_e(t_f)$ and $\varnothing_e(t_f)$ are the filter's estimated 1σ bounds,

η determines the number of standard deviations the volume encloses.

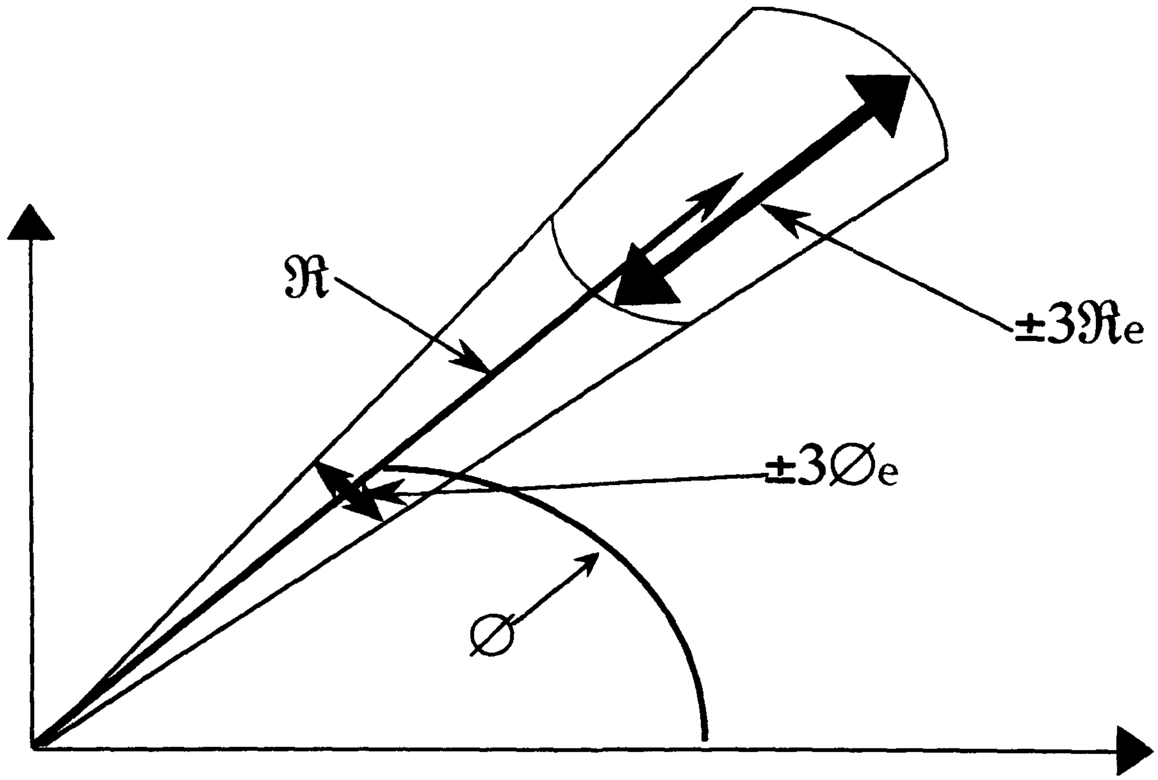

Figure 1-2 Defining the Kill Zone

Parts of the problem which require investigation include: (1) How do the estimation errors of $\Re(t)$ and $\varnothing(t)$ propagate as a function of the time-to-intercept (T_{TI}) parameter? (2) How do aircraft maneuvers affect the T_{TI}, central intercept point, and associated errors which define the volume cross-section? (3) What laser measurement parameters and assumptions have the greatest impacts on the ability to predict the volume cross-section? (4) How do dynamic elements used (e.g., missile dynamics, ladar errors, Kalman filter models, navigation errors, etc.) affect the final volume cross-section parameters? (5) How do scenario initial conditions such as initial missile/aircraft state values, allowed aircraft maneuvers, and specifics of a given scenario problem affect the estimation results?

Figure 1-3 illustrates the relationships between the various timing elements which hypothetically combine to define the T_{TI} parameter required to predict the kinetic kill zone of a tracking missile. In Figure 1-3 time-to-go (T_{TG}) is defined as the scenaric time remaining before the missile-to-aircraft range equals the missile fusing range, $T_{\underline{s}}$ is the filter-state propagation time between measurement updates, $T_{\underline{p}}$ is the processing time for the estimation filter's last measurement update, $T_{\underline{e}}$ is the filter's required estimation processing time to predict a volume cross-section, and $T_{\underline{d}}$ is the cannister deployment time to intercept the volume. Note that the possibility of achieving kinetic kill necessarily requires that

$$T_{TG} > T_{TI} = T_p + T_e + T_d \qquad (1\text{-}2)$$

where

T_{TG} is the time to aircraft-missile impact,
T_{TI} is the time to kinetic kill of the missile,
T_p is the final measurement processing time,
T_e is the volume estimation time, and
T_d is the cannister deployment time.

1.3 Summary of Current Knowledge

The kinetic kill zone estimation problem is largely a system level integration of several smaller problems. Several of these smaller problems have already been adequately solved, and other parts are concurrently under investigation which include use of a guided kinetic kill projectile, and state estimation of a homing missile using a ladar.

Predicting the future state of a homing missile first requires accurate estimation of the missile's current kinematic states. Cusumano and Deponte used an

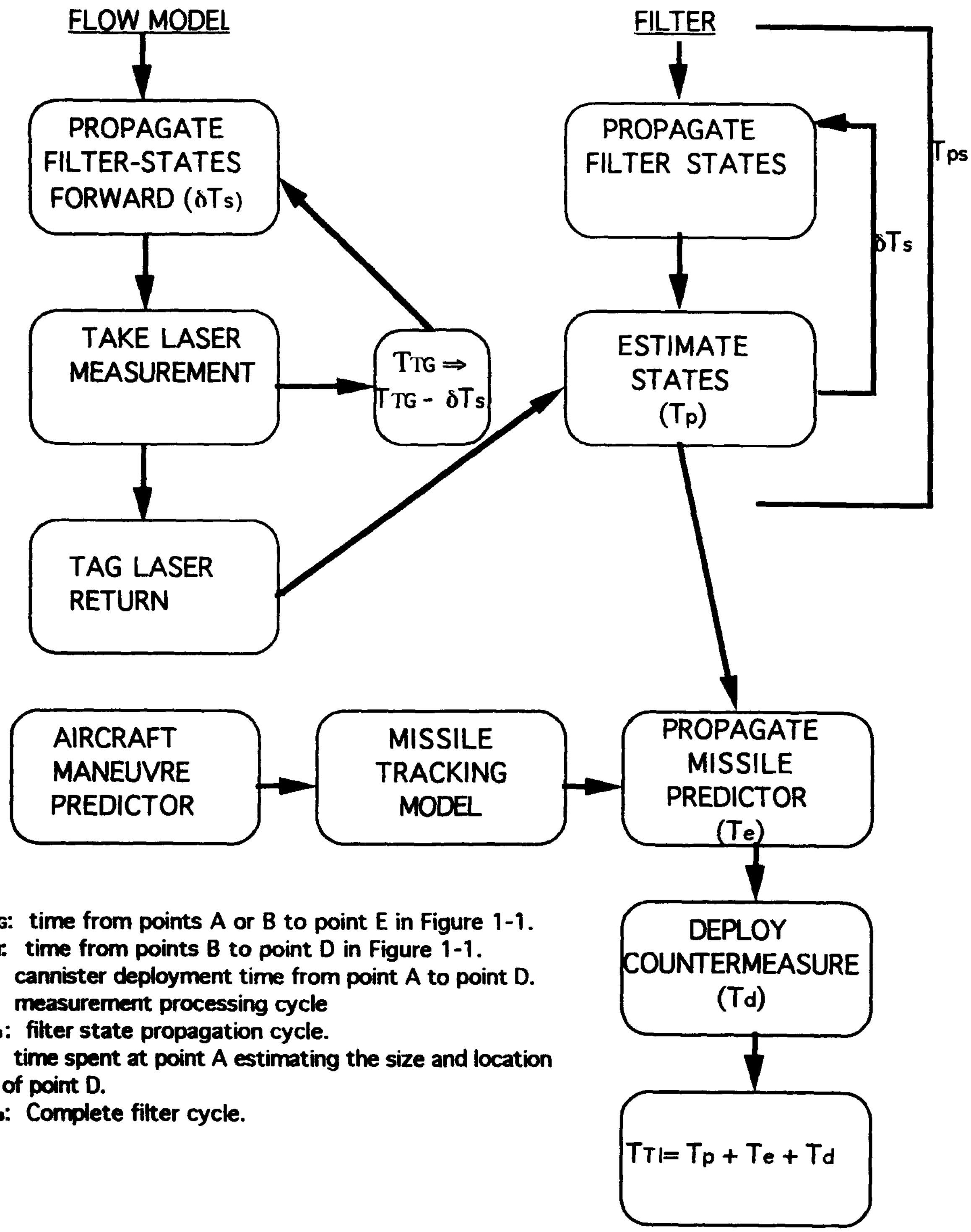

T_{TG}: time from points A or B to point E in Figure 1-1.
T_{TI}: time from points B to point D in Figure 1-1.
T_d: cannister deployment time from point A to point D.
T_p: measurement processing cycle
δT_s: filter state propagation cycle.
T_e: time spent at point A estimating the size and location of point D.
T_{ps}: Complete filter cycle.

Figure 1-3 TTI Parameter Flow Chart

(This figure illustrates a typical timing sequence necessary to complete a missile intercept.)

onboard radar to track a homing missile [5,11]. Measurements taken by the radar were processed by an extended Kalman filter, which produced sufficiently accurate state estimates of the homing missile for tracking purposes. An in-depth analysis of the Kalman filter estimation problem was performed to minimize estimation errors of the missile states. Cusumano and Deponte focused on state reduction of the missile dynamics model. The authors developed a 5th order missile dynamics truth model, and tested reduced order missile models (zero to 4th order) for relative performance in a filter model. The test results indicated that filter performance increased only marginally as the filter model complexity was increased from a zero order to a fourth order missile model [5:]. The kinematic equations of motion between the aircraft and missile had been developed in previous thesis work by Lutter [8,10]. Together, the thesis work by Lutter, and that by Cusumano and DePonte, provide a good foundation for target tracker extended Kalman filtering.

Negast, in his thesis, analyzed the performance of various Global Positioning Satellite (GPS)/INS integration approaches versus the Completely Integrated Reference Instrumentation System (CIRIS) used to test INS's at Holloman AFB, NM [13: 1-1]. The analysis included a twenty-two state DGPS/INS (GPS/INS with differential corrections) Kalman filter which was practical for airborne implementations. A summary of the twenty-two state filter's achieved performance is presented in Table 1-1. [13: Appendix I].

Note that Table 1-1 only presents results for INS states of interest to the kill zone estimation problem. Also note that while the reported acceleration errors are not directly available from Negast's thesis, they are considered to be obtainable from typical INS accelerometers. Because the kill zone estimation problem has been defined with a constant altitude, planar geometry, only north and east velocity and acceleration errors are required. Because the volume cross-section is always defined in $\Re(t)$ and $\varnothing(t)$ coordinates relative to the friendly aircraft, knowledge of precise aircraft position is irrelevant to the kill zone estimation problem, and the applicable INS position errors have been omitted from Table 1-1. Vertical position remains only as an aid to estimating the scenario altitude for missile drag considerations. The discussion of all modelling considerations is deferred to Chapter II.

Table 1-1 DGPS-INS Performance Results

INS State	RMS Errors
North Velocity	< 0.1 ft/sec
East Velocity	< 0.1 ft/sec
North Acceleration	50×10^{-6} x true value
East Acceleration	50×10^{-6} x true value
Vertical Position	9 ft

Rockwell International is currently testing the concept of using a guided sphere to intercept a missile and achieve kinetic kill [15]. The sphere uses an onboard sensor and small lateral thrusters to provide proportional navigation guidance corrections for small errors in the estimated intercept point. The use of a "smart" projectile with lateral thrust simplifies the required missile trajectory estimation problem. Furthermore, Rockwell's initial testing of the guided sphere has been primarily limited to space scenarios, where the missile flight path is more stable, time-to-go (T_{TG}) is not a critical parameter, and the missile flies a preprogrammed ballistic trajectory (i.e. the missile is not reacting to the uncertain movements of an evading aircraft).

This thesis differs from the Rockwell efforts, in that this thesis assumes the use of an unguided spread of projectiles to accomplish the missile kill. Successfully using a "dumb" projectile necessarily requires accurate estimation of the future missile trajectory. It has been suggested that a priori knowledge of future aircraft maneuvers is key to investigating the kinetic kill zone problem [20]. The combination of special aircraft maneuvers, along with accurate estimation of the future flight trajectory of a homing missile, may enable one to force the missile onto a path which optimizes the kinetic kill zone.

1.4 Assumptions

This thesis assumes that the encountered homing missile uses proportional navigation or a derivative thereof (including pure pursuit, lead-angle, constant bearing etc.) as the primary guidance law, regardless of the type of seeker head employed (such as active/semi-active radar, infrared, home-on-jam, optical etc.). This thesis exploits the known attributes of proportional navigation guidance independent of the region of the electromagnetic spectrum in which the missile seeker head operates.

This thesis further assumes that available Missile Warning Receiver (MWR) technologies will provide accurate initial estimates of four parameter sets. First, Time-to-Go (T_{TG}), provides the time remaining before missile impact with the evading aircraft. The T_{TG} provided must be large enough to allow problem execution. (What defines this sufficient time is an output parameter of this thesis). Second, the MWR verifies existence of a tracking missile which starts the scenario. Third, the MWR estimates the initial angular position of the tracking missile. This is particularly important, since a ladar has excellent angular resolution -- less than 50 μrad has been demonstrated -- but is very poor at initial acquisition in a large field of view. Fourth, the MWR provides initial estimates for other filter states and covariances as available. Such MWR technology is currently under development by Wright Laboratory's Avionics Directorate's Electronic Warfare Division, ECM Advanced Development Branch, Electro-optics Group (WL/AAWD-2).

Mr Kevin McKamey, program manager for WL/AAWD-2's current MWR development, has provided the initial condition values summarized in Table 1-2 as being valid based on expected MWR technology developments [12].

Restrictions are enforced on the allowed maneuvers of the evading aircraft. Two justifications are given for this assumption. The missile is primarily being controlled by its proportional navigation guidance law which commands the

Table 1-2 MWR Provided Initial Conditions

Initial Parameter	RMS Error
Range	3.0 meters
Range Rate	5.0 meter/sec
Angle	2.0 mrad
Time-to-go	10% error

missile to intercept the target aircraft. Therefore the aircraft trajectory becomes in essence a series of guidance and control commands given to the missile. If the aircraft were allowed to perform a random maneuver during the TTI, the aircraft maneuver would become equivalent to a random guidance command given to the missile. However if the allowed maneuvers of the aircraft are benign such that they can be accurately estimated by an extended Kalman filter a priori, the maneuvers instead become a control command given to the missile to force a favorable outcome.

While an easily predictable maneuver is somewhat restrictive, the restrictions are considered justifiable given that this thesis represents a first approach to the kill zone problem. As such this thesis focuses on modeling and analyzing the kill zone volume, and not on optimally modeling an evading aircraft.

Assuming that the kill zone can adequately be predicted with readily predictable aircraft maneuvers, more defensive maneuvers can be added later provided they meet the following condition: The filter must have an adequate means of consistently and accurately estimating *apriori* the aircrafts maneuver. Selecting a benign aircraft trajectory for this study fulfills that condition. As a final note, restricting the allowed aircraft maneuvers does not equate to exact knowledge of aircraft maneuvers actually being executed (which can never be truly known), but rather serves to enhance the accuracy to which an aircraft maneuver is known. Sensitivity of the final predicted kill zone volume to this known maneuver precision is analyzed.

Since this thesis depends heavily on the use of previous thesis studies, most notably Cusumano and Deponte, and Negast, it assumes the models developed in those thesis studies, and the results obtained are correct.

There is currently no known accepted method of determining a homing missile's T_{TG} in a dynamic environment involving evasive aircraft maneuvers. The T_{TG} problem is largely driven by unknown and undeterminable future maneuver relations between the missile and aircraft. As such, T_{TG} as previously defined is always changing. In order for a predicted volume at a predicted T_{TI} to make physical sense, a good estimate of T_{TG} needs to be available. For purposes of solving the thesis problem, an overly simplistic T_{TG} model is developed and used with the understanding that such technology is under development [12]. This thesis treats T_{TG} as an analysis parameter so that the results presented are independent of current T_{TG} estimation problems.

1.5 Scope

This thesis begins with the detection of a homing missile already in flight that is tracking the friendly aircraft. Initial conditions in Table 1-2 are provided by the MWR and include a valid missile detection, angular direction (in milliradians), T_{TG} and initial filter conditions for all state values an MWR would require to process detection, position, and T_{TG}. The thesis model predicts an intercept point and a bounded volume at a specified remaining T_{TG} and T_{TI}. The central intercept location of the kill zone volume is in general not a single point but rather a solution which generates the point based on key input parameters such as T_{TG}, initial position, final T_{TI}, allowed aircraft maneuvers, and measurement rates, as well as all the associated error tolerances for these parameters. This thesis does not address any of the kinematic problems associated with the actual deployment of the kinetic kill cannister. For purposes of this thesis, a prediction of a "good volume cross-section" is assumed as lethal to a homing missile. This thesis makes maximum use of existing missile trajectory, internal missile dynamics, and INS error models, and Kalman filter models developed in previous thesis studies. This thesis focuses on analyzing the kinetic kill zone volume and determines how changing each of the assumed input parameters changes the output volume parameters.

Figure 1-4 shows a block diagram representation of the thesis model. The dynamics equations describing the desired aircraft maneuvers (a) are programmed into the Kalman filter's state equations. Pilot deviation from the filter-programmed trajectory, is represented by an appropriate noise strength driving the extended Kalman filter's aircraft state covariances. The true aircraft trajectory (A) is generated assuming a constant speed/constant angle-rate turn driven by pilot-induced noise. Jinking maneuvers are not used since they would tend to be unpredictable by the filter and would therefore degrade the final solution. Noise corrupted measurements of the true aircraft trajectory (b) are provided to the filter from the INS. The true missile dynamics (C,D) are simulated using a modified version of Cusumano and Deponte's 5th order missile model [5]. The ladar takes measurements between the true missile position (E) and the true aircraft position (B) to provide the extended Kalman filter with noise corrupted measurements of range, range rate, angle, and angle rate (f). The filter then updates current filter state estimates with the ladar and INS measurements (g) and propagates the states forward one measurement period to generate new state estimates for the next measurement cycle. An indepth analysis of these system functions is provided in Chapter II.

1.6 Approach and Methodology

The Kalman filter is simulated using a Multimode Simulation for Optimal Filter Evaluation (MSOFE) software [3]. An extended Kalman filter model is used to estimate the nonlinear truth model states. The system truth model generates aircraft flight dynamics internally. The simulation assumes filter access (during measurement cycle) to a GPS-aided INS based on a twenty-two state Kalman filter comparable to that presented in the Negast thesis [13]. All computer simulations are run using Standard FORTRAN 77 code.

There are four major parts of the extended Kalman Filter model: (1) the friendly aircraft INS states, (2) the missile flight dynamics model, (3) the ladar measurement model, and (4) the missile body dynamics model. The final volume cross-section is generated by propagating the filter's steady state kinematics estimation results forward by the T_{II} parameter.

The thesis uses a parametric approach to analyzing the various elements. First a general baseline performance model is established using low (or zero where appropriate) noise strengths and simple aircraft and missile trajectories. Specific problem parameters of interest are varied from the baseline model to determine kinetic kill zone sensitivity to that parameter. Then multiple parametric studies are accomplished using more complex scenarios, to determine how the parameters of interest inter-relate. Parameters to be analyzed include noise strengths used, aircraft trajectories, missile approach angles, required T_{II}, and missile dynamics.

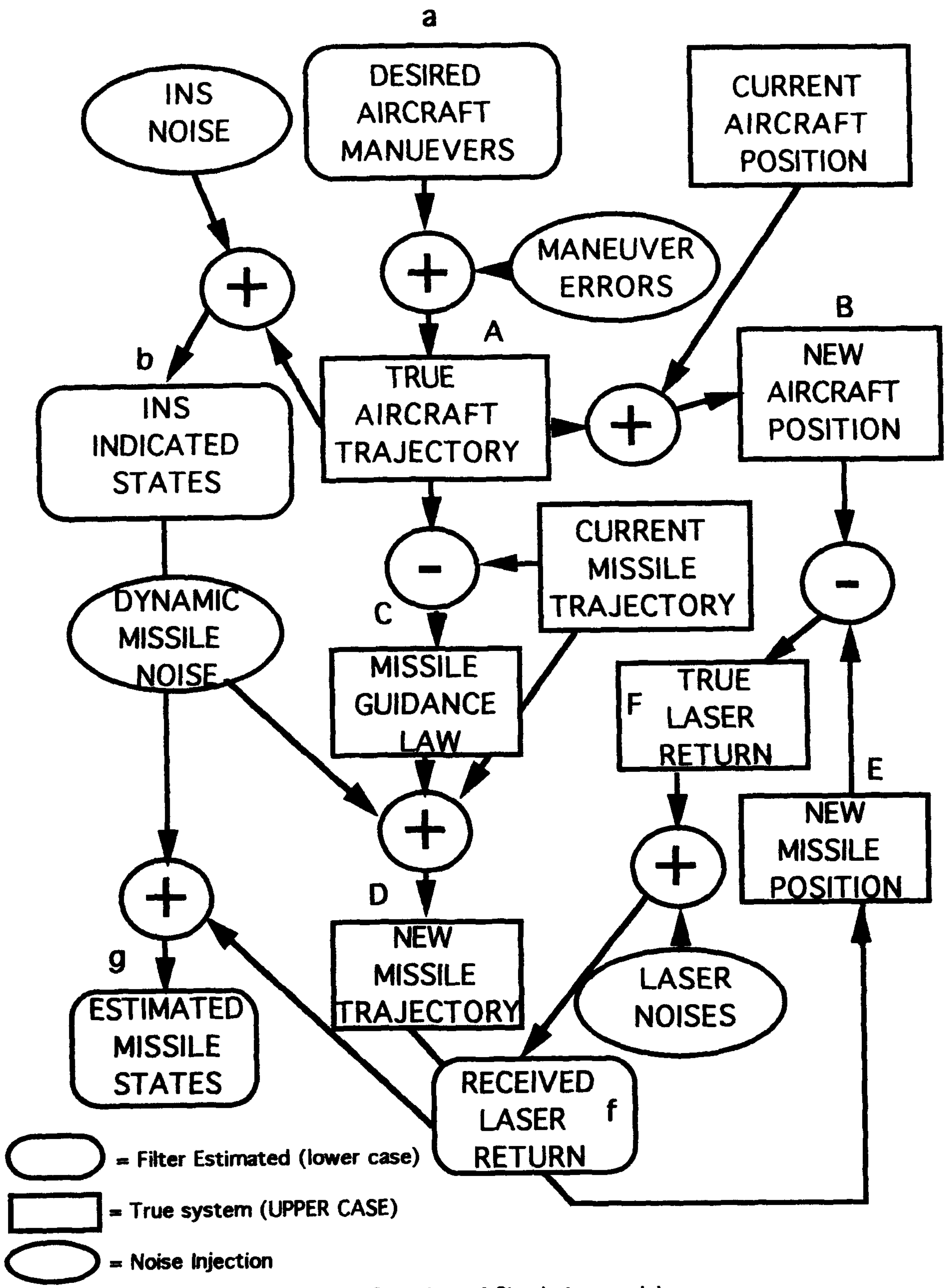

Fig 1-4 Overview of Simulation model

1.7 Summary

Chapter I introduced and defined the kinetic kill zone problem under study in this thesis. Section 1.1 presented the background rationale for performing this study, with a specific problem statement and established research goals following in Section 1.2. Previous research and other related work which made significant contributions to this study was summarized in Section 1.3. Section 1.4 presented the basic assumptions underlying the problem definition as presented in Section 1.2, and gave rationale supporting those assumptions where applicable. Section 1.5 scoped the work to be accomplished in this thesis study and overviewed the simulation model developed in detail in Chapter II. Section 1.6 concluded the chapter with a discussion of simulation methods, and parametric analysis techniques used to accomplish the established research goals.

Chapter II develops mathematical equations for the filter and truth models used in this study. System and filter states are established. System dynamic and measurement noise models are developed. Finally any special initial conditions (mean or covariance) used by the models are presented with supporting justification.

Chapter III overviews the simulation runs conducted to parametrically analyze the kinetic kill zone estimation problem. The simulations focus on three primary areas; the missile-aircraft scenario geometry, variation of the assumed ladar parameters, and variation of the assumed aircraft parameters. High and low performance baselines are established for the aircraft and ladar parametric studies.

Chapter IV presents the simulation results. Particular attention is focused on how the predicted volume varies as a function of range, time, and the parameters under study. Cross-section figures of merit are established as a means of standardizing the analysis. Best case and worst case baselines are established for performance comparisons. Parameters which had either very large or negligible influence on the predicted volume are presented.

Chapter V presents the thesis study's primary conclusions. The kinetic kill zone prediction approach presented in this thesis (i.e. extended Kalman filtering using propagated covariance estimates to predict the cross-section statistics) is analyzed in terms of its feasibilty based on the Chapter IV results. Recommendations for continued research are also presented here.

II The Simulation Models

2.0 Introduction

Chapter II develops the models presented in Figure 1-4 in detail. Discussion starts with the missile and aircraft dynamics. Appropriate coordinate frames are established for the missile and aircraft dynamics in Section 2.1. Kinematic equations of motion are then developed using the established coordinate frames in Section 2.2. Special considerations such as missile drag, internal missile dynamics, and aircraft maneuver dynamics are also covered in Section 2.2. Section 2.3 follows with a discussion of truth states and filter states selected from the dynamics equations developed in Section 2.2. Section 2.4 discusses the noise terms used in the truth and filter models, including system process noise, filter Q (dynamic noise strength) values, sources of ladar measurement noise, and INS measurement noise. (Note that, in this context, INS measurement noise is taken to mean the DGPS/INS filter's uncertainty about state values when the INS filter is requested to supply an INS update to the tracking filter. Since an INS filter model was not developed for this thesis, the tracker-requested INS updates are processed as measurements from an external source.) The chapter concludes with a discussion of initial conditions presented in Sections 2-4 and 2-5.

2.1 Reference Frames

There are four reference frames used in developing the system dynamics model. The four reference frames illustrated in Figure 2-1(a-b) include the aircraft's and missile's reference frame (a), the aircraft-to-missile relative coordinate frame (b), and the missile-to-aircraft relative coordinate frame (b). The aircraft receives friendly aircraft kinematic measurement updates, defined in north-east-down (NED) coordinates, (the aircraft reference frame) which are supplied by an onboard Inertial Navigation Subsystem aided with Global Positioning Satellite updates and Differential Corrections (INS/DGPS). The

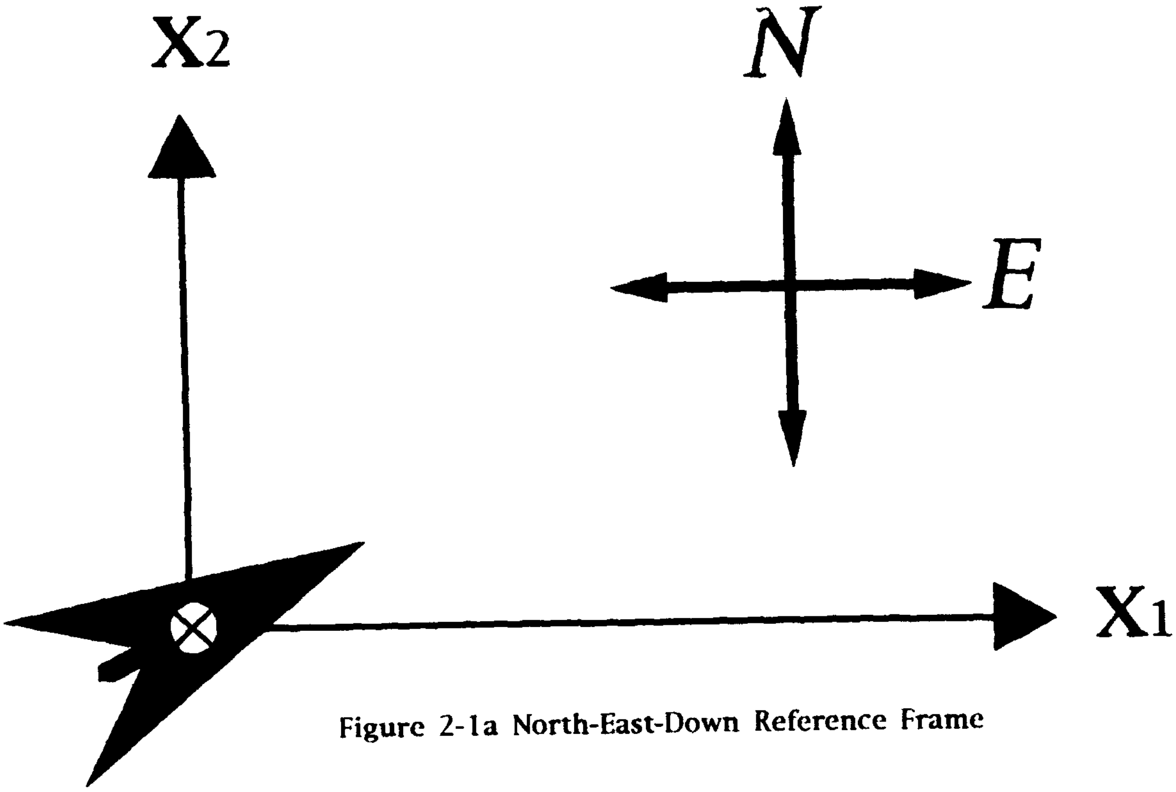

Figure 2-1a North-East-Down Reference Frame

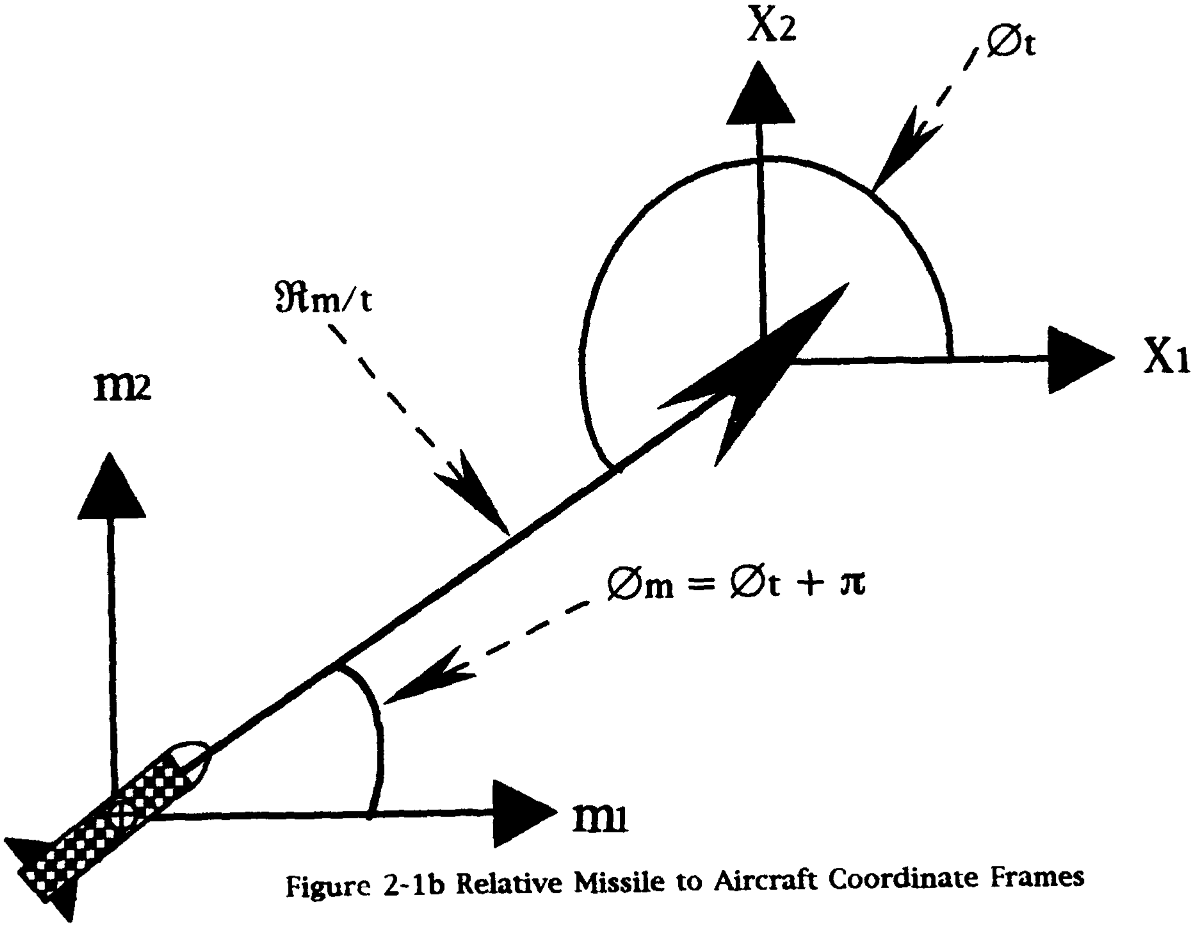

Figure 2-1b Relative Missile to Aircraft Coordinate Frames

aircraft-to-missile reference frame is defined in $(R_t, \emptyset_t)$ coordinates originating at the aircraft. Relative missile-to-aircraft kinematic measurements are supplied by the ladar to the aircraft's Kalman filter in this reference frame. The missile-to-aircraft reference frame is defined in $(R_m = R_t, \emptyset_m = \emptyset_t + \pi)$ coordinates. The missile uses relative kinematic measurements obtained in the missile-to-aircraft coordinate system to generate the appropriate lateral accelerations, A_L, which guide the missile to the aircraft. Since no direct access is available to the missile's kinematic states, the missile's reference frame is free to be chosen in any appropriate coordinates and the NED coordinates used by the aircraft are chosen for convenience.

Since this thesis study is limited to an in-the-plane analysis, all references to NED coordinates are assumed to be at constant altitude (down reference is fixed constant) and all references to $(R,\emptyset)$ coordinates are assumed to lie in a constant altitude plane.

2.2 Developing The Simulation Model

Development starts with an aircraft flying a specified trajectory in the aircraft coordinate frame. A missile is assumed to be tracking the aircraft with sufficient closing velocity to achieve intercept. The missile is positioned in $(R_m$ $\emptyset_m)$ coordinates, using the missile-to-aircraft reference frame. $\emptyset_m$ is defined as being counterclockwise from east in the aircraft reference system. The respective aircraft and missile headings are defined as

$$\beta_m = \text{ARCTAN}\,(V_{mn} / V_{me}) \tag{2-1}$$

$$\beta_t = \text{ARCTAN}\,(V_{tn} / V_{te}) \tag{2-2}$$

where

β_m is the missile heading,

β_t is the aircraft heading,

V_{mn} is the missile's north velocity component,

V_{me} is the missile's east velocity component,
V_{tn} is the aircraft's north velocity component,
V_{te} is the aircraft's east velocity component.

Since the missile reference frame is coupled to the aircraft reference frame by the commanded lateral accelerations, acceleration must necessarily be propagated as a state. To this effect, equations of acceleration are taken from Symon which describe acceleration in $(\mathfrak{R}, \varnothing)$ coordinates [17].

$$a_r = \partial^2\mathfrak{R}/\partial t^2 - \mathfrak{R}(\partial\varnothing/\partial t)^2 \qquad (2\text{-}3)$$

$$a_\varnothing = \mathfrak{R}(\partial^2\varnothing/\partial t^2) + 2\,(\partial\mathfrak{R}/\partial t)\,(\partial\varnothing/\partial t) \qquad (2\text{-}4)$$

where
a_r is the radial acceleration,
$a_\varnothing$ is the tangential acceleration.

Using the state definitions provided later in Table 2-2, (for a discussion on the selection of filter and system states see Section 2.3) a coordinate transformation between (X,Y) -or- NED and $(\mathfrak{R},\varnothing)$ coordinates, and properties of vectors, the missile and aircraft NED referenced accelerations are rewritten in the missile to aircraft reference frame, using the coordinate transformation matrix.

$$\begin{bmatrix} X' \\ Y' \end{bmatrix} = \begin{bmatrix} \cos\beta & \sin\beta \\ -\sin\beta & \cos\beta \end{bmatrix} \begin{bmatrix} X \\ Y \end{bmatrix} \qquad (2\text{-}5)$$

where $\beta = \varnothing_m - (\beta_m$ or β_t respectively),
and
β_m is the missile heading,
β_t is the aircraft heading,
$\varnothing_m$ is the missile to aircraft line-of-sight.

The transformed missile acceleration (from NED to $(\mathfrak{R},\varnothing)$ coordinates) becomes

$$|a_m| = (\,(\partial V_{mn}/\partial t)^2 + (\partial V_{me}/\partial t)^2\,)^{1/2} \qquad (2\text{-}6a)$$

$$a_{r_m} = |a_m| COS(\varnothing_m - ARCTAN((\partial V_{mn}/\partial t)/(V_{me}/\partial t))) \tag{2-6b}$$

$$a_{\varnothing m} = - |a_m| SIN(\varnothing_m - ARCTAN((\partial V_{mn}/\partial t)/(\partial V_{mn}/\partial t))) \tag{2-6c}$$

where

$|a_m|$ is the magnitude of the missile acceleration vector,

a_{r_m} is the radial missile acceleration,

$a_{\varnothing m}$ is the tangential missile acceleration.

Using the same transformation on the aircraft acceleration vector yields

$$|a_t| = ((\partial V_{tn}/\partial t)^2 + (\partial V_{te}/\partial t)^2)^{1/2} \tag{2-7a}$$

$$a_{r_t} = |a_t| COS(\varnothing_m - ARCTAN((\partial V_{tn}/\partial t)/(\partial V_{te}/\partial t))) \tag{2-7b}$$

$$a_{\varnothing t} = - |a_t| SIN(\varnothing_m - ARCTAN((\partial V_{tn}/\partial t)/(\partial V_{te}/\partial t))) \tag{2-7c}$$

where

$|a_t|$ is the magnitude of the aircraft acceleration vector,

a_{r_t} is the radial aircraft acceleration,

$a_{\varnothing t}$ is the tangential aircraft acceleration.

The relative missile-to-aircraft acceleration vector in the missile-to-aircraft reference frame is derived by subtracting Equation set (2-6) from Equation set (2-7) to yield:

$$a_{r_{mt}} = a_{r_m} - a_{r_t} \tag{2-8}$$

$$a_{\varnothing mt} = a_{\varnothing m} - a_{\varnothing t} \tag{2-9}$$

Combining Equations (2-8) and (2-9) with Equations (2-1) and (2-2) yields the following expressions for radial acceleration and angular acceleration:

$$\partial^2 \mathfrak{R}/\partial t^2 = a_{r_t} - a_{r_m} + \mathfrak{R}(\partial \varnothing/\partial t)^2 \tag{2-10}$$

$$\partial^2 \varnothing/\partial t^2 = (a_{\varnothing t} - a_{\varnothing m} - 2(\partial \mathfrak{R}/\partial t)(\partial \varnothing/\partial t))/\mathfrak{R} \tag{2-11}$$

This concludes the development of the kinematic model. The section continues with a development of missile and aircraft dynamics. State selection is deferred to Section 2.3.

2.2.1 The 5^{th} Order Missile Model

Cusumano and De Ponte developed a 5^{th} order missile truth model which was used as a performance benchmark against which to evaluate lower order filter models shown in Figure 2-2 [5]. The truth model autopilot had time-varying poles and zeros which altered the overall autopilot transfer function slightly with time. The 5^{th} order missile model was selected to represent the truth model's internal missile dynamics for this thesis. However, the time-varying poles and zeros were replaced by constant values equal to the time-zero values. This was done based on the recommendation of Cusumano and De Ponte, since the time-varying transfer function's dominant poles and zeros did not change significantly from their time-zero values, and the time-zero autopilot transfer function was always a good approximation to the time varying autopilot transfer function [5].

2.2.2 Series To Parallel Conversion

The autopilot portion of the 5^{th} order missile model is implemented as a decoupled transfer function, shown in Figure 2-3, by doing a partial fraction expansion on the autopilot transfer function [7]. The autopilot was converted in order to decouple the autopilot poles and zeros in the MSOFE computer code. Decoupling the states allowed pole and zero values to be altered more easily. The residues of the decoupled states, listed in Table 2-1, are evaluated as

$$r_i = (s + p_i)\, H(s) \Big|_{s = -p_i} \tag{2-12}$$

where

r_i is the residue of pole p_i,

p_i is the current pole under evaluation,

H(s) is the 5^{th} order missile's transfer function,

s is a Laplace transform variable.

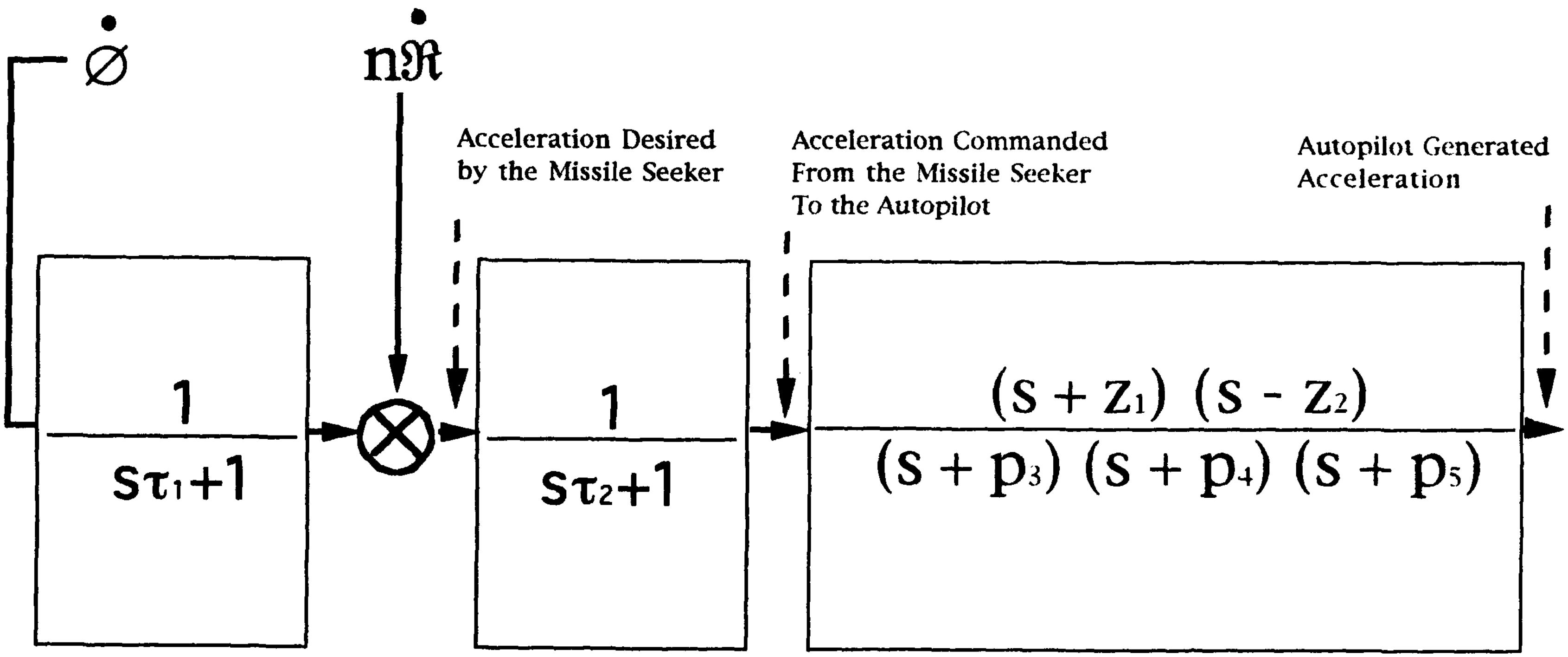

$1/\tau_1 = 13.33$
$1/\tau_2 = 3.33$
$p_3 = 3.06$
$p_4 = 21.88$
$p_5 = 63.34$
$z_1 = 33.34$
$z_2 = 31.10$

Figure 2-2 5th Order Cusumano and Deponte Missile Guidance Strip

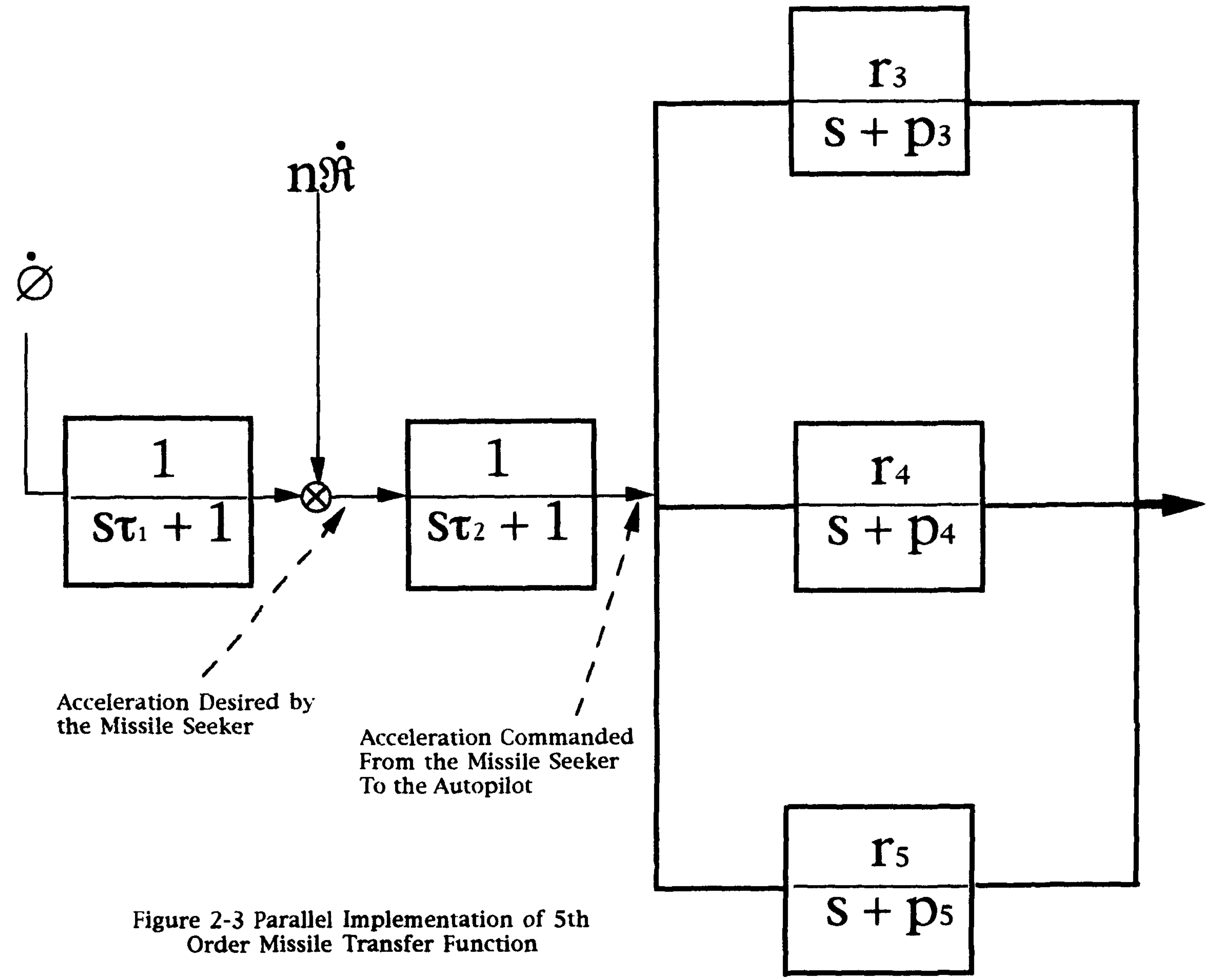

Figure 2-3 Parallel Implementation of 5th Order Missile Transfer Function

Table 2-1 Converted Autopilot Poles

5th Order Missile Pole	Converted Residue Values
s + 3.33	3.33 (no change)
s + 13.33	13.33 (no change)
s + 3.06	- .998751 (r3)
s + 21.88	+ .783663 (r4)
s + 63.34	+ 1.12986 (r5)
DC Gain	-3.964

2.2.3 The Missile Guidance Law

The missile generates lateral acceleration (A_L) in response to aircraft maneuvers according to the proportional navigation guidance law

$$A_{Lcomd}(s) = n\ s\Re(s)\ s\varnothing(s) \qquad (2\text{-}13a)$$

$$A_L(s) = A_{Lcomd}(s)\ H(s) \qquad (2\text{-}13b)$$

where

$A_L(s)$ is the missile's generated lateral acceleration,
$A_{Lcomd}(s)$ is the guidance law's commanded lateral acceleration,
n is a constant of proportional navigation between 3 and 6 [22],
$s\Re(s)$ is the range-rate between the missile and aircraft,
$s\varnothing(s)$ is the line-of-sight rate between the missile and aircraft,
H(s) is the 5^{th} order missile transfer function.

2.2.4 Atmospheric Effects

The missile used in this simulation is assumed to be in a post-burnout, coast-to-intercept phase of flight. The missile is therefore assumed to be constant mass and kinetically limited. The missile has two drag terms which significantly affect the missile's future flight trajectory. Both the coefficient of drag, C_D, and the coefficient of lift, C_L, generate drag force acting in opposition to the missile's current velocity vector. However, the coefficient of lift also produces a lift force perpendicular to the missile velocity vector. The amount of lift force generated is controlled by the missile's guidance law and transfer function from Equation (2-13). The amount of additional forward drag induced by the coefficient of lift is a function of the lift force requested.

The detailed development of the two drag coefficients is covered thoroughly in Zarchan [22], but is summarized here for completeness. The coefficient of drag is a function of four deterministic parameters - the air density (ρ), the missile surface area (cross-section) to mass ratio (S/M), the speed of sound (γ), the scenario altitude (h) - and the coefficient of zero lift (C_{DO}). The coefficient of lift is a function of the air density (ρ), the missile surface-to-mass ratio (S/M), the missile velocity (V_m) and the commanded lateral acceleration (A_{Lcomd}) [22]. The drag equations are

air density	$\rho = 0.002378\, e^{-(h/30{,}000)}$ (slg/ft^3)	(2-14)
coefficient of drag	$C_D = 0.5\, \rho\, S/M\, C_{DO}$	(2-15)
coefficient of lift	$C_L = 2\, A_{Lcomd}/(S/M\ \rho\, V_m^2)$	(2-16)
drag acceleration	$A_D(t) = -(\, C_D + C_{DL}\,)\, V_m^2$	(2-17)

where

A_{Lcomd} is the commanded lateral acceleration,
$A_D(t)$ is the total missile drag due to lift induced and normal drag,
C_{DO} is the no-lift induced drag,
C_{DL} is the lift induced drag.
V_m is the missile velocity (magnitude).

Cusumano and De Ponte further develop the C_{DL} and C_{DO} terms in their thesis work [5]:

zero lift drag $\quad C_{DO} = 2\,\gamma^{1/2} / V_m^{1/2}$ (2-18)

lift induced drag $\quad C_{DL} = 4\,A_{Lcomd}^2 / (\rho^2\,(S/M)^2\,V_m^3\,\gamma)$ (2-19)

where γ is the speed of sound in air.

2.2.5 Aircraft Maneuver Generator

All aircraft maneuvers are assumed to be benign for this simulation for two reasons. When the filter switches from the track mode, in which the filter continues to converge the state covariances, to the predict mode, the filter propagates the state covariances forward by the desired intercept time (T_{TI}). Because the filter accesses a priori information, no measurements from either the ladar or the INS are accessible during this extended cycle. All anticipated aircraft maneuvers act as control inputs to the missile's flight trajectory, as coupled through the proportional navigation guidance laws. The filter estimate of the aircraft trajectory therefore accounts for two processes through white noise of strength Q(t). The noise strength reflects limitations in the filter's aircraft trajectory model, and the pilot's limited ability to execute the desired maneuver without error. A benign trajectory simplifies the analysis and allows the filter to model the nominal aircraft trajectory accurately. The benign trajectory is also easier for the pilot to track, resulting in an appropriate decrease in Q(t).

The filter equations are developed as follows assuming a constant speed constant angle-rate turn [17]:

|acceleration| $\quad V_t^2/R_{turn} = 9.8\,G_{level} = \omega^2\,R_{turn}$ (2-20)

position $\quad X_{te}(t) = R_{turn}\,COS(\omega t + \theta)$ (2-21a)

$Y_{tn}(t) = R_{turn}\,SIN(\omega t + \theta)$ (2-21b)

velocity $\quad V_{te}(t) = -\omega R_{turn} SIN(\omega t + \theta)$ (2-22a)

$V_{tn}(t) = \omega R_{turn} COS(\omega t + \theta)$ (2-22b) acceleration $A_{te}(t) = -\omega^2 R_{turn} COS(\omega t + \theta)$ (2-23a)

$A_{tn}(t) = -\omega^2 R_{turn} SIN(\omega t + \theta)$ (2-22b)

jerk $J_{te}(t) = \omega^3 R_{turn} SIN(\omega t + \theta)$ (2-24a)

$J_{tn}(t) = -\omega^3 R_{turn} COS(\omega t + \theta)$ (2-24b)

where

V_t is the aircraft's velocity (magnitude),

G_{level} is the turn acceleration in g's,

R_{turn} is the turn radius,

ω is the angle-rate of the turn in rad/sec,

θ is a phase angle determined by the aircraft's initial velocity heading,

and all kinematic terms are derived in the NED reference frame.

The equations of circular motion (Equations (2-20) through (2-24)) are selected to model the aircraft motion for the following reasons: (1) The trajectory is easily modeled mathematically by both the filter and the truth system; (2) The trajectory is easily executed by a pilot; (3) The trajectory meets qualifications of being a benign "easily predictable" trajectory; (4) The trajectory is a subset of potential evasive maneuvers which may be included as part of a follow-on analysis.

2.3 State Selection

The state selection process (for both the truth model and the filter model) begins with a summary of the three key facts which dictated the choice of reference frames. 1) All aircraft INS measurements occur in the NED reference frame. 2) All aircraft ladar measurements occur in the aircraft-to-missile reference frame (i.e. polar coordinates originating from the aircraft). 3) The missile navigates using target information obtained in the missile-to-aircraft reference frame (i.e. polar coordinates originating at the missile). Because the most complicated dynamics occur in the missile-to-aircraft reference frame (i.e. the missile guidance commands), it is chosen as the primary reference frame for the truth and filter models.

2.3.1 The Truth States

The state selection process begins with Equations (2-10) and (2-11), which describe radial and angular acceleration, respectively, in the missile-to-aircraft reference frame. From the two equations ten states are selected. They include range, range-rate, angle, angle-rate, north missile velocity, east missile velocity, north aircraft velocity, east aircraft velocity, north aircraft acceleration and east aircraft acceleration. The four aircraft states are measurable directly from the aircraft INS. The ladar provides relative aircraft-to-missile measurements of range, range-rate, angle and angle-rate. The missile velocity states are measured by combining the absolute aircraft measurements, available from the INS, with the relative velocity measurements available from the ladar. All ten kinematic states are therefore observable with respect to the assumed INS and ladar measurements. Missile velocity is propagated as acceleration driven by drag, Equations (2-18) and (2-19), and (guidance law commanded) lateral acceleration, Equation (2-13). As seen from Equations (2-18) and (2-19), drag is a function of absolute missile velocity, hence the reason for propagating both absolute and relative missile kinematics.

The missile transfer function, H(s), contains five internal states (ref. Figure 2-3) which are selected. The proportional navigation constant, n, is a parameter. From Equations (2-18) and (2-19), two additional parameters are chosen - the scenario altitude, h, and the missile's surface to mass ratio (S/M). No additional states are required to model missile drag.

Aircraft kinematics are taken from Equations (2-20) thru (2-24b). Two new states representing aircraft velocity are added along with g-level which is a parameter. R_{turn}, ω, and θ can be calculated internally from the states and parameters already available and are not needed as separate states. A summary of selected truth model states is provided in Table 2-2A.

Table 2-2A Truth Model States

TRUTH STATE	DEFINITION OF STATE VARIABLE	UNITS OF STATE VARIABLE
$X_s(1)$	True Missile Velocity X Direction	m / sec
$X_s(2)$	True Missile Velocity Y Direction	m / sec
$X_s(3)$	True Line-of-Sight Angle	radians (rad)
$X_s(4)$	True Line-of-Sight Rate	rad / sec
$X_s(5)$	True Missile-to-Aircraft Range	meters (m)
$X_s(6)$	True Range-Rate	m / sec
$X_s(7)$	Aircraft East Velocity	m / sec
$X_s(8)$	Aircraft North Velocity	m / sec
$X_s(9)$	Aircraft East Acceleration	m / sec^2
$X_s(10)$	Aircraft North Acceleration	m / sec^2
$X_s(11)$	Seeker Bandwidth	rad / sec
$X_s(12)$	Seeker-Commanded Lateral Acceleration	m / sec^2
$X_s(13)$-(15)	Missile Autopilot Transfer Function	m / sec^2
A_L	Generated Lateral Acceleration	$\Sigma X_s(13) \Leftrightarrow X_s(15)$
n	Pro-Nav Parameter of Missile	const (Val = 3.0 - 6.0)
h	Scenario Altitude	feet
S/M	Missile's Surface-to-Mass Ratio	m^2 / kg

2.3.2 The Filter States

Filter states are chosen identical to the truth states except as noted here. All variables listed as parameters (except g-level) in the truth model are considered as unknown constants by the filter and are therefore modeled as the outputs of integrators driven by white pseudo-noise. The unknown constants include n, S/M, and h. In addition, the unknown missile transfer function is modelled as a perfect direct feedthrough with an appropriate increase in the filter's missile dynamics noise strnegth and in the pseudo-noise strength driving n. Although the simulations are set up to be strictly in-the-plane (contant altitude) scenarios, missile drag is a function of altitude (albeit a weak one). It is not expected that altitude estimations will have a significant impact on filter performance. Altitude has been included anyway since it will not degrade filter performance. If one seeks to optimize the filter design, altitiude estimation can be removed without significantly changing filter performance. The selection of filter states is summarized in Table 2-2B.

Table 2-2B Filter Model States

FILTER STATE	DEFINITION OF STATE VARIABLE	UNITS OF STATE VARIABLE
$X_f(1)$	Est. Missile Velocity X Direction	m / sec
$X_f(2)$	Est. Missile Velocity Y Direction	m / sec
$X_f(3)$	Est. Line-of-Sight Angle	radians (rad)
$X_f(4)$	Est. Line-of-Sight Rate	rad / sec
$X_f(5)$	Est. Missile-to-Aircraft Range	meters (m)
$X_f(6)$	Est. Range-Rate	m / sec
$X_f(7)$	Time-to-Go Estimate	seconds (sec)
$X_f(8)$	Est. of Pro-Nav Parameter	constant 4.5 nominal
$X_f(9)$	Est. Surface-to- Mass Ratio	m^2 / kg
$X_f10)$	Est. Missile Lateral Acceleration	m / sec^2
$X_f(11)$	Est. Scenario Altitude	feet
$X_f(12)$	Aircraft East Velocity	m / sec
$X_f(13)$	Aircraft East Acceleration	m / sec^2
$X_f(14)$	Aircraft North Velocity	m / sec
$X_f(15)$	Aircraft East Acceleration	m / sec^2

2.4 The Noise Terms

All noise used to drive the model can be categorized in one of four types: system process noise, INS related measurement noise, ladar measurement noise, and filter parameter estimation (or tuning) noise. Process noise is a representation of unmodelled, or partially modelled real dynamic effects. Process noise always refers to noise terms driving the truth model states $\underline{x}_s(t)$. Tuning noise represents uncertainty in the filter's dynamic model and can, but does not necessarily, represent real dynamic effects. Ladar measurement noise represents limitations in the measurement accuracy. INS measurement noise represents the INS filter's estimated uncertainty, which is propagated in the INS filter as a state covariance. The kill zone estimation filter periodically accesses the INS filter, to update the kill zone estimator's propagated aircraft states. The INS filter's estimated covariance becomes the kill zone estimation filter's measurement noise at the prescribed update time.

2.4.1 Process Noise

Process noise enters the model through the truth model dynamic equations as [9]

$$\partial \underline{x}(t)/\partial t = \underline{f}\{t,\underline{x}(t)\} + \underline{G}\{t,\underline{x}(t)\}\underline{w}(t) \qquad (2\text{-}25)$$

where

$\underline{x}(t)$ is the vector of states previously defined in Table 2-1,
$f\{t,x(t)\}$ is a vector of nonlinear dynamic equations developed in Section 2-1,
$\underline{G}\{t,\underline{x}(t)\}$ is a vector of noise shaping terms,
$\underline{w}(t)$ is a vector of "white noises" which partially drive the system dynamics.

Aircraft Process Noise The aircraft's acceleration states ($\underline{x}_{s9}(t)$, $\underline{x}_{s10}(t)$) are given a process noise which models the pilot's inability to execute a perfect maneuver. When the filter switches from the track mode (in which the filter converges the covariance estimates for each state to its steady state value) to the predictor mode (in which the filter tries to predict the missile trajectory), the filter loses all access to measurement updates. The filter assumes a nominal aircraft trajectory which is to be perfectly executed. Since the aircraft trajectory represents a control input to the tracking missile (as coupled through the lateral acceleration guidance commands), any deviation from the filter's assumed trajectory will cause a corresponding error in the filter's estimate of the missile trajectory. Most pilots are capable of sustaining constant velocity, constant gee-level maneuvers within ± 0.1 g for at least 30 second intervals [4], a much larger time interval than a typical kinetic kill zone scenario would last. Since the 0.1 g acceleration error is controlled and bounded by the pilot, the acceleration error is more typical of a measurement noise than a dynamic process noise. A noise strength, $Q(t)$, of $(0.1\ g)^2/sec$ is considered an adequate approximation to represent the pilot induced trajectory error.

Missile Process Noise Figure 2-4a shows a missile seekerhead. The missile body axis is shown with vector (a), the missile seeker axis with vector (b) and the target LOS with vector (c). The angle between vectors (b) and (c) is the missile's tracking error, and is measured by the missile seeker. The tracking error is represented on the horizontal axis of Figure 2.5(a & b). The moving target's angle-rate in the missile-to-aircraft reference frame causes a change in vector (b) relative to (c) and hence a change in the tracking error. The tracking error is passed to an amplifier (Figure 2.5) which generates an appropriate angle-rate signal to null the tracking error, thus allowing the missile to track the target. The generated angle-rate is then fed back through an integrator and subtracted from the original tracking error [19].

As seen from Figure 2-5, the magnitude of the nulling angle-rate signal is proportional to the tracking error represented by the sloped gain curve. Two curves are presented in Figure 2-5. The top curve represents a "loose" tracking loop, while the bottom curve represents a "tight" tracking loop. Both curves show a saturation gain which represents the maximum angle rate the amplifier can

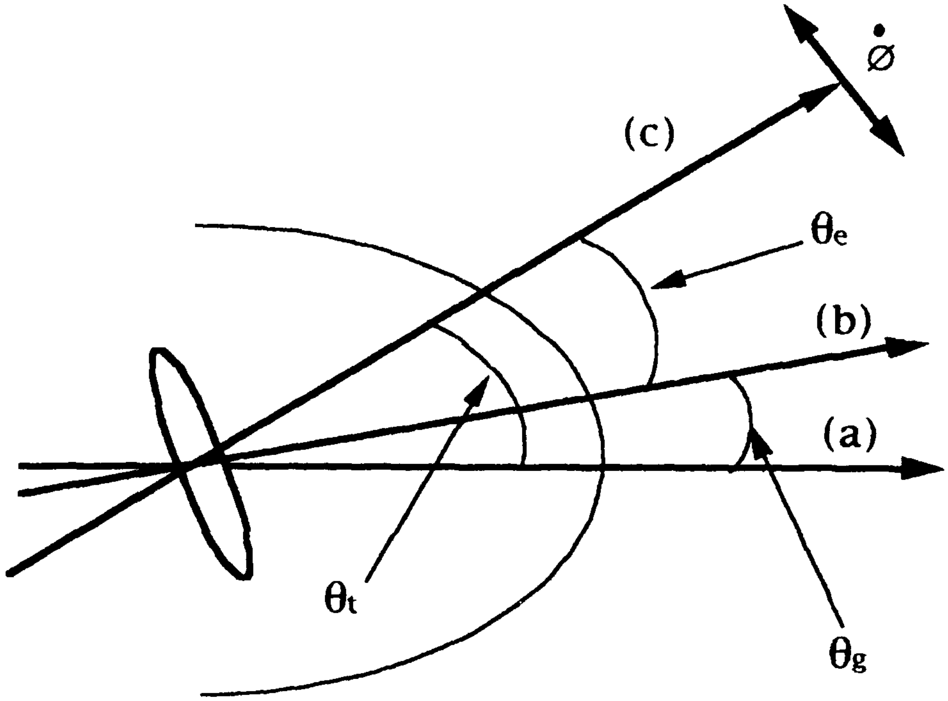

Figure 2-4a Missile Seeker Head

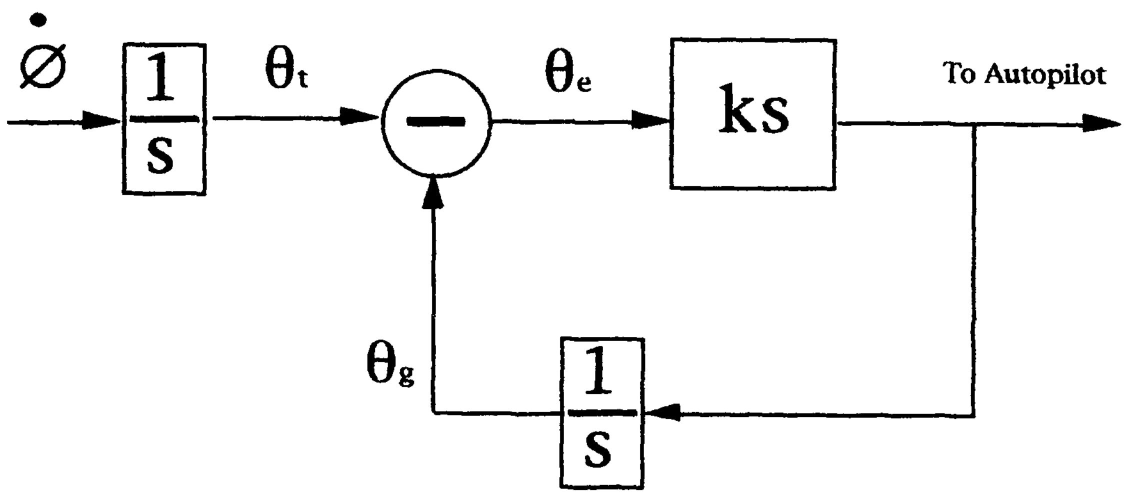

Figure 2-4b Missile Seeker Tracking Loop

generate. Below the saturation gain is a corresponding angle which represents the tracking error that generates saturation (and hence the maximum tracking error allowed before break-lock). The angle resolution of the amplifier is assumed to be between 5% and 10% of the saturation angle. The amplifier is assumed to be updated with new tracking errors at the seeker scan-rate of 100 Hz [19].

The minimum resolvable tracking angle for Figure 2-5a is taken as 10% of $\theta_{error\ max}$ or 0.1°. The minimum resolvable tracking angle for Figure 2-5b $\theta_{error\ min}$, is taken as 5% or 0.005°. The two tracking errors are multiplied by their corresponding amplifier gains to generate angle-rate errors of

$$\text{maximum error-rate } (600/\text{sec})(1/200^{\circ}) = 3^{\circ}/\text{sec} \qquad (2\text{-}26a)$$

$$\text{minimum error-rate } (15/\text{sec})(1/10^{\circ}) = 1.5^{\circ}/\text{sec} \qquad (2\text{-}26b)$$

which gets passed to the missile autopilot at 100 Hz. Thus a good range for a Q(t) value is between $900^{\circ 2}/\text{sec}^3$ and $225^{\circ 2}/\text{sec}^3$ where Q(t) is defined as the white noise diffusion strength [19].

The second noise source represents the missile autopilot's ability to produce identical missile accelerations, given identical acceleration commands from the seeker. Figure 2-6 shows a reproduced oscilloscope plot of autopilot acceleration error versus frequency for an actual missile analyzed at the Electronic Warfare Division's DIME facility, Wright Laboratory, Avionics Directorate [19]. The plot shows the autopilot transfer function to be an approximate first-order lag with a 300 Hz cutoff frequency and DC gain of about 0.08 g's. The error plot can be modelled approximately as

$$\text{autopilot acceleration error} \qquad 0.08(g)\, 2000 / (s + 2000) \qquad (2\text{-}27)$$

Since the autopilot error bandwidth is much greater than the autopilot transfer function bandwidth in the Cusumano and DePonte model (Figure 2-2), the autopilot noise can be modelled as white noise of strength $(0.08\ g)^2/\text{second}$.

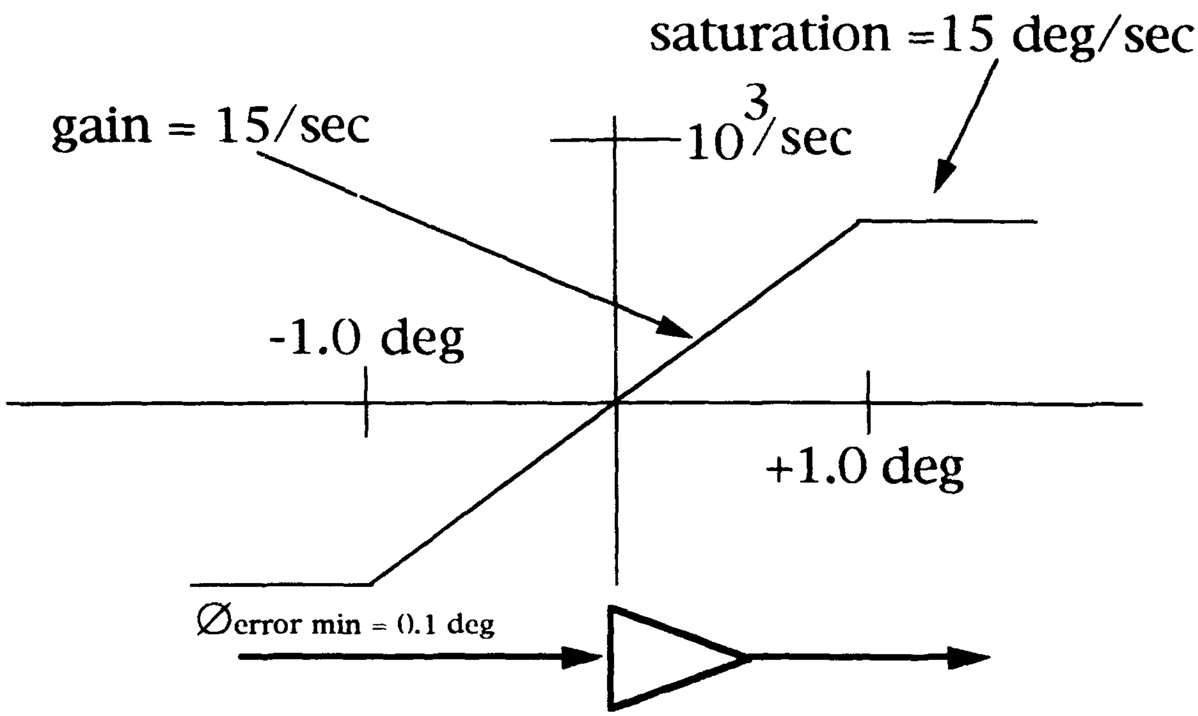

Figure 2.5a Seeker Amplifier Gain Curve 1.0 deg Tracking Error

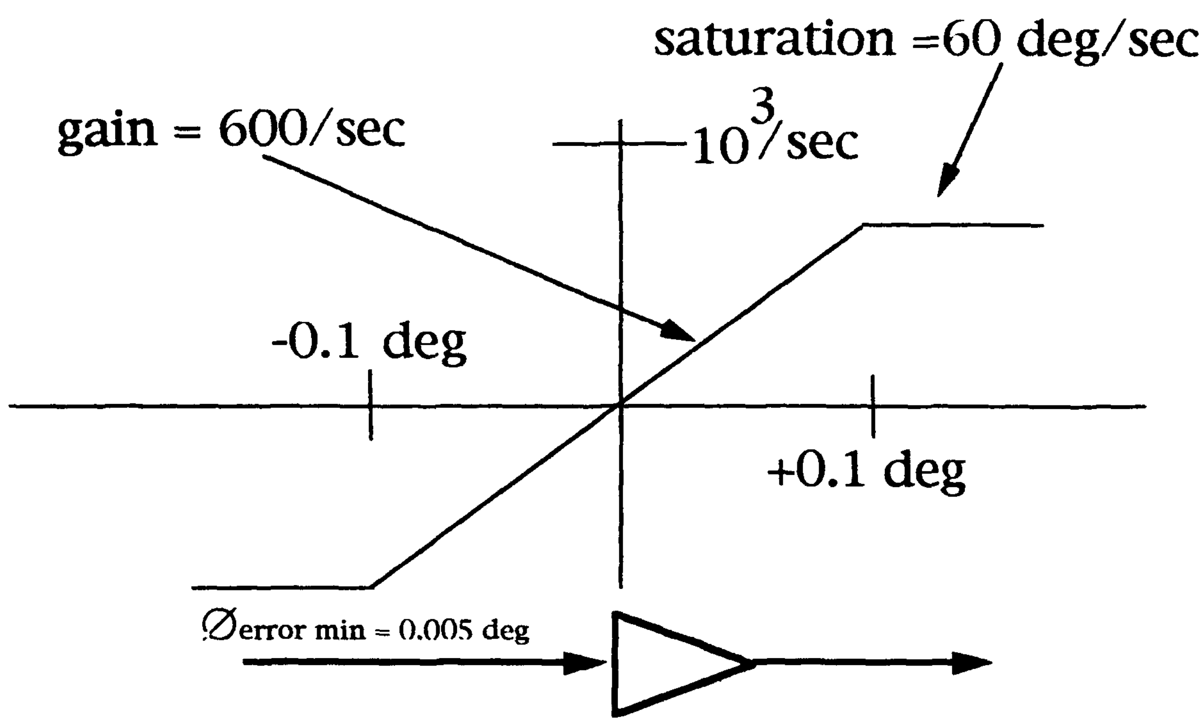

Figure 2.5b Seeker Amplifier Gain Curve 0.1 deg Tracking Error

Figure 2-6 Autopilot Acceleration Error Vs Frequency

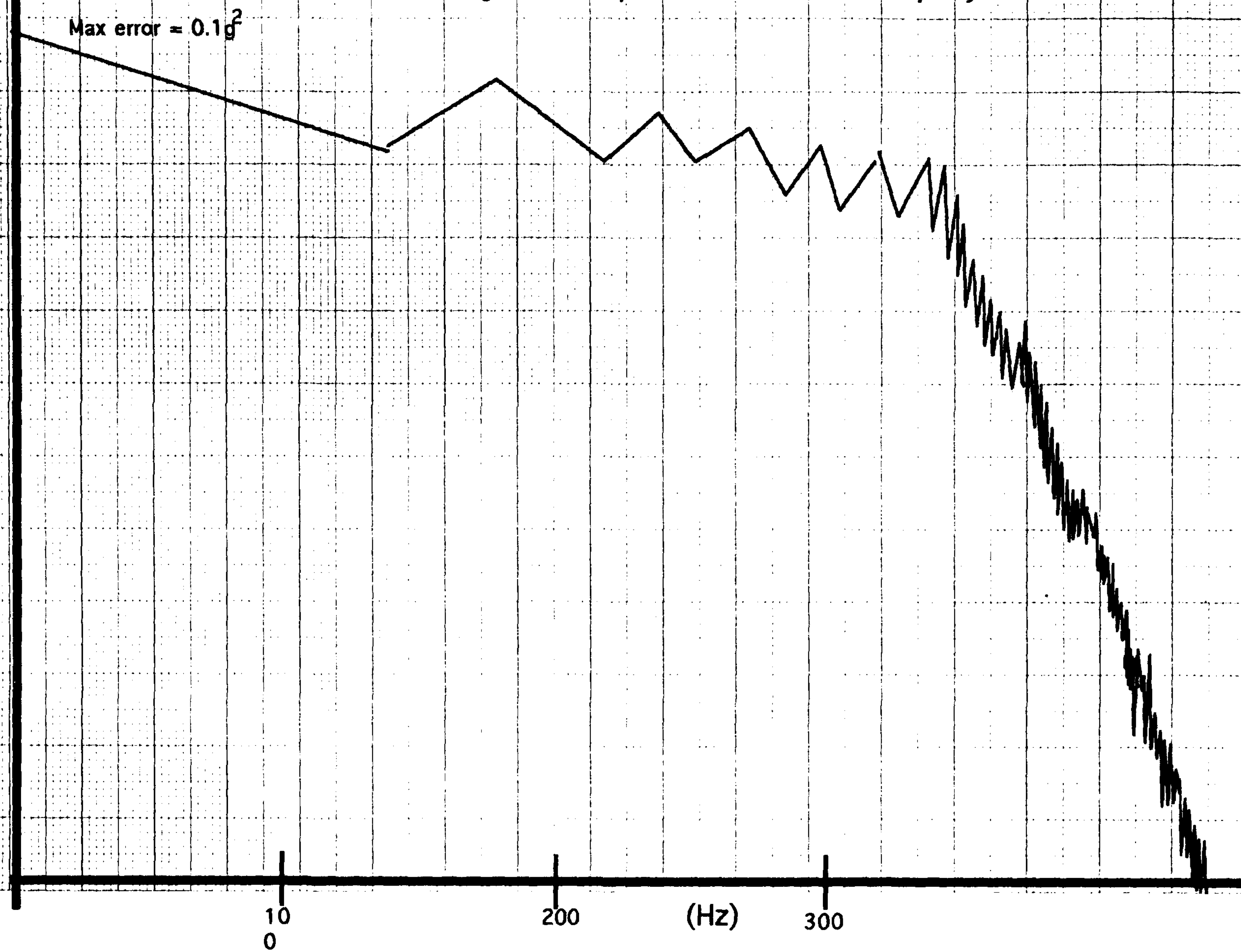

2.4.2 Filter Tuning Noise

The filter is given pseudo-noise for the proportional navigation constant (n), the missile's Surface to Mass Ratio (S/M), and the estimated scenario altitude (h) as shown in Equations (2-28 a-c)

$$\partial n/\partial t = 0.0 + w_n(t) \tag{2-28a}$$

$$\partial h/\partial t = 0.0 + w_h(t) \tag{2-28b}$$

$$\partial(S/M)/\partial t = 0.0 + w_{(S/M)}(t) \tag{2-28c}$$

The pseudo-noise is added to compensate for initial filter uncertainties for the two missile parameters, and the scenario altitude. Noise is also added to the filter's lateral acceleration estimate and the aircraft acceleration states. The missile noise allows the filter to track the fifth-order truth missile. The aircraft acceleration noise allows the filter to track the pilot-induced maneuver errors discussed in Section 2.4.1. All noise strengths are left as tuning parameters for the filter. In tuning the filter, the noise strengths are kept as small as possible to allow acquisition and track. The "low noise" tuning philosophy sacrifices filter settling time to achieve a better final volume estimate through slower diffusion of tuning noise into the final volume estimate.

2.4.3 Ladar Measurement Noise

Ladar measurement noise originates form three sources: Turbulence noise affects the ladar's detector array resolution of angle and angle-rate, $\varnothing(t)$ and $\partial\varnothing(t)/\partial t$, measurement; receiver processing delay noise which degrades range, $R(t)$, measurement; and spectral frequency resolution which degrades range-rate measurement, $\partial R/\partial t$. Noise statistics are provided in Table 2-3.

Figure 2-7 shows the structure of a typical ladar tracking system system. The primary subsystems include the laser, the receiver optics, the infrared detector array, and the signal processing elements. The laser transmits a pulse which is steered to the expected location of the missile through use of beam control

Table 2-3 Ladar Measurement Noise

MEASUREMENT TYPE	RMS Value
Range	0.5 meter
Range-rate	2 meter/sec
Angle	40.0 μrad
Angle-rate	2.0 mrad/sec

optics and slew mirrors (a). The laser beam divergence is set to equal the FOV of the detector array. The missile scattered laser return is focused by the receiver optics onto the detector plane (b). When the received pulse crosses a set detection threshold, the pulse is tagged by the next available clock pulse from the receiver clock (c). Since the transmitted pulse is released by a signal from the transmitter clock, (presumed to be in synch with the receiver clock), the range is calculated from the elapsed clock time.

Turbulence effects are modeled using the refractive index structure parameter C_n^2. The C_n^2 parameter provides an approximate means of estimating the rms angle error caused by propagation through a turbulent atmosphere, and is given by Equation (2-29) [16].

$$C_n^2 = 4.2\ 10^{-14}\ h^{-1/3}\ e^{-h/h_0} \tag{2-29}$$

$$\langle\theta^2\rangle = C_n^2\ \Re\ D_0^{-1/3} \tag{2-30}$$

where,

C_n^2 is the refractive index structure parameter,

h is the scenario altitude,

h_0 is 3200 meters,

$\Re$ is the target range,

$\langle\theta^2\rangle$ is the mean squared beam wander angle,

D_0 is the optic diameter.

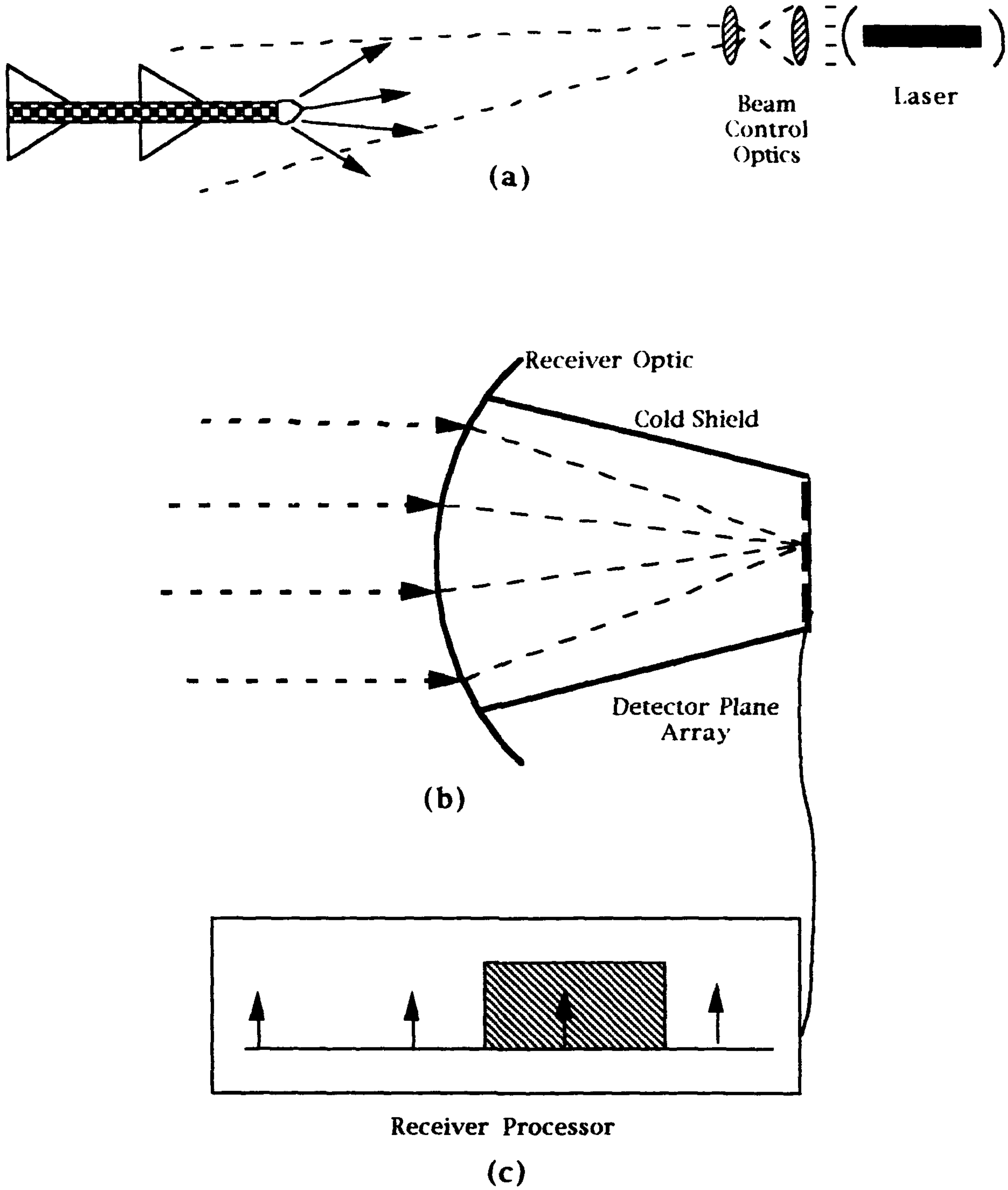

Figure 2-7 A Typical Ladar System

The received signal is picked up by the detector array (shown in Figure 2-8) which maps the system FOV into the individual detector element FOV's. An angle error signal is then generated by the receiver which enables the ladar to measure angle and angle rate. The FOV of the ladar is determined by the number of detectors in the detector array, the scan-rate (the ratio of the ladar's FOV to the detector array FOV) - assumed to be one - and the instantaneous FOV of each detector [Seyrafi].

$$\text{Ladar FOV} \qquad \alpha_L^{1/2} = n_d^{1/2}\, k_{scan}^{1/2}\, \alpha_d^{1/2} \qquad (2\text{-}31)$$

where

$\alpha_L^{1/2}$ is the FOV plane angle,
n_d is the number of detectors (256),
k_{scan} is the scan-rate (assumed to be one),
$\alpha_d^{1/2}$ is the detector FOV plane angle (40 μrad assumed).

Normally in optics, FOV angles are given as solid angles. However since this thesis is limited to a planar analysis, the notation $\alpha^{1/2}$ is used to represent planar angles. Since the FOV of the ladar is small (640 μrad under the assumed conditions), the ladar depends on the IR staring array of the MWR to perform low resolution angular tracking. The ladar is then cued in to allow high resolution angle measurements.

Figure 2-8 shows part of a 16 x 16 element detector array. Each detector maps into one part of the receiver FOV. The inner solid circle represents the focused return signal. The outer ring represents the one sigma error bound, $<\theta^2>^{1/2}$, which determines the angular resolution of the ladar. The value of $<\theta^2>^{1/2}$ has been demonstrated to about 40 μrad in tested systems, and is verifiable using Equations (2-29) and (2-30). Because $\alpha_d^{1/2}$ of each detector is 40 μrad, the outer ring would normally be approximately equal to the individual detector size, but has been enlarged in Figure 2-8 for illustration purposes.

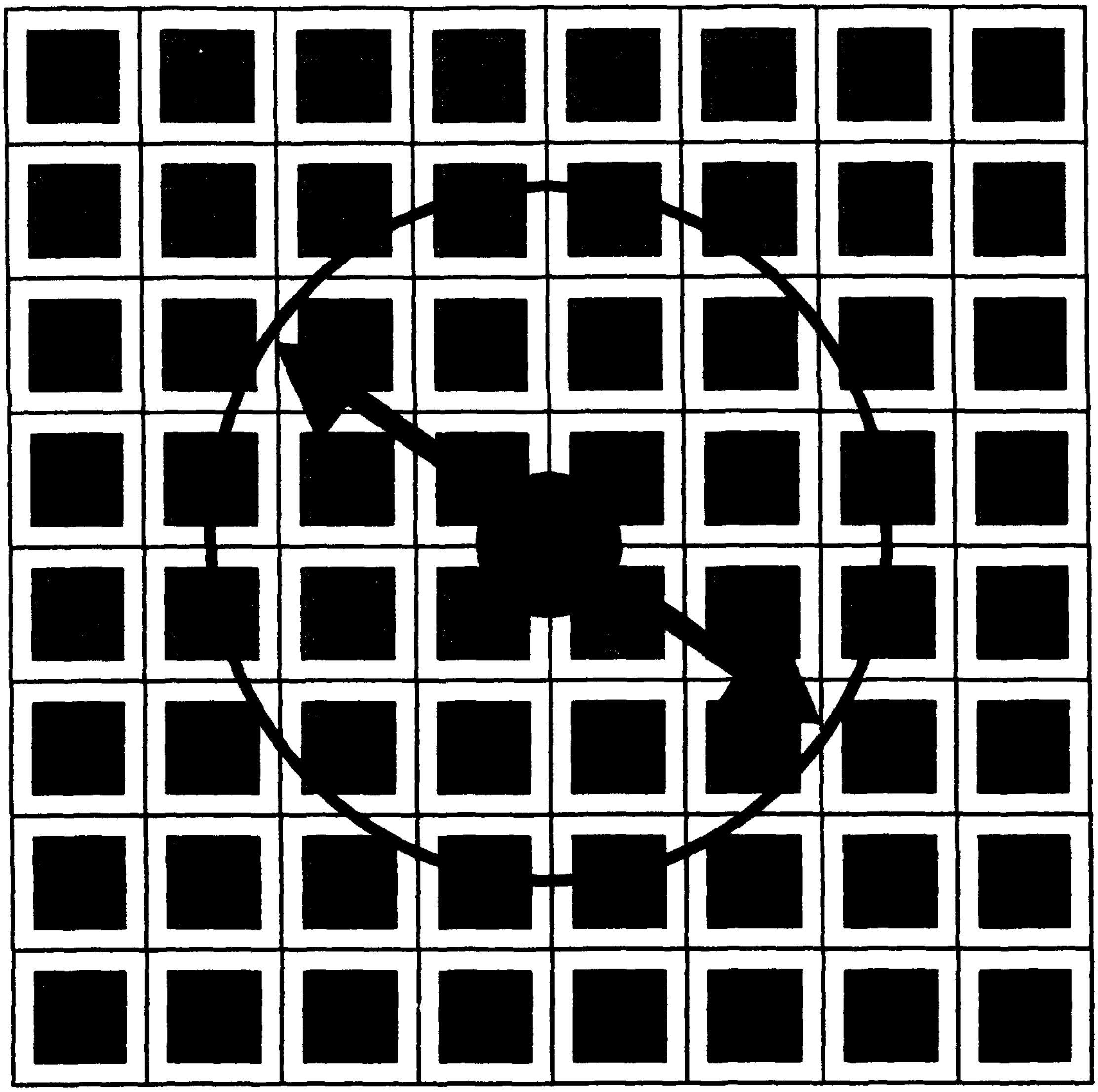

Figure 2-8 Angular Resolution

Most detector noise sources, such as bandwidth noise, dark current, shot noise, etc., affect the signal-to-noise ratio of the detector and hence the maximum effective range of return pulse detection [2]. For a typical 1.064 μm Nd:YAG pulsed laser, the maximum detection range is well over 30 km in clear atmosphere. Since the scenarios studied in this analysis are well under that range (typically 10 km or less) receiver detection noise is not considered applicable. The detector noises do not affect the range and angle resolution of the receiver.

Most receivers use a silicon based detector head with variable but measurable rise times of between 2 - 50 ns. The rise times are accurately measured and can be compensated for by the detection software. Therefore detector rise time does not significantly affect range resolution.

When a laser pulse is transmitted and received, an internal receiver clock keeps track of the transmit and receive times through an integer count of the elapsed clock periods. Therefore the Time of Launch (T_{OL}) and Time of Arrival (T_{OA}) resolution of the ladar cannot exceed the resolution of the receiver clock. Current laser trackers can support a T_{OA} resolution of about 2.5 ns, as illustrated in Figure 2-9 [21]. With a similar T_{OL} resolution, this gives a receiver clock induced range error of:

range error $$\Re_e = \pm T_{clock}\, n_{air}\, c \tag{2-32}$$

where

T_{clock} is the receiver clock's resolution (2.5×10^{-9} sec),
n_{air} is the index of refraction of air from Equation (2-33),
c is the speed of light in a vacuum (2.998×10^8 m/sec).

From Equation (2-32) the rms range error is approximately 0.75 meters.

Atmospheric turbulence is another potential source of ladar range measurement noise. The speed of light in any non-vacuum medium is given by the speed of light in vacuum, c, divided by the index of refraction in that medium, with the index of a vacuum, n_0, defined as 1.0. According to Goodman, the index of refraction of air, n_{air}, varies as a function of laser wavelength, λ, atmospheric pressure, P, and absolute temperature, T [7]:

index of air $$n_{air} = 1 + 77.6\,(1 + 7.52 \times 10^{-3}\,\lambda^{-2})\,P \times 10^{-6}/T \tag{2-33}$$

where

λ is the wavelength in μm (1.064),
T is the atmospheric temperature in K°,
P is the atmospheric pressure in millibars.

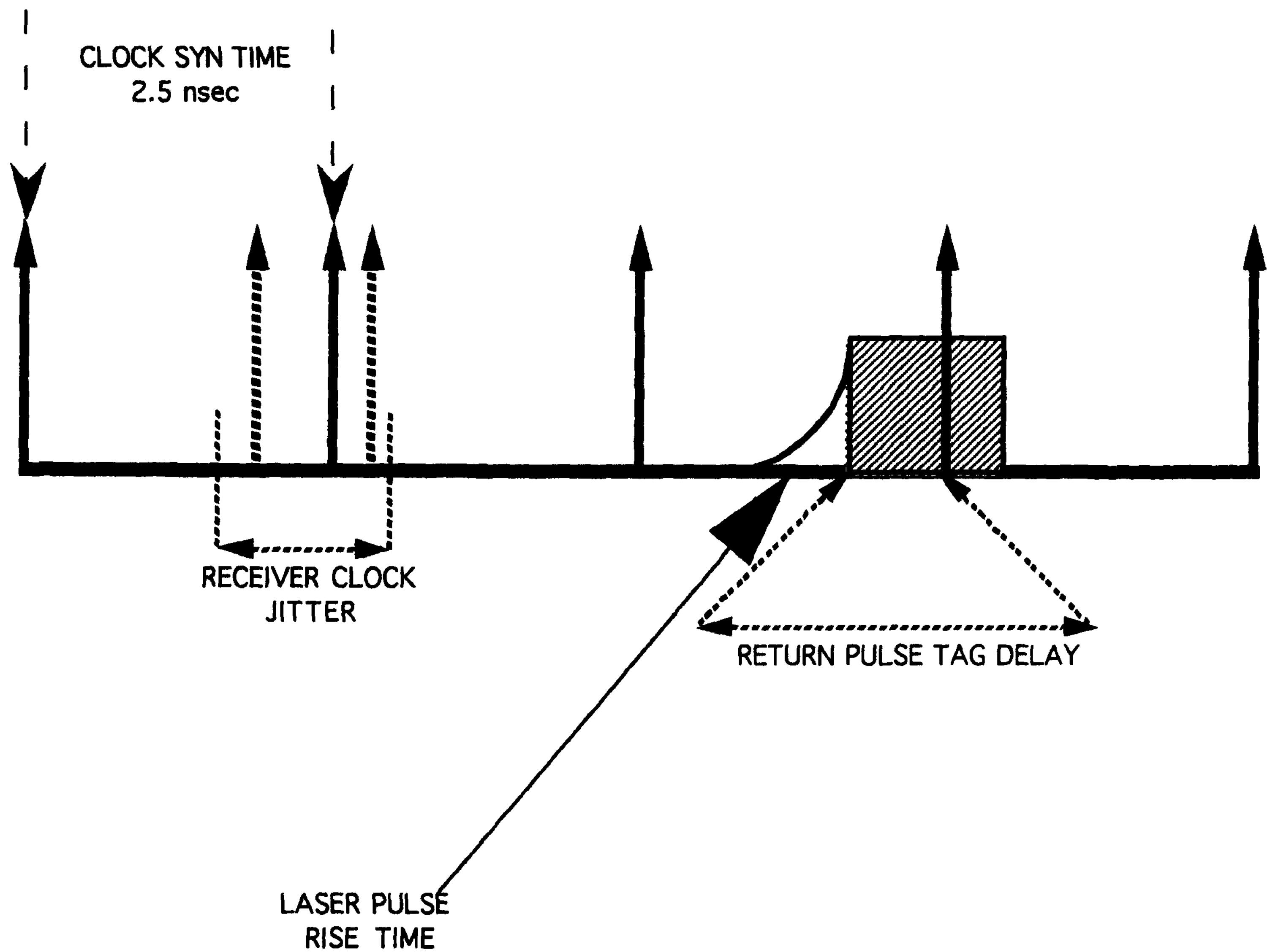

Figure 2-9 Receiver Timing Diagram

Turbulence is caused by small scale variations in atmospheric temperature and pressure. The net effect of turbulence is to cause a corresponding variation of the index of refraction, and therefore of the speed of propagation. Because range is a large scale measurement, the effective index of refraction will be an average of the total of all refraction indexes traversed appropriately scaled to account for propagation distances crossed with that index. When the average effect is accounted for, turbulence has a negligible effect on range error at the ranges of interest. This argument is made on three premises: That index variation is a linear function of pressure, that the index only varies slightly with pressure, and that the total pressure variations encountered must average to approximately the nominal atmospheric pressure. When all three premises hold, the net range error caused by atmospheric turbulence is less than 10^{-5} x total distance propagated, or less than 0.1 meter per 10 km of tracking range. Since the scenarios encountered in this study are usually simulated at ranges under 10 km, the effect of turbulence on range measurement is negligible.

The ladar range-rate noise can be calculated using Equation (2-34) [16:237]

$$\Delta f = 2\,(\partial \Re(t)/\partial t)\,/\,\lambda \tag{2-34}$$

where

Δf is the Doppler frequency shift,

$\partial \Re(t)/\partial t)$ is the range-rate,

λ is the laser wavelength,

by setting the frequency shift equal to the frequency resolution of a heterodyne receiver. (A heterodyne receiver uses a frequency mixer to generate a beat pattern between a received signal and a reference signal. The frequency of the beat pattern determines the frequency difference between the received signal and the reference signal.) A 1.0 m/sec range-rate resolution requires a receiver frequency resolution of approximately 2.0 MHz. Seyrafi verifies that range-rate accuracies less than 1.0 m/sec are achievable [16:238].

2.5 The Initial Conditions

Initial conditions are established by setting up a particular scenario of interest. Initial missile range and tracker angles are chosen, along with missile velocity, aircraft heading, aircraft turning rate, the proportional navigation constant, the missile's surface-to-mass ratio, and scenario altitude. The specific initial conditions chosen for these variables are left to the problem parameter under investigation.

The initial conditions are assumed to be handed off from a Missile Warning Receiver (MWR) onboard the aircraft. Initial conditions to be provided include range, range-rate, time-to-go, and LOS angle. Values for the rms errors of the initial conditions are based on minimum performance goals established by Mr Kevin McCamey, Program Manager of the Electronic Countermeasures Advanced Development Branch Missile Warning Program[12], and are provided in Table (2-4).

Initial covariance estimates for the aircraft states are assumed to be available from the GPS/INS. GPS/INS covariance values are obtained from Negast [13] using the twenty-two state GPS/INS model in steady state. Table (2-5) contains

Table 2-4 MWR Provided Initial Conditions

Initial Parameter	RMS Error
Range	3.0 meters
Range Rate	5.0 meter/sec
Angle	2.0 mrad
Time-to-go	10% error

the rms errors associated with the aircraft states. These same rms errors are used in the measurement update cycles for the aircraft states, since they are assumed to be continuously available from the navigation system.

Table 2-5 INS Provided Initial Conditions

INS State	RMS Error
North Velocity	0.03 meter/sec
East Velocity	0.03 meter/sec
Vertical Position	9 feet

The filter's proportional navigation parameter, n, is given an initial covariance of 0.25 guaranteeing that, with an initial estimate of 4.5, the parameter's full range (3 to 6) is covered within the 3σ bounds. The filter's missile surface-to-mass ratio is given a covariance of $(0.0008)^2$ to cover the expected range (0.005 to .0001) with an initial estimate of 0.0025 m^2/kg.

2.6 The Summarized Truth and Filter Model Equations

This section presents the actual model equations and noise matrices used in simulation. A rigorous presentation of extended Kalman filtering is not presented, nor are the equations associated with extended Kalman filtering. Knowledge of the subject is assumed on the part of the reader. For a rigorous treatement of extended Kalman filtering refer to Maybeck [9].

The system dynamics are developed in Section 2.2, the state selections summarized in Table 2-2, and the process and measurement noise terms presented in Section 2.4. The following is a summarized list of the actual truth model and filter model equations used in simulation. All variables and notation used here is consistent with that used throughout the chapter. The states are as defined in

Table 2.2a and 2-2b. The truth and sytem models are described by two general equations [9]:

$$\partial \underline{x}/\partial t = \underline{f}[\underline{x}(t),t] + \underline{G}(t)\underline{w}(t) \tag{2-35}$$

$$\underline{z}(t_i) = \underline{h}[\underline{x}(t_i),t_i] + \underline{v}(t_i) \tag{2-36}$$

where

$\underline{f}[\underline{x}(t),t]$ is a vector of non-linear state equations describing system dynamics,
$\underline{x}(t)$ is a vector of states from either Table 2-2A or Table 2-2B,
$\underline{w}(t)$ is a vector of dynamic process noises,
$\underline{G}(t)$ is a non-linear noise shaping matrix,
$\underline{z}(t_i)$ is a vector of system measurements,
$\underline{h}[\underline{x}(t_i),t_i]$ is a vector of non-linear measurement equations,
$\underline{v}(t_i)$ is a vector of measurement noises or uncertainties.

2.6.1 The Truth Model Dynamics

Equation Sets (2-37) and (2-38) define the true dynamics vector $\partial \underline{x}_s/\partial t$:

$$\partial x_{s1}/\partial t = - f1V_m^{1/2}x_{s1} - f_2A_L^2 + A_Lx_{s2}/V_m \tag{2-37a}$$

$$\partial x_{s2}/\partial t = - f1V_m^{1/2}x_{s2} - f_2A_L^2 - A_Lx_{s1}/V_m \tag{2-37b}$$

$$\partial x_{s3}/\partial t = x_{s4} \tag{2-37c}$$

$$\partial x_{s4}/\partial t = \{ - A_t\mathrm{Sin}[x_{s3} - \mathrm{ArcTan}(x_{s10}/x_{s9})] + A_m\mathrm{Sin}[x_{s3} - \mathrm{ArcTan}(\partial x_{s2}/\partial t / \partial x_{s1}/\partial t)] + x_{s6}x_{s4} \} /x_{s5} \tag{2-37d}$$

$$\partial x_{s5}/\partial t = x_{s6} \tag{2-37e}$$

$$\partial x_{s6}/\partial t = A_t\mathrm{Cos}[x_{s3} - \mathrm{ArcTan}(x_{s10}/x_{s9})] - A_m\mathrm{Cos}[x_{s3} - \mathrm{ArcTan}(\partial x_{s2}/\partial t / \partial x_{s1}/\partial t)] + x_{s5}x_{s4}^2 \tag{2-37f}$$

$$\partial x_{s7}/\partial t = x_{s9} \tag{2-37g}$$

$$\partial x_{s8}/\partial t = x_{s10} \tag{2-37h}$$

$$\partial x_{s9}/\partial t = \omega^3R_{turn}\mathrm{Sin}(\omega t+\theta) + w_9(t) \tag{2-37i}$$

$$\partial x_{s10}/\partial t = - \omega^3R_{turn}\mathrm{Cos}(\omega t+\theta) + w_{10}(t) \tag{2-37j}$$

$$\partial x_{s11}/\partial t = - 13.33x_{s11} + 13.33x_{s4} + w_{11}(t) \tag{2-37k}$$

$$\partial x_{s12}/\partial t = - 3.33x_{s12} + 3.33nx_{s11}x_{s6} \tag{2-37l}$$

$$\partial x_{s13}/\partial t = - 3..06x_{s13} - 4(.998751)x_{s12} + w_{13}(t) \tag{2-37m}$$

$$\partial x_{s14}/\partial t = -3..06x_{s14} - 4(.783663)x_{s12} \quad (2\text{-}37n)$$

$$\partial x_{s15}/\partial t = -3..06x_{s15} - 4(1.12986)x_{s12} \quad (2\text{-}37o)$$

and

$$V_m = (x_{s1}{}^2 + x_{s2}{}^2)^{1/2} \quad (2\text{-}38a)$$

$$A_m = (\partial x_{s1}/\partial t^2 + \partial x_{s2}/\partial t^2)^{1/2} \quad (2\text{-}38b)$$

$$A_t = (x_{s9}{}^2 + x_{s10}{}^2)^{1/2} \quad (2\text{-}38c)$$

$$A_L = x_{s13} + x_{s14} + x_{s15} \quad (2\text{-}38d)$$

$$f_1 = 1.29\, e^{-(h/30{,}000)}\, S/M_Y{}^{1/2} \quad (2\text{-}38e)$$

$$f_2 = 2.0/(1.29\, e^{-(h/30{,}000)}\, S/M_Y) \quad (2\text{-}38f)$$

2.6.2 The Truth Model Measurements

Equation Set (2-39) defines the true measurement vector $\underline{z}_s(t_i)$:

$$z_{s1} = -(x_{s6}+v_{s6})\mathrm{Cos}(x_{s3}+v_{s3}) + (x_{s5}+v_{s5})(x_{s4}+v_{s4})\mathrm{Sin}(x_{s3}+v_{s3}) + (x_{s7}+v_{s7}) \quad (2\text{-}39a)$$

$$z_{s2} = -(x_{s6}+v_{s6})\mathrm{Sin}(x_{s3}+v_{s3}) - (x_{s5}+v_{s5})(x_{s4}+v_{s4})\mathrm{Cos}(x_{s3}+v_{s3}) + (x_{s8}+v_{s8}) \quad (2\text{-}39b)$$

$$z_{s3} = x_{s3} + v_{s3} \quad (2\text{-}39c)$$

$$z_{s4} = x_{s4} + v_{s4} \quad (2\text{-}39d)$$

$$z_{s5} = x_{s5} + v_{s5} \quad (2\text{-}39e)$$

$$z_{s6} = x_{s6} + v_{s6} \quad (2\text{-}39f)$$

$$z_{s7} = x_{s7} + v_{s7} \quad (2\text{-}39g)$$

$$z_{s8} = x_{s8} + v_{s8} \quad (2\text{-}39h)$$

$$z_{s9} = x_{s9} + v_{s9} \quad (2\text{-}39i)$$

$$z_{s10} = x_{s10} + v_{s10} \quad (2\text{-}39j)$$

2.6.3 The Truth Model Noise Strength

Table 2-6 presents the noise strength values used in the dynamic's $Q(t)$ matrix and in the measurement's $R(t_i)$ matrix. Each noise strength is presented with its accompanying subscripted r_m or q_{nn} term to identify matix location. All matrix entries not explicitly specified in the table are assumed to be zero.

Table 2-6 Truth Model Noise Terms

R Entry	Strength	Q Entry	Strength
r_3	$1.6E^{-10}$	$q_{9,9}$	1.0
r_4	$4.0E^{-6}$	$q_{10,10}$	1.0
r_5	0..25	$q_{11,11}$	15.0
r_6	1.0	$q_{13,13}$	.64
r_7	.01		
r_8	0.01		
r_9	$25.0E^{-10}$		
r_{10}	$25.0E^{-10}$		

2.6.4 The Filter Model Dynamics

Equation Sets (2-40) and (2-41) define the filter dynamics vector $\partial \underline{x}_f/\partial t$:

$$\partial x_{f1}/\partial t = -f1V_m^{1/2}x_{f1} - f_2A_L^2 + A_Lx_{f2}/V_m \quad (2\text{-}40a)$$

$$\partial x_{f2}/\partial t = -f1V_m^{1/2}x_{f2} - f_2A_L^2 - A_Lx_{f1}/V_m \quad (2\text{-}40b)$$

$$\partial x_{f3}/\partial t = x_{f4} \quad (2\text{-}40c)$$

$$\partial x_{f4}/\partial t = \{ -A_t \operatorname{Sin}[x_{f3} - \operatorname{ArcTan}(x_{f15} / x_{f13})] + A_m \operatorname{Sin}[x_{f3} - \operatorname{ArcTan}(\partial x_{f2}/\partial t/ \partial x_{f1}/\partial t)] + x_{f6}x_{f4} \} / x_{f5} \quad (2\text{-}40d)$$

$$\partial x_{f5}/\partial t = x_{f6} \quad (2\text{-}40e)$$

$$\partial x_{f6}/\partial t = A_t \operatorname{Cos}[x_{f3} - \operatorname{ArcTan}(x_{f15} / x_{f13})] - A_m \operatorname{Cos}[x_{f3} - \operatorname{ArcTan}(\partial x_{f2}/\partial t / \partial x_{f1}/\partial t)] + x_{f5}x_{f4}^2 \quad (2\text{-}40f)$$

$$\partial x_{f7}/\partial t = 0.0 \ (x_{f7} = 1.5x_{f5}/x_{f6}) \quad (2\text{-}40g)$$

$$\partial x_{f8}/\partial t = 0.0 + w_{f8}(t) \quad (2\text{-}40h)$$

$$\partial x_{f9}/\partial t = 0.0 + w_{f9}(t) \quad (2\text{-}40i)$$

$$\partial x_{f10}/\partial t = 0.0 + w_{f10}(t) \qquad (2\text{-}40j)$$

$$\partial x_{f11}/\partial t = 0.0 + w_{f11}(t) \qquad (2\text{-}40k)$$

$$\partial x_{f12}/\partial t = x_{f13} \qquad (2\text{-}40l)$$

$$\partial x_{f13}/\partial t = \omega^3 R_{turn} \mathrm{Sin}(\omega t+\theta) + w_{f13}(t) \qquad (2\text{-}40m)$$

$$\partial x_{f14}/\partial t = x_{f15} \qquad (2\text{-}40n)$$

$$\partial x_{f15}/\partial t = -\omega^3 R_{turn} \mathrm{Cos}(\omega t+\theta) + w_{f15}(t) \qquad (2\text{-}40o)$$

and

$$V_m = (x_{f1}{}^2 + x_{f2}{}^2)^{1/2} \qquad (2\text{-}41a)$$

$$A_m = (\partial x_{f1}/\partial t^2 + \partial x_{f2}/\partial t^2)^{1/2} \qquad (2\text{-}41b)$$

$$A_t = (x_{f13}{}^2 + x_{f15}{}^2)1/2 \qquad (2\text{-}41c)$$

$$A_L = n\ Xf4\ Xf6 + x_{f10} \qquad (2\text{-}41d)$$

$$f_1 = 1.29\ e^{-(x_{f11}/30{,}000)}\ x_{f9}\ \gamma^{1/2} \qquad (2\text{-}41e)$$

$$f_2 = 2.0/(1.29\ e^{-(x_{f11}/30{,}000)}\ x_{f9}\ \gamma) \qquad (2\text{-}41f)$$

2.6.5 The Filter Measurement Matrix

Equation Set (2-42) presents the filter measurement vector $\underline{z}_s(t_i)$:

$$z_{f1} = -(x_{f6}+v_{f6})\mathrm{Cos}(x_{f3}+v_{f3}) + (x_{f5}+v_{f5})(x_{f4}+v_{f4})\mathrm{Sin}(x_{f3}+v_{f3}) + (x_{f12}+v_{f12}) \qquad (2\text{-}42a)$$

$$z_{f2} = -(x_{f6}+v_{f6})\mathrm{Sin}(x_{f3}+v_{f3}) - (x_{f5}+v_{f5})(x_{f4}+v_{f4})\mathrm{Cos}(x_{f3}+v_{f3}) + (x_{f14}+v_{f14}) \qquad (2\text{-}42b)$$

$$z_{f3} = x_{f3} + v_{f3} \qquad (2\text{-}42c)$$

$$z_{f4} = x_{f4} + v_{f4} \qquad (2\text{-}42d)$$

$$z_{f5} = x_{f5} + v_{f5} \qquad (2\text{-}42e)$$

$$z_{f6} = x_{f6} + v_{f6} \qquad (2\text{-}42f)$$

$$z_{f12} = x_{f12} + v_{f12} \qquad (2\text{-}42g)$$

$$z_{f13} = x_{f13} + v_{f13} \qquad (2\text{-}42h)$$

$$z_{f14} = x_{f14} + v_{f14} \qquad (2\text{-}42i)$$

$$z_{f15} = x_{f15} + v_{f15} \qquad (2\text{-}42j)$$

The filters measurement matrix ($\underline{H}$) is formed by taking the partial derivatives of Equations (2-42 a-j) with respect to the 15 filter states. The $\underline{H}$ matrix is:

$$
\begin{bmatrix}
0 & 0 & a & b & c & d & 0 & 0 & 0 & 0 & 0 & 1 & 0 & 0 & 0 \\
0 & 0 & e & f & g & h & 0 & 0 & 0 & 0 & 0 & 0 & 1 & 0 & 0 \\
0 & 0 & 1 & 0 & 0 & 0 & 0 & 0 & 0 & 0 & 0 & 0 & 0 & 0 & 0 \\
0 & 0 & 0 & 1 & 0 & 0 & 0 & 0 & 0 & 0 & 0 & 0 & 0 & 0 & 0 \\
0 & 0 & 0 & 0 & 1 & 0 & 0 & 0 & 0 & 0 & 0 & 0 & 0 & 0 & 0 \\
0 & 0 & 0 & 0 & 0 & 1 & 0 & 0 & 0 & 0 & 0 & 0 & 0 & 0 & 0 \\
0 & 0 & 0 & 0 & 0 & 0 & 0 & 0 & 0 & 0 & 0 & 1 & 0 & 0 & 0 \\
0 & 0 & 0 & 0 & 0 & 0 & 0 & 0 & 0 & 0 & 0 & 0 & 1 & 0 & 0 \\
0 & 0 & 0 & 0 & 0 & 0 & 0 & 0 & 0 & 0 & 0 & 0 & 0 & 1 & 0 \\
0 & 0 & 0 & 0 & 0 & 0 & 0 & 0 & 0 & 0 & 0 & 0 & 0 & 0 & 1
\end{bmatrix}
$$

where

$$a = x_{f6}\mathrm{Sin}(x_{f3}) + x_{f5}x_{f4}\mathrm{Cos}(x_{f3}) \qquad (2\text{-}43a)$$

$$b = x_{f5}\mathrm{Sin}(x_{f3}) \qquad (2\text{-}43b)$$

$$c = x_{f4}\mathrm{Sin}(x_{f3}) \qquad (2\text{-}43c)$$

$$d = \mathrm{Cos}(x_{f3}) \qquad (2\text{-}43d)$$

$$e = -\,x_{f6}\mathrm{Cos}(x_{f3}) + x_{f5}x_{f4}\mathrm{Sin}(x_{f3}) \qquad (2\text{-}43e)$$

$$f = -\,x_{f5}\mathrm{Cos}(x_{f3}) \qquad (2\text{-}43f)$$

$$g = -\,x_{f4}\mathrm{Cos}(x_{f3}) \qquad (2\text{-}43g)$$

$$h = -\,\mathrm{Sin}(x_{f3}) \qquad (2\text{-}43h)$$

2.6.6 The Filter Model Noise Strength

Table 2-7 presents the noise strength values used in the filter dynamic's $Q(t)$ matrix and in the filter measurement's $R(t_i)$ matrix. Each noise strength is presented with its accompanying subscripted r_{mn} or q_{mn} term to identify matix location. All matrix entries not explicitly specified in the table are assumed to be zero.

Table 2-7 Filter Model Noise Terms

R Entry	Strength	Q Entry	Strength
$r_{1,1}$	$a_{1,1}$	$q_{8,8}$	.25
$r_{2,2}$	$b_{2,2}$	$q_{9,9}$	1.0
$r_{3,3}$	1.6 E^{-10}	$q_{10,10}$	64.0
$r_{4,4}$	4.0 E^{-6}	$q_{11,11}$	1.0 E^{-8}
$r_{5,5}$	0.25	$q_{13,13}$	1.0
$r_{6,6}$	1.0	$q_{15,15}$	1.0
$r_{7,12}$	.01		
$r_{8,13}$	25.0 E^{-10}		
$r_{9,14}$	.01		
$r_{10,15}$	25.0 E^{-10}		

where

$$a_{1,1} = r_{4,4} x_{f5}^2 \mathrm{Sin}(x_{f3}) + r_{6,6} \mathrm{Cos}(x_{f3}) \quad (2\text{-}44a)$$

$$b_{2,2} = r_{4,4} x_{f5}^2 \mathrm{Cos}(x_{f3}) + r_{6,6} \mathrm{Sin}(x_{f3}) \quad (2\text{-}44b)$$

2.7 Summary

Chapter II developed the truth model and filter model used in the simulation studies conducted for this thesis. Section 2.1 defined the simulation reference frames and gave rationale for their selection. Section 2.2 developed the kinematic equations describing aircraft and missile motion. Section 2.3 described the selection of truth model and filter states based on the equations developed in Section 2.2. Section 2.4 presented the noise sources driving the aircraft dynamics, missile dynamics, and ladar measurements, and gave rationale for the noise strengths used in the simulation models. Section 2.5 covered the selection of initial conditions which were considered to have special relevance to the simulation model. Section 2.6 summarized the state equations, measurement equations and noise matrices used in the simulation. The next chapter overviews the simulation runs conducted in this study. Each run focuses on an individual parameter viewed to be significant in determining filter either performance or truth model behavior.

III The Simulation Runs

3.0 Introduction

This chapter presents an overview of the computer simulations conducted while researching the kinetic kill zone estimation problem. All computer simulations presented in this thesis study were accomplished on SUN SPARC II workstations, using the MSOFE simulation software [3], and standard FORTRAN 77 computer code. Chapter III only presents parameters varied in each run (and the values used in simulation). Actual simulation results are presented in Chapter IV. Section 3.1 presents the missile-aircraft geometry run series. Eight runs were made to analyze the effect of the missile approach angle on the ability to predict the kill zone. Section 3.2 presents the ladar run series, conducted to analyze how ladar measurement parameters affect the ability to predict the kill zone. Each measurement is first varied independently, then all measurements are varied simultaneously, and finally the ladar measurement rate is varied from 60 Hz to 30 Hz. Section 3.3 presents a run series conducted to analyze how specific aircraft parameters affect the final predicted volume. Section 3.4 presents a worst case performance baseline. (The best case performance baseline is taken from Section 3.1.)

As a final note, certain terminology consistently used throughout this Chapter needs a brief clarification. The term "run series" always refers to a collective set of all runs done to analyze one of three major subgroups affecting kill zone prediction: missile-aircraft geometry, the ladar, or aircraft specific parameters. The term "run set" always refers to a sequence of runs made to analyze one specific parameter within a run series. The term "run," by itself, always refers to a single computer simulation.

3.1 The Missile Approach Angle Run Series

The missile approach angle simulations presented here are conducted to analyze the impacts of missile engagement geometry on the final volume predictions achieved. For all missile approach angle simulations, the aircraft is assumed to be initially heading east at 300 m/s and starting a 3 g turn to the north. (The aircraft maneuver chosen as a baseline condition against which a comparative analysis is later performed. The airspeed and turn-rate were selected as being a typical mid-range value.) Missile engagements are taken in $\pi/4$ intervals starting at 0.0 radians and measured in the missile-to-aircraft reference frame (i.e., the initial LOS is defined looking from the missile to the aircraft). Initial missile speed is 1500 m/s for all aspect angles. Table 3-1 summarizes the initial conditions used in the eight missile approach angle runs.

Due to the extensive variations in missile kinematics which results from the different aspect angles, there are significant differences in two missile initial conditions other than approach angle. The two variable initial conditions are range and missile surface-to-mass ratio. The variations in these missile initial conditions are driven primarily by the dynamics of a post-burnout coasting missile. In each aspect angle, the set of initial conditions which resulted in the best missile kinematics ("best" from a simulation viewpoint, not necessarily from a cross-section prediction viewpoint) is ultimately chosen.

The missile's surface to mass ratio, S/M, is set near the minimum of the normal expected range (0.0001 to 0.005 m^2/kg) for the $\pi/4$ approach angle because $\pi/4$ is a very benign dynamic approach angle, and the missile is initially chasing the aircraft. Reducing S/M increases the coasting performance of the missile and therefore allows a longer missile flight time. The increased range and missile flight time allows the final kill zone volume to be more easily analyzed as a function of range and simulation time (see Chapter IV). As the initial missile Table

3-1 Missile Approach Angle Series

Approach Angle	Range	Missile East Velocity	Missile North Velocity	Missile Surface to Mass Ratio
0.0	5000 m	1500 m/s	0.0 m/s	.0003 m^2/kg
$\pi/4$	5300 m	1200 m/s	900 m/s	.0001 m^2/kg
$\pi/2$	10000 m	300 m/s	1470 m/s	.0003 m^2/kg
$3\pi/4$	3000 m	-900 m/s	1200 m/s	.0006 m^2/kg
π	5000 m	-1500 m/s	0.0 m/s	.0004 m^2/kg
$5\pi/4$	12000 m	-900 m/s	-1200 m/s	.0003 m^2/kg
$3\pi/2$	7000 m	300 m/s	-1470 m/s	.0003 m^2/kg
$7\pi/4$	3000 m	1200 m/s	-900 m/s	.0006 m^2/kg

approach changes from tail-chase to head-on approach, the missile's S/M also increases to allow the missile better turning performance at the expense of poorer coasting performance. (Refer to Chapter II Subsection 2.2.4 for the relationships between S/M and missile drag). All missile approach angle trajectory plots, filter plots and cross-section prediction plots are presented in Appendix A.

There are two aspect angles, $3\pi/4$ and $7\pi/4$, in which the simulation fails altogether.). The simulation results indicate that the missile is unable to maintain track on the aircraft for the $3\pi/4$ and $7\pi/4$ approach angle's, so these geometries are presented now and are not included with the results presented in Chapter IV.

Figure 3-1 shows a vector diagram explaining why the $3\pi/4$ (and by analogy the $7\pi/4$) missile shot dynamics failed. The missile commands lateral acceleration, as given in Equation (2- 13), proportional to the LOS-rate in the missile-to-aircraft reference frame. As seen from Figure 3-1, there are three factors which contribute to the total LOS-rate: drag induced LOS-rate, range-closure induced

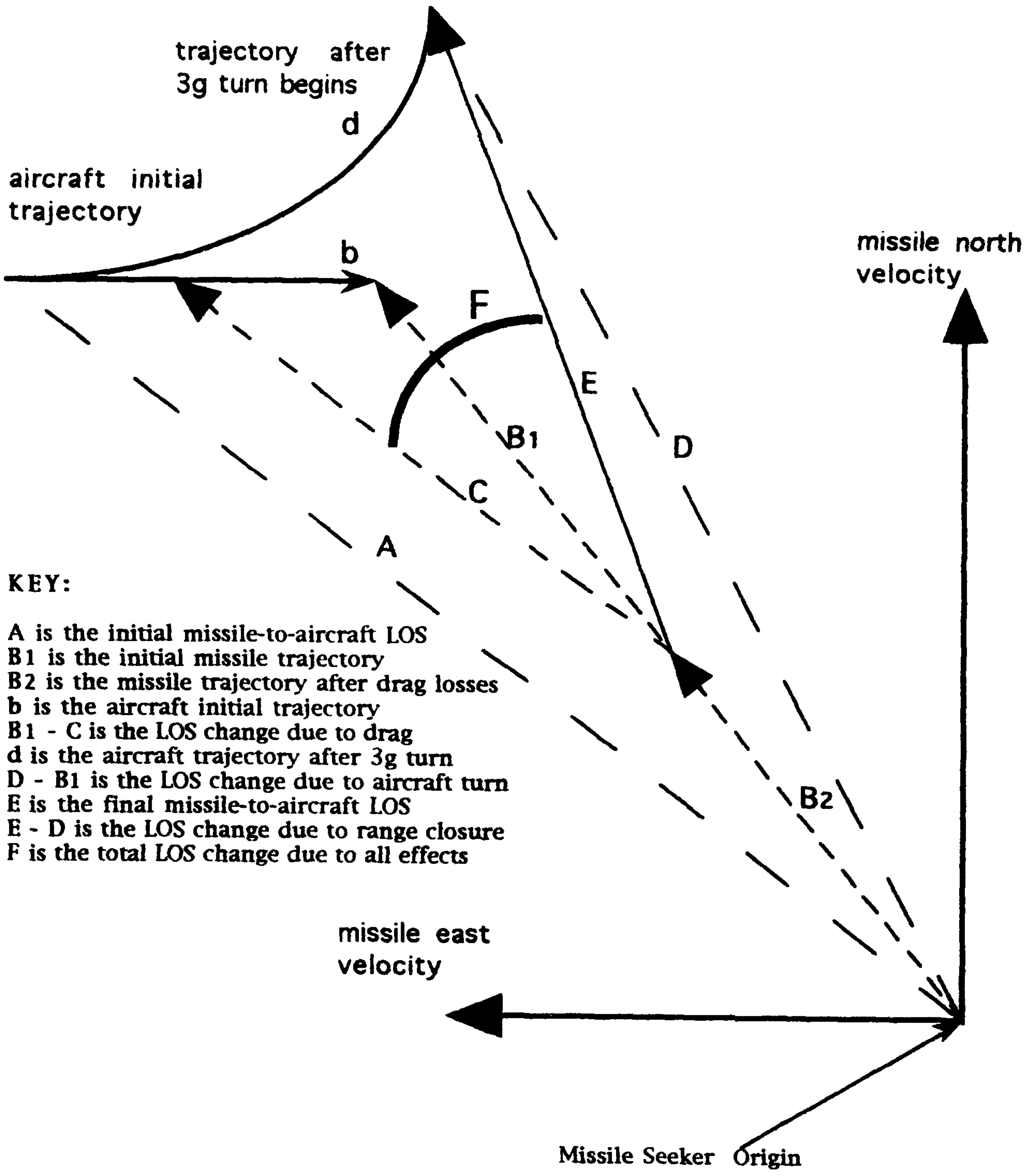

Figure 3-1 Failed Missile Kinematics

LOS-rate, and aircraft turn induced LOS-rate. The scenario starts with an aircraft trajectory defined by b, a missile trajectory defined by B1, and an LOS defined by A. If no aircraft and missile trajectory changes occur, the LOS vector, A, never changes and the missile intercepts the aircraft. When missile drag is added to the scenario, the missile's trajectory changes to B_2, and a drag induced LOS-rate occurs given by the angle B_1 - C. When the aircraft turn is added to the scenario, the aircraft trajectory changes from b to d and the turn induced LOS-rate is given by the angle D - B_1. When range closure is considered a third source of LOS-rate is given by the angle E - D. The combined angle-rate is given by the arc F. In the $3\pi/4$ scenario, the drag induced LOS-rate is acting against the turn induced LOS rate. When the missile commands lift to null the aircraft's turn induced LOS rate, the missile's lift-drag acts to increase the missile-to-aircraft LOS-rate. The harder the missile turns, the harder the missile needs to turn. This effect is heightened by the range closure, which is severe for a forward quarter missile approach. The missile literally turns itself to death.

3.2 The Ladar Noise Run Series

The ladar simulations presented here were conducted to analyze the impacts of the assumed ladar measurement parametrics on the results achieved. All ladar noise run series are simulated from the $\pi/4$ missile approach angle, shown in Figure 3-2, using identical initial conditions and random number seeds for each run. The only parameter changed for each run is the specific parameter under investigation. Table 3-2 shows the values used for the ladar measurement noise during the ladar run series. The baseline values are selected based on the ladar's rms errors as developed in Chapter II. The other values are generated by redoubling the baseline values as one crosses the table from left to right. The angle-rate measurement is only doubled twice since it is believed that an angle-rate measurement error of 16.0 mrad/s is not of practical value.

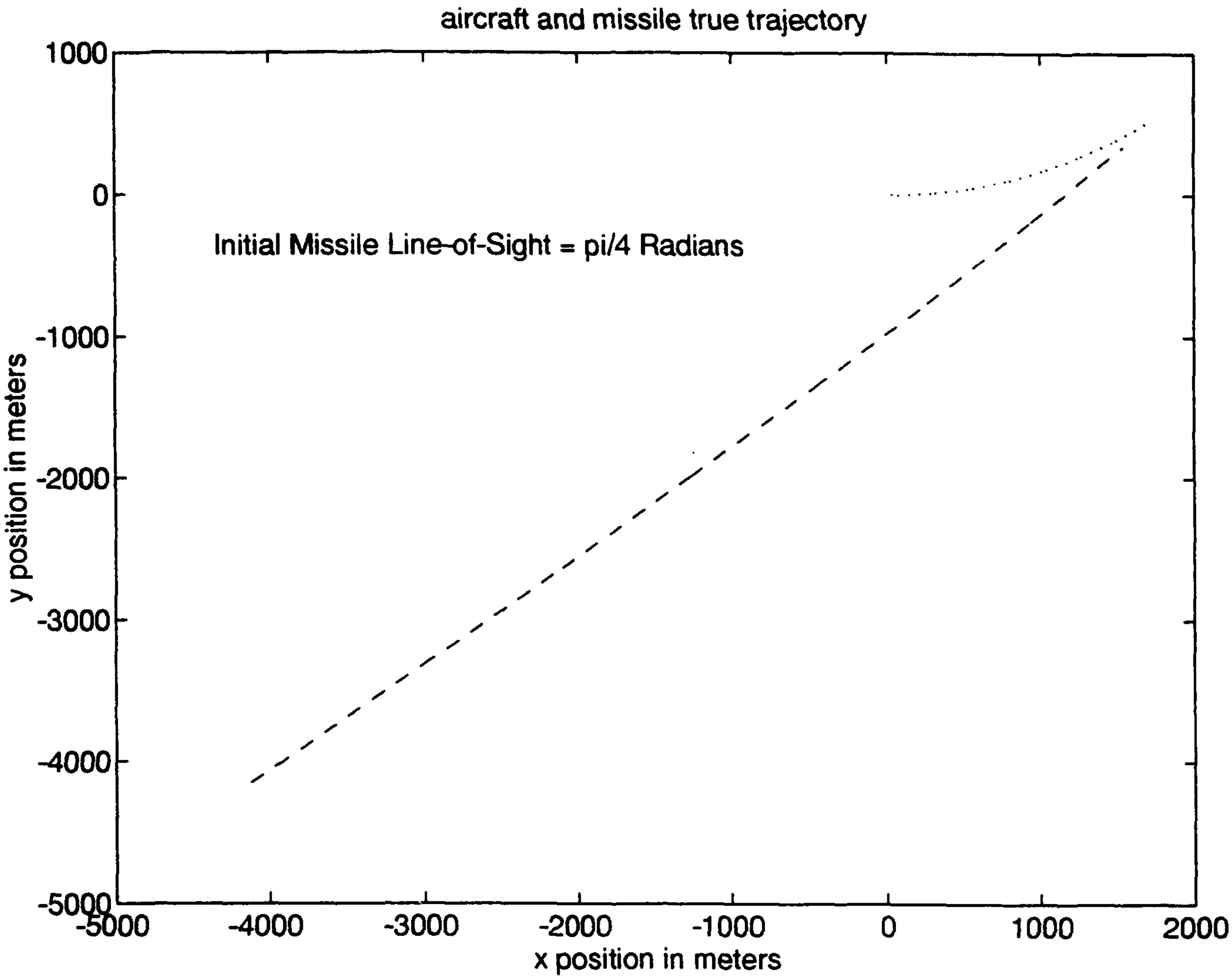
aircraft and missile true trajectory
1000
0
-1000
-2000
-3000
-4000
-5000
y position in meters
Initial Missile Line-of-Sight = pi/4 Radians
-5000
-4000
-3000
-2000
-1000
0
1000
2000
x position in meters

Table 3-2 RMS Ladar Noise

Measurement	Baseline Value	2nd Value	3rd Value	4th value
Range	0.5 meters	1.0 meters	2.0 meters	4.0 meters
Range-rate	1.0 m/s	2.0 m/s	4.0 m/s	8.0 m/s
Angle	40 μrad	80 μrad	160 μrad	250 μrad
Angle-rate	2.0 mrad/s	2.0 mrad/s	4.0 mrad/s	8.0 mrad/s

Table 3-3 presents a summary of the ladar series runs. The first column lists each run set contained in the ladar series. The second column gives the parameter under study in that run-set. The values used under the "Parameter Varied" column are listed in Table 3-2. All parameters not listed in the "Parameter Varied" column are left at the baseline values (column two, Table 3-2) for the entire run set. The entry "all" indicates that all parameters listed in Table 3-2 are varied simultaneously from the baseline. The baseline laser pulse-rate is 60 Hz, with a run set accomplished at 30 Hz for comparison as requested by the thesis sponsor [20]. The last column, "Filter vs. System" indicates differences between the filter's assumed rms measurement noise, and the actual rms measurement noise corrupting the system. The entry "same" indicates that the truth model's and filter model's ladar rms measurement noise are identical for the parameter under study. The entry "filter high" indicates that the filter's noise strength is varied while the system noise strength remains at baseline. The entry "filter low" indicates that the filter noise strength is kept at baseline while the system noise is varied.

As is evident from Table 3-2 and 3-3, the ladar series addresses five objectives: (1) Each ladar measurement is analyzed independently to determine the effect of rms noise on the final volume estimate; (2) All ladar measurements are analyzed as a group to determine the effect of ladar measurement quality on the

Table 3-3 Ladar Series Run Sets

Run Set	Parameter Varied	Filter vs. System
Range	Range only	same
Range-rate	Range-rate only	same
Angle	Angle only	same
Angle-rate	Angle-rate only	same
60 Hz	all simultaneously	same
Range-f	Range only	filter tuned high
Range-s	Range only	filter tuned low
Range-rate-f	Range-rate only	filter tuned high
Range-rate-s	Range-rate only	filter tuned low
Angle-f	Angle only	filter tuned high
Angle-s	Angle only	filter tuned low
Angle-rate-f	Angle-rate only	filter tuned high
Angle-rate-s	Angle-rate only	filter tuned low
all-f	all simultaneously	filter tuned high
all-s	all simultaneously	filter tuned low
30 Hz	all simultaneously	same

final volume estimate; (3) The ladar sampling rate is analyzed to determine its impact on the final volume estimate; (4) The ladar is tested against cases where the filter assumed measurements are more accurate than the true measurements actually are; (5) The ladar is tested against cases where the filter assumed measurements are less accurate than the true measurements actually are. Since the turbulence model used throughout this thesis study assumes benign turbulence, the effects of this assumption need to be explored. The filter "high" and filter "low" run sets are conducted to determinetwo things: (1) Does over modelling turbulence noise in the filter seriously degrade cross-section estimates? and (2) Does undermodeling turbulence noise in the filter cause the estimated cross-section to not capture the true missile trajectory as it should? All ladar run series plots are presented in Appendices B (range), C (range-rate), D (angle), E (angle-rate) and F (pulse-rate).

3.3 The Aircraft Run Series

The aircraft run series has three objectives: (1) To study how the assumed DGPS/INS accuracies affect the final kill zone volume; (2) To study how the aircraft turn rate affects the final kill zone volume; and (3) To study how pilot-induced maneuver error affects the final kill zone volume. To accomplish these objectives, one run set is generated for each parameter under study, using the $\pi/4$ geometry with the same random number seeds and initial conditions as in the ladar series. The simulation model originally presented in Figure 1-4 assumes that acceleration measurements can be provided from the aircraft's navigation subsystem. The DGPS/INS run set removes all aircraft acceleration measurements to determine the impacts of not having acceleration measurements available, and also varies the aircraft's velocity measurement noise strengths (as shown in Table 3-4) to determine how the naivigation subsystem's estimated errors affect the predicted cross-section. The DGPS/INS filter plots and volume plots are contained in Appendix H. The aircraft turn rate set is generated by resetting the DGPS/INS to the normal values presented in Table 2-5, and varying the aircraft's assumed turn rate from 0.0 g to 5.0 g in 1.0 g increments. The aircraft turn rate filter plots and volume plots are contained in Appendix I. Finally the pilot induced maneuver error is analyzed by varying the aircraft process noise strength (Section 2-4) from 0.0 to $(0.5g)^2/s$ in $(0.1g)^2/s$ increments. The pilot induced maneuver error plots are contained in Appendix G.

Table 3-4 Assumed DGPS/INS Velocity Errors

Run	North Velocity Error	East Velocity Error
1	0.1 meter/second	0.1 meter/second
2	0.5 meter/second	0.5 meter/second
3	1.0 meter/second	1.0 meter/second
4	5.0 meter/second	5.0 meter/second

3.4 High Noise Baseline Run

One final run is made to establish a worst case volume baseline. The "high noise" baseline is established by taking the worst assumed noise and measurement conditions, from each run set, and using those conditions together in a single run. The $\pi/4$ geometry with a 60 Hz ladar is selected for consistency. Table 3-5 summarizes the 1σ noise strengths used to establish the high noise baseline. The plots are discussed in Chapter IV.

3.5 Summary

This Chapter summarizes the MSOFE simulation runs conducted in analyzing the kinetic kill zone prediction problem. The parameters analyzed are divided into

Table 3-5 High Noise Baseline Run Conditions

Ladar Measurement	1σ Noise Strength	Aircraft Parameter	1σ Noise Strength
Range	4.0 meters	North Velocity	5.0 m/s
Range-rate	8.0 m/s	East Velocity	5.0 m/s
Angle	250 μrad	Turn-rate	5.0 g
Angle-rate	8.0 mrad/s	pilot error	0.5 g

three major groups - or series. The aircraft-missile geometry is discussed in Section 3.1. The ladar measurement parameters are covered in Section 3.2. The aircraft parameters are covered in Section 3.3. The $\pi/4$ missile approach angle geometry is used as a best case performance baseline for the run series' conducted in Section 3.2 and Section 3.3. A worst case performance baseline is developed for the same run series' in Section 3.4 using the worst case noise strengths from each run set.

The next chapter presents the simulation results. For the missile appraoch angle run series the results are compared to analyze actual versus expected results. Two run sets are selected from the missile approach angle run series to analyze the effect of true range on the predicted cross-section. For the remaining run series, baseline performance criteria and volume cross-section figures of merit are established as performance comparison tools.

IV Results and Analysis

4.0 Introduction

This chapter presents results for the simulation series discussed in Chapter III. The chapter structure parallels the structure in Chapter III, with a subsection designated for each major run series. Each subsection presents the results obtained from that run series, a brief summary of the results and, where applicable, expected results. Discussion focuses in three primary areas, explanation of the results, the results' effect on the predicted volume cross-section, and, where applicable, a discussion on deviations from the expected results.

Filter and volume cross-section plots for the $\pi/4$ missile approach angle are presented in this chapter since that geometry is used as the baseline for all run series except the missile approach angle run series. Other filter plots and cross-section estimation plots are contained in the appendices, and are referenced as needed.

4.1 Missile Approach Angle Run Series Results

Table 4-1 summarizes the results of the runs conducted in the missile approach angle run series. The initial missile approach angle is found in column one. For each approach angle, a set of volume plots is generated (Appendix A). The best cross-section prediction (best is based on both the final cross-section predicted, and the true missile trajectory being within the filter estimated cross-section) for each approach angle is presented in column six. Each volume cross-section prediction is made by removing all filter measurements and allowing the filter covariance estimates to diverge (hereafter referred to as filter divergence) for one second. Columns two through six each possess two sets of numbers. The first number represents the filter statistics at the time of filter covariance release, and the second set, after the filter is allowed to diverge for one second. (For example row two of Table 4-1 reads: The filter took measurements until $t = 5.0$ seconds and then made a volume prediction for $t = 6.0$ seconds. At 5.0 seconds the filter estimated range is 900 (m) with an estimated rms error of 0.148 (m) and the estimated LOS rms error is 16.8 (μrad). After 1 second of propagation into the future, the range is estimated as 200 (m) with a filter estimated 16.6 (m) rms error, and with a filter estimated LOS rms error of 4.18 (mrad).) The volume cross-section

Table 4-1 Summary of Missile Approach Angle Run Series Results

Approach Angle (radians)	Time (seconds)	Δ Range (meters)	Δ Angle (mrad)	Range (meters)	Cross-Section (m^2)
0.0	3.5 - 4.5	.152 / 12.6	.0232 / 2.36	1500 / 1050	.0053 / 31.2
π/4	5.0 - 6.0	.148 / 16.6	.0168 / 4.18	900 / 200	.0022 / 13.9
π/2	4.0 - 5.0	.150 / 8.67	.0159 / .530	1800 / 1000	.0043 / 4.59
3π/4	missile failed to track				
π	2.5 - 3.5	.150 / 11.7	.0157 / .982	1700 / 700	.0070 / 8.76
5π/4	7.0-8.0	.148 / 2.95	.0171 / 2.72	1900 / 800	.0048 / 31.5
3π/2	3.5 - 4.5	.149 / 19.0	.0158 / .368	2300 / 1150	.126 / 8.04
7π/4	missile failed to track				

estimate provided in column six is calculated based on Equation (1-1) with two exceptions - a small angle approximation is used (since the largest angle in Table 4-1 is 4 mrad and the small angle approximation greatly simplifies calculations), and the cross-section values are based on 1σ values instead of the 3σ values (again just to simplify calculations) used in Equation (1-1). Equation 4-1 presents the small angle approximation form used in calculating the cross-sections:

$$\text{Volume Cross-Section} = (\partial\mathfrak{R})\,(\mathfrak{R}\partial\varnothing) \qquad (4\text{-}1)$$

where

$\mathfrak{R}$ is the filter estimated range (col 5),

$\partial\mathfrak{R}$ is the filter estimated range rms error (col 3),

$\partial\emptyset$ is the filter estimated angle error (col 4).

Two missile approach angle run sets, the $\pi/4$ and $5\pi/4$ geometries, are selected for additional study to determine possible relationships between predicted volume cross-section and missile range. The two missile approach angles are selected from the eight missile approach angles available because these simulations have longer range and longer simulation run times than the other six missile approach angles, thus providing more possible data points for study. For each of these two approach angles, the filter is run for a specified amount of time and is then allowed to diverge for one second generating a cross-section prediction. The filter run-time (before divergence) starts at 1.0 seconds for the first run, and is increased by 0.5 seconds for each additional run. The filter is propagated to each specified time using the same initial conditions and random number seeds, and is then diverged for one second to generate a volume cross-section prediction. It is thought that a relationship between estimated volume cross-section and range can be established. Because the volume cross-section given in Equation (4-1) is linear versus range, a "tilted-bathtub" pattern similar to that shown in Figure 4-1 is expected. The "tilted-bathtub" pattern has three distinct parts, the initial slope which represents the period before the filter actually converges to the optimal missile states, the linear region where the filter covariance estimates are assumed to be stable and slowly changing, and the cross-section estimate decreases inversely with range, and the final tail where the range approaches zero causing the filter to go unstable. When the missile-to-aircraft range approaches zero, small changes in the range cause very large changes in the LOS and LOS-rate. This causes the simulation dynamics to go numerically

Figure 4-1 Expected "Bathtub" Pattern for Cross-Section vs Range

unstable. The tracking missile seeker experiences the same problem. To compensate for this effect, missiles are preprogrammed with a special flight trajectory which is activated when the missile-to-aircraft tracking errors exceed a prescribed limit. The activation of the flight trajectory causes the missile to enter the "endgame scenario" in which it no longer uses proportional navigation as a guidance law. In the filter, this stage is marked by a sudden rapid growth in the filter covariances followed by an integration failure within MSOFE. These effects, which ultimately determined the scenario time length, can be seen in Figure A-86 Appendix A.

Figure 4-2 (a & b) shows a series of volume cross-section predictions for the $\pi/4$ geometry. Figure 4-2a shows the volume cross-section at filter release as a function of range. Figure 4-2b shows the volume cross-section after one second of filter divergence. Note that the subdivisions on the range axis do not correlate from Figure 4-2a to Figure 4-2b. The range axis is not scaled relative to range, but rather relative to time. The range values shown are taken at 0.5 second intervals beginning at 1.0 seconds in Figure 4-2a. Since Figure 4-2b represents a 1.0 second prediction, its range axis is shifted two range subdivisions (or one second in time) to the right. For instance the initial cross-section estimate at range = 4200 (Figure 4-2a) corresponds to the diverged cross-section estimate at range = 3000 (Figure 4-2b)). Figure 4-3 (a & b) is similarly aligned. Figures 4-2a and 4-3a show that the expected relationship between cross-section estimation and range is achieved at the initial filter release. However, as seen in Figures 4-2b and 4-3b, that same relationship does not exist after divergence. Figure 4-3a also contains two outlier points. The mid-range point is caused by a brief filter tracking error and is not significant. The end-range point is caused by the "zero range" divergence which is now starting to occur. The expected "zero range" divergence does infact occur but can not be shown in the figures because when it occurs, the filter divergence is so severe it crashes the computer simulations (usually in less than 0.1 seconds). (For an example of range induced filter divergence see Appendix A Figure A-86.) In the first section of the "bathtub" curve, the filter does not estimate larger volumes, but instead tends to lose track of the true missile trajectory during divergence, resulting in bad cross-section predictions.

Figure 4-2a Initial Cross-Section vs. Range (pi/4)

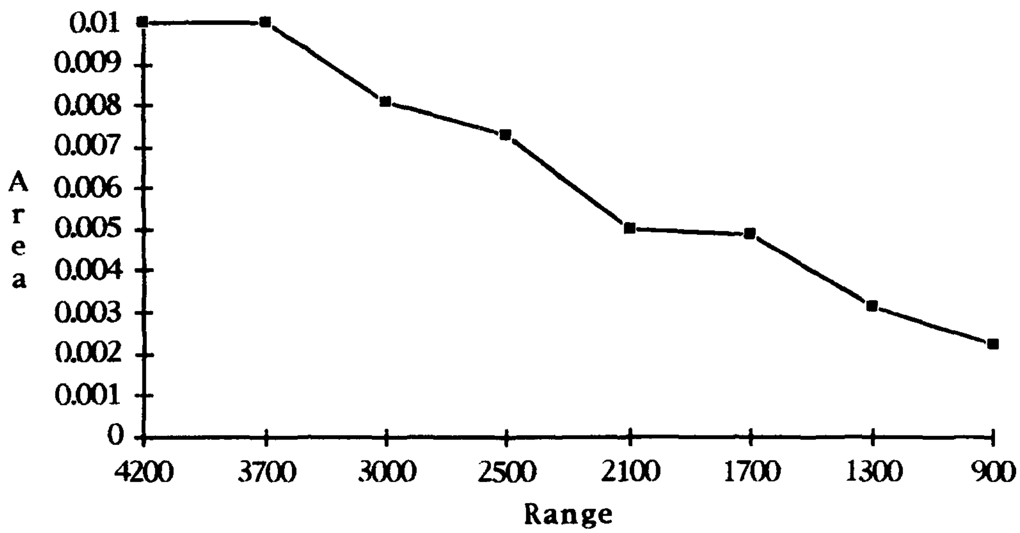

Figure 4-2b Cross-Section vs Range After One Second Divergence (pi/4)

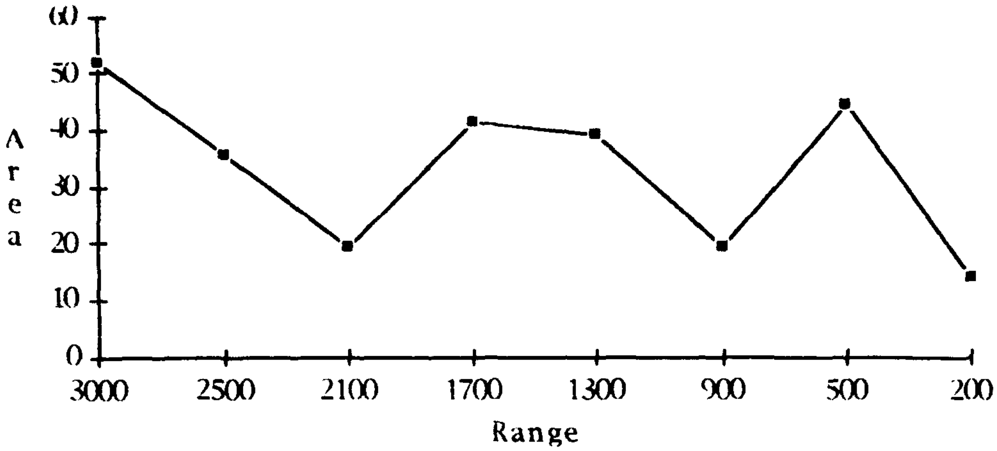

Figure 4-3a Initial Cross-Section vs Range (5pi/4)

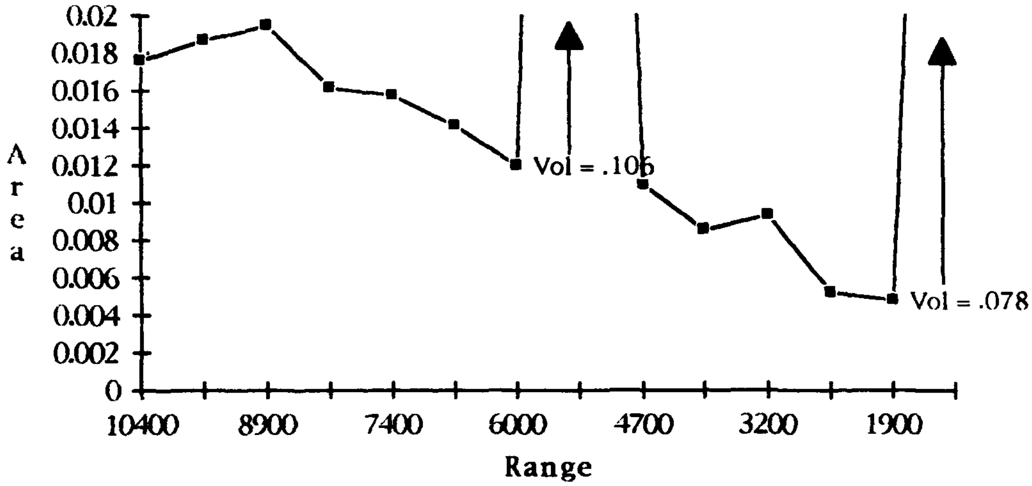

4.2 The Performance Baselines

The $\pi/4$ missile approach angle is used in all the remaining simulations conducted. The $\pi/4$ geometry (reference Figure 3-2 for a pictorial) is selected

Figure 4-3b Cross-Section vs Range After One Second Divergence (5Pi/4)

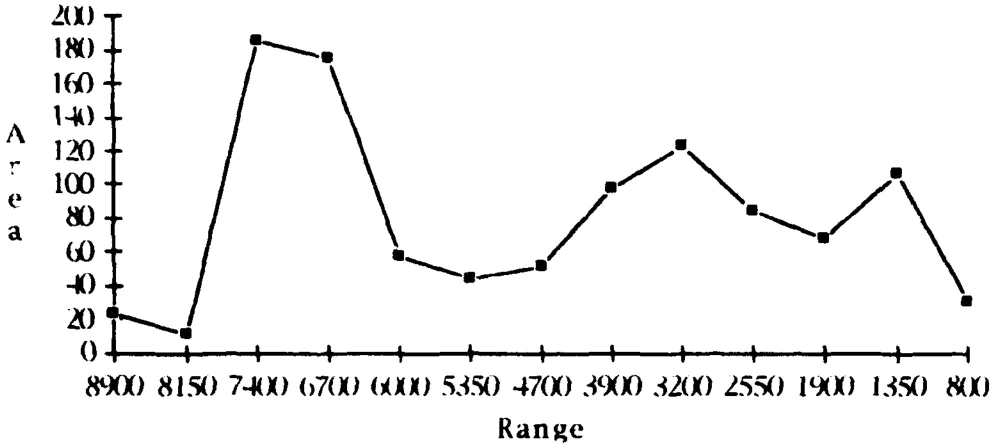

because the dynamics in that geometry are least sensitive to system effects likely to cause simulation failure (such as the previously discussed zero range effect). All simulations are conducted using identical initial conditions and random number seeds with the exception of the parameter currently under study. The baseline conditions are established as indicated in Table 3-2.

Filter plots showing range, range-rate angle and angle-rate errors are presented in Figure 4-4 (a-d). Figure 4-4 (e-f) presents a three second filter divergence for the low noise baseline initiated three seconds after simulation start. All remaining simulations are conducted using identical filter divergence criteria.

A high noise performance baseline is similarly established using the $\pi/4$ geometry and conditions listed in Table 3-5. The high noise baseline filter plots are presented in Figure 4-5 (a-d), with the three-second filter divergence plots in Figure 4-5 (e-f) respectively. The intention is to establish a comparative performance range between the low noise baseline results and the high noise baseline results. The primary figures of merit for the comparison are the filter estimated rms errors after one second and three seconds of filter divergence. Throughout this analysis true errors are only considered to the extent that they

Figure 4-4 (a and b)

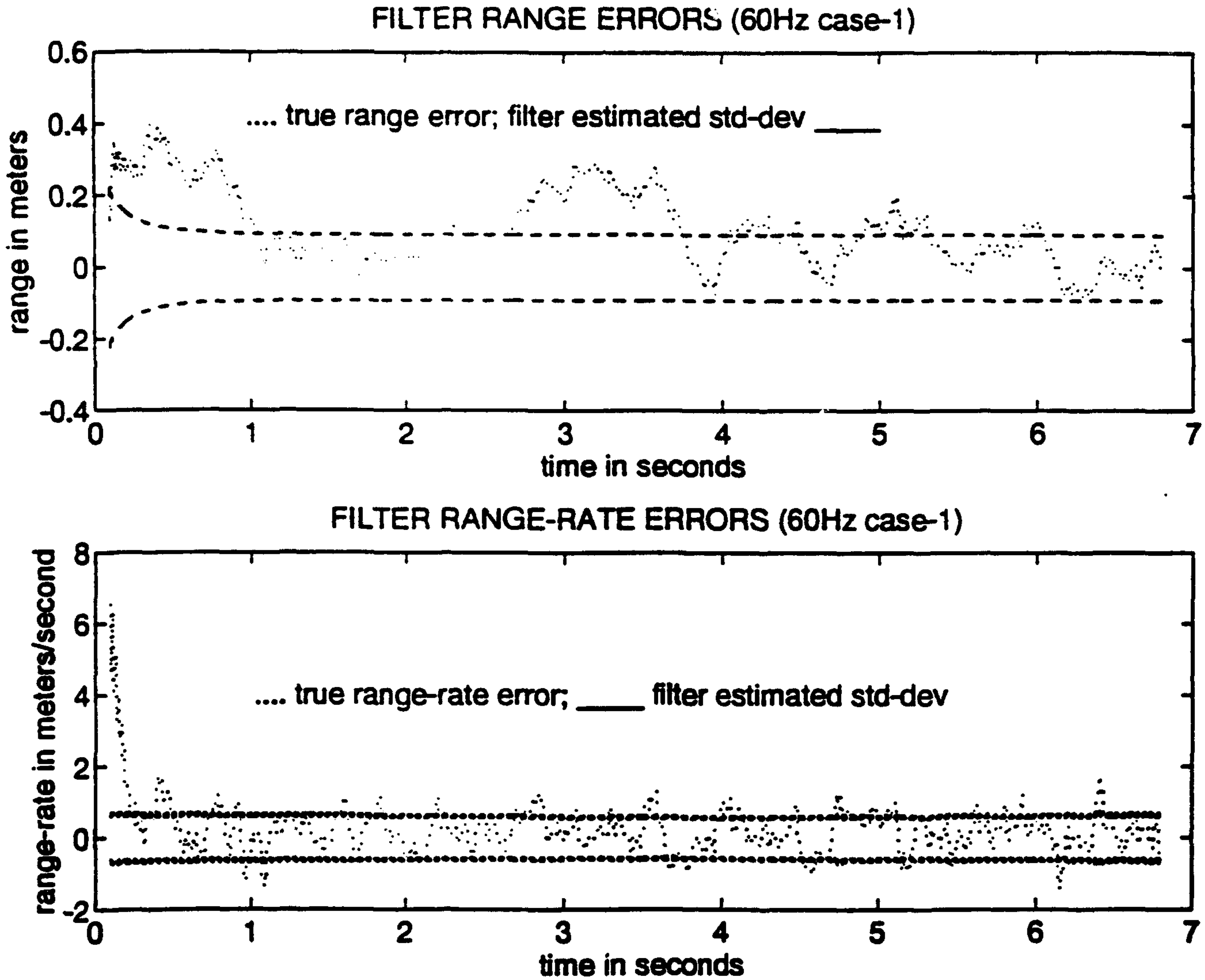

Figure 4-4 (c and d)

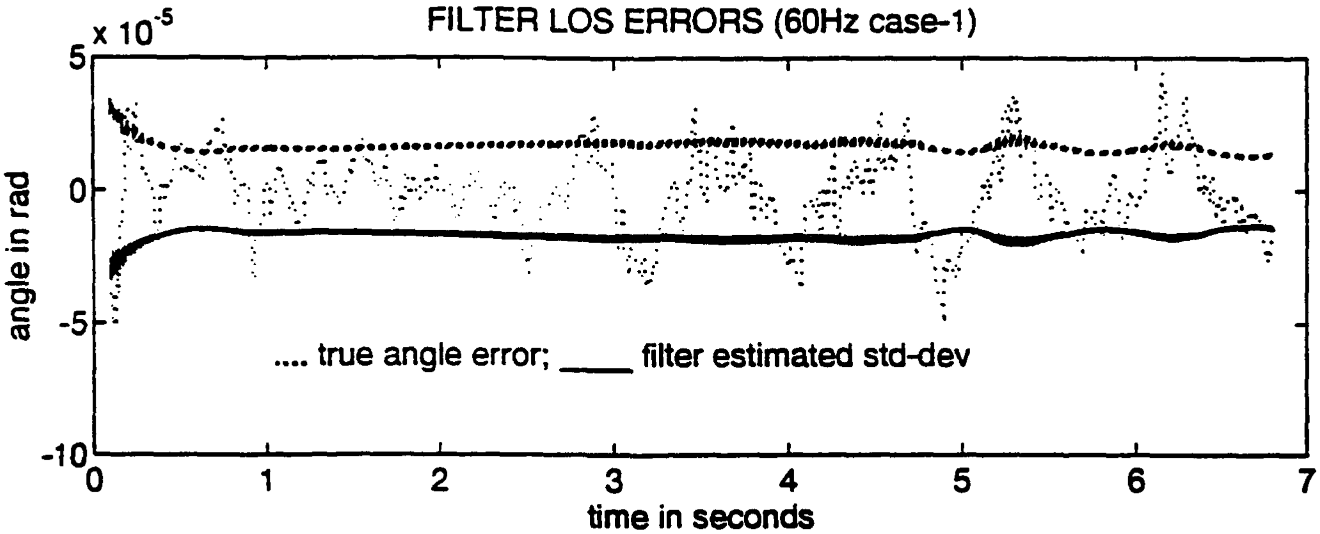

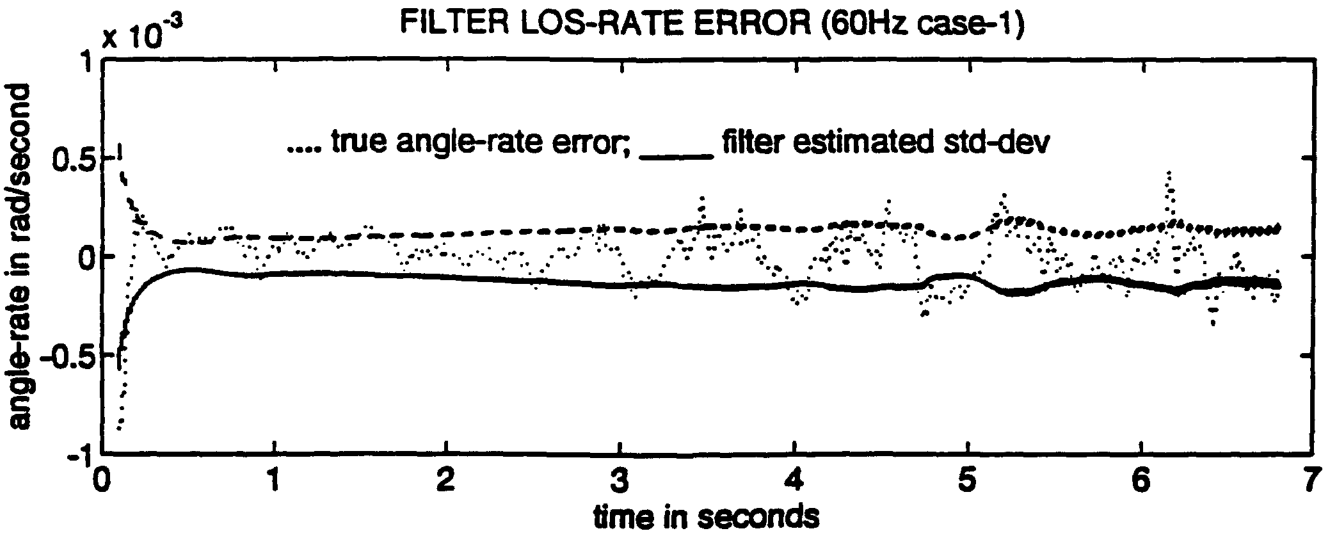

Figure 4-4 (e and f)

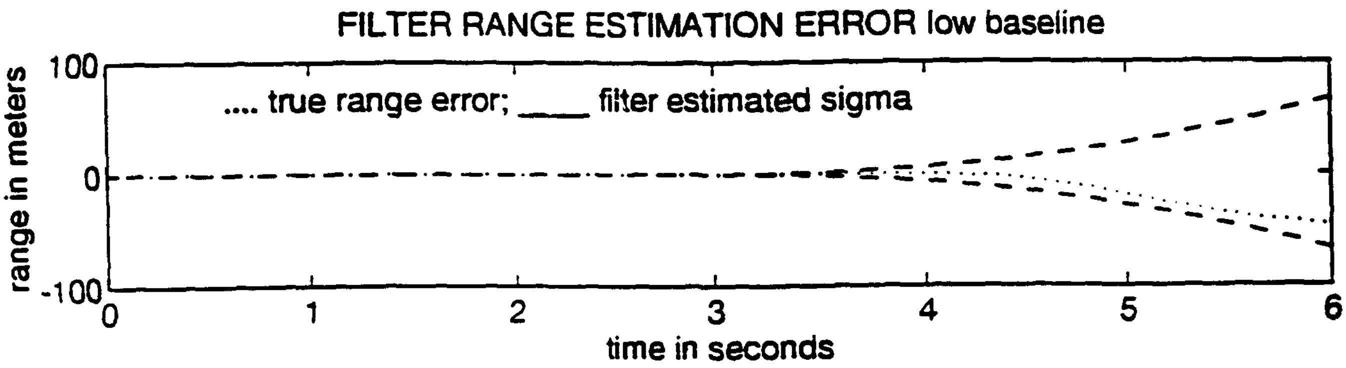

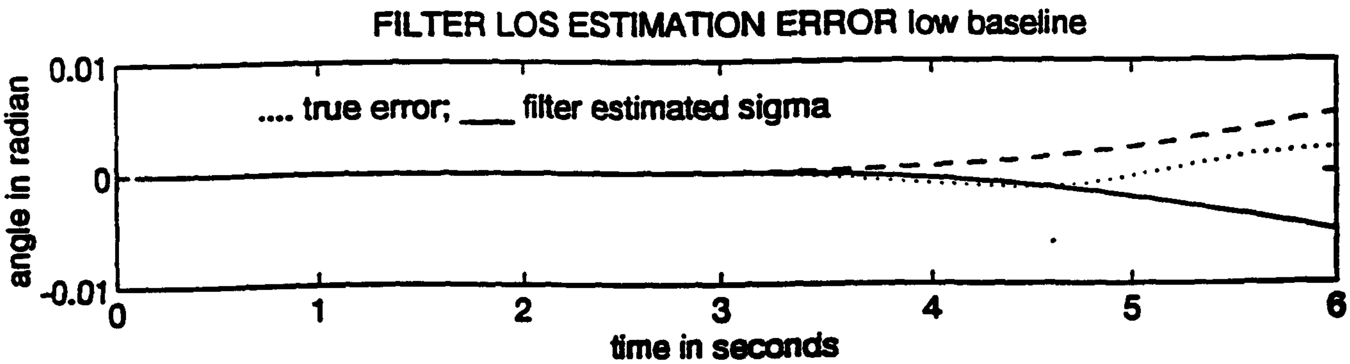

Figure 4-5 (a and b)

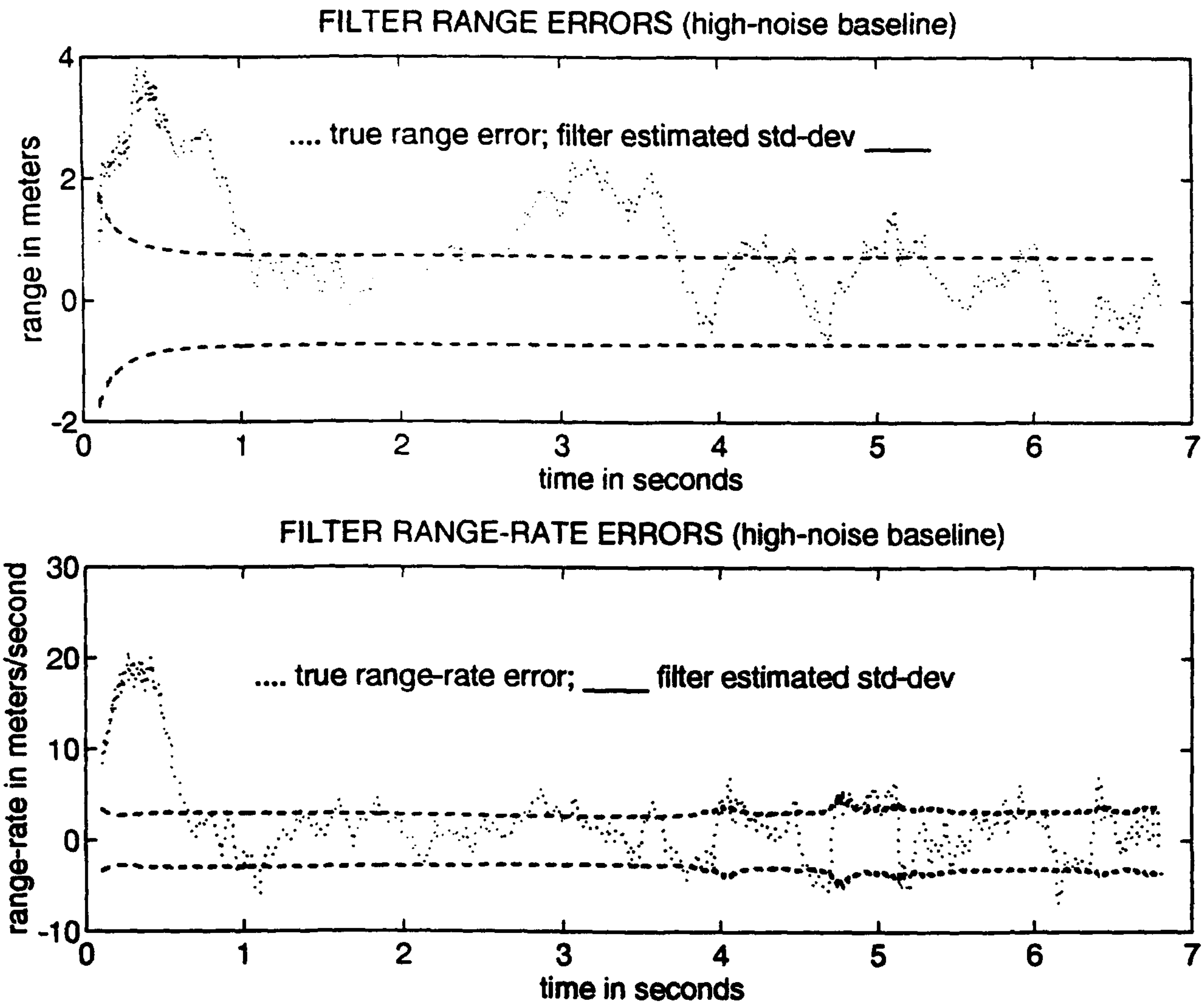

Figure 4-5 (c and d)

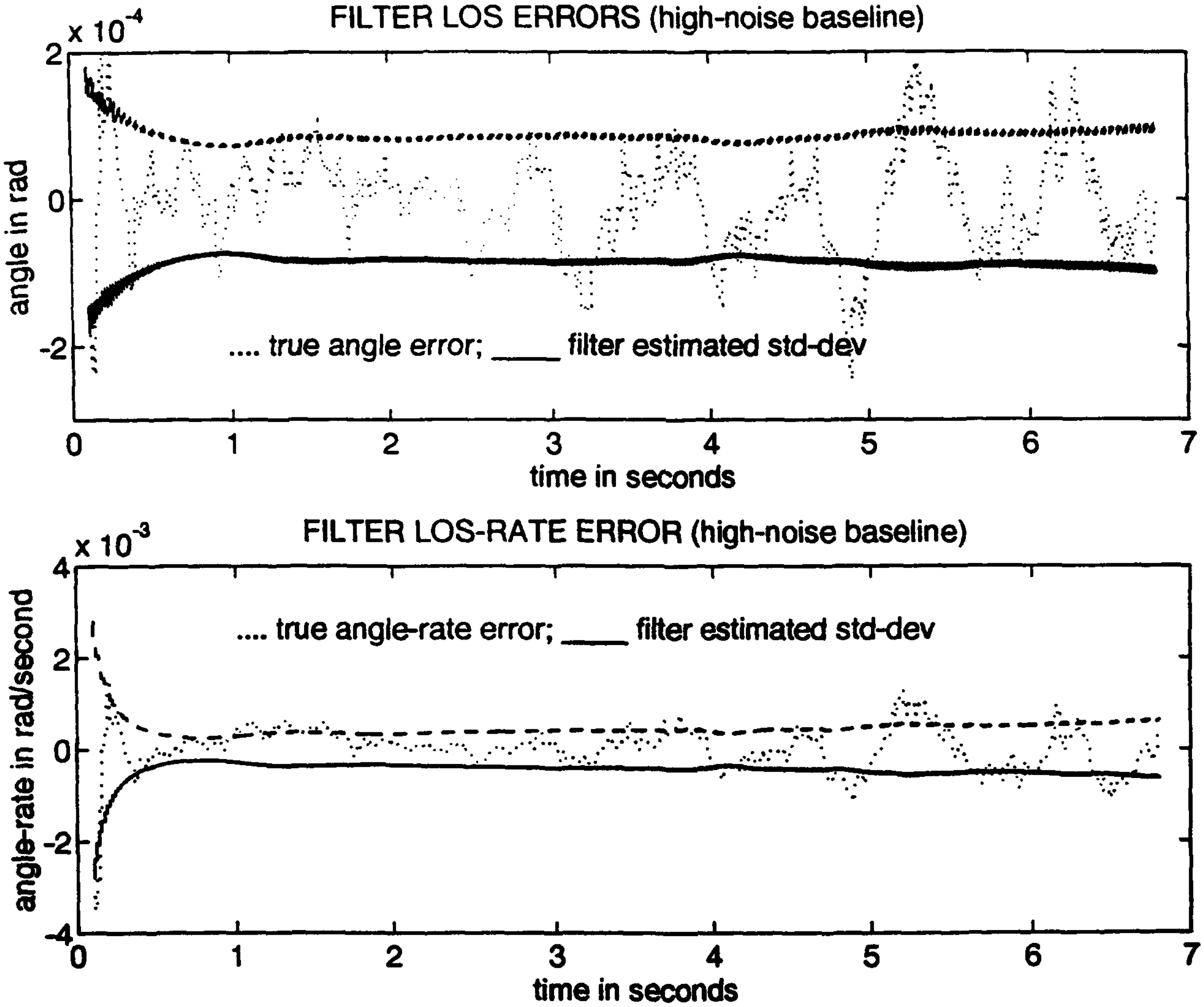

Figure 4-5 (e and f)

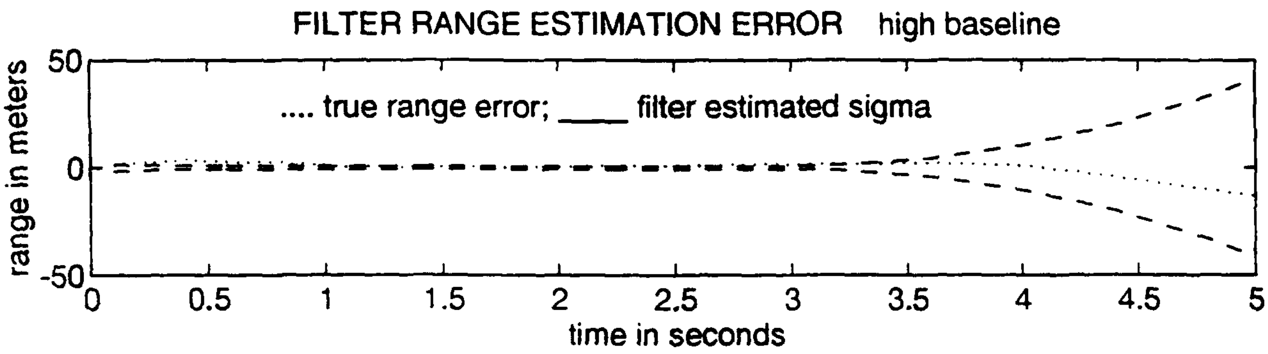

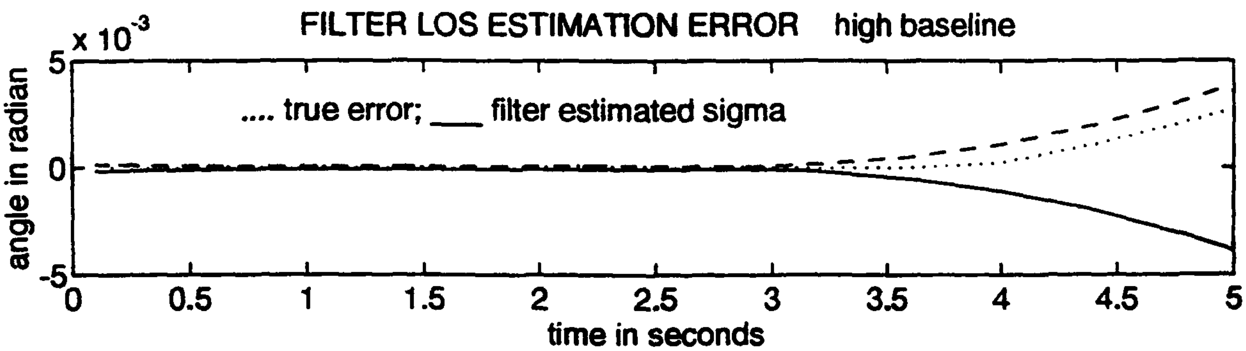

are sufficiently (by at least one standard deviation) outside the filter's estimated rms errors indicating an invalid cross-section prediction. The use of filter estimated statistics is as an analysis technique is used throughout this thesis as a method of analyzing the filter predicted volume. It is not the intent of this thesis to study issues particular to optimal extended Kalman filter design. More will be said about the results of this assumption in Chapter V. The high noise baseline divergence plots only go out to five seconds. The three second divergence goes unstable shortly after two seconds of propagation, so the three second worst case performance can not be established. The filter estimated rms error for the baseline simulations are summarized in Table 4-2.

Table 4-2 Baseline Performance Results

Baseline Noise	One Second Divergence rms Range Error	rms Angle Error	Three Second Divergence rms Range Error	rms Angle Error
low	6.336 (m)	537.5 (μrad)	67.61	5.33 mrad
high	10.4 (m)	1.11 (mrad)	failed n/a	failed n/a

4.3 The Ladar Run Series Results

The parameters studied in the ladar series run sets are summarized in Tables 3-2 and 3-3. The results are summarized in Tables 4-3 (a-e). All values presented in the first column are the rms noise values used in simulation. The values marked with an "L" indicate that the truth model (only) uses the values given in the table while the filter remains at baseline conditions. The values marked with an "H" indicate that the filter model (only) uses the values given in the table while the truth model remains at baseline. The unmarked column one entries indicate that both the truth model and the filter model use these values. Columns two through seven give the filter estimated rms errors at initial filter release, after one second of filter divergence and after three seconds of filter divergence.

The result of the individual ladar measurement study indicates that no one ladar measurement dominates the overall volume prediction at either one second or three seconds of filter divergence. Similarly dropping the ladar pulse-rate to 30 Hz also does not significantly affect the figures of merit. Table 4-3 shows that, with the exception of two failed angle simulations, the final predicted volume after three seconds of divergence never consistently exceeds 50% of the value established by the baseline, and in some cases even bettered the established performance baseline. The results suggest that the variation in predicted volume as a function of ladar parameter variation is not large enough to be statistically significant using only filter estimated statistics. Monte-Carlo simulations (which

Table 4-3a Ladar Range Results

RMS Noise Value	Initial Filter Release		One Second		Three Seconds	
	RMS Range Error	RMS Angle Error	RMS Range Error	RMS Angle Error	RMS Range Error	RMS Angle Error
1.0 m	0.129	16.5	6.10	461	59.4	3690
2.0 m	0.193	17.7	7.85	802	91.85	8180
4.0 m	0.327	16.8	6.66	622	72.16	5850
1.0 m L	.129	17.5	6.91	713	77.9	6380
2.0 m L	.193	16.9	6.11	546	61.5	4520
4.0 m L	.327	17.6	7.18	753	86.1	7390
1.0 m H	.0906	17.5	7.20	756	85.3	6860
2.0 m H	.091	17.2	6.12	584	62.1	4690
4.0 m H	.091	17.0	6.33	528	164	4320

All range values are given in units of meters.

All angle values are given in units of micro-radians.

Table 4-3b Ladar Range-Rate Results

RMS Noise Value	Initial Filter Release		One Second		Three Seconds	
	RMS Range Error	RMS Angle Error	RMS Range Error	RMS Angle Error	RMS Range Error	RMS Angle Error
2.0 m/s	0.133	16.9	7.63	701	87.2	7540
4.0 m/s	0.165	16.4	7.49	476	65.16	3930
8.0 m/s	.199	16.8	7.83	447	64.26	3360
2.0 m/s L	.125	17.1	7,13	620	72.2	5610
4.0 m/s L	.166	17.5	8.92	855	110	10400
8.0 m/s L	.199	17.1	8.15	531	68.7	4390
2.0 m/s H	.0906	17.4	6.84	701	80.1	6460
4.0 m/s H	.091	17.1	7.16	750	98.7	7670
8.0 m/s H	.0905	13.6	9.33	377	130	2440

All range values are given in units of meters.

All angle values are given in units of micro-radians.

Table 4-3c Ladar Angle Results

RMS Noise Value	Initial Filter Release		One Second		Three Seconds	
	RMS Range Error	RMS Angle Error	RMS Range Error	RMS Angle Error	RMS Range Error	RMS Angle Error
80 μrad	.0906	28.2	6.39	630	67.81	5400
160 μrad	.0906	45.8	5.39	458	49.5	2990
250 μrad	divergence failed					
80 μrad L	.0906	28.3	6.84	746	84.2	7460
160 μrad L	.0905	47.7	7.10	845	92.3	7920
250 μrad L	divergence failed					
80 μrad H	.0906	17.4	6.88	707	81.1	7010
160 μrad H	.091	17.3	6.82	691	83.2	6430
250 μrad H	.0902	16.8	5.22	374	48.6	6430

All range values are given in units of meters.

All angle values are given in units of micro-radians.

Table 4-3d Ladar Angle-Rate Results

RMS Noise Value	Initial Filter Release		One Second		Three Seconds	
	RMS Range Error	RMS Angle Error	RMS Range Error	RMS Angle Error	RMS Range Error	RMS Angle Error
4.0 mr/s	.0907	17.8	6.78	681	74.8	6150
8.0 mr/s	.0907	17.5	6.21	595	64.8	5020
4.0 mr/s L	.091	13.7	6.40	562	65.0	4470
8.0 mr/s L	.091	17.6	6.35	610	66.4	5170
4.0 mr/s H	.0905	16.8	6.27	611	70.3	5470
8.0 mr/s H	.0905	17.1	7.01	715	86.3	7380

All range values are given in units of meters.

All angle values are given in units of micro-radians.

Table 4-3e Ladar Pulse-Rate Results

RMS Noise Value	Initial Filter Release		One Second		Three Seconds	
	RMS Range Error	RMS Angle Error	RMS Range Error	RMS Angle Error	RMS Range Error	RMS Angle Error
60 Hz-2	.180	30.1	7.33	761	77.9	6240
60 Hz-3	.350	53.1	8.20	864	87.3	6990
60 Hz-4	.720	79.1	9.81	966	88.1	7320
30 Hz-1	.125	21.3	7.86	750	81.3	7250
30 Hz-2	.247	36.0	8.11	616	72.3	5070
30 Hz-3	.494	70.1	9.75	1008	42.8	8380
30 Hz-4	.986	99.5	10.6	864	79.5	5620

All range values are given in units of meters.

All angle values are given in units of micro-radians.

unfortunately are not used in this thesis study) are required to establish any meaningful conclusions on the relationships between predicted volume size and rms ladar noise.

There are two notable exceptions to these results. The simulation dynamics are more sensitive to rms angle noise, than to rms range, range-rate and angle-rate noise as is seen from Table 4-3c. The angle noise sensitivity does not appear in the volume predictions, but rather within the system dynamics themselves. At higher rms angle noise the filter becomes unstable.

The second notable exception is found by close analysis of the results presented in Table 4-4e. For each ladar pulse-rate, four cases are tested (60 Hz-1 is the low noise baseline presented in Table 4-2) using the rms measurement noise sets from Table (3-2). At the initial filter release time, there is a strong relationship between estimated volume and noise strength. A similar relationship exists between the filter estimated volume and ladar pulse-rate at filter release. For the 60 Hz pulse-rate, the relationship between volume and ladar noise, although still present, is less prevalent for one second of filter divergence and even more so after three seconds of filter divergence. For the 30 Hz pulse-rate, there is a marginal relationship between ladar noise and filter estimated range error after one second of filter divergence. There is no evidence of relationship between filter estimated range error and ladar noise for 30 Hz after three seconds of divergence. There is no evidence of relationship between filter estimated angle error and ladar noise for either divergence at 30 Hz. Further discussion of Table 4-3e results is deferred to Chapter V.

4.4 The Aircraft Run Series Results

Simulations in the aircraft run series are conducted using the criteria established in Section 3.3 and Table 3-4. For consistency a $\pi/4$ missile approach angle is used, as discussed in Section 4-2. Throughout the aircraft run series, no aircraft acceleration measurements are assumed to be available from the navigation system. All other parameters (except the one under study in the particular run set) are held at the baseline values. The aircraft run series investigates the effects of assumed INS measurement noise, assumed pilot error noise, and aircraft turn rate on the predicted volume cross-section.

The low noise baseline results presented in Table 4-2 assume a $(0.1g)^2$/sec pilot induced aircraft trajectory error. The baseline value is taken from the development in Chapter II. Since the baseline value is based on an ad hoc estimated noise strength (see the discussion on pilot induced error in Section 2.4), this parametric analysis is performed to assess the impact of assumed pilot induced error on the predicted cross-section. Table 4-4 presents the results obtained as the assumed pilot induced error is increased. From the Table 4-4 results, two observations are made. The filter's cross-section estimate at filter release appears to be constant, indicating that the velocity measurements provided by the navigation subsystem are capable of filtering out the pilot induced noise strength as long as measurements are available. For the one-second and three-second filter divergences, there is no obvious relationship between pilot induced error and estimated cross-section, indicating the need for Monte-Carlo analysis.

Table 4-5 presents the results of the INS run set and Table 4-6 presents the results of the aircraft turn rate run set. The results are consistent with those

Table 4-4 Pilot Induced Error Results

Mean Squared Noise Strength	Initial Filter Release		One Second		Three Seconds	
	RMS Range Error	RMS Angle Error	RMS Range Error	RMS Angle Error	RMS Range Error	RMS Angle Error
$(0.2g)^2$/s	.0906	17.1	5.88	934	58.3	3940
$(0.3g)^2$/s	.0906	17.2	7.17	761	96.5	7880
$(0.4g)^2$/s	.0906	16.8	6.26	606	71.6	5490
$(0.5g)^2$/s	.0906	17.4	6.27	576	67.1	4610

All range values are given in units of meters.

All angle values are given in units of micro-radians.

observed in the pilot induced error run set (i.e., no relationship between parametric variations and predicted volume cross-section at either one or three seconds of divergence). For purposes of comparison, the baseline values presented in Table 4-2 include an assumed 0.1m/s velocity error (with acceleration measurements) and a 3.0 g aircraft turn. Table 4-5 results for the cross-section at initial filter release shows that filter estimated range and angle errors do not change with an increase in assumed aircraft velocity measurements. The same results from Table 4-5 indicate that it may be possible to eliminate acceleration measurements from the filter model altogether, as performance without acceleration measurements is only marginally above baseline performance (at initial filter release). Table 4-6 results at initial filter release, show that aircraft turn rate does affect initial cross-section estimates. Neither table shows a relationship between the parameter under study and the filter estimated cross-section at either one or three seconds of divergence, again indicating the need for Monte-Carlo simulation.

4.5 The PRONAV Parameter Pseudo-Noise

The results of the parametric studies conducted to this point yield no conclusive results concerning which model parameter has the largest impact on

Table 4-5 INS Velocity Measurement Error Results

RMS Velocity Error	Initial Filter Release		One Second		Three Seconds	
	RMS Range Error	RMS Angle Error	RMS Range Error	RMS Angle Error	RMS Range Error	RMS Angle Error
0.5 m/s	.0906	17.5	7.40	798	99.2	8480
1.0 m/s	.0906	17.5	6.86	689	76.5	6320
5.0 m/s	.0906	17.4	6.76	677	76.2	6190

All range values are given in units of meters.

All angle values are given in units of micro-radians

Table 4-6 Aircraft Turn Rate Results

Aircraft Turn Rate	Initial Filter Release		One Second		Three Seconds	
	RMS Range Error	RMS Angle Error	RMS Range Error	RMS Angle Error	RMS Range Error	RMS Angle Error
1.0 g turn	.0906	16.4	6.72	494	70.3	4230
2.0 g turn	.0906	15.7	4.82	200	38.6	7880
4.0 g turn	.0906	17.1	6.26	606	71.6	5490
5.0 g turn	.0910	18.2	6.27	576	67.1	4610

All range values are given in units of meters.

All angle values are given in units of micro-radians

the divergence of the volume cross-section. This prompts further simulation to research exactly what model parameter does have a dominant impact on the filter divergence. The ladar measurement noise, the INS noise, the pilot induced error, the aircraft maneuver, and the scenario conditions have all been subjected to parametric analysis and none have shown a strong relationship between the parametric variations and the filter predicted cross-section after either one or three seconds of filter divergence. Only three possible candidates remain, the proportional navigation (Pro-Nav) constant (n) pseudo-noise, the filter's surface-to-mass ratio (S/M) pseudo-noise, and the lateral acceleration tuning noise. The Pro-Nav constant's pseudo-noise turns out to be the driver. (Like the parameters studied earlier, the surface-to-mass ratio and lateral acceleration noise strengths have no discernable effect on the predicted volume cross-section.) The Pro-Nav constant is given an initial diffusion strength Q(t) of $(.5)^2$/sec. This Q(t) value allows the filter to occasionally lose track of the system dynamics, particularly in harsher dynamic scenarios where the missile require larger lateral accelerations. The Q(t) value is increased to $(2)^2$/sec to facilitate better lateral acceleration tracking (which it does). However, on filter release the Pro-Nav constant diffusion strength is now dominating the covariance spread (and hence the predicted volume cross-section). To investigate, the aircraft turn rate set is resimulated using a Q(t) of $(.5)^2$/sec for the Pro-Nav constant. The results of the new run set are presented in Table 4-7. A second run set is simulated using the baseline conditions and varying the Pro-Nav constant noise diffusion strength for direct comparison. These results are presented in Table 4-8.

Table 4-7 Aircraft Turn Rate Results Using New Pro-Nav Constant Q(t)

Aircraft Turn Rate	Initial Filter Release		One Second		Three Seconds	
	RMS Range Error	RMS Angle Error	RMS Range Error	RMS Angle Error	RMS Range Error	RMS Angle Error
0.1 g turn	.0906	13.7	6.70	439	69.1	1720
1.0 g turn	.0906	13.4	5.28	182	50.4	1100
2.0 g turn	.0906	13.5	4.82	200	38.6	1320
3.0 g turn	.0906	13.8	4.09	171	27.5	1090
4.0 g turn	divergence failed 0.5 seconds after release					
5.0 g turn	divergence failed 0.26 seconds after release					

All range values are given in units of meters.

All angle values are given in units of micro-radians

Table 4-8 n Parameter Q(t) vs Baseline Comparison

Q(t)	Initial Filter Release		One Second		Three Seconds	
	Range	Angle	Range	Angle	Range	Angle
baseline	.0906	15.4	6.34	538	67.6	5330
$(1.0)^2$/sec	.0905	15.3	5.21	370	45.4	3020
$(0.5)^2$/sec	.0906	13.8	4.09	171	27.5	1320

All range values are given in units of meters.

All angle values are given in units of micro-radians

The results in Table 4-8 show a definite correlation between the Pro-Nav constant diffusion strength and the filter divergence. Although the divergence correlation is strong for both range and angle divergence, there is stronger divergence in the angle. Table 4-7 results verify that the filter's estimated cross-section is significantly smaller at all divergences when using a lower Pro-Nav constant Q(t). Table 4-7 also verifies that the lower Q(t) value does not allow adequate tracking when the scenario dynamics require higher missile lateral acceleration as seen from the failed divergences under aircraft 4.0 g and 5.0 g turns.

4.6 Summary

This chapter presents the simulation results obtained from the kill zone volume parametric analysis described in Chapter III. In general the initial volume cross-section at filter release varied as expected with the parameter under study. However, the volume cross-section after three seconds of divergence is, in general, independent of the parameter under study. New simulations are conducted to investigate why the filter predicted three second cross-section is independent of ladar measurement noise, assumed INS rms errors, pilot error and aircraft turn rate. It is found that the tuning pseudo-noise used on the filter's estimation of the proportional navigation parameter (n) is dominating the filter divergence. The other parameters effects can not be adequately ascertained without Monte-Carlo simulation.

Chapter V summarizes the research accomplished in this thesis study. The work presented in Chapters I to IV is briefly reviewed, the main conclusions of the thesis study are presented, and recommendations for continued research are made based on these conclusions. In particular, certain results presented in this chapter are reviewed in light of the Pro-Nav constant induced filter divergence, and in light of the obvious need for Monte-Carlo simulation.

V Conclusions and Recommendations

5.0 Introduction

The conclusions presented in this chapter are based on the results presented in Chapter IV. The assumptions and analysis techniques used to scope this thesis study are summarized. The conclusions focus on the impact of the Pro-Nav parameter's noise diffusion and its effect on the other simulation results. Research recommendations are made based on the conclusions presented in this chapter, the assumptions outlined in Chapter I and the model limitations from Chapter II. The chapter ends with an overall thesis summary.

5.1 Review of Thesis Assumptions

Proper interpretation of the results presented in Chapter IV first requires a review of the assumptions made in Chapters I and II which scope the thesis and define the limitations of the simulation model. Therefore, as a first step to presenting conclusions, the modelling assumptions on which those conclusions are based, are now presented.

A benign and easily tracked aircraft trajectory is chosen to simplify model dynamics. The simple trajectory also reduces required missile lateral acceleration, obstensibly making the filter's tracking and predicting functions easier. From a mission standpoint flying a benign trajectory may not be desirable or even possible.

The analyses performed throughout this thesis use filter computed statistics as the benchmark of performance. This may be true of an optimally designed and tuned filter, which has been thoroughly tested with Monte-Carlo analysis, but no such design and analysis has been performed as part of this thesis. This thesis looks past optimal filter design issues to get a first glimpse at how the filter computes and propagates the predicted volume cross-section. This thesis study is intended as only the first in a series of studies on the complex subject of kinetic kill zone prediction, as such specific design issues have been surpassed to get a big picture look at the whole volume prediction problem.

The missile model used in this thesis assumes a post burnout coast-to-intercept missile flight with no endgame guidance. As such the missile simulations conducted are limited to those in which a kinetically limited missile is capable of adequately tracking the target. The envelope of possible engagement scenarios can be significantly expanded by using a thrusting missile model in future analyses. The missile endgame guidance should also be considered particularly when using a thrusting missile model. Most missiles have lateral acceleration limits between 24 g and 40 g. The non-thrusting missile is not kinetically capable of exceeding about 14 g in lateral acceleration before bleeding off airspeed and stalling. A thrusting missile may be capable of exceeding this limit and therefore needs to consider the addition of an endgame trajectory when specific acceleration limits are exceeded.

The initial ladar rms measurement errors developed in Chapter II are based on a benign atmospheric turbulence model. A good jet-wash turbulence model has not yet been developed. More adequate measurement statistics based on the active turbulence caused by jet-wash and missile flight needs to be added to the ladar model. This thesis overcomes the model limitation by treating the assumed ladar measurement errors as parameters of study.

The simulations are limited to a constant altitude plane throughout this study. The baro-altimeter (vertical position) measurements used in this thesis, are useful within the context of a constant altitude simulation, but are not realistic if the missile is not confined to the aircraft's altitude plane. A three dimensional simulation definitely addresses the issue of observing missile altitude. Should however, a two dimensional model be selected for continued analysis, the altimeter measurements should be removed from the model.

During simulation the missile truth model used a Pro-Nav constant of 4.5. The filter estimate of the Pro-Nav constant consistently settled to -4.5. A thorough search was made to hunt for a possible sign error in the code to explain the negative filter estimate, but came up empty. The simulation results indicate that the missile does track the aircraft in both the filter and truth models (see trajectory plots in Appendix A). All tests which attempted to switch the sign bias of the filter model led to almost immediate simulation because the filter initially tried to laterally accelerate in the wrong direction. Thus the negative bias for the filter estimate of the Pro-Nav gain remains unexplained. It is mentioned here as a warning to future researchers who may be interested in using the FORTRAN code developed during this study.

5.2 Conclusions

Discussion now returns to the ladar run series results presented in Table 4-3c and Table 4-3e. It is believed that the angle measurement's 250 μrad rms error runs fails during filter divergence because the Pro-Nav constant's noise diffusion has its largest impact on angle divergence. Spreading the ladar angle measurements while maintaining tight ladar measurements of range, range-rate and angle-rate, causes an imbalance in the filter covariance estimates which in-turn causes filter instability during propagation without measurement.

The data from Table 4-3e is reconsidered under scrutiny of the Pro-Nav constant's noise diffusion. The data is presented in a new format in Table 5-1. Column one of the table lists the runs being compared. The notation 60 Hz 1-2 indicates that the results from the 60 Hz case 1 run are being compared to the results from the 60 Hz case 2 run (Table 4-3e). The notation 30-60 (1) indicates that the 30 Hz case 1 run is being compared to the 60 Hz case 1 run. The results indicate that at filter release time the filter estimated rms range and angle errors basically follow the ladar's assumed rms measurement errors. In each case as the assumed rms error is doubled, the filter estimated range error doubles and the filter estimated angle error almost doubles. The results also indicate that there is an approximate 30% increase in filter estimated errors

Table 5-1 Range and Angle Divergence Correlations

Runs Compared	Initial Filter Release		One Second		Three Seconds	
	Range Δ%	Angle Δ%	Range Δ%	Angle Δ%	Range Δ%	Angle Δ%
60 Hz 1-2	98.7%	95.5%	11.6%	42.0%	11.5%	17.1%
60 Hz 2-3	94.4%	76.4%	11.9%	13.5%	11.2%	12.0%
60 Hz 3-4	105.7%	49.0%	19.6%	11.8%	0.92%	4.7%
30 Hz 1-2	97.6%	69%	3.2%	no corr	no corr	no corr
30 Hz 2-3	100%	94.7%	20%	no corr	no corr	no corr
30 Hz 3-4	99.6%	41.2%	8.7%	no corr	no corr	no corr
30-60 (1)	38.0%	38.3%	no corr	no corr	no corr	no corr
30-60 (2)	37.2%	19.6%	no corr	no corr	no corr	no corr
30-60 (3)	41.1%	32.0%	no corr	no corr	no corr	no corr
30-60 (4)	36.9%	25.8%	no corr	no corr	no corr	no corr

when the pulse-rate is decreased from 60 Hz to 30 Hz. After one second of divergence, however the percentage change in filter estimated errors have dropped to about 15% for 60 Hz and 10% (range only) for 30 Hz as the assumed ladar measurement errors double. The Table results also show that doubling the assumed ladar measurement accuracy yields less improvement in volume prediction at 30 Hz than at 60 Hz.

The conclusion that the Pro-Nav constant's pseudo-noise strength drives the filter divergence without measurements, supports the observations made in Section 4.1. Figure 4-2b and Figure 4-3b both indicate that, at filter release, a relationship between estimated range and estimated volume size exists as expected. The same relationship is not observed after one second of filter divergence. As a final note, the claim is not being made that no relationship exists between filter estimated ladar measurement noise and filter estimated cross-section, or estimated range and estimated cross-section, but only that the relationships are small compared to that observed from variations in the Pro-Nav constant's diffusion strength. Determining the impacts of either the assumed rms ladar noise or the filter estimated range, on the post divergence filter estimated cross-section, requires Monte-Carlo simulation which is not done in this study.

This thesis investigates the use of an extended Kalman filter (EKF) to predict the kinetic kill zone. The EKF approach is not the only valid approach to such a complex problem. Although the initial EKF approach's results obtained in this study are not considered favorable, the EKF approach cannot be ruled out as invalid based on Section 5.1 assumptions (i.e no Monte-Carlo simulations are conducted, and the filter used is not optimally designed and tuned for the kinetic kill zone problem).

5.3 Recommendations

The EKF approach to the kinetic kill zone estimation problem represents only one of many possible approaches. Given the results presented and their ensuing conclusions, further research is necessary to determine if the EKF approach is an optimum approach. There are considerable processing and time line risks associated with an EKF approach only a few of which are presented in Chapter I. Despite the risk, the EKF approach is used because it is thought that an EKF approach offers performance advantages over other possible approaches. Given the resulting dominance of the filter's Pro-Nav constant noise strength, it is not clear whether an optimally designed EKF will offer these performance advantages. In light of this, it is recommended that alternative approaches to the kinetic kill zone estimation problem be studied.

There are three things which are relatively certain about the kinetic kill zone estimation problem. They are (1) at any given time, a single ladar measurement represents a reasonably accurate measurement of current missile location and velocity, (2) the missile is guiding itself towards the target using some form of proportional navigation, and (3) the missile must traverse the space between the missile's current position and the aircraft estimated trajectory in order to intercept the aircraft.

A possible new approach could perform Monte-Carlo analysis on the missile flight path itself in order to establish a mean and estimated rms missile flight trajectory. The aircraft and missile starting locations remain fixed, while missile dynamic models are subjected to random variations, to generate statistics on the possible missile trajectory to intercept. The results can be used as a database to aid in the kill zone estimation problem. The only online estimation that occurs, is linear projection of the missile location based on the ladar measurements. The processing timeline risk goes away since such calculations can probably be accomplished within a few milliseconds. Maximum use is then made of the ladar measurements accuracy since system reaction can be almost instantaneous. This allows maximum latitude in selecting an optimum intercept time and location which is not driven the by stringent processing timelines that an EKF approach requires.

Should the EKF approach to the kinetic kill zone estimation problem be explored further, the following recommendations are made.

(1) A need exists for Monte-Carlo simulation to accurately assess the impacts of parametric variations on model performance. Specific conclusions about the effects of rms ladar measurement errors, pilot induced trajectory error, aircraft turn-rate, and estimated rms INS errors on the final estimated cross-section could not be made based solely on the results of filter computed statistics.

(2) The possibility of Q-switching the Pro-Nav constant's pseudo-noise strength needs study to determine if a high initial diffusion strength can be used to enhance tracking performance, and a lower diffusion strength used for volume estimation. This may require the aircraft to perform specific or restricted maneuvers to enhance the performance of the Q-switched filter (which inturn may not be desirable from a mission standpoint as discussed earlier).

(3) This study uses a post burnout coast-to-intercept missile scenario. The following missile model changes are recommended: The missile should be initially thrusting, with the possibility of going into coast; The simulated missile should have an endgame guidance capability to allow more complete simulations. The implementation of three dimensional simulations can be accomplished at a more advanced stage.

(4) This study uses a benign turbulence model and accounts for the inadequacies in the model by performing a parametric study on assumed ladar noises. A more accurate representation of aircraft turbulence should be included in the next study. In the event that an accurate jet wash turbulence model does not exist, measurements need to be made to determine turbulence induced measurement errors more completely.

(5) Processing time requirements may be a potential problem when using the EKF approach to kinetic kill zone estimation, especially as advanced models are developed. The timing diagram presented in Figure 1-3 requires online filter estimation in faster than real time. Given the complexity of the model used in simulation and additional complexities which would become part of an actual system, it is not certain that faster than real time simulation can be achieved. Alternatives to filter processing may need investigation just on this point alone.

(6) Accurate assessment of time-to-go requires an ability to estimate missile endgame guidance. Any time-to-go model which does not take this into consideration is highly suspect in performance results.

(7) No attempt is made to optimize the filter model design used throughout this simulation. An optimized filter design may (or may not) provide additional performance benefits which need to be understood and characterized.

5.3 Overall Summary

This thesis investigates using an extended Kalman filter to predict a kinetic kill zone for aircraft self defense against homing missiles. The problem is studied using FORTRAN simulations conducted on Sun SPARC II Workstations, and includs a software simulation package called MSOFE [3. The simulation model is limited to constant altitude planar analysis and assums benign easily predictable aircraft maneuvers, a kinetically limited missile, and a 60 Hz laser radar operating in a benign turbulence environment. The overall simulation goal is to predict a volume cross-section relative to the aircraft's future position, which the missile would have to fly through at a specific time. Assumptions and parameters of the developed model are systematically studied to determine that parameter's impact on the predicted volume cross-section. It is found that the filter pseudo-noise used to drive the filter's estimation of the missile's proportional navigation constant has the largest impact on the estimated volume cross-section. Other parameter impacts are generally small enough in comparison, so as to be unaccessible without Monte-Carlo simulation.

Bibliography

1. Blakelock, John H. Automatic Control of Missiles and Aircraft. New York: John Whiley and Sons, Inc, 1965.

2. Boyd, Robert W. Radiometry and the Detection of Optical Radiation . New York: John Whiley and Sons, Inc, 1983.

3. Carson, Neal A. and Stanton H. Musick. User's Manual for a Multimode Simulation for Optimal Filter Evaluation (MSOFE). AFWAL-TR-88-1138, Wright-Patterson AFB OH: Avionics Laboratory, AFWAL/AARN-2, 1990.

4. Clark, Dean. *F-16 Fighter Pilot, USAF.* Wright Patterson AFB, OH. Personal Interview. 26 October 1993.

5. Cusumano, Salvatore J. and Manuel DePonte Jr. An Extended Kalman Filter Fire Control System Aainst Air-to-Air Missiles. MS thesis, AFIT/GE/EE/77-13. School of Engineering, Air Force Institute of Technology (AU), Wright-Patterson AFB OH, February 1978 (AD-A055179).

6. Etter, D. M. Structured Fortran 77 for Engineers and Scientists. The Benjamin/Cummings Publishing Company, Inc. 1983.

7. Goodman, Joseph P. Statistical Optics. John Wiley & Sons, Inc., 1985.

8. Lutter, Robert N. Application of an Extended Kalman Filter to an Advanced Fire Control System. MS thesis, AFIT/GE/EE/76-31. School of Engineering, Air Force Institute of Technology (AU), Wright-Patterson AFB OH, December 1976.

9. Maybeck, Peter S. Stochastic Models, Estimation and Control (vol 2). San Diego: Academic Press, Inc., 1982.

10. Maybeck, P. S., J. G. Reid, and R. N. Lutter. "Application of an Extended Kalman Filter to an Advanced Fire Control System," Proceedings of the 1977 IEEE Conference on Decision and Control, New Orleans, LA, December 1977.

11. Maybeck, P. S., S. J. Cusumano, M. DePonte Jr., and J. E. Negro. "Enhanced Fire Control System Filtering via Refined Air-to-Air Missile Acceleration Modeling," IEEE Transactions on Automatic Control (vol AC-24 no 6). Dec 1979.

12. McCamey, Kevin J. *Program Manager, Advanced Development Program Office, Electronic Warfare Division.* WL/AAWD-2 Wright-Patterson AFB OH. Personal Interview. 20 May 1992.

13. Negast, William J. Incorporation of Differential Global Positioning System Measurements Using an Extended Kalman Filter for Improved Reference System Performance. MS thesis, AFIT/GE/ENG/91D-41. School of Engineering, Air Force Institute of Technology, (AU), Wright-Patterson AFB OH, December 1991 (AD-A243742).

14. Reid, J. Gary. Linear System Fundementals: Continuous and Discrete, Classical and Modern. McGraw-Hill Inc, 1983.

15. Rockwell International Rocketdyne Division. Aircraft Self Defense. Presentation notes. April 1993.

16. Seyrafi, Khalil and S. A. Hovanessian. Introduction to Electro-Optical Imaging and Tracking Systems. Norwood, MA: Artech House, Inc., 1993.

17. Symon, Keith R. Mechanics. Addison-Wesley Publishing Company, 1971.

18. Tipler, Paul A. Physics. Rochester, MI: Worth Publishers, Inc. 1982.

19. Vogel, George. *Program Manager, Active Electronic Warfare Program Office, Electronic Warfare Division* WL/AAWW-3 Wright-Patterson AFB OH. Personal Interview. 15 September 1993.

20. Warner, Duane A. *Program Manager, Advanced Development Program Office, Electronic Warfare Division* WL/AAWD-2 Wright-Patterson AFB OH. Personal Interview. 20 November 1992.

21. Wunderlich, Mark. *Program Manager, Advanced Development Program Office, Electronic Warfare Division* WL/AAWD-2, Wright Patterson AFB OH, Personal Interview. March 1993.

22. Zarchan, Paul. Tactical and Strategic Missile Guidance. Washington DC: American Institute of Aeronautics and Astronautics, Inc., 1990.

Appendix A

This appendix contains simulation plots for the missile approach angle run series. The aircraft is initially heading east and beginning a 3 g turn to the north. All measurement noises and dynamic noise strengths are set at baseline values. Eight missile shots are taken at $\pi/4$ intervals beginning with 0.0 radians and ending with $7\pi/4$ radians. Each run has a trajectory plot, estimated range and range error plots, estimated LOS and LOS error plots, and a series of one second filter divergence plots used to estimate the volume cross-section. The number of volume cross-section estimations made for each approach angle vary. The $3\pi/2$ approach angle has two LOS plot sets. The second LOS plot is taken to the maximum possible simulation time to illustrate the zero range induced filter divergence.

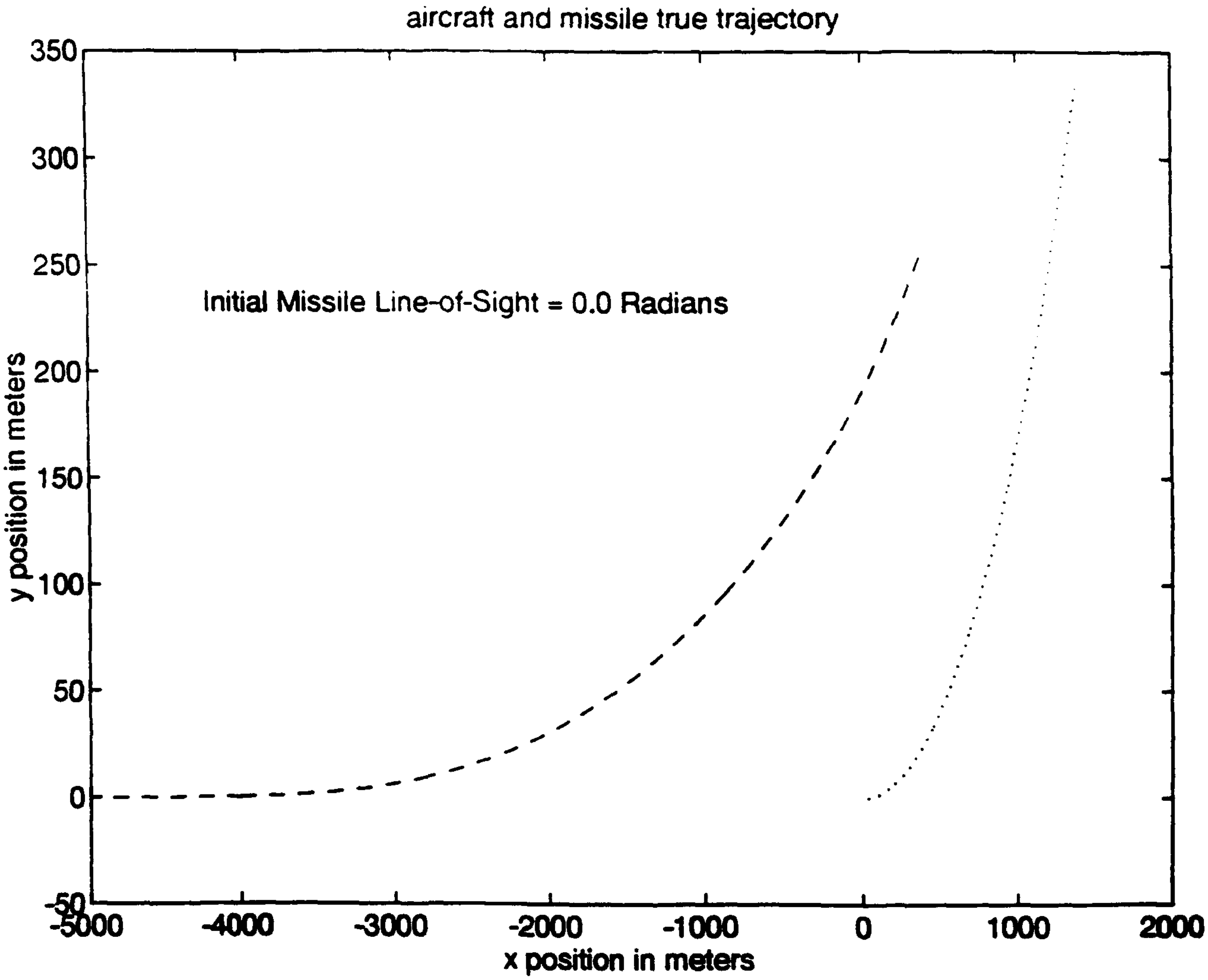
aircraft and missile true trajectory
Initial Missile Line-of-Sight = 0.0 Radians
y position in meters
x position in meters
350
300
250
200
150
100
50
0
-50
-5000
-4000
-3000
-2000
-1000
0
1000
2000

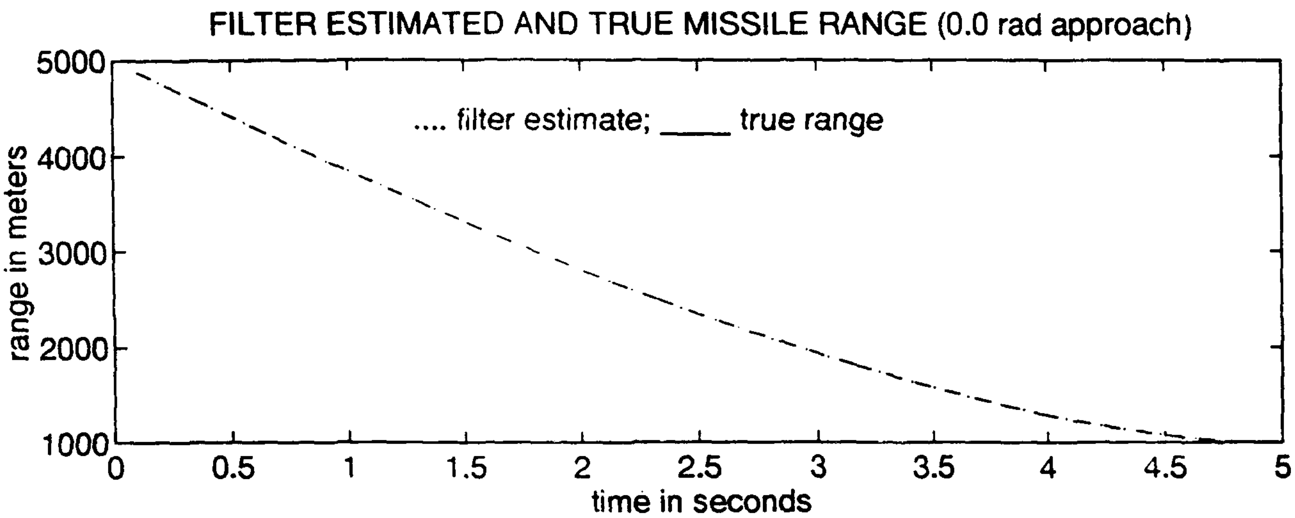
FILTER ESTIMATED AND TRUE MISSILE RANGE (0.0 rad approach)
.... filter estimate; ____ true range
range in meters
5000
4000
3000
2000
1000
0
0.5
1
1.5
2
2.5
3
3.5
4
4.5
5
time in seconds

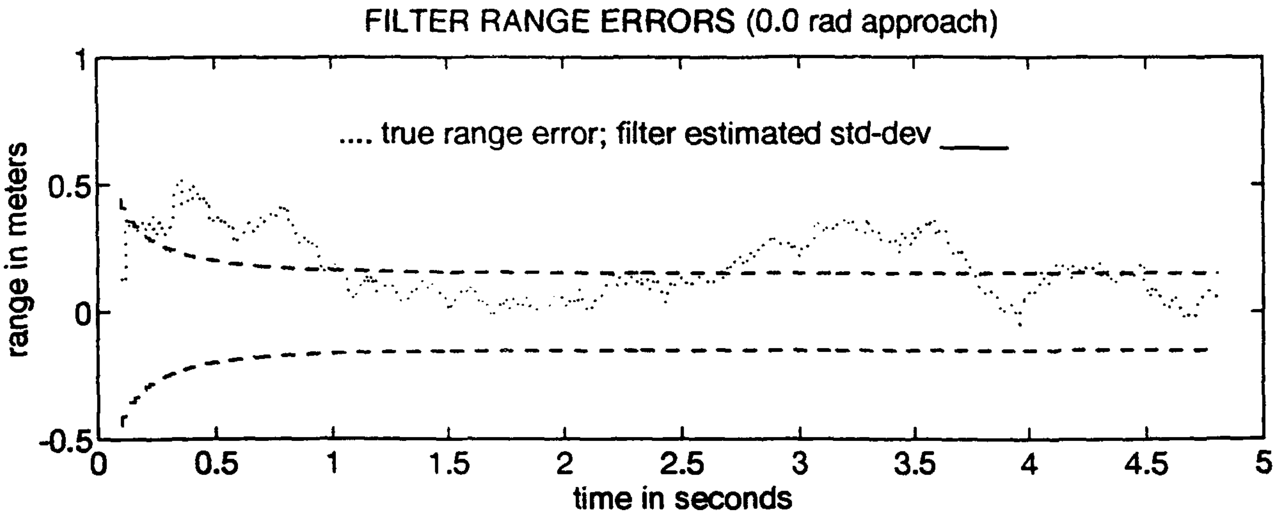
FILTER RANGE ERRORS (0.0 rad approach)
.... true range error; filter estimated std-dev ____
range in meters
1
0.5
0
-0.5
0
0.5
1
1.5
2
2.5
3
3.5
4
4.5
5
time in seconds

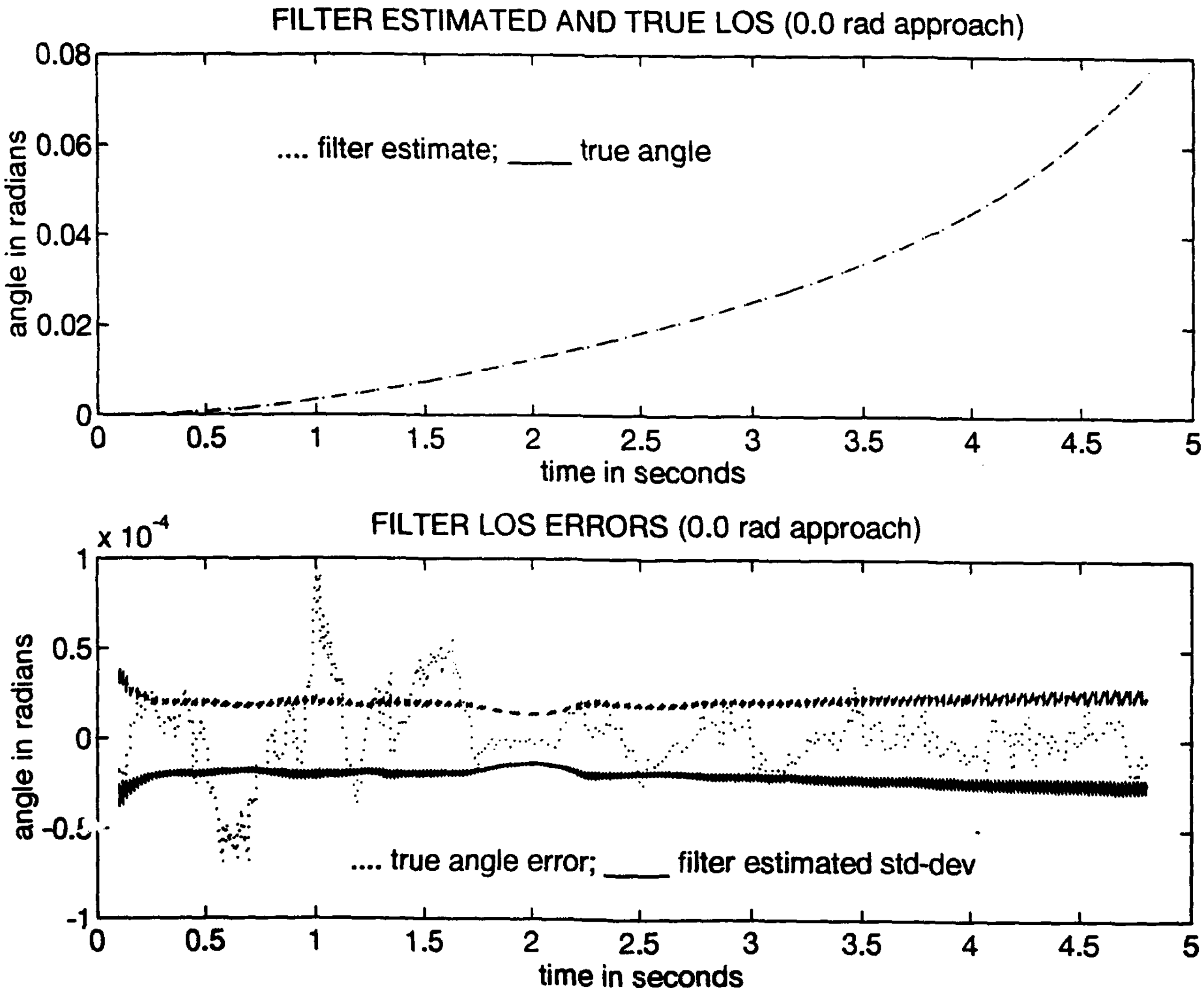
FILTER ESTIMATED AND TRUE LOS (0.0 rad approach)
.... filter estimate; ____ true angle
angle in radians
time in seconds
0.08
0.06
0.04
0.02
0
0
0.5
1
1.5
2
2.5
3
3.5
4
4.5
5
FILTER LOS ERRORS (0.0 rad approach)
x 10^-4
.... true angle error; ____ filter estimated std-dev
angle in radians
time in seconds
1
0.5
0
-0.5
-1
0
0.5
1
1.5
2
2.5
3
3.5
4
4.5
5

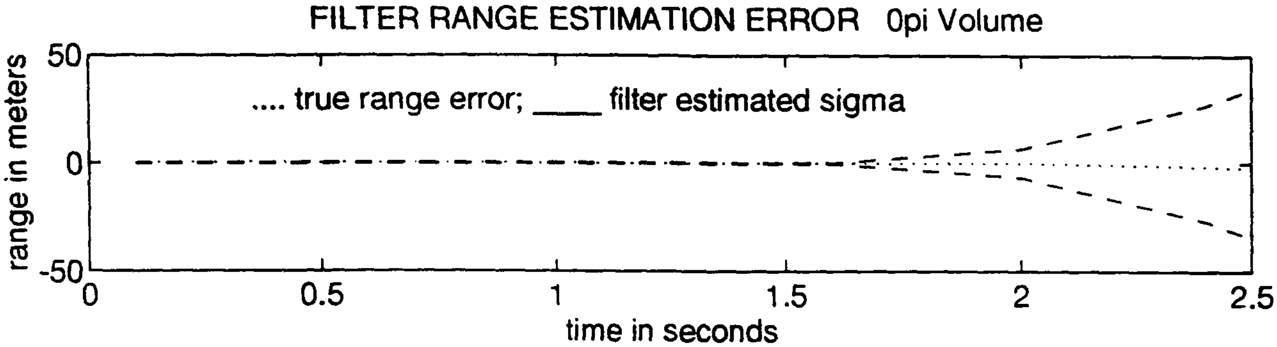
FILTER RANGE ESTIMATION ERROR   0pi Volume
.... true range error; ____ filter estimated sigma
range in meters
50
0
-50
0
0.5
1
1.5
2
2.5
time in seconds

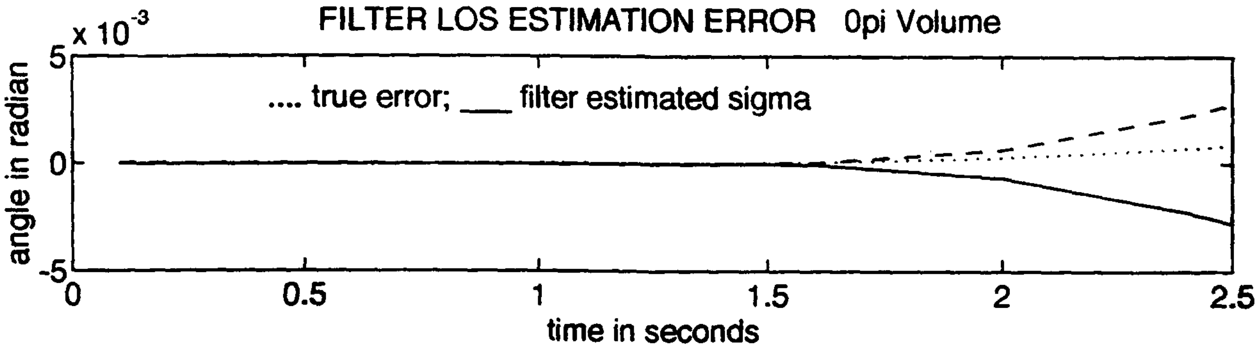
FILTER LOS ESTIMATION ERROR   0pi Volume
x 10^-3
.... true error; ___ filter estimated sigma
angle in radian
5
0
-5
0
0.5
1
1.5
2
2.5
time in seconds

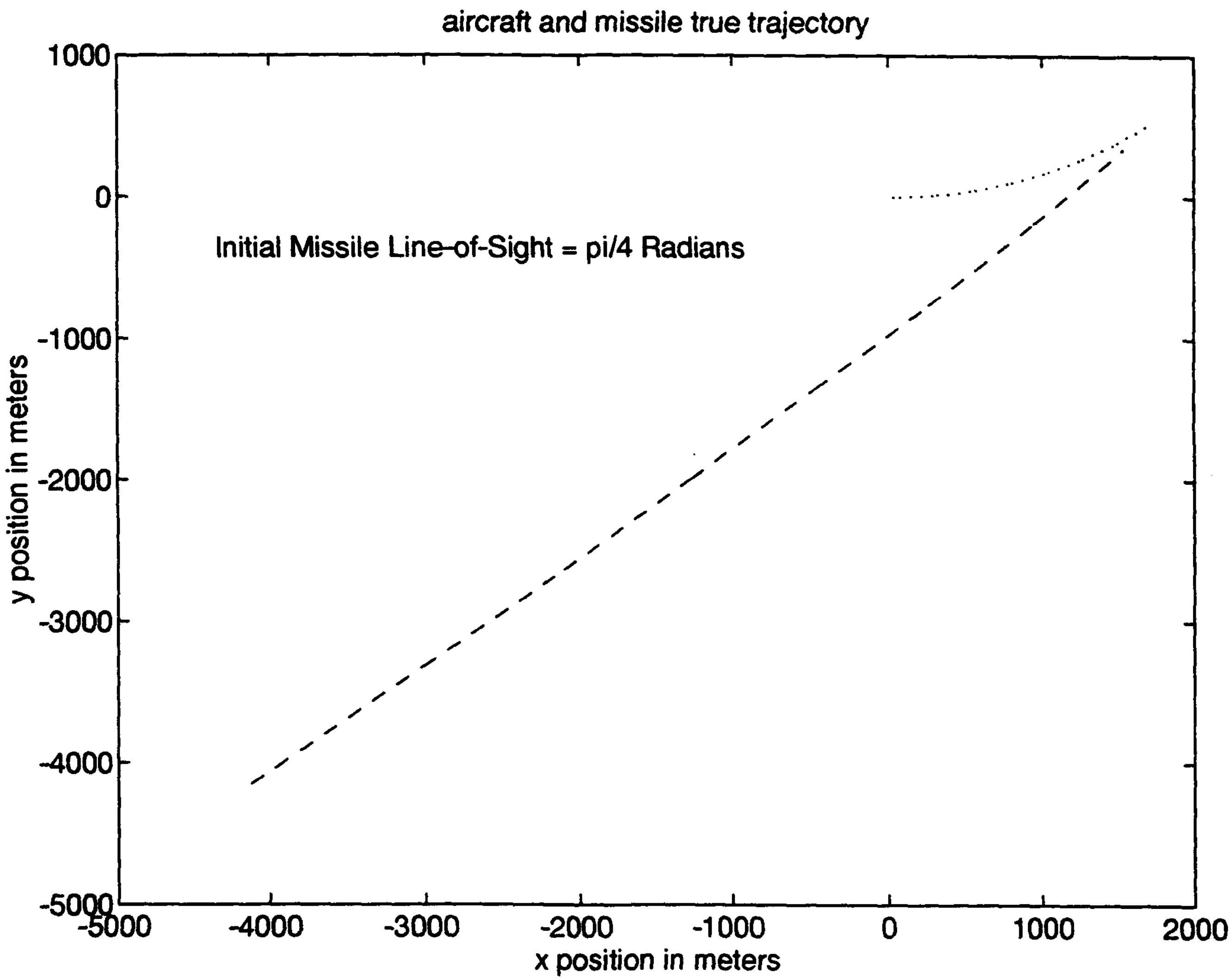
aircraft and missile true trajectory
Initial Missile Line-of-Sight = pi/4 Radians
y position in meters
x position in meters
1000
0
-1000
-2000
-3000
-4000
-5000
-5000
-4000
-3000
-2000
-1000
0
1000
2000

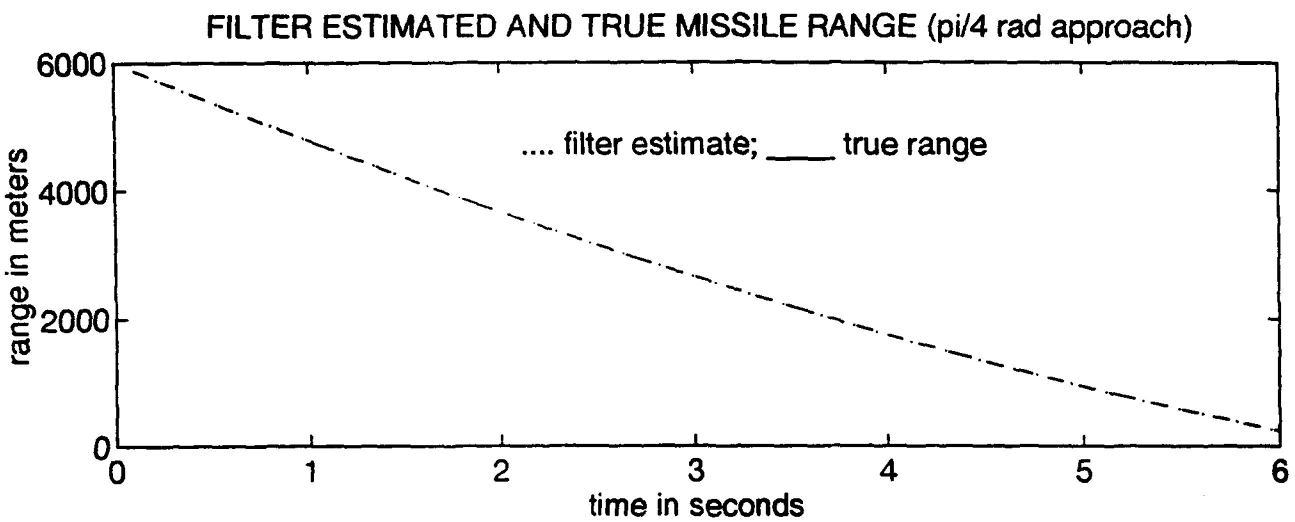
FILTER ESTIMATED AND TRUE MISSILE RANGE (pi/4 rad approach)
.... filter estimate; ____ true range
range in meters
time in seconds

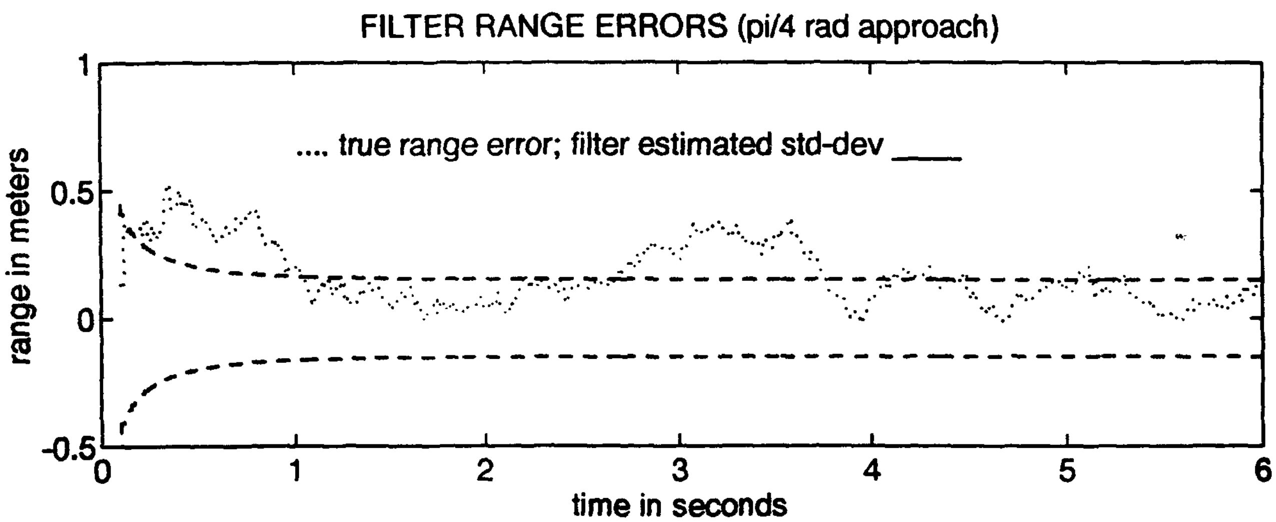
FILTER RANGE ERRORS (pi/4 rad approach)
.... true range error; filter estimated std-dev ____
range in meters
time in seconds

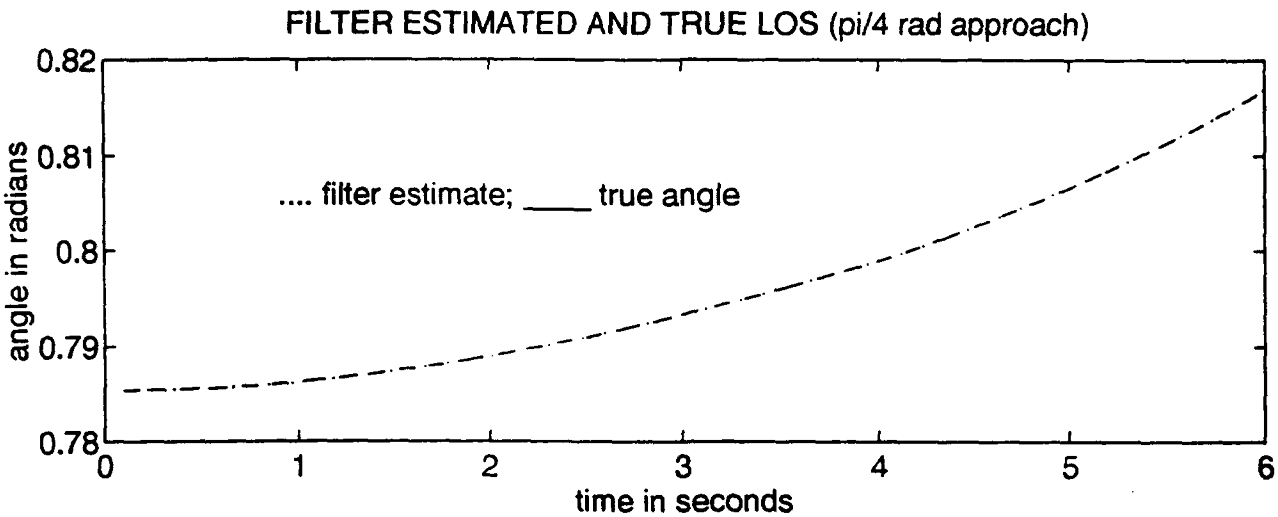
FILTER ESTIMATED AND TRUE LOS (pi/4 rad approach)
.... filter estimate; ____ true angle
angle in radians
time in seconds
0.82
0.81
0.8
0.79
0.78
0
1
2
3
4
5
6

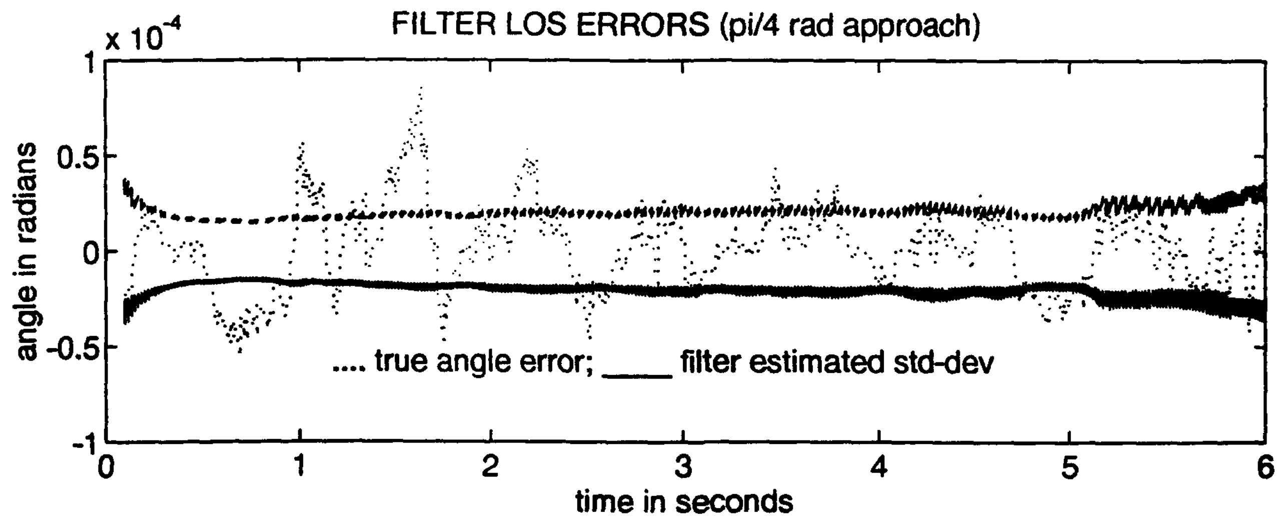
FILTER LOS ERRORS (pi/4 rad approach)
x 10^-4
.... true angle error; ____ filter estimated std-dev
angle in radians
time in seconds
1
0.5
0
-0.5
-1
0
1
2
3
4
5
6

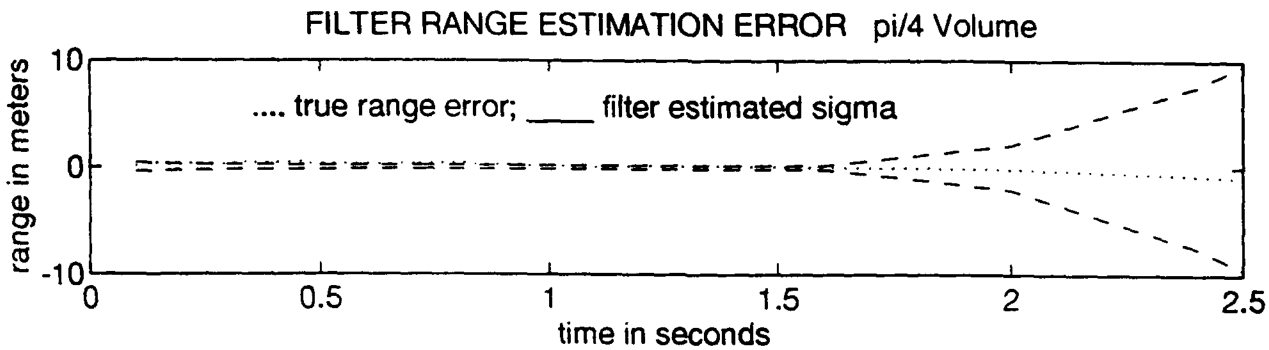
FILTER RANGE ESTIMATION ERROR pi/4 Volume
.... true range error; ____ filter estimated sigma
range in meters
10
0
-10
0
0.5
1
1.5
2
2.5
time in seconds

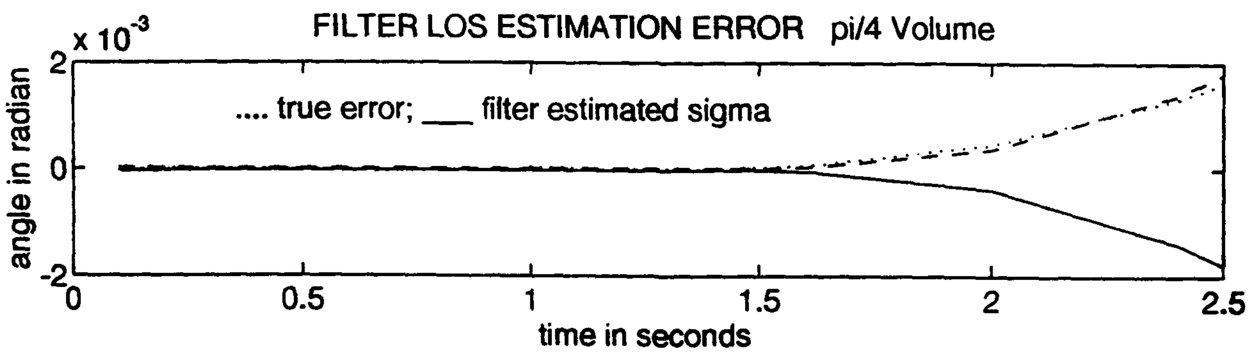
FILTER LOS ESTIMATION ERROR pi/4 Volume
x 10^-3
.... true error; ___ filter estimated sigma
angle in radian
2
0
-2
0
0.5
1
1.5
2
2.5
time in seconds

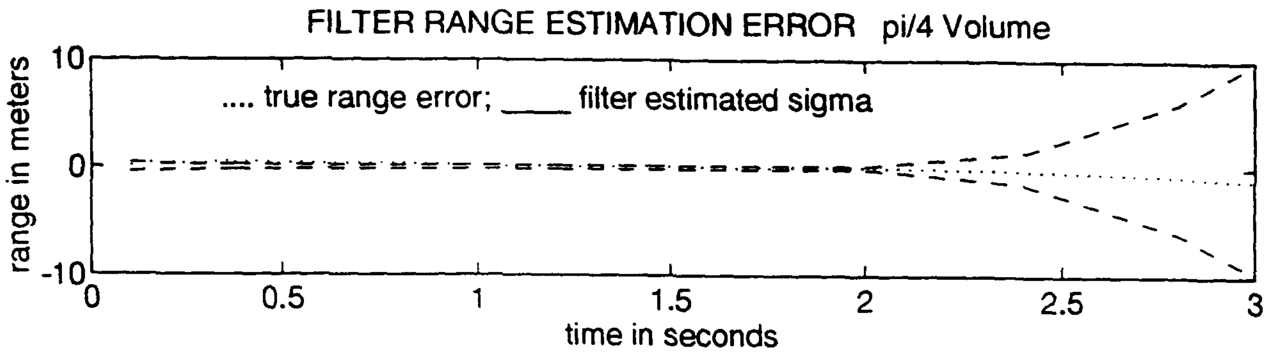
FILTER RANGE ESTIMATION ERROR pi/4 Volume
.... true range error; ____ filter estimated sigma
range in meters
10
0
-10
0
0.5
1
1.5
2
2.5
3
time in seconds

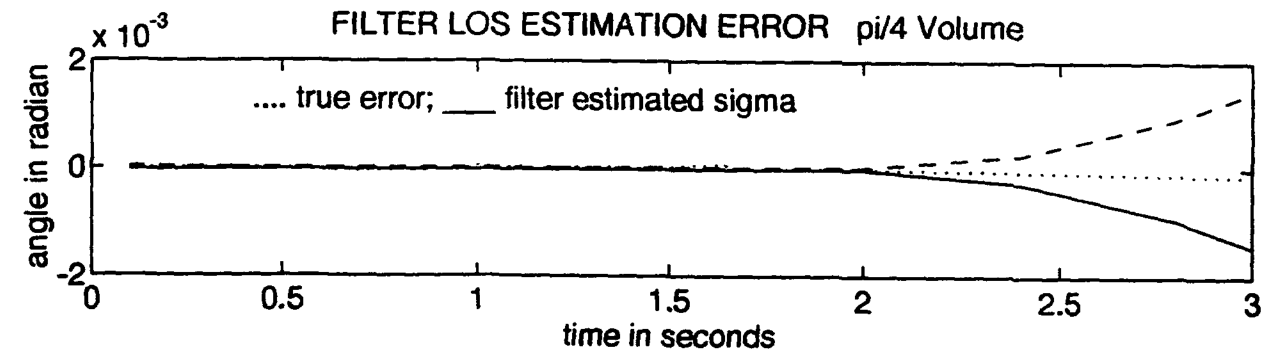
FILTER LOS ESTIMATION ERROR pi/4 Volume
x 10-3
.... true error; ___ filter estimated sigma
angle in radian
2
0
-2
0
0.5
1
1.5
2
2.5
3
time in seconds

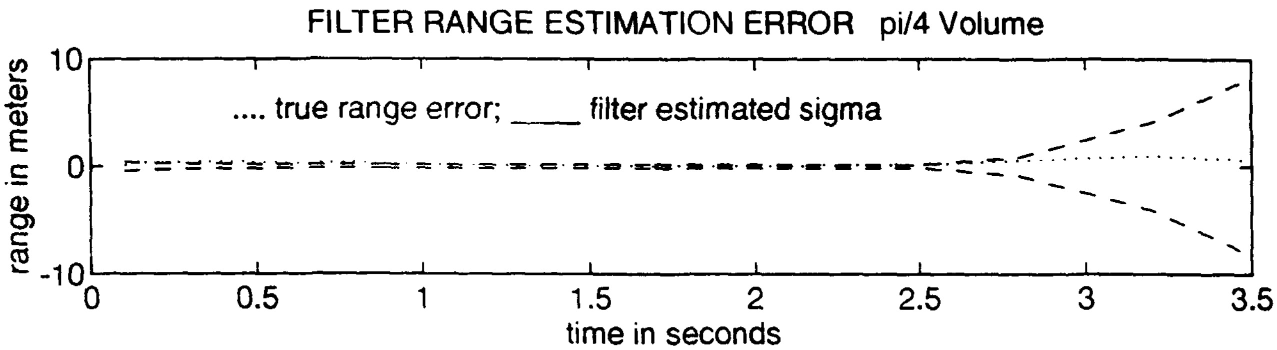
FILTER RANGE ESTIMATION ERROR pi/4 Volume
.... true range error; ____ filter estimated sigma
range in meters
10
0
-10
0
0.5
1
1.5
2
2.5
3
3.5
time in seconds

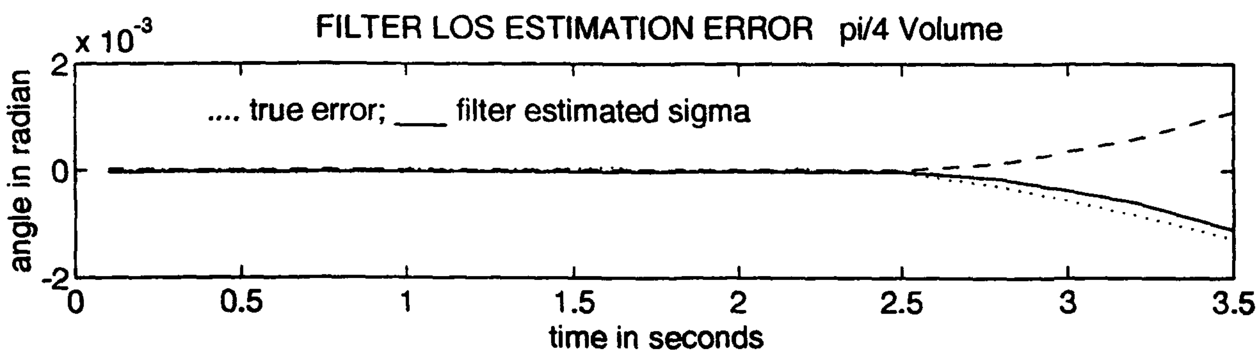
FILTER LOS ESTIMATION ERROR pi/4 Volume
x 10^-3
.... true error; ____ filter estimated sigma
angle in radian
2
0
-2
0
0.5
1
1.5
2
2.5
3
3.5
time in seconds

FILTER RANGE ESTIMATION ERROR pi/4 Volume

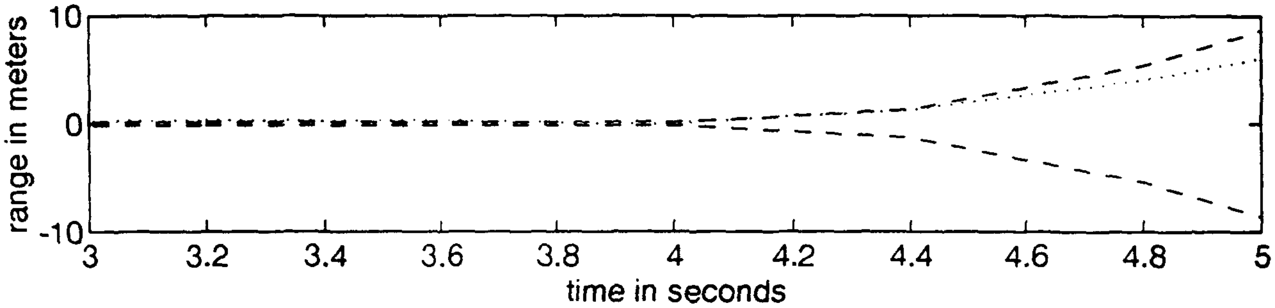

.... true error; ____ filter estimated sigma
.... true range error; ____ filter estimated sigma

FILTER LOS ESTIMATION ERROR pi/4 Volume

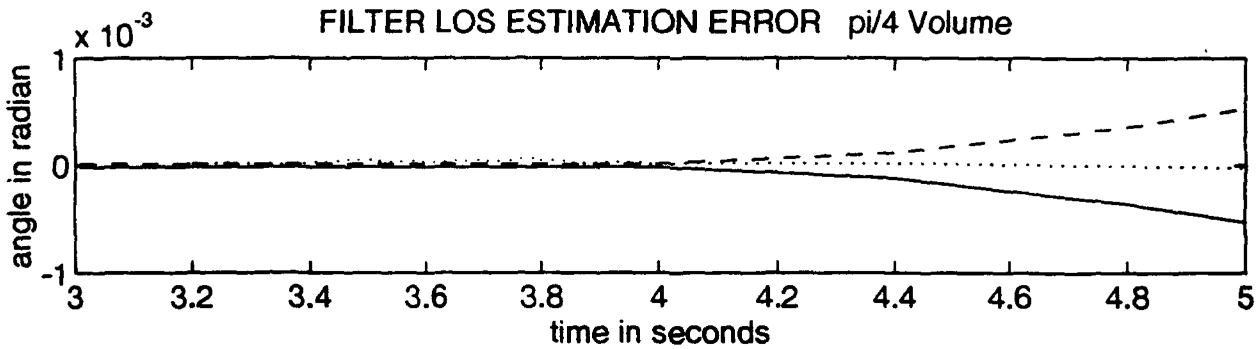

FILTER RANGE ESTIMATION ERROR   pi/4 Volume

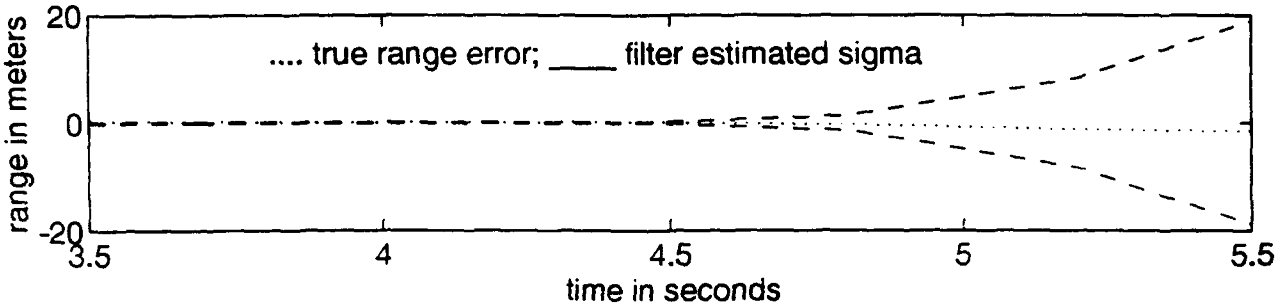

FILTER LOS ESTIMATION ERROR   pi/4 Volume

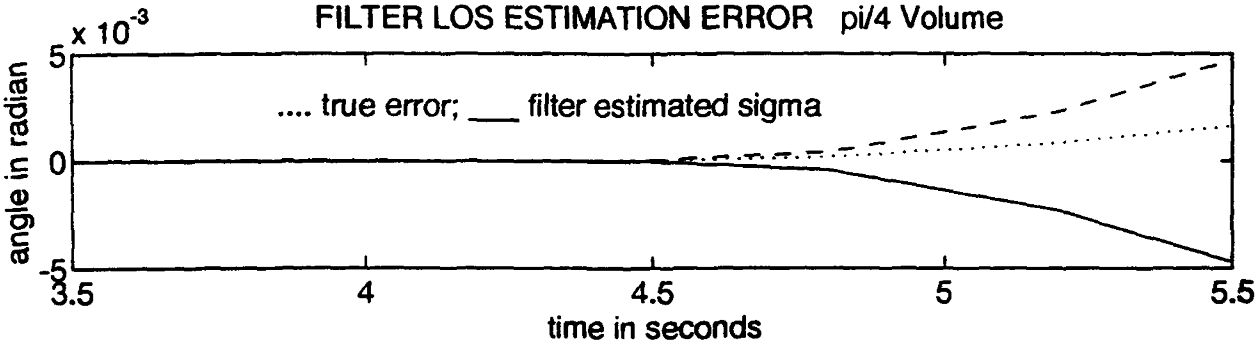

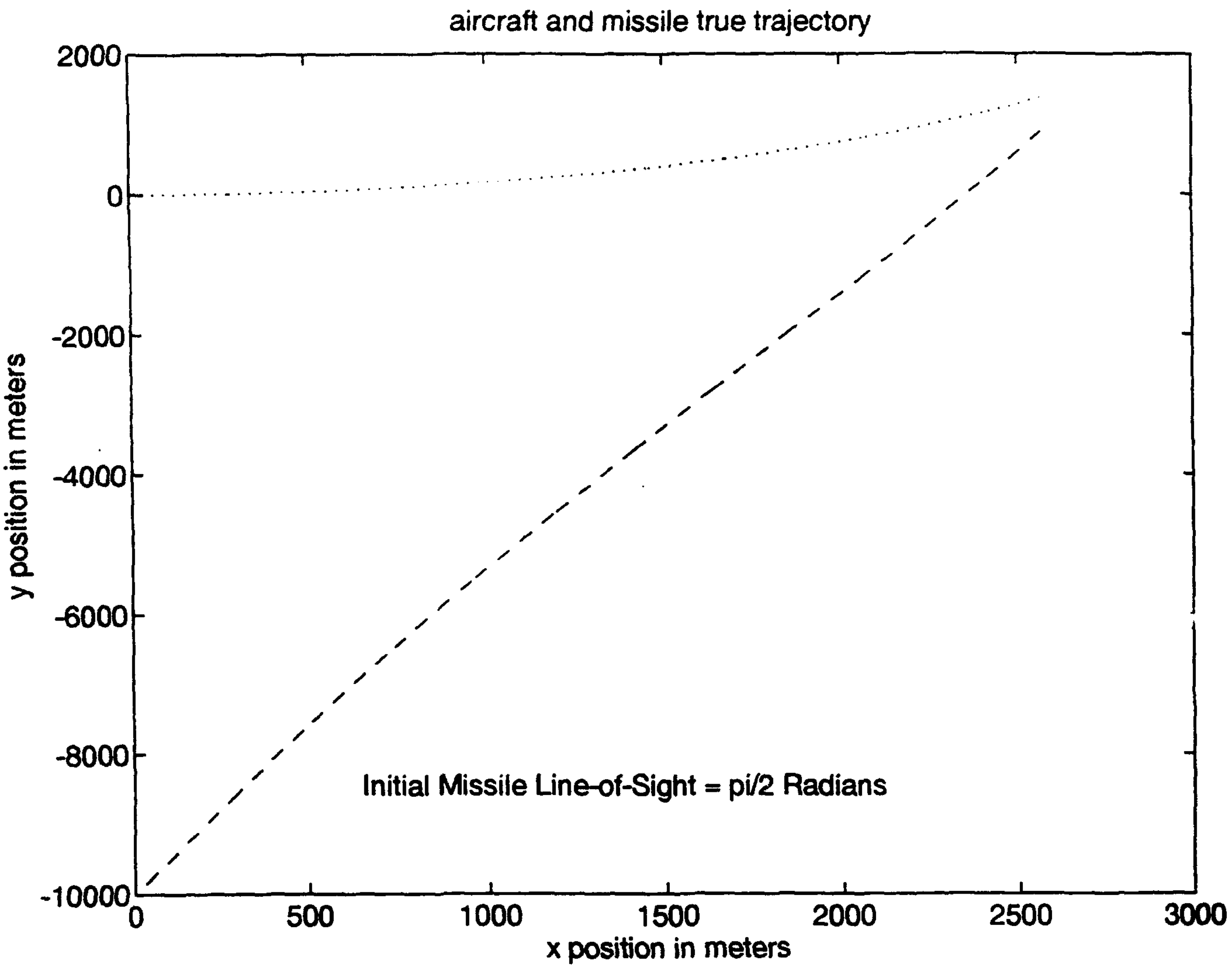

aircraft and missile true trajectory
2000
0
-2000
-4000
-6000
-8000
-10000
0
500
1000
1500
2000
2500
3000
x position in meters
y position in meters
Initial Missile Line-of-Sight = pi/2 Radians

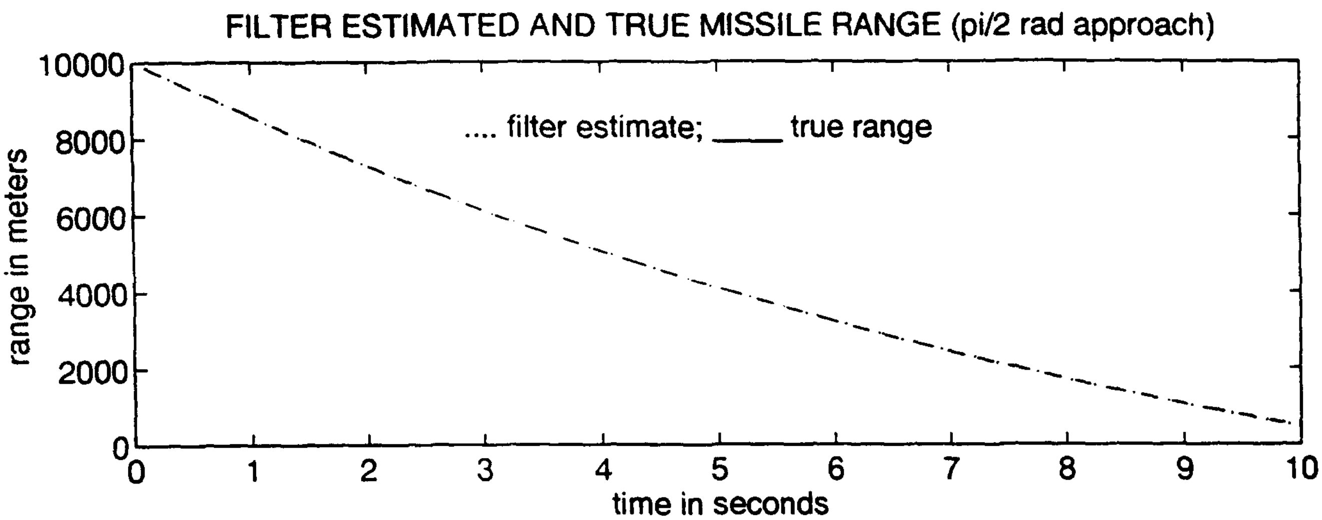
FILTER ESTIMATED AND TRUE MISSILE RANGE (pi/2 rad approach)
.... filter estimate; ____ true range
range in meters
time in seconds
10000
8000
6000
4000
2000
0
0
1
2
3
4
5
6
7
8
9
10

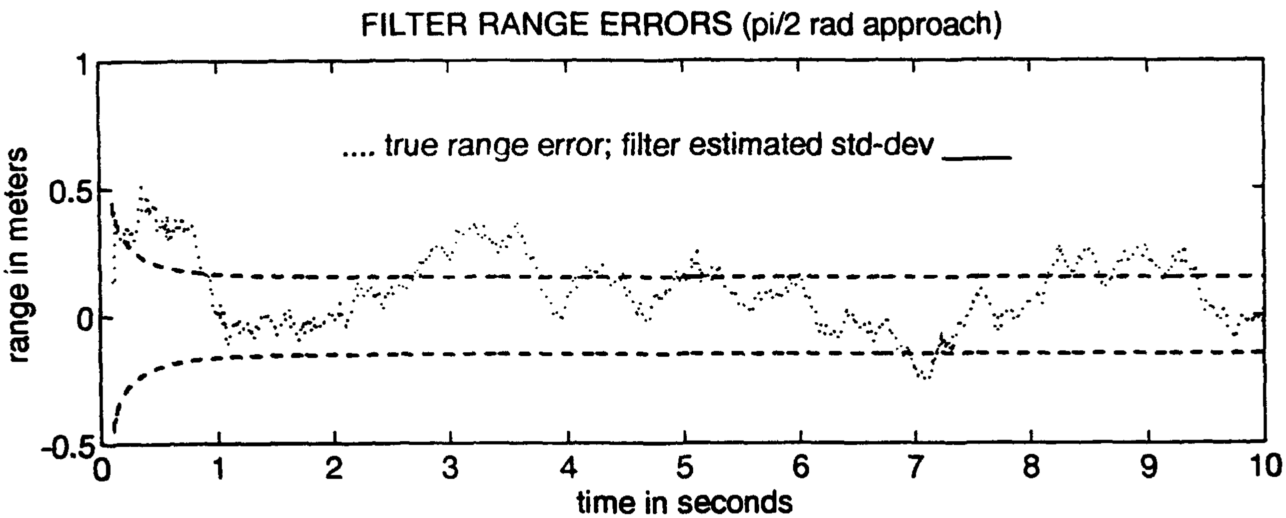
FILTER RANGE ERRORS (pi/2 rad approach)
.... true range error; filter estimated std-dev ____
range in meters
time in seconds
1
0.5
0
-0.5
0
1
2
3
4
5
6
7
8
9
10

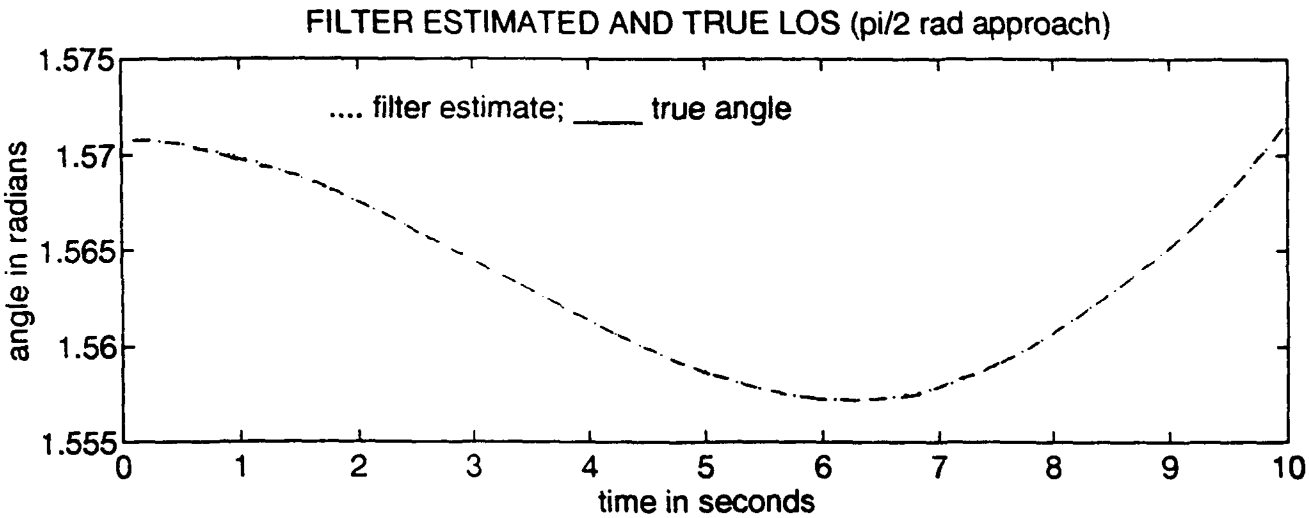

FILTER ESTIMATED AND TRUE LOS (pi/2 rad approach)
.... filter estimate; ____ true angle
angle in radians
1.575
1.57
1.565
1.56
1.555
0
1
2
3
4
5
6
7
8
9
10
time in seconds

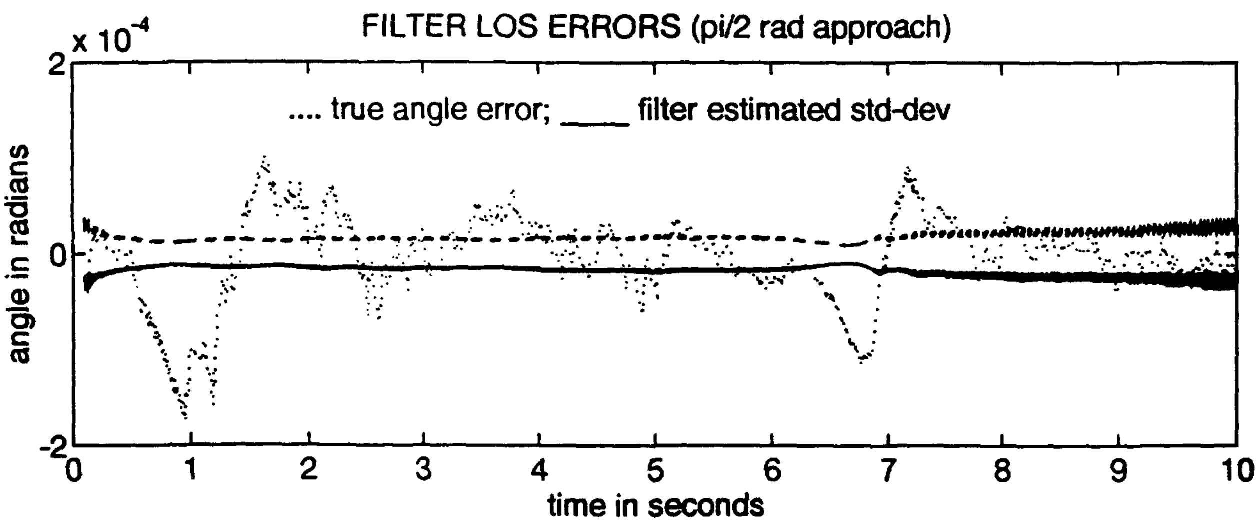

FILTER LOS ERRORS (pi/2 rad approach)
x 10^-4
.... true angle error; ____ filter estimated std-dev
angle in radians
2
0
-2
0
1
2
3
4
5
6
7
8
9
10
time in seconds

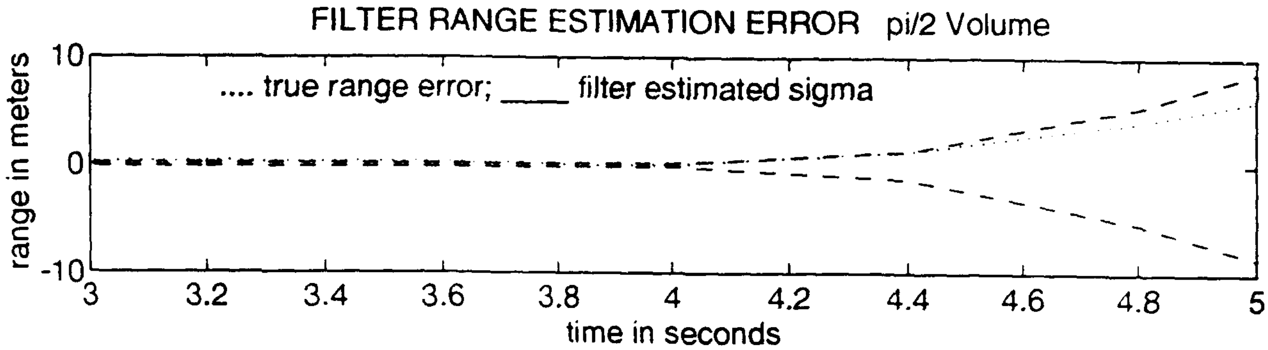
FILTER RANGE ESTIMATION ERROR pi/2 Volume
.... true range error; ____ filter estimated sigma
range in meters
10
0
-10
3
3.2
3.4
3.6
3.8
4
4.2
4.4
4.6
4.8
5
time in seconds

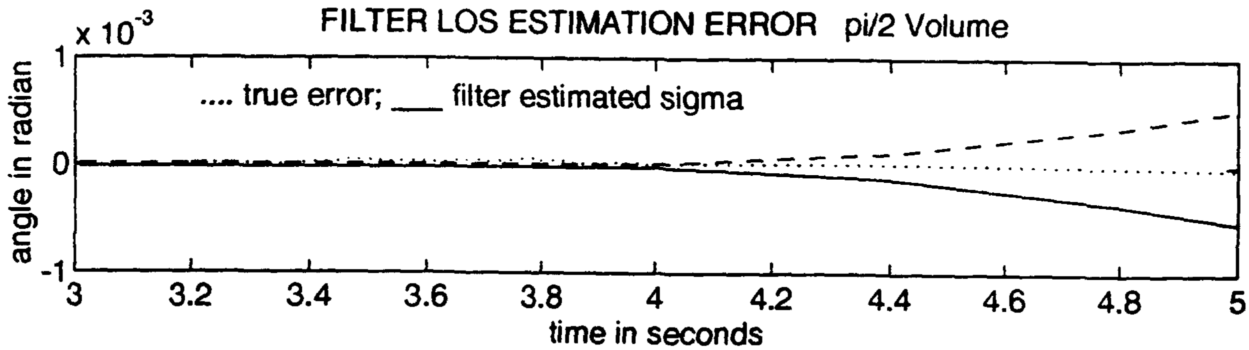
FILTER LOS ESTIMATION ERROR pi/2 Volume
x 10^-3
.... true error; ___ filter estimated sigma
angle in radian
1
0
-1
3
3.2
3.4
3.6
3.8
4
4.2
4.4
4.6
4.8
5
time in seconds

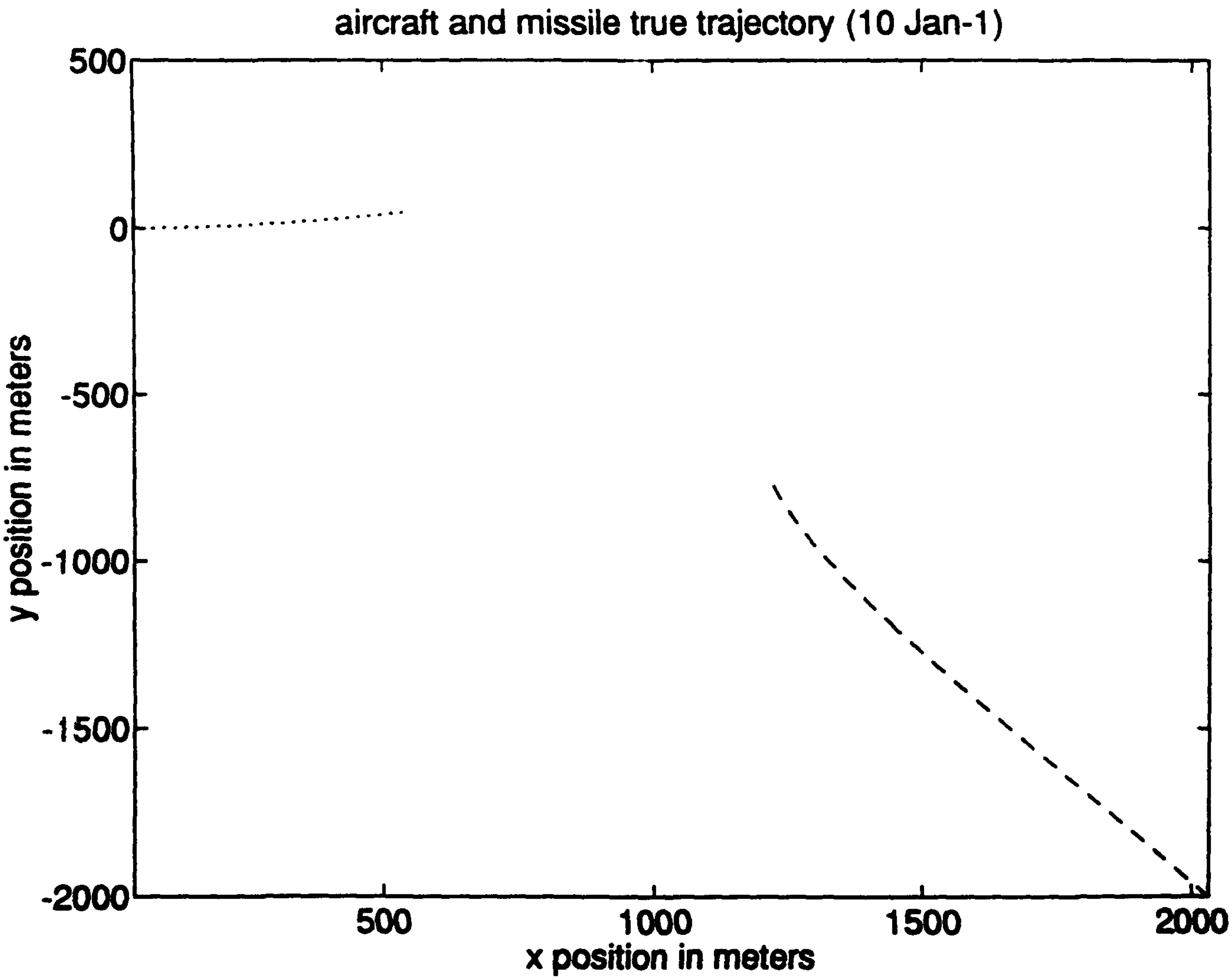
aircraft and missile true trajectory (10 Jan-1)
500
0
-500
-1000
-1500
-2000
y position in meters
500
1000
1500
2000
x position in meters

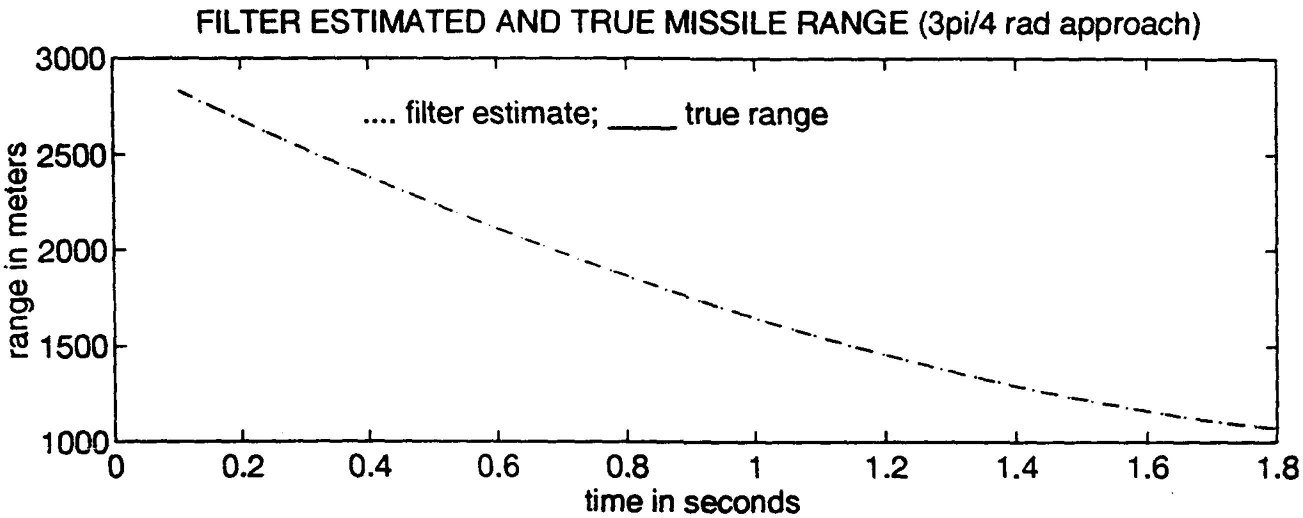
FILTER ESTIMATED AND TRUE MISSILE RANGE (3pi/4 rad approach)
.... filter estimate; ____ true range
range in meters
time in seconds
3000
2500
2000
1500
1000
0
0.2
0.4
0.6
0.8
1
1.2
1.4
1.6
1.8

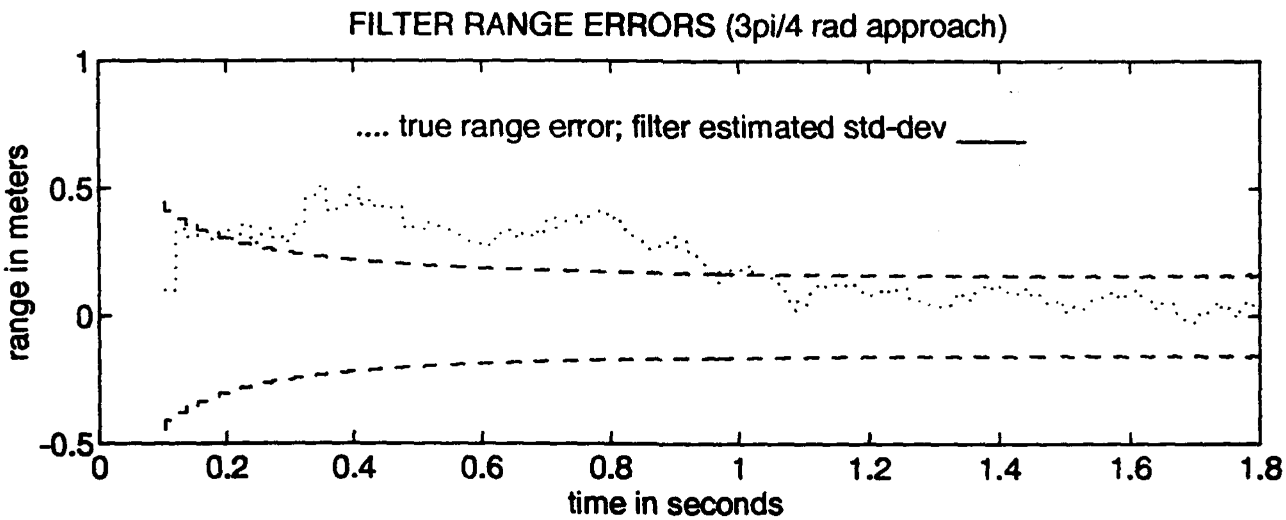
FILTER RANGE ERRORS (3pi/4 rad approach)
.... true range error; filter estimated std-dev ____
range in meters
time in seconds
1
0.5
0
-0.5
0
0.2
0.4
0.6
0.8
1
1.2
1.4
1.6
1.8

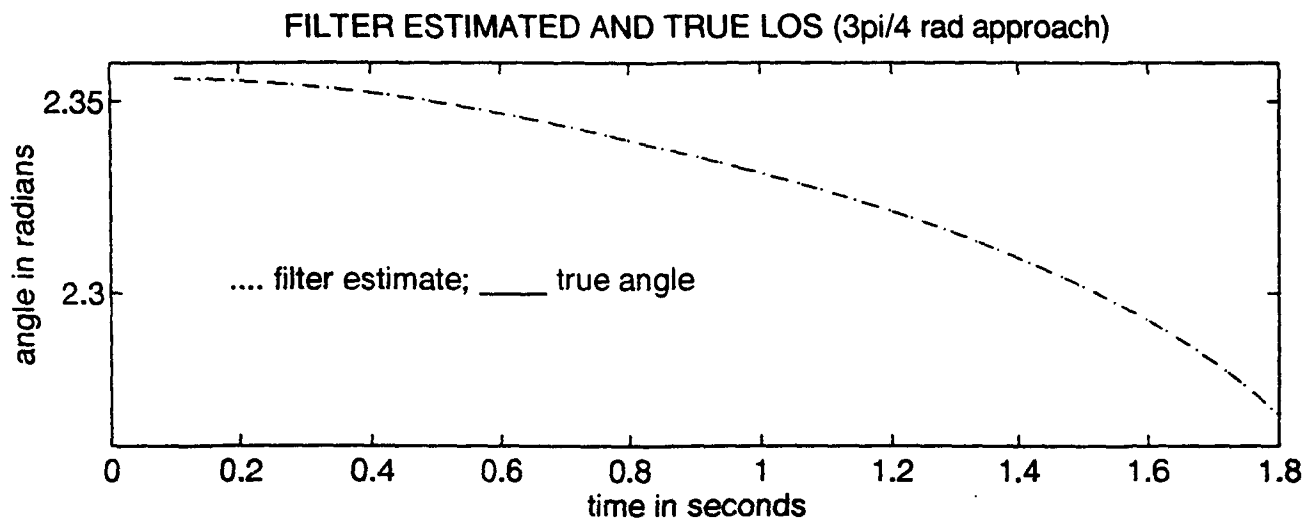
FILTER ESTIMATED AND TRUE LOS (3pi/4 rad approach)
2.35
2.3
angle in radians
.... filter estimate; ____ true angle
0
0.2
0.4
0.6
0.8
1
1.2
1.4
1.6
1.8
time in seconds

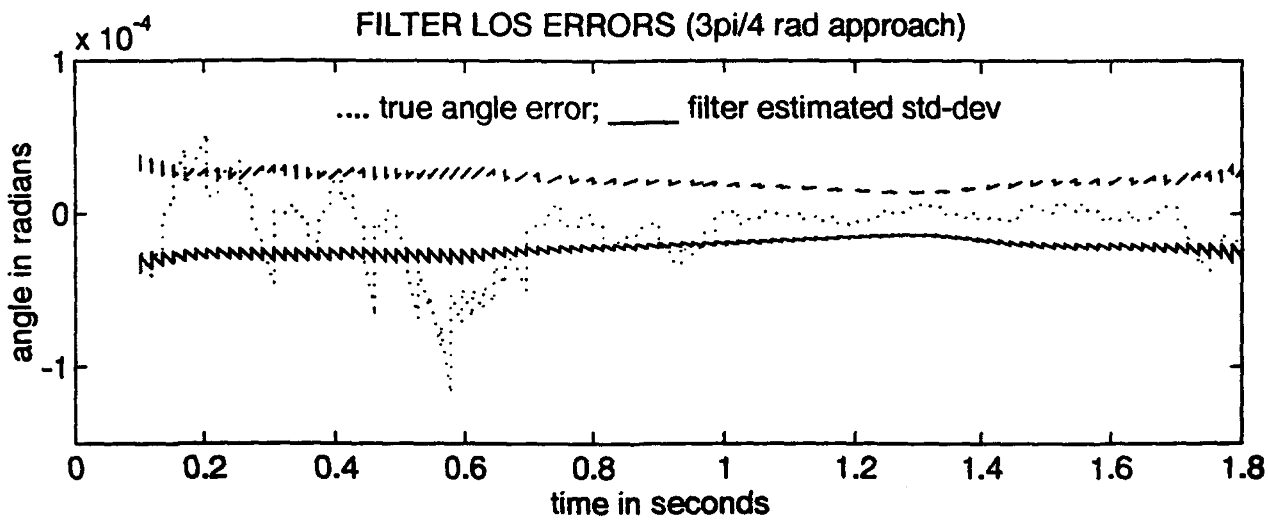
x 10^-4
FILTER LOS ERRORS (3pi/4 rad approach)
1
0
-1
angle in radians
.... true angle error; ____ filter estimated std-dev
0
0.2
0.4
0.6
0.8
1
1.2
1.4
1.6
1.8
time in seconds

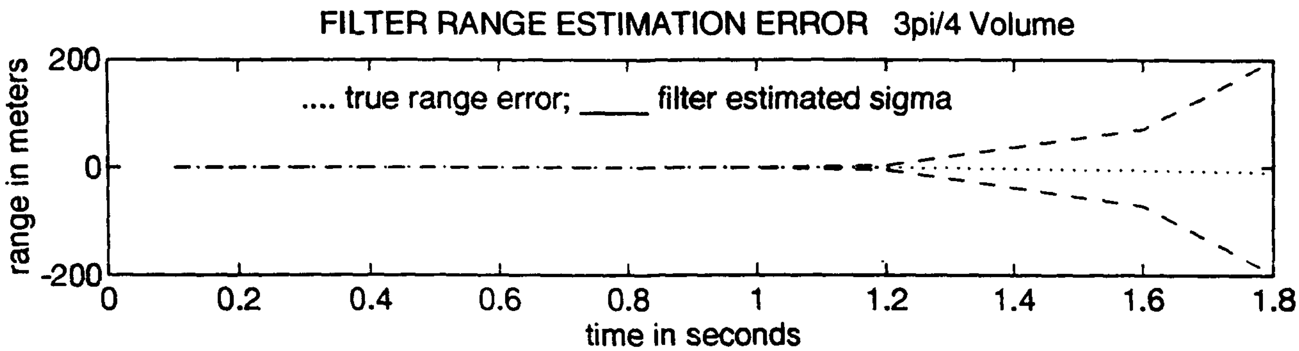

FILTER RANGE ESTIMATION ERROR 3pi/4 Volume
.... true range error; ____ filter estimated sigma
range in meters
200
0
-200
0
0.2
0.4
0.6
0.8
1
1.2
1.4
1.6
1.8
time in seconds

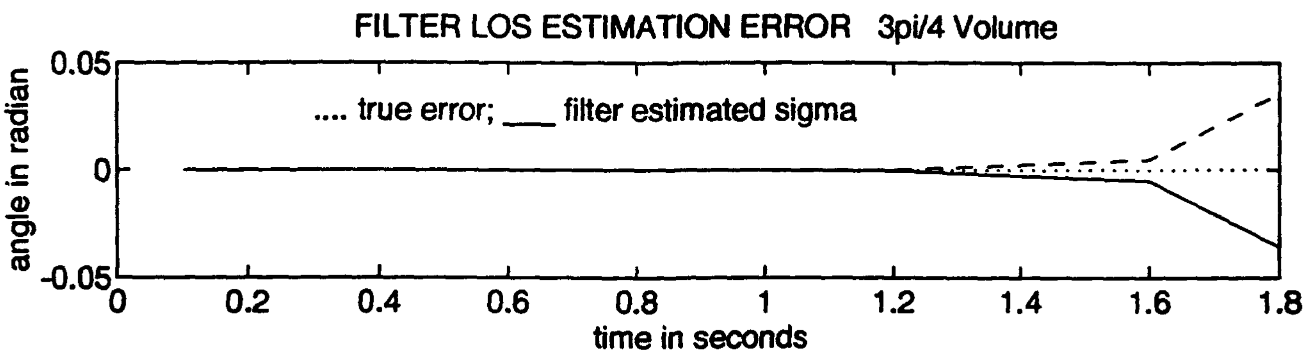

FILTER LOS ESTIMATION ERROR 3pi/4 Volume
.... true error; ___ filter estimated sigma
angle in radian
0.05
0
-0.05
0
0.2
0.4
0.6
0.8
1
1.2
1.4
1.6
1.8
time in seconds

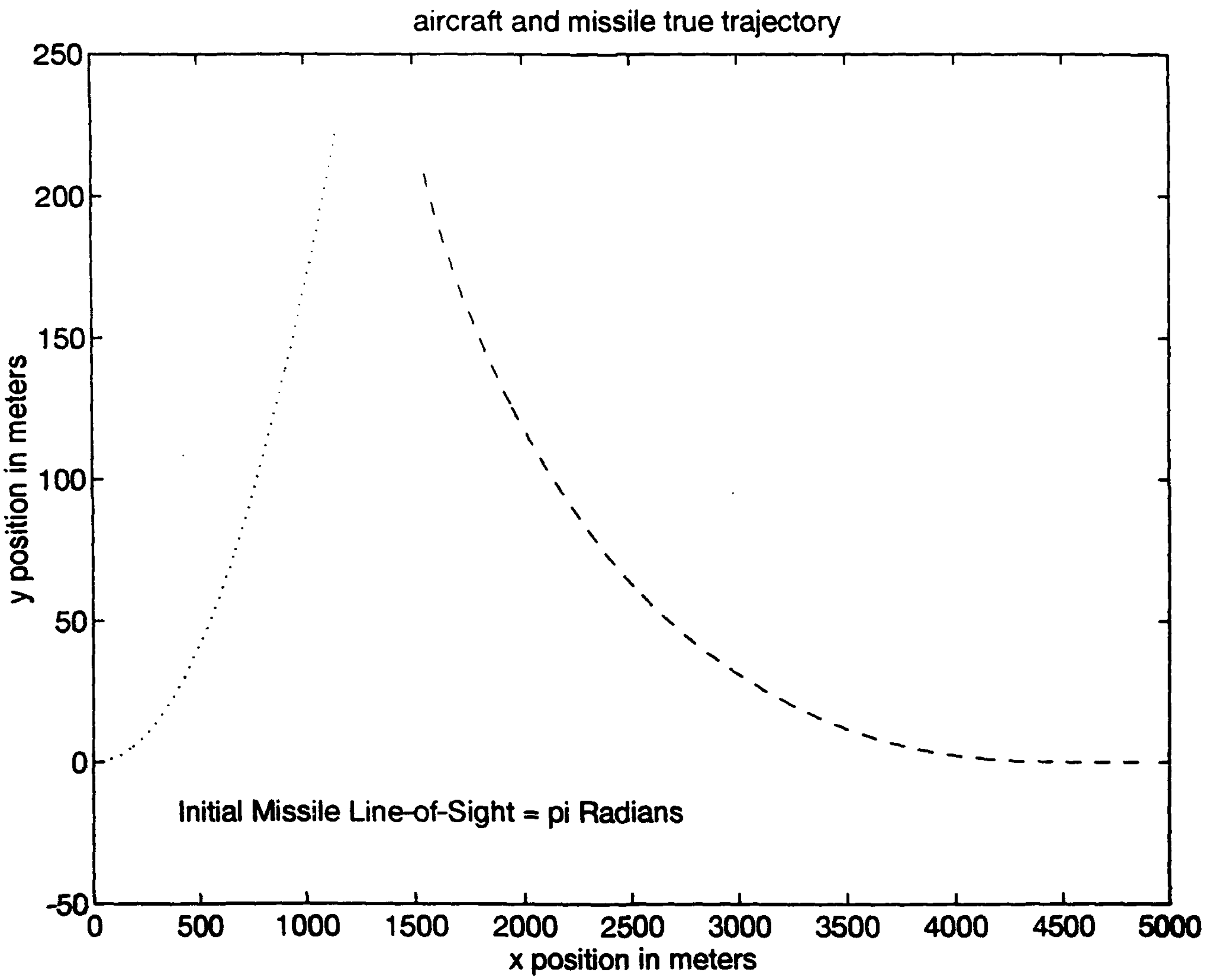
aircraft and missile true trajectory
250
200
150
100
50
0
-50
y position in meters
0
500
1000
1500
2000
2500
3000
3500
4000
4500
5000
x position in meters
Initial Missile Line-of-Sight = pi Radians

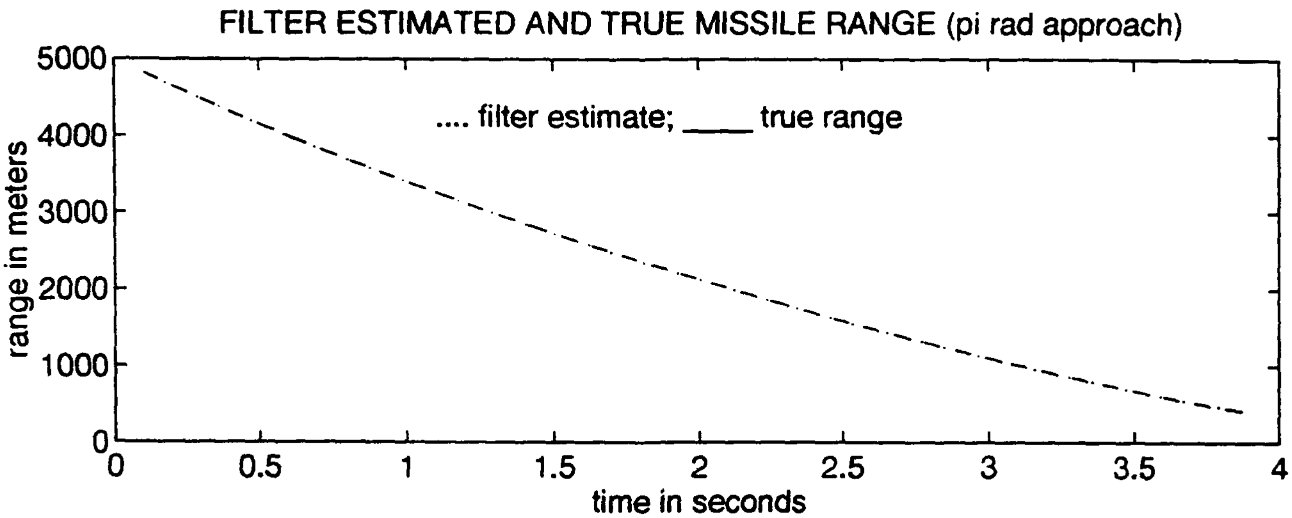
FILTER ESTIMATED AND TRUE MISSILE RANGE (pi rad approach)
.... filter estimate; ____ true range
range in meters
5000
4000
3000
2000
1000
0
0
0.5
1
1.5
2
2.5
3
3.5
4
time in seconds

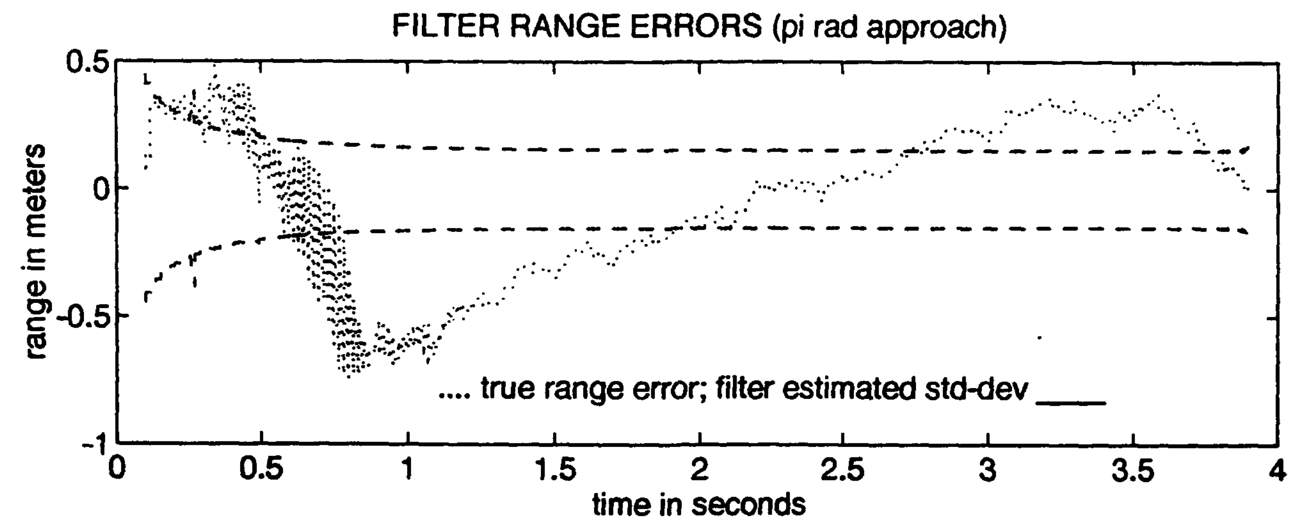
FILTER RANGE ERRORS (pi rad approach)
.... true range error; filter estimated std-dev ____
range in meters
0.5
0
-0.5
-1
0
0.5
1
1.5
2
2.5
3
3.5
4
time in seconds

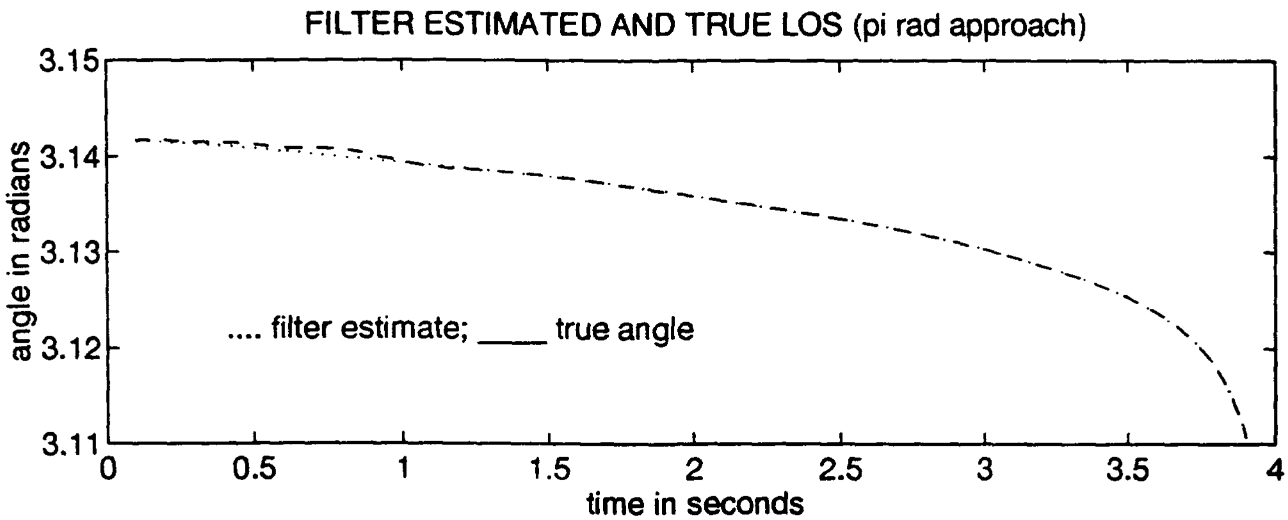
FILTER ESTIMATED AND TRUE LOS (pi rad approach)
angle in radians
3.15
3.14
3.13
3.12
3.11
.... filter estimate; _____ true angle
0
0.5
1
1.5
2
2.5
3
3.5
4
time in seconds

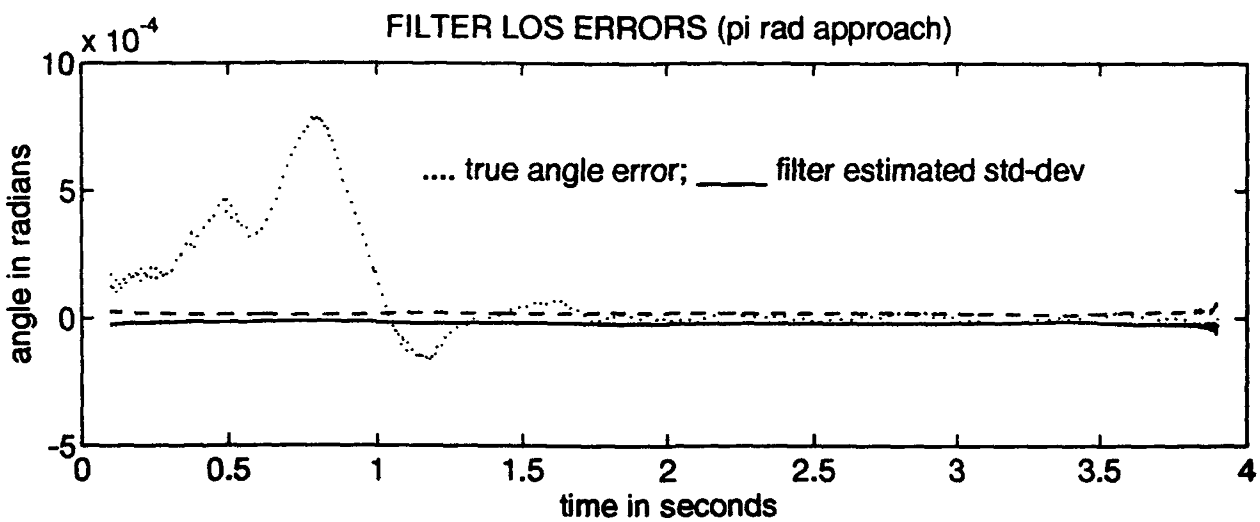
FILTER LOS ERRORS (pi rad approach)
x 10^-4
10
5
0
-5
angle in radians
.... true angle error; _____ filter estimated std-dev
0
0.5
1
1.5
2
2.5
3
3.5
4
time in seconds

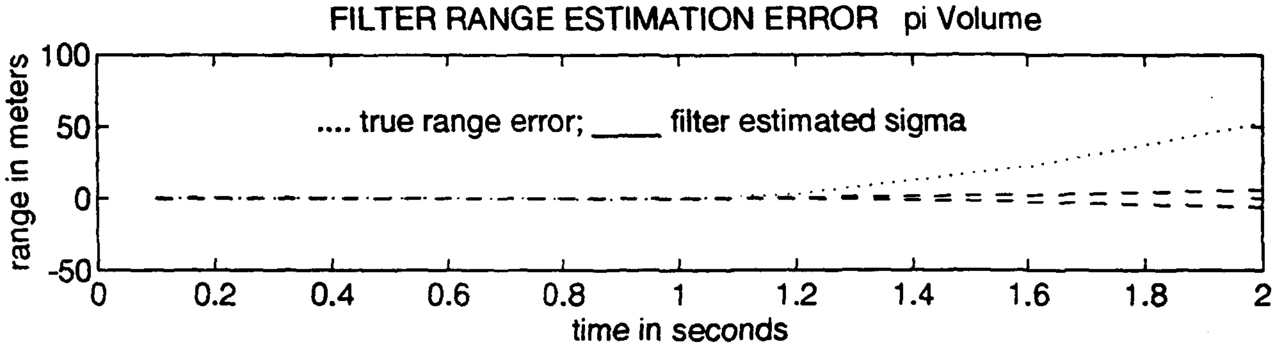
FILTER RANGE ESTIMATION ERROR pi Volume
.... true range error; ____ filter estimated sigma
range in meters
100
50
0
-50
0
0.2
0.4
0.6
0.8
1
1.2
1.4
1.6
1.8
2
time in seconds

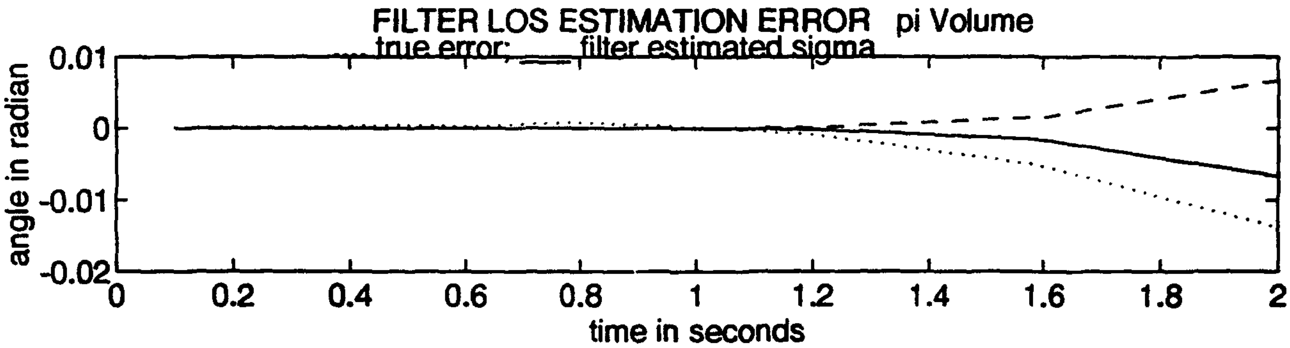
FILTER LOS ESTIMATION ERROR pi Volume
.... true error; ____ filter estimated sigma
angle in radian
0.01
0
-0.01
-0.02
0
0.2
0.4
0.6
0.8
1
1.2
1.4
1.6
1.8
2
time in seconds

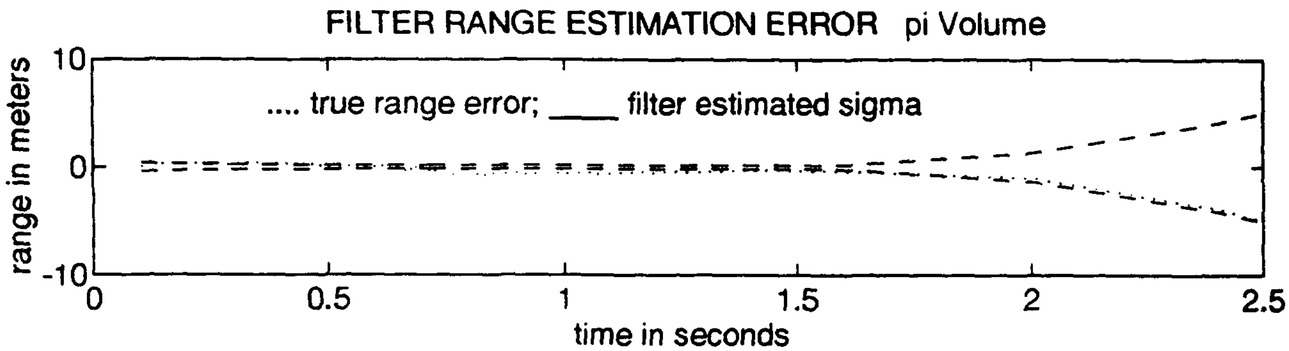
FILTER RANGE ESTIMATION ERROR pi Volume
.... true range error; ____ filter estimated sigma
range in meters
10
0
-10
0
0.5
1
1.5
2
2.5
time in seconds

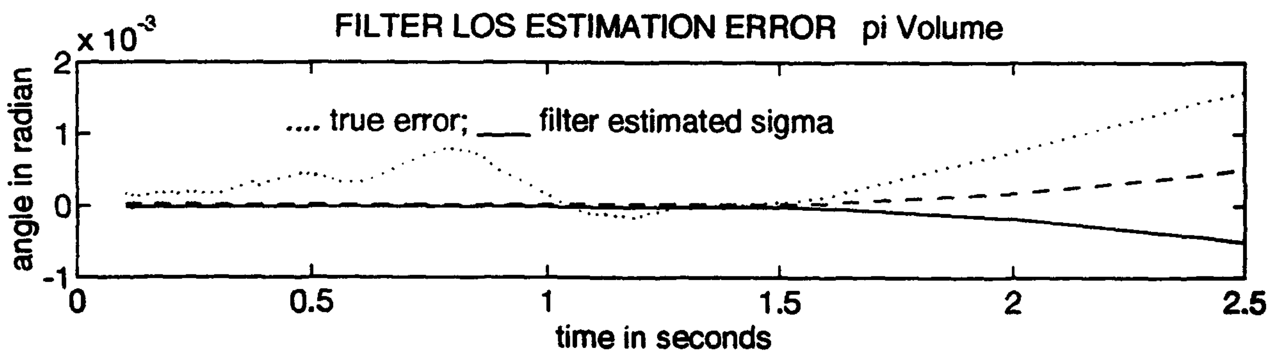
FILTER LOS ESTIMATION ERROR pi Volume
x 10^-3
.... true error; ___ filter estimated sigma
angle in radian
2
1
0
-1
0
0.5
1
1.5
2
2.5
time in seconds

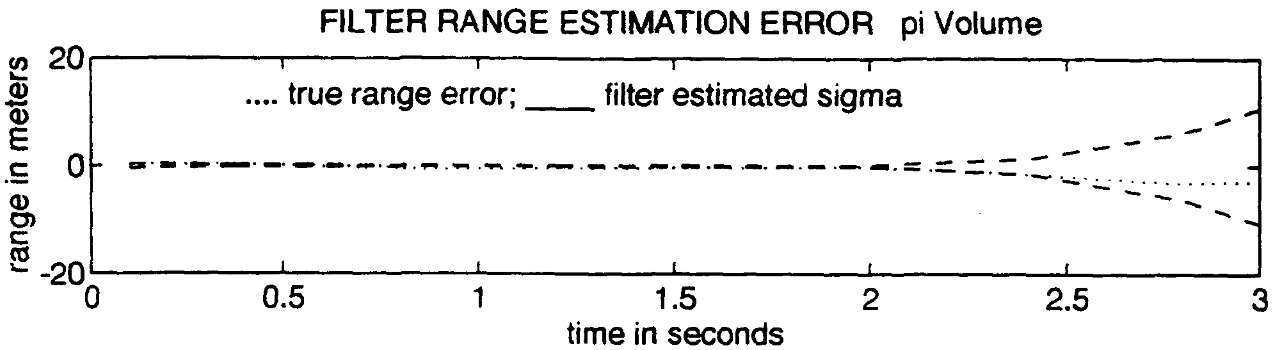
FILTER RANGE ESTIMATION ERROR pi Volume
.... true range error; ____ filter estimated sigma
range in meters
20
0
-20
0
0.5
1
1.5
2
2.5
3
time in seconds

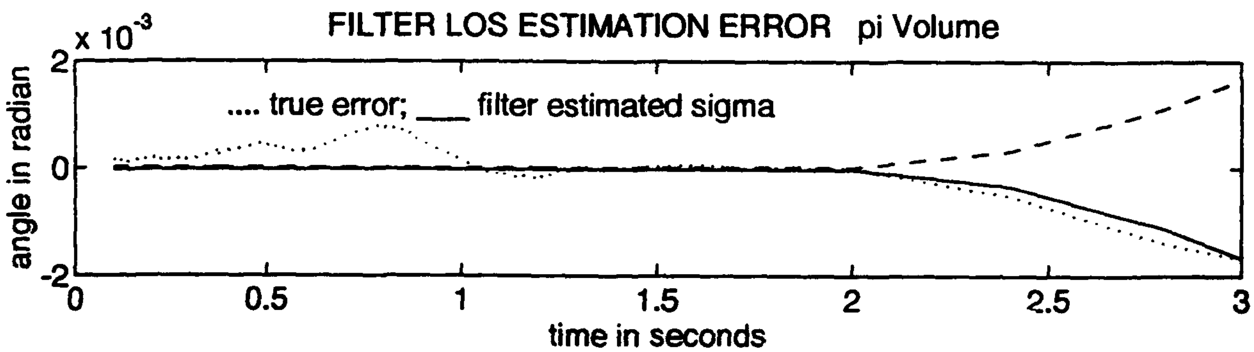
FILTER LOS ESTIMATION ERROR pi Volume
x 10-3
.... true error; ___ filter estimated sigma
angle in radian
2
0
-2
0
0.5
1
1.5
2
2.5
3
time in seconds

FILTER RANGE ESTIMATION ERROR pi Volume

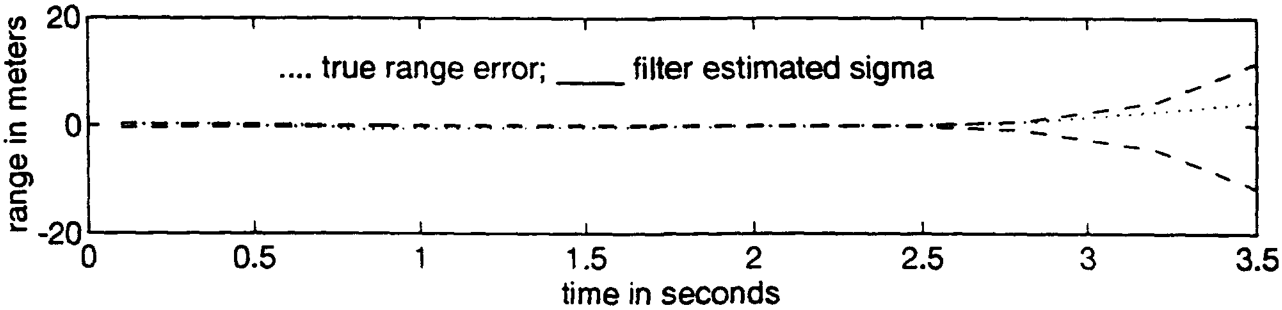

FILTER LOS ESTIMATION ERROR pi Volume

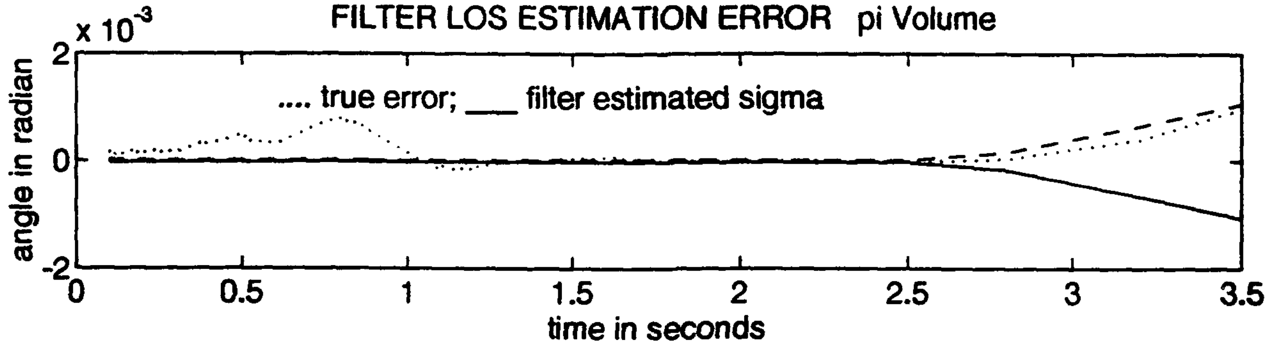

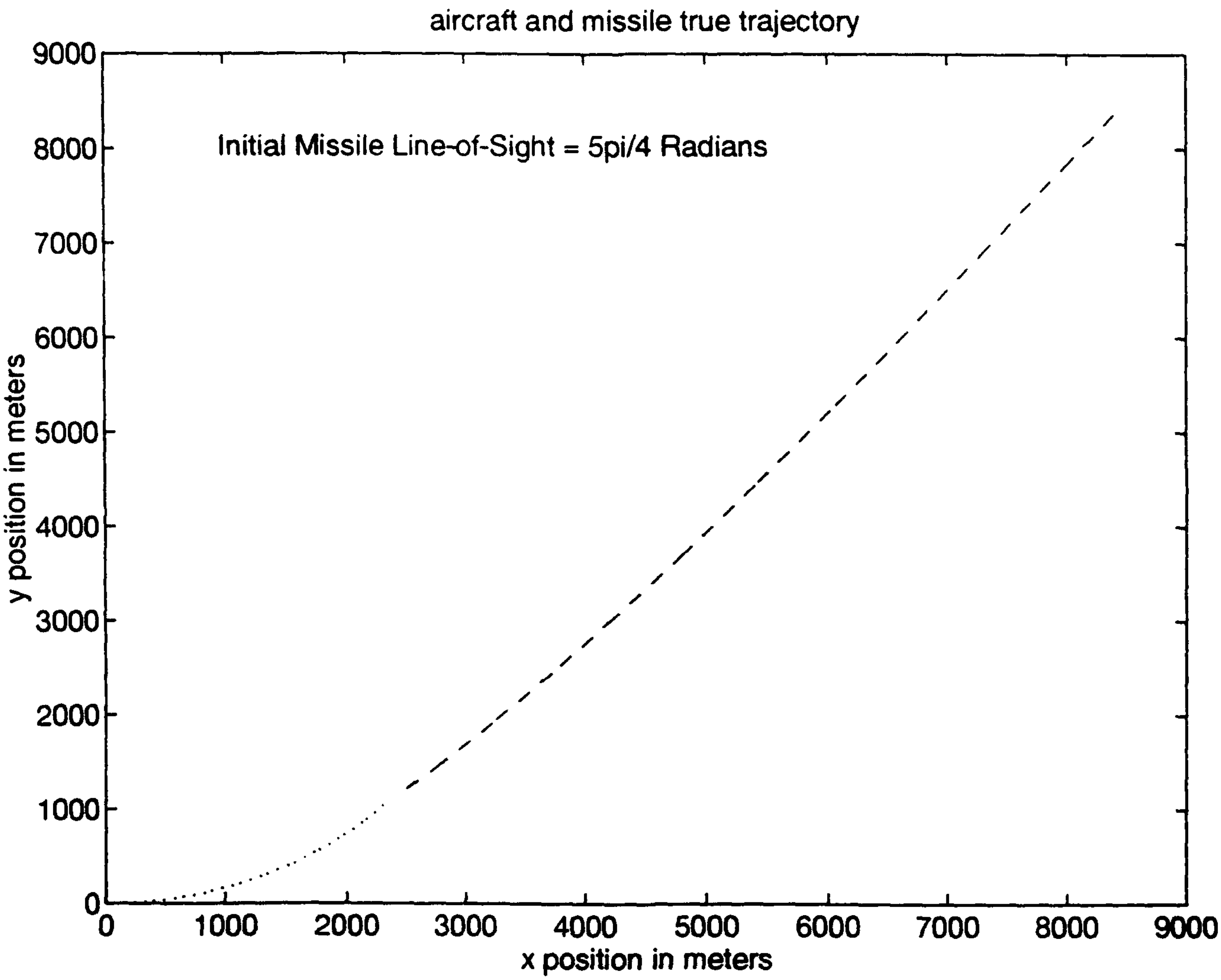
aircraft and missile true trajectory
Initial Missile Line-of-Sight = 5pi/4 Radians
y position in meters
x position in meters
0
1000
2000
3000
4000
5000
6000
7000
8000
9000

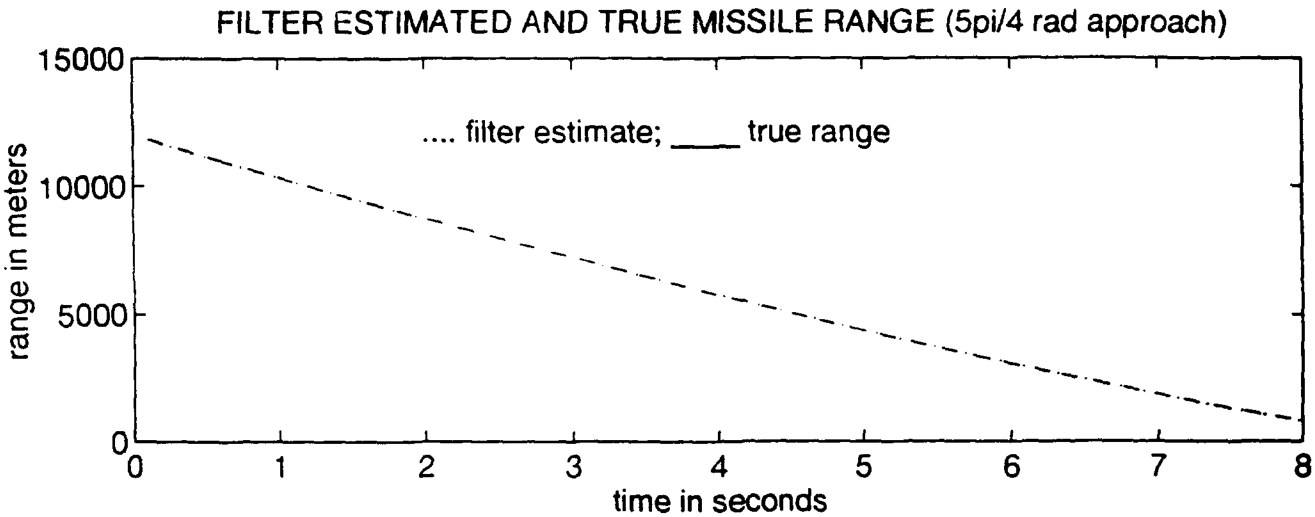
FILTER ESTIMATED AND TRUE MISSILE RANGE (5pi/4 rad approach)
.... filter estimate; ____ true range
range in meters
time in seconds
15000
10000
5000
0
0
1
2
3
4
5
6
7
8

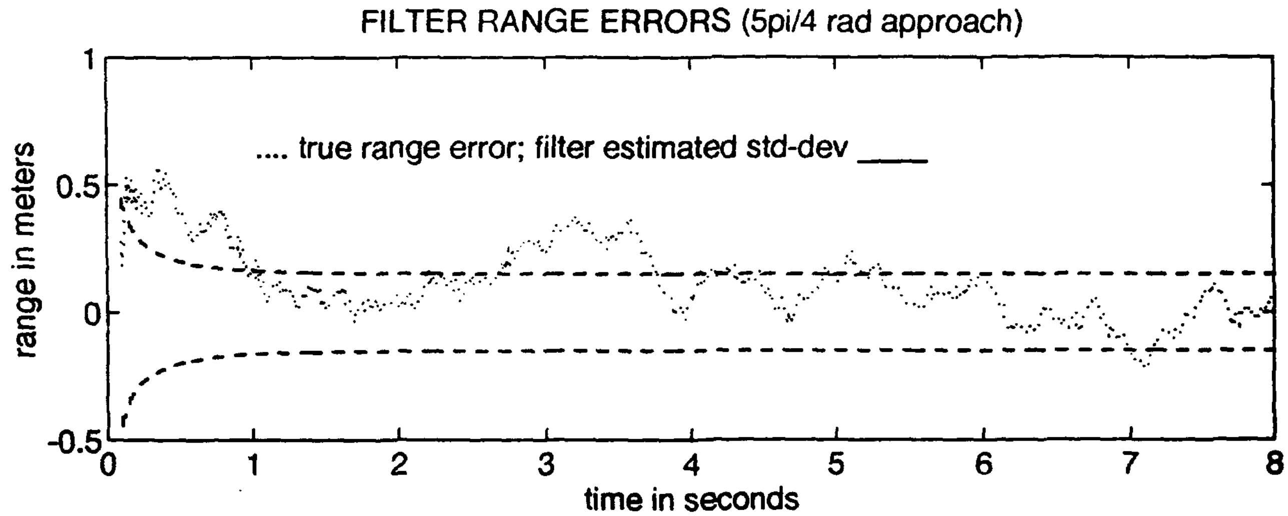
FILTER RANGE ERRORS (5pi/4 rad approach)
.... true range error; filter estimated std-dev ____
range in meters
time in seconds
1
0.5
0
-0.5
0
1
2
3
4
5
6
7
8

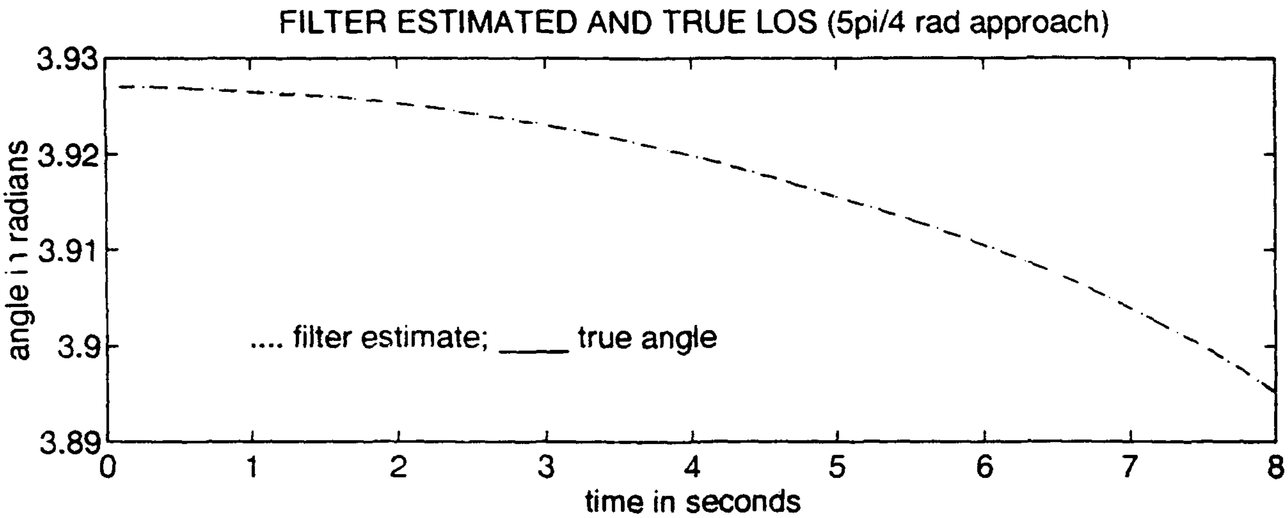
FILTER ESTIMATED AND TRUE LOS (5pi/4 rad approach)
3.93
3.92
3.91
3.9
3.89
angle in radians
.... filter estimate; ____ true angle
0
1
2
3
4
5
6
7
8
time in seconds

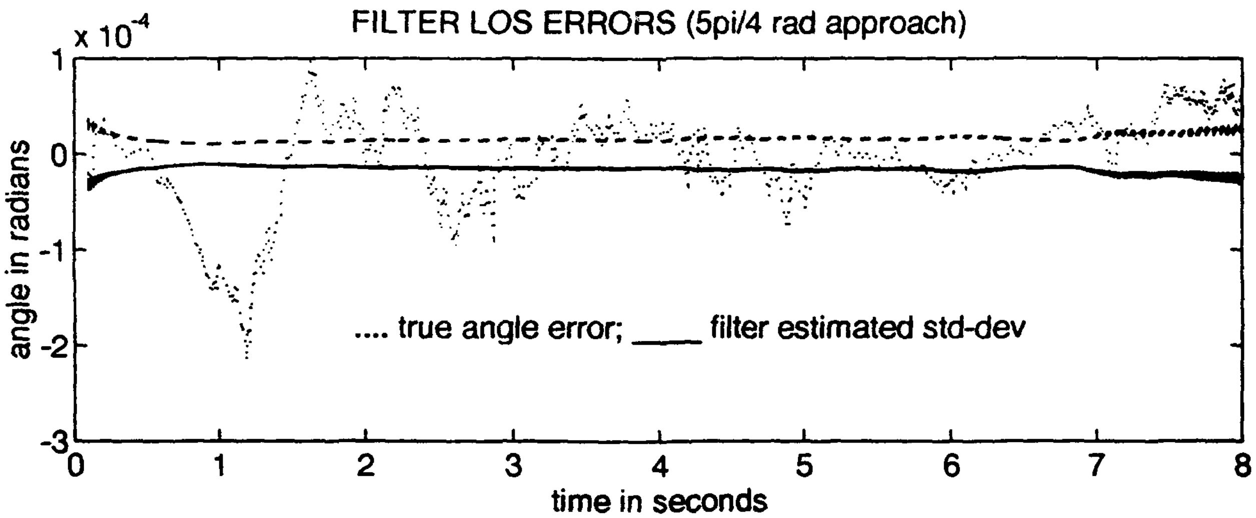
FILTER LOS ERRORS (5pi/4 rad approach)
x 10^-4
1
0
-1
-2
-3
angle in radians
.... true angle error; ____ filter estimated std-dev
0
1
2
3
4
5
6
7
8
time in seconds

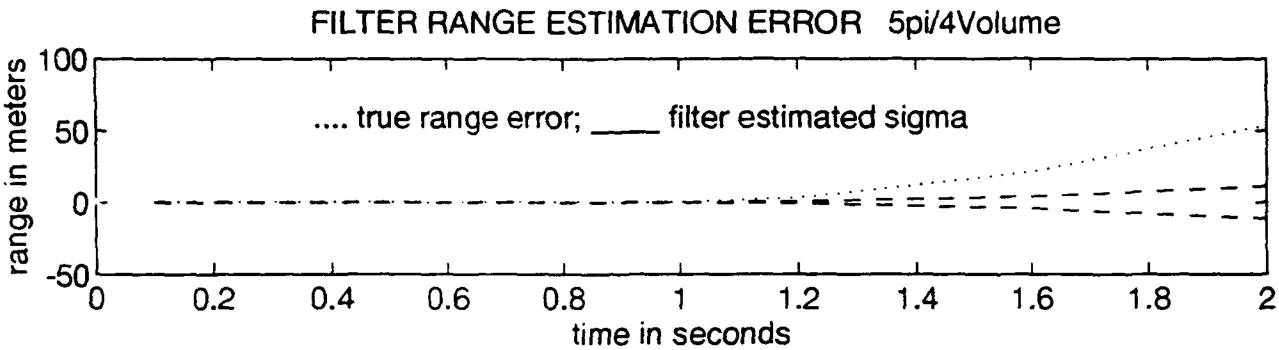
FILTER RANGE ESTIMATION ERROR 5pi/4Volume
.... true range error; ____ filter estimated sigma
range in meters
100
50
0
-50
0
0.2
0.4
0.6
0.8
1
1.2
1.4
1.6
1.8
2
time in seconds

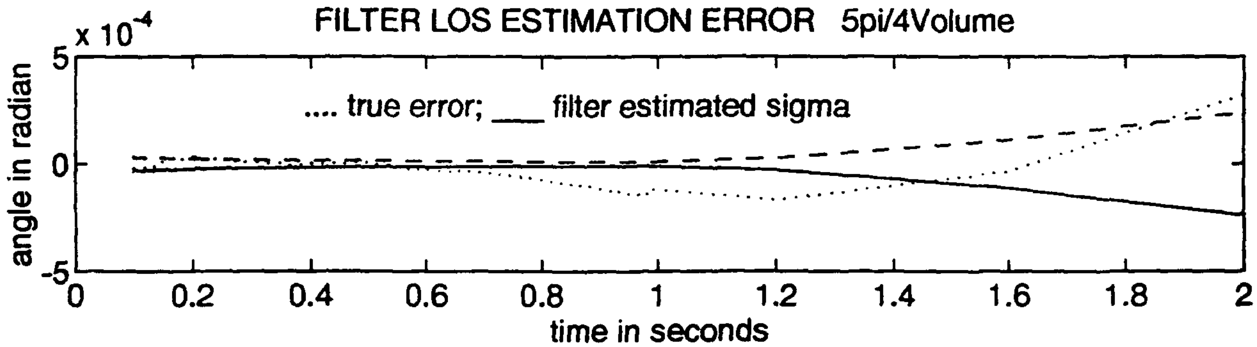
FILTER LOS ESTIMATION ERROR 5pi/4Volume
x 10^-4
.... true error; ___ filter estimated sigma
angle in radian
5
0
-5
0
0.2
0.4
0.6
0.8
1
1.2
1.4
1.6
1.8
2
time in seconds

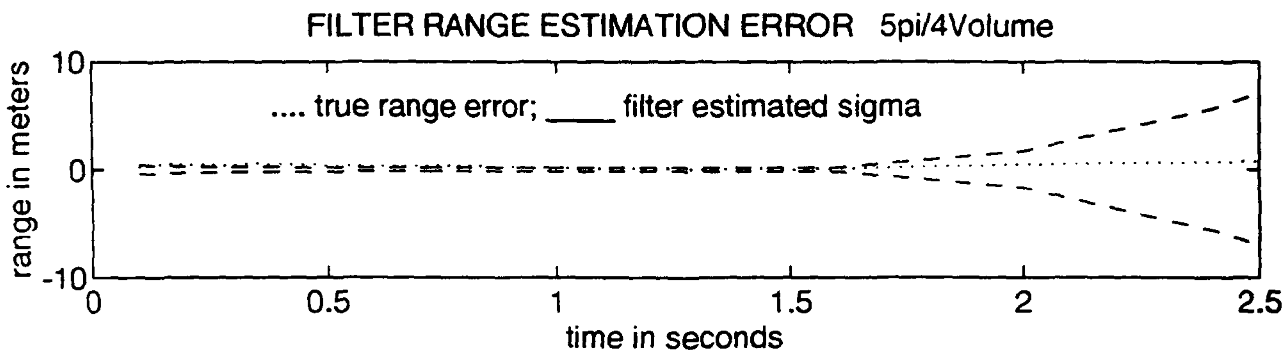
FILTER RANGE ESTIMATION ERROR 5pi/4Volume
.... true range error; ____ filter estimated sigma
range in meters
10
0
-10
0
0.5
1
1.5
2
2.5
time in seconds

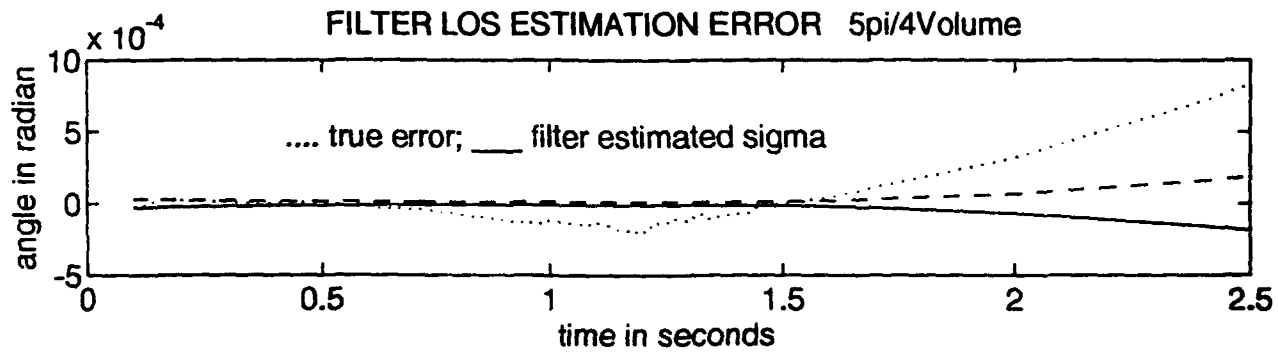
FILTER LOS ESTIMATION ERROR 5pi/4Volume
x 10^-4
.... true error; ___ filter estimated sigma
angle in radian
10
5
0
-5
0
0.5
1
1.5
2
2.5
time in seconds

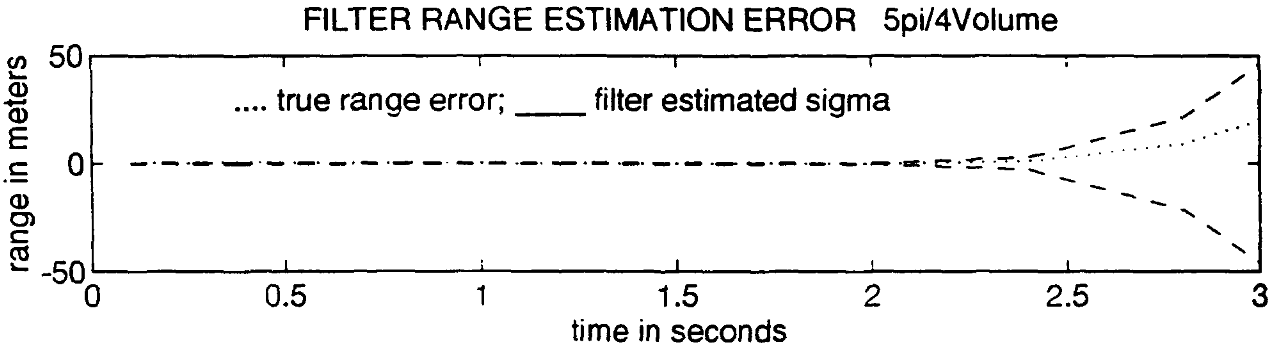

FILTER RANGE ESTIMATION ERROR 5pi/4Volume
.... true range error; ____ filter estimated sigma
range in meters
50
0
-50
0
0.5
1
1.5
2
2.5
3
time in seconds

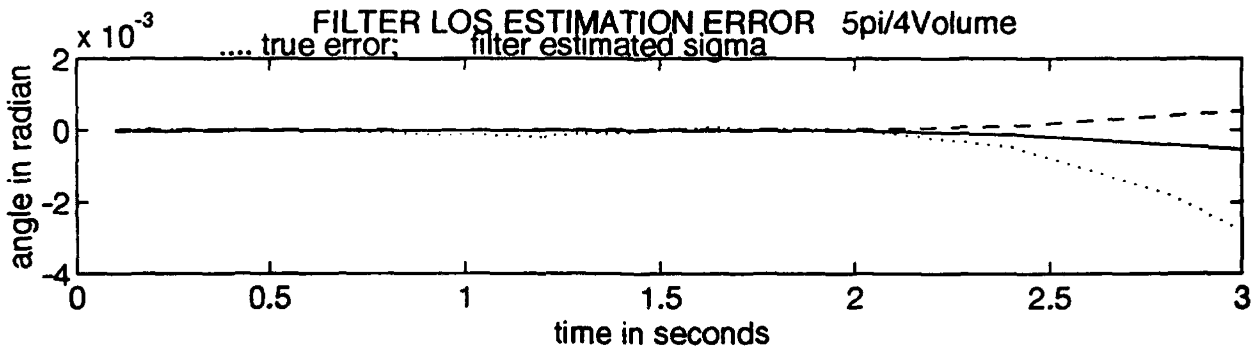

FILTER LOS ESTIMATION ERROR 5pi/4Volume
x 10^-3
.... true error; filter estimated sigma
angle in radian
2
0
-2
-4
0
0.5
1
1.5
2
2.5
3
time in seconds

FILTER RANGE ESTIMATION ERROR 5pi/4Volume

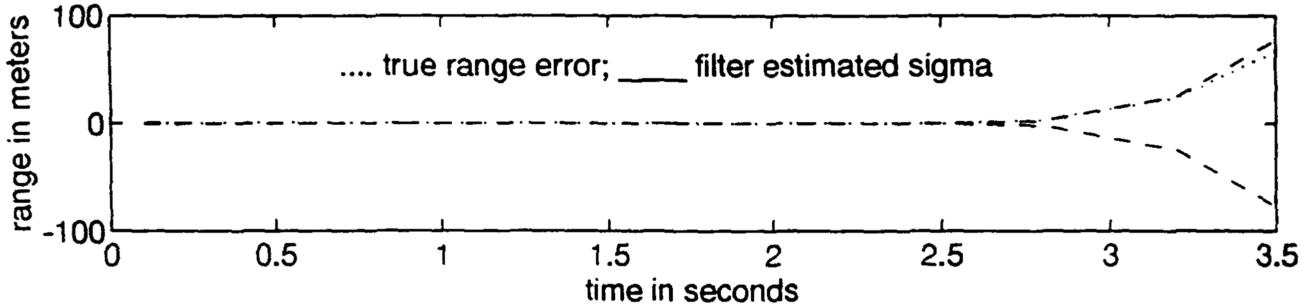

FILTER LOS ESTIMATION ERROR 5pi/4Volume

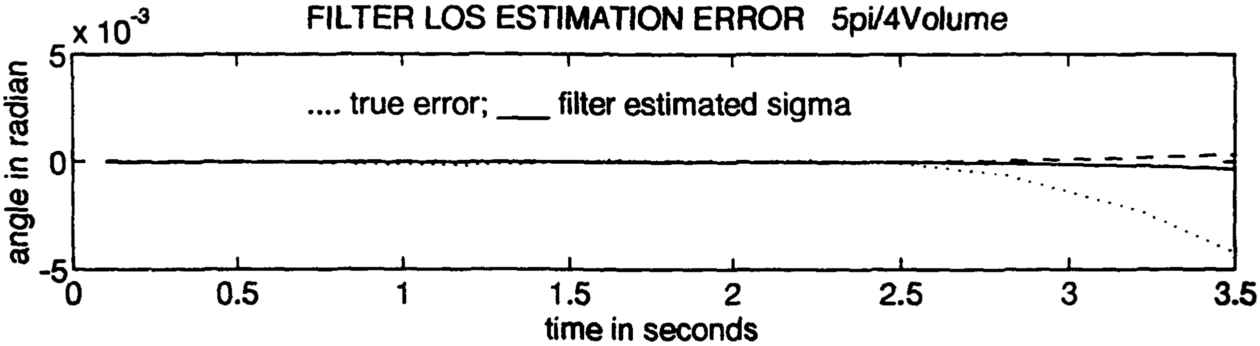

FILTER RANGE ESTIMATION ERROR 5pi/4Volume

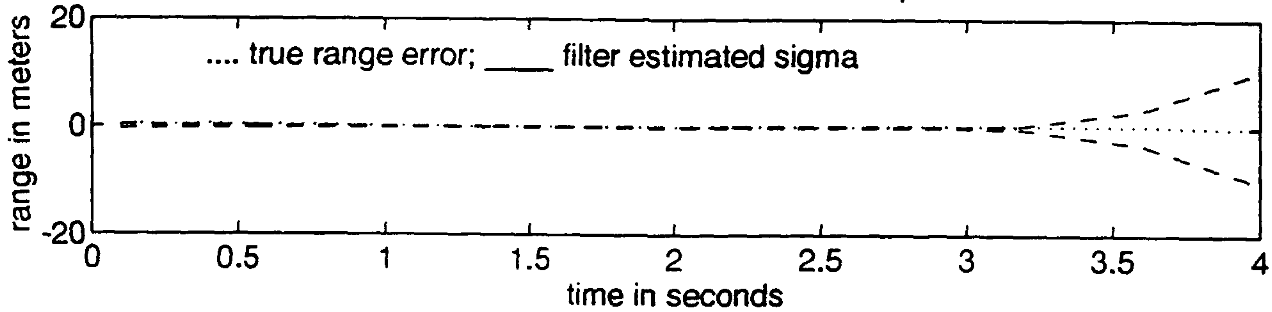

FILTER LOS ESTIMATION ERROR 5pi/4Volume

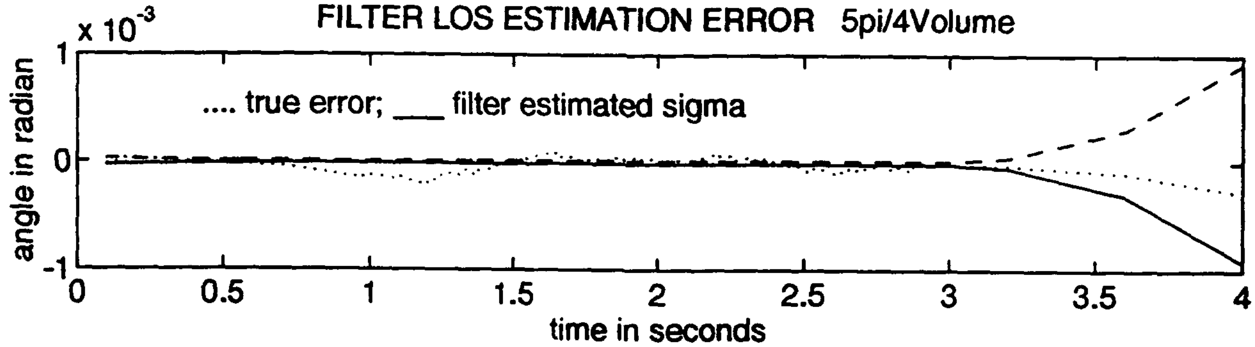

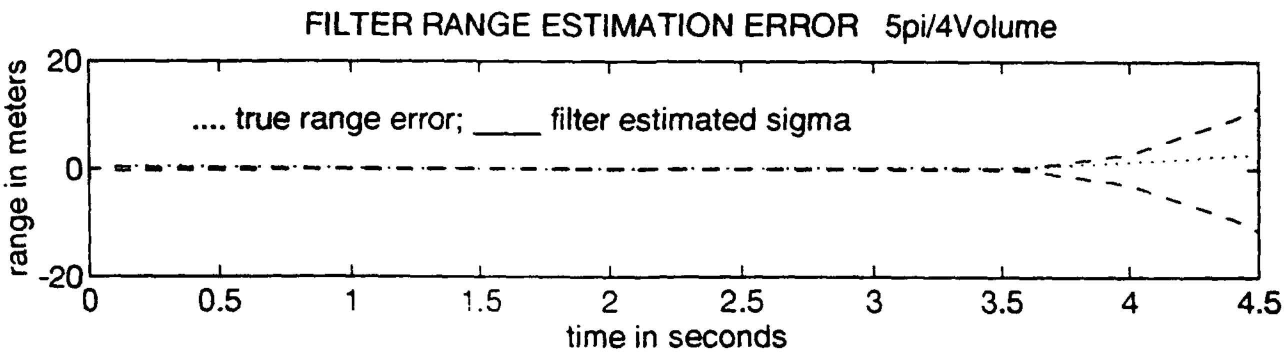
FILTER RANGE ESTIMATION ERROR 5pi/4Volume
.... true range error; ____ filter estimated sigma
range in meters
20
0
-20
0
0.5
1
1.5
2
2.5
3
3.5
4
4.5
time in seconds

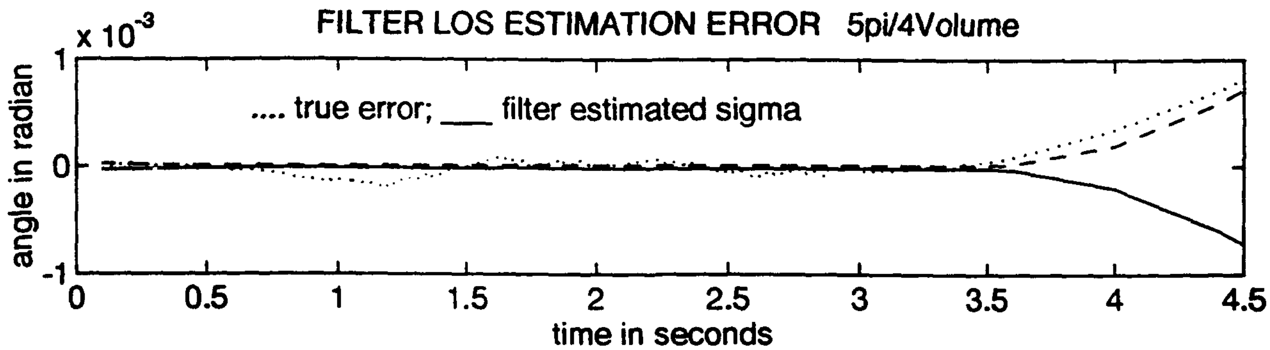
FILTER LOS ESTIMATION ERROR 5pi/4Volume
x 10^-3
.... true error; ___ filter estimated sigma
angle in radian
1
0
-1
0
0.5
1
1.5
2
2.5
3
3.5
4
4.5
time in seconds

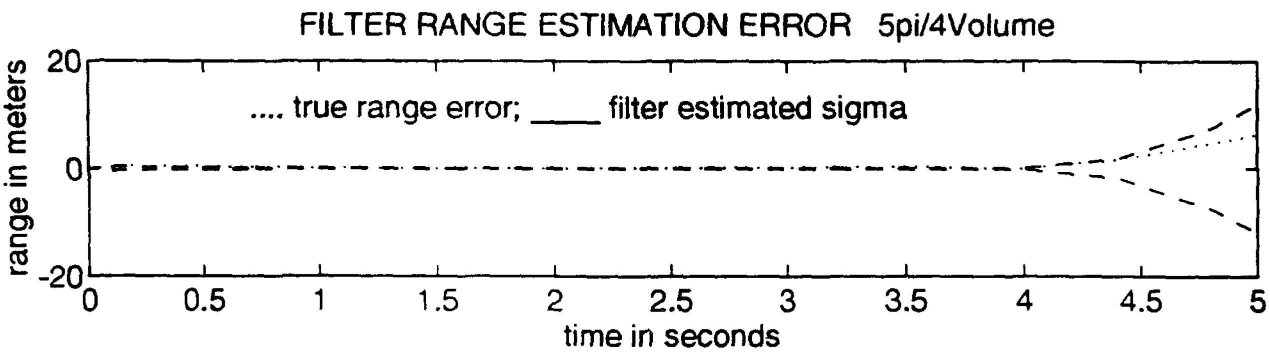
FILTER RANGE ESTIMATION ERROR 5pi/4Volume
.... true range error; ____ filter estimated sigma
range in meters
20
0
-20
0
0.5
1
1.5
2
2.5
3
3.5
4
4.5
5
time in seconds

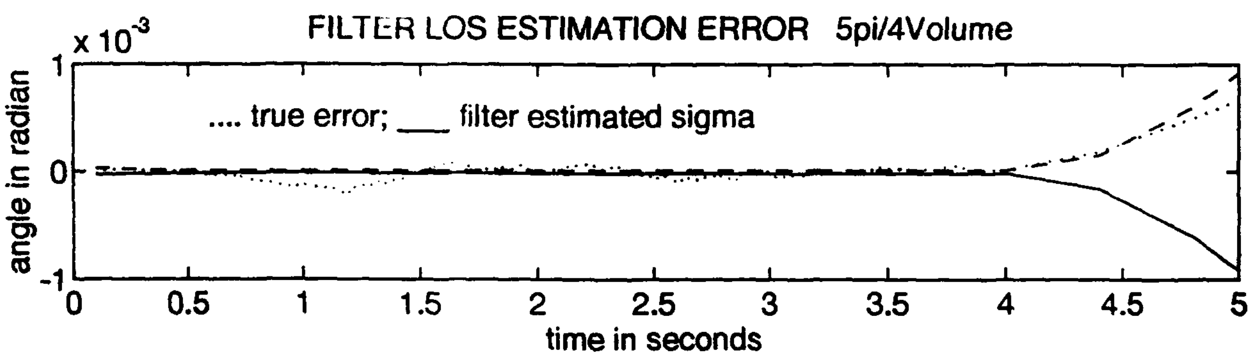
FILTER LOS ESTIMATION ERROR 5pi/4Volume
x 10-3
.... true error; ___ filter estimated sigma
angle in radian
1
0
-1
0
0.5
1
1.5
2
2.5
3
3.5
4
4.5
5
time in seconds

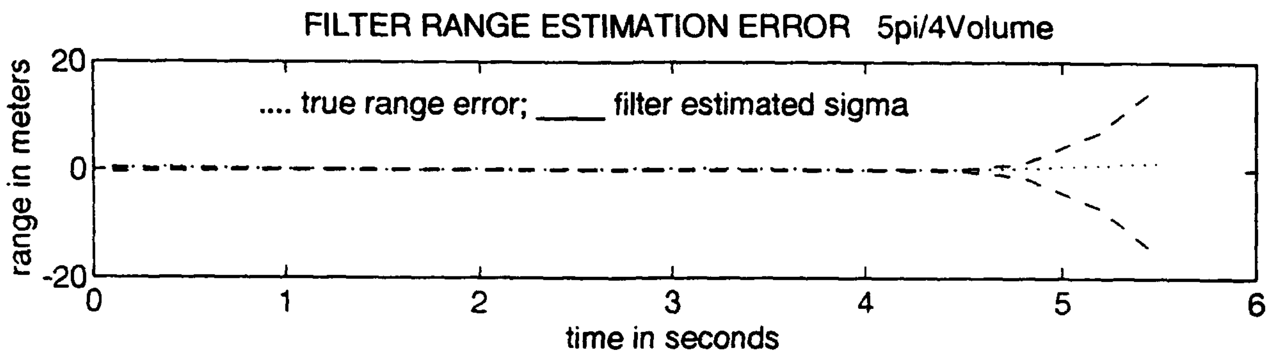
FILTER RANGE ESTIMATION ERROR 5pi/4Volume
.... true range error; ____ filter estimated sigma
range in meters
20
0
-20
0
1
2
3
4
5
6
time in seconds

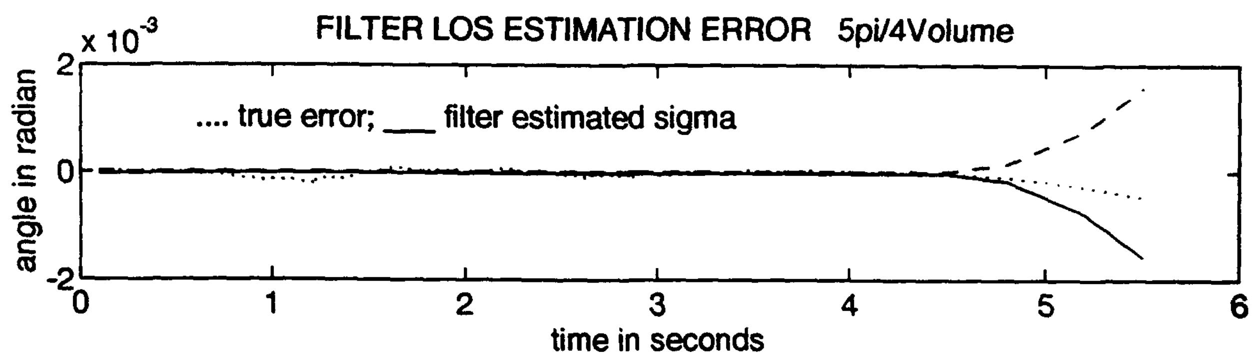
FILTER LOS ESTIMATION ERROR 5pi/4Volume
x 10^-3
.... true error; ___ filter estimated sigma
angle in radian
2
0
-2
0
1
2
3
4
5
6
time in seconds

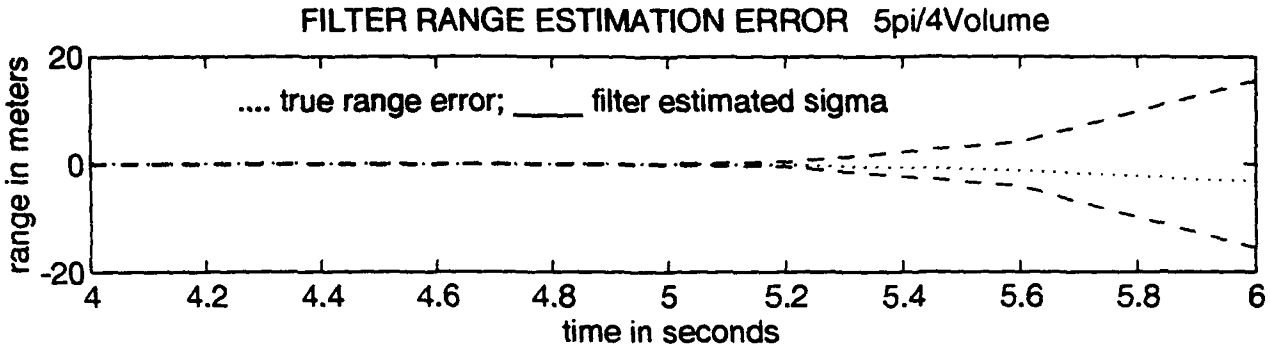
FILTER RANGE ESTIMATION ERROR 5pi/4Volume
.... true range error; ____ filter estimated sigma
range in meters
20
0
-20
4
4.2
4.4
4.6
4.8
5
5.2
5.4
5.6
5.8
6
time in seconds

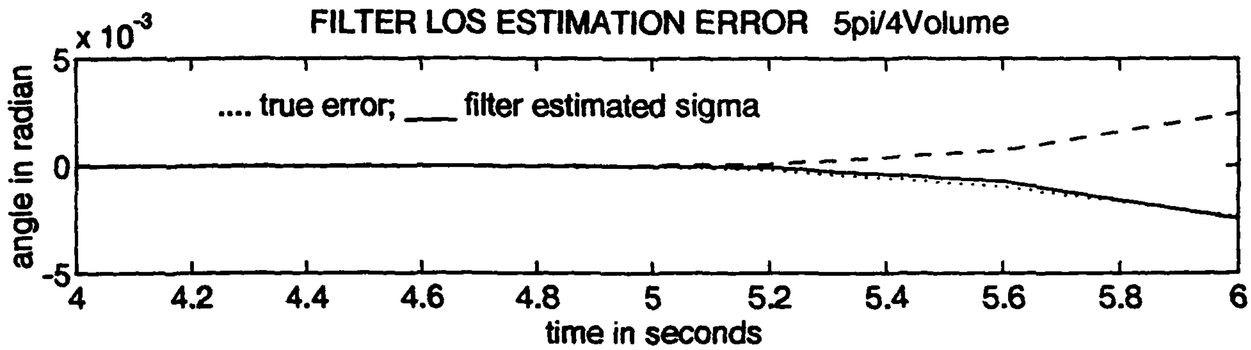
FILTER LOS ESTIMATION ERROR 5pi/4Volume
x 10^-3
.... true error; ___ filter estimated sigma
angle in radian
5
0
-5
4
4.2
4.4
4.6
4.8
5
5.2
5.4
5.6
5.8
6
time in seconds

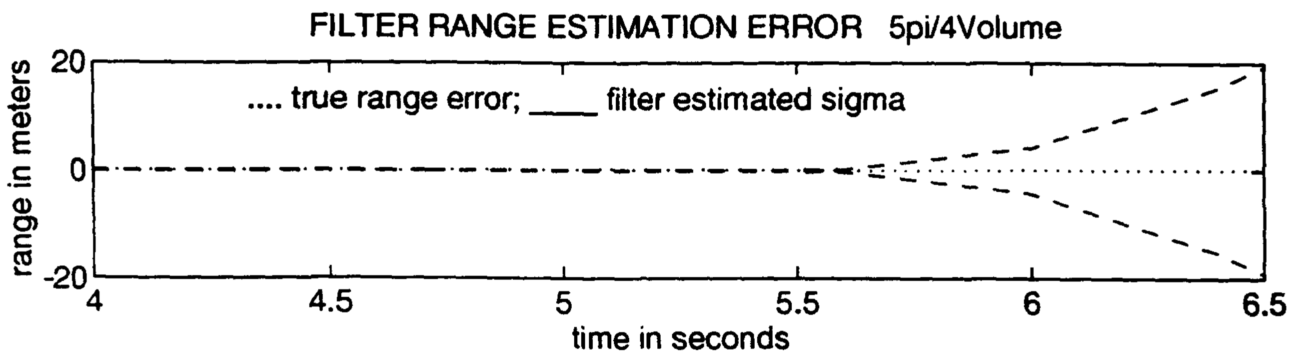
FILTER RANGE ESTIMATION ERROR 5pi/4Volume
.... true range error; ____ filter estimated sigma
range in meters
20
0
-20
4
4.5
5
5.5
6
6.5
time in seconds

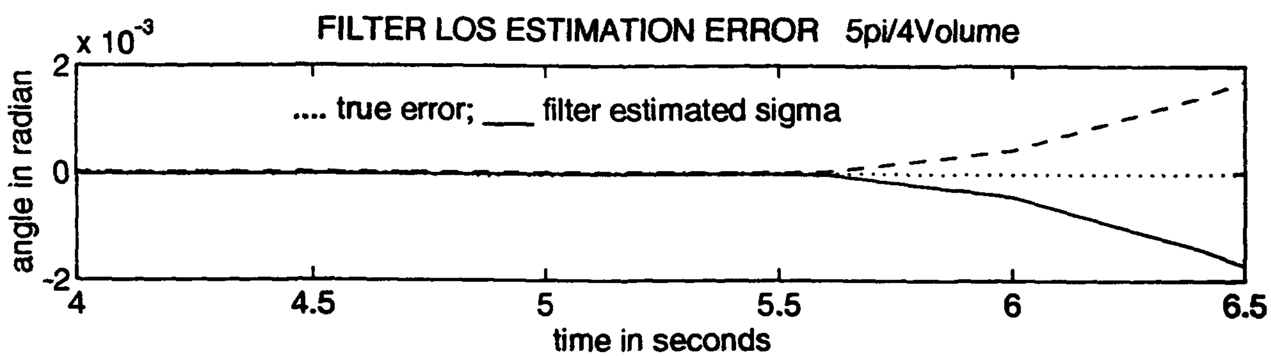
FILTER LOS ESTIMATION ERROR 5pi/4Volume
x 10^-3
.... true error; ___ filter estimated sigma
angle in radian
2
0
-2
4
4.5
5
5.5
6
6.5
time in seconds

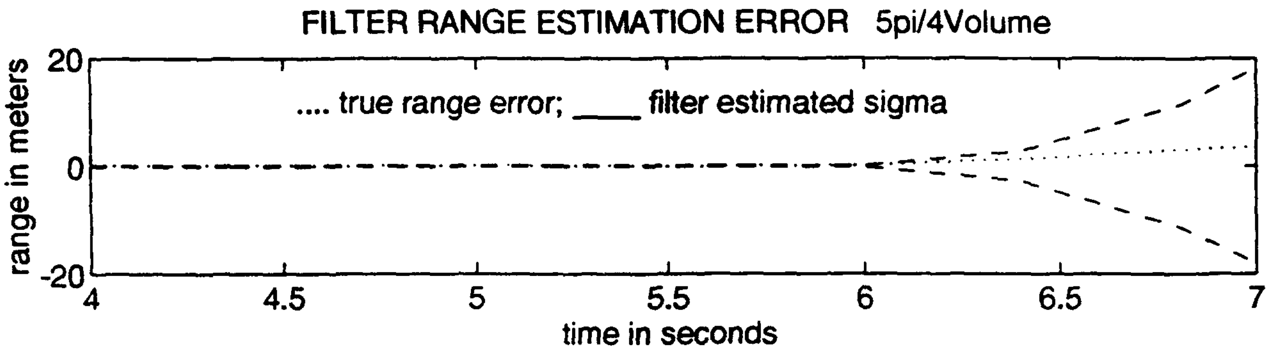
FILTER RANGE ESTIMATION ERROR 5pi/4Volume
.... true range error; ____ filter estimated sigma
range in meters
20
0
-20
4
4.5
5
5.5
6
6.5
7
time in seconds

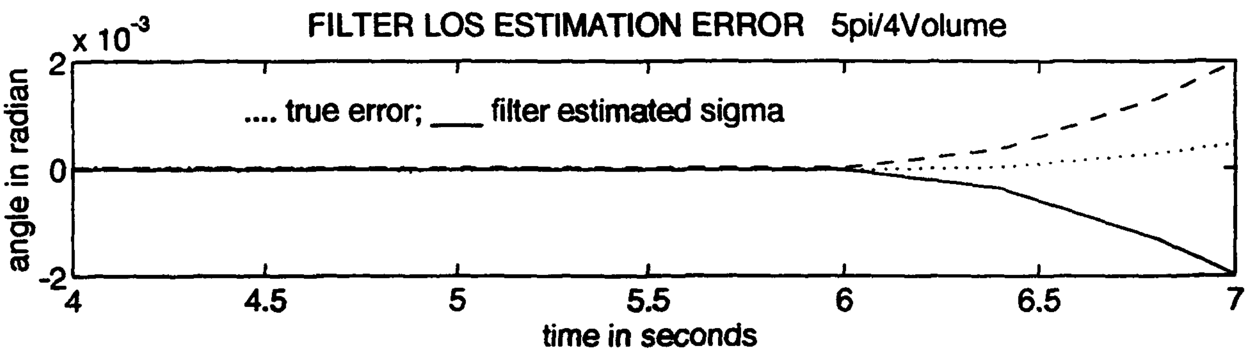
FILTER LOS ESTIMATION ERROR 5pi/4Volume
x 10-3
.... true error; ___ filter estimated sigma
angle in radian
2
0
-2
4
4.5
5
5.5
6
6.5
7
time in seconds

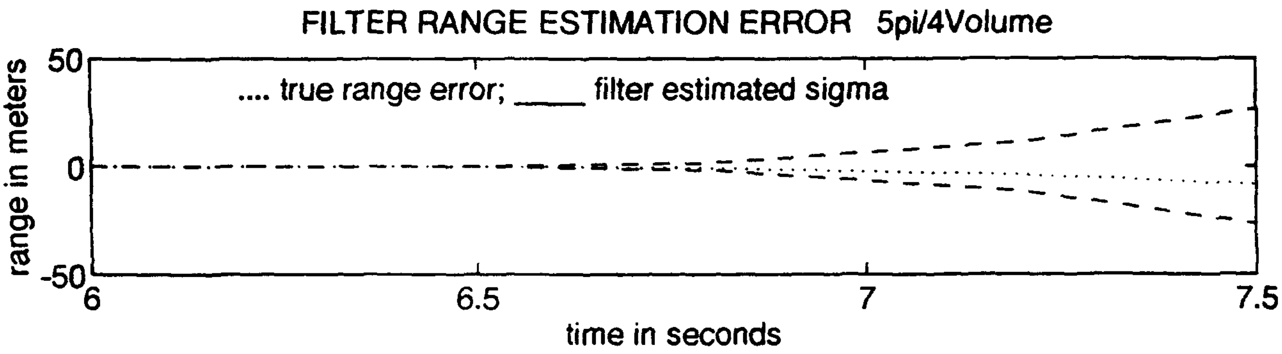
FILTER RANGE ESTIMATION ERROR 5pi/4Volume
.... true range error; ____ filter estimated sigma
range in meters
50
0
-50
6
6.5
7
7.5
time in seconds

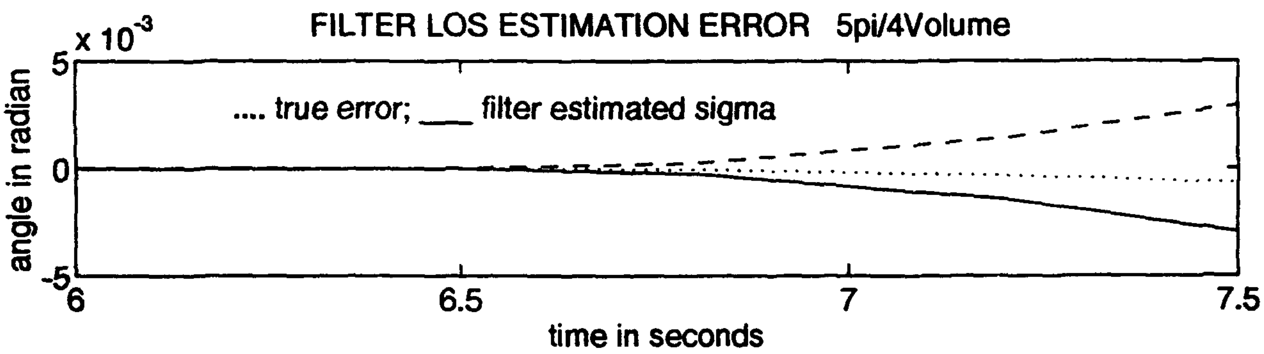
FILTER LOS ESTIMATION ERROR 5pi/4Volume
x 10^-3
.... true error; ___ filter estimated sigma
angle in radian
5
0
-5
6
6.5
7
7.5
time in seconds

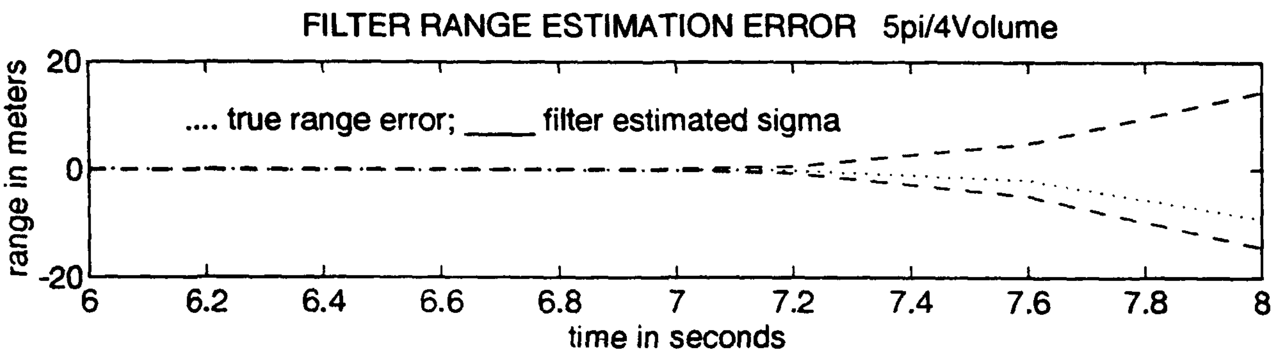
FILTER RANGE ESTIMATION ERROR 5pi/4Volume
.... true range error; ____ filter estimated sigma
range in meters
20
0
-20
6
6.2
6.4
6.6
6.8
7
7.2
7.4
7.6
7.8
8
time in seconds

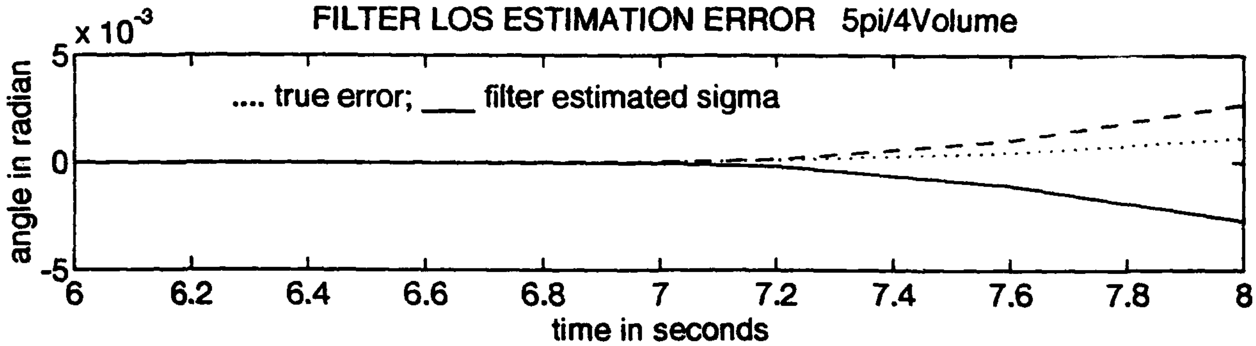
FILTER LOS ESTIMATION ERROR 5pi/4Volume
x 10^-3
.... true error; ___ filter estimated sigma
angle in radian
5
0
-5
6
6.2
6.4
6.6
6.8
7
7.2
7.4
7.6
7.8
8
time in seconds

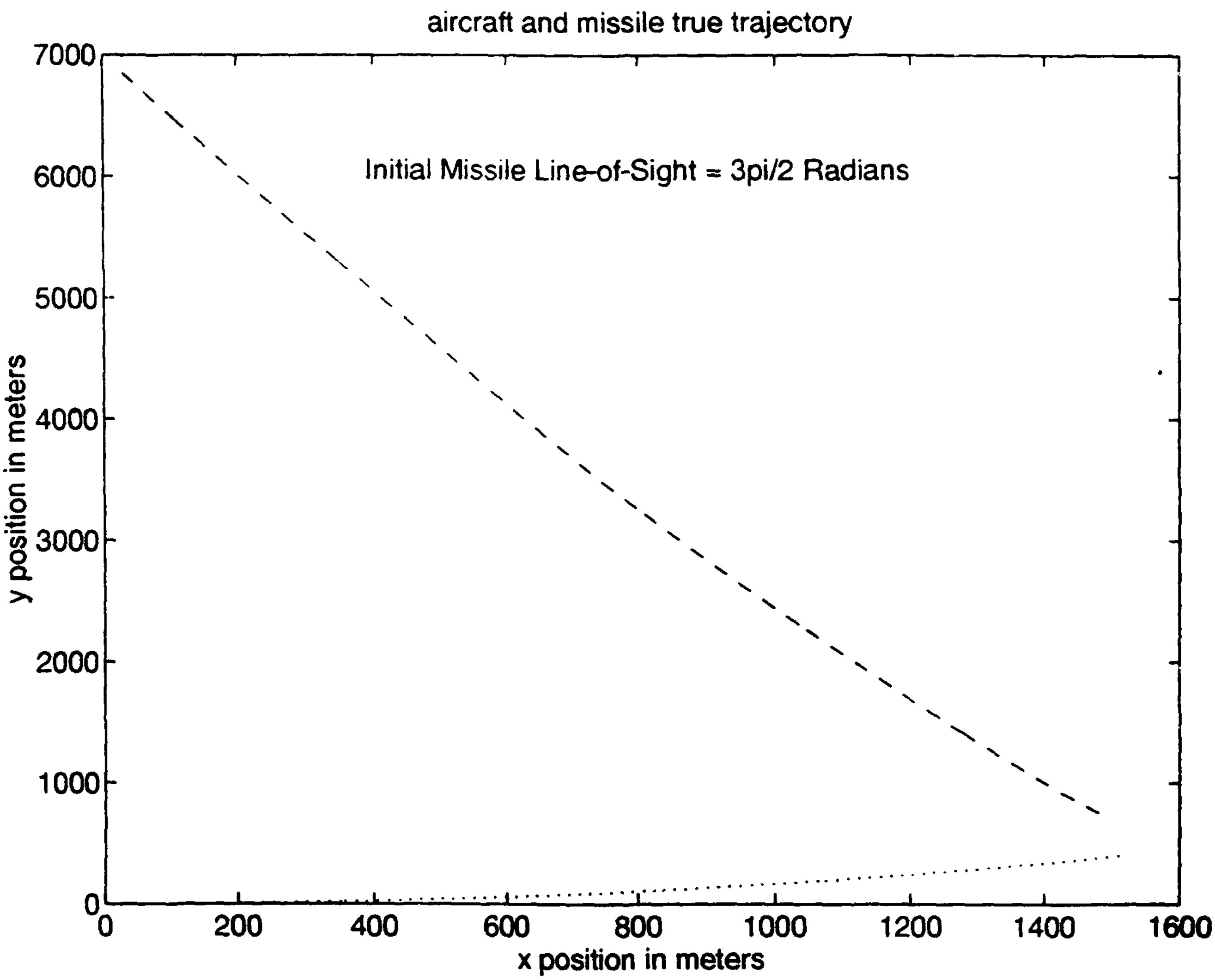
aircraft and missile true trajectory
Initial Missile Line-of-Sight = 3pi/2 Radians
y position in meters
x position in meters
7000
6000
5000
4000
3000
2000
1000
0
0
200
400
600
800
1000
1200
1400
1600

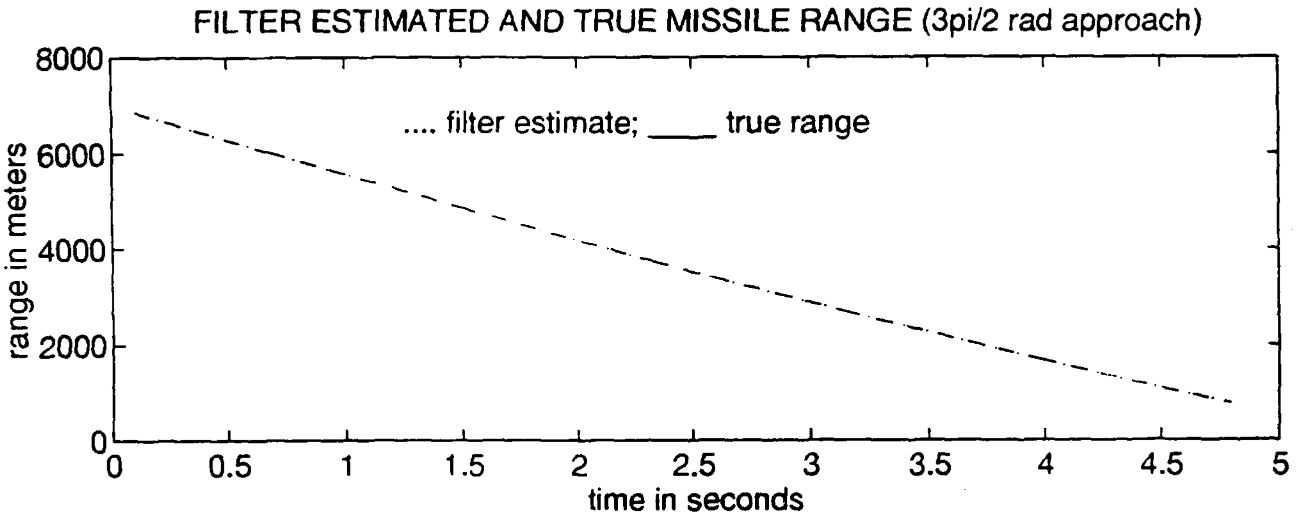
FILTER ESTIMATED AND TRUE MISSILE RANGE (3pi/2 rad approach)
.... filter estimate; ____ true range
range in meters
time in seconds

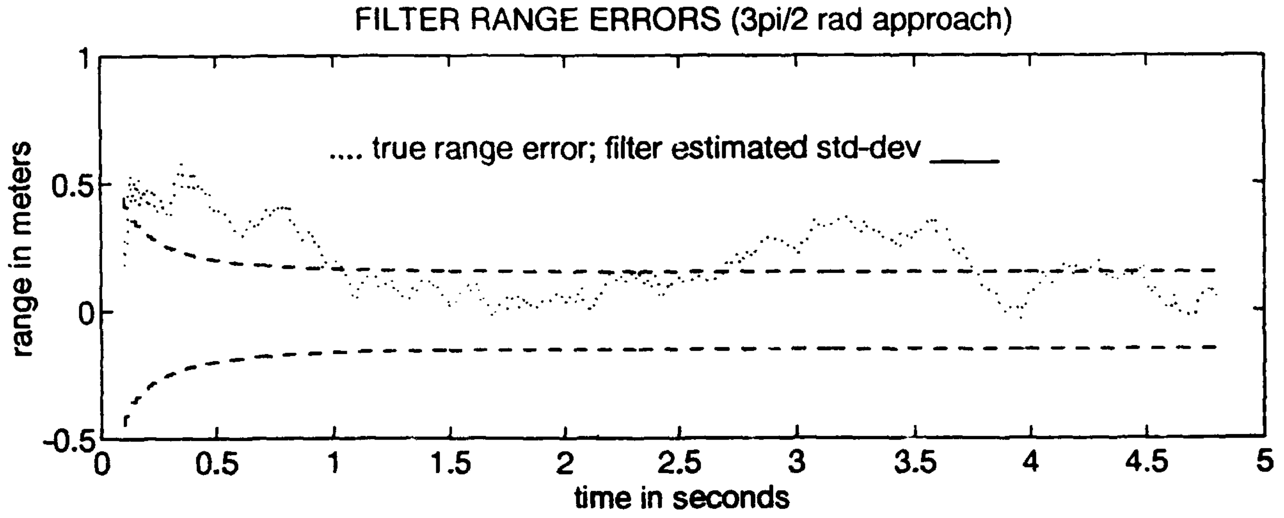
FILTER RANGE ERRORS (3pi/2 rad approach)
.... true range error; filter estimated std-dev ____
range in meters
time in seconds

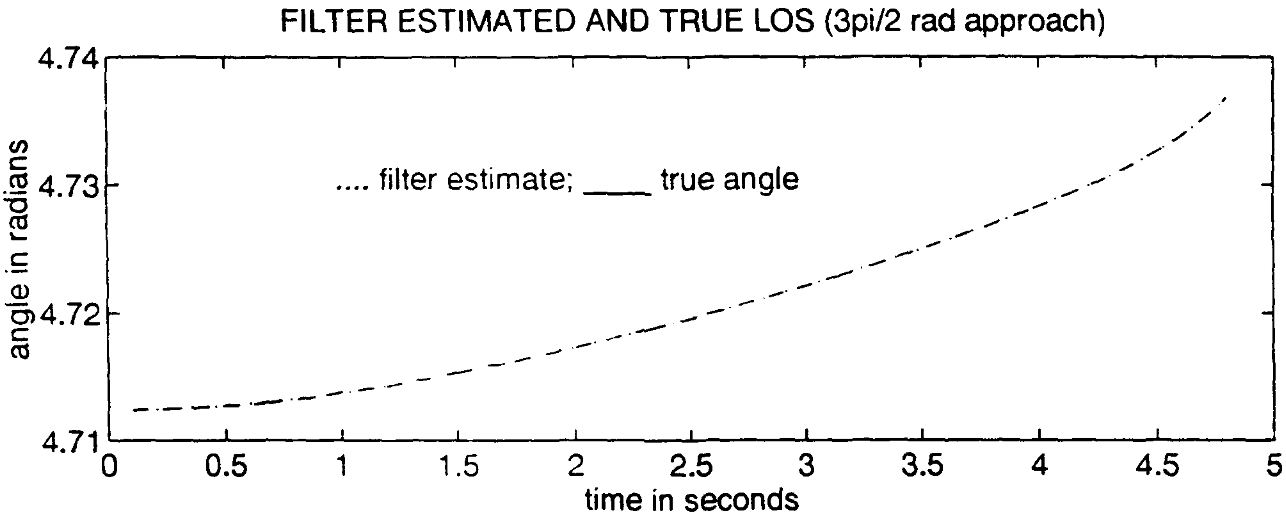
FILTER ESTIMATED AND TRUE LOS (3pi/2 rad approach)
.... filter estimate; ____ true angle
angle in radians
time in seconds
4.74
4.73
4.72
4.71
0
0.5
1
1.5
2
2.5
3
3.5
4
4.5
5

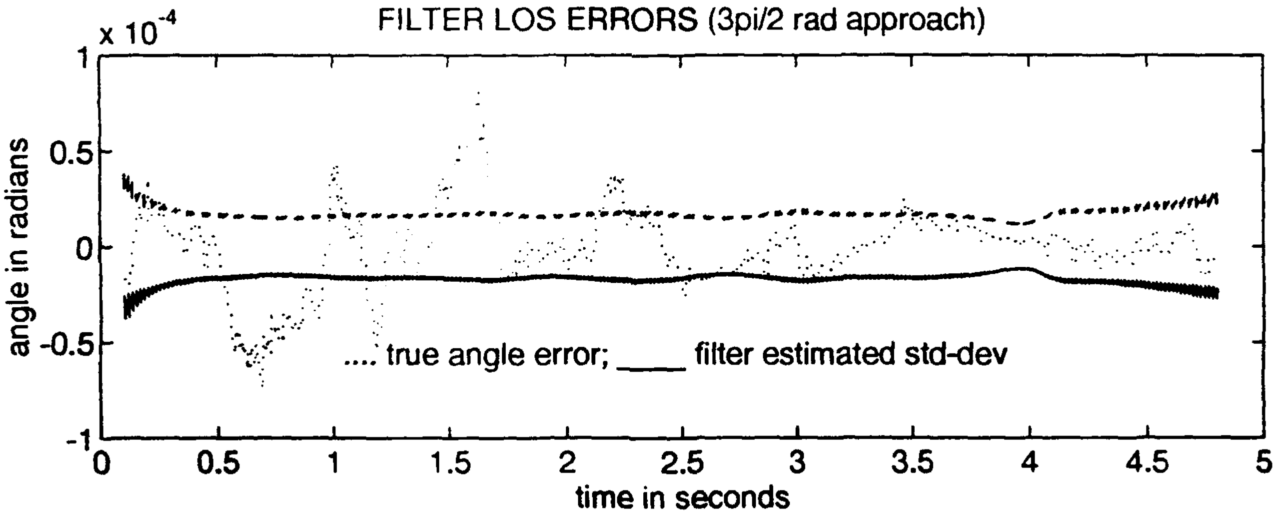
FILTER LOS ERRORS (3pi/2 rad approach)
x 10^-4
.... true angle error; ____ filter estimated std-dev
angle in radians
time in seconds
1
0.5
0
-0.5
-1
0
0.5
1
1.5
2
2.5
3
3.5
4
4.5
5

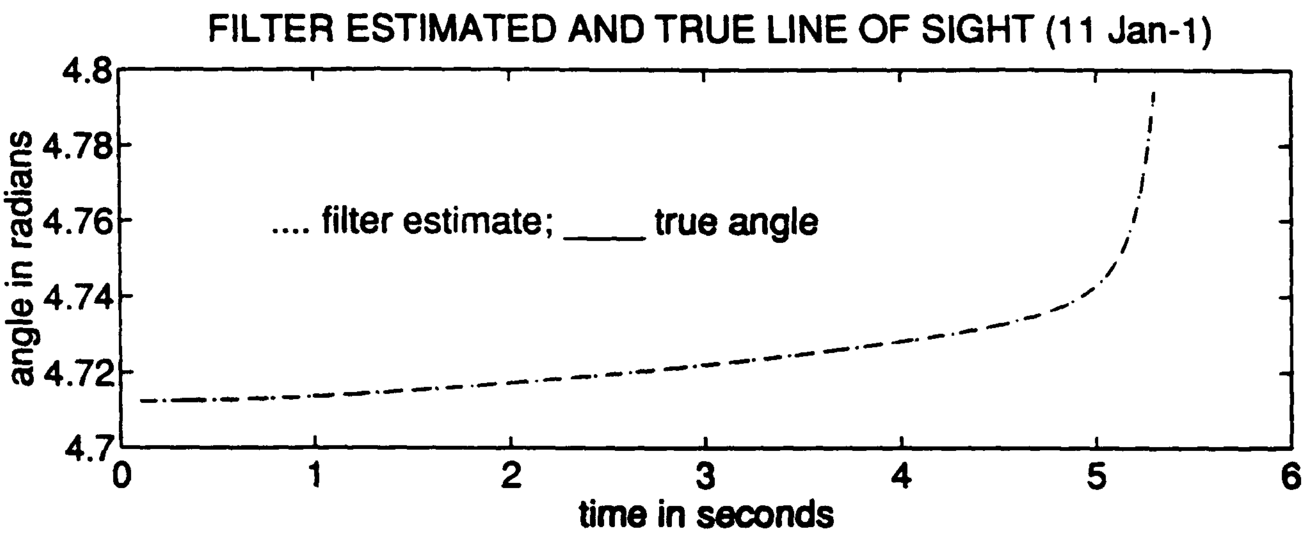
FILTER ESTIMATED AND TRUE LINE OF SIGHT (11 Jan-1)
angle in radians
.... filter estimate; ____ true angle
4.8
4.78
4.76
4.74
4.72
4.7
0
1
2
3
4
5
6
time in seconds

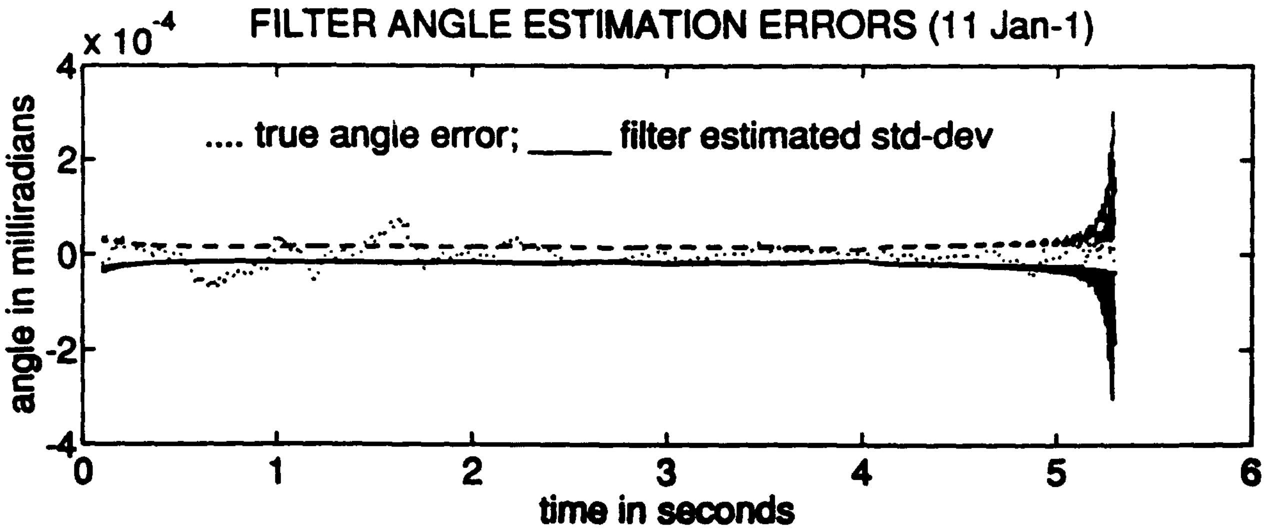
FILTER ANGLE ESTIMATION ERRORS (11 Jan-1)
x 10^-4
angle in milliradians
.... true angle error; ____ filter estimated std-dev
4
2
0
-2
-4
0
1
2
3
4
5
6
time in seconds

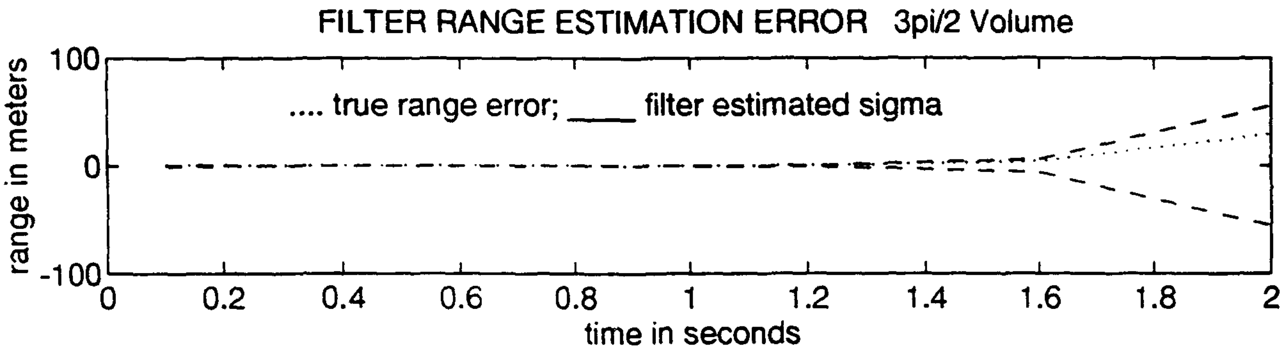
FILTER RANGE ESTIMATION ERROR 3pi/2 Volume
.... true range error; ____ filter estimated sigma
range in meters
100
0
-100
0
0.2
0.4
0.6
0.8
1
1.2
1.4
1.6
1.8
2
time in seconds

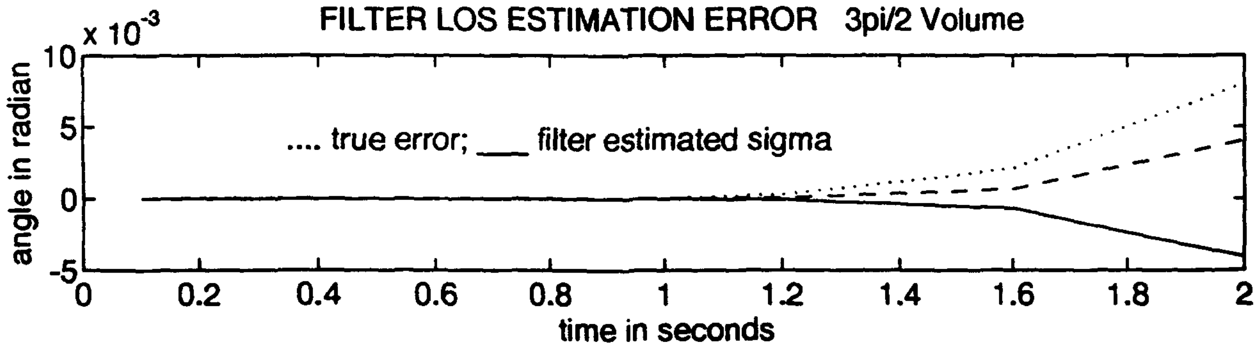
FILTER LOS ESTIMATION ERROR 3pi/2 Volume
x 10^-3
.... true error; ___ filter estimated sigma
angle in radian
10
5
0
-5
0
0.2
0.4
0.6
0.8
1
1.2
1.4
1.6
1.8
2
time in seconds

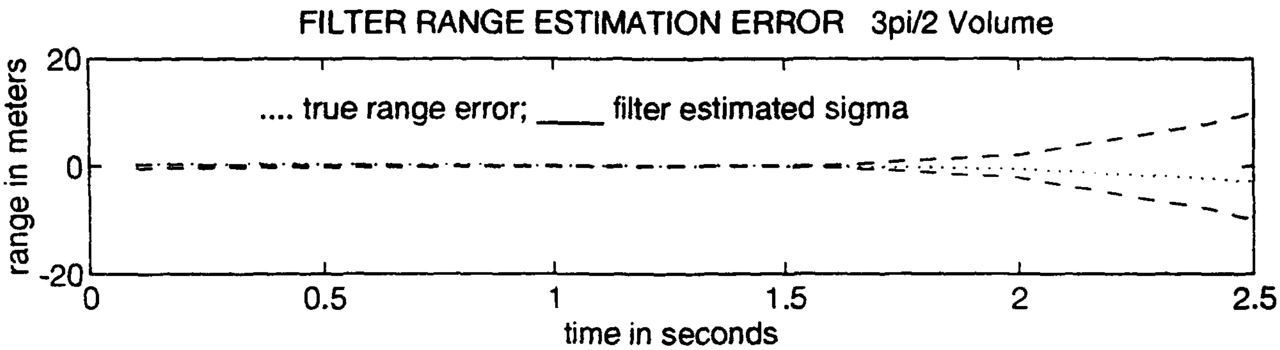
FILTER RANGE ESTIMATION ERROR 3pi/2 Volume
.... true range error; ____ filter estimated sigma
range in meters
20
0
-20
0
0.5
1
1.5
2
2.5
time in seconds

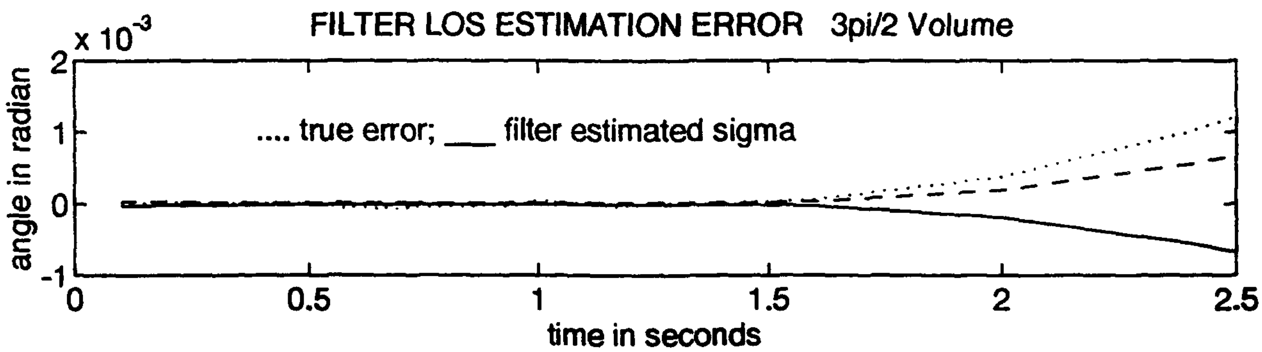
FILTER LOS ESTIMATION ERROR 3pi/2 Volume
x 10^-3
.... true error; ___ filter estimated sigma
angle in radian
2
1
0
-1
0
0.5
1
1.5
2
2.5
time in seconds

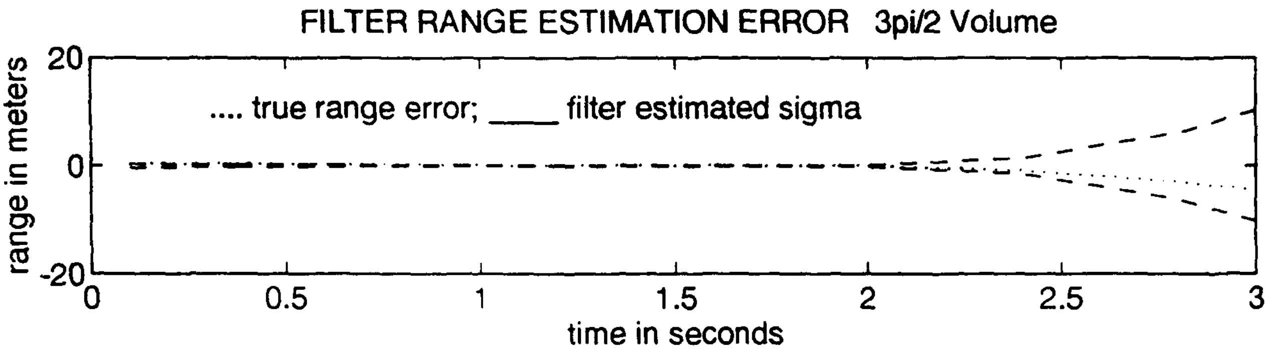

FILTER RANGE ESTIMATION ERROR 3pi/2 Volume
.... true range error; ____ filter estimated sigma
range in meters
20
0
-20
0
0.5
1
1.5
2
2.5
3
time in seconds

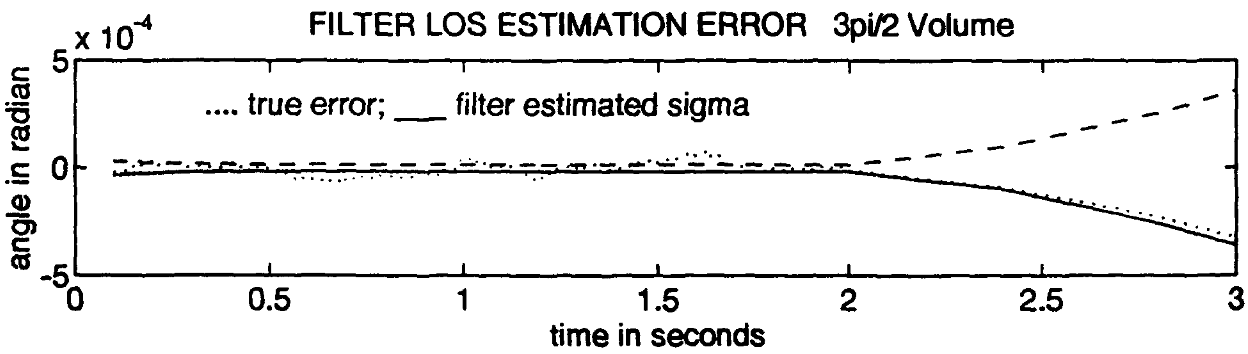

FILTER LOS ESTIMATION ERROR 3pi/2 Volume
x 10^-4
.... true error; ___ filter estimated sigma
angle in radian
5
0
-5
0
0.5
1
1.5
2
2.5
3
time in seconds

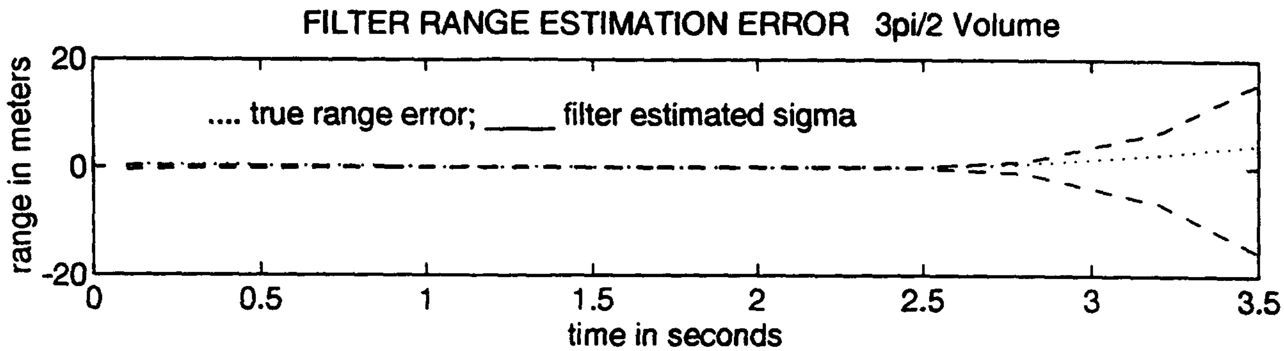
FILTER RANGE ESTIMATION ERROR 3pi/2 Volume
.... true range error; ____ filter estimated sigma
range in meters
20
0
-20
0
0.5
1
1.5
2
2.5
3
3.5
time in seconds

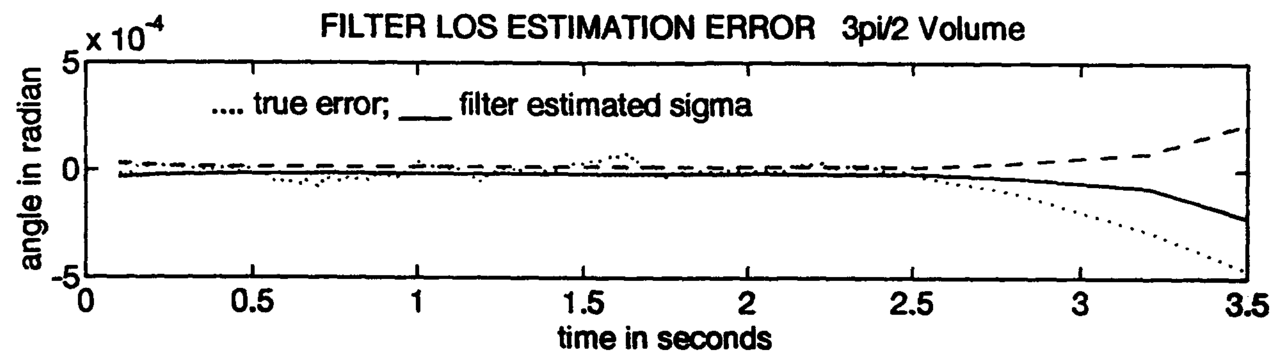
FILTER LOS ESTIMATION ERROR 3pi/2 Volume
x 10^-4
.... true error; ___ filter estimated sigma
angle in radian
5
0
-5
0
0.5
1
1.5
2
2.5
3
3.5
time in seconds

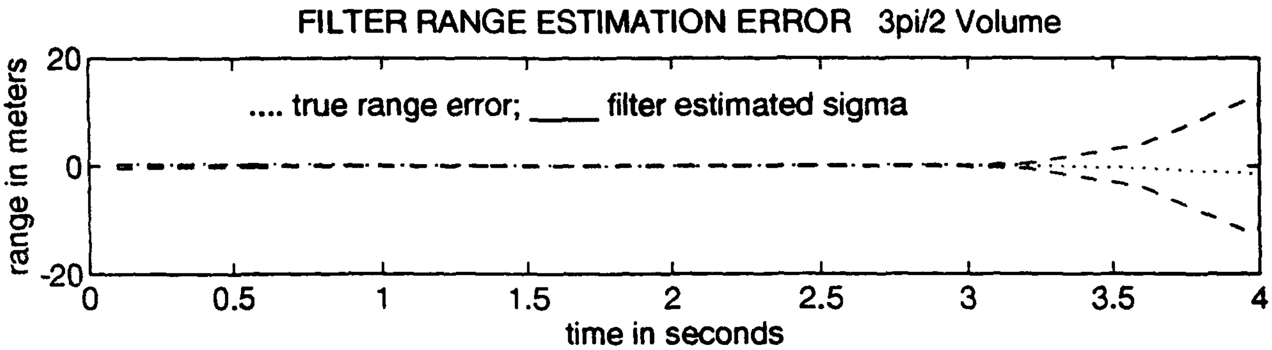
FILTER RANGE ESTIMATION ERROR 3pi/2 Volume
.... true range error; ____ filter estimated sigma
range in meters
20
0
-20
0
0.5
1
1.5
2
2.5
3
3.5
4
time in seconds

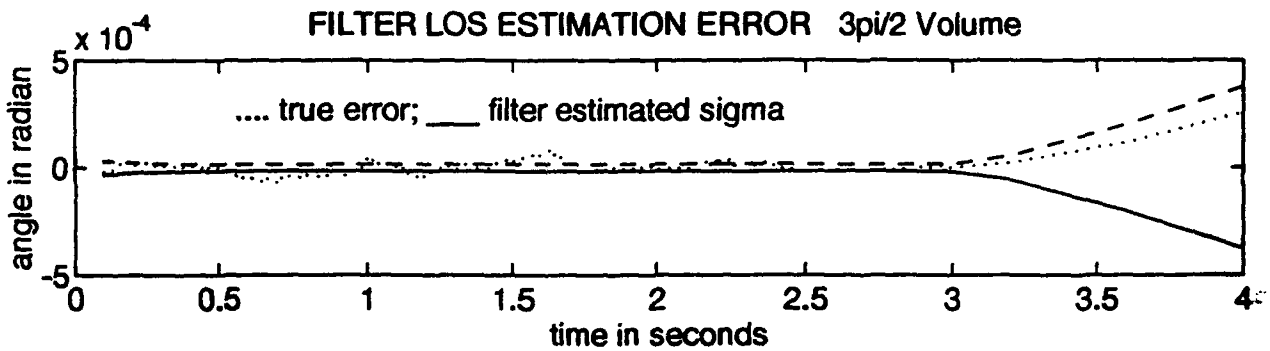
FILTER LOS ESTIMATION ERROR 3pi/2 Volume
x 10^-4
.... true error; ___ filter estimated sigma
angle in radian
5
0
-5
0
0.5
1
1.5
2
2.5
3
3.5
4
time in seconds

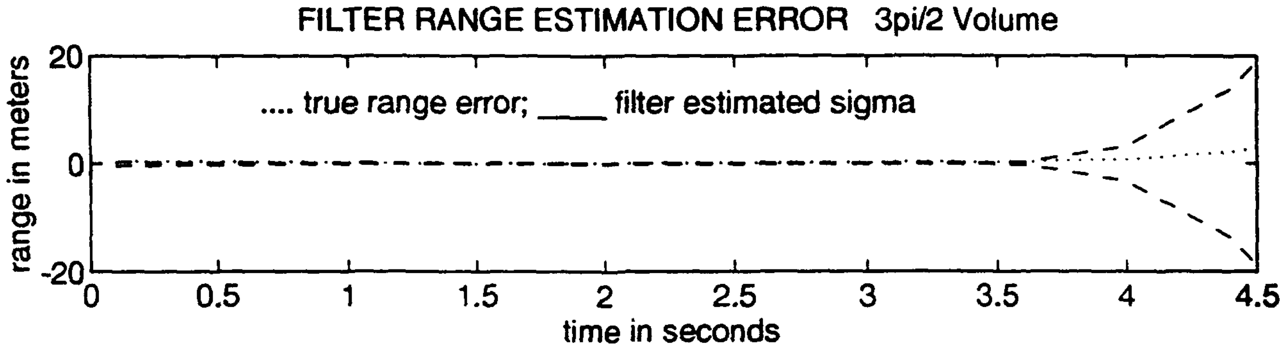

FILTER RANGE ESTIMATION ERROR 3pi/2 Volume
.... true range error; ____ filter estimated sigma
range in meters
20
0
-20
0
0.5
1
1.5
2
2.5
3
3.5
4
4.5
time in seconds

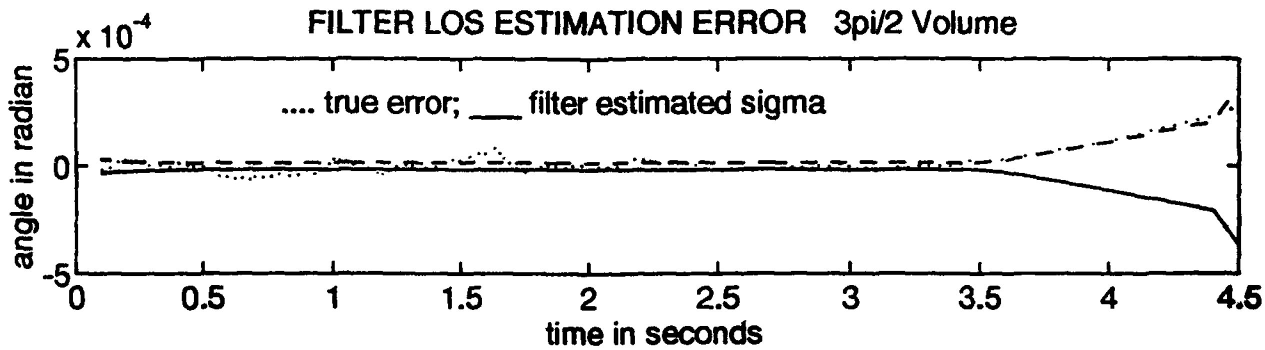

FILTER LOS ESTIMATION ERROR 3pi/2 Volume
x 10^-4
.... true error; ___ filter estimated sigma
angle in radian
5
0
-5
0
0.5
1
1.5
2
2.5
3
3.5
4
4.5
time in seconds

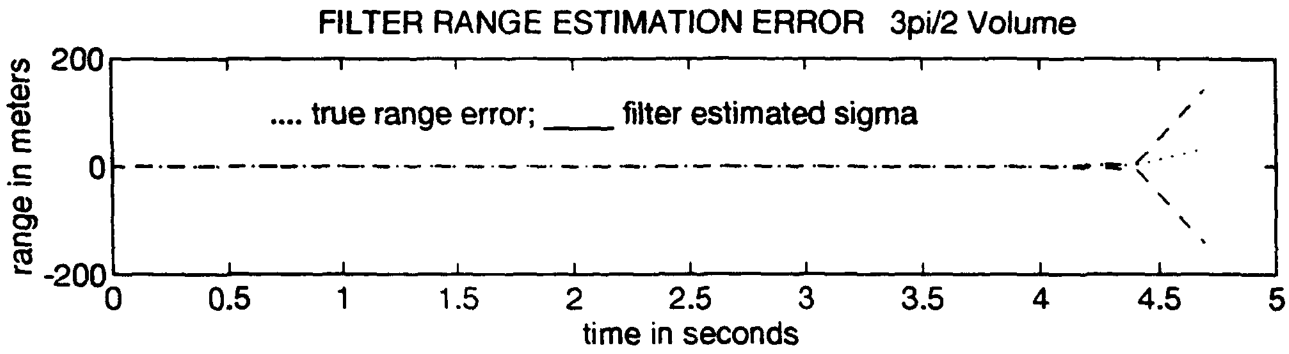
FILTER RANGE ESTIMATION ERROR 3pi/2 Volume
.... true range error; ____ filter estimated sigma
range in meters
200
0
-200
0
0.5
1
1.5
2
2.5
3
3.5
4
4.5
5
time in seconds

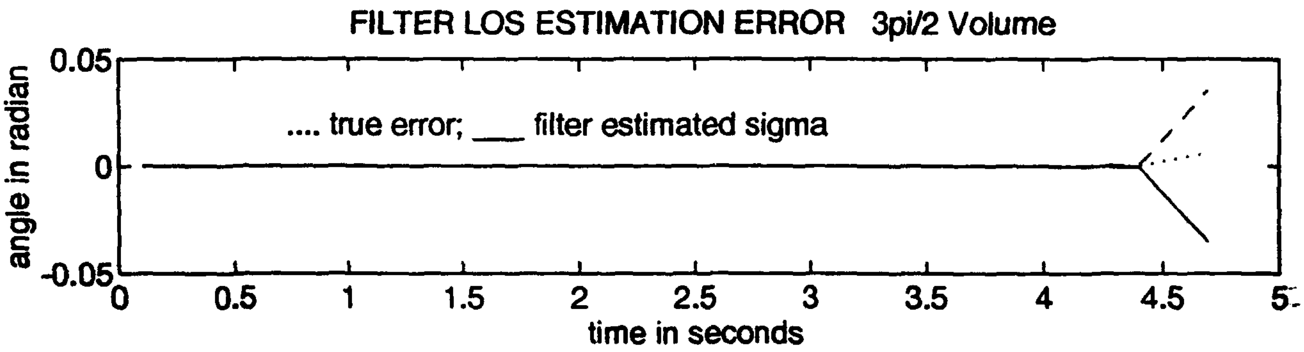
FILTER LOS ESTIMATION ERROR 3pi/2 Volume
.... true error; ___ filter estimated sigma
angle in radian
0.05
0
-0.05
0
0.5
1
1.5
2
2.5
3
3.5
4
4.5
5
time in seconds

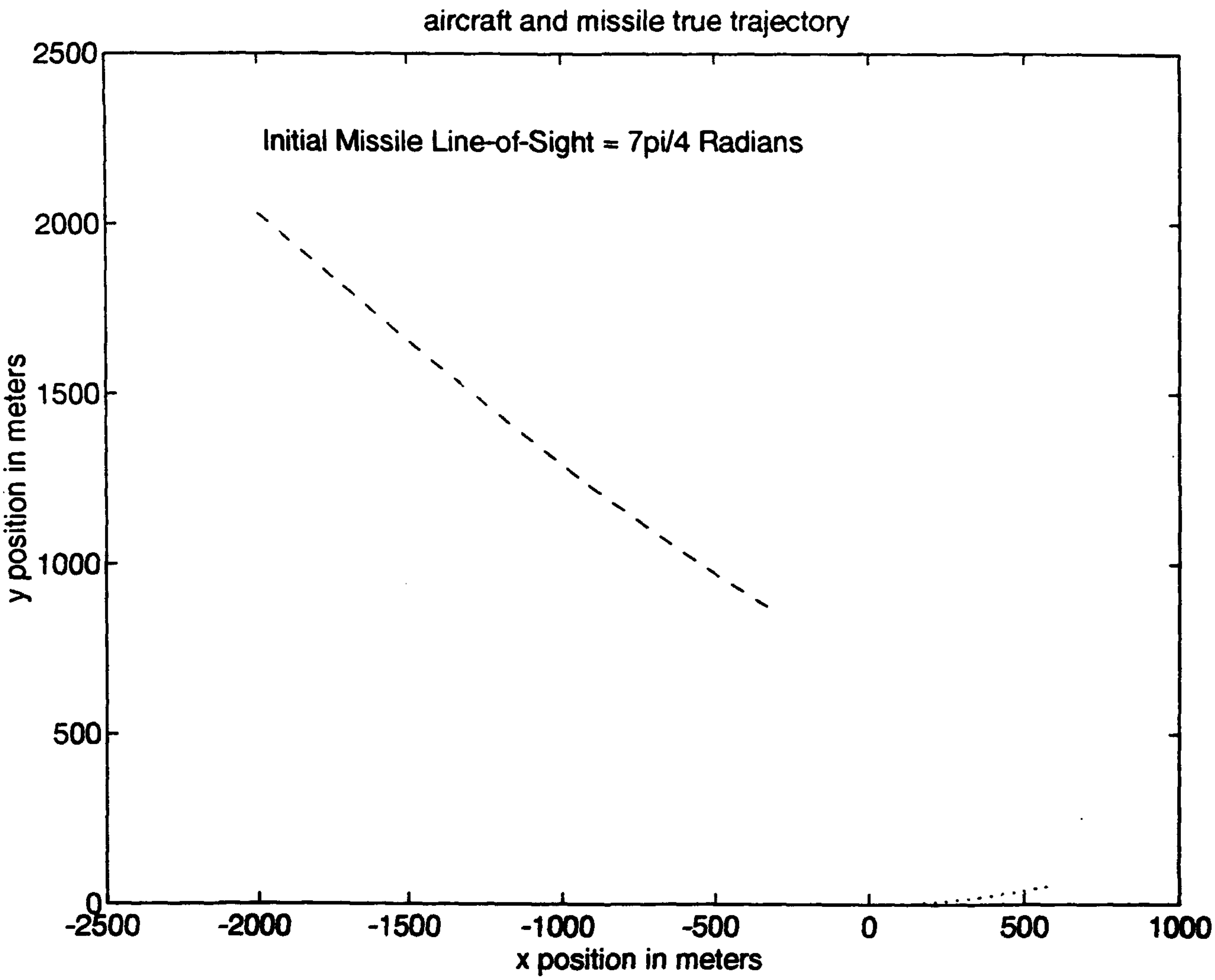
aircraft and missile true trajectory
Initial Missile Line-of-Sight = 7pi/4 Radians
2500
2000
1500
1000
500
0
y position in meters
-2500
-2000
-1500
-1000
-500
0
500
1000
x position in meters

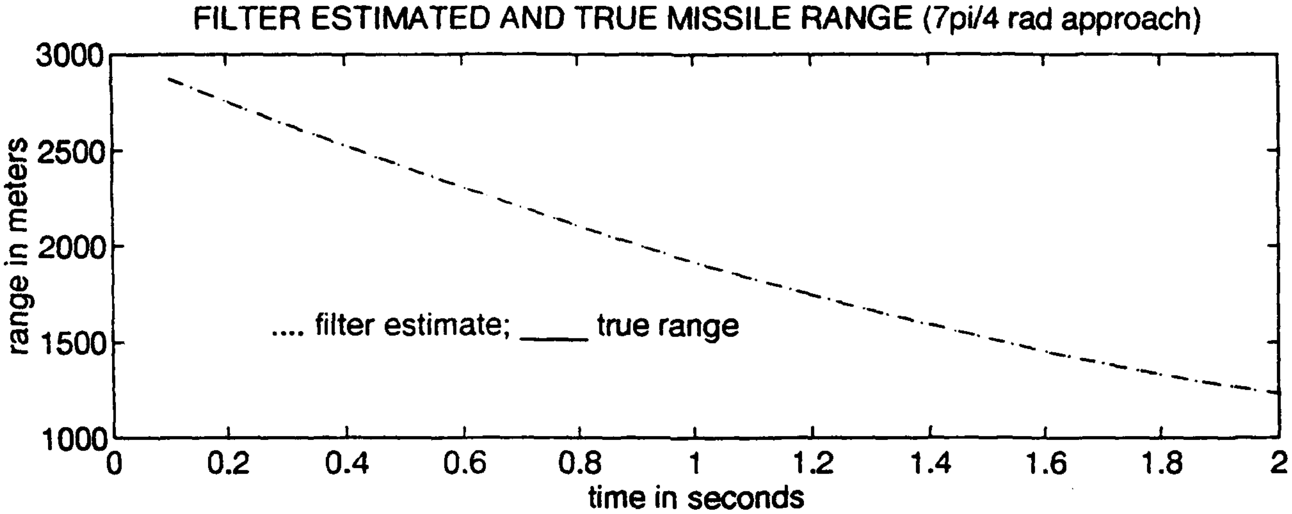
FILTER ESTIMATED AND TRUE MISSILE RANGE (7pi/4 rad approach)
range in meters
3000
2500
2000
1500
1000
.... filter estimate; ____ true range
0
0.2
0.4
0.6
0.8
1
1.2
1.4
1.6
1.8
2
time in seconds

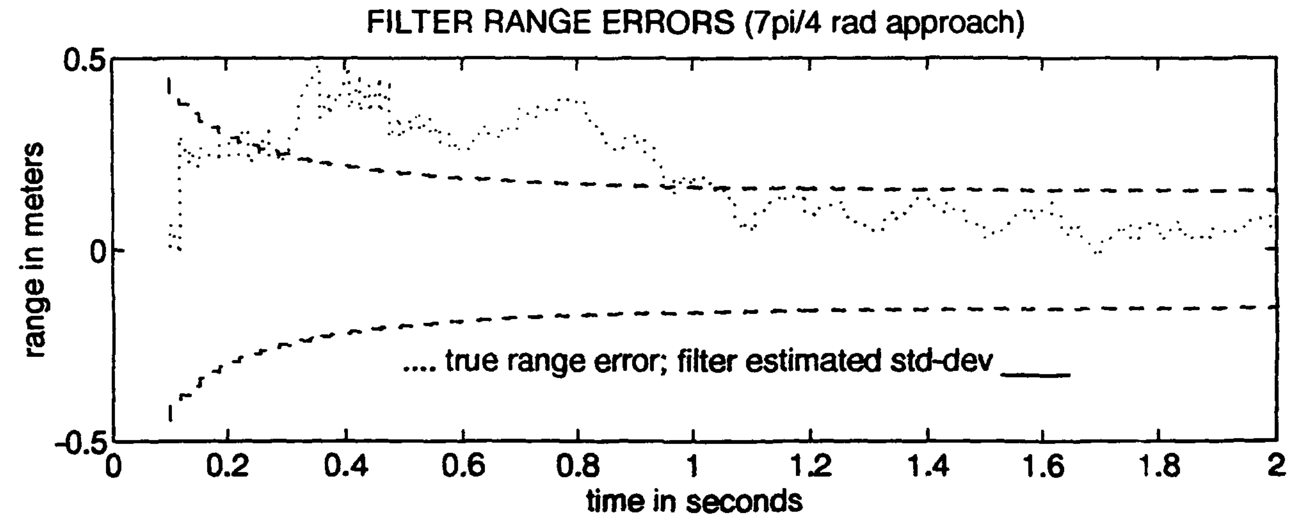
FILTER RANGE ERRORS (7pi/4 rad approach)
range in meters
0.5
0
-0.5
.... true range error; filter estimated std-dev ____
0
0.2
0.4
0.6
0.8
1
1.2
1.4
1.6
1.8
2
time in seconds

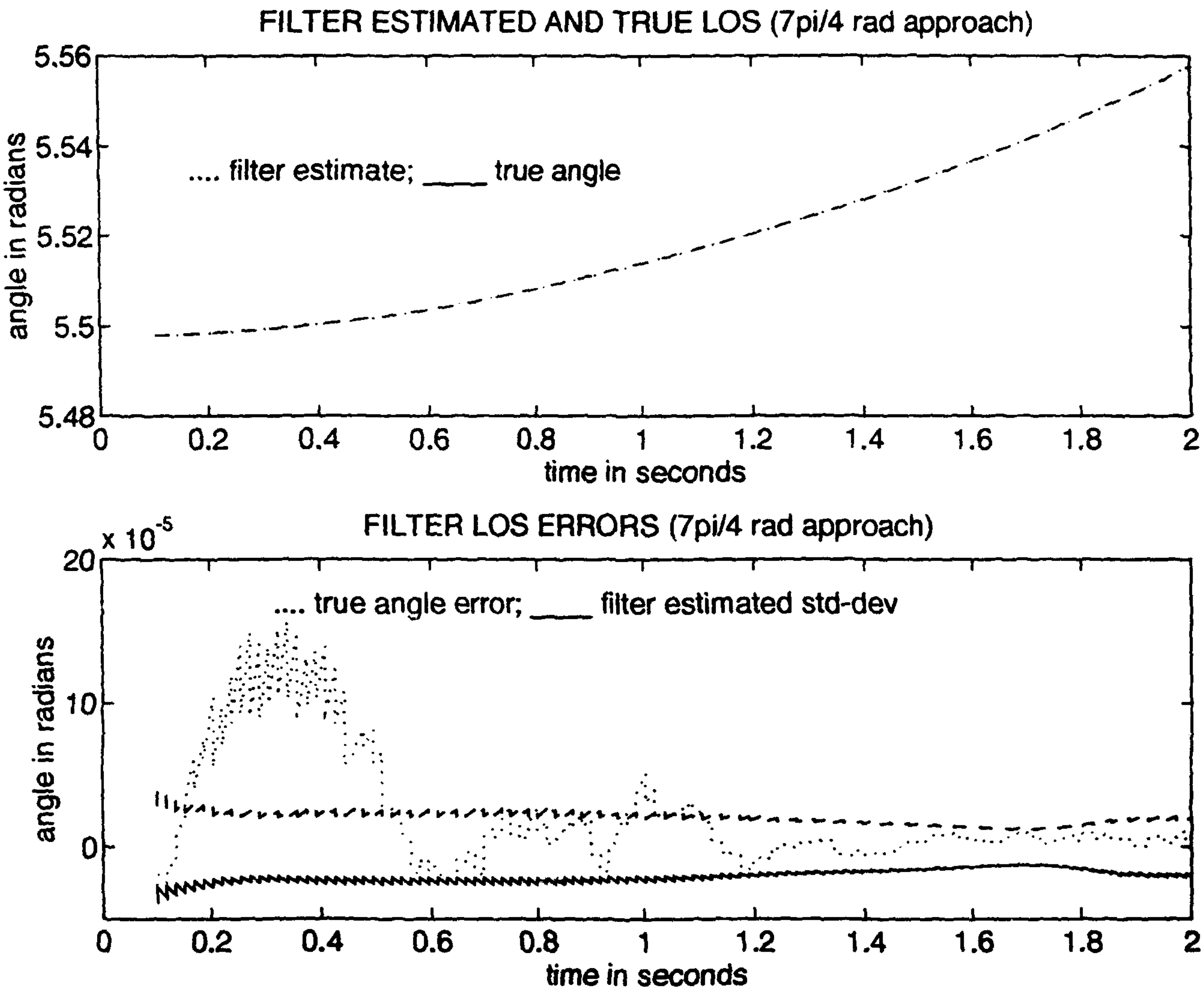
FILTER ESTIMATED AND TRUE LOS (7pi/4 rad approach)
.... filter estimate; ____ true angle
angle in radians
5.56
5.54
5.52
5.5
5.48
0
0.2
0.4
0.6
0.8
1
1.2
1.4
1.6
1.8
2
time in seconds
FILTER LOS ERRORS (7pi/4 rad approach)
x 10^-5
.... true angle error; ____ filter estimated std-dev
angle in radians
20
10
0
time in seconds

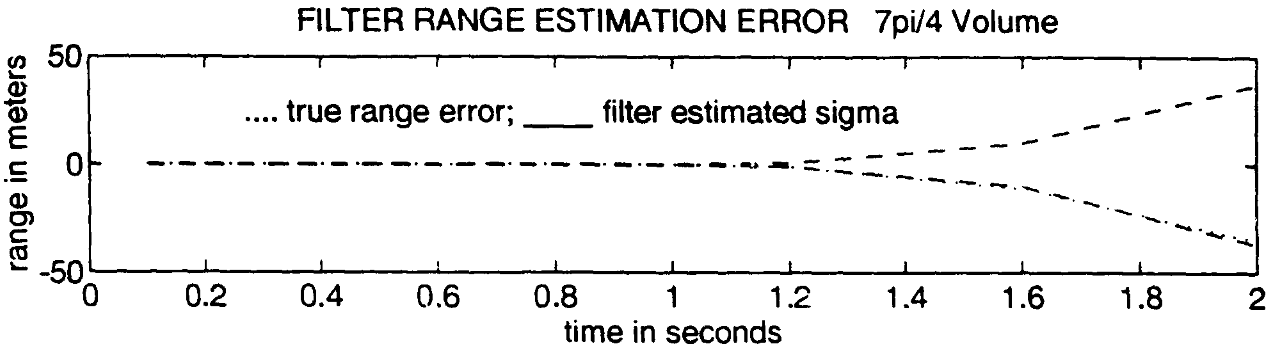
FILTER RANGE ESTIMATION ERROR 7pi/4 Volume
.... true range error; ____ filter estimated sigma
range in meters
50
0
-50
0
0.2
0.4
0.6
0.8
1
1.2
1.4
1.6
1.8
2
time in seconds

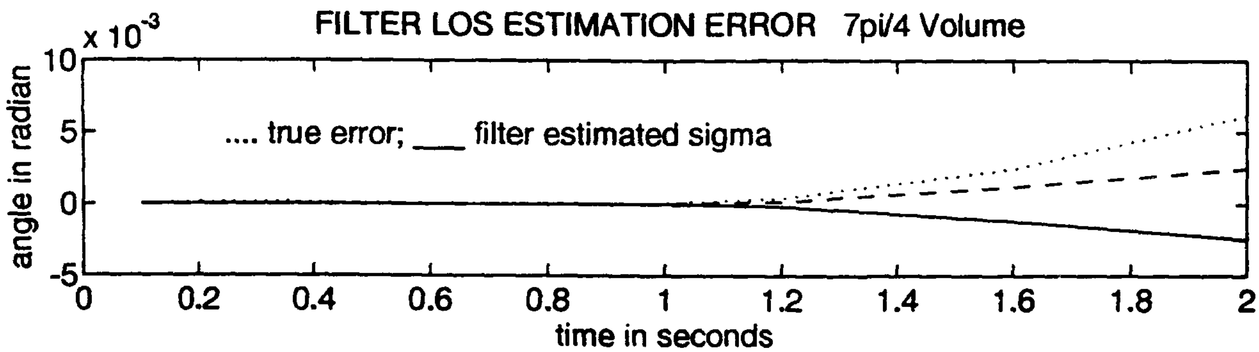
FILTER LOS ESTIMATION ERROR 7pi/4 Volume
x 10-3
.... true error; ___ filter estimated sigma
angle in radian
10
5
0
-5
0
0.2
0.4
0.6
0.8
1
1.2
1.4
1.6
1.8
2
time in seconds

Appendix B

This appendix contains simulation plots for the ladar range noise run set. The aircraft is initially heading east and beginning a 3 g turn to the north. All measurement noises (except range) and dynamic noise strengths are set at baseline values. The missile is launched from the $\pi/4$ approach angle. Each run has a trajectory plot, estimated range errors, range-rate errors, LOS errors and LOS-rate errors. Estimated range and LOS plots are found in the $\pi/4$ missile approach angle run plots in Appendix A. The baseline (see Figure 4-4) range measurement error is 0.5 meters, with additional runs made for range errors of 1.0, 2.0 and 4.0 meters. Each plot set contains filter divergence plots of range error and angle error for a three second divergence from three to six seconds. The divergence plots, which define the volume cross-section, are used for performance comparison versus the baseline. In Figures B-2 thru B-19 both the filter and truth model measurement noises are varied from the baseline. In Figures B-20 thru B-37 only the filter measurement noise is varied above baseline (i.e., the filter noise is set "high"). In Figures B-38 thru B-55 only the true measurement noise is varied above baseline (i.e., the filter noise is set "low").

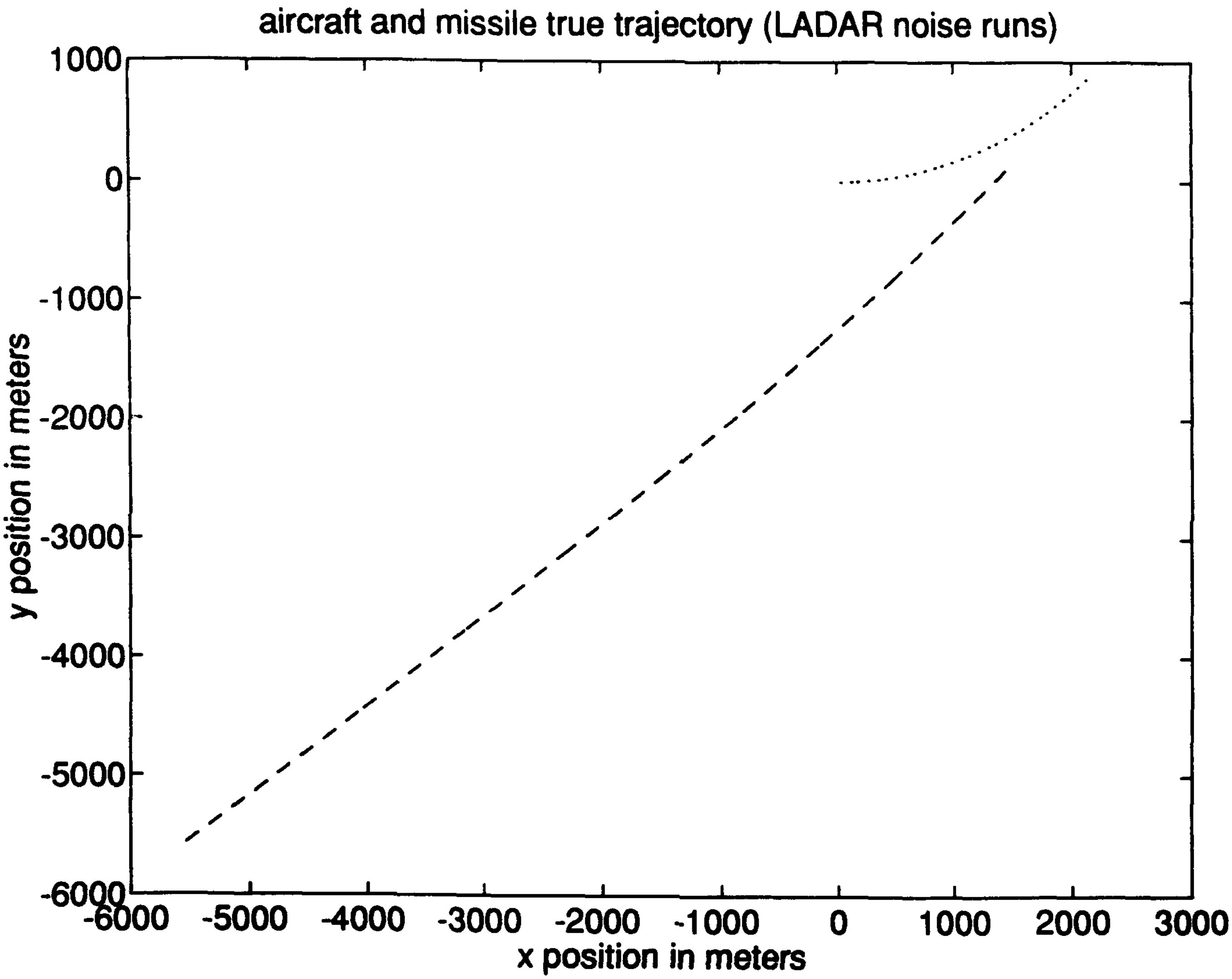
aircraft and missile true trajectory (LADAR noise runs)
1000
0
-1000
-2000
-3000
-4000
-5000
-6000
y position in meters
-6000
-5000
-4000
-3000
-2000
-1000
0
1000
2000
3000
x position in meters

FILTER RANGE ERRORS (range = 1.0)

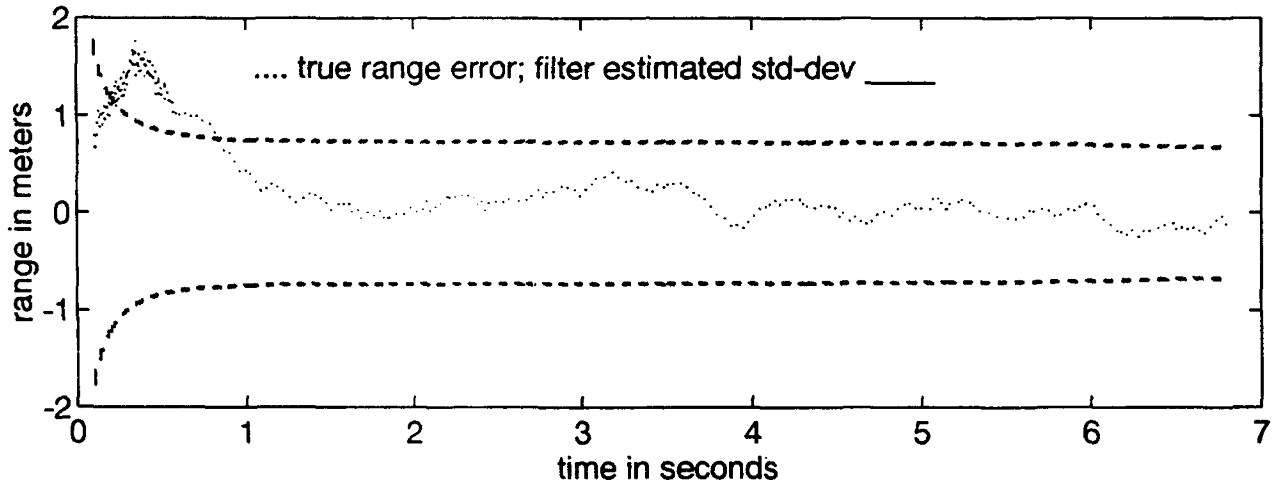

FILTER RANGE-RATE ERRORS (range = 1.0)

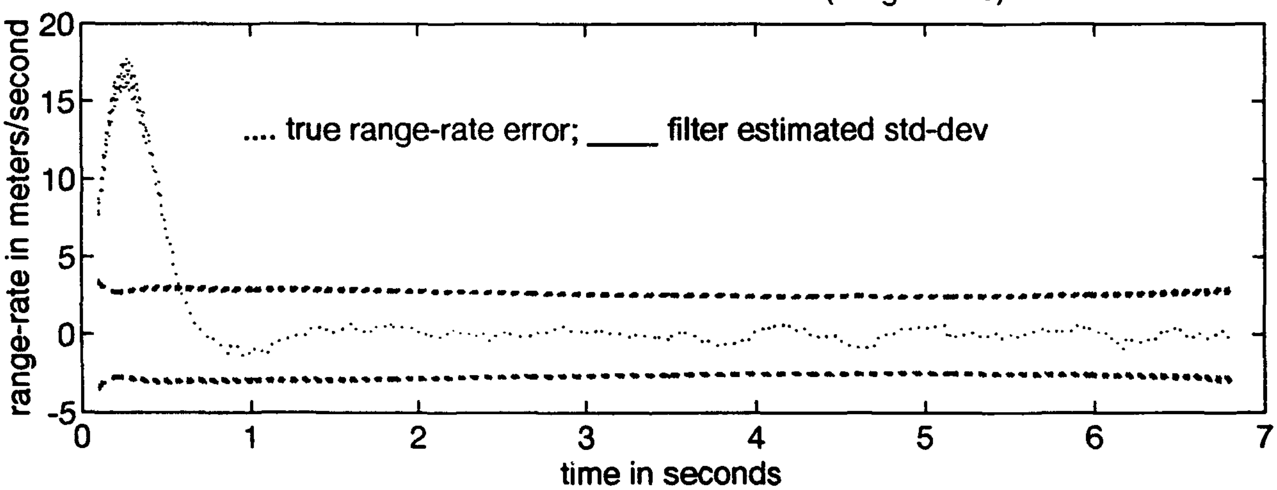

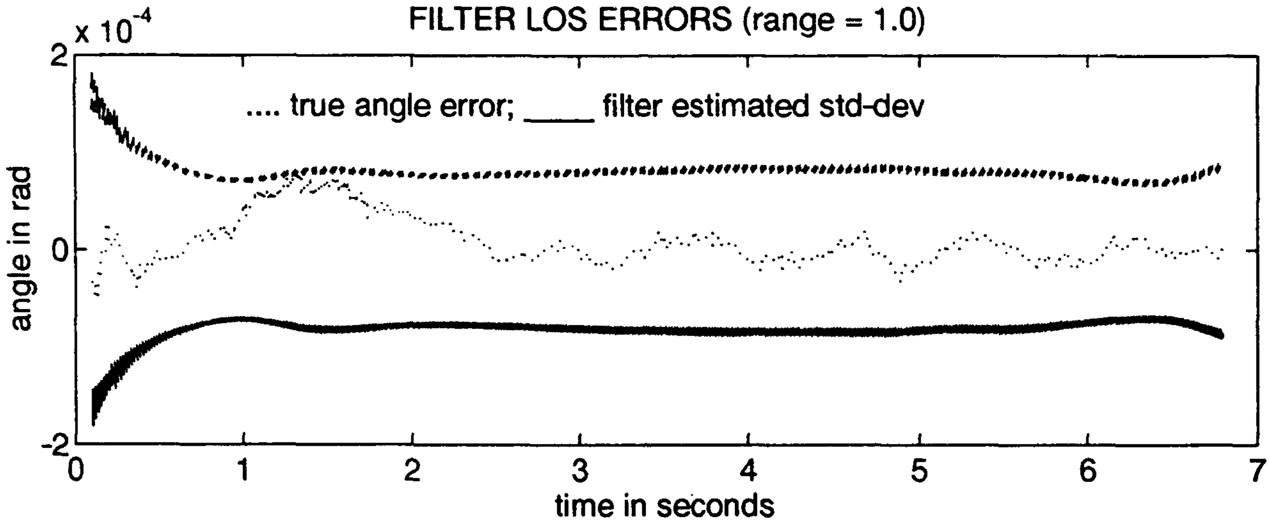

FILTER LOS ERRORS (range = 1.0)
x 10^-4
.... true angle error; _____ filter estimated std-dev
angle in rad
time in seconds
2
0
-2
0
1
2
3
4
5
6
7

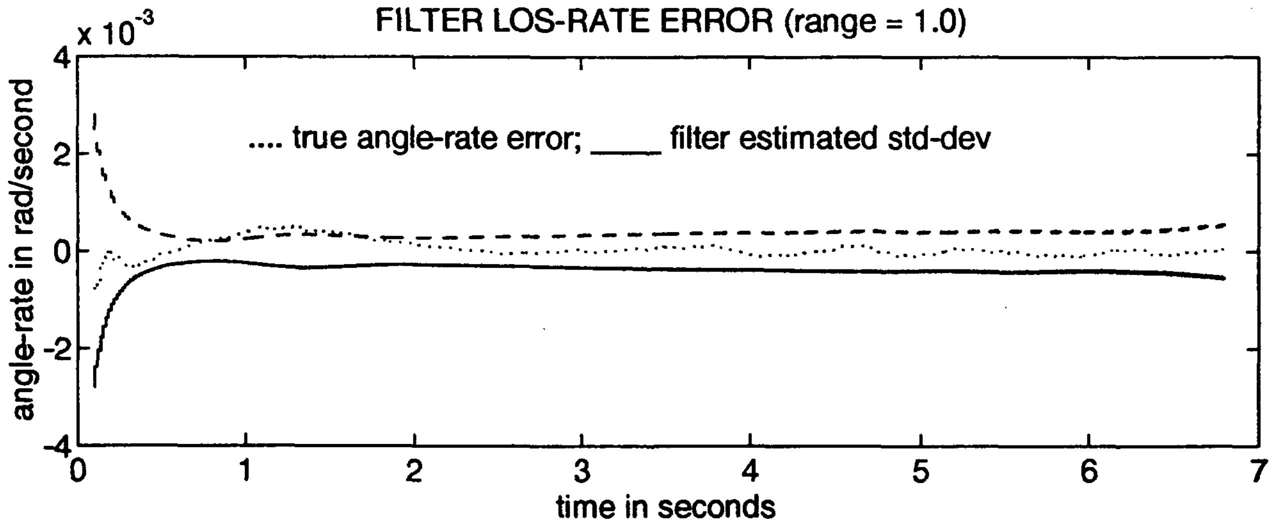

FILTER LOS-RATE ERROR (range = 1.0)
x 10^-3
.... true angle-rate error; _____ filter estimated std-dev
angle-rate in rad/second
time in seconds
4
2
0
-2
-4
0
1
2
3
4
5
6
7

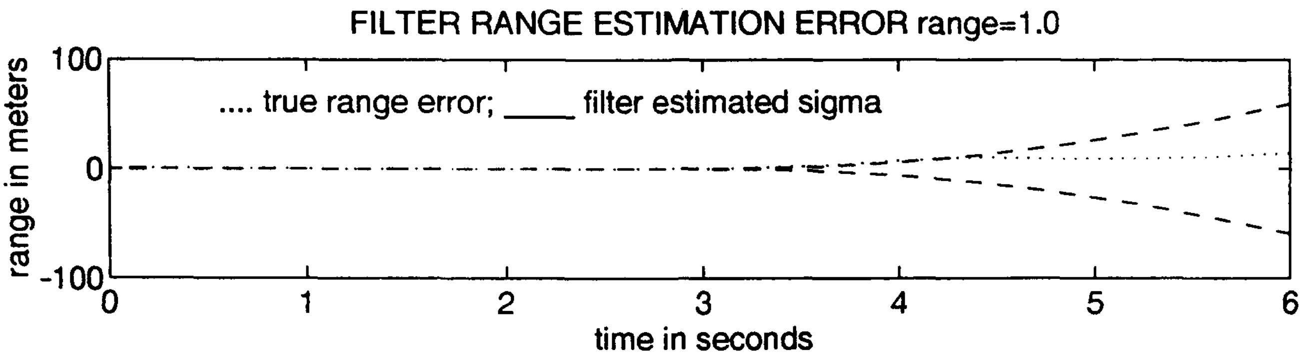
FILTER RANGE ESTIMATION ERROR range=1.0
.... true range error; ____ filter estimated sigma
range in meters
100
0
-100
0
1
2
3
4
5
6
time in seconds

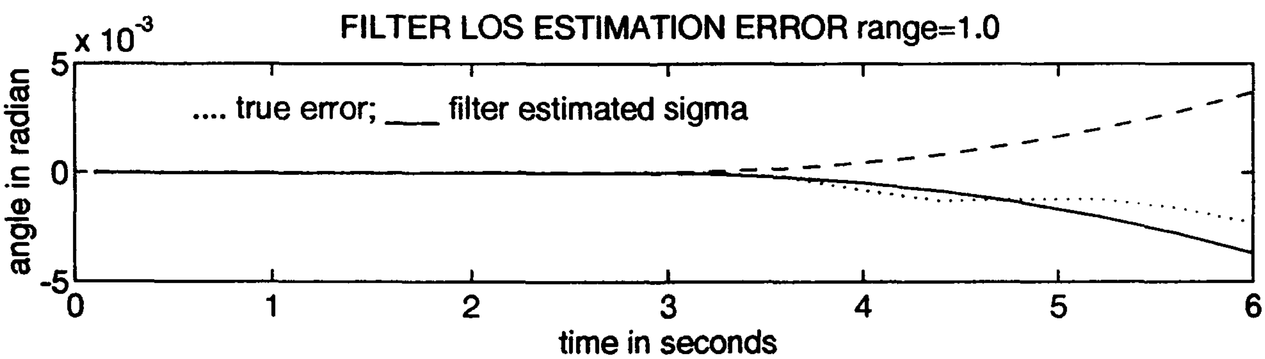
x 10^-3
FILTER LOS ESTIMATION ERROR range=1.0
.... true error; ___ filter estimated sigma
angle in radian
5
0
-5
0
1
2
3
4
5
6
time in seconds

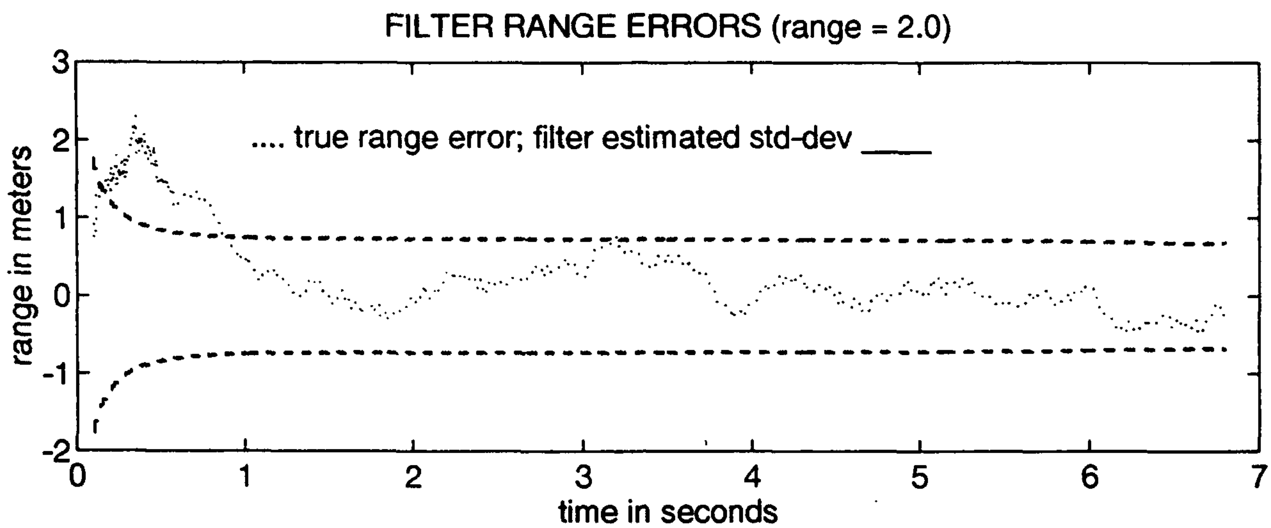
FILTER RANGE ERRORS (range = 2.0)
.... true range error; filter estimated std-dev ____
range in meters
time in seconds
3
2
1
0
-1
-2
0
1
2
3
4
5
6
7

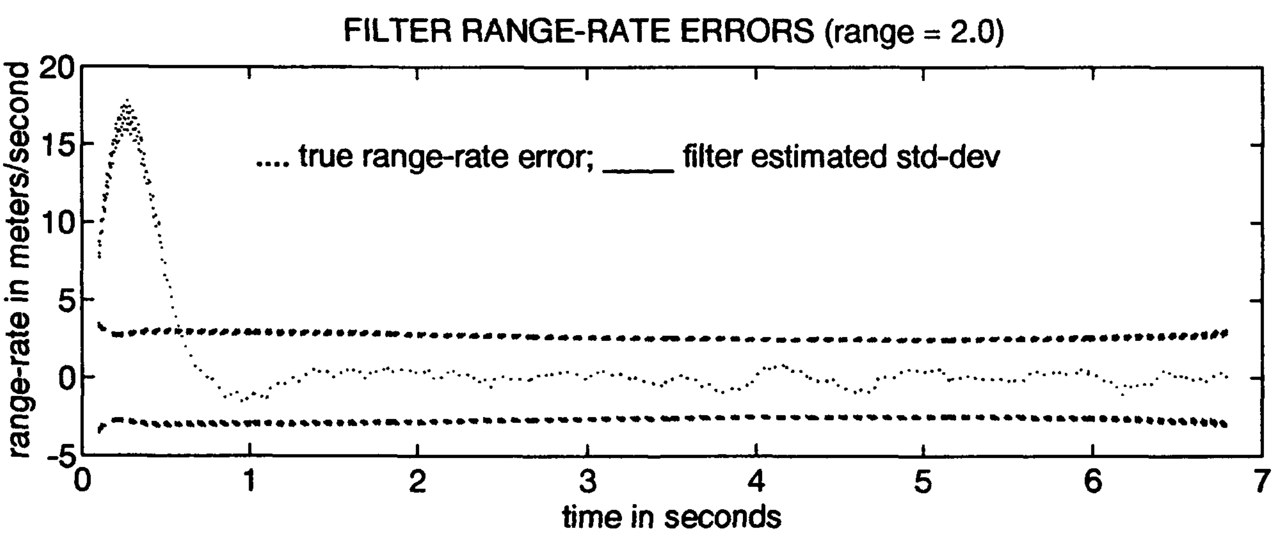
FILTER RANGE-RATE ERRORS (range = 2.0)
.... true range-rate error; ____ filter estimated std-dev
range-rate in meters/second
time in seconds
20
15
10
5
0
-5
0
1
2
3
4
5
6
7

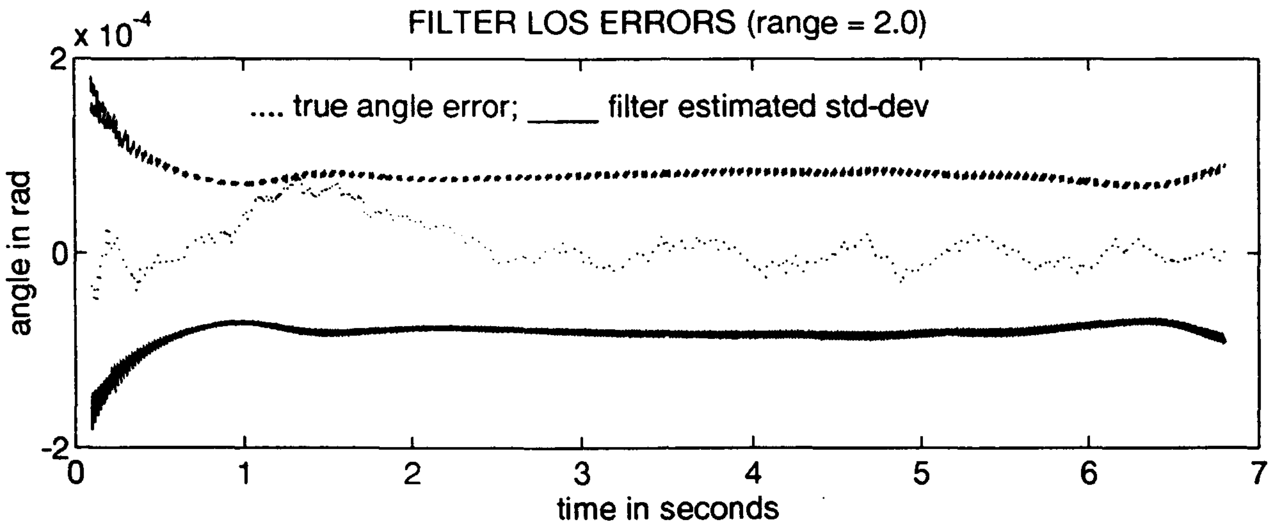
FILTER LOS ERRORS (range = 2.0)
x 10^-4
.... true angle error; ____ filter estimated std-dev
angle in rad
time in seconds
2
0
-2
0 1 2 3 4 5 6 7

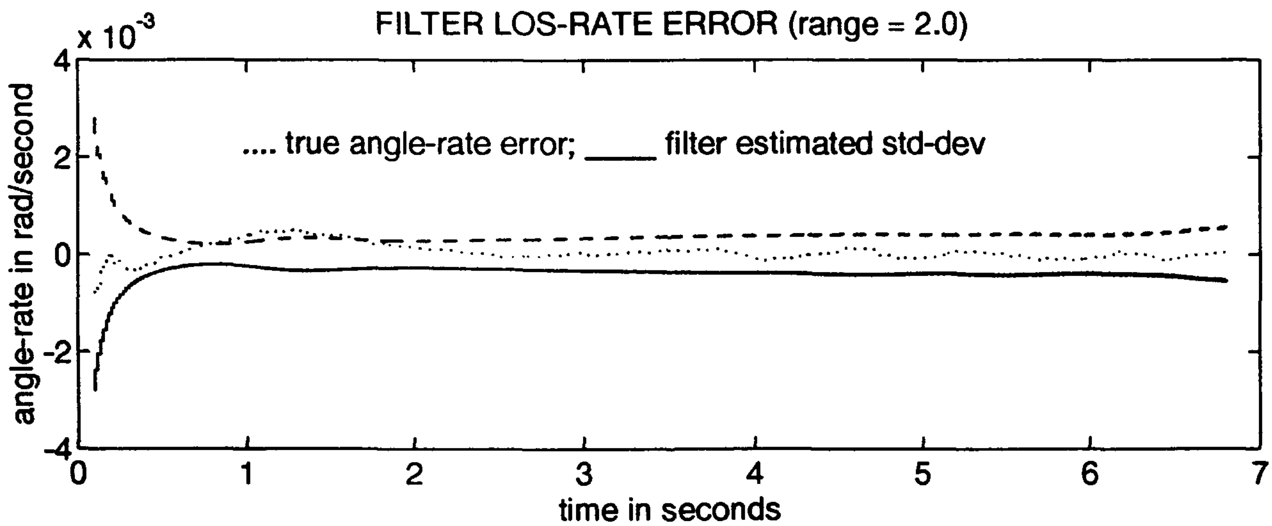
FILTER LOS-RATE ERROR (range = 2.0)
x 10^-3
.... true angle-rate error; ____ filter estimated std-dev
angle-rate in rad/second
time in seconds
4
2
0
-2
-4
0 1 2 3 4 5 6 7

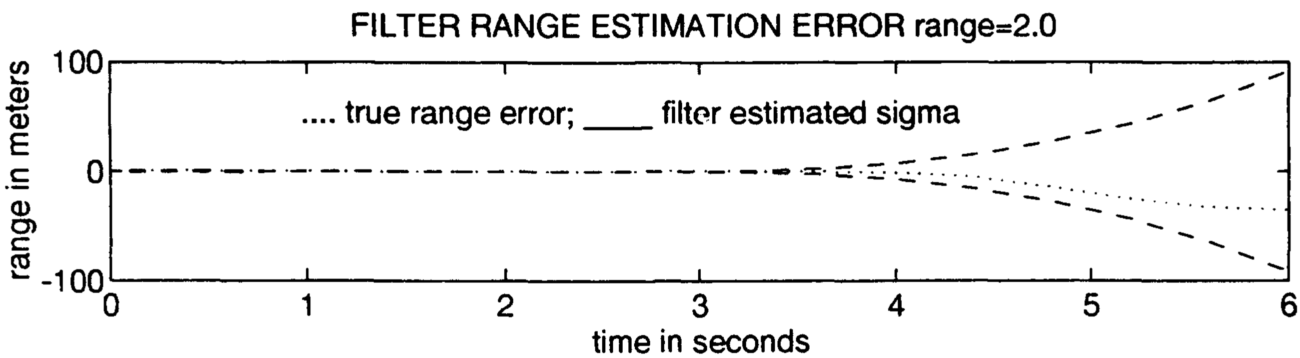

FILTER RANGE ESTIMATION ERROR range=2.0
.... true range error; ____ filter estimated sigma
range in meters
100
0
-100
0
1
2
3
4
5
6
time in seconds

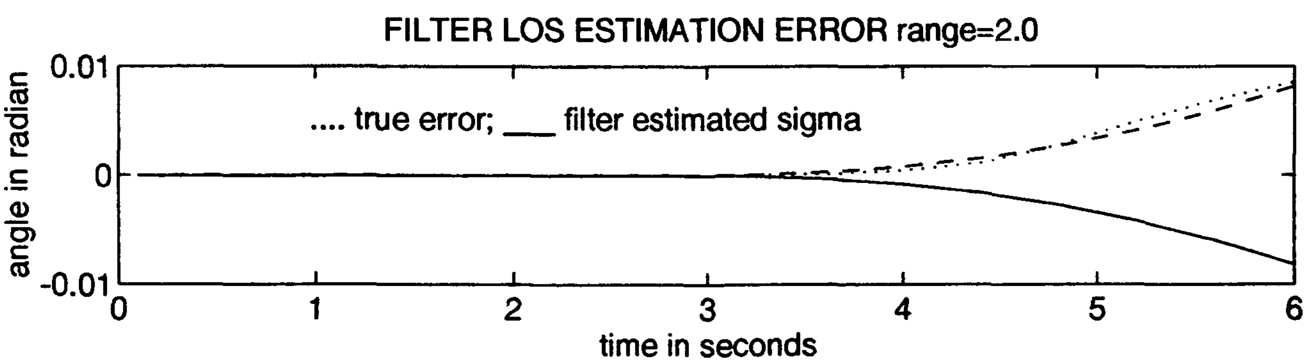

FILTER LOS ESTIMATION ERROR range=2.0
.... true error; ___ filter estimated sigma
angle in radian
0.01
0
-0.01
0
1
2
3
4
5
6
time in seconds

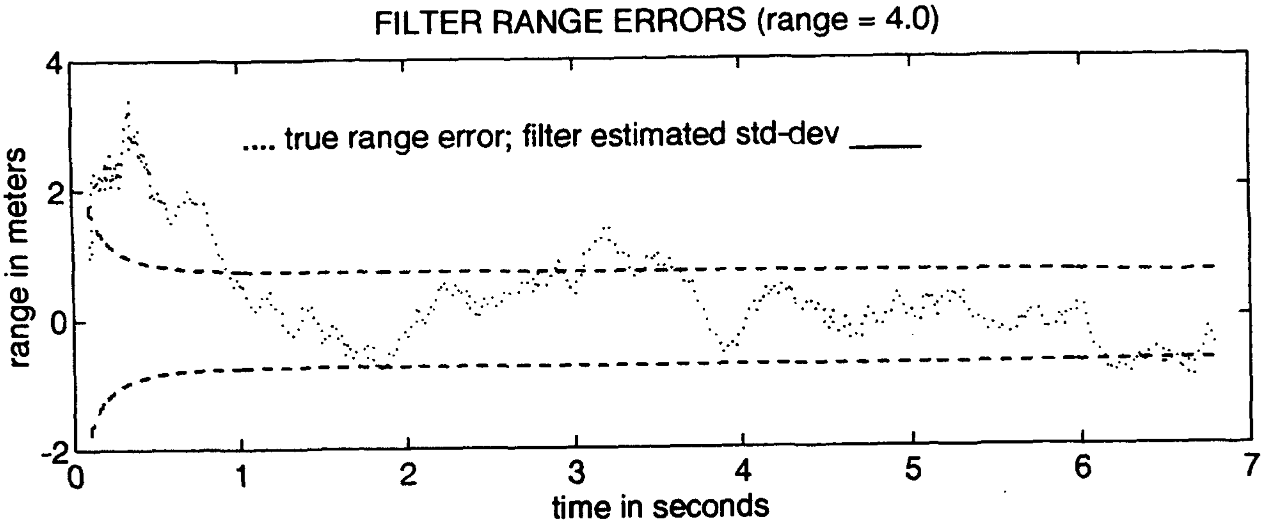

FILTER RANGE ERRORS (range = 4.0)
.... true range error; filter estimated std-dev ____
range in meters
time in seconds
4
2
0
-2
0
1
2
3
4
5
6
7

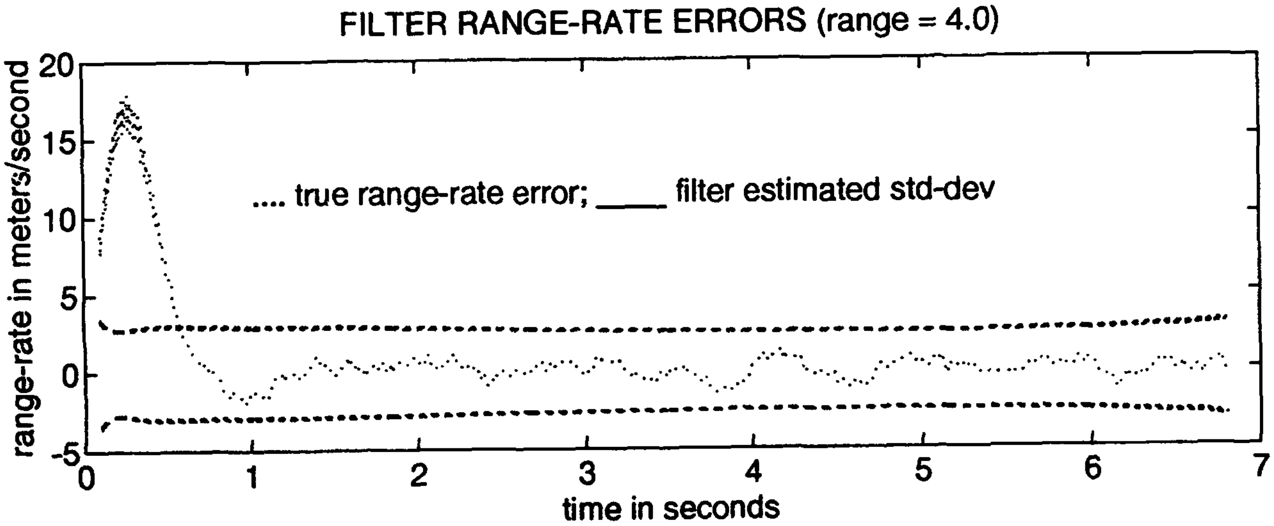

FILTER RANGE-RATE ERRORS (range = 4.0)
.... true range-rate error; ____ filter estimated std-dev
range-rate in meters/second
time in seconds
20
15
10
5
0
-5
0
1
2
3
4
5
6
7

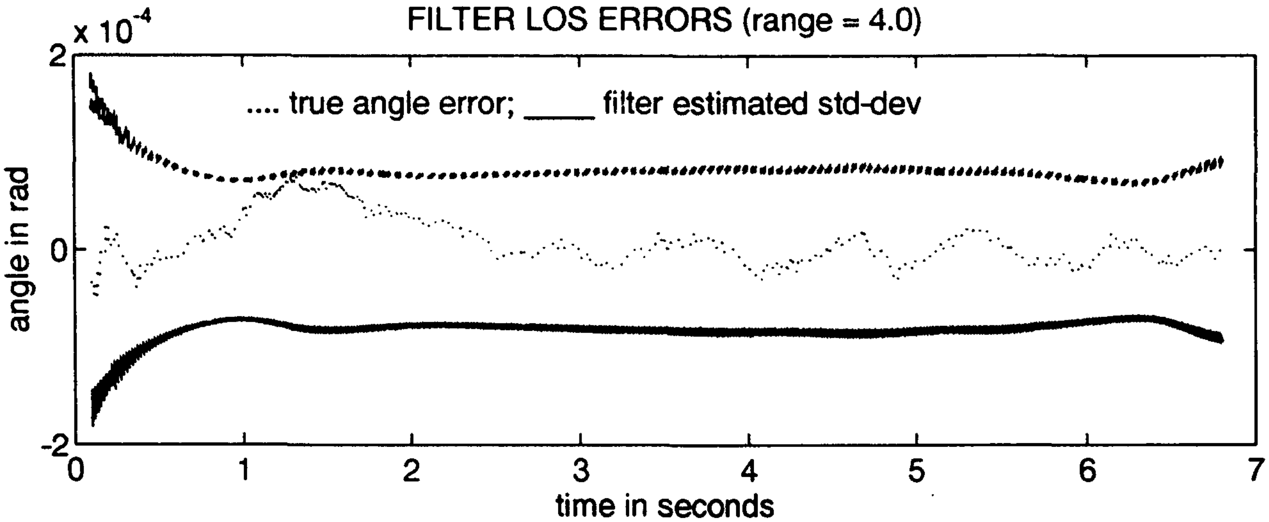
FILTER LOS ERRORS (range = 4.0)
x 10^-4
.... true angle error; _____ filter estimated std-dev
angle in rad
time in seconds
2
0
-2
0
1
2
3
4
5
6
7

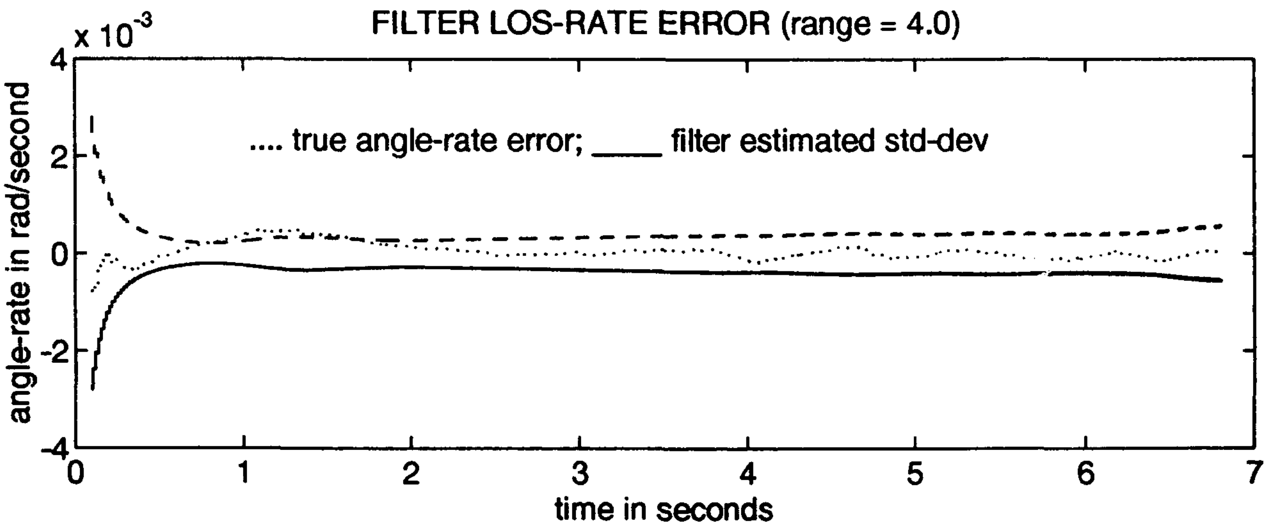
FILTER LOS-RATE ERROR (range = 4.0)
x 10^-3
.... true angle-rate error; ____ filter estimated std-dev
angle-rate in rad/second
time in seconds
4
2
0
-2
-4
0
1
2
3
4
5
6
7

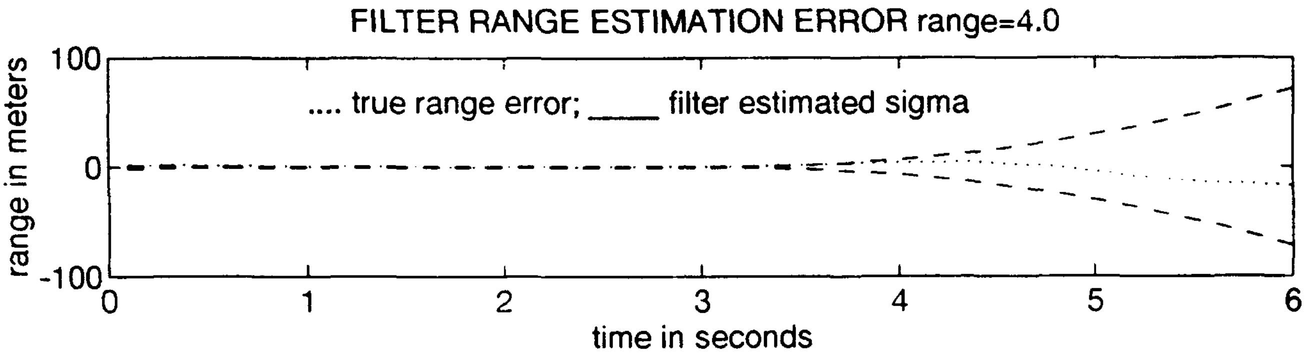
FILTER RANGE ESTIMATION ERROR range=4.0
.... true range error; ____ filter estimated sigma
range in meters
100
0
-100
0
1
2
3
4
5
6
time in seconds

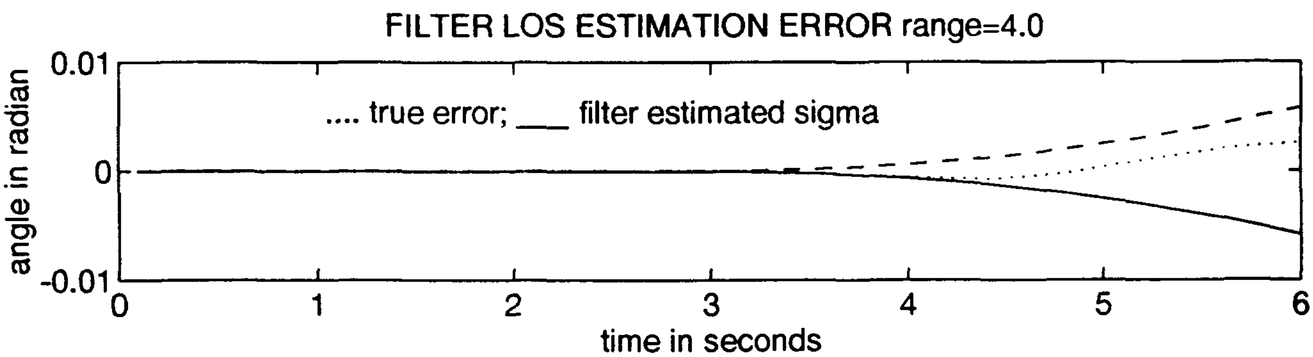
FILTER LOS ESTIMATION ERROR range=4.0
.... true error; ___ filter estimated sigma
angle in radian
0.01
0
-0.01
0
1
2
3
4
5
6
time in seconds

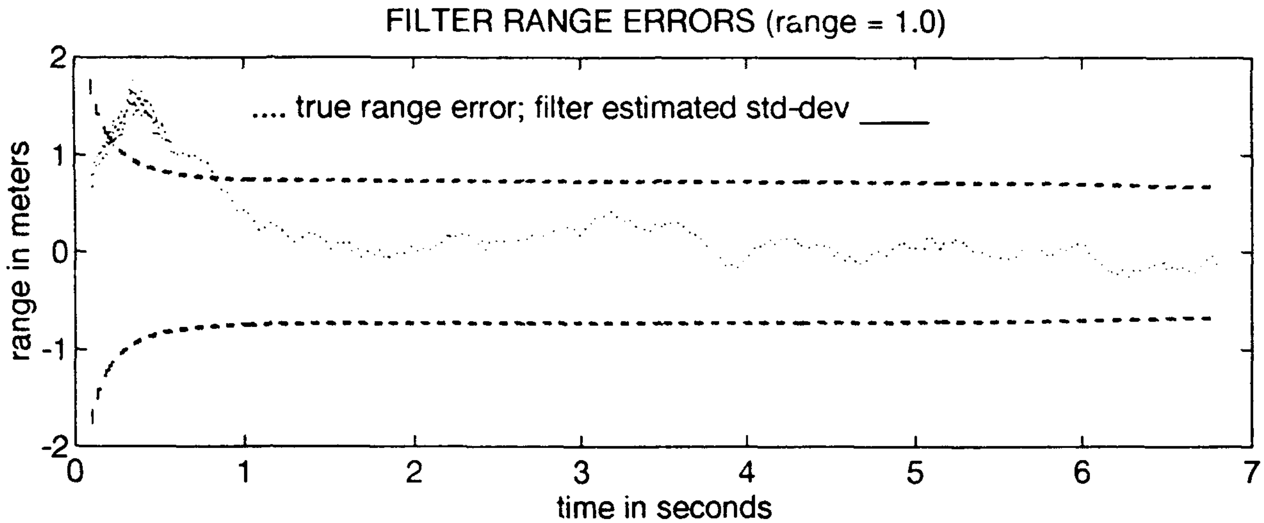
FILTER RANGE ERRORS (range = 1.0)
.... true range error; filter estimated std-dev ____
range in meters
time in seconds
2
1
0
-1
-2
0
1
2
3
4
5
6
7

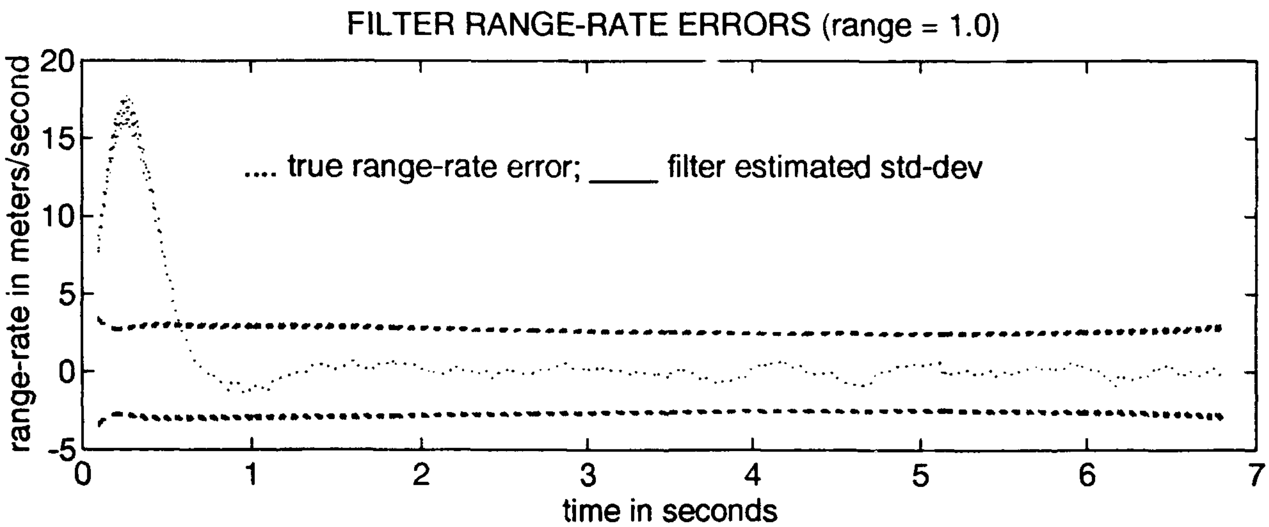
FILTER RANGE-RATE ERRORS (range = 1.0)
.... true range-rate error; ____ filter estimated std-dev
range-rate in meters/second
time in seconds
20
15
10
5
0
-5
0
1
2
3
4
5
6
7

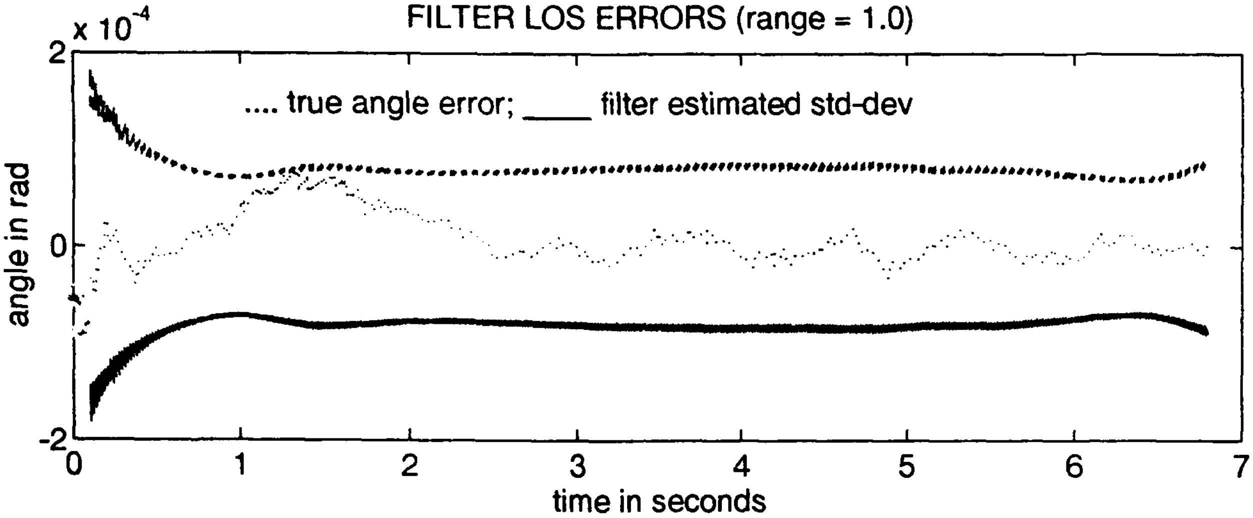
FILTER LOS ERRORS (range = 1.0)
x 10^-4
.... true angle error; ____ filter estimated std-dev
angle in rad
time in seconds
2
0
-2
0 1 2 3 4 5 6 7

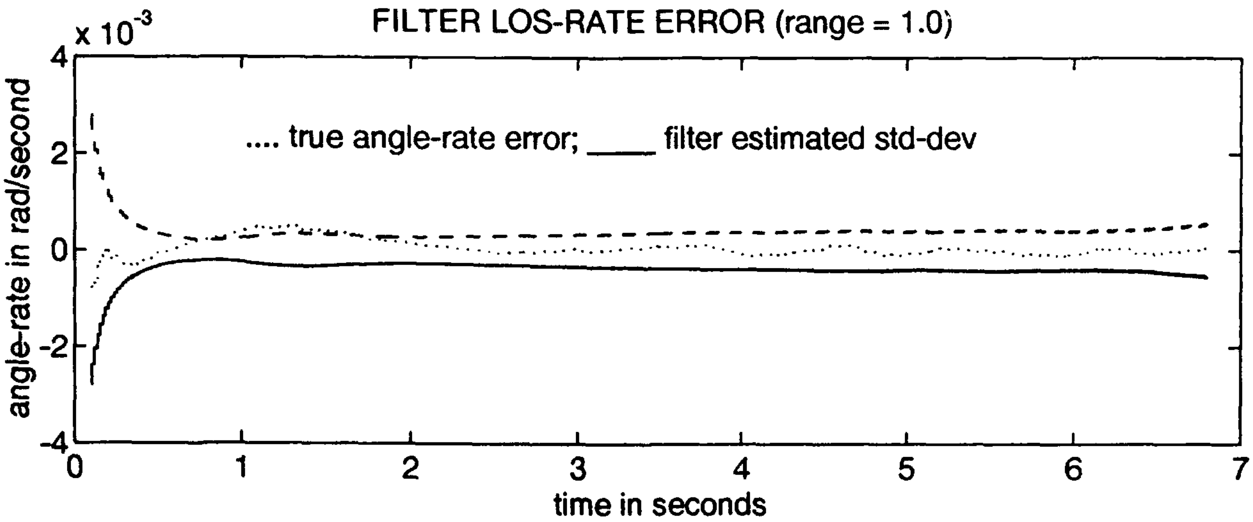
FILTER LOS-RATE ERROR (range = 1.0)
x 10^-3
.... true angle-rate error; ____ filter estimated std-dev
angle-rate in rad/second
time in seconds
4
2
0
-2
-4
0 1 2 3 4 5 6 7

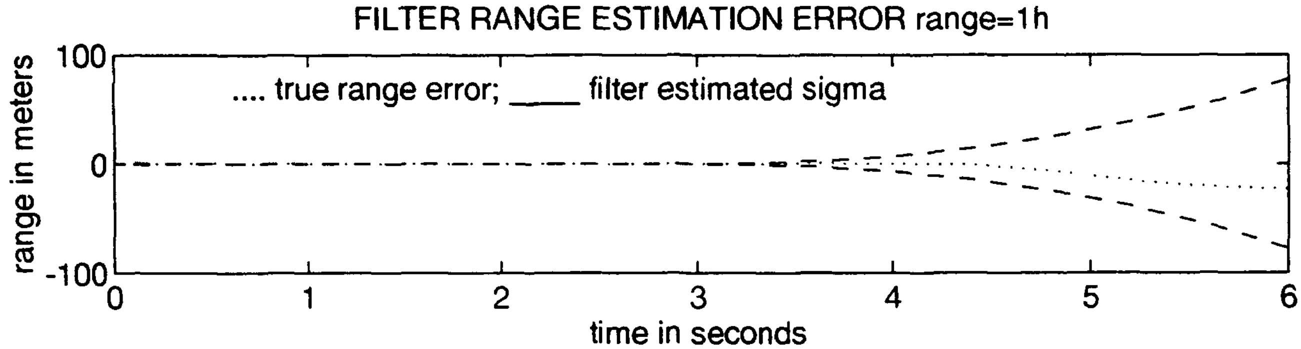
FILTER RANGE ESTIMATION ERROR range=1h
.... true range error; ____ filter estimated sigma
range in meters
100
0
-100
0
1
2
3
4
5
6
time in seconds

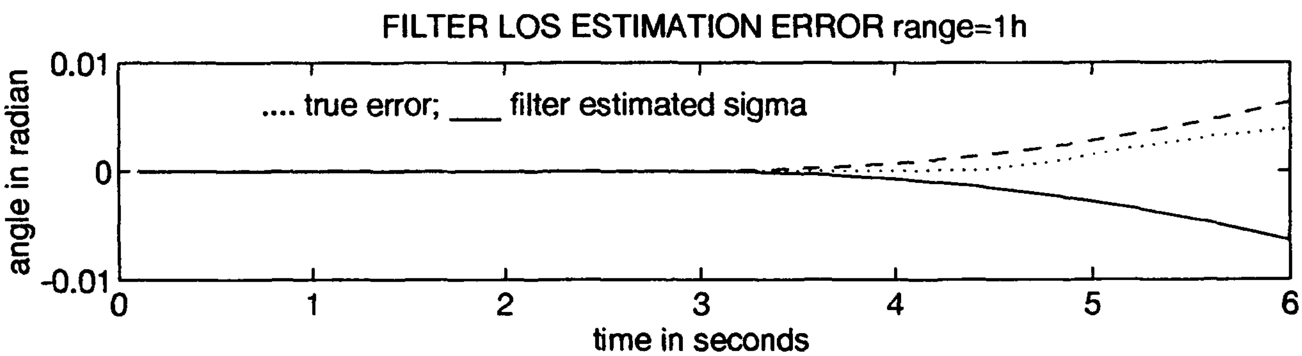
FILTER LOS ESTIMATION ERROR range=1h
.... true error; ___ filter estimated sigma
angle in radian
0.01
0
-0.01
0
1
2
3
4
5
6
time in seconds

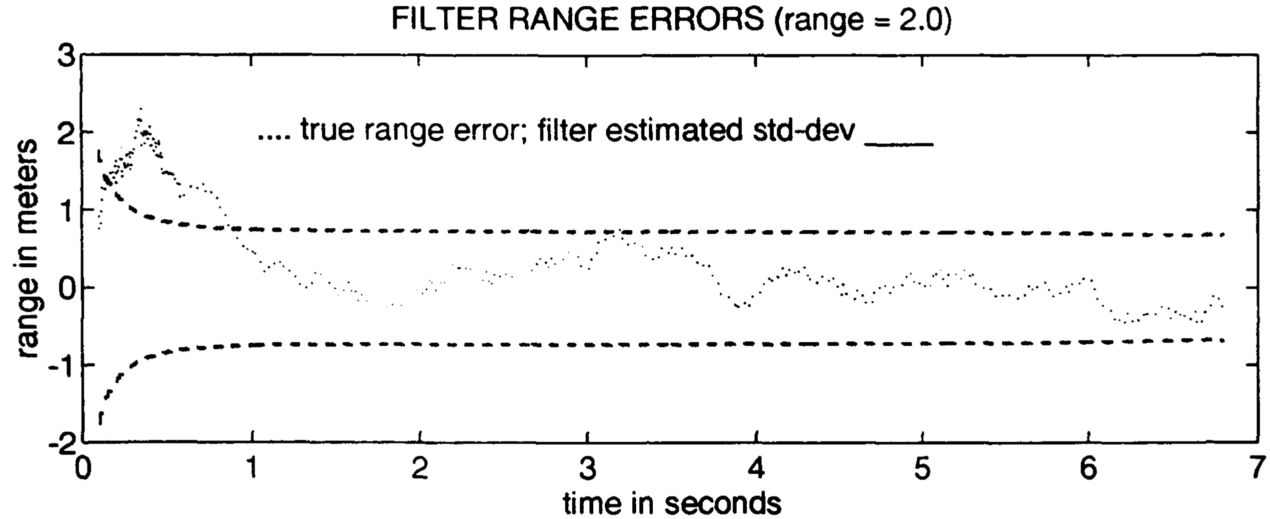
FILTER RANGE ERRORS (range = 2.0)
.... true range error; filter estimated std-dev ____
range in meters
3
2
1
0
-1
-2
0
1
2
3
4
5
6
7
time in seconds

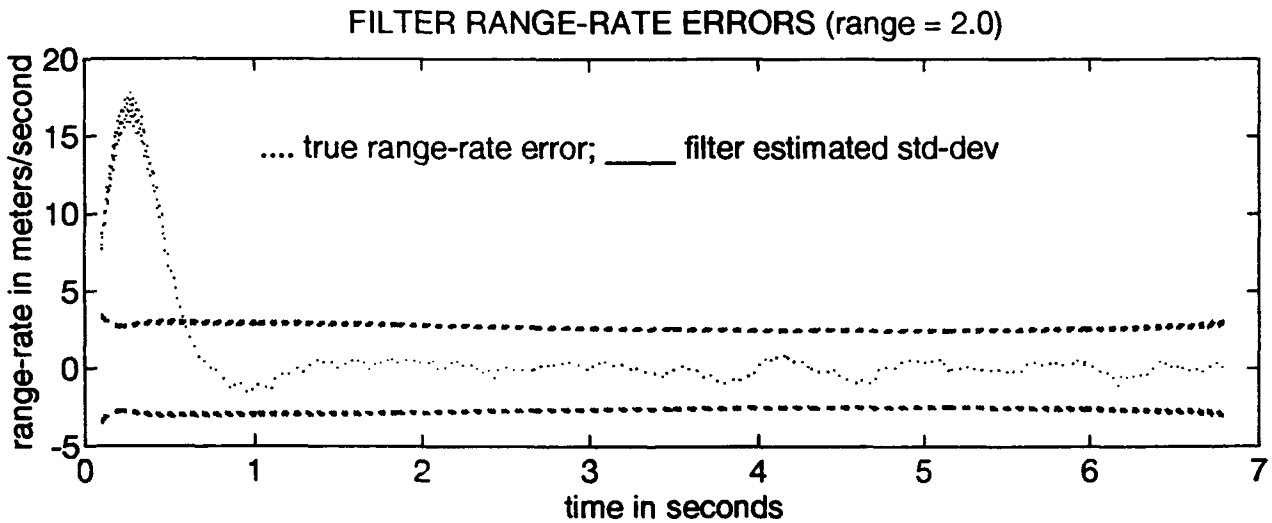
FILTER RANGE-RATE ERRORS (range = 2.0)
.... true range-rate error; ____ filter estimated std-dev
range-rate in meters/second
20
15
10
5
0
-5
0
1
2
3
4
5
6
7
time in seconds

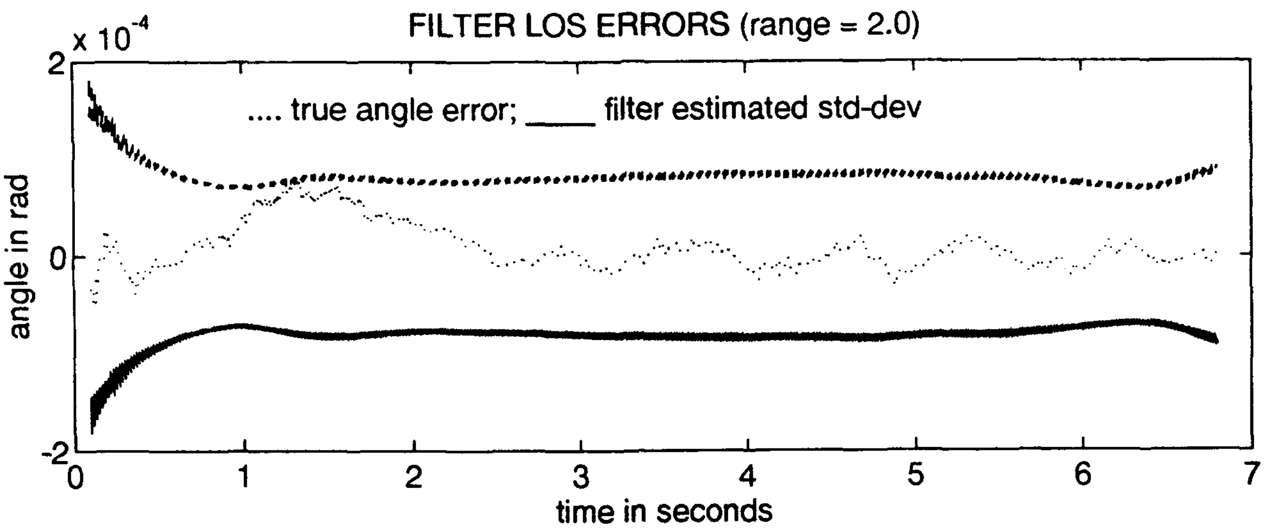
FILTER LOS ERRORS (range = 2.0)
x 10^-4
.... true angle error; ____ filter estimated std-dev
angle in rad
2
0
-2
0
1
2
3
4
5
6
7
time in seconds

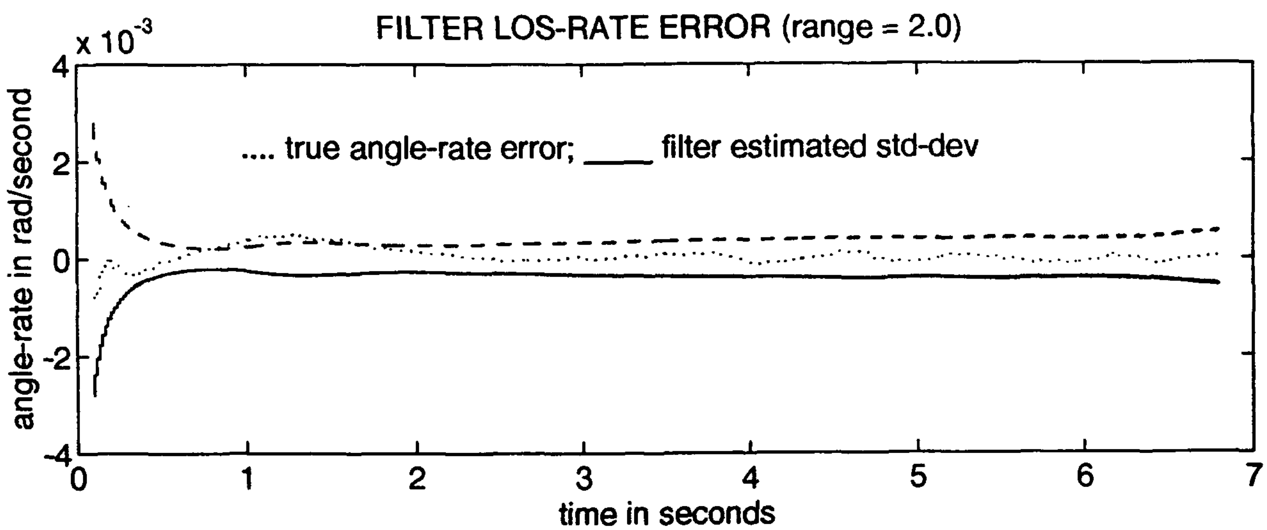
FILTER LOS-RATE ERROR (range = 2.0)
x 10^-3
.... true angle-rate error; ____ filter estimated std-dev
angle-rate in rad/second
4
2
0
-2
-4
0
1
2
3
4
5
6
7
time in seconds

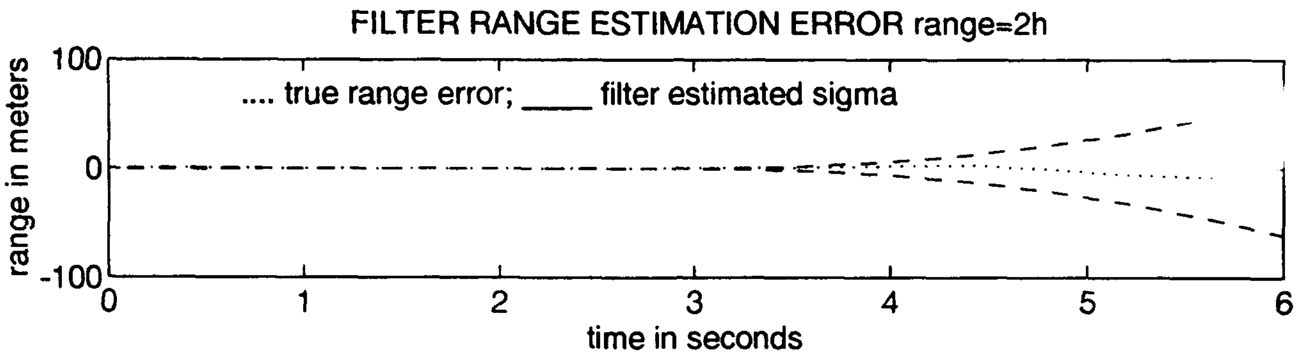
FILTER RANGE ESTIMATION ERROR range=2h
100
0
-100
range in meters
.... true range error; ____ filter estimated sigma
0
1
2
3
4
5
6
time in seconds

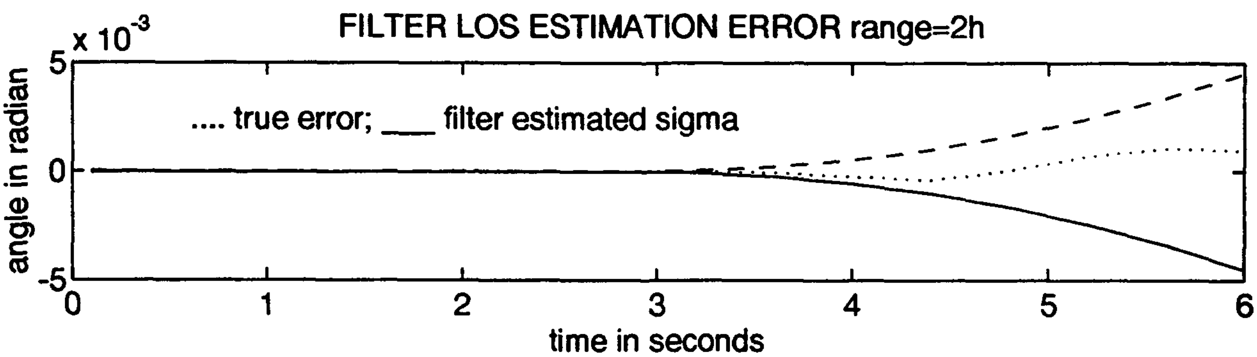
FILTER LOS ESTIMATION ERROR range=2h
x 10^-3
5
0
-5
angle in radian
.... true error; ___ filter estimated sigma
0
1
2
3
4
5
6
time in seconds

FILTER RANGE ERRORS (range = 4.0)

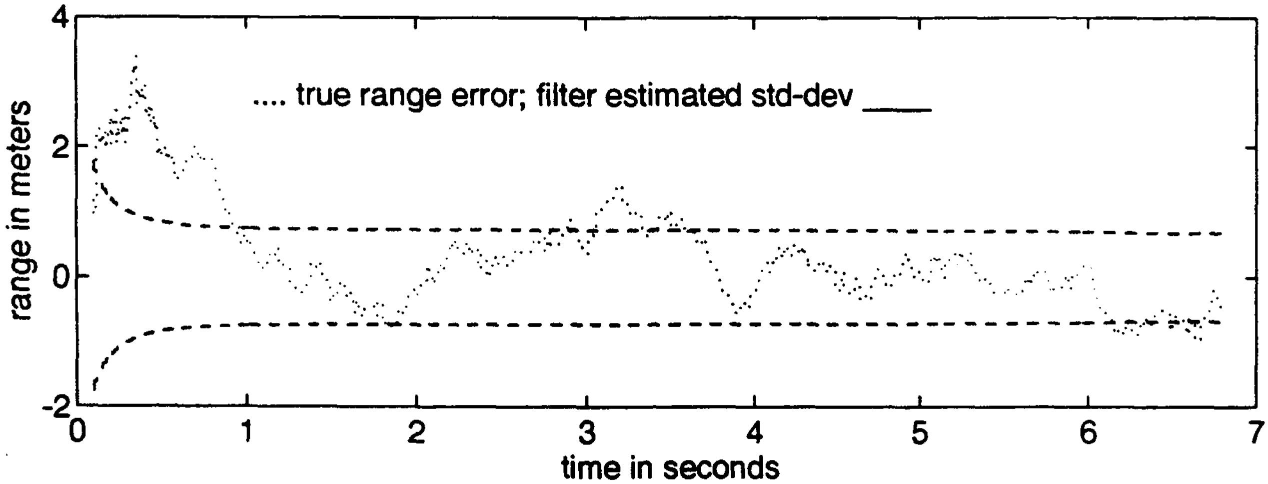

FILTER RANGE-RATE ERRORS (range = 4.0)

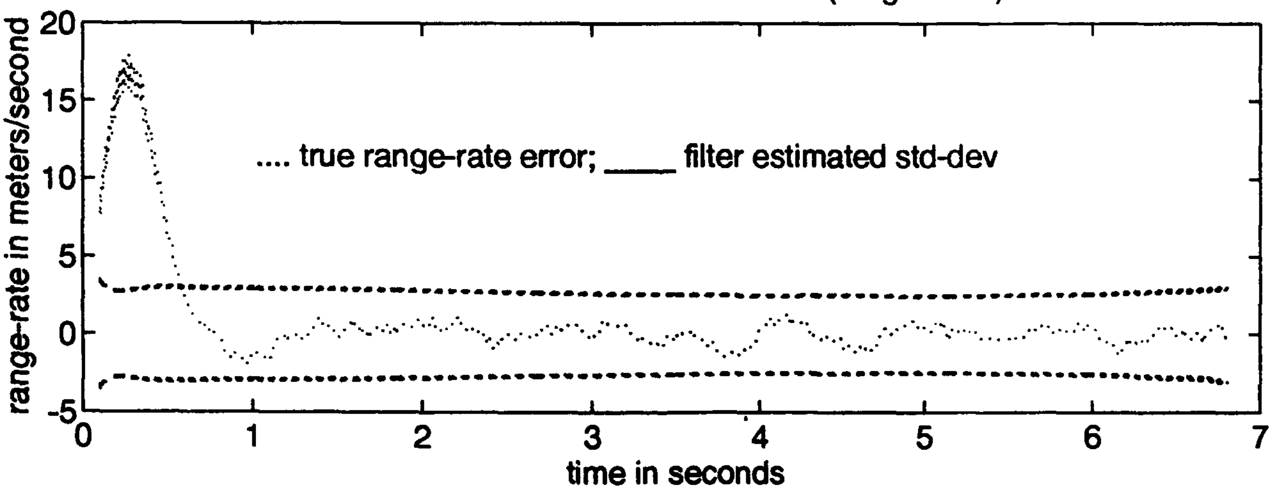

FILTER LOS ERRORS (range = 4.0)

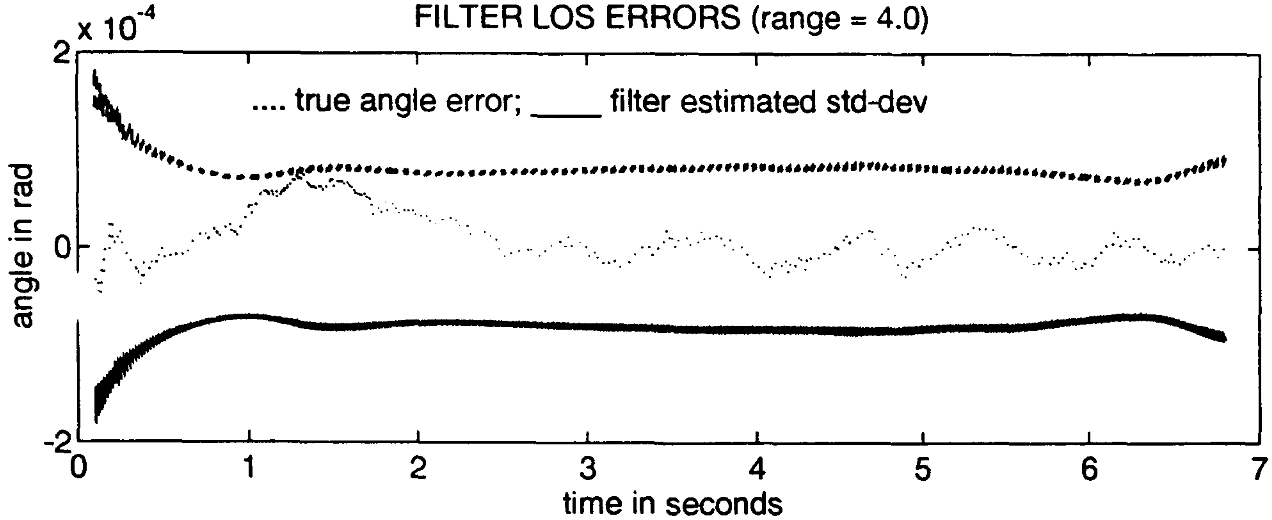

FILTER LOS-RATE ERROR (range = 4.0)

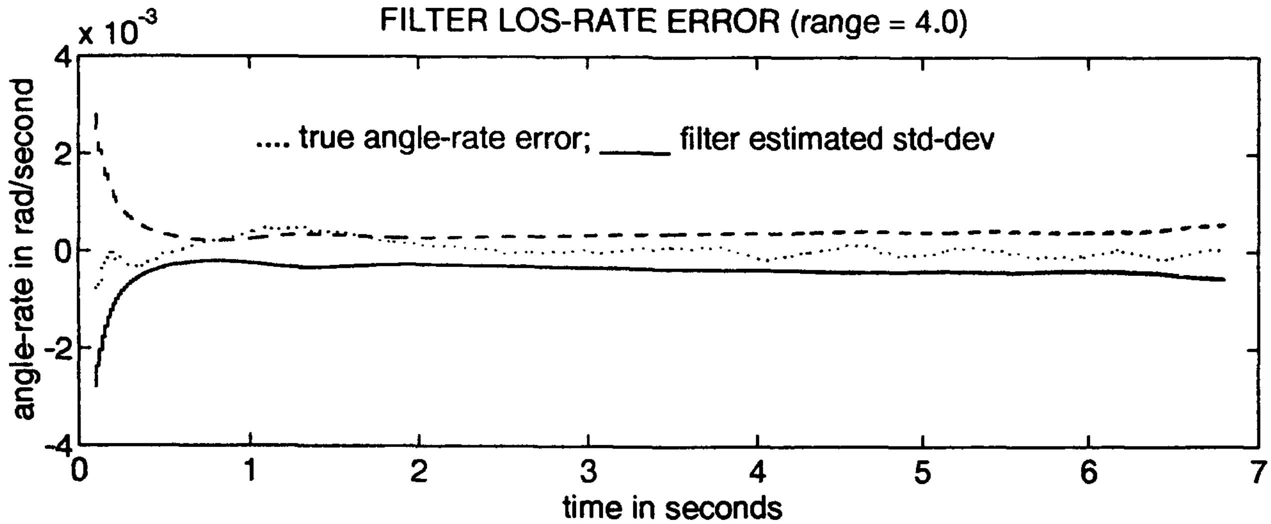

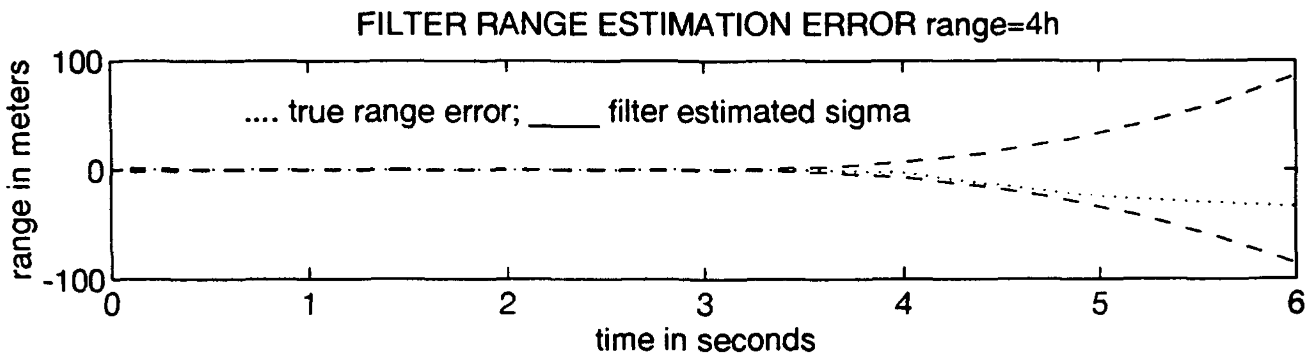
FILTER RANGE ESTIMATION ERROR range=4h
.... true range error; ____ filter estimated sigma
range in meters
100
0
-100
0
1
2
3
4
5
6
time in seconds

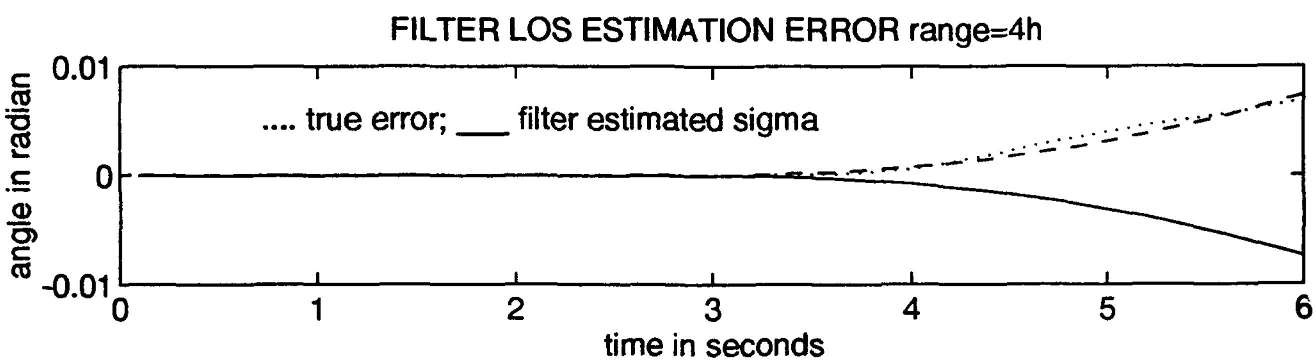
FILTER LOS ESTIMATION ERROR range=4h
.... true error; ___ filter estimated sigma
angle in radian
0.01
0
-0.01
0
1
2
3
4
5
6
time in seconds

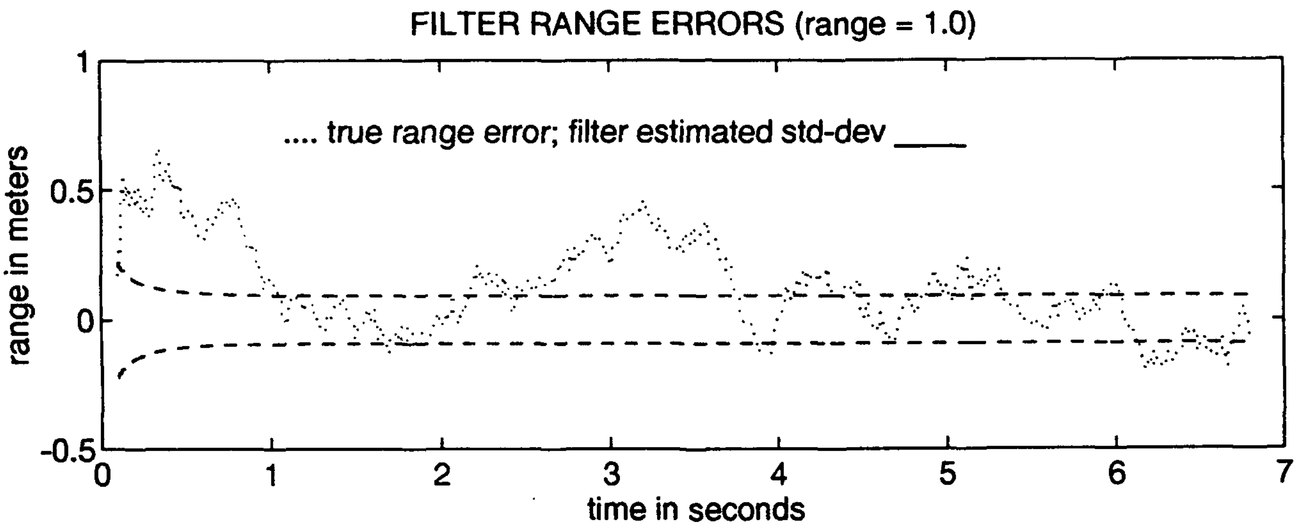
FILTER RANGE ERRORS (range = 1.0)
.... true range error; filter estimated std-dev ____
range in meters
1
0.5
0
-0.5
0
1
2
3
4
5
6
7
time in seconds

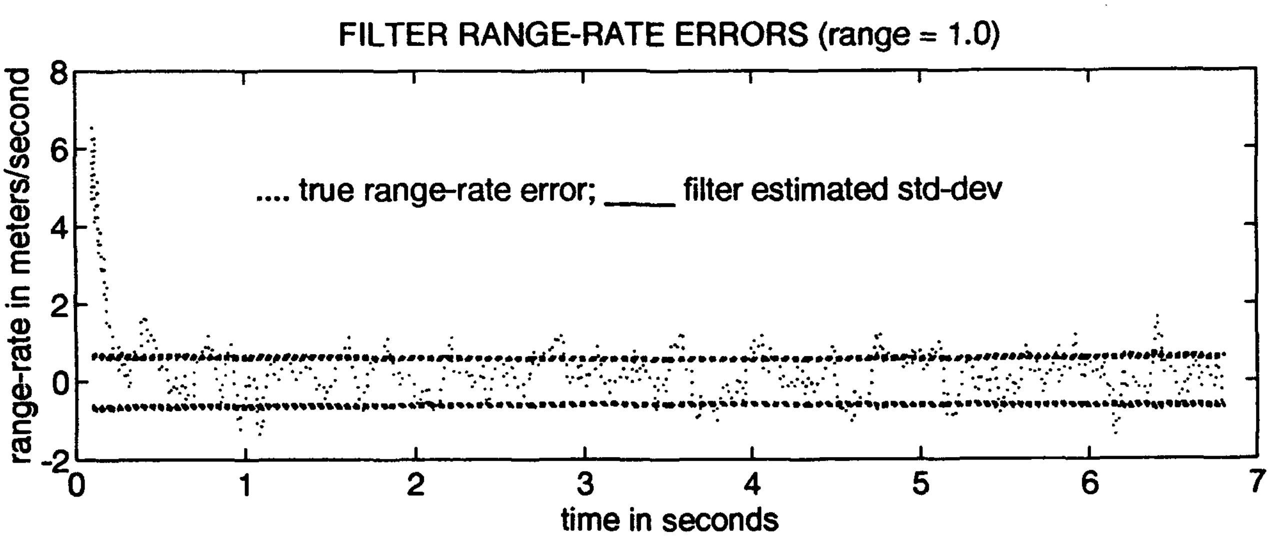
FILTER RANGE-RATE ERRORS (range = 1.0)
.... true range-rate error; ____ filter estimated std-dev
range-rate in meters/second
8
6
4
2
0
-2
0
1
2
3
4
5
6
7
time in seconds

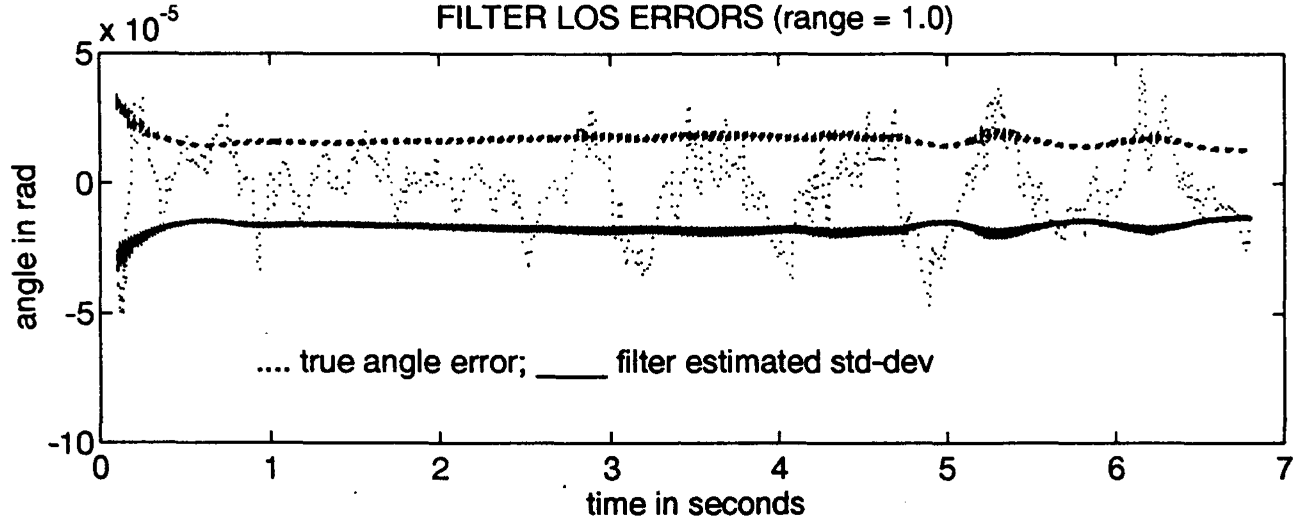
FILTER LOS ERRORS (range = 1.0)
x 10^-5
5
0
-5
-10
angle in rad
.... true angle error; ____ filter estimated std-dev
0
1
2
3
4
5
6
7
time in seconds

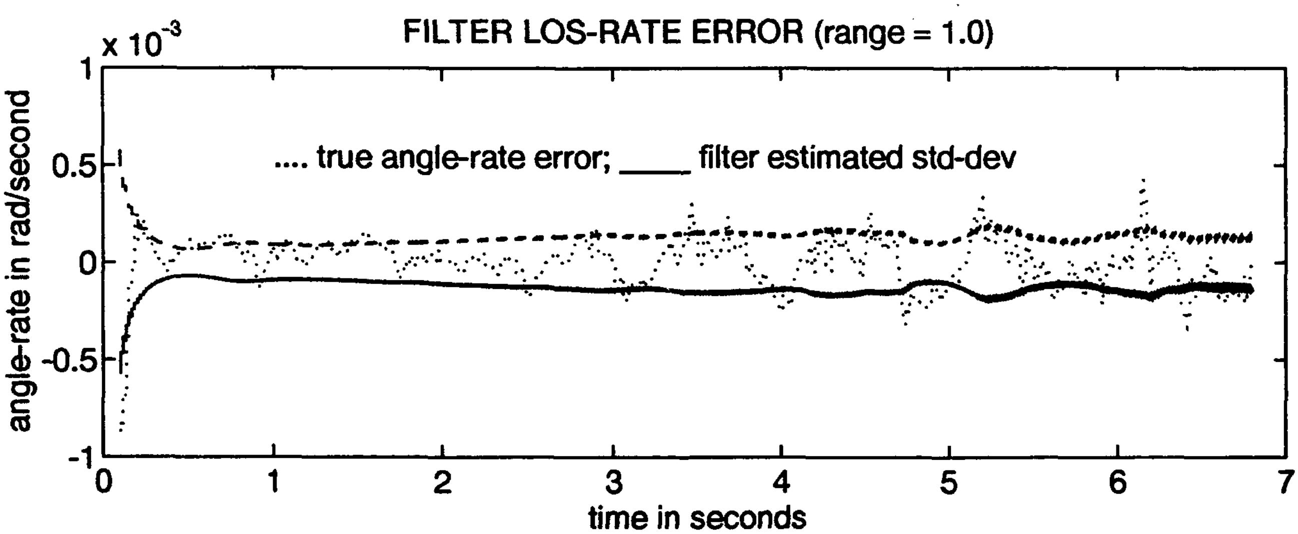
FILTER LOS-RATE ERROR (range = 1.0)
x 10^-3
1
0.5
0
-0.5
-1
angle-rate in rad/second
.... true angle-rate error; ____ filter estimated std-dev
0
1
2
3
4
5
6
7
time in seconds

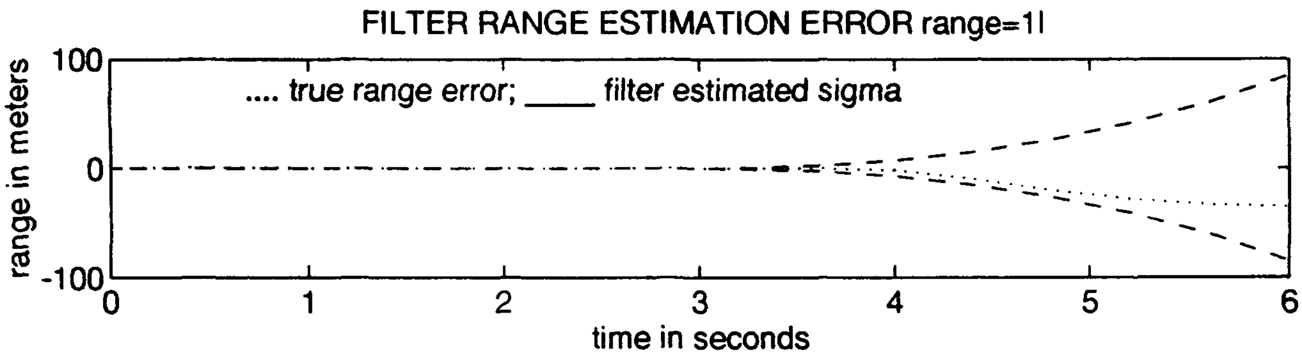
FILTER RANGE ESTIMATION ERROR range=1l
.... true range error; ____ filter estimated sigma
range in meters
100
0
-100
0
1
2
3
4
5
6
time in seconds

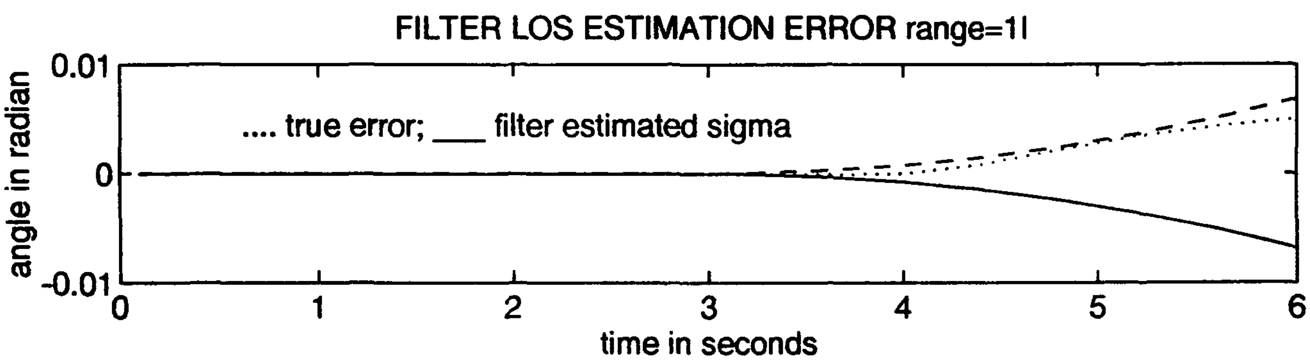
FILTER LOS ESTIMATION ERROR range=1l
.... true error; ___ filter estimated sigma
angle in radian
0.01
0
-0.01
0
1
2
3
4
5
6
time in seconds

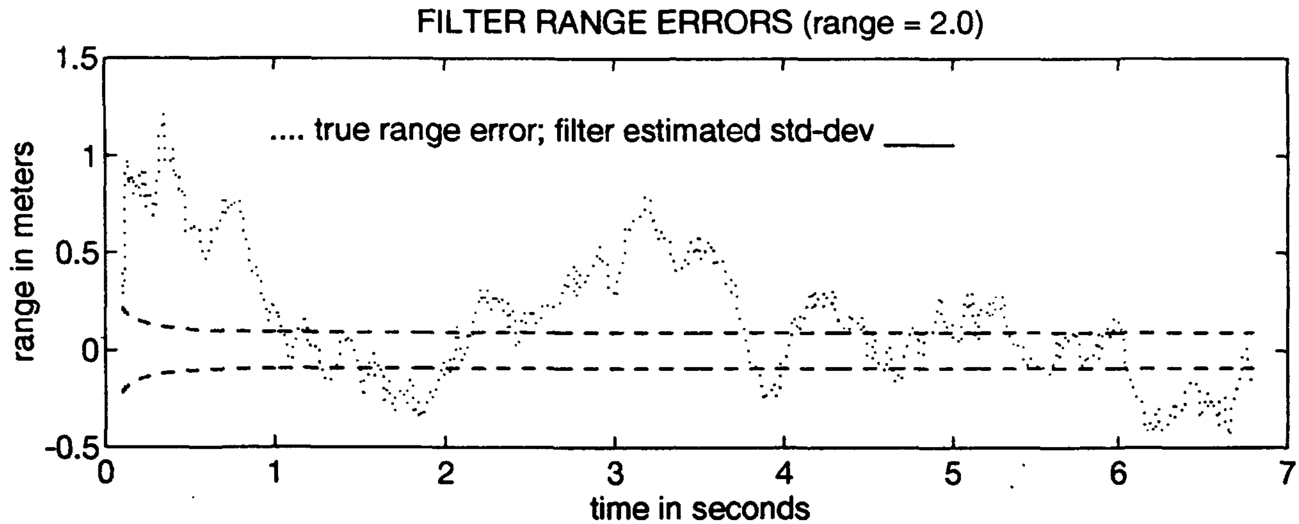
FILTER RANGE ERRORS (range = 2.0)
.... true range error; filter estimated std-dev ____
range in meters
time in seconds
1.5
1
0.5
0
-0.5
0
1
2
3
4
5
6
7

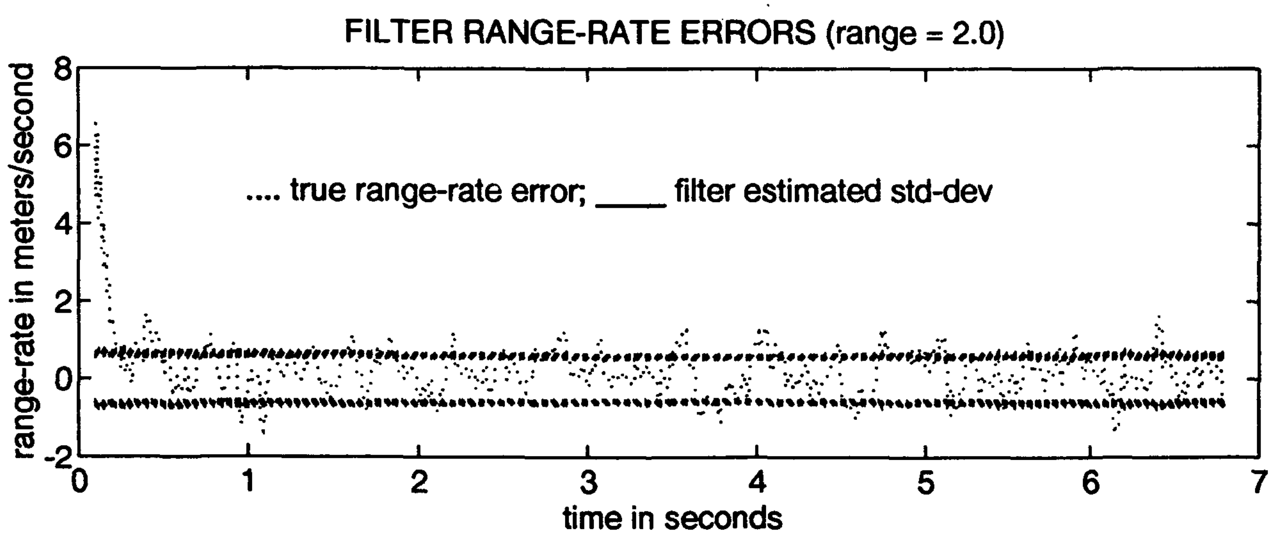
FILTER RANGE-RATE ERRORS (range = 2.0)
.... true range-rate error; ____ filter estimated std-dev
range-rate in meters/second
time in seconds
8
6
4
2
0
-2
0
1
2
3
4
5
6
7

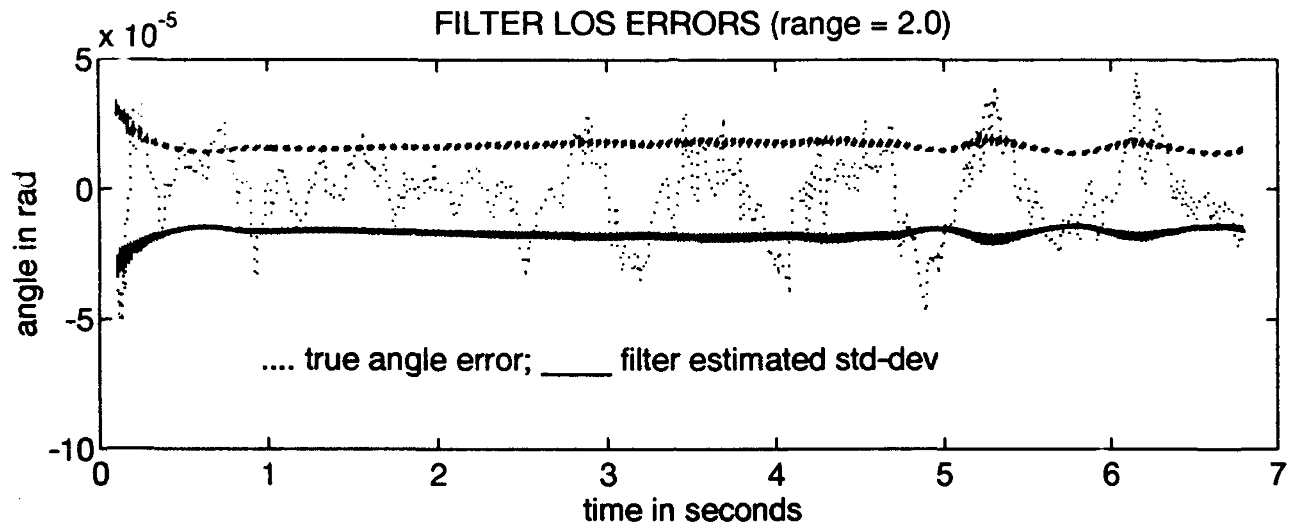
FILTER LOS ERRORS (range = 2.0)
x 10^-5
5
0
-5
-10
angle in rad
.... true angle error; ____ filter estimated std-dev
0
1
2
3
4
5
6
7
time in seconds

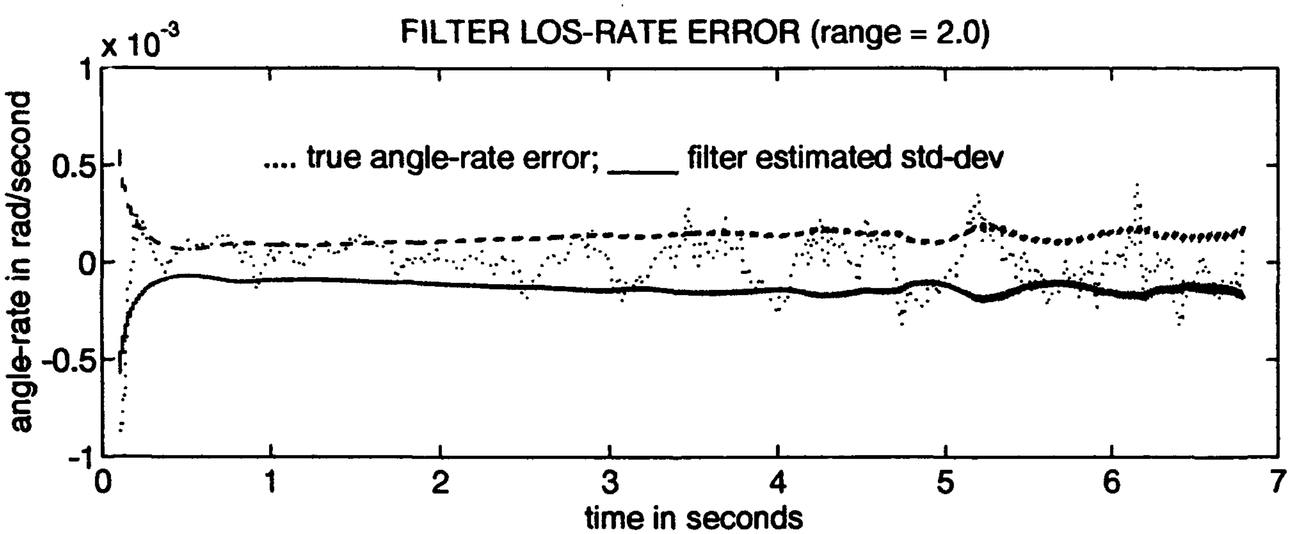
FILTER LOS-RATE ERROR (range = 2.0)
x 10^-3
1
0.5
0
-0.5
-1
angle-rate in rad/second
.... true angle-rate error; ____ filter estimated std-dev
0
1
2
3
4
5
6
7
time in seconds

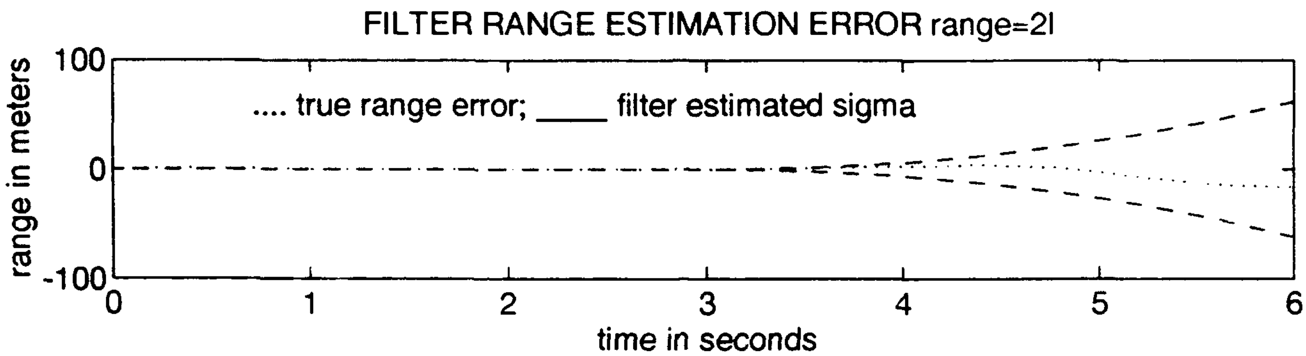
FILTER RANGE ESTIMATION ERROR range=2l
.... true range error; ____ filter estimated sigma
range in meters
100
0
-100
0
1
2
3
4
5
6
time in seconds

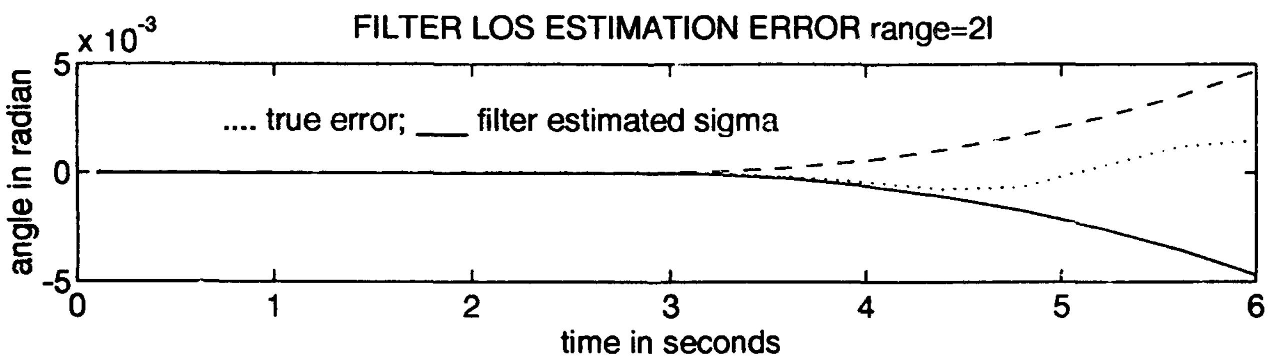
FILTER LOS ESTIMATION ERROR range=2l
x 10^-3
.... true error; ___ filter estimated sigma
angle in radian
5
0
-5
0
1
2
3
4
5
6
time in seconds

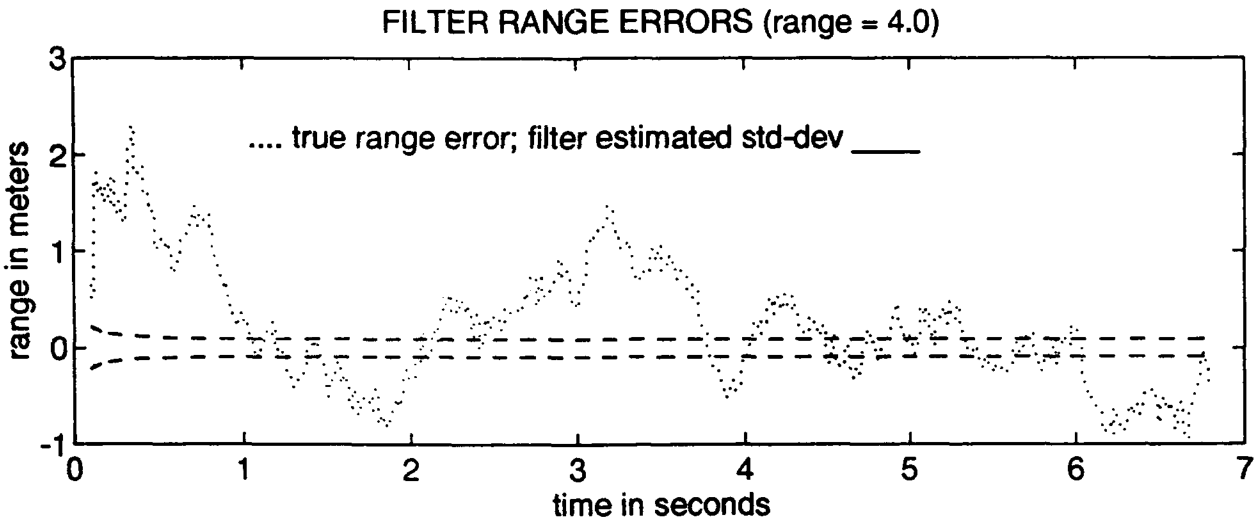
FILTER RANGE ERRORS (range = 4.0)
.... true range error; filter estimated std-dev ____
range in meters
time in seconds
3
2
1
0
-1
0
1
2
3
4
5
6
7

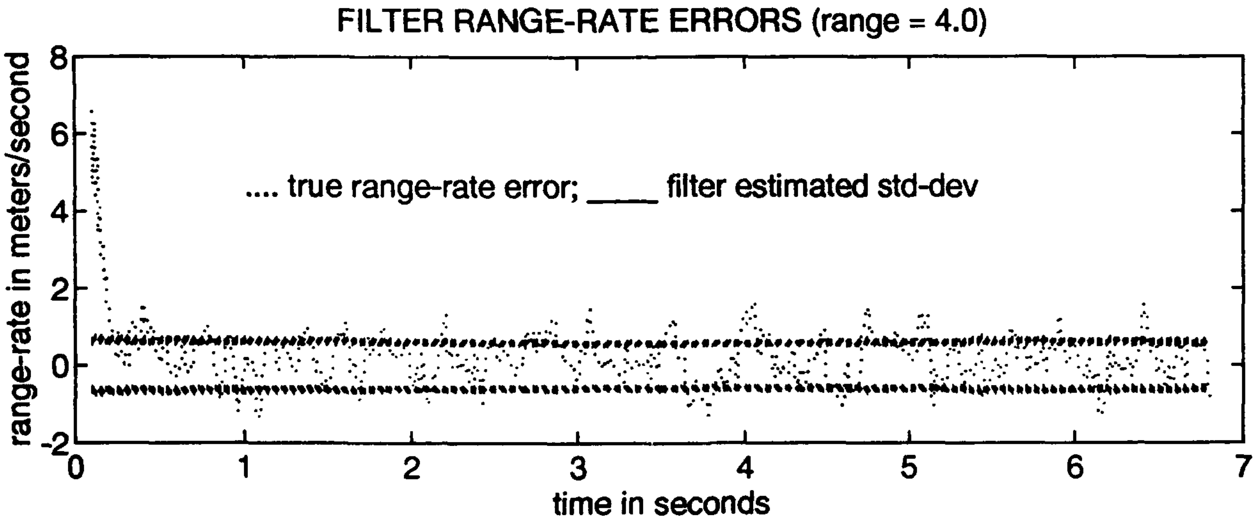
FILTER RANGE-RATE ERRORS (range = 4.0)
.... true range-rate error; ____ filter estimated std-dev
range-rate in meters/second
time in seconds
8
6
4
2
0
-2
0
1
2
3
4
5
6
7

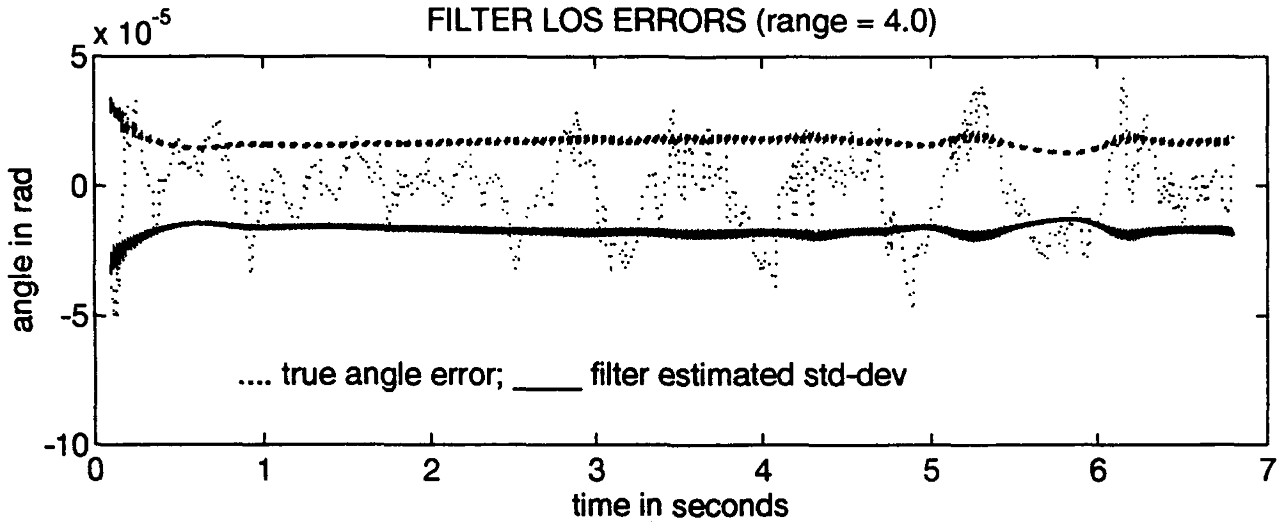
FILTER LOS ERRORS (range = 4.0)
x 10^-5
5
0
-5
-10
angle in rad
.... true angle error; ____ filter estimated std-dev
0
1
2
3
4
5
6
7
time in seconds

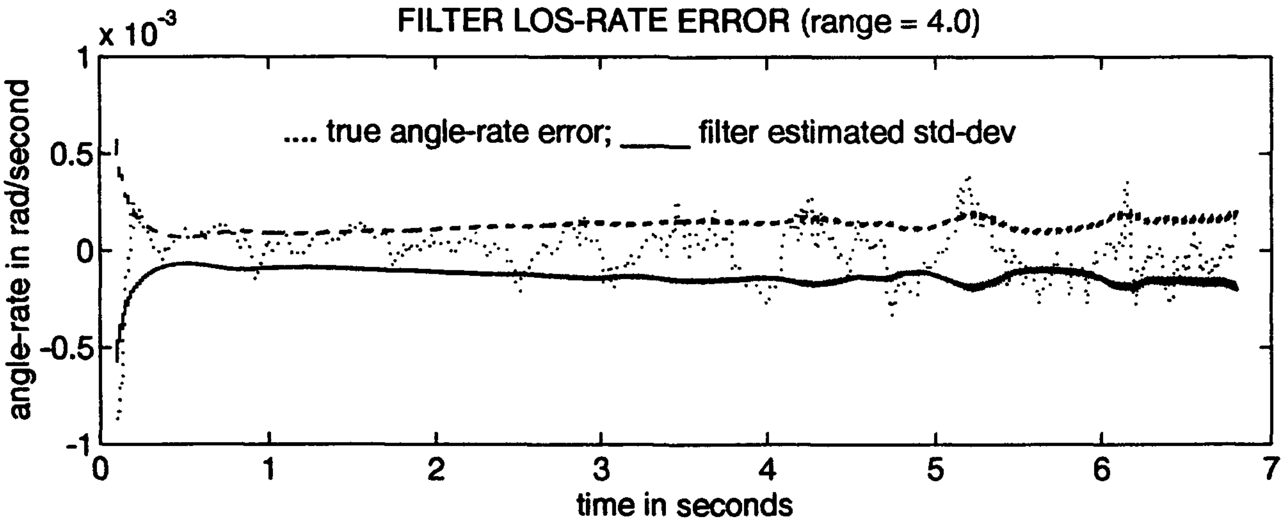
FILTER LOS-RATE ERROR (range = 4.0)
x 10^-3
1
0.5
0
-0.5
-1
angle-rate in rad/second
.... true angle-rate error; ____ filter estimated std-dev
0
1
2
3
4
5
6
7
time in seconds

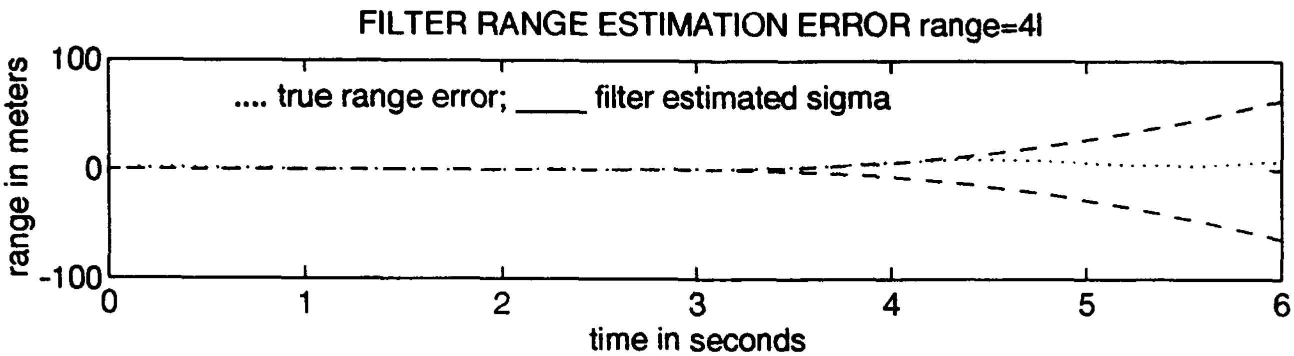
FILTER RANGE ESTIMATION ERROR range=4l
.... true range error; ____ filter estimated sigma
range in meters
100
0
-100
0
1
2
3
4
5
6
time in seconds

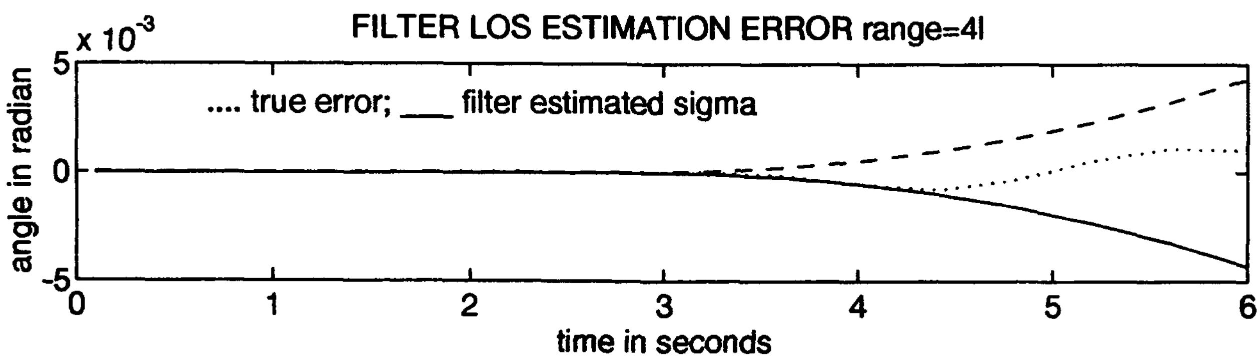
FILTER LOS ESTIMATION ERROR range=4l
x 10-3
.... true error; ___ filter estimated sigma
angle in radian
5
0
-5
0
1
2
3
4
5
6
time in seconds

Appendix C

This appendix contains simulation plots for the ladar range-rate noise run set. The aircraft is initially heading east and beginning a 3 g turn to the north. All measurement noises (except range-rate) and dynamic noise strengths are set at baseline values. The missile is launched from the $\pi/4$ approach angle. Each run has a trajectory plot, estimated range errors, range-rate errors, LOS errors and LOS-rate errors. Estimated range and LOS plots are found in the $\pi/4$ missile approach angle run plots in Appendix A. The baseline (see Figure 4-4) range-rate measurement error is 1.0 m/sec, with additional runs made for range-rate errors of 2.0, 4.0 and 8.0 m/sec. Each plot set contains filter divergence plots of range error and angle error for a three second divergence from three to six seconds. The divergence plots, which define the volume cross-section, are used for performance comparison versus the baseline. In Figures C-2 thru C-19 both the filter and truth model measurement noises are varied from the baseline. In Figures C-20 thru C-37 only the filter measurement noise is varied above baseline (i.e., the filter noise is set "high"). In Figures C-38 thru C-55 only the true measurement noise is varied above baseline (i.e., the filter noise is set "low").

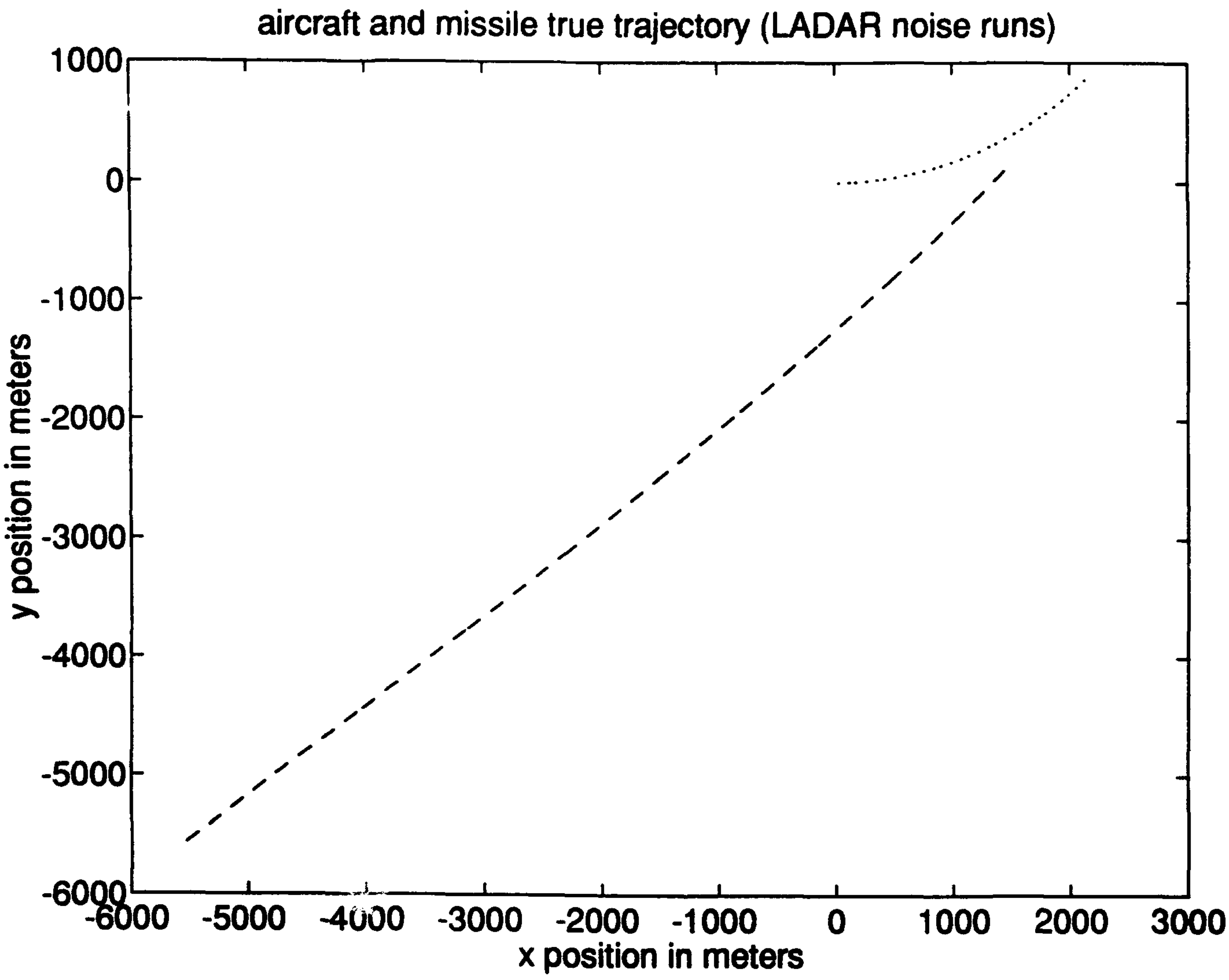
aircraft and missile true trajectory (LADAR noise runs)
1000
0
-1000
-2000
-3000
-4000
-5000
-6000
y position in meters
-6000
-5000
-4000
-3000
-2000
-1000
0
1000
2000
3000
x position in meters

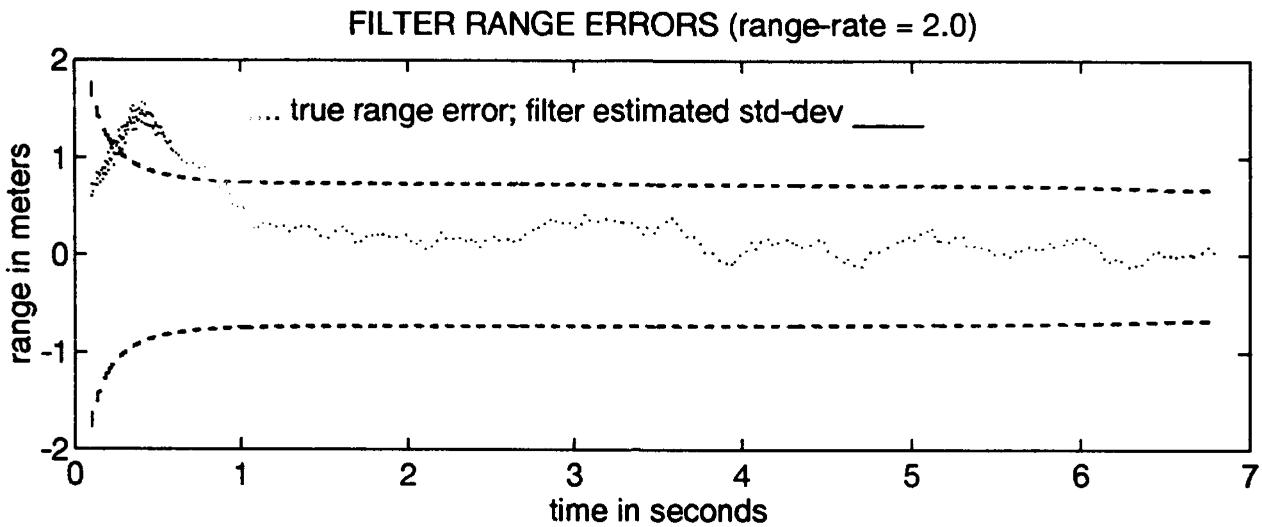
FILTER RANGE ERRORS (range-rate = 2.0)
.... true range error; filter estimated std-dev ____
range in meters
2
1
0
-1
-2
0
1
2
3
4
5
6
7
time in seconds

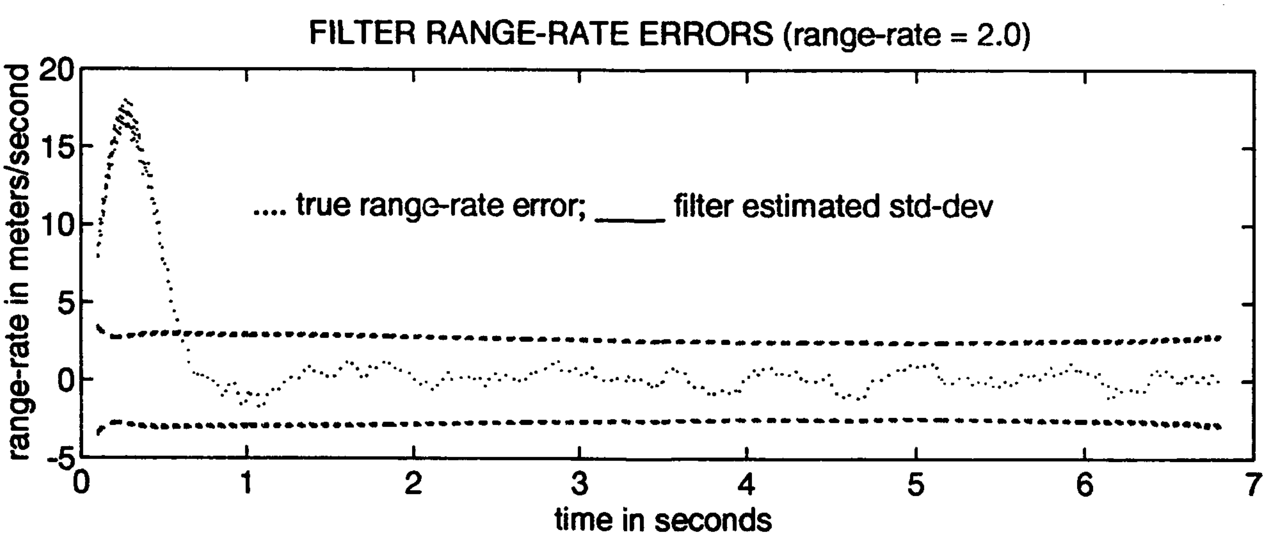
FILTER RANGE-RATE ERRORS (range-rate = 2.0)
.... true range-rate error; ____ filter estimated std-dev
range-rate in meters/second
20
15
10
5
0
-5
0
1
2
3
4
5
6
7
time in seconds

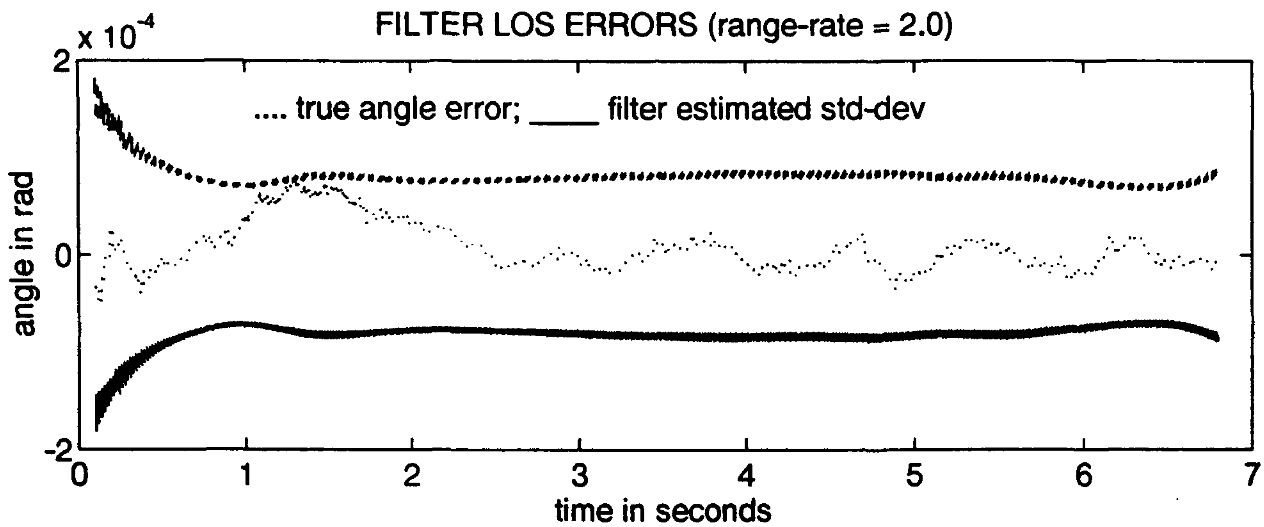
FILTER LOS ERRORS (range-rate = 2.0)
x 10^-4
.... true angle error; ____ filter estimated std-dev
angle in rad
2
0
-2
0
1
2
3
4
5
6
7
time in seconds

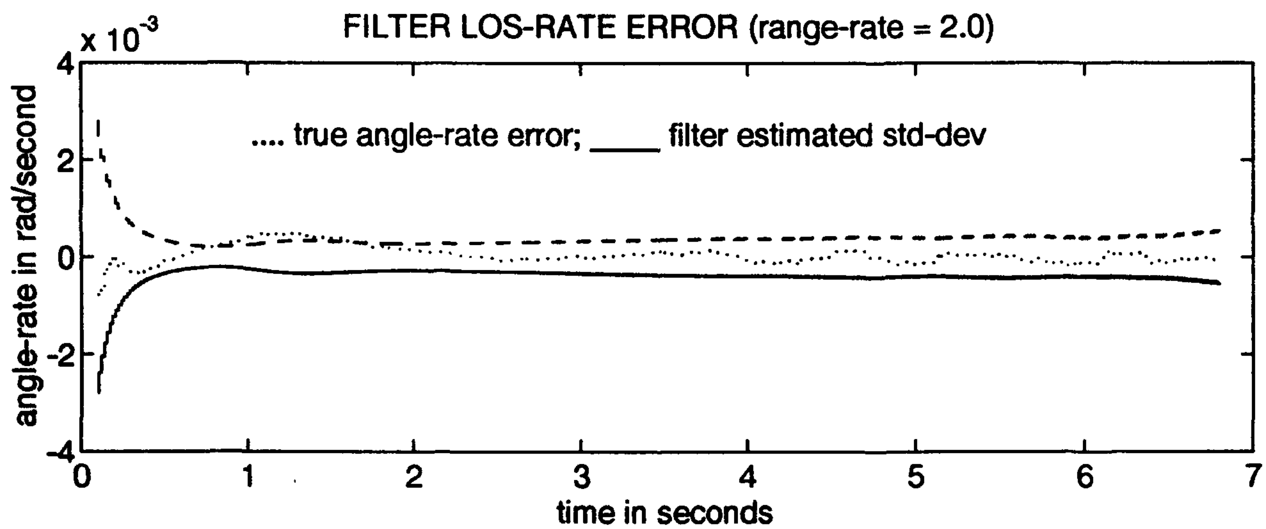
FILTER LOS-RATE ERROR (range-rate = 2.0)
x 10^-3
.... true angle-rate error; ____ filter estimated std-dev
angle-rate in rad/second
4
2
0
-2
-4
0
1
2
3
4
5
6
7
time in seconds

FILTER RANGE ESTIMATION ERROR range-rate=2.0

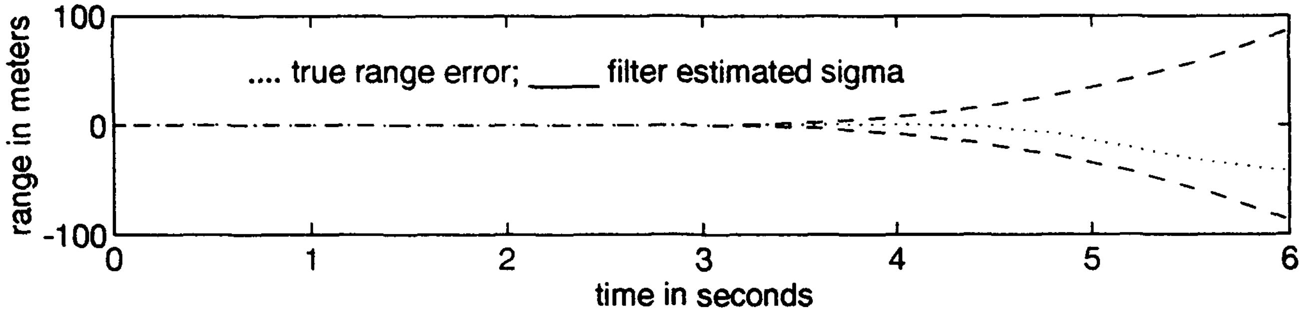

FILTER LOS ESTIMATION ERROR range-rate=2.00

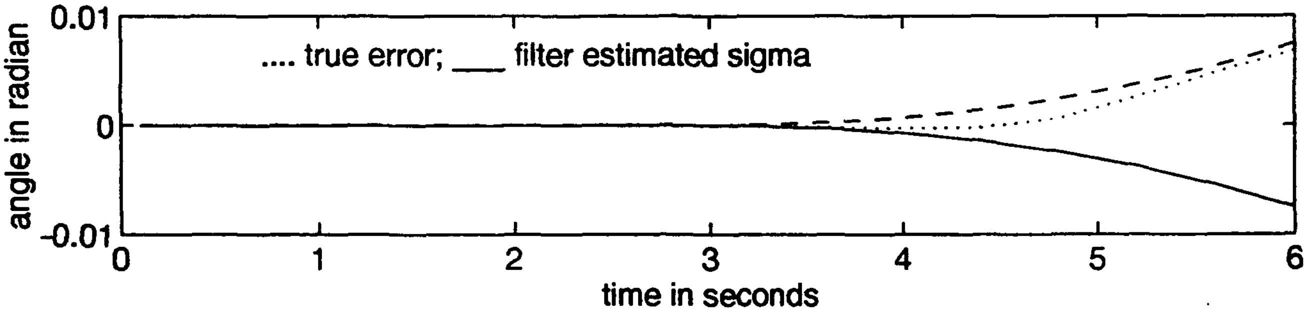

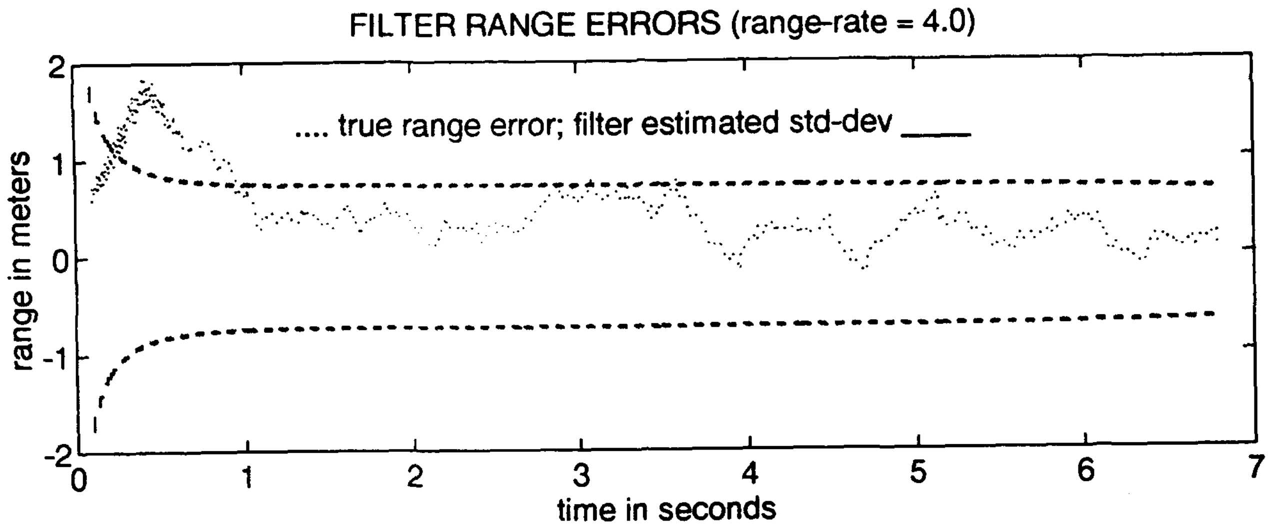
FILTER RANGE ERRORS (range-rate = 4.0)
.... true range error; filter estimated std-dev _____
range in meters
time in seconds

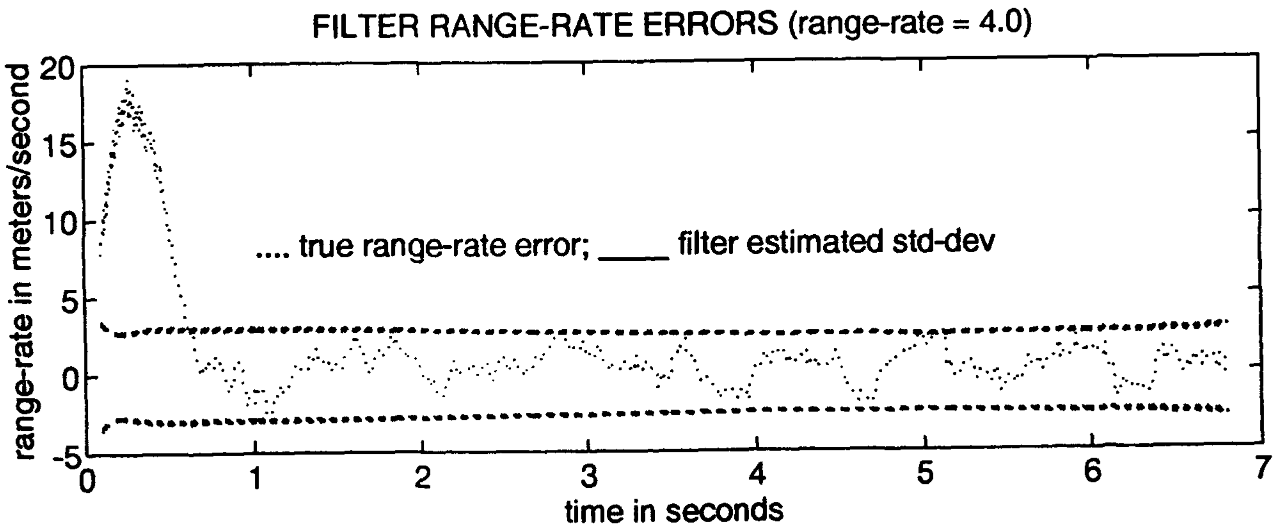
FILTER RANGE-RATE ERRORS (range-rate = 4.0)
.... true range-rate error; _____ filter estimated std-dev
range-rate in meters/second
time in seconds

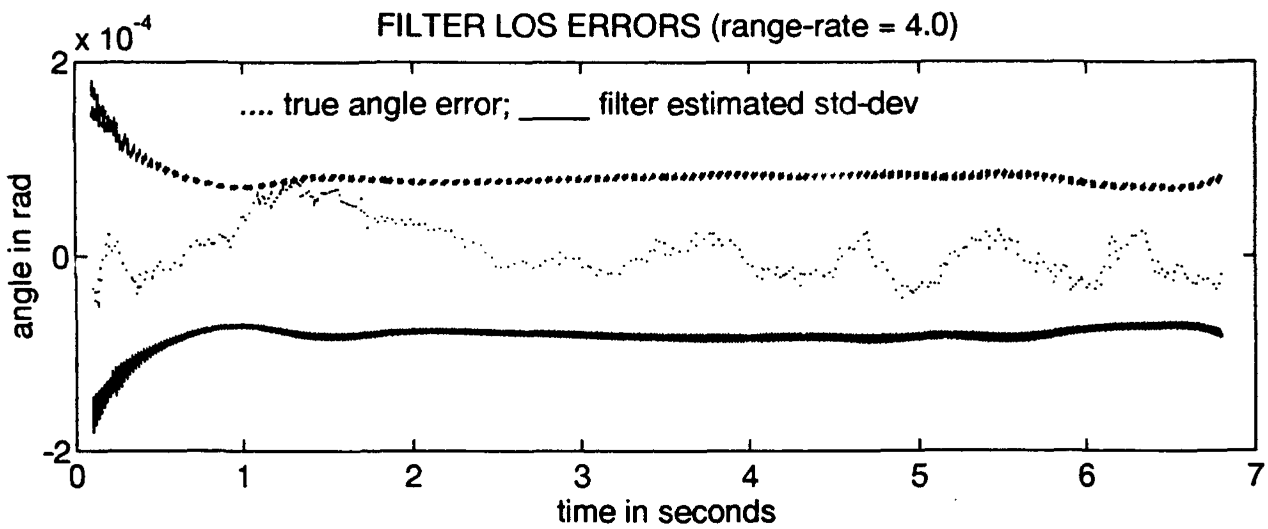
FILTER LOS ERRORS (range-rate = 4.0)
x 10^-4
.... true angle error; ____ filter estimated std-dev
angle in rad
2
0
-2
0
1
2
3
4
5
6
7
time in seconds

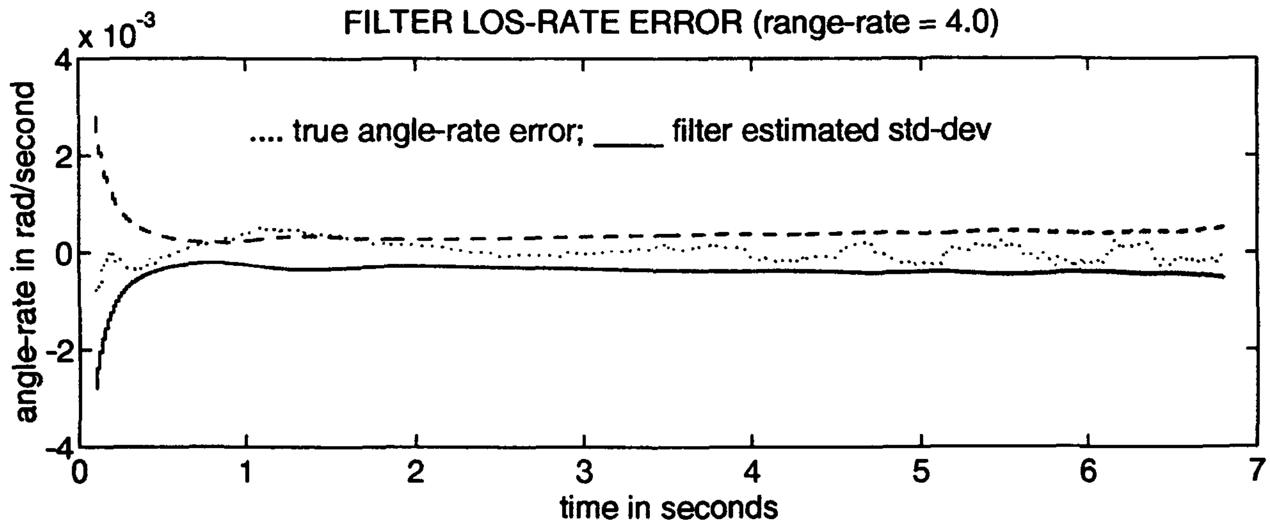
FILTER LOS-RATE ERROR (range-rate = 4.0)
x 10^-3
.... true angle-rate error; ____ filter estimated std-dev
angle-rate in rad/second
4
2
0
-2
-4
0
1
2
3
4
5
6
7
time in seconds

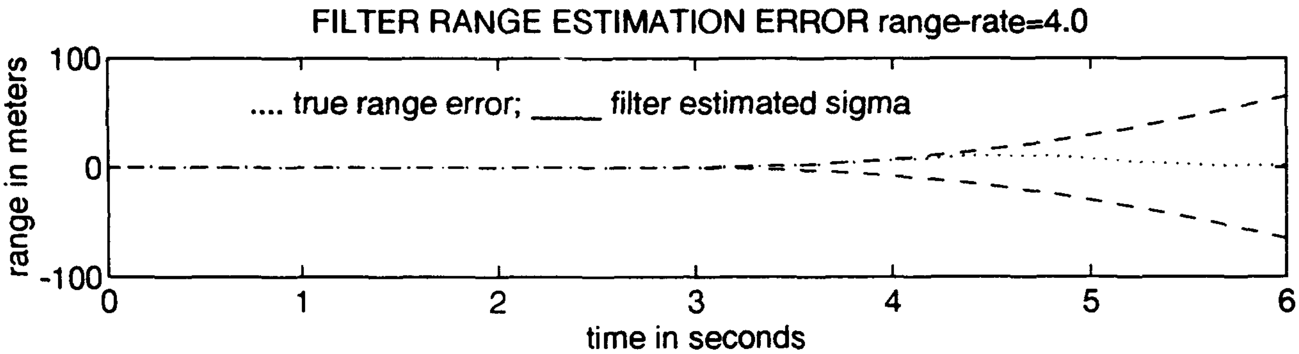
FILTER RANGE ESTIMATION ERROR range-rate=4.0
.... true range error; _____ filter estimated sigma
range in meters
100
0
-100
0
1
2
3
4
5
6
time in seconds

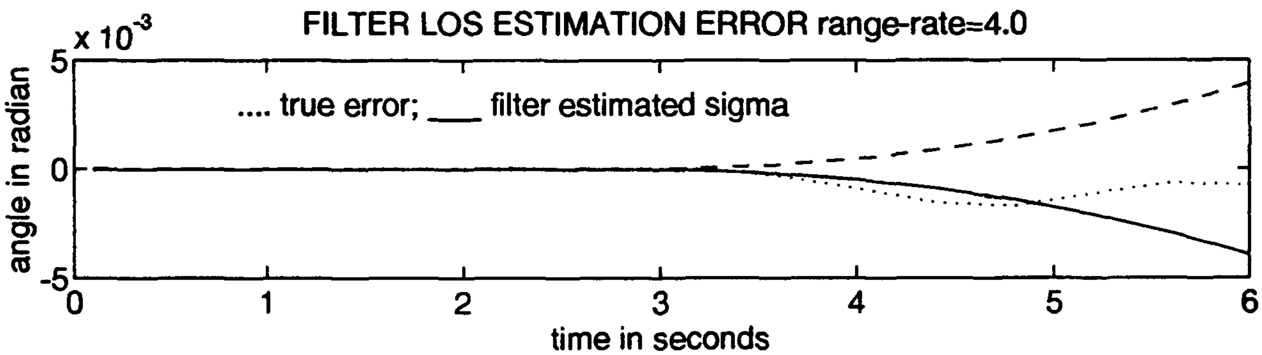
FILTER LOS ESTIMATION ERROR range-rate=4.0
x 10^-3
.... true error; ___ filter estimated sigma
angle in radian
5
0
-5
0
1
2
3
4
5
6
time in seconds

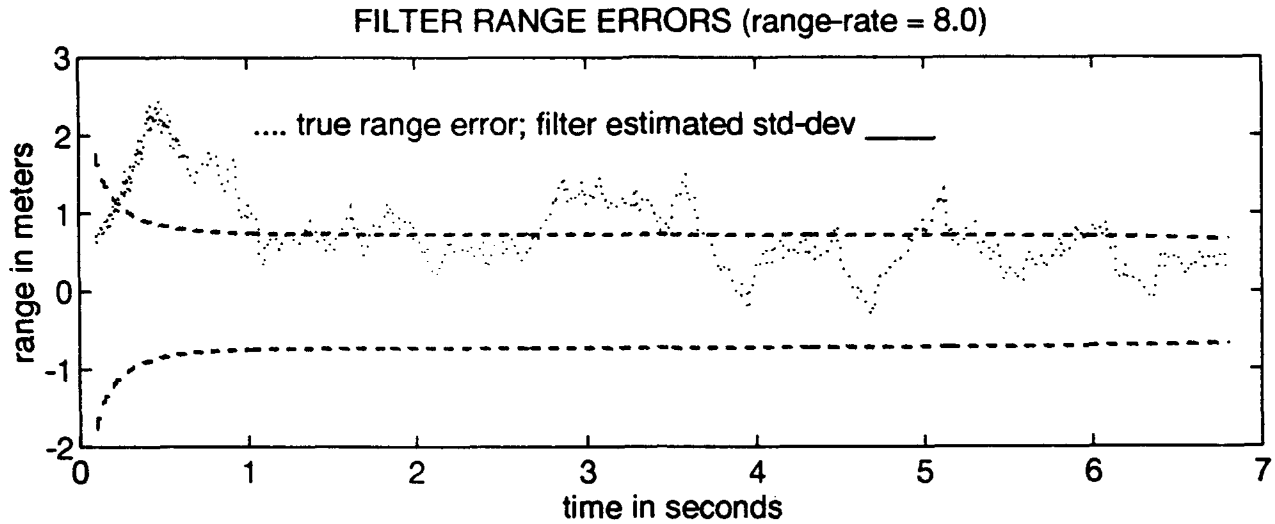
FILTER RANGE ERRORS (range-rate = 8.0)
.... true range error; filter estimated std-dev _____
range in meters
3
2
1
0
-1
-2
0
1
2
3
4
5
6
7
time in seconds

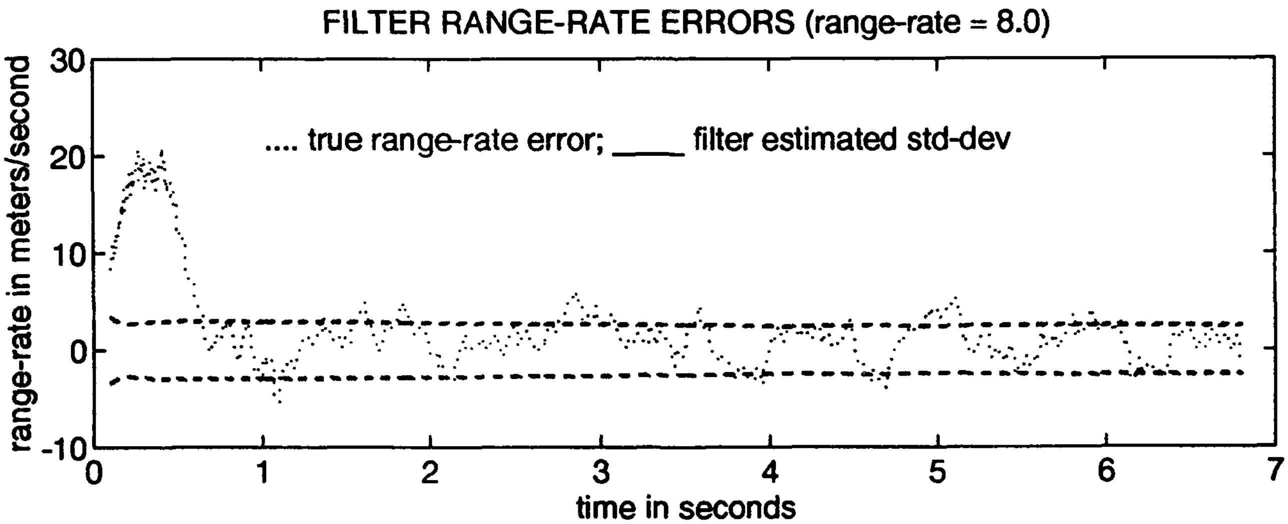
FILTER RANGE-RATE ERRORS (range-rate = 8.0)
.... true range-rate error; _____ filter estimated std-dev
range-rate in meters/second
30
20
10
0
-10
0
1
2
3
4
5
6
7
time in seconds

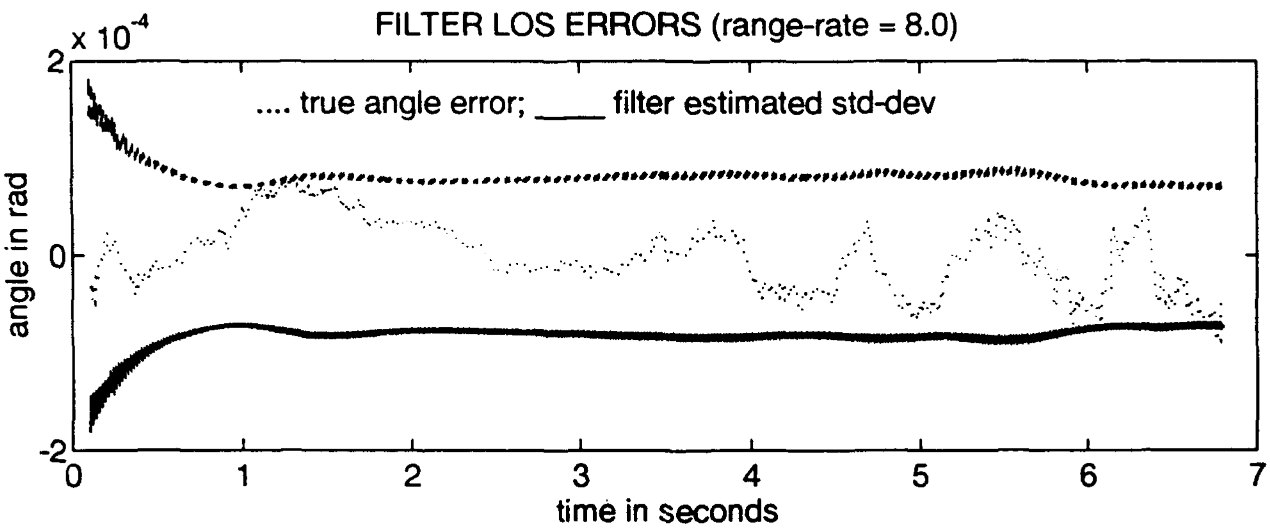
FILTER LOS ERRORS (range-rate = 8.0)
x 10^-4
.... true angle error; ____ filter estimated std-dev
angle in rad
time in seconds
2
0
-2
0 1 2 3 4 5 6 7

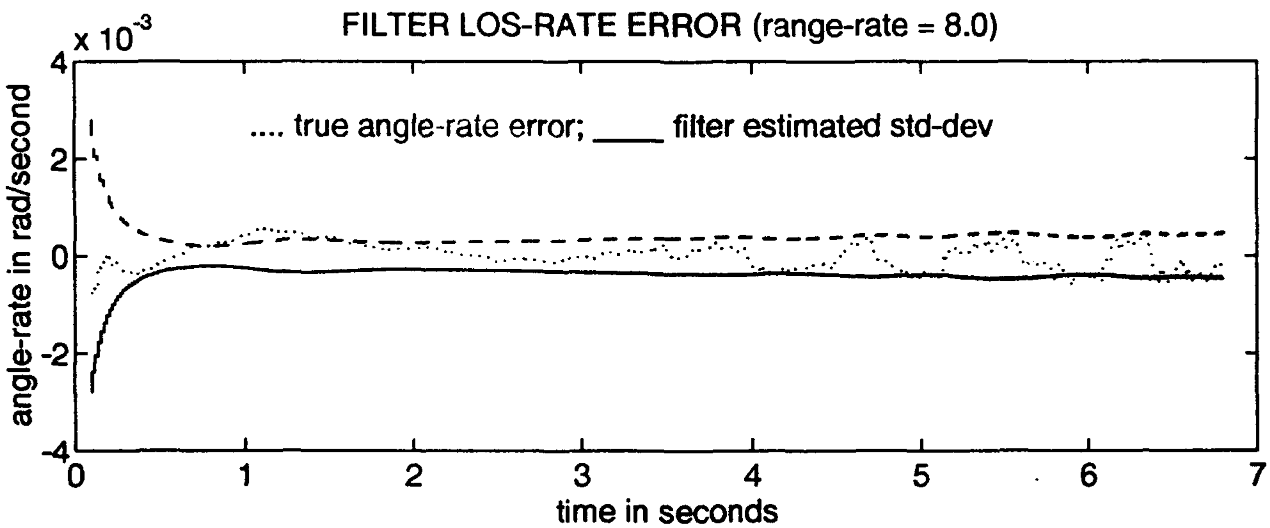
FILTER LOS-RATE ERROR (range-rate = 8.0)
x 10^-3
.... true angle-rate error; ____ filter estimated std-dev
angle-rate in rad/second
time in seconds
4
2
0
-2
-4
0 1 2 3 4 5 6 7

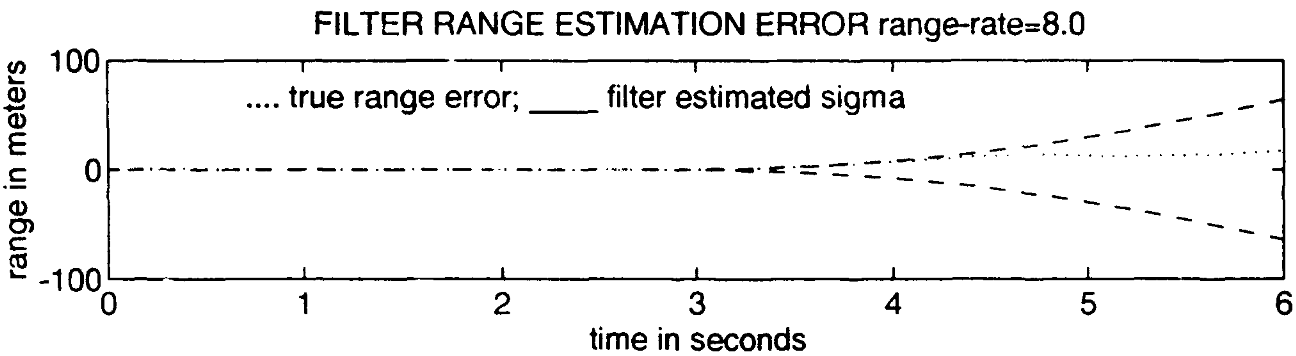
FILTER RANGE ESTIMATION ERROR range-rate=8.0
.... true range error; ____ filter estimated sigma
range in meters
100
0
-100
0
1
2
3
4
5
6
time in seconds

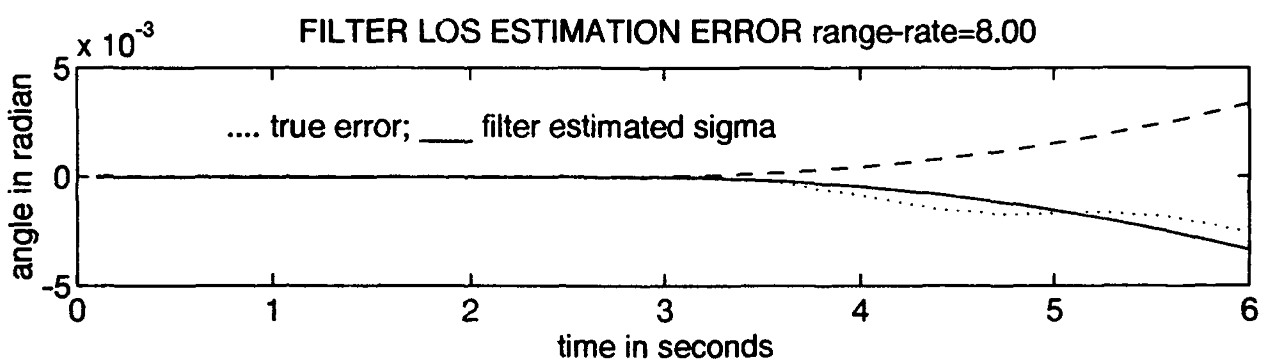
FILTER LOS ESTIMATION ERROR range-rate=8.00
x 10-3
.... true error; ____ filter estimated sigma
angle in radian
5
0
-5
0
1
2
3
4
5
6
time in seconds

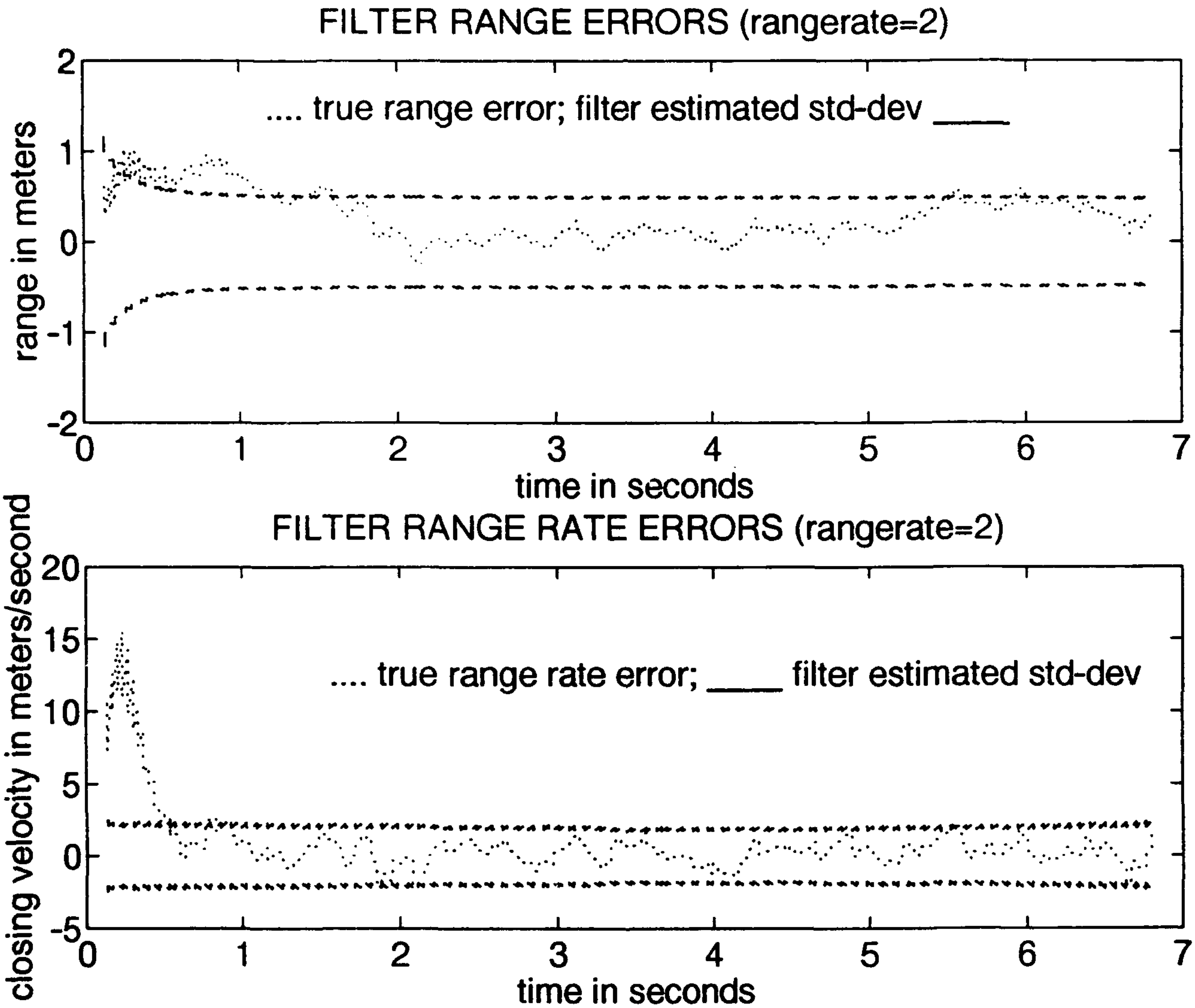
FILTER RANGE ERRORS (rangerate=2)
.... true range error; filter estimated std-dev ____
range in meters
2
1
0
-1
-2
0
1
2
3
4
5
6
7
time in seconds
FILTER RANGE RATE ERRORS (rangerate=2)
.... true range rate error; ____ filter estimated std-dev
closing velocity in meters/second
20
15
10
5
0
-5
0
1
2
3
4
5
6
7
time in seconds

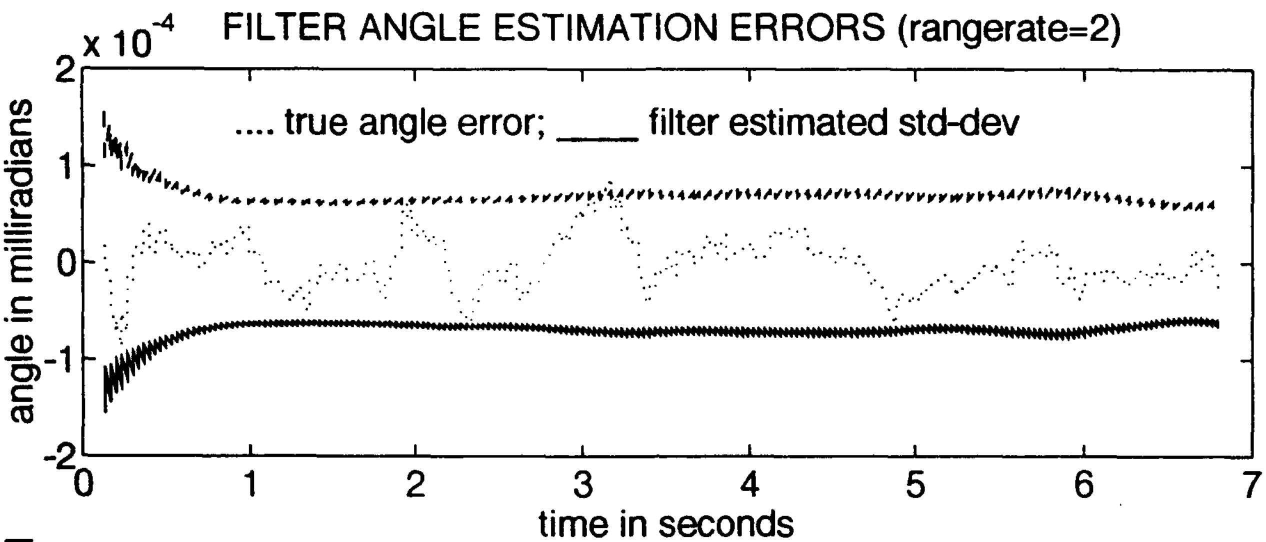
x 10^-4
FILTER ANGLE ESTIMATION ERRORS (rangerate=2)
.... true angle error; ____ filter estimated std-dev
angle in milliradians
2
1
0
-1
-2
0
1
2
3
4
5
6
7
time in seconds

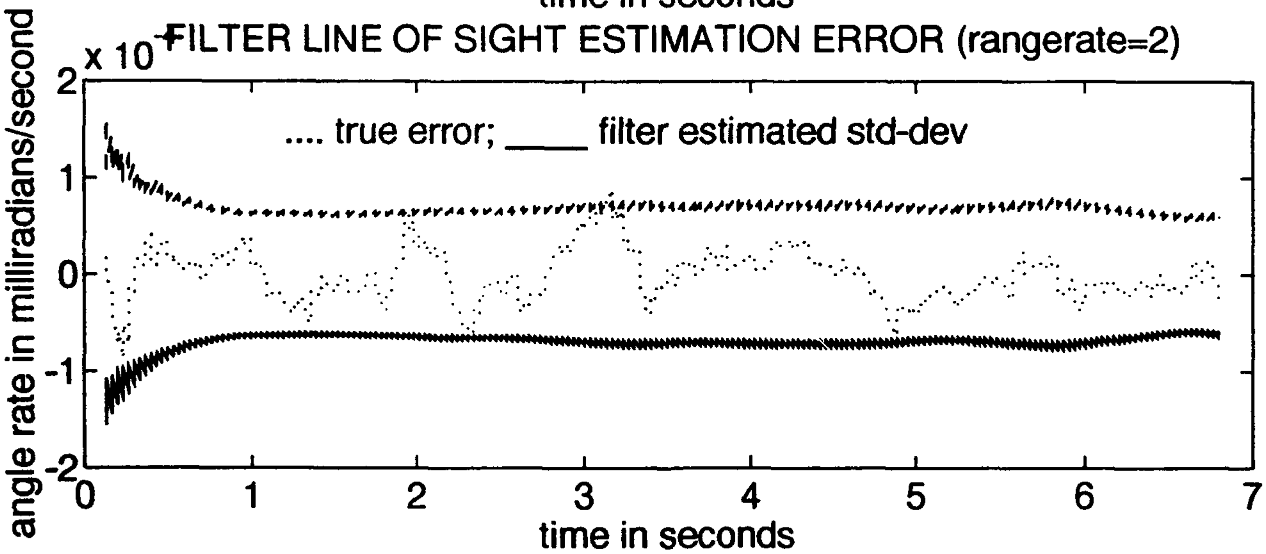
x 10^-4
FILTER LINE OF SIGHT ESTIMATION ERROR (rangerate=2)
.... true error; ____ filter estimated std-dev
angle rate in milliradians/second
2
1
0
-1
-2
0
1
2
3
4
5
6
7
time in seconds

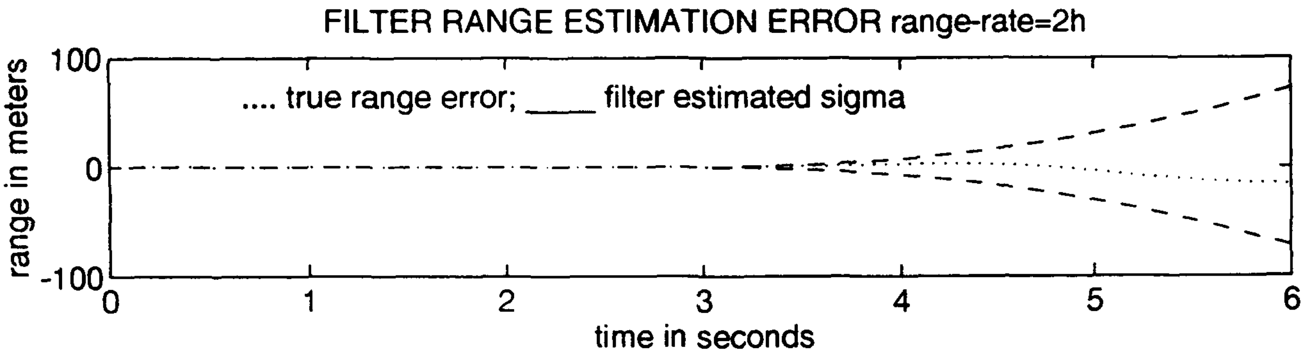
FILTER RANGE ESTIMATION ERROR range-rate=2h
.... true range error; ____ filter estimated sigma
range in meters
100
0
-100
0
1
2
3
4
5
6
time in seconds

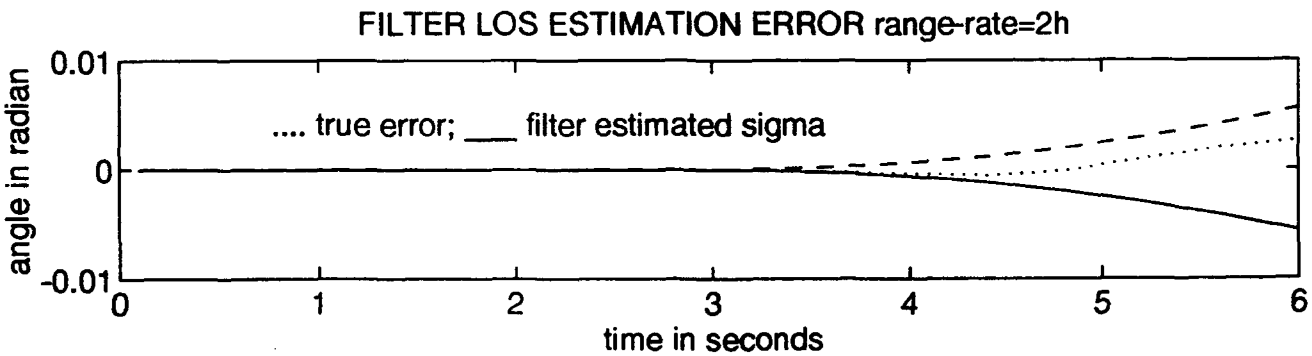
FILTER LOS ESTIMATION ERROR range-rate=2h
.... true error; ___ filter estimated sigma
angle in radian
0.01
0
-0.01
0
1
2
3
4
5
6
time in seconds

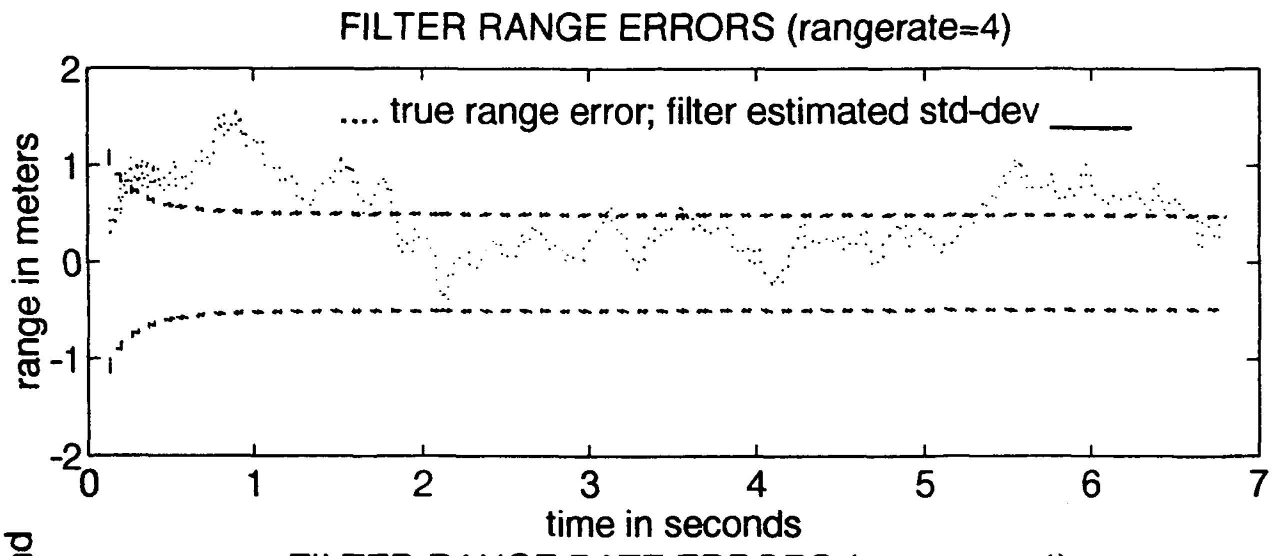
FILTER RANGE ERRORS (rangerate=4)
.... true range error; filter estimated std-dev _____
range in meters
time in seconds

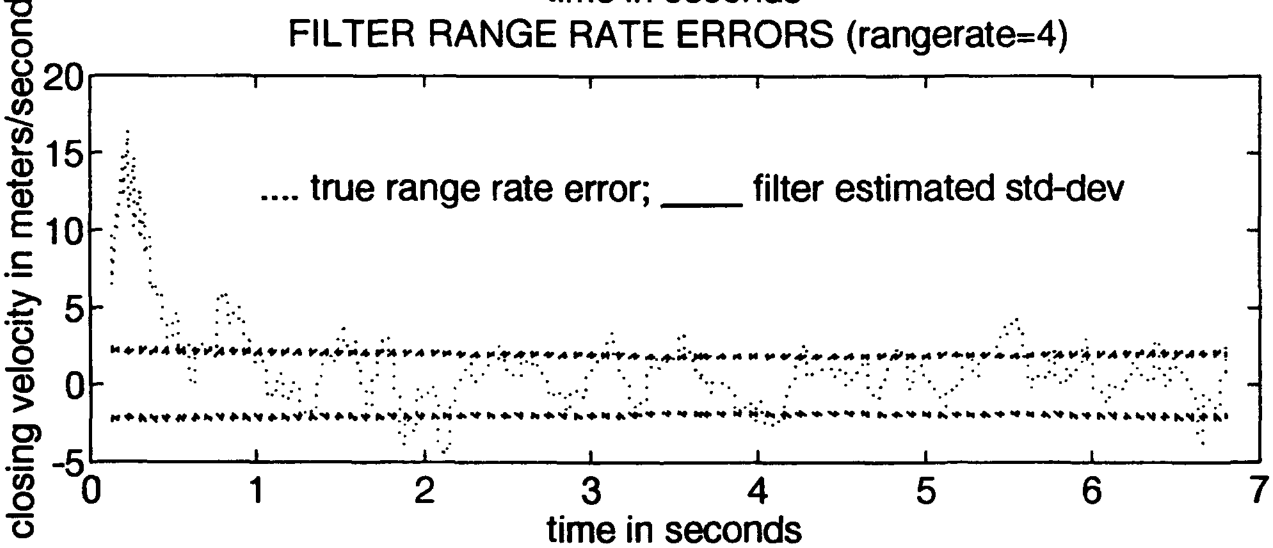
FILTER RANGE RATE ERRORS (rangerate=4)
.... true range rate error; _____ filter estimated std-dev
closing velocity in meters/second
time in seconds

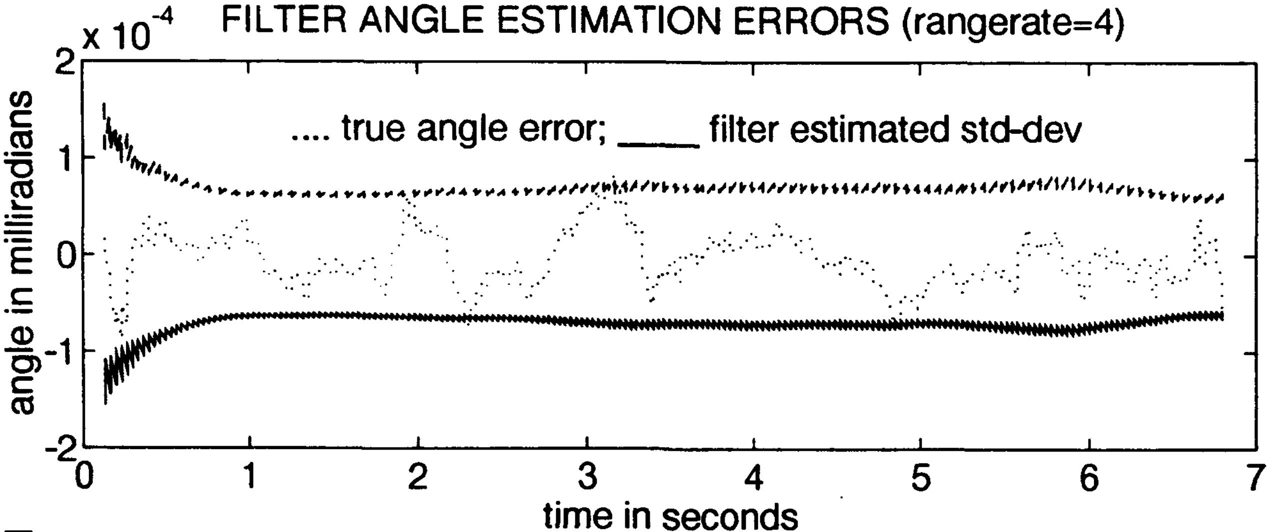
x 10^-4
FILTER ANGLE ESTIMATION ERRORS (rangerate=4)
.... true angle error; _____ filter estimated std-dev
angle in milliradians
2
1
0
-1
-2
0
1
2
3
4
5
6
7
time in seconds

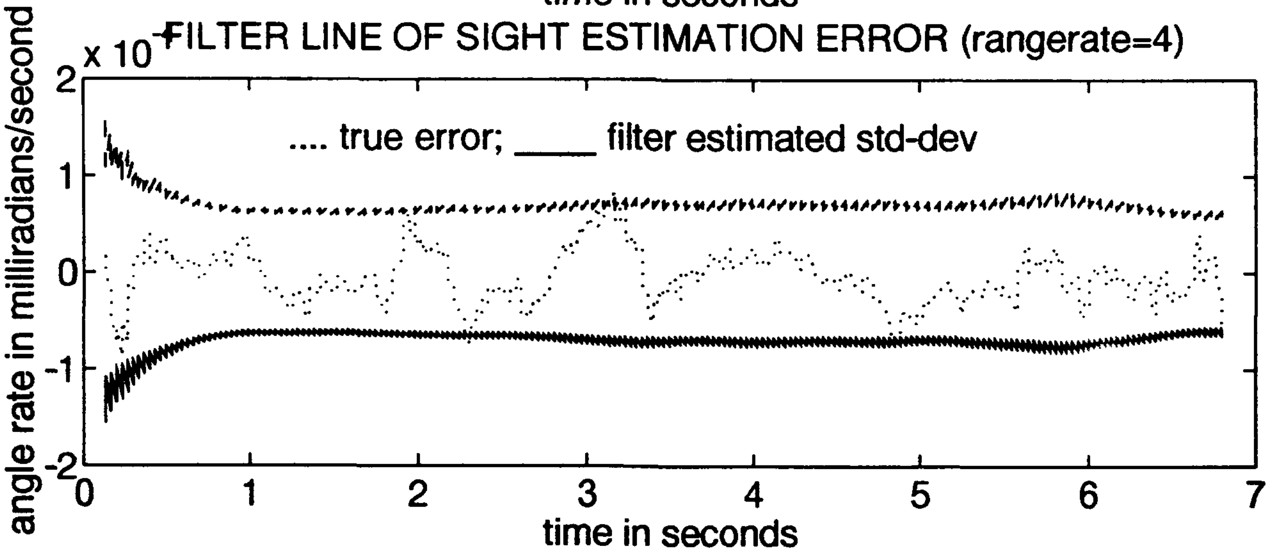
x 10^-4
FILTER LINE OF SIGHT ESTIMATION ERROR (rangerate=4)
.... true error; _____ filter estimated std-dev
angle rate in milliradians/second
2
1
0
-1
-2
0
1
2
3
4
5
6
7
time in seconds

FILTER RANGE ESTIMATION ERROR range-rate=4h

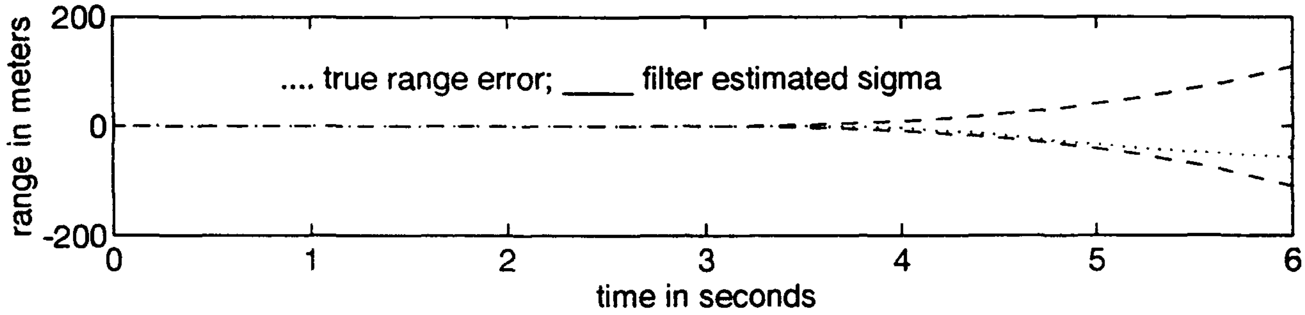

FILTER LOS ESTIMATION ERROR range-rate=4h

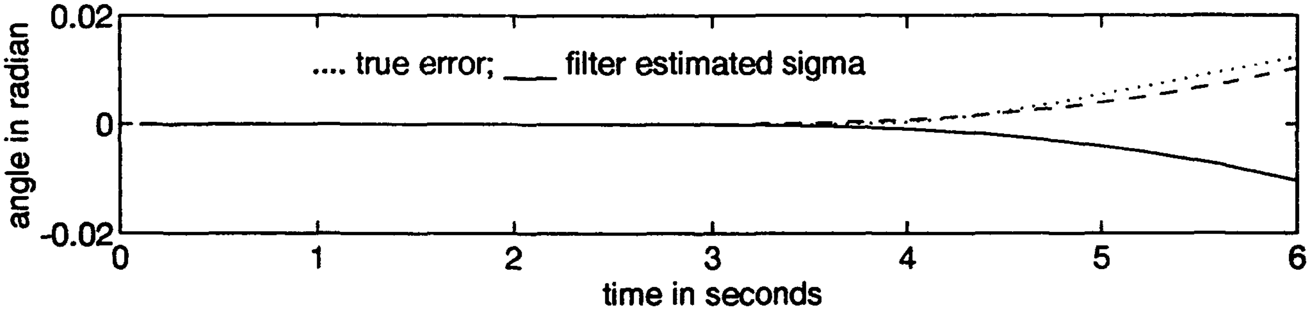

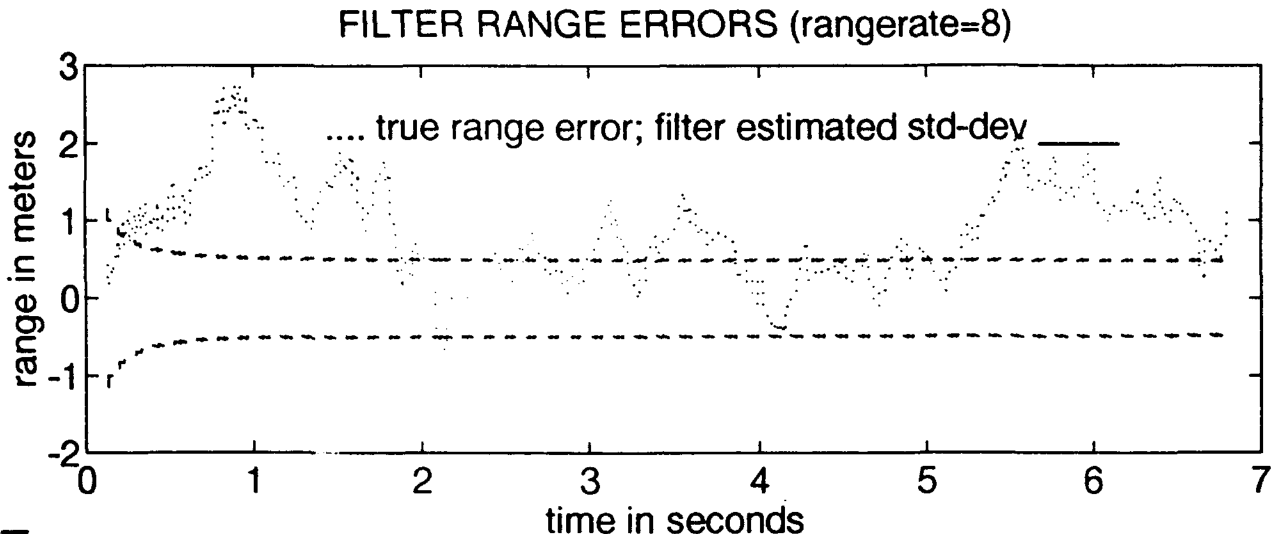
FILTER RANGE ERRORS (rangerate=8)
.... true range error; filter estimated std-dev ____
range in meters
time in seconds

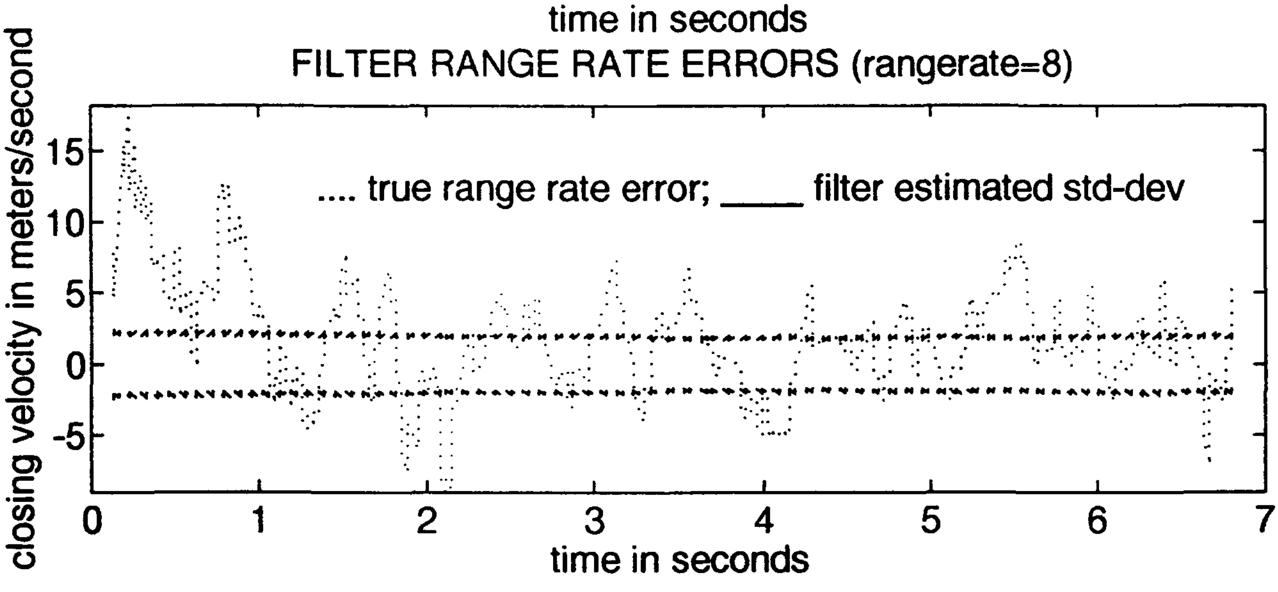
FILTER RANGE RATE ERRORS (rangerate=8)
.... true range rate error; ____ filter estimated std-dev
closing velocity in meters/second
time in seconds

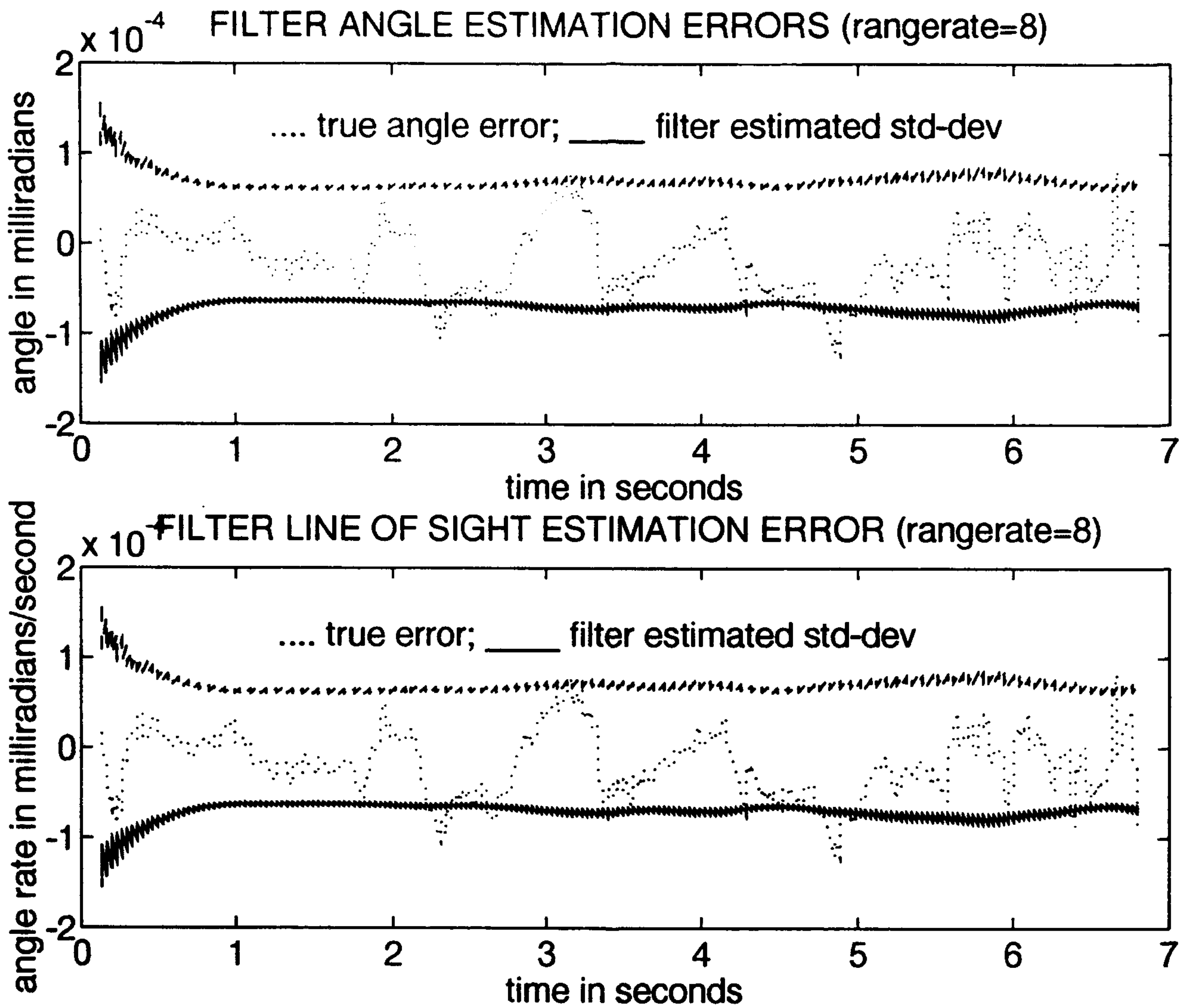
FILTER ANGLE ESTIMATION ERRORS (rangerate=8)
x 10^-4
.... true angle error; _____ filter estimated std-dev
angle in milliradians
time in seconds
FILTER LINE OF SIGHT ESTIMATION ERROR (rangerate=8)
x 10^-4
.... true error; _____ filter estimated std-dev
angle rate in milliradians/second
time in seconds

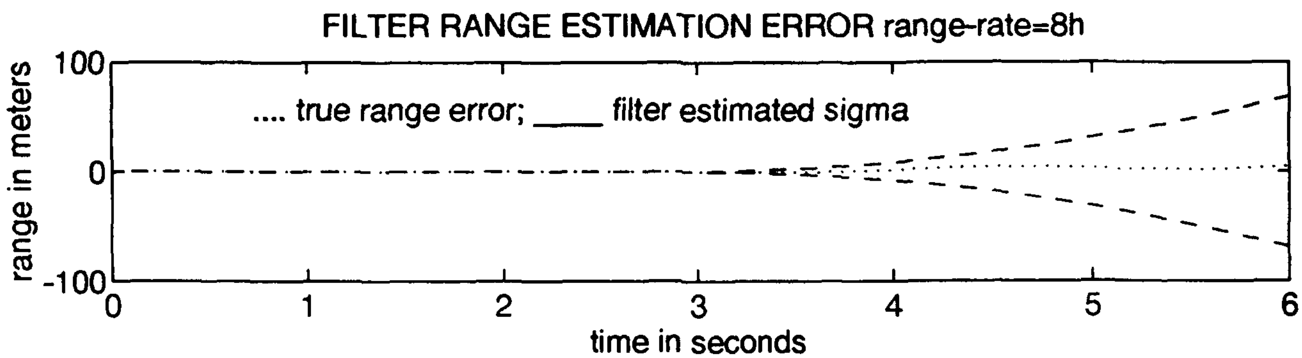
FILTER RANGE ESTIMATION ERROR range-rate=8h
.... true range error; ____ filter estimated sigma
range in meters
100
0
-100
0
1
2
3
4
5
6
time in seconds

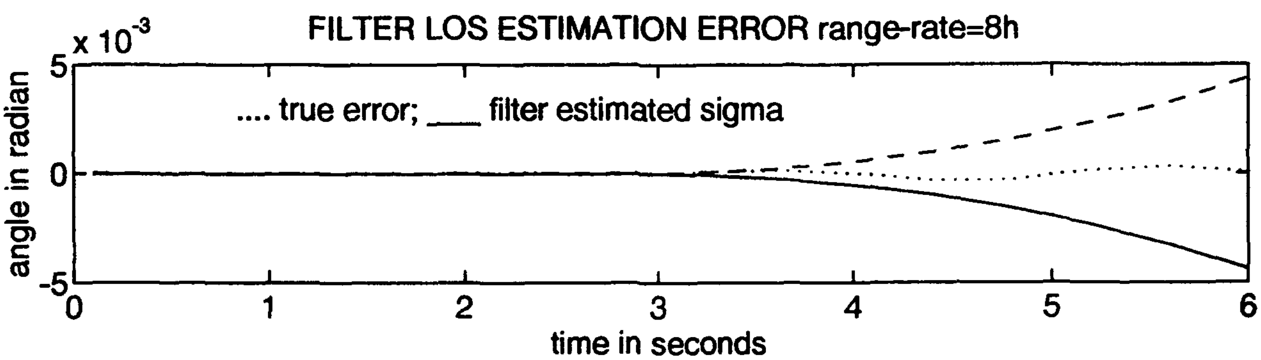
FILTER LOS ESTIMATION ERROR range-rate=8h
x 10^-3
.... true error; ___ filter estimated sigma
angle in radian
5
0
-5
0
1
2
3
4
5
6
time in seconds

FILTER LOS ERRORS (range-rate = 2.0)

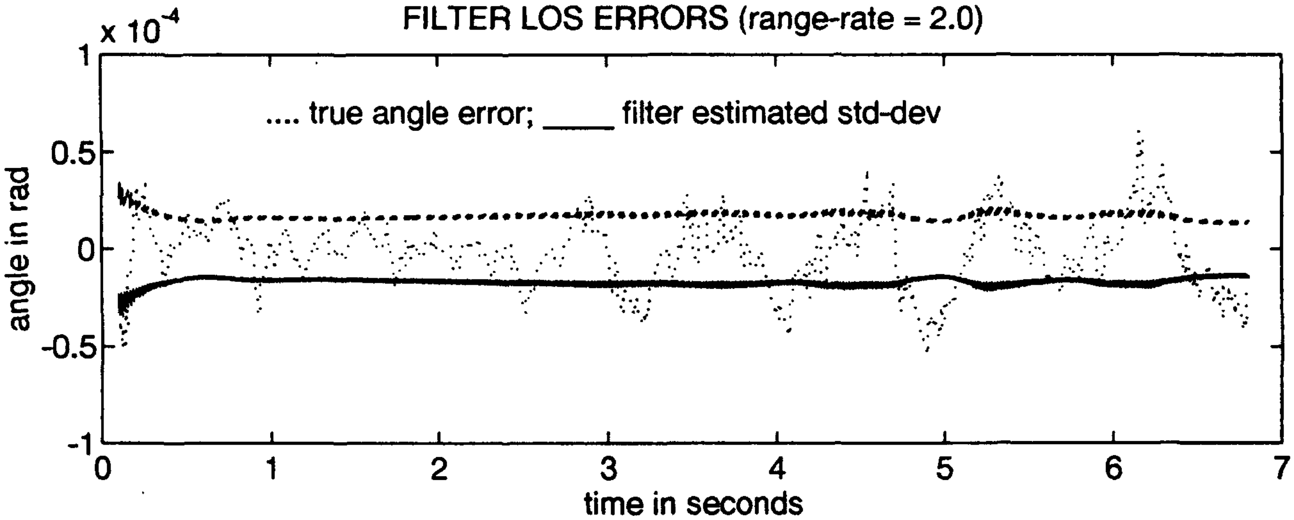

FILTER LOS-RATE ERROR (range-rate = 2.0)

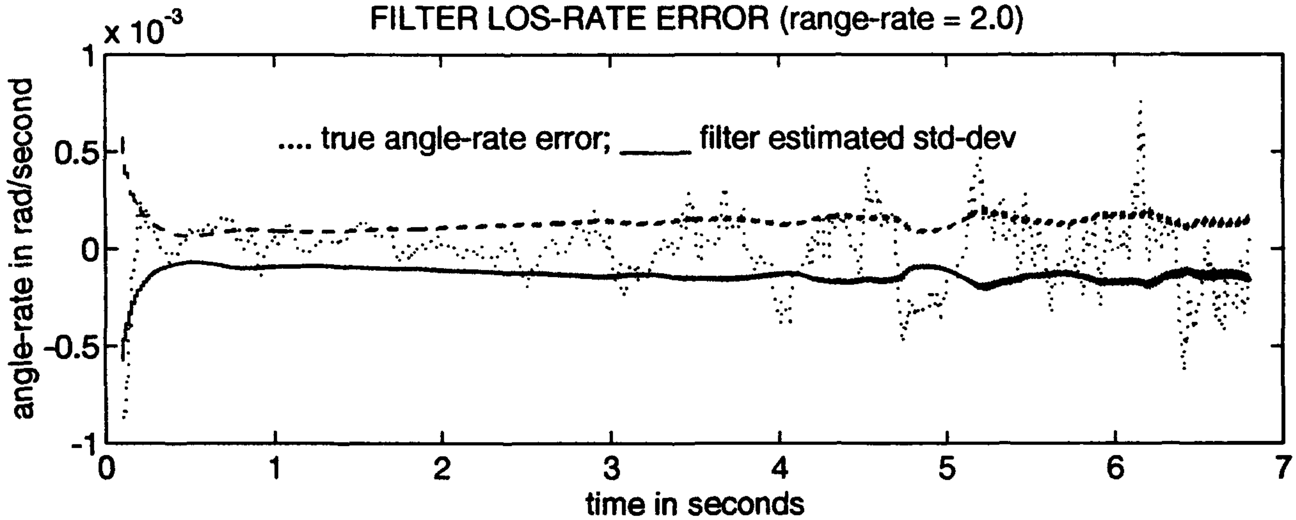

FILTER RANGE ERRORS (range-rate = 2.0)

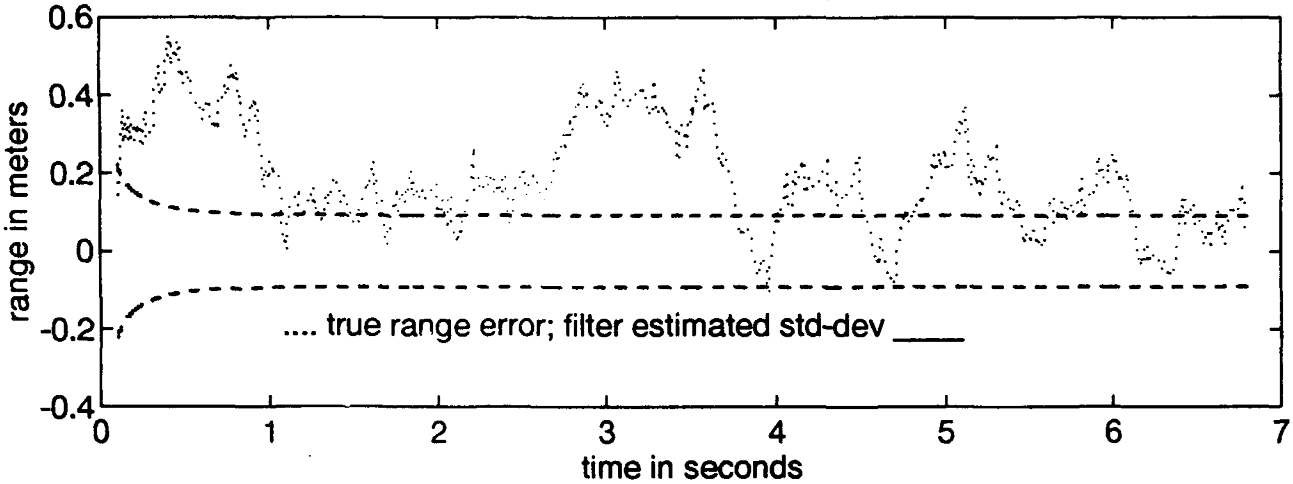

FILTER RANGE-RATE ERRORS (range-rate = 2.0)

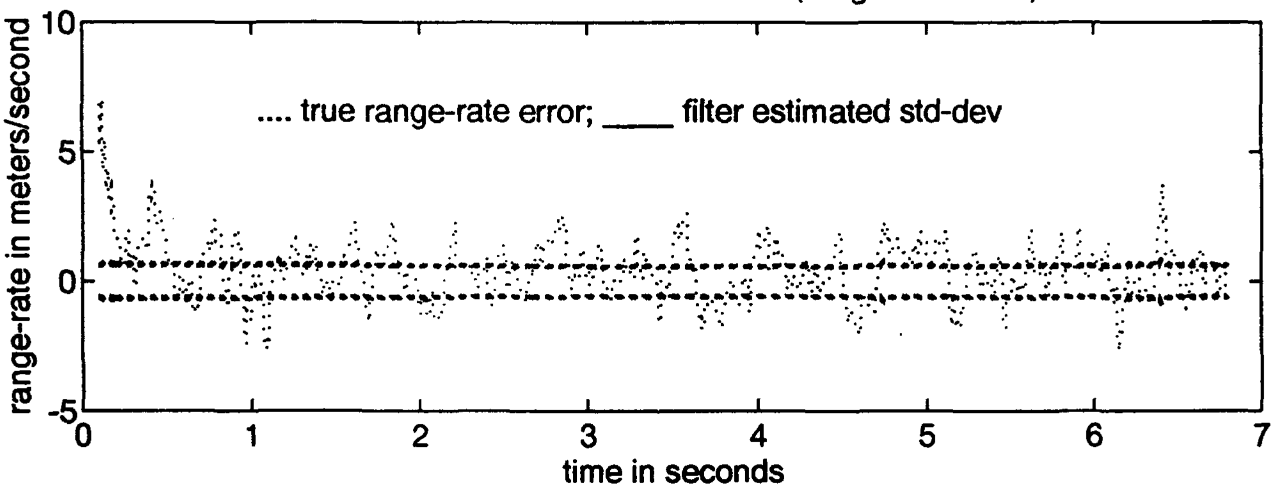

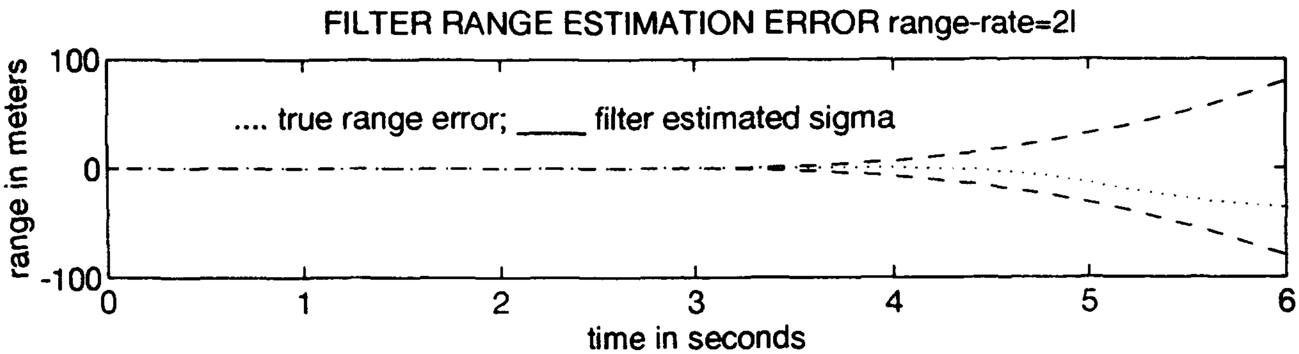
FILTER RANGE ESTIMATION ERROR range-rate=2l
.... true range error; ____ filter estimated sigma
range in meters
100
0
-100
0
1
2
3
4
5
6
time in seconds

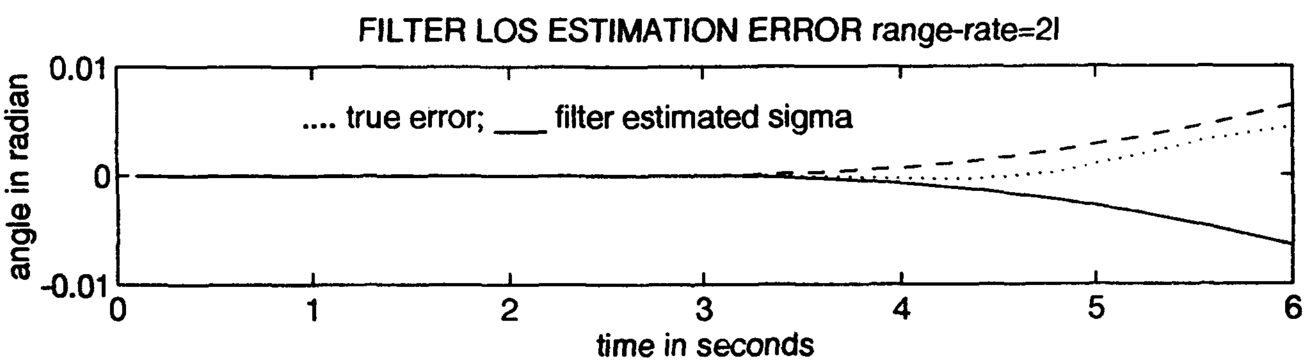
FILTER LOS ESTIMATION ERROR range-rate=2l
.... true error; ___ filter estimated sigma
angle in radian
0.01
0
-0.01
0
1
2
3
4
5
6
time in seconds

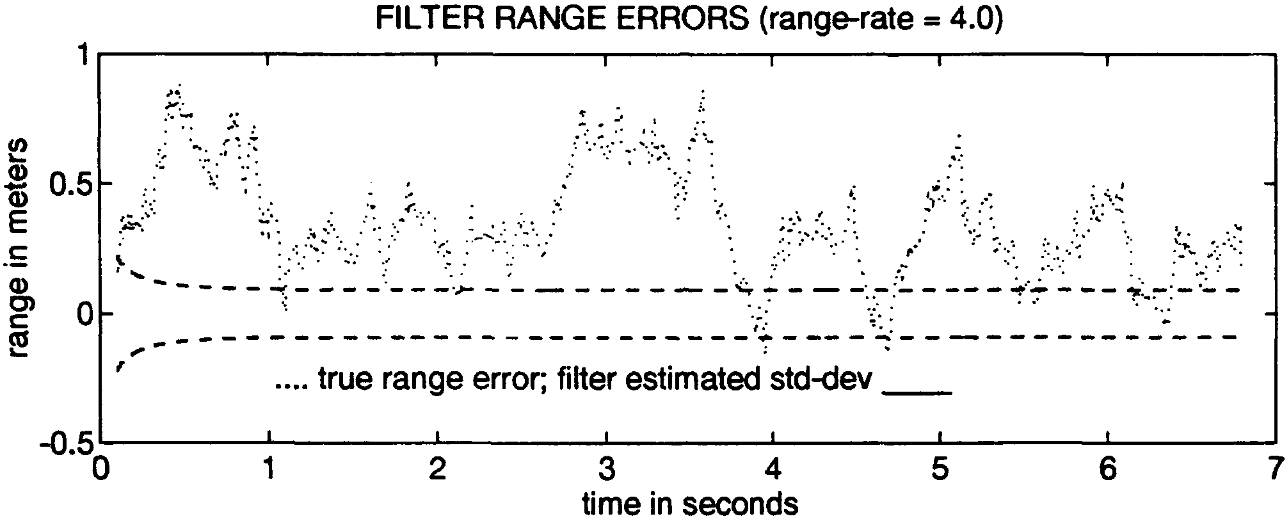
FILTER RANGE ERRORS (range-rate = 4.0)
range in meters
1
0.5
0
-0.5
.... true range error; filter estimated std-dev ____
0
1
2
3
4
5
6
7
time in seconds

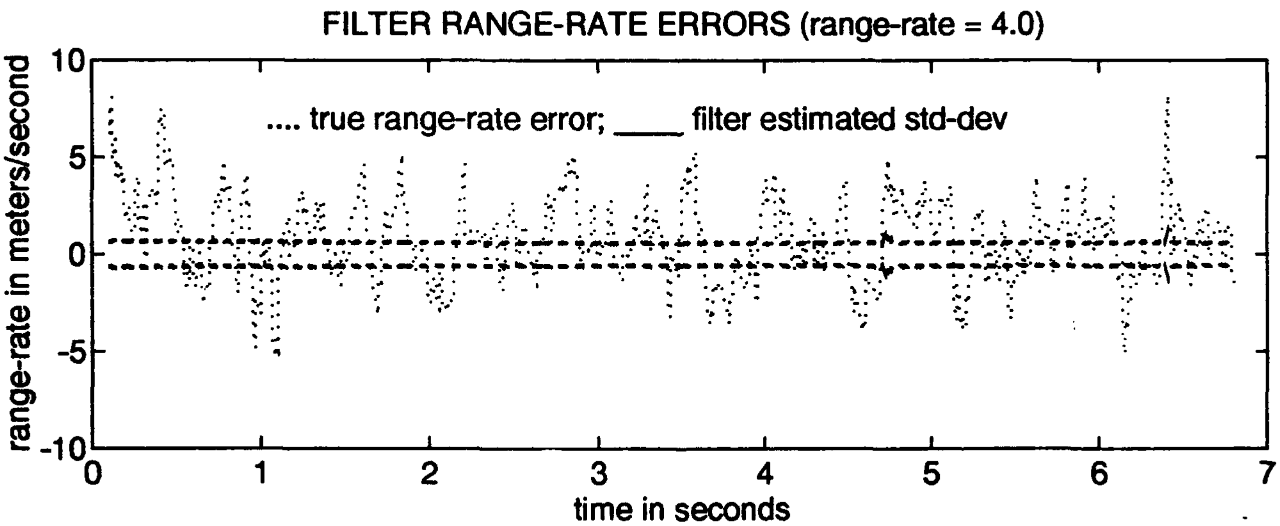
FILTER RANGE-RATE ERRORS (range-rate = 4.0)
range-rate in meters/second
10
5
0
-5
-10
.... true range-rate error; ____ filter estimated std-dev
0
1
2
3
4
5
6
7
time in seconds

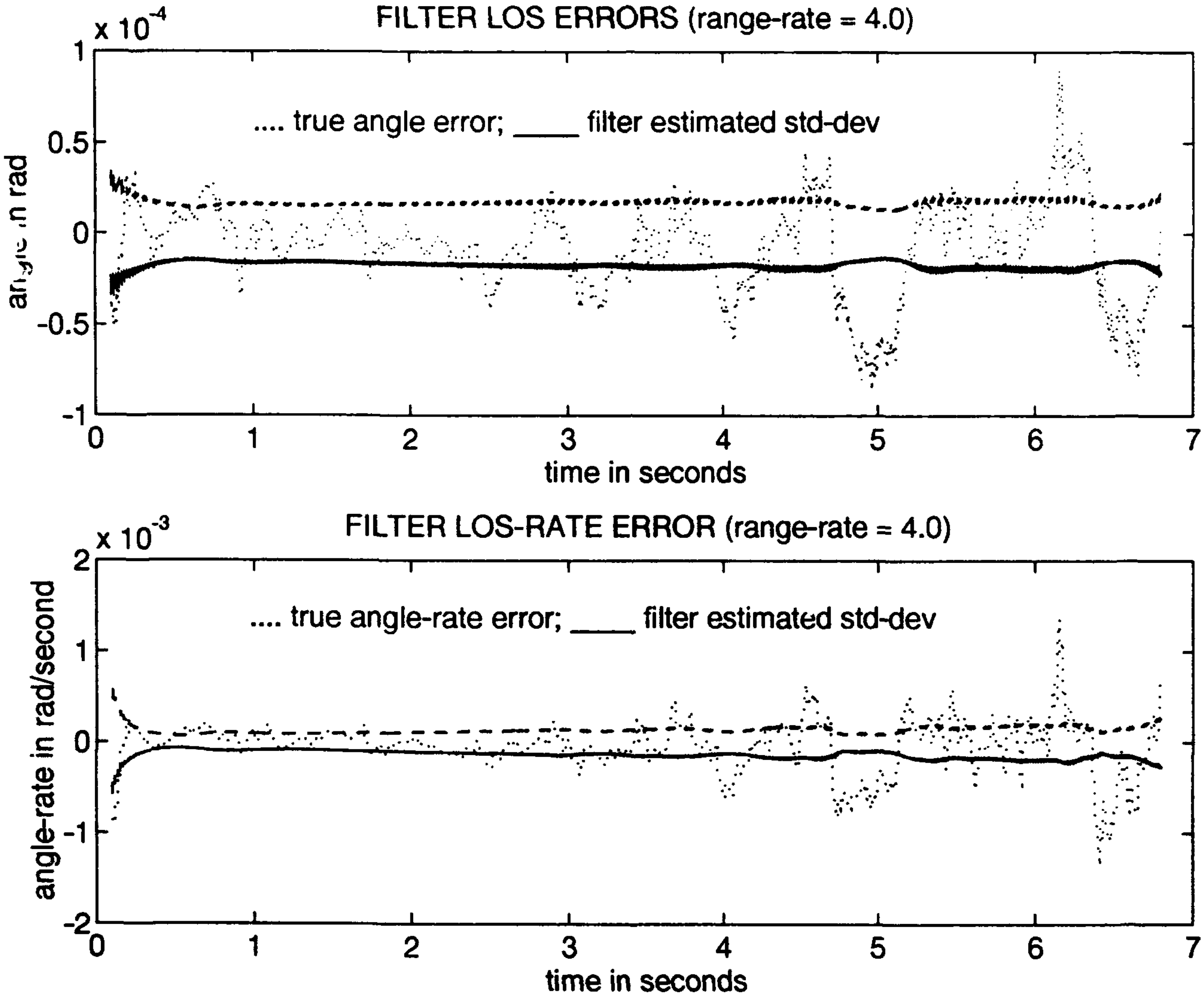
FILTER LOS ERRORS (range-rate = 4.0)
x 10^-4
.... true angle error; _____ filter estimated std-dev
time in seconds
FILTER LOS-RATE ERROR (range-rate = 4.0)
x 10^-3
.... true angle-rate error; _____ filter estimated std-dev
angle-rate in rad/second
time in seconds

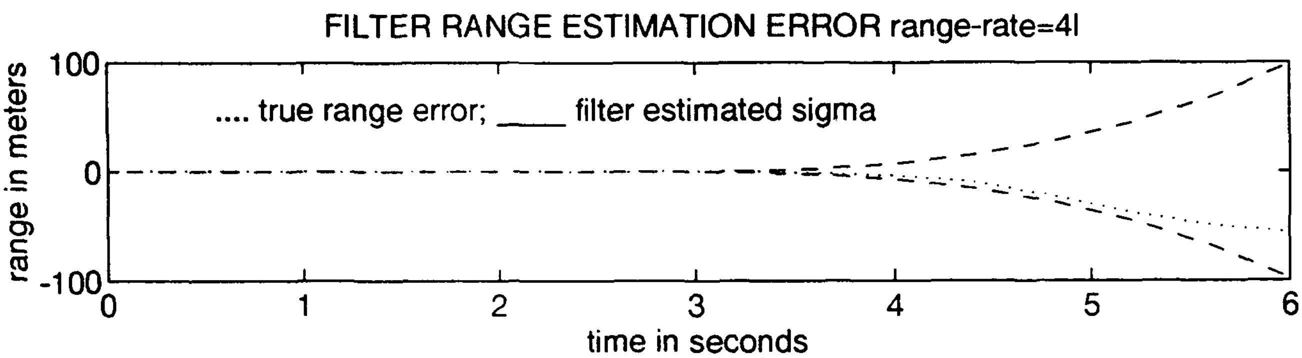

FILTER RANGE ESTIMATION ERROR range-rate=4l
.... true range error; _____ filter estimated sigma
range in meters
100
0
-100
0
1
2
3
4
5
6
time in seconds

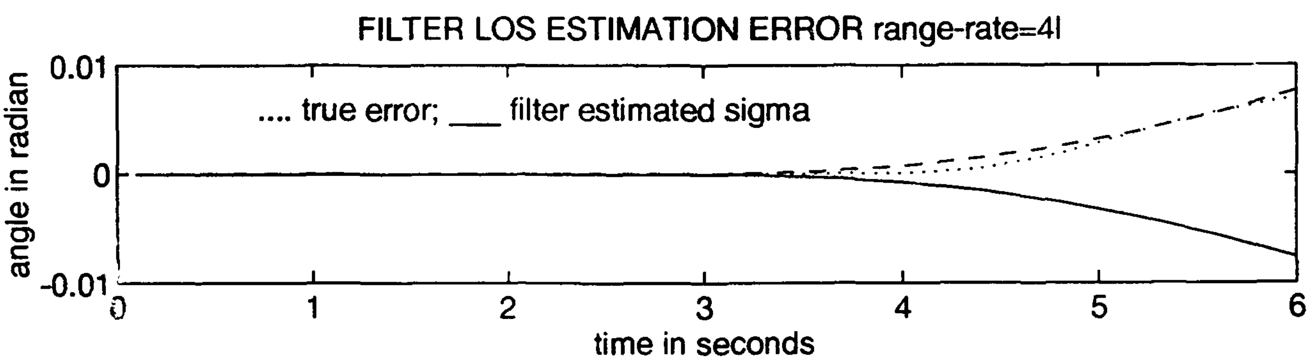

FILTER LOS ESTIMATION ERROR range-rate=4l
.... true error; ___ filter estimated sigma
angle in radian
0.01
0
-0.01
0
1
2
3
4
5
6
time in seconds

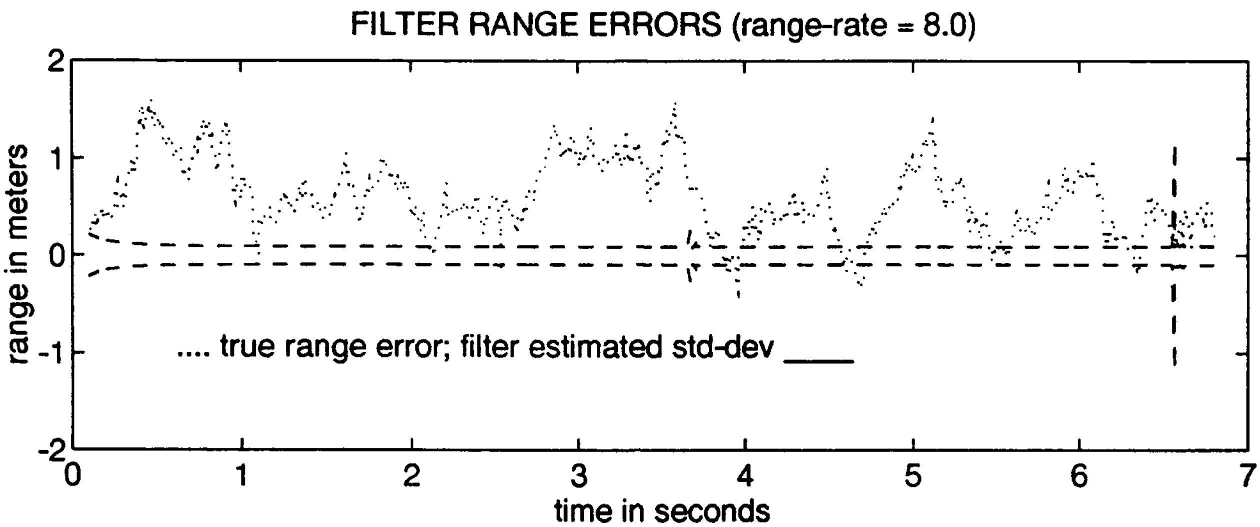
FILTER RANGE ERRORS (range-rate = 8.0)
range in meters
.... true range error; filter estimated std-dev ____
time in seconds
2
1
0
-1
-2
0
1
2
3
4
5
6
7

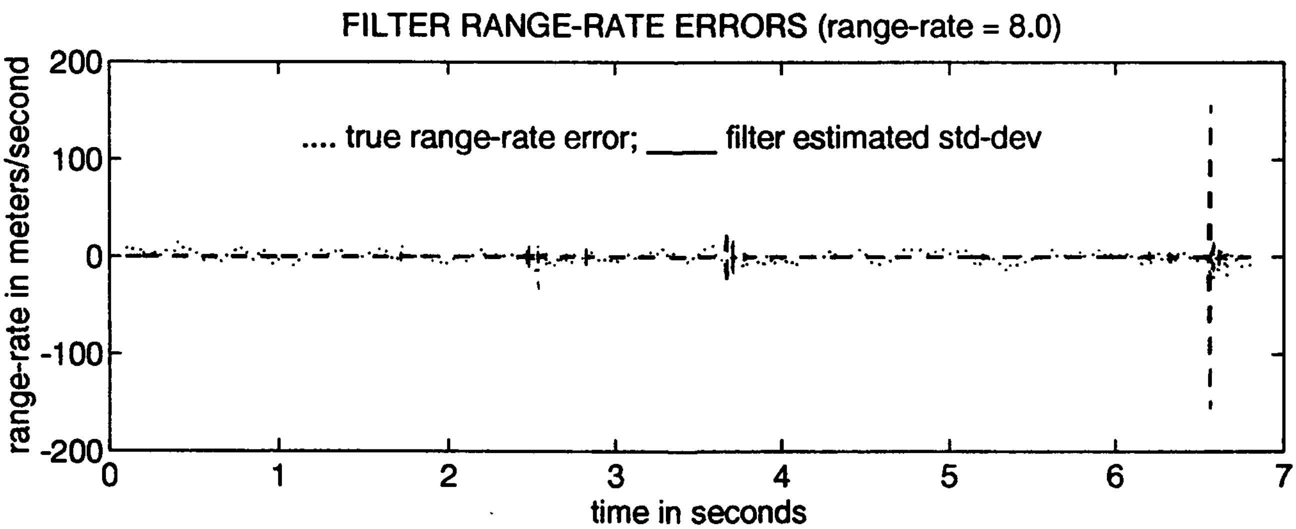
FILTER RANGE-RATE ERRORS (range-rate = 8.0)
range-rate in meters/second
.... true range-rate error; ____ filter estimated std-dev
time in seconds
200
100
0
-100
-200
0
1
2
3
4
5
6
7

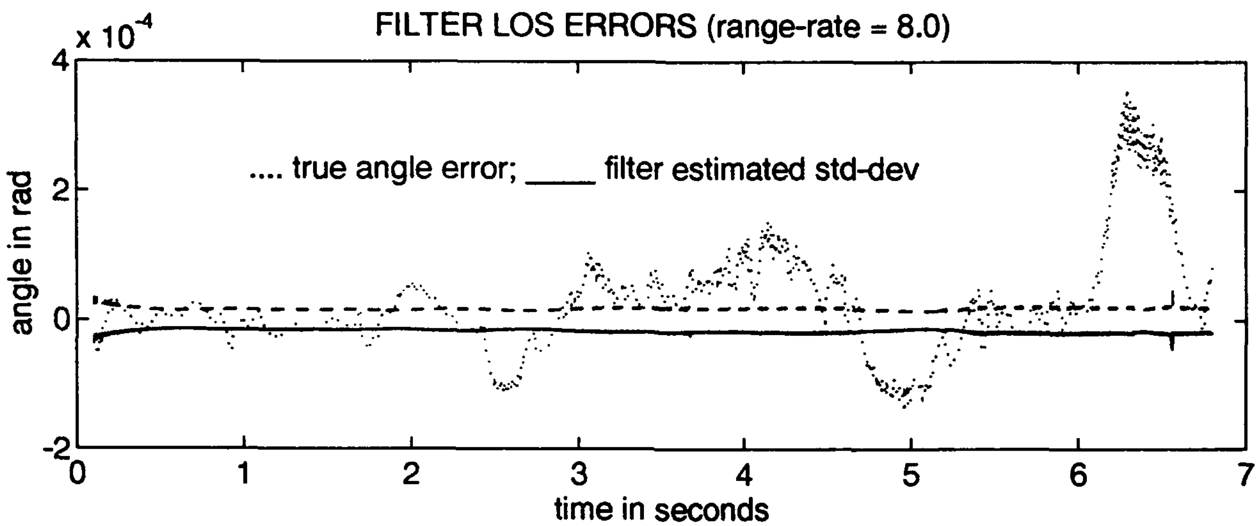
FILTER LOS ERRORS (range-rate = 8.0)
x 10^-4
.... true angle error; ____ filter estimated std-dev
angle in rad
4
2
0
-2
0
1
2
3
4
5
6
7
time in seconds

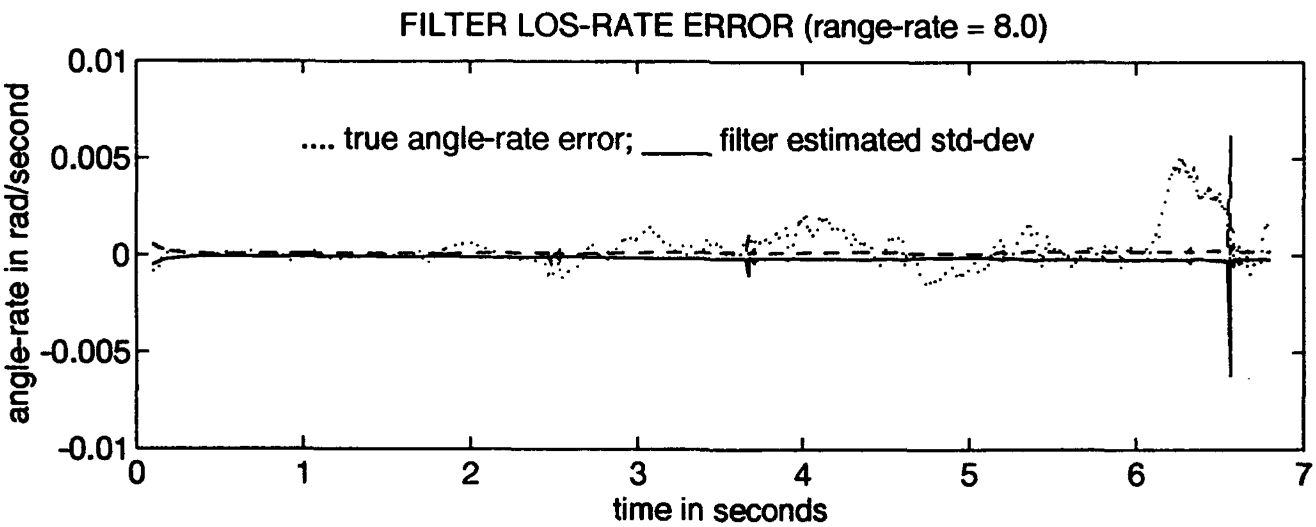
FILTER LOS-RATE ERROR (range-rate = 8.0)
.... true angle-rate error; ____ filter estimated std-dev
angle-rate in rad/second
0.01
0.005
0
-0.005
-0.01
0
1
2
3
4
5
6
7
time in seconds

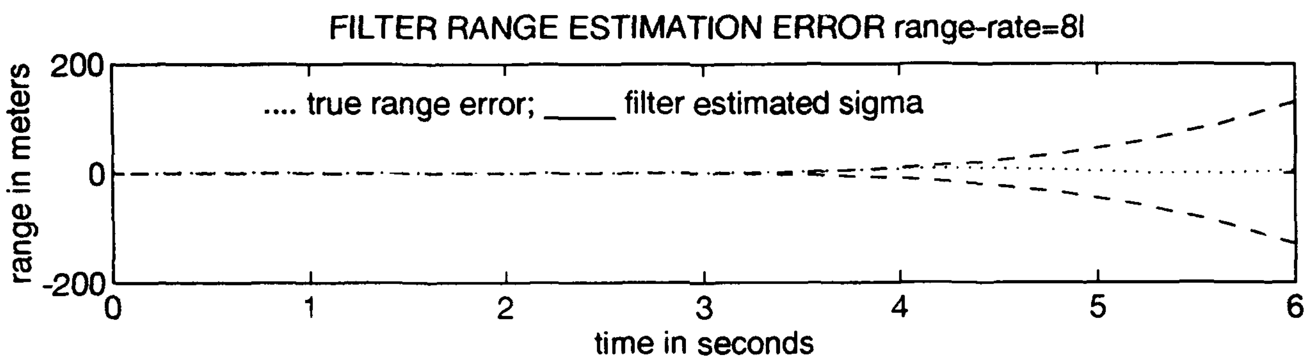
FILTER RANGE ESTIMATION ERROR range-rate=8l
.... true range error; ____ filter estimated sigma
range in meters
200
0
-200
0
1
2
3
4
5
6
time in seconds

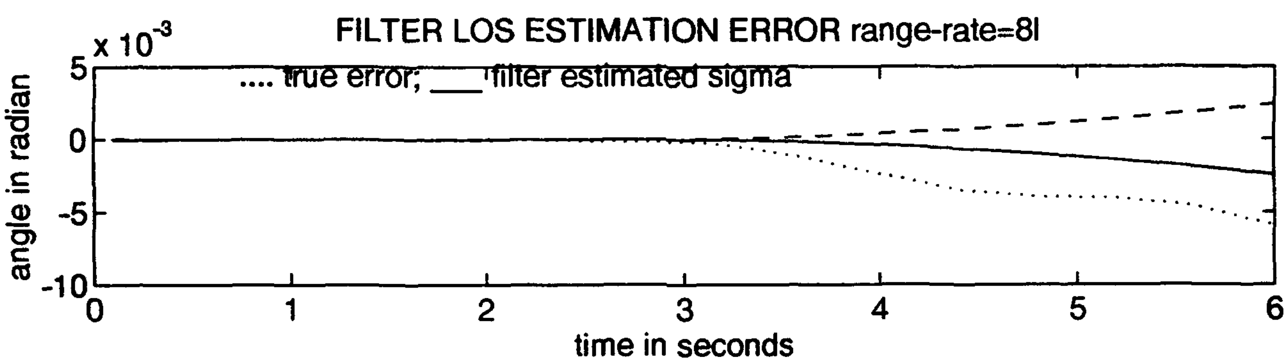
FILTER LOS ESTIMATION ERROR range-rate=8l
x 10^-3
.... true error; ____ filter estimated sigma
angle in radian
5
0
-5
-10
0
1
2
3
4
5
6
time in seconds

Appendix D

This appendix contains simulation plots for the ladar angle noise run set. The aircraft is initially heading east and beginning a 3 g turn to the north. All measurement noises (except angle) and dynamic noise strengths are set at baseline values. The missile is launched from the $\pi/4$ approach angle. Each run has a trajectory plot, estimated range errors, range-rate errors, LOS errors and LOS-rate errors. Estimated range and LOS plots are found in the $\pi/4$ missile approach angle run plots in Appendix A. The baseline (see Figure 4-4) angle measurement error is 40 μrad, with additional runs made for angle errors of 80, 160 and 250 μrad. Each plot set contains filter divergence plots of range error and angle error for a three second divergence from three to six seconds. The divergence plots, which define the volume cross-section, are used for performance comparison versus the baseline. In Figures D-2 thru D-17 both the filter and truth model measurement noises are varied from the baseline. In Figures D-18 thru D-33 only the filter measurement noise is varied above baseline (i.e., the filter noise is set "high"). In Figures D-34 thru D-51 only the true measurement noise is varied above baseline (i.e., the filter noise is set "low"). There are no divergence plots for the "both varied", and "filter high" runs at 250 μrad because divergence failed during simulation and plots could not be generated.

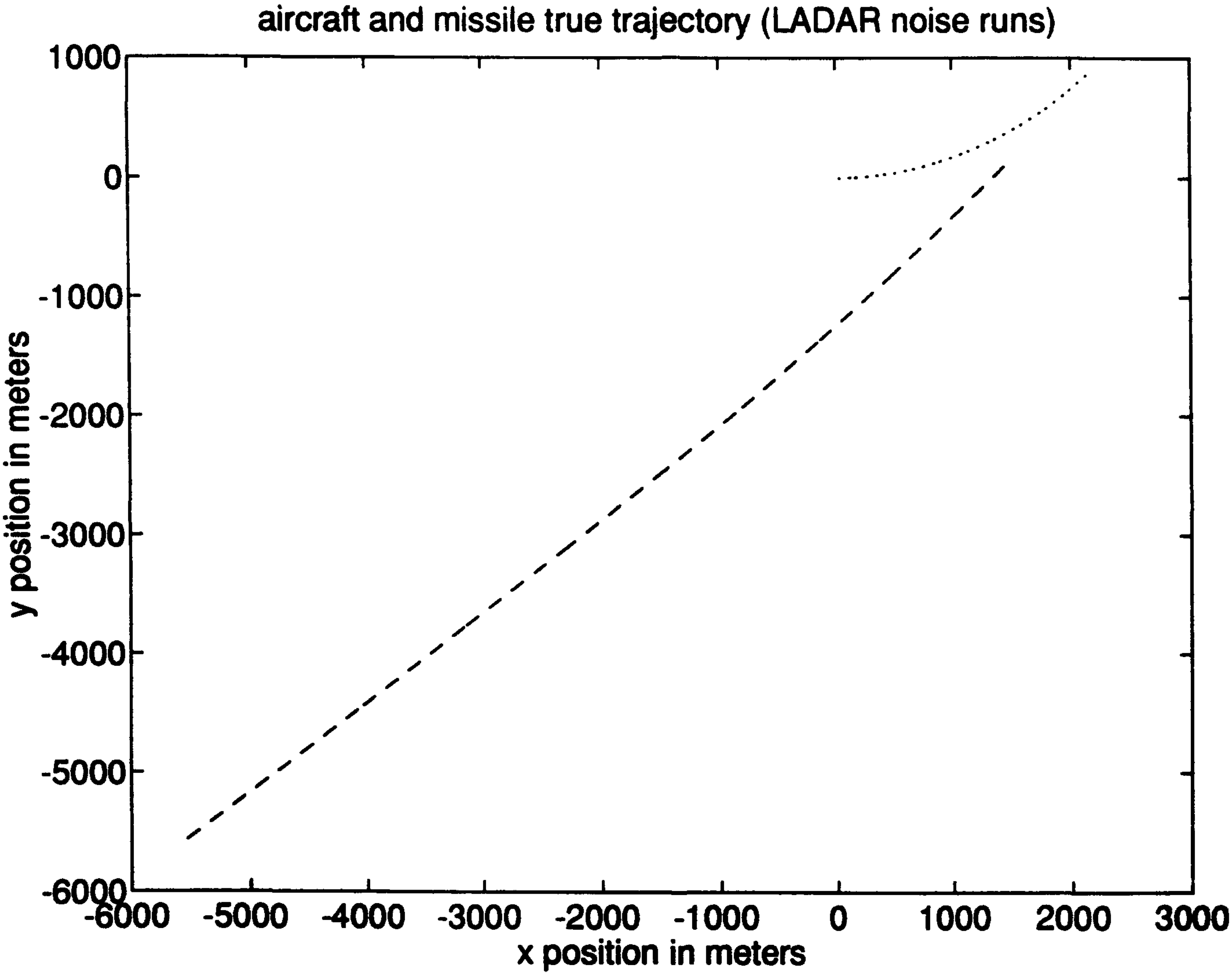

aircraft and missile true trajectory (LADAR noise runs)
y position in meters
x position in meters
1000
0
-1000
-2000
-3000
-4000
-5000
-6000
-6000
-5000
-4000
-3000
-2000
-1000
0
1000
2000
3000

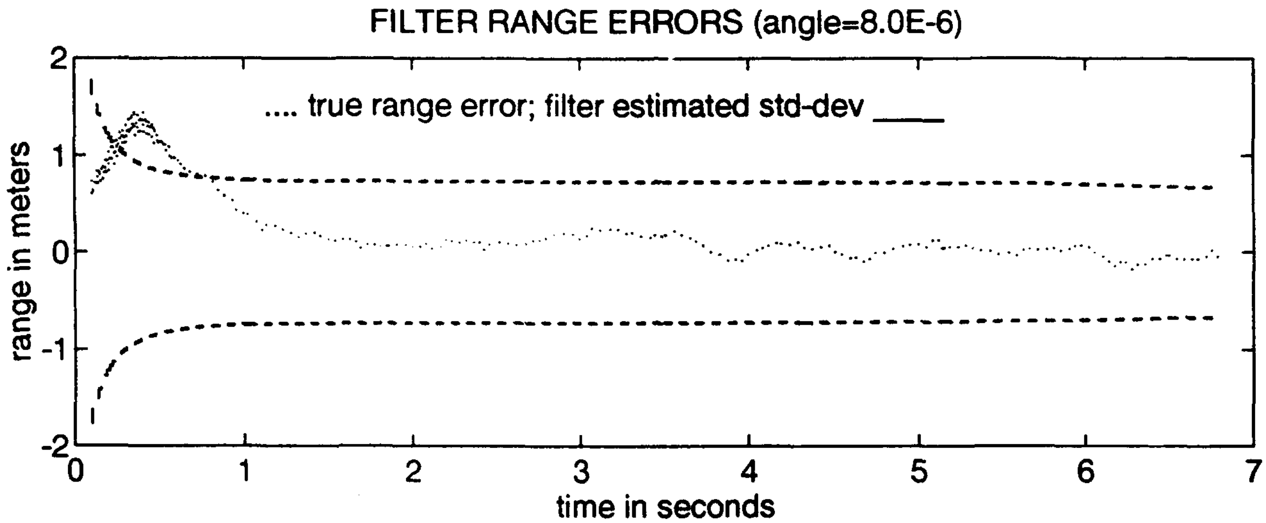
FILTER RANGE ERRORS (angle=8.0E-6)
.... true range error; filter estimated std-dev ____
range in meters
time in seconds
2
1
0
-1
-2
0
1
2
3
4
5
6
7

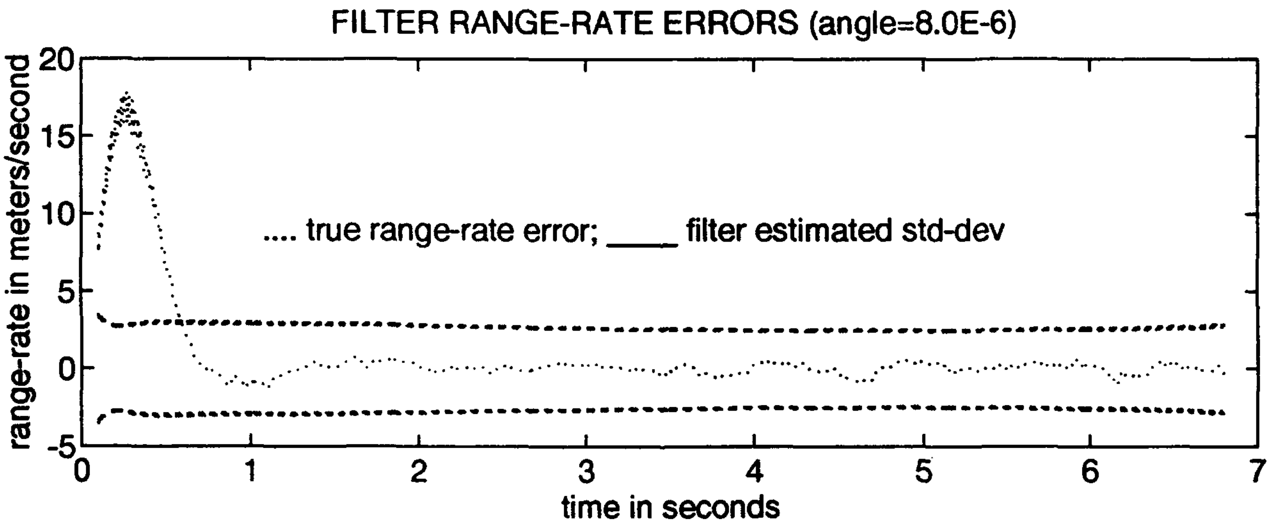
FILTER RANGE-RATE ERRORS (angle=8.0E-6)
.... true range-rate error; ____ filter estimated std-dev
range-rate in meters/second
time in seconds
20
15
10
5
0
-5
0
1
2
3
4
5
6
7

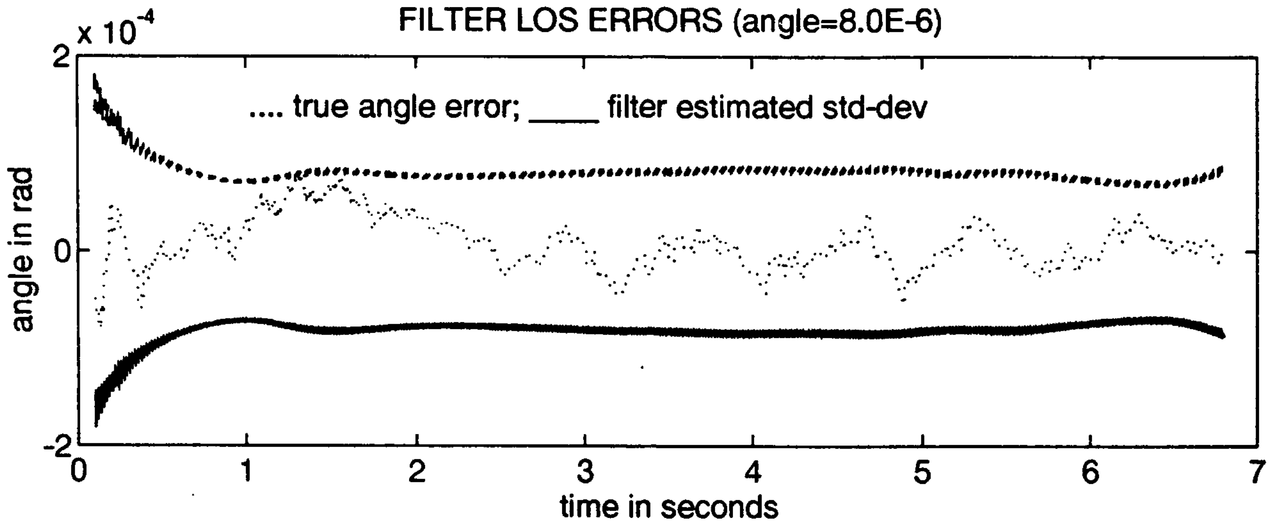
FILTER LOS ERRORS (angle=8.0E-6)
x 10^-4
.... true angle error; _____ filter estimated std-dev
angle in rad
time in seconds
2
0
-2
0
1
2
3
4
5
6
7

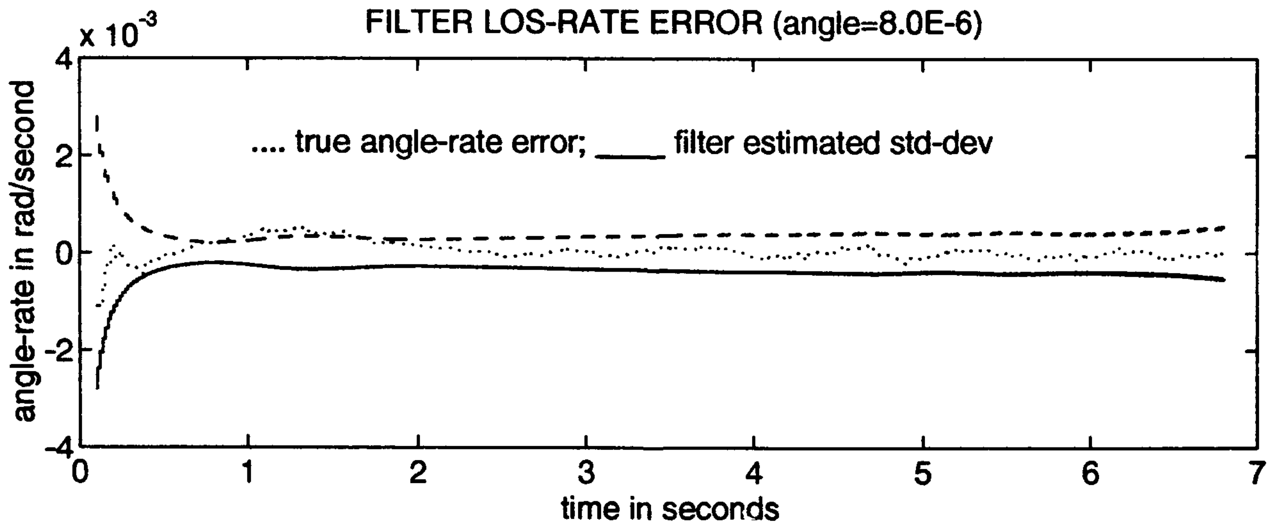
FILTER LOS-RATE ERROR (angle=8.0E-6)
x 10^-3
.... true angle-rate error; _____ filter estimated std-dev
angle-rate in rad/second
time in seconds
4
2
0
-2
-4
0
1
2
3
4
5
6
7

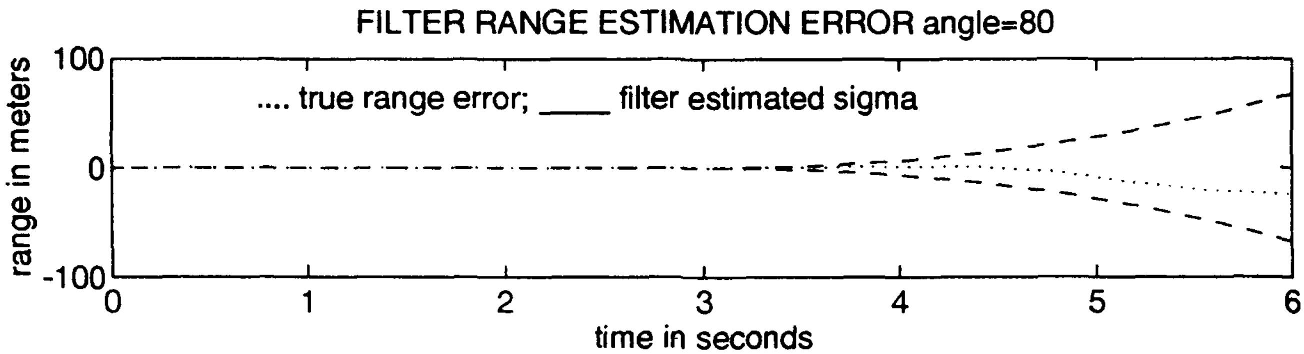
FILTER RANGE ESTIMATION ERROR angle=80
.... true range error; _____ filter estimated sigma
range in meters
100
0
-100
0
1
2
3
4
5
6
time in seconds

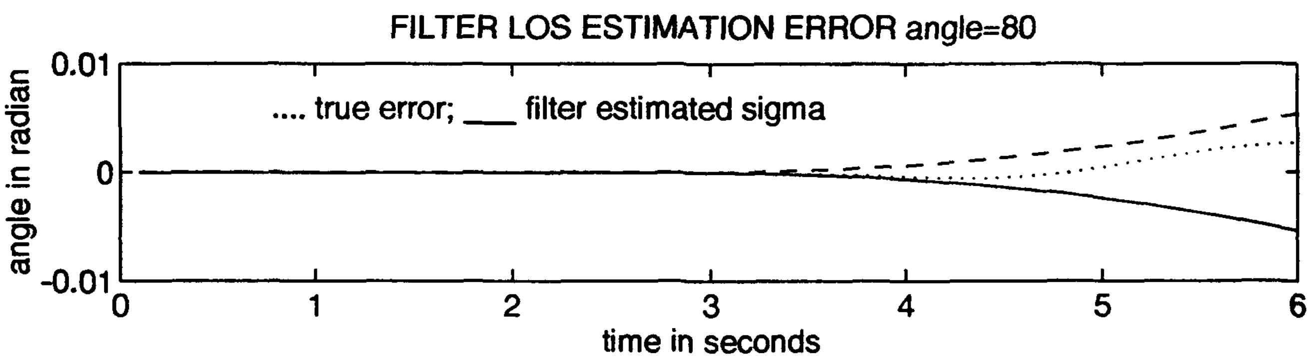
FILTER LOS ESTIMATION ERROR angle=80
.... true error; ___ filter estimated sigma
angle in radian
0.01
0
-0.01
0
1
2
3
4
5
6
time in seconds

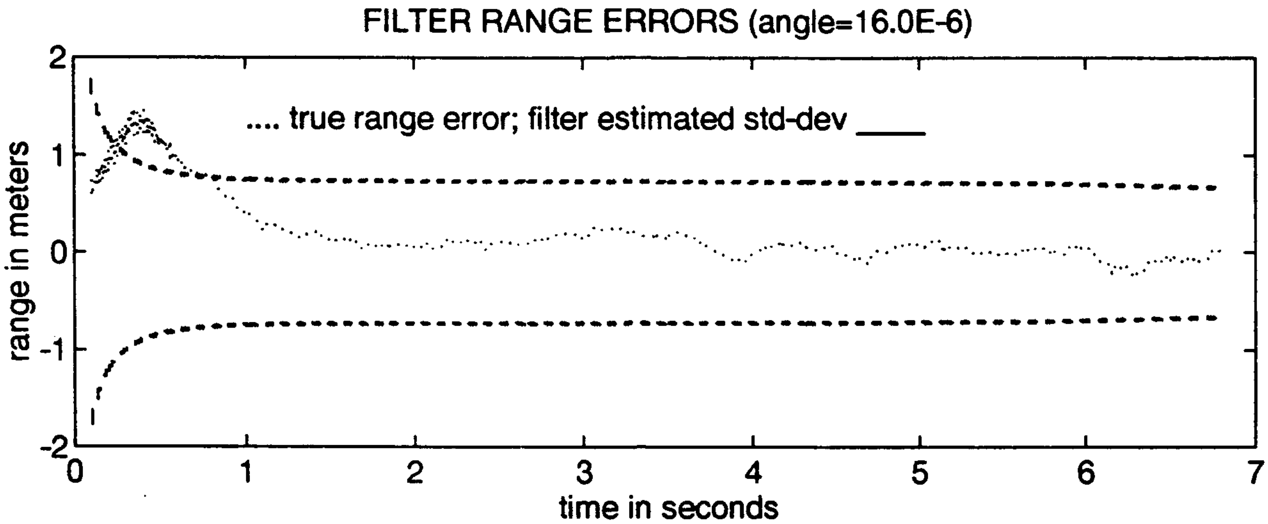
FILTER RANGE ERRORS (angle=16.0E-6)
.... true range error; filter estimated std-dev ____
range in meters
time in seconds
2
1
0
-1
-2
0
1
2
3
4
5
6
7

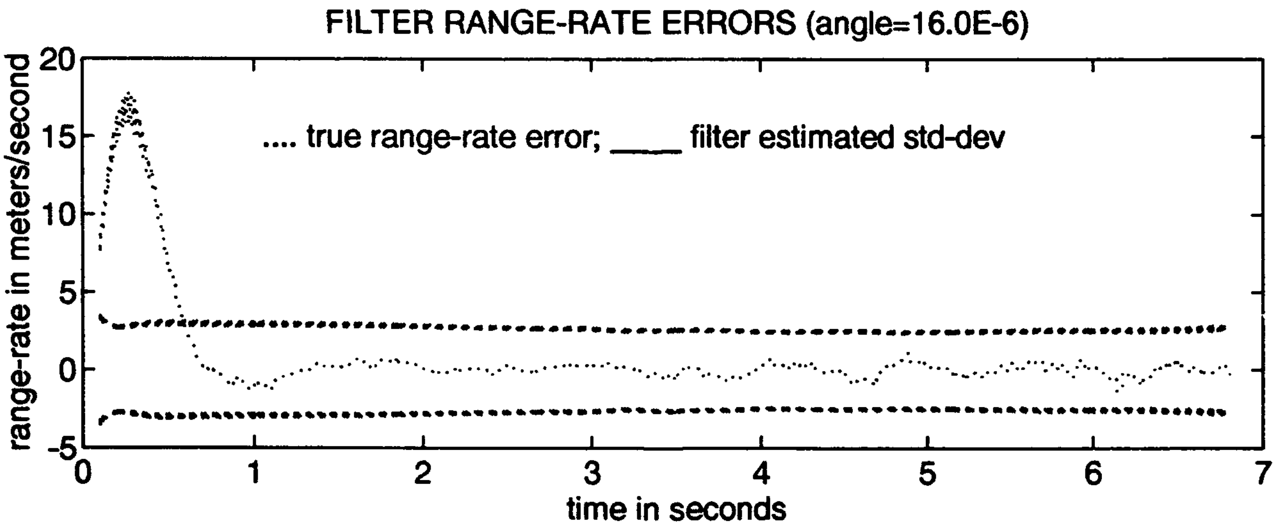
FILTER RANGE-RATE ERRORS (angle=16.0E-6)
.... true range-rate error; ____ filter estimated std-dev
range-rate in meters/second
time in seconds
20
15
10
5
0
-5
0
1
2
3
4
5
6
7

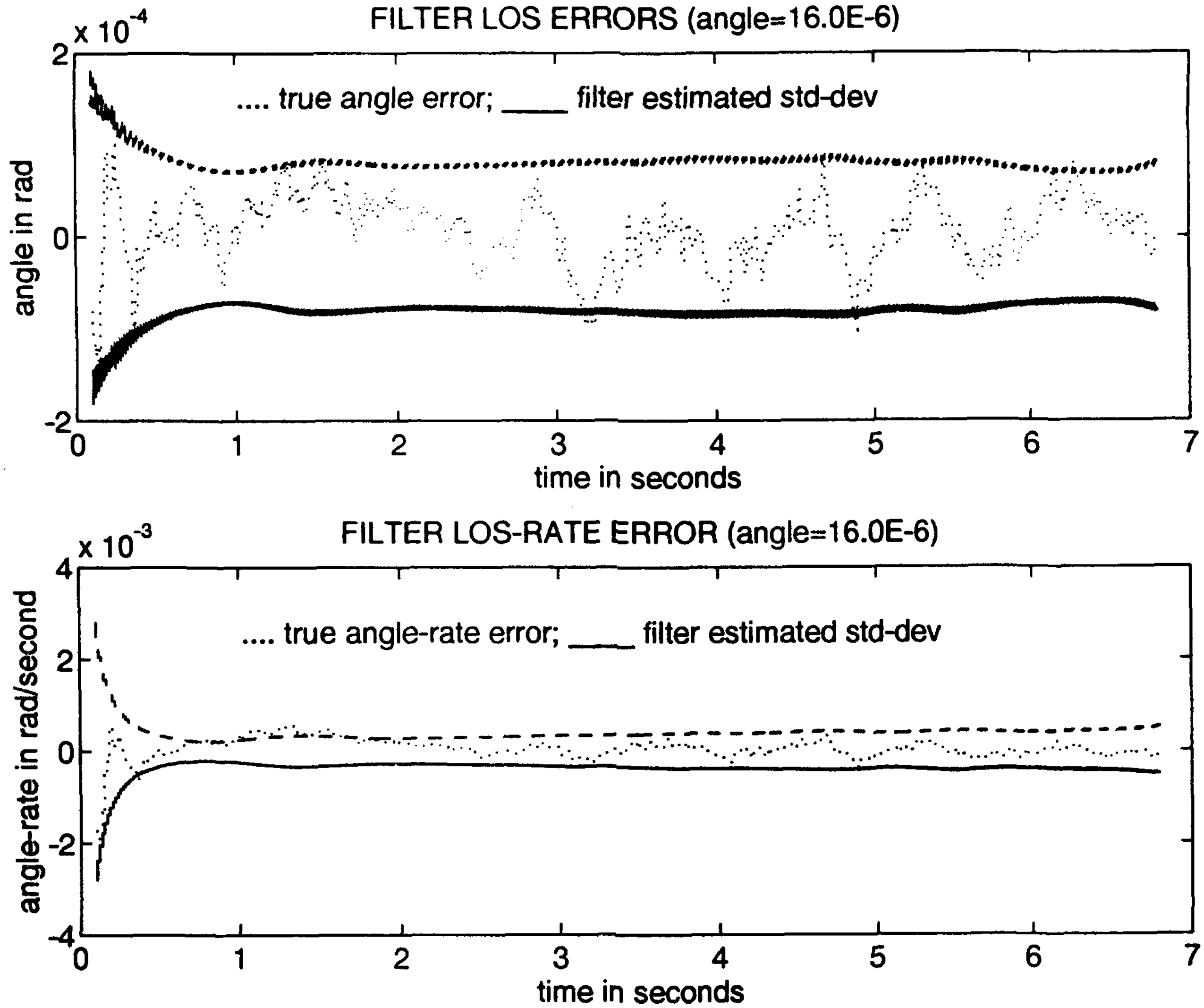
FILTER LOS ERRORS (angle=16.0E-6)
x 10^-4
.... true angle error; ____ filter estimated std-dev
angle in rad
time in seconds
FILTER LOS-RATE ERROR (angle=16.0E-6)
x 10^-3
.... true angle-rate error; ____ filter estimated std-dev
angle-rate in rad/second
time in seconds

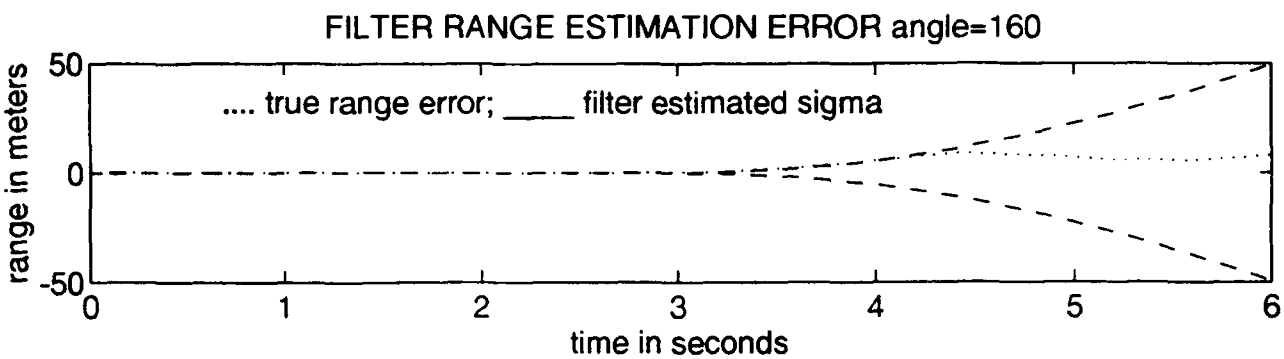
FILTER RANGE ESTIMATION ERROR angle=160
.... true range error; _____ filter estimated sigma
range in meters
50
0
-50
0
1
2
3
4
5
6
time in seconds

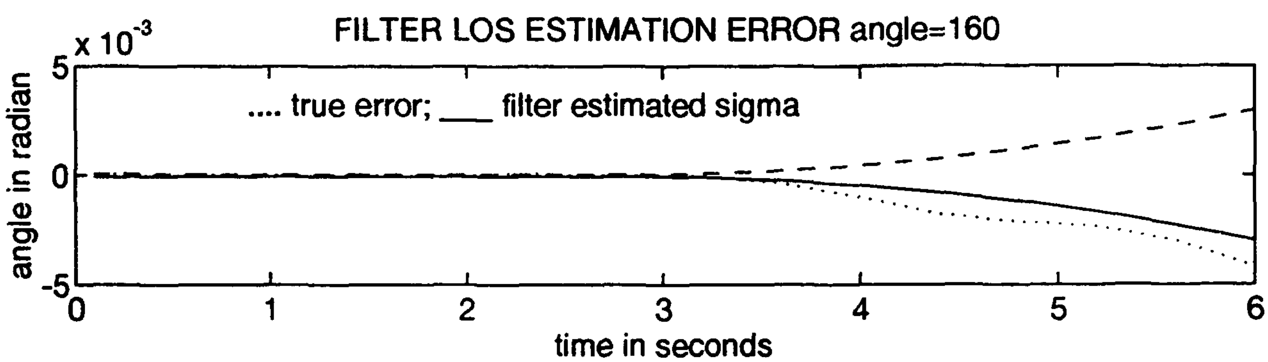
FILTER LOS ESTIMATION ERROR angle=160
x 10^-3
.... true error; ___ filter estimated sigma
angle in radian
5
0
-5
0
1
2
3
4
5
6
time in seconds

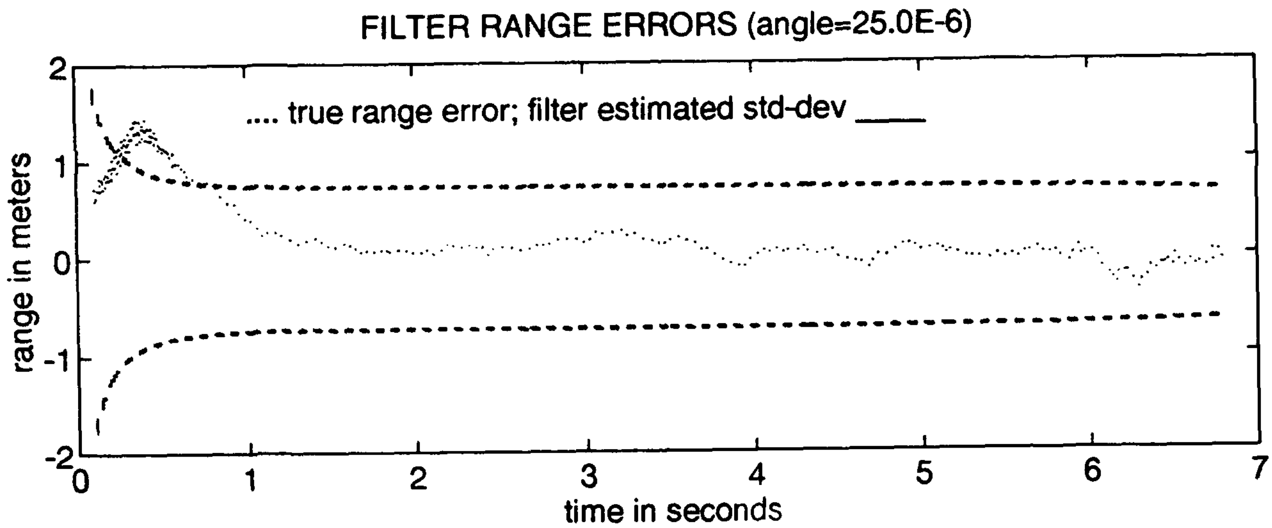
FILTER RANGE ERRORS (angle=25.0E-6)
.... true range error; filter estimated std-dev ____
range in meters
2
1
0
-1
-2
0
1
2
3
4
5
6
7
time in seconds

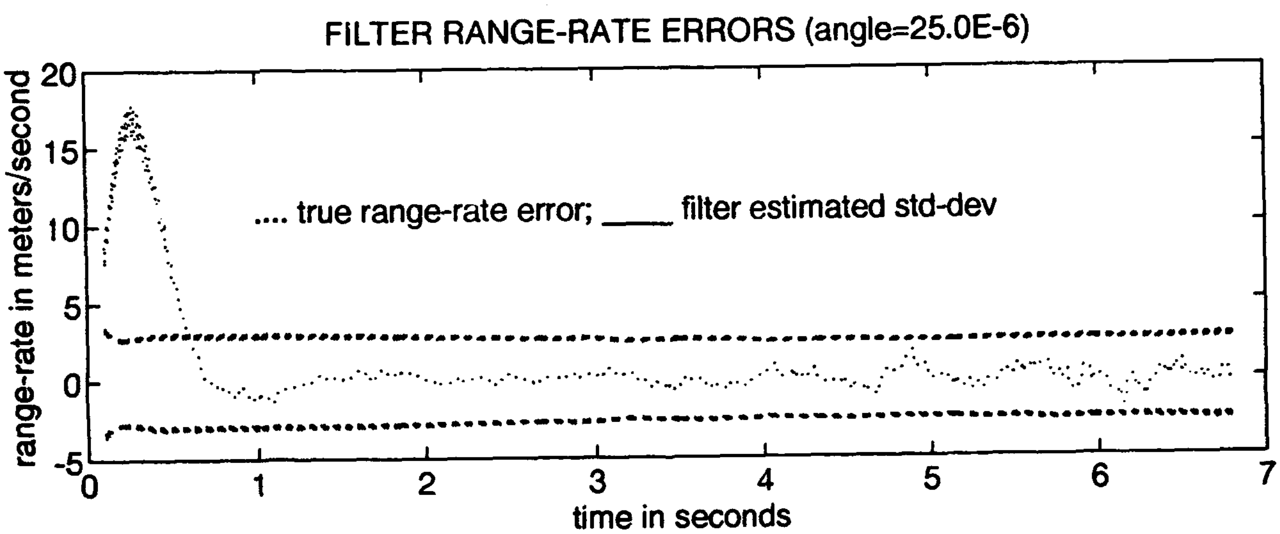
FILTER RANGE-RATE ERRORS (angle=25.0E-6)
.... true range-rate error; ____ filter estimated std-dev
range-rate in meters/second
20
15
10
5
0
-5
0
1
2
3
4
5
6
7
time in seconds

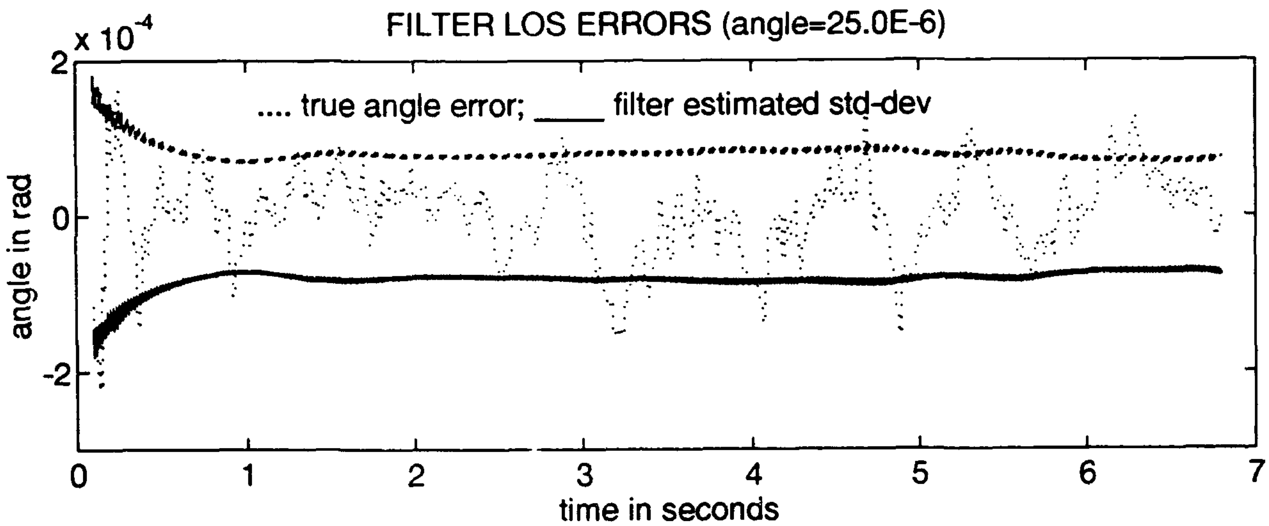
FILTER LOS ERRORS (angle=25.0E-6)
x 10^-4
.... true angle error; ____ filter estimated std-dev
angle in rad
time in seconds

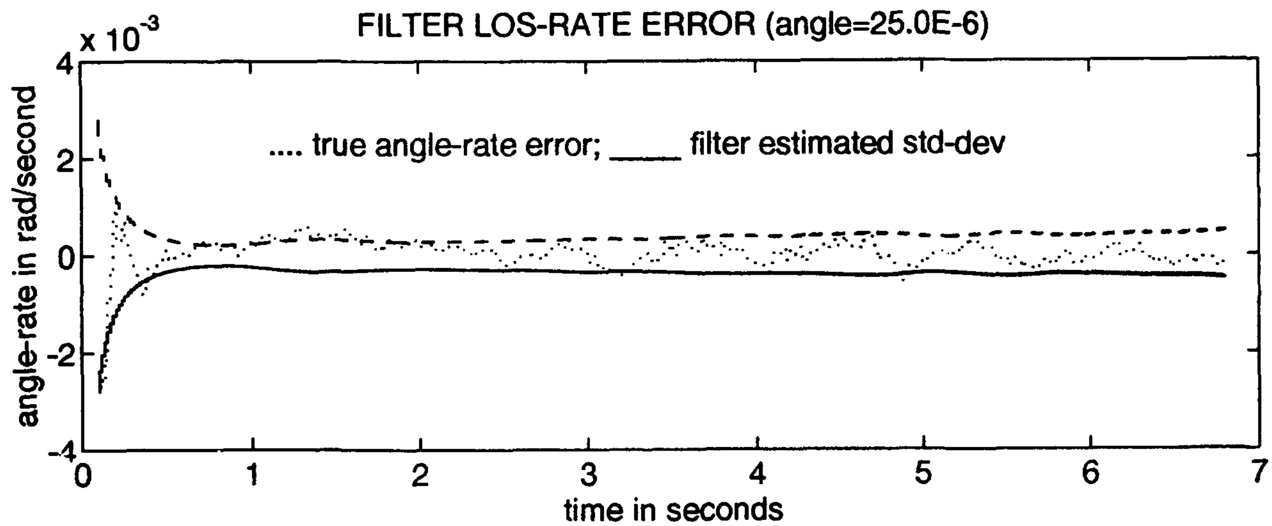
FILTER LOS-RATE ERROR (angle=25.0E-6)
x 10^-3
.... true angle-rate error; ____ filter estimated std-dev
angle-rate in rad/second
time in seconds

FILTER RANGE ERRORS (angle=8.0E-6)

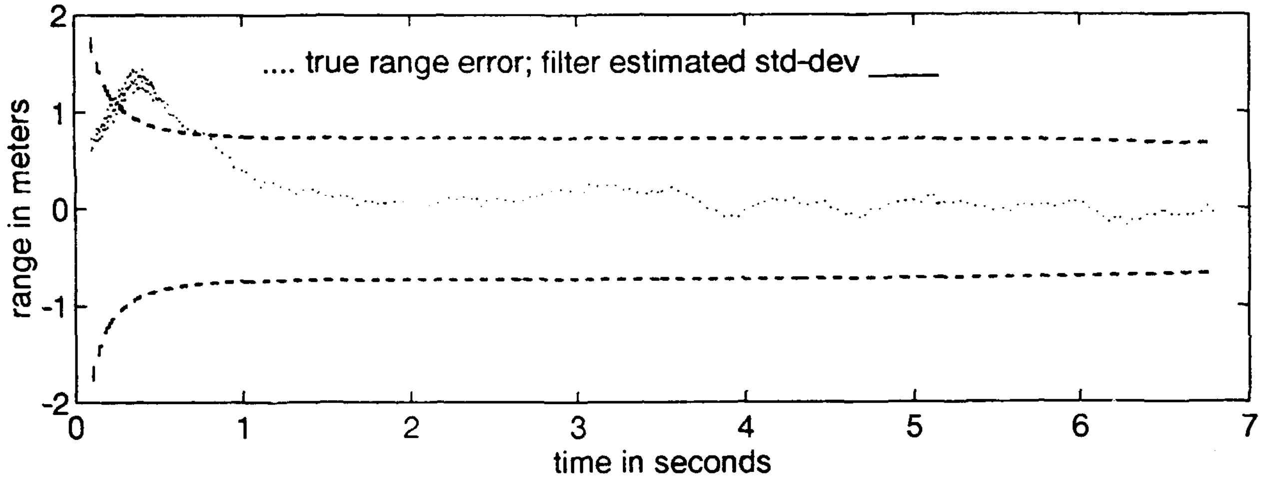

FILTER RANGE-RATE ERRORS (angle=8.0E-6)

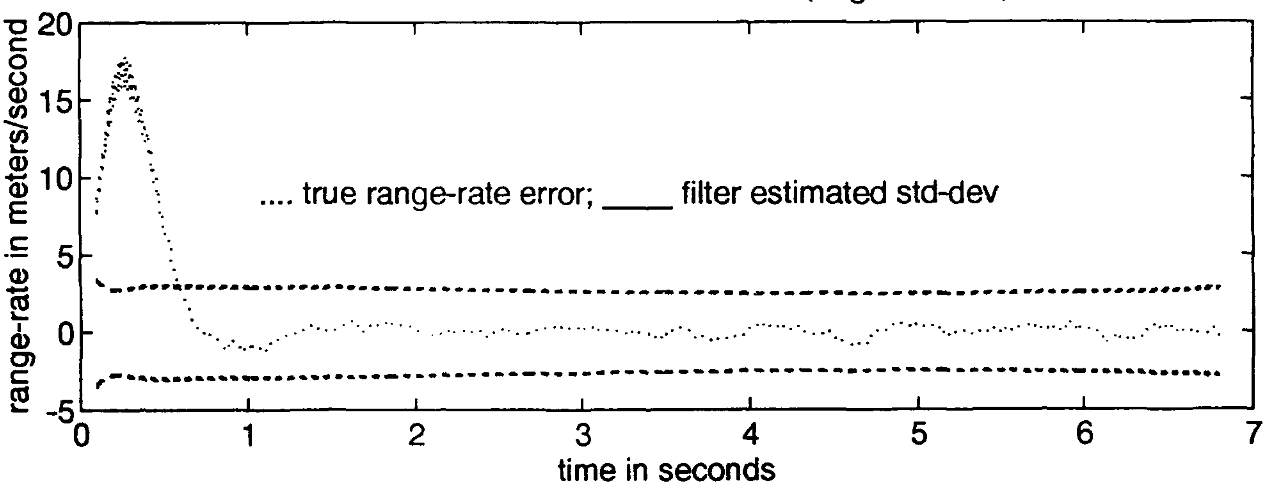

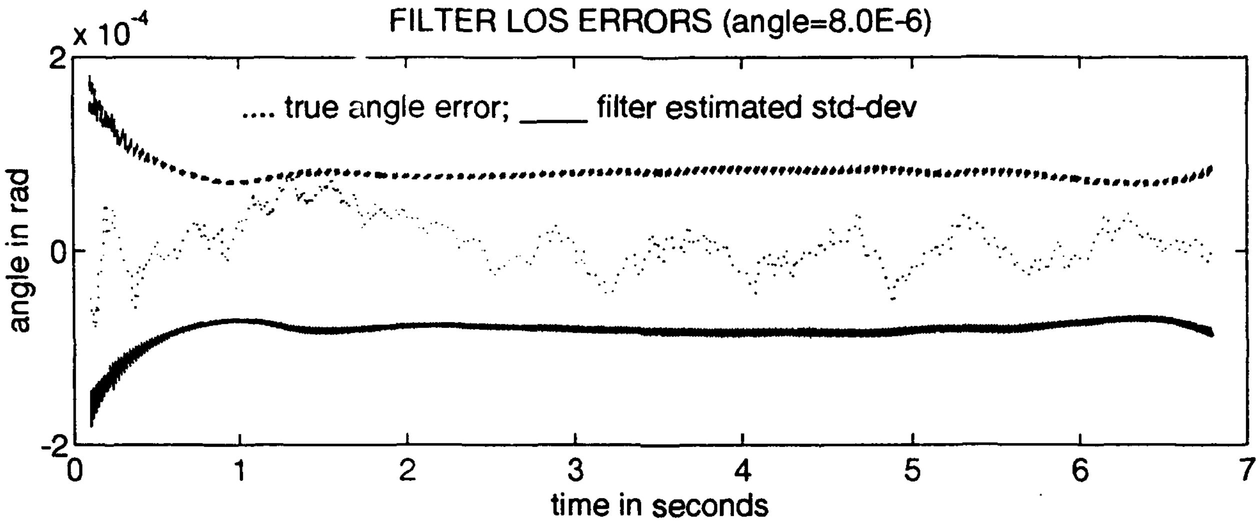

FILTER LOS ERRORS (angle=8.0E-6)
x 10^-4
.... true angle error; ____ filter estimated std-dev
angle in rad
2
0
-2
0
1
2
3
4
5
6
7
time in seconds

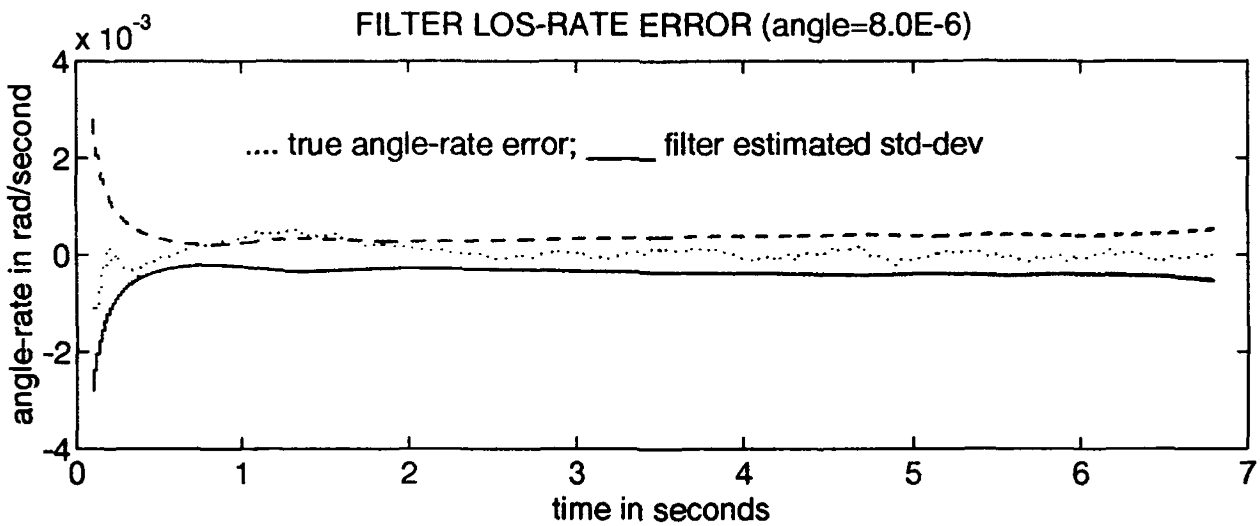

FILTER LOS-RATE ERROR (angle=8.0E-6)
x 10^-3
.... true angle-rate error; ____ filter estimated std-dev
angle-rate in rad/second
4
2
0
-2
-4
0
1
2
3
4
5
6
7
time in seconds

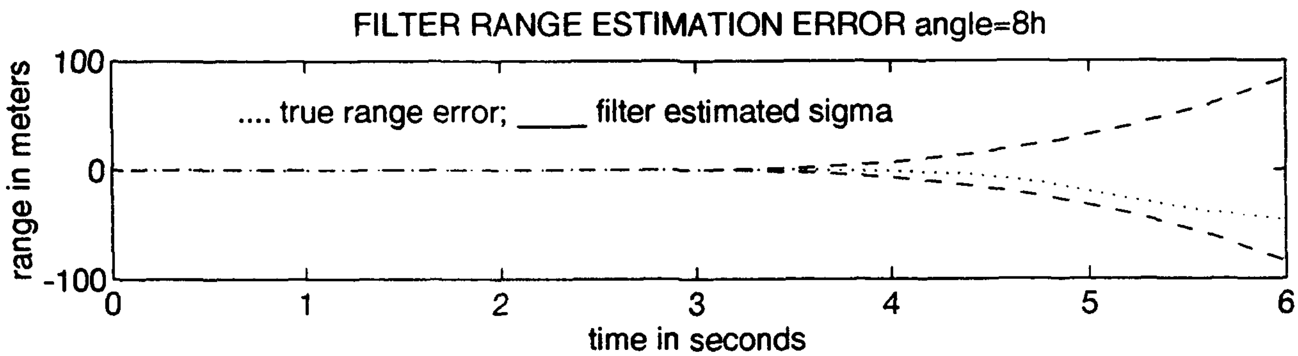
FILTER RANGE ESTIMATION ERROR angle=8h
.... true range error; ____ filter estimated sigma
range in meters
100
0
-100
0
1
2
3
4
5
6
time in seconds

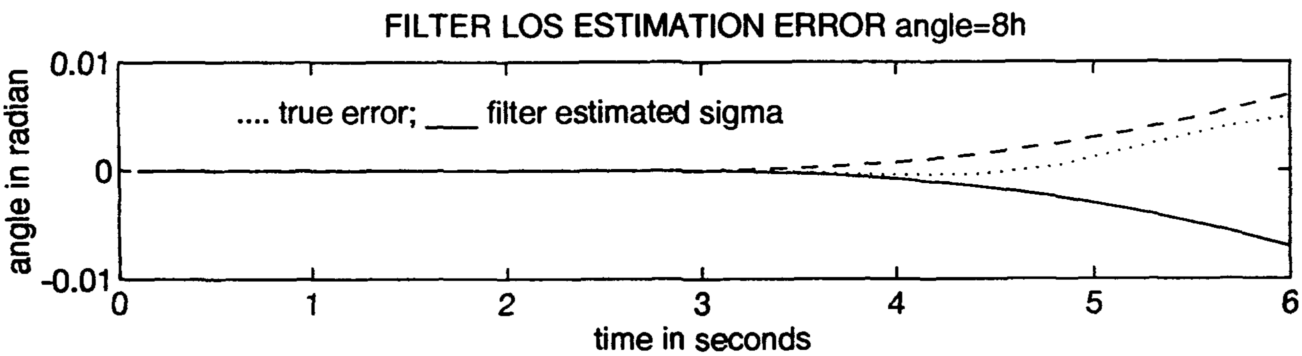
FILTER LOS ESTIMATION ERROR angle=8h
.... true error; ___ filter estimated sigma
angle in radian
0.01
0
-0.01
0
1
2
3
4
5
6
time in seconds

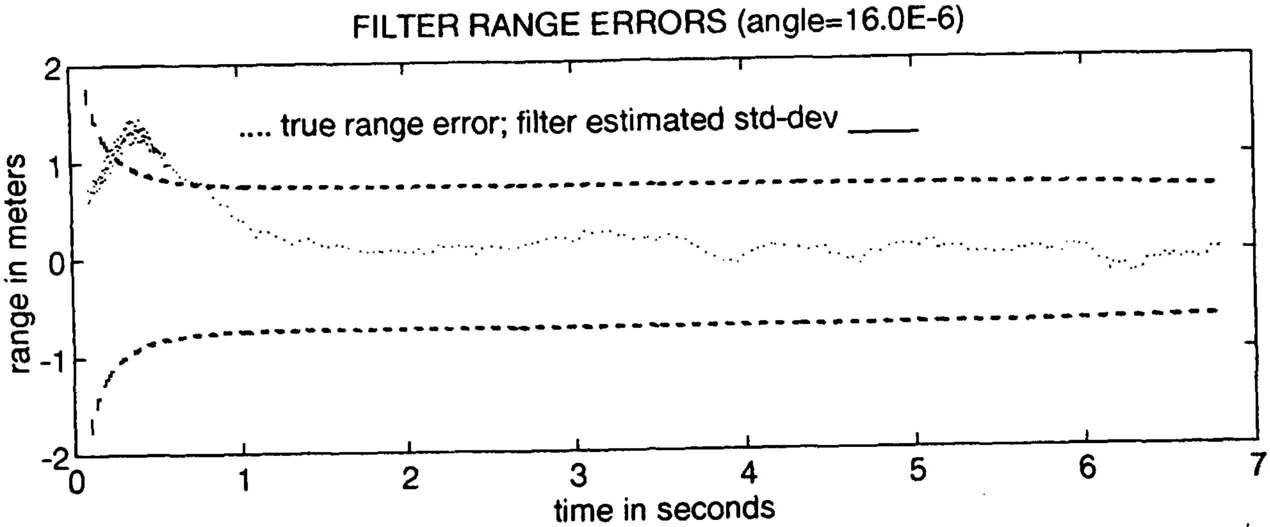

FILTER RANGE ERRORS (angle=16.0E-6)
.... true range error; filter estimated std-dev _____
range in meters
time in seconds

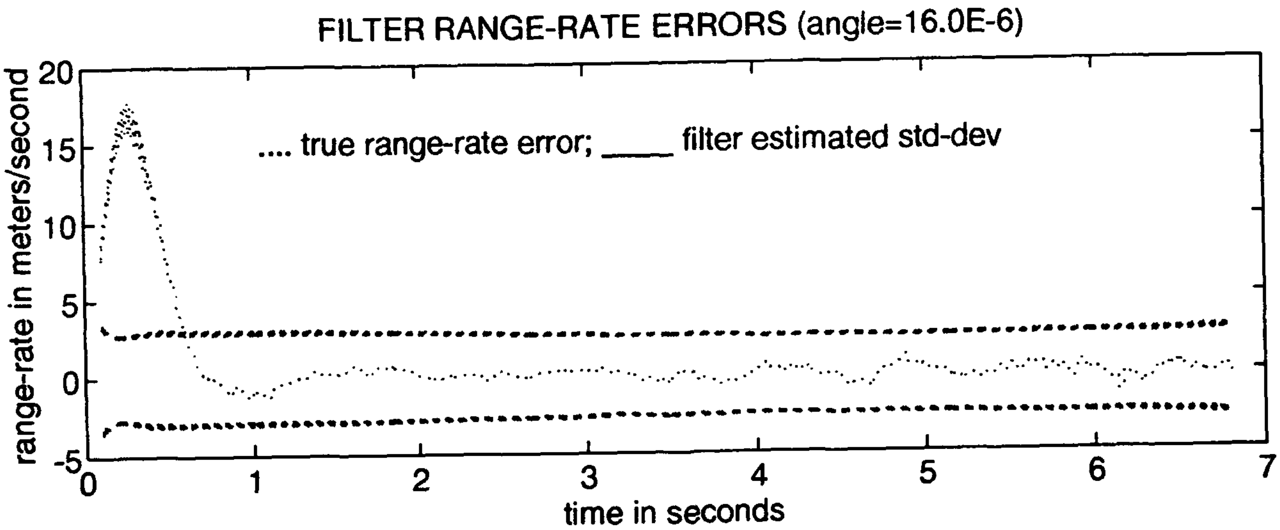

FILTER RANGE-RATE ERRORS (angle=16.0E-6)
.... true range-rate error; _____ filter estimated std-dev
range-rate in meters/second
time in seconds

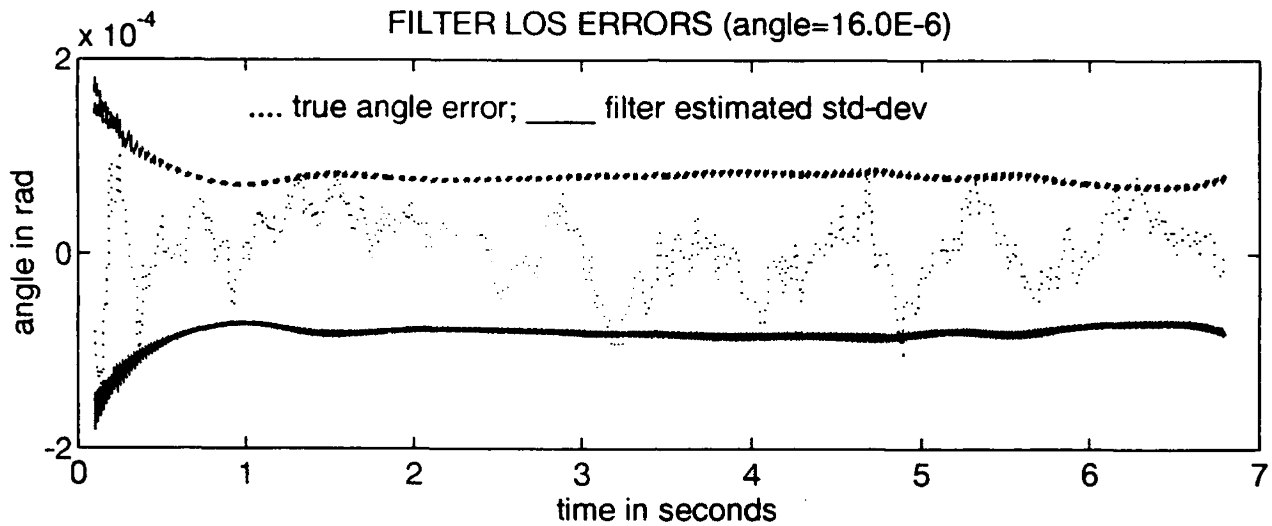
FILTER LOS ERRORS (angle=16.0E-6)
x 10^-4
.... true angle error; _____ filter estimated std-dev
angle in rad
time in seconds
2
0
-2
0
1
2
3
4
5
6
7

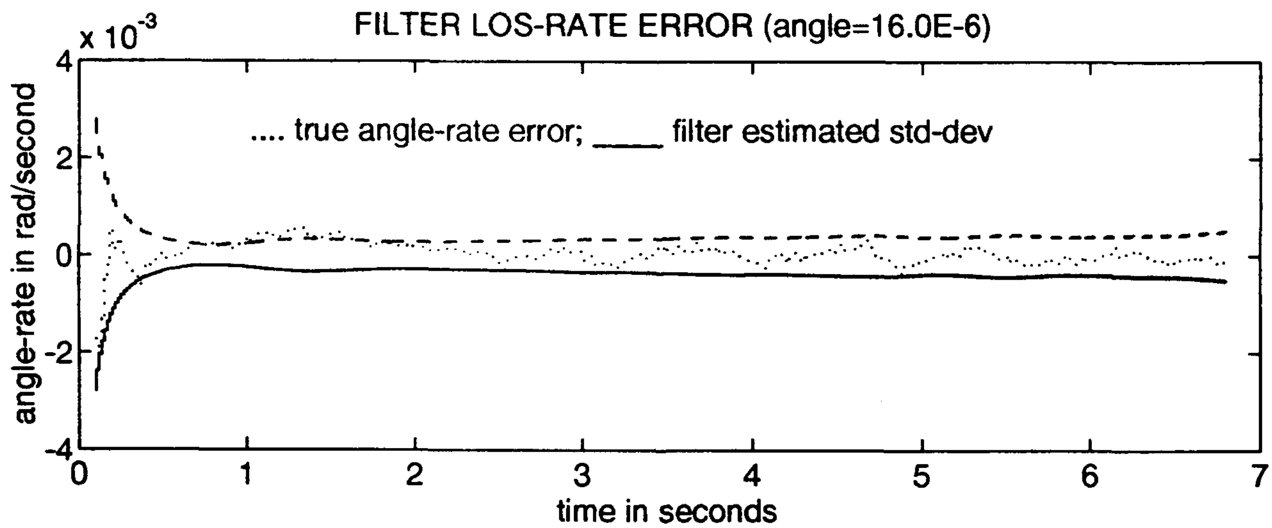
FILTER LOS-RATE ERROR (angle=16.0E-6)
x 10^-3
.... true angle-rate error; _____ filter estimated std-dev
angle-rate in rad/second
time in seconds
4
2
0
-2
-4
0
1
2
3
4
5
6
7

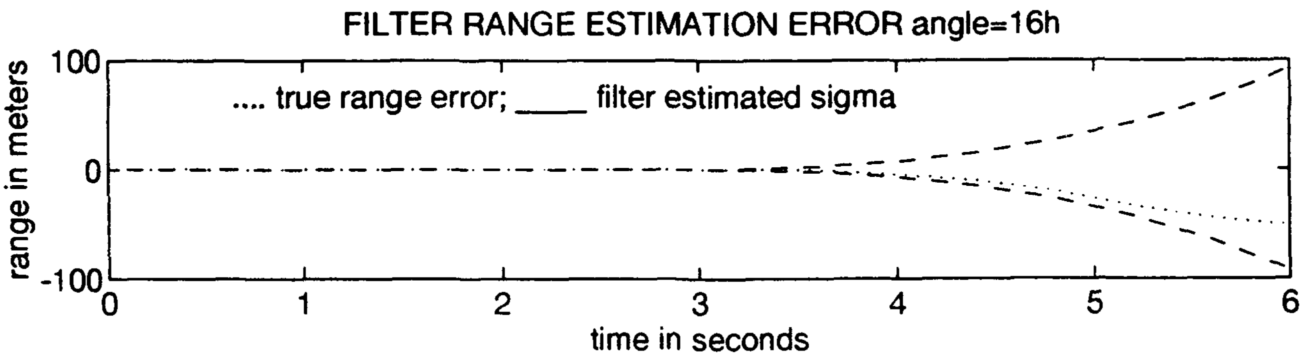
FILTER RANGE ESTIMATION ERROR angle=16h
.... true range error; ____ filter estimated sigma
range in meters
100
0
-100
0
1
2
3
4
5
6
time in seconds

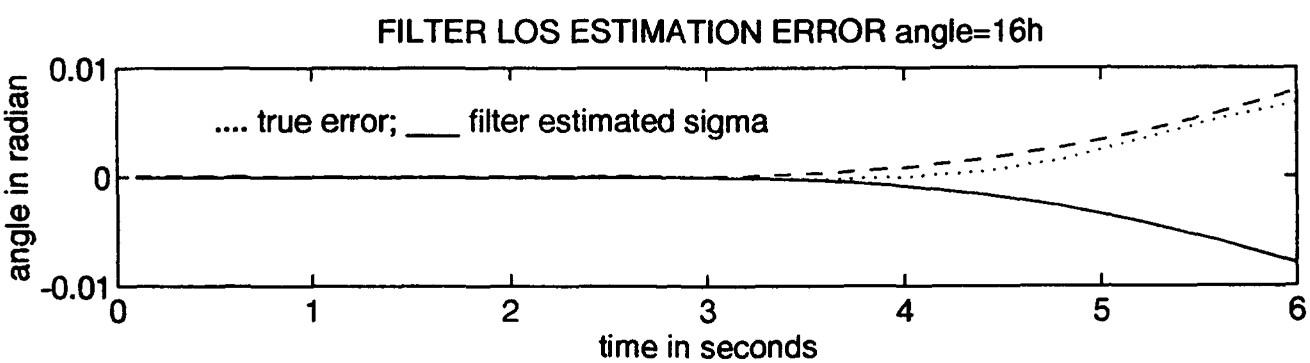
FILTER LOS ESTIMATION ERROR angle=16h
.... true error; ___ filter estimated sigma
angle in radian
0.01
0
-0.01
0
1
2
3
4
5
6
time in seconds

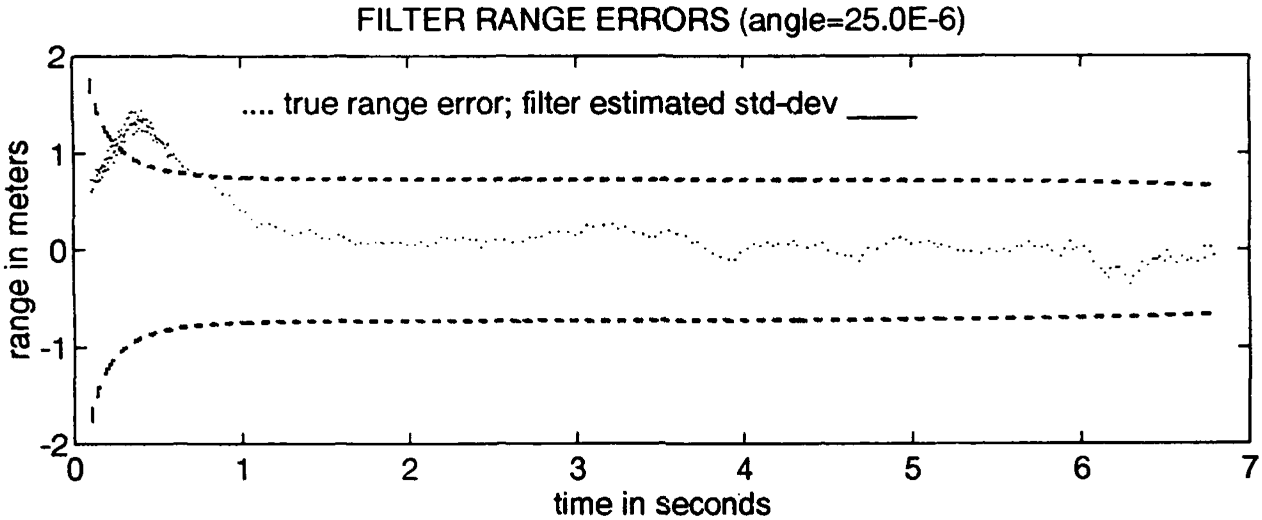
FILTER RANGE ERRORS (angle=25.0E-6)
.... true range error; filter estimated std-dev ____
range in meters
2
1
0
-1
-2
0
1
2
3
4
5
6
7
time in seconds

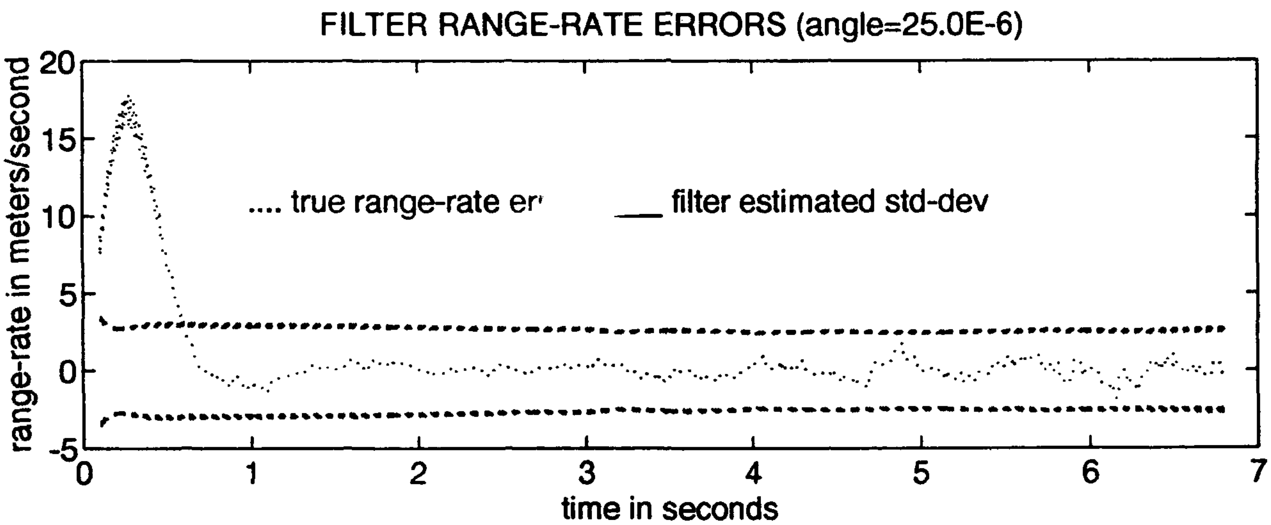
FILTER RANGE-RATE ERRORS (angle=25.0E-6)
.... true range-rate er
____ filter estimated std-dev
range-rate in meters/second
20
15
10
5
0
-5
0
1
2
3
4
5
6
7
time in seconds

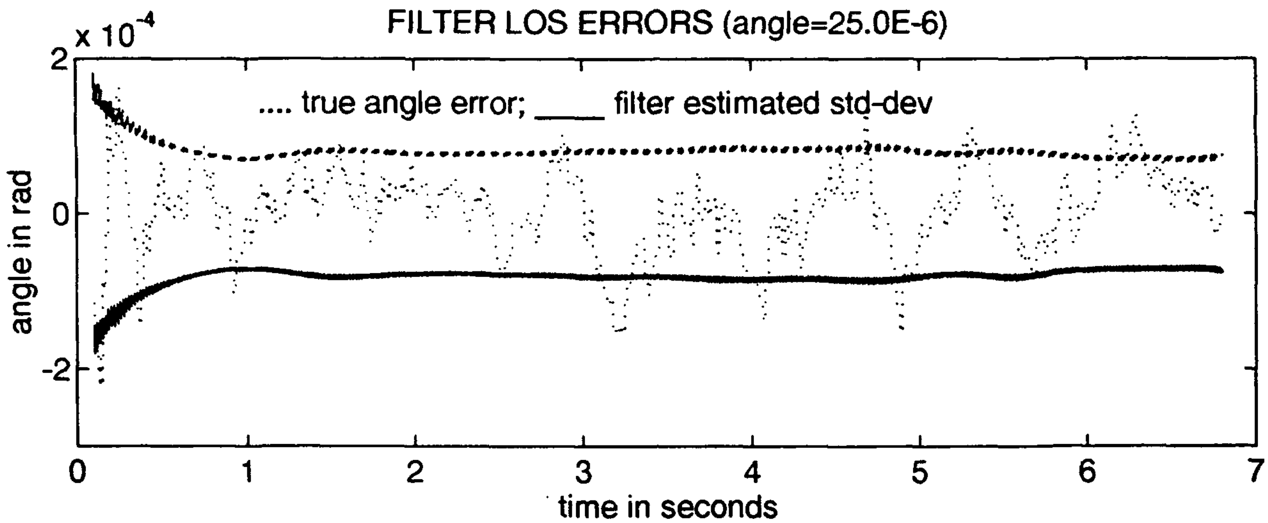
FILTER LOS ERRORS (angle=25.0E-6)
x 10^-4
.... true angle error; ____ filter estimated std-dev
angle in rad
time in seconds

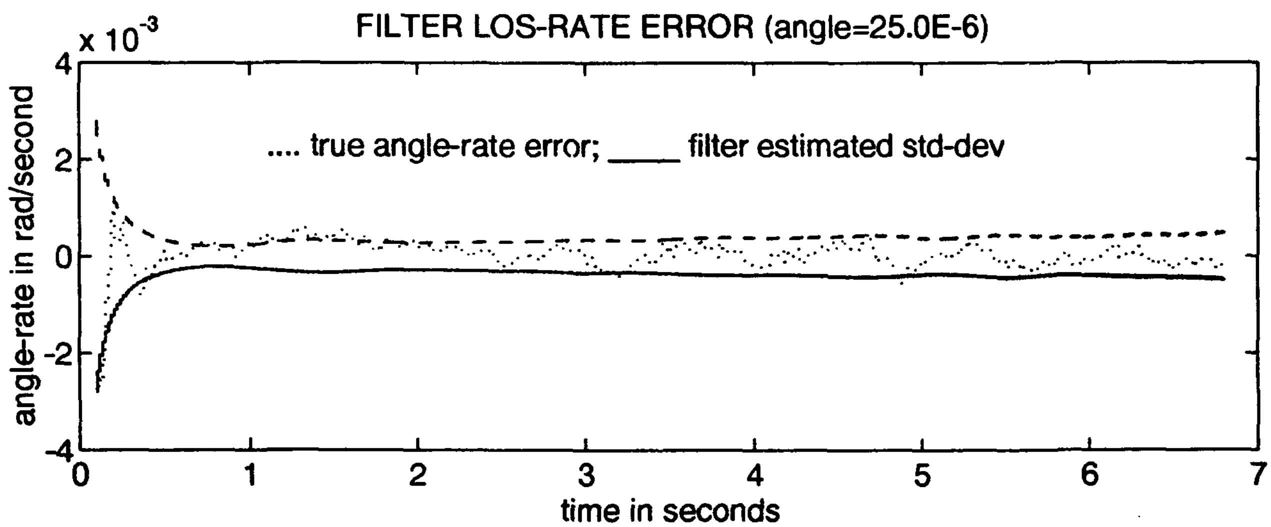
FILTER LOS-RATE ERROR (angle=25.0E-6)
x 10^-3
.... true angle-rate error; ____ filter estimated std-dev
angle-rate in rad/second
time in seconds

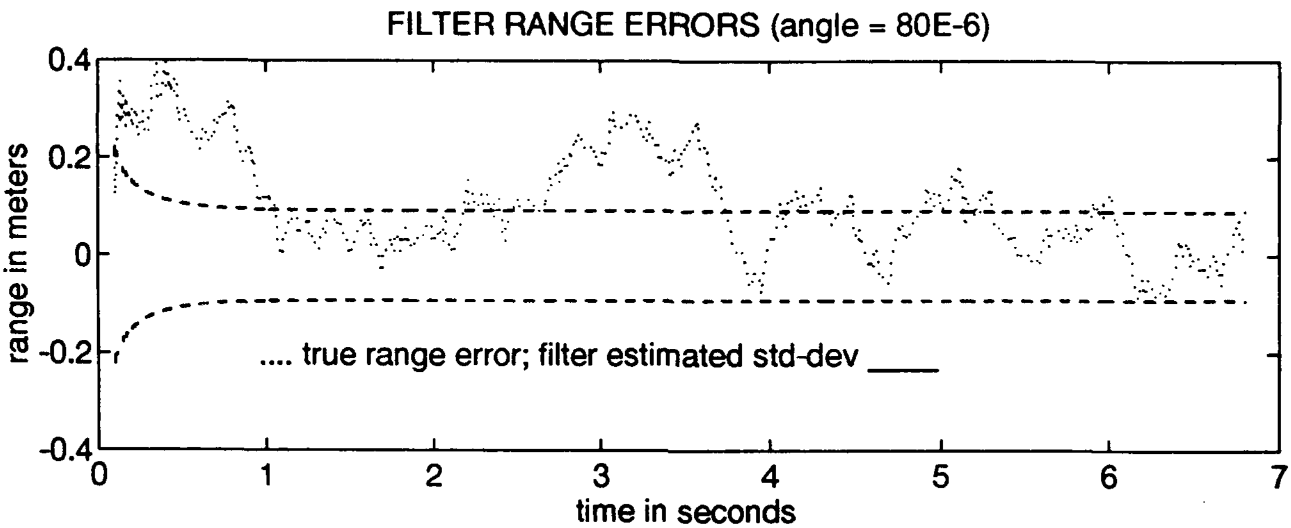
FILTER RANGE ERRORS (angle = 80E-6)
range in meters
0.4
0.2
0
-0.2
-0.4
.... true range error; filter estimated std-dev ____
0
1
2
3
4
5
6
7
time in seconds

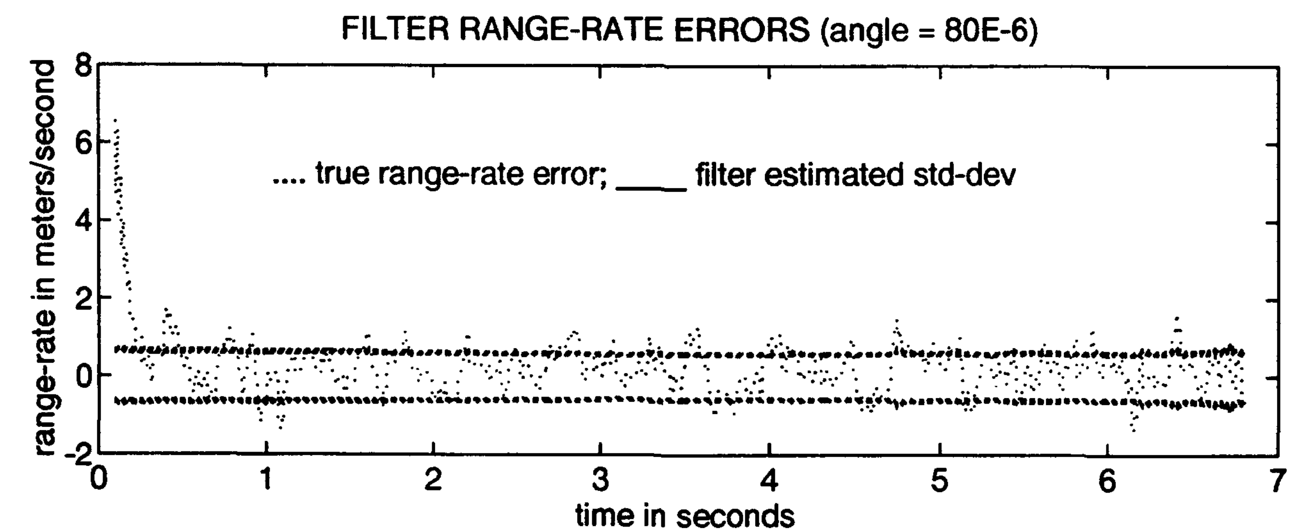
FILTER RANGE-RATE ERRORS (angle = 80E-6)
range-rate in meters/second
8
6
4
2
0
-2
.... true range-rate error; ____ filter estimated std-dev
0
1
2
3
4
5
6
7
time in seconds

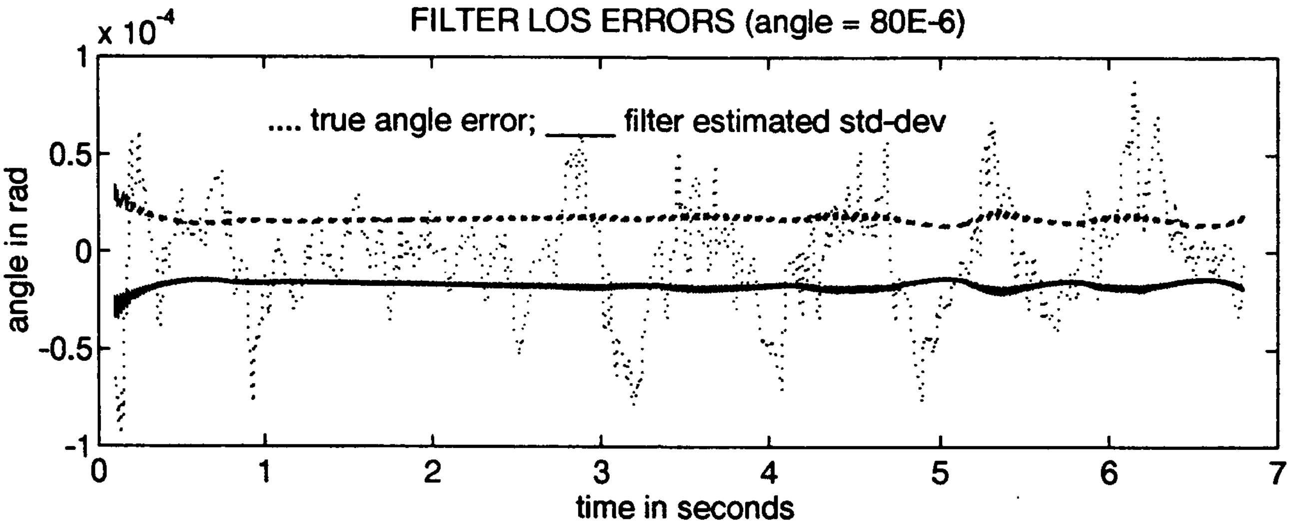
x 10^-4
FILTER LOS ERRORS (angle = 80E-6)
.... true angle error; _____ filter estimated std-dev
angle in rad
1
0.5
0
-0.5
-1
0
1
2
3
4
5
6
7
time in seconds

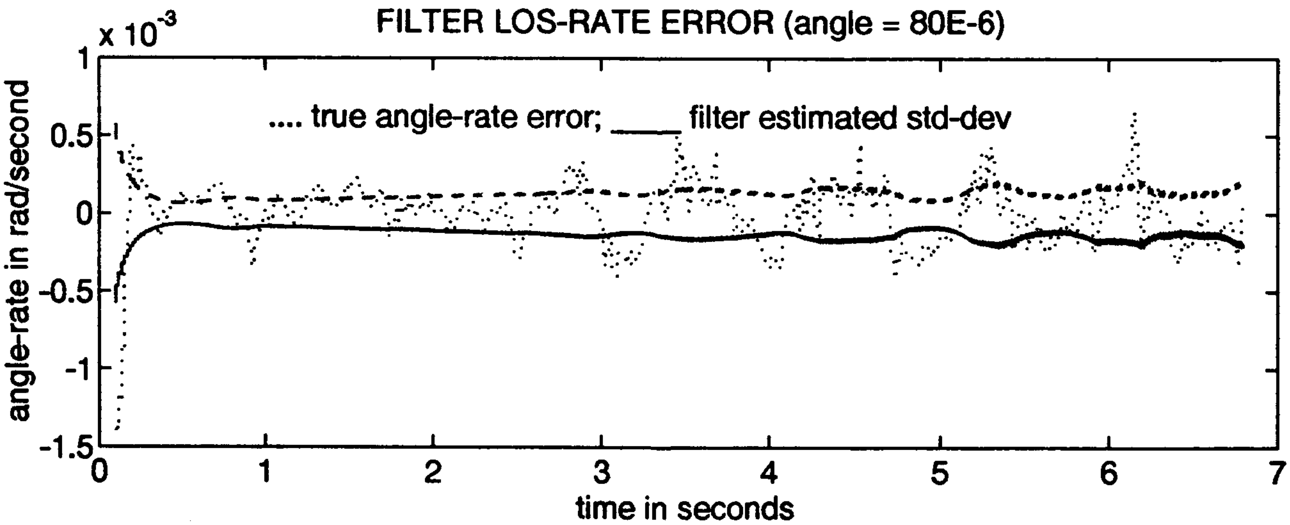
x 10^-3
FILTER LOS-RATE ERROR (angle = 80E-6)
.... true angle-rate error; _____ filter estimated std-dev
angle-rate in rad/second
1
0.5
0
-0.5
-1
-1.5
0
1
2
3
4
5
6
7
time in seconds

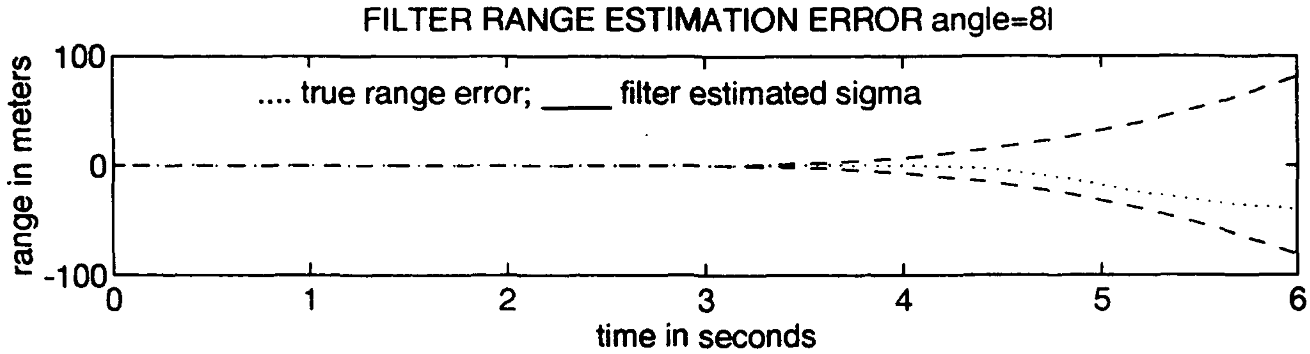
FILTER RANGE ESTIMATION ERROR angle=8l
.... true range error; ____ filter estimated sigma
range in meters
100
0
-100
0
1
2
3
4
5
6
time in seconds

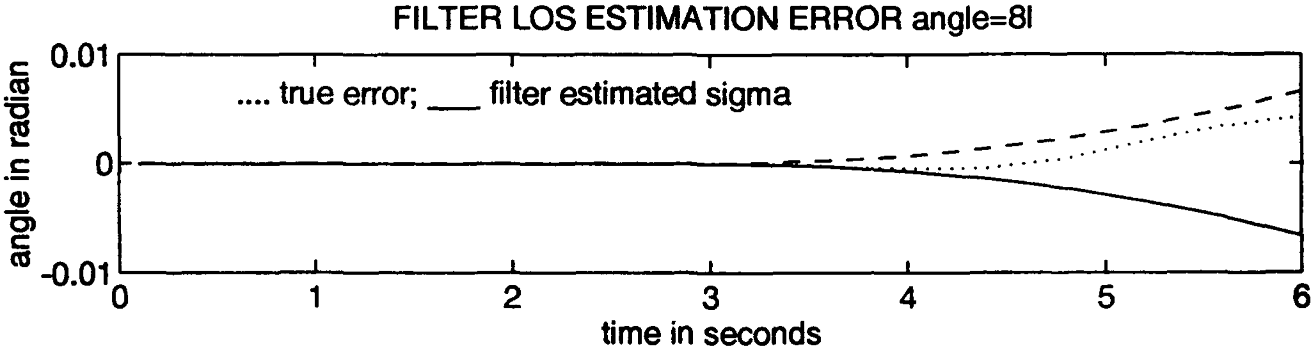
FILTER LOS ESTIMATION ERROR angle=8l
.... true error; ___ filter estimated sigma
angle in radian
0.01
0
-0.01
0
1
2
3
4
5
6
time in seconds

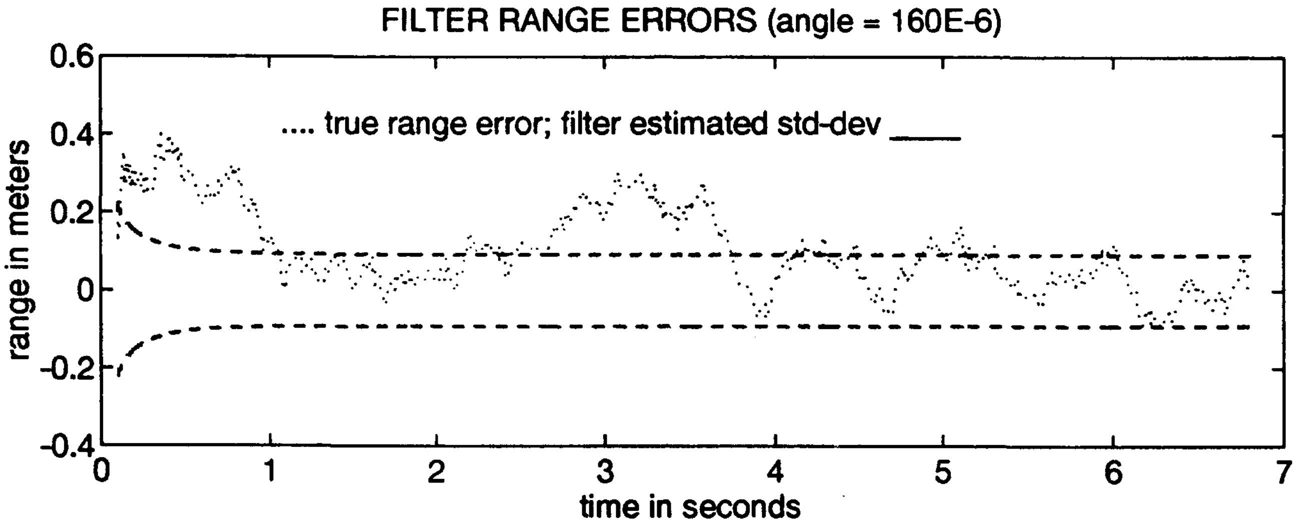
FILTER RANGE ERRORS (angle = 160E-6)
.... true range error; filter estimated std-dev ____
range in meters
0.6
0.4
0.2
0
-0.2
-0.4
0
1
2
3
4
5
6
7
time in seconds

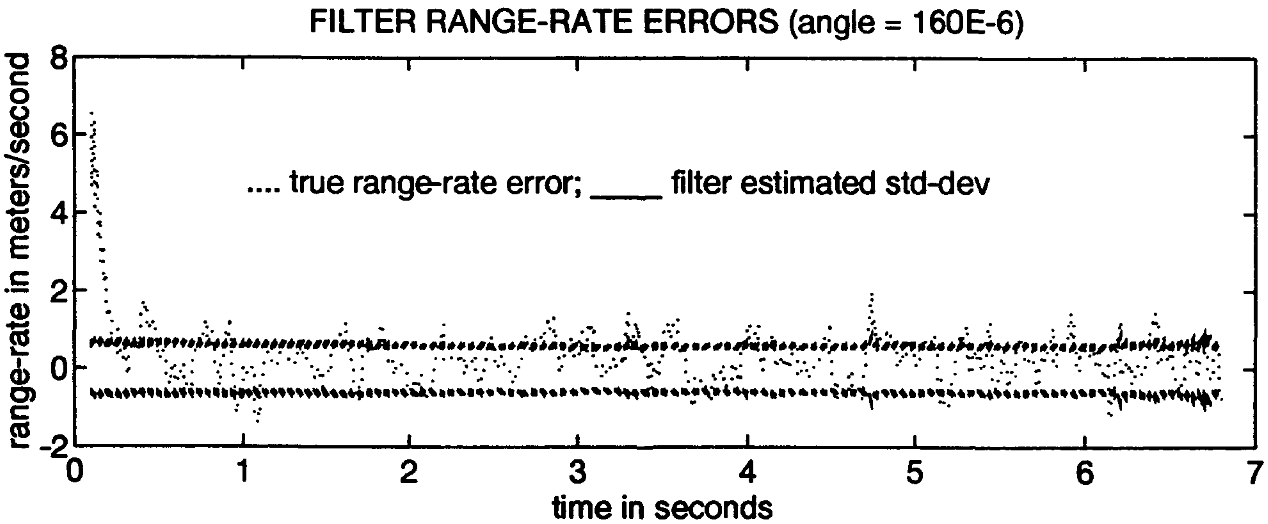
FILTER RANGE-RATE ERRORS (angle = 160E-6)
.... true range-rate error; ____ filter estimated std-dev
range-rate in meters/second
8
6
4
2
0
-2
0
1
2
3
4
5
6
7
time in seconds

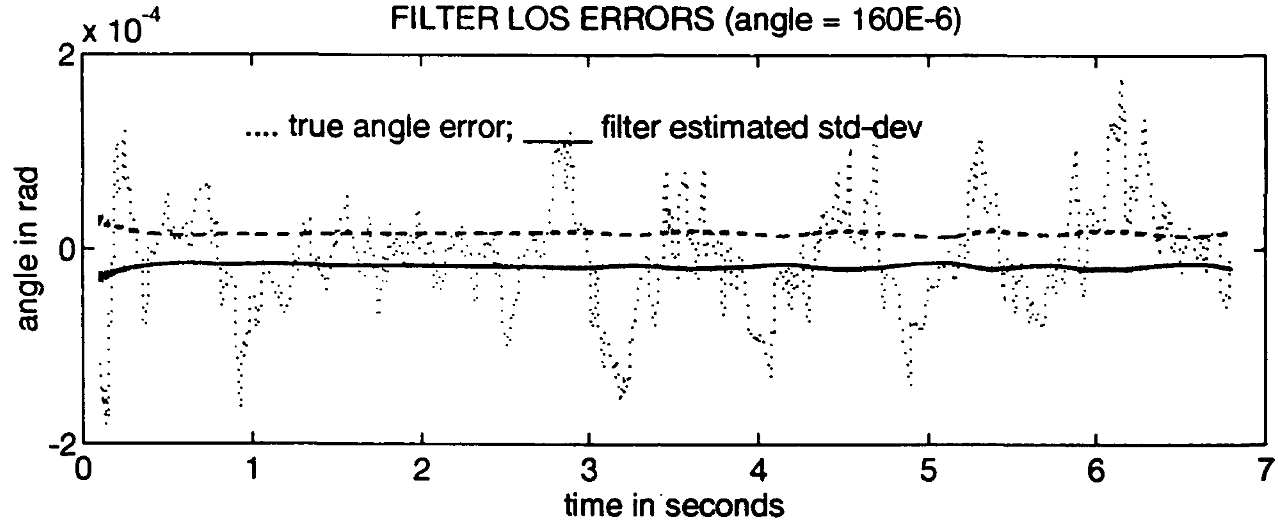
FILTER LOS ERRORS (angle = 160E-6)
x 10^-4
.... true angle error; ____ filter estimated std-dev
angle in rad
2
0
-2
0
1
2
3
4
5
6
7
time in seconds

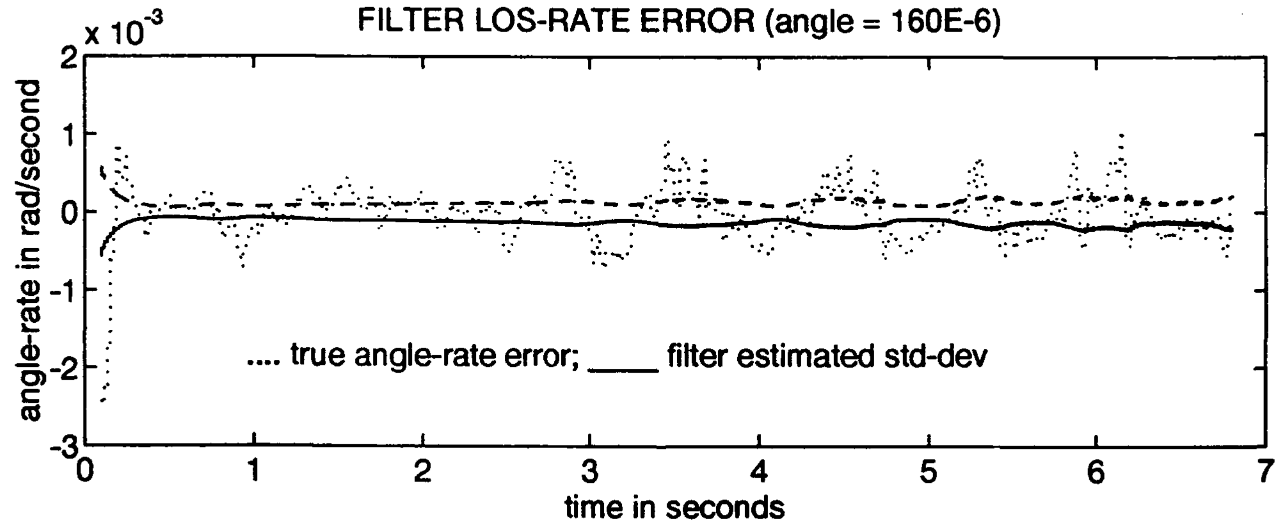
FILTER LOS-RATE ERROR (angle = 160E-6)
x 10^-3
.... true angle-rate error; ____ filter estimated std-dev
angle-rate in rad/second
2
1
0
-1
-2
-3
0
1
2
3
4
5
6
7
time in seconds

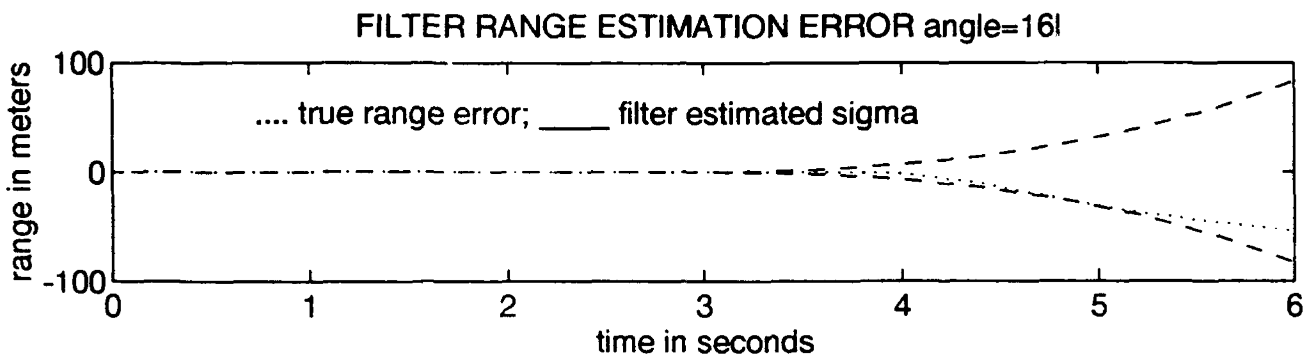

FILTER RANGE ESTIMATION ERROR angle=16l
.... true range error; ____ filter estimated sigma
range in meters
100
0
-100
0
1
2
3
4
5
6
time in seconds

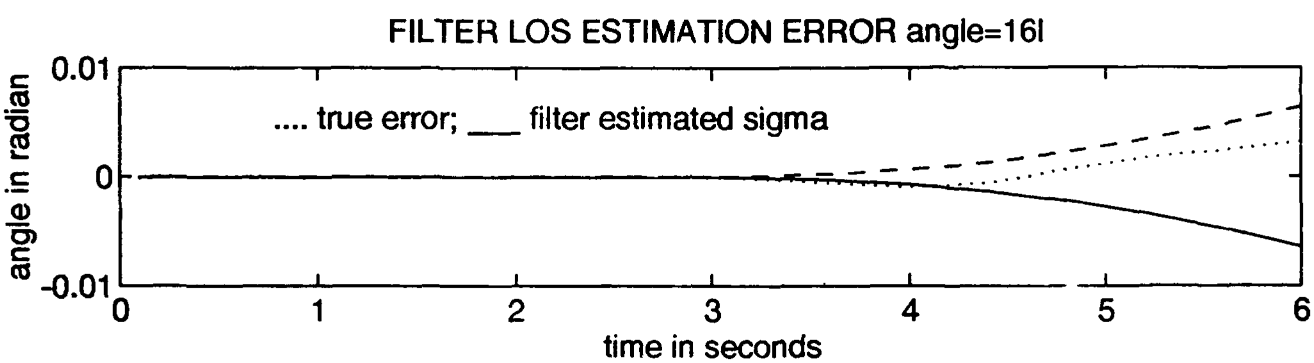

FILTER LOS ESTIMATION ERROR angle=16l
.... true error; ___ filter estimated sigma
angle in radian
0.01
0
-0.01
0
1
2
3
4
5
6
time in seconds

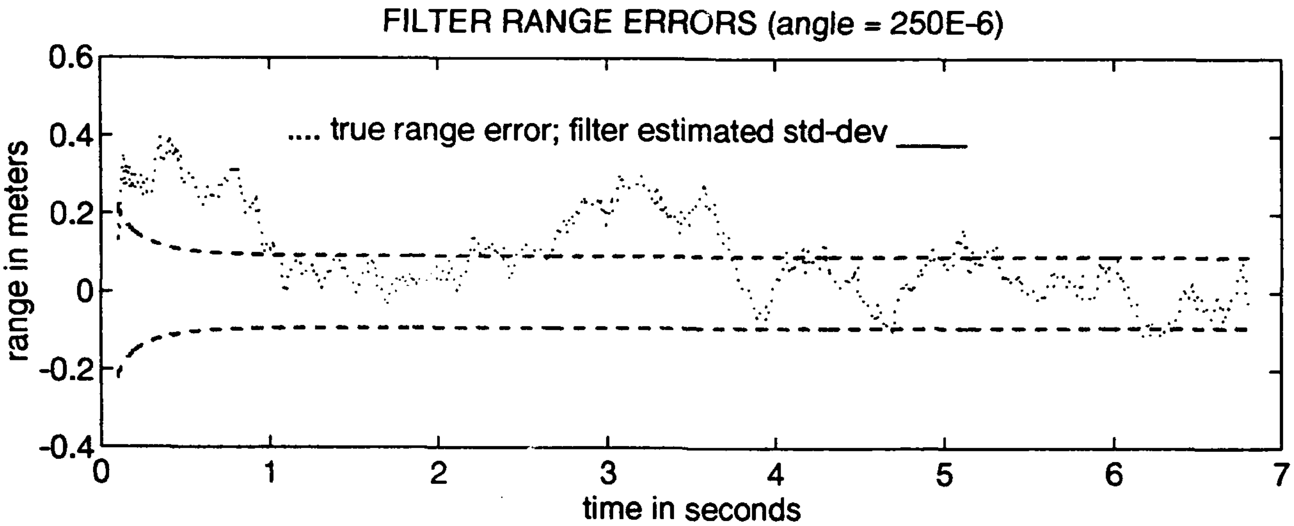
FILTER RANGE ERRORS (angle = 250E-6)
.... true range error; filter estimated std-dev ____
range in meters
0.6
0.4
0.2
0
-0.2
-0.4
0
1
2
3
4
5
6
7
time in seconds

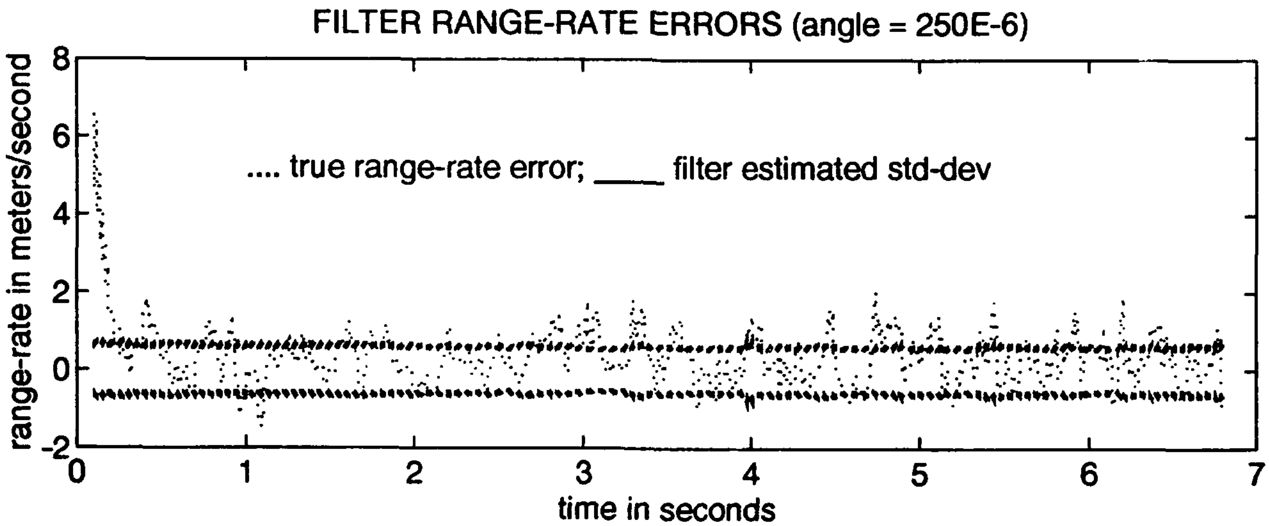
FILTER RANGE-RATE ERRORS (angle = 250E-6)
.... true range-rate error; ____ filter estimated std-dev
range-rate in meters/second
8
6
4
2
0
-2
0
1
2
3
4
5
6
7
time in seconds

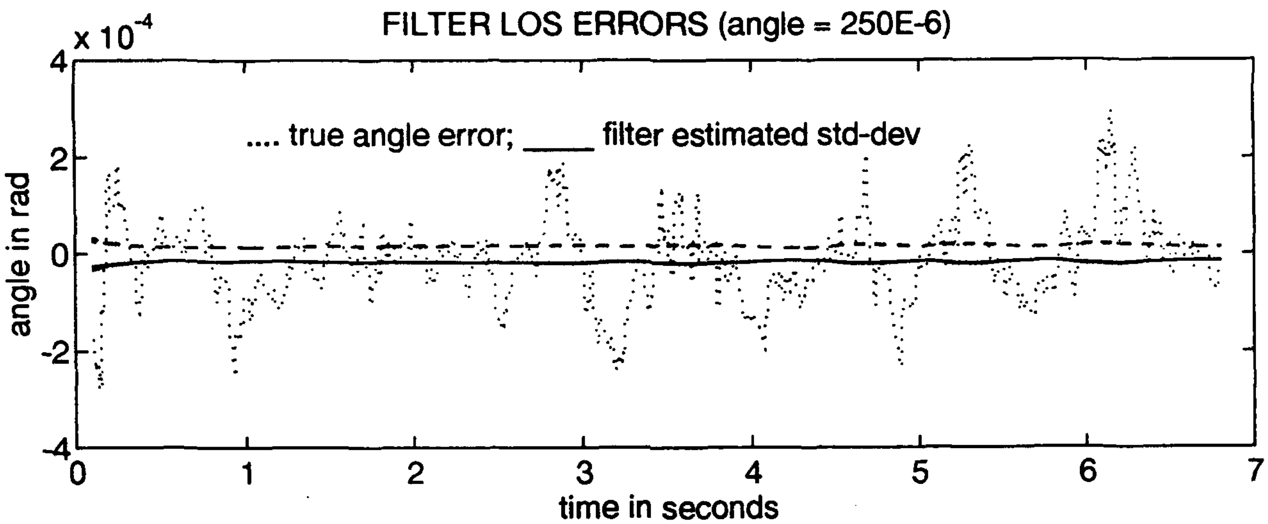
FILTER LOS ERRORS (angle = 250E-6)
x 10^-4
.... true angle error; _____ filter estimated std-dev
angle in rad
time in seconds
4
2
0
-2
-4
0
1
2
3
4
5
6
7

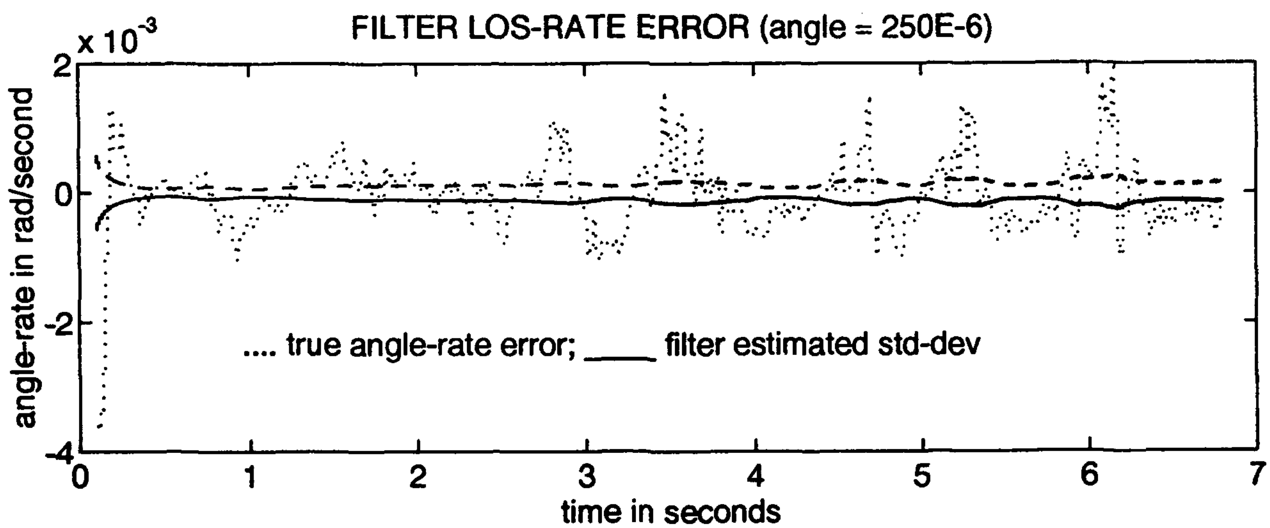
FILTER LOS-RATE ERROR (angle = 250E-6)
x 10^-3
.... true angle-rate error; _____ filter estimated std-dev
angle-rate in rad/second
time in seconds
2
0
-2
-4
0
1
2
3
4
5
6
7

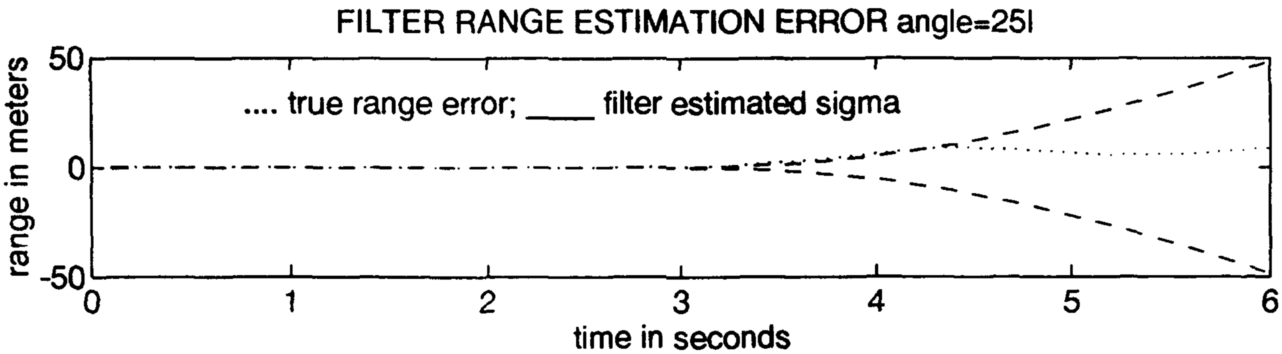
FILTER RANGE ESTIMATION ERROR angle=25l
.... true range error; ____ filter estimated sigma
range in meters
50
0
-50
0
1
2
3
4
5
6
time in seconds

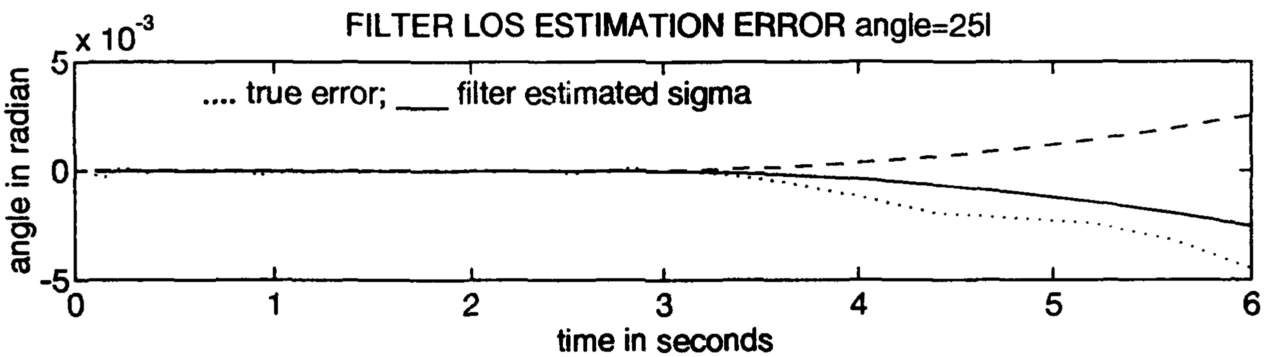
FILTER LOS ESTIMATION ERROR angle=25l
x 10^-3
.... true error; ___ filter estimated sigma
angle in radian
5
0
-5
0
1
2
3
4
5
6
time in seconds

Appendix E

This appendix contains simulation plots for the ladar angle-rate noise run set. The aircraft is initially heading east and beginning a 3 g turn to the north. All measurement noises (except angle-rate) and dynamic noise strengths are set at baseline values. The missile is launched from the $\pi/4$ approach angle. Each run has a trajectory plot, estimated range errors, range-rate errors, LOS errors and LOS-rate errors. Estimated range and LOS plots are found in the $\pi/4$ missile approach angle run plots in Appendix A. The baseline (see Figure 4-4) angle-rate measurement error is 2.0 mrad/sec, with additional runs made for angle-rate errors of 4.0 and 8.0 mrad/sec. Each plot set contains filter divergence plots of range error and angle error for a three second divergence from three to six seconds. The divergence plots, which define the volume cross-section, are used for performance comparison versus the baseline. In Figures E-2 thru E-13 both the filter and truth model measurement noises are varied from the baseline. In Figures E-14 thru E-25 only the filter measurement noise is varied above baseline (i.e., the filter noise is set "high"). In Figures E-26 thru E-37 only the true measurement noise is varied above baseline (i.e., the filter noise is set "low").

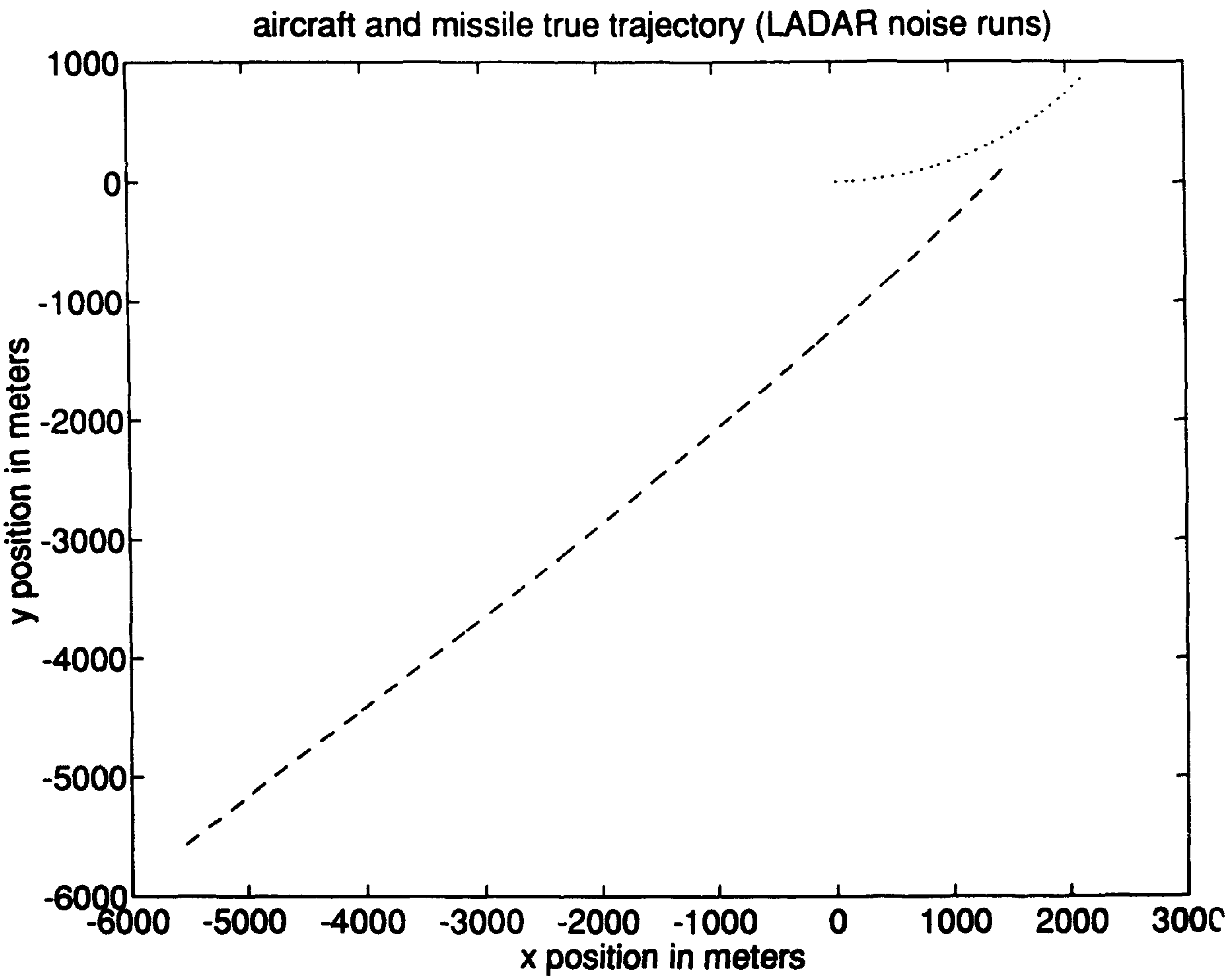
aircraft and missile true trajectory (LADAR noise runs)
1000
0
-1000
-2000
-3000
-4000
-5000
-6000
-6000
-5000
-4000
-3000
-2000
-1000
0
1000
2000
3000
x position in meters
y position in meters

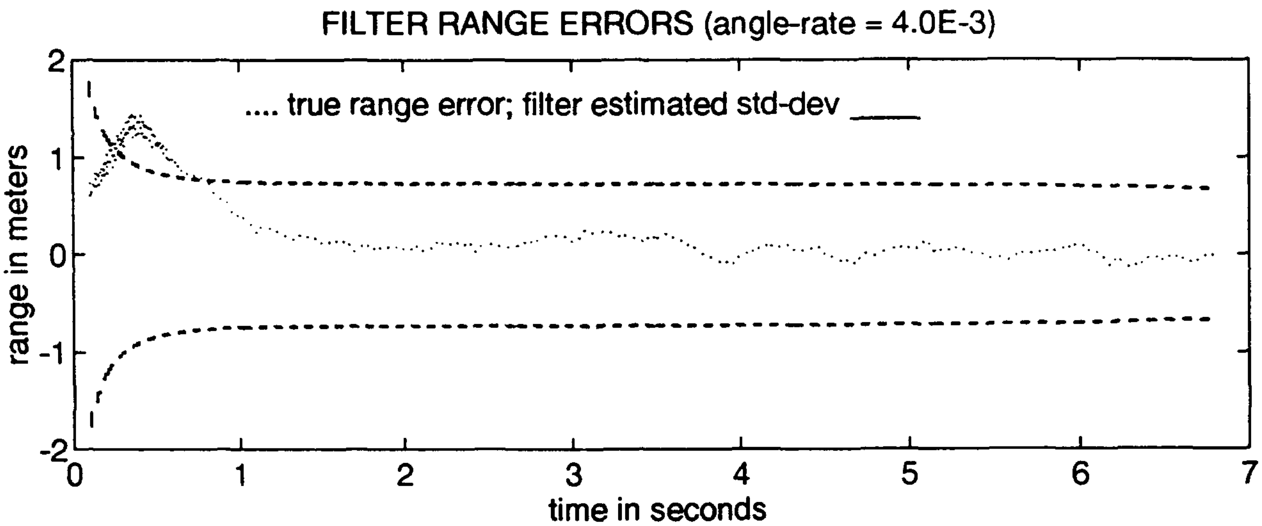

FILTER RANGE ERRORS (angle-rate = 4.0E-3)
.... true range error; filter estimated std-dev ____
range in meters
time in seconds

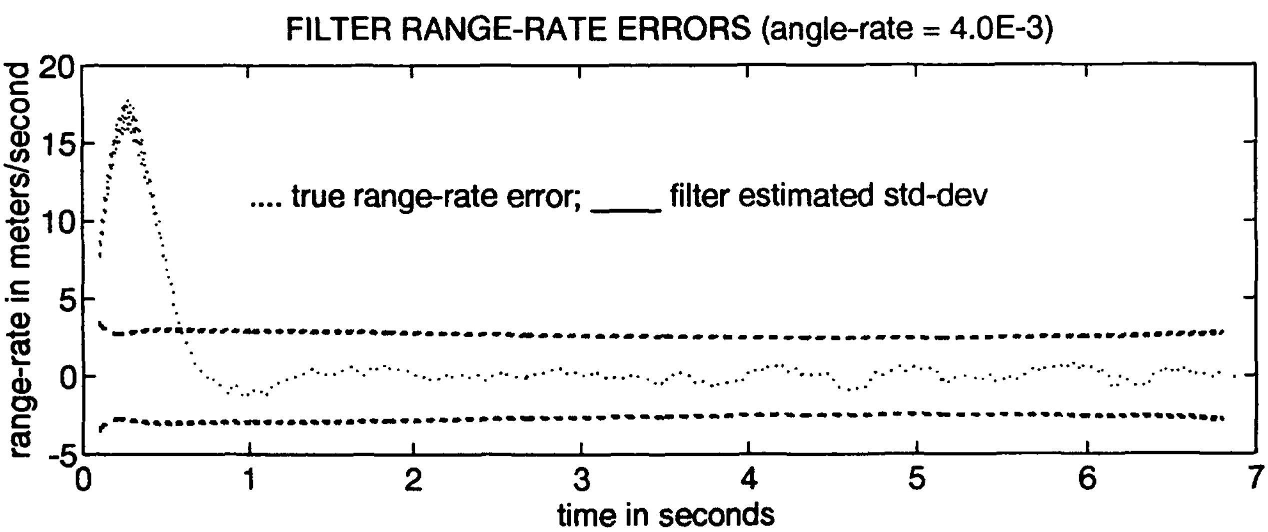

FILTER RANGE-RATE ERRORS (angle-rate = 4.0E-3)
.... true range-rate error; ____ filter estimated std-dev
range-rate in meters/second
time in seconds

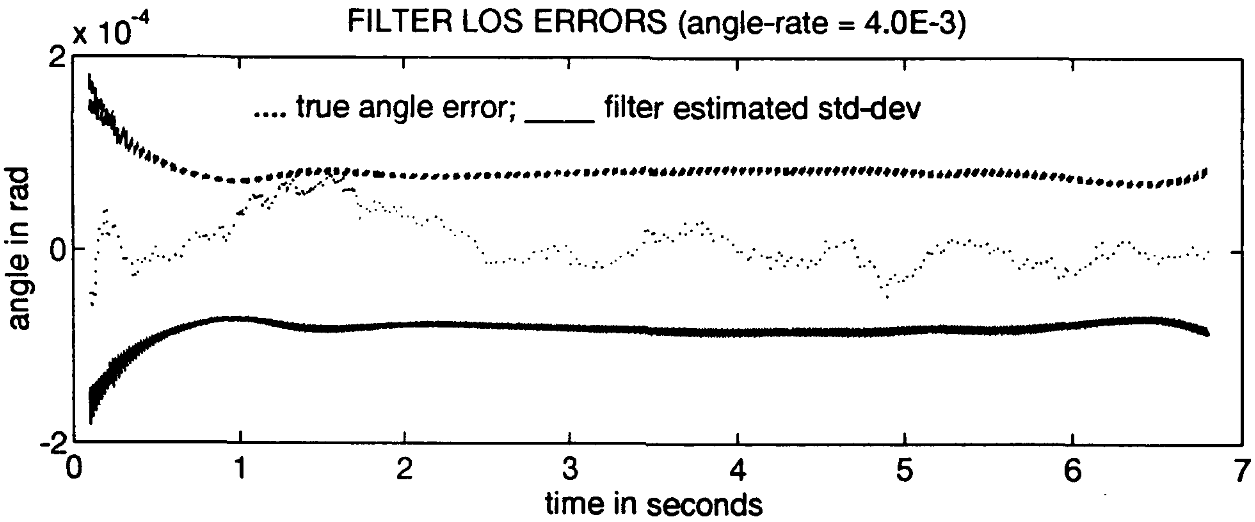
FILTER LOS ERRORS (angle-rate = 4.0E-3)
x 10^-4
.... true angle error; _____ filter estimated std-dev
angle in rad
time in seconds
2
0
-2
0
1
2
3
4
5
6
7

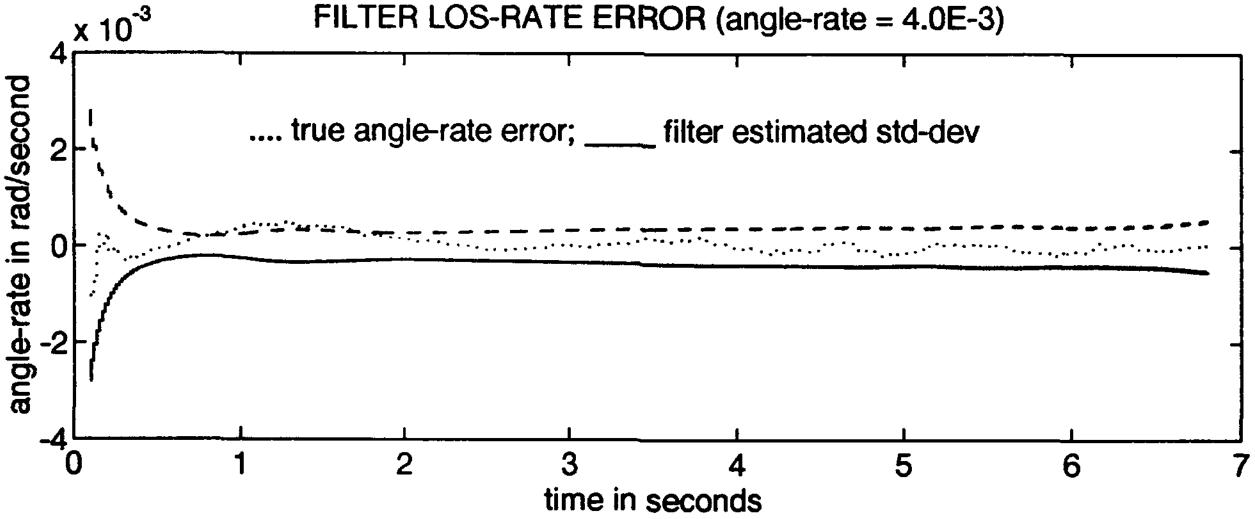
FILTER LOS-RATE ERROR (angle-rate = 4.0E-3)
x 10^-3
.... true angle-rate error; _____ filter estimated std-dev
angle-rate in rad/second
time in seconds
4
2
0
-2
-4
0
1
2
3
4
5
6
7

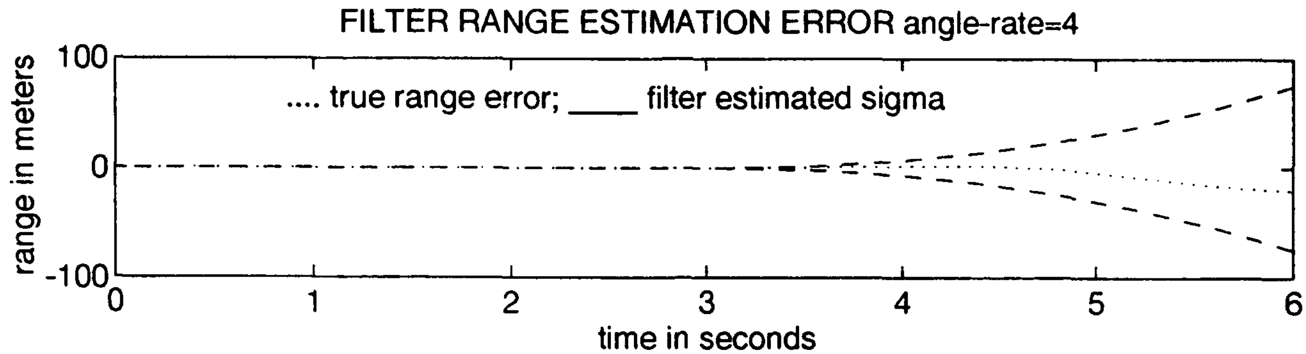
FILTER RANGE ESTIMATION ERROR angle-rate=4
.... true range error; ____ filter estimated sigma
range in meters
100
0
-100
0
1
2
3
4
5
6
time in seconds

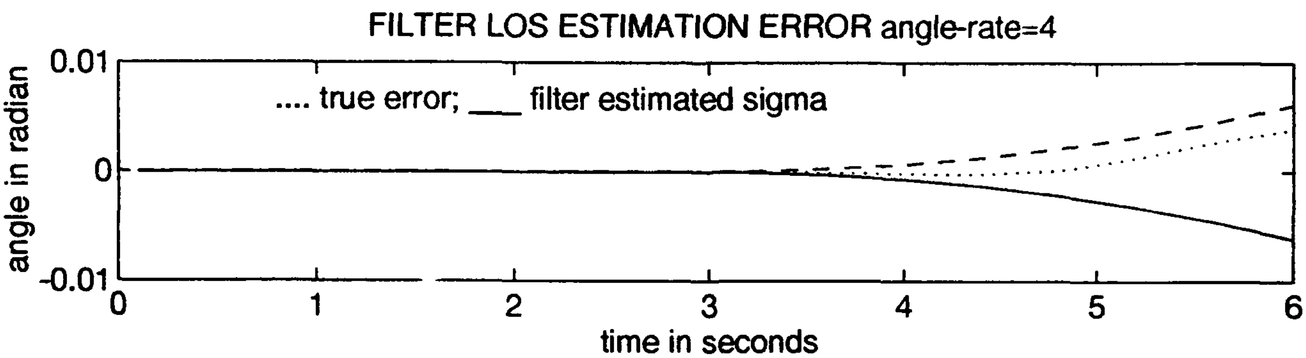
FILTER LOS ESTIMATION ERROR angle-rate=4
.... true error; ___ filter estimated sigma
angle in radian
0.01
0
-0.01
0
1
2
3
4
5
6
time in seconds

FILTER RANGE ERRORS (angle-rate = 8.0E-3)

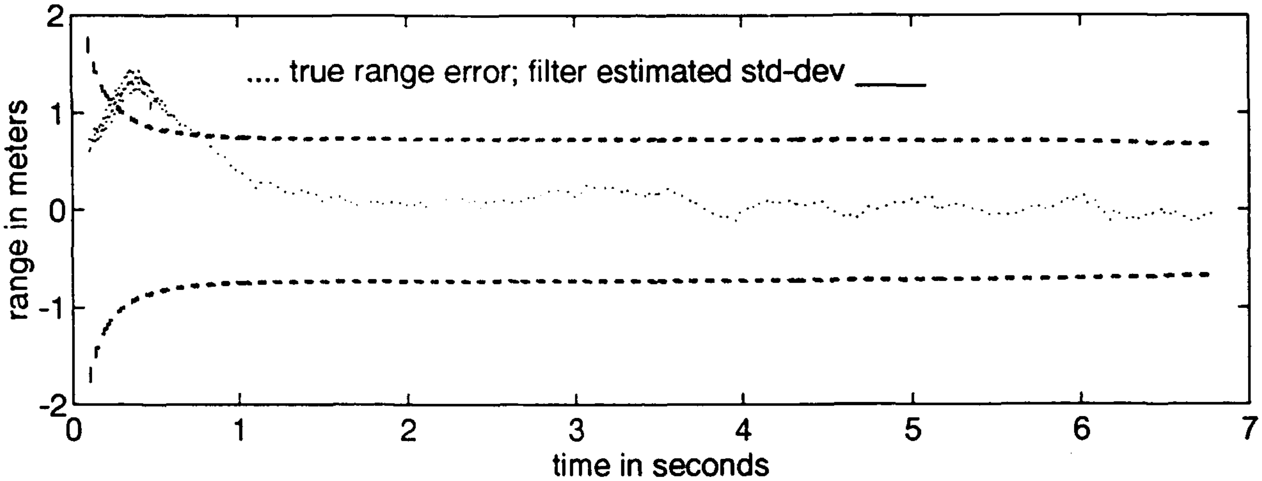

FILTER RANGE-RATE ERRORS (angle-rate = 8.0E-3)

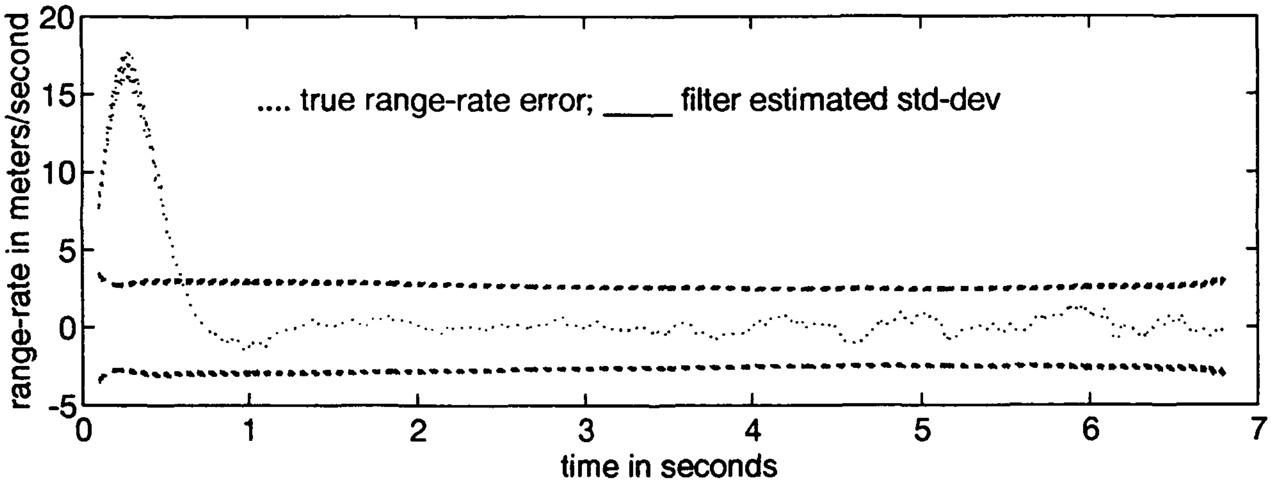

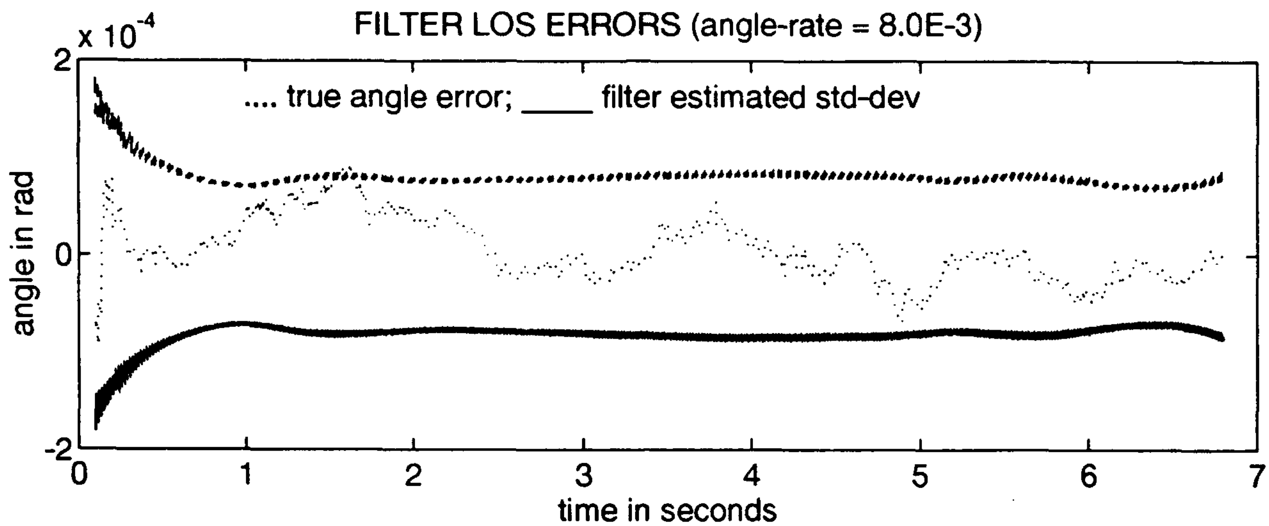

FILTER LOS ERRORS (angle-rate = 8.0E-3)
x 10^-4
.... true angle error; ____ filter estimated std-dev
angle in rad
time in seconds
2
0
-2
0 1 2 3 4 5 6 7

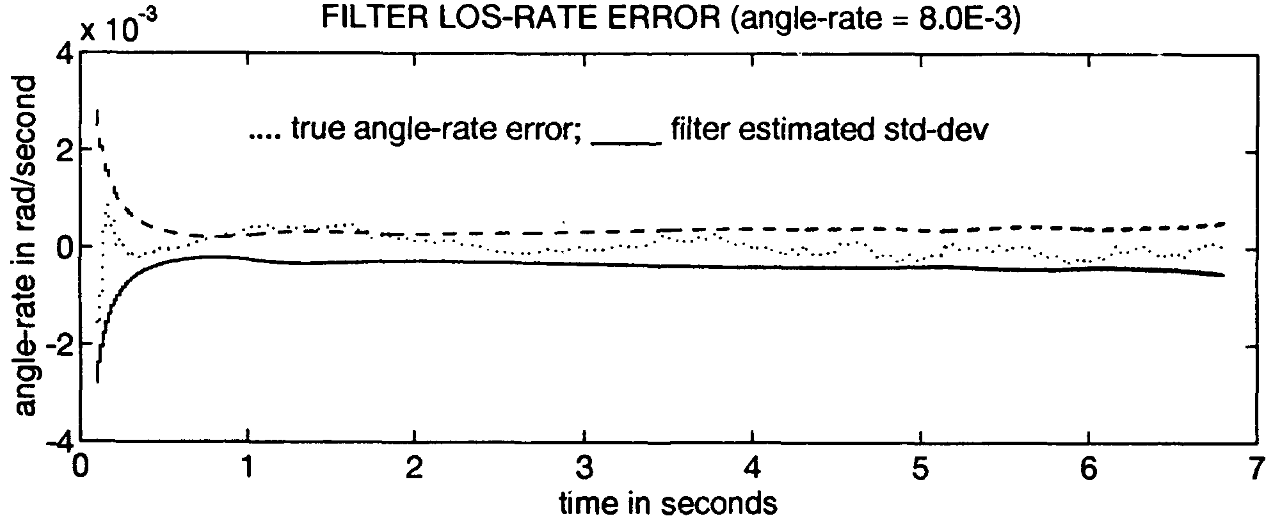

FILTER LOS-RATE ERROR (angle-rate = 8.0E-3)
x 10^-3
.... true angle-rate error; ____ filter estimated std-dev
angle-rate in rad/second
time in seconds
4
2
0
-2
-4
0 1 2 3 4 5 6 7

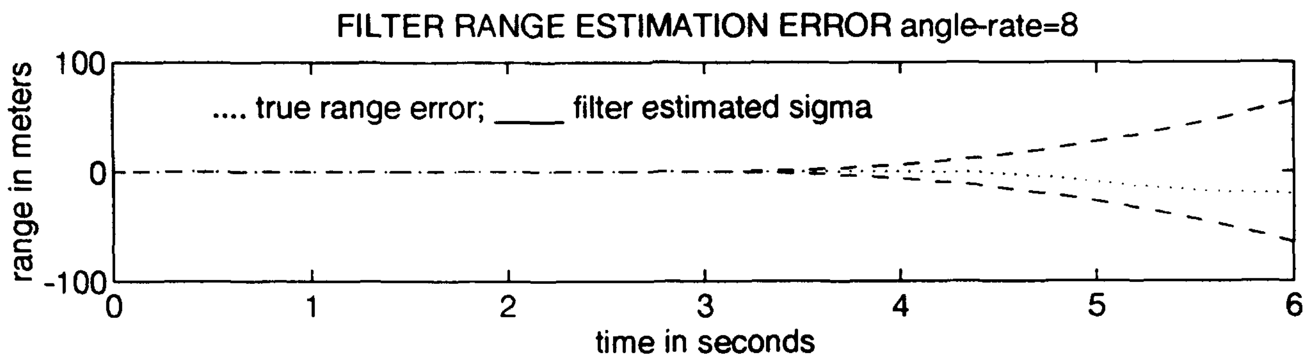
FILTER RANGE ESTIMATION ERROR angle-rate=8
.... true range error; ____ filter estimated sigma
range in meters
100
0
-100
0
1
2
3
4
5
6
time in seconds

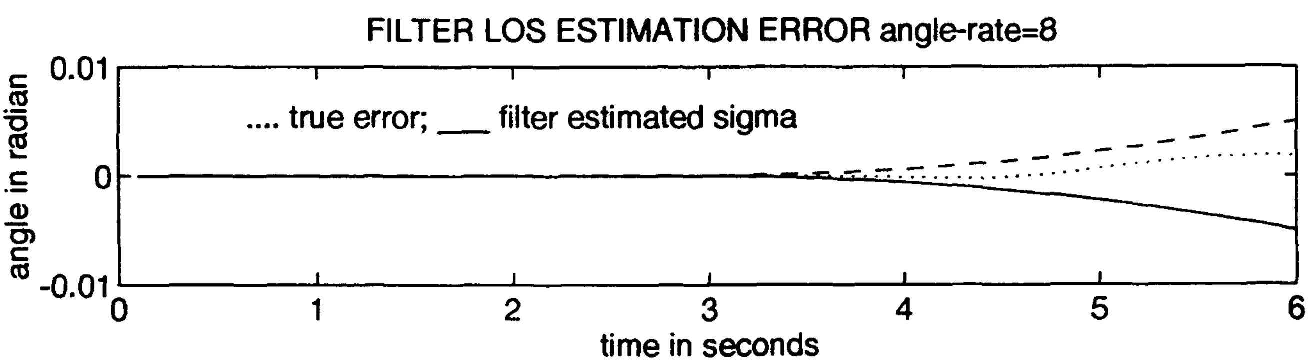
FILTER LOS ESTIMATION ERROR angle-rate=8
.... true error; ___ filter estimated sigma
angle in radian
0.01
0
-0.01
0
1
2
3
4
5
6
time in seconds

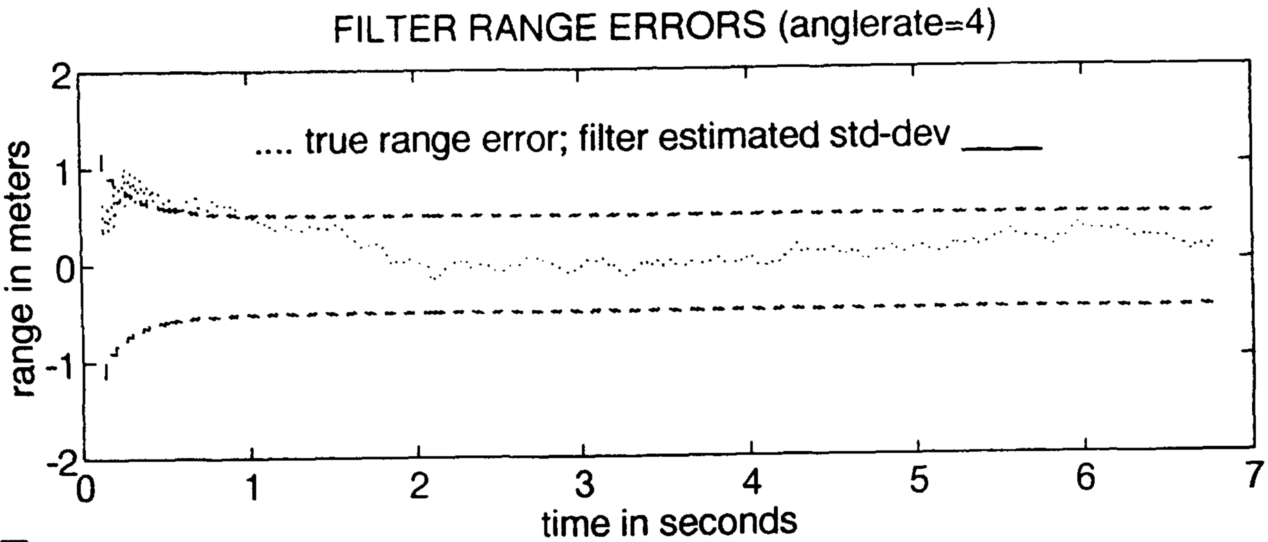
FILTER RANGE ERRORS (anglerate=4)
.... true range error; filter estimated std-dev ____
range in meters
2
1
0
-1
-2
0
1
2
3
4
5
6
7
time in seconds

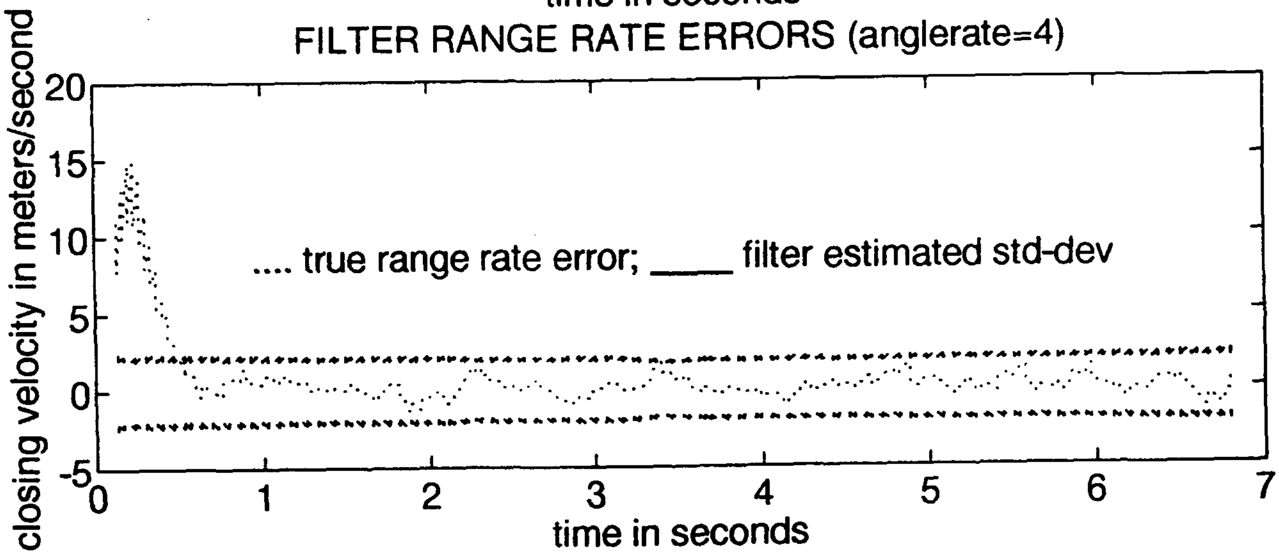
FILTER RANGE RATE ERRORS (anglerate=4)
.... true range rate error; ____ filter estimated std-dev
closing velocity in meters/second
20
15
10
5
0
-5
0
1
2
3
4
5
6
7
time in seconds

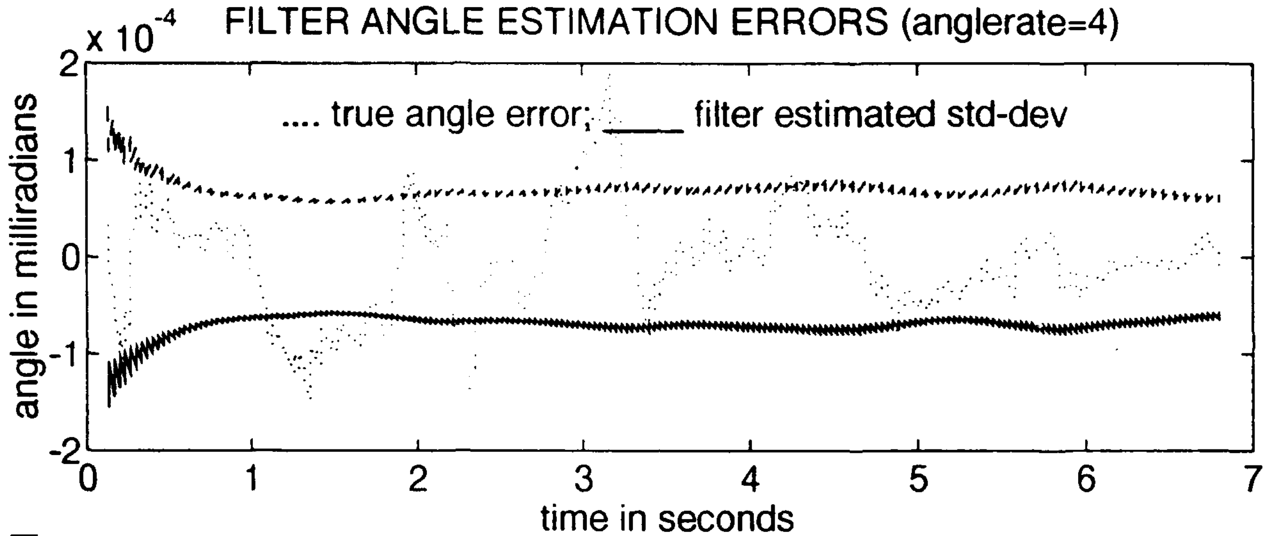
FILTER ANGLE ESTIMATION ERRORS (anglerate=4)
x 10^-4
.... true angle error; _____ filter estimated std-dev
angle in milliradians
2
1
0
-1
-2
0
1
2
3
4
5
6
7
time in seconds

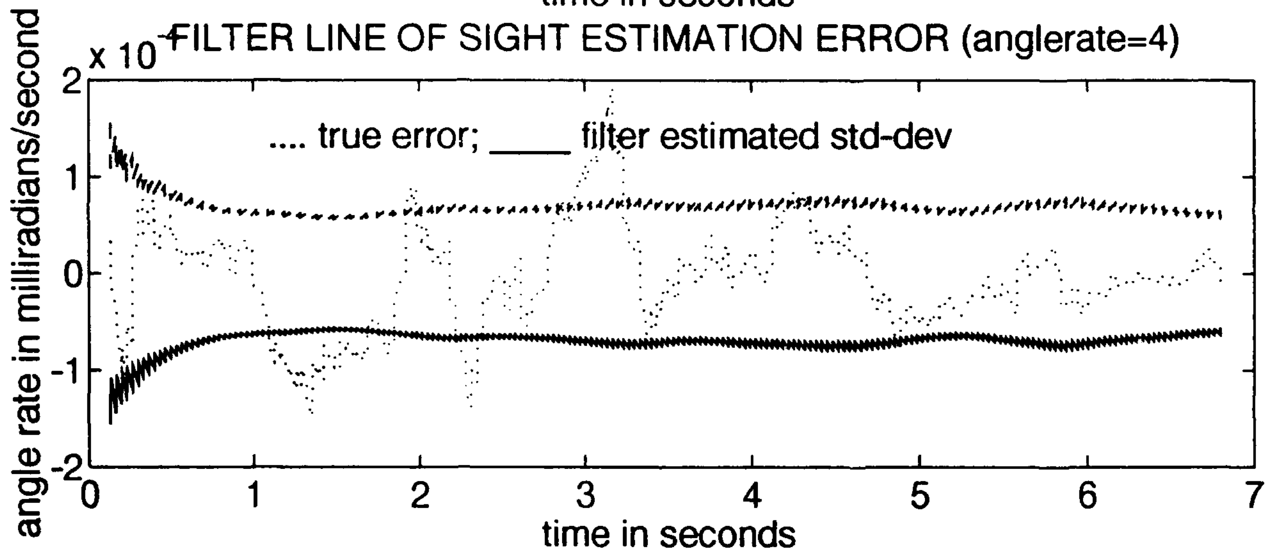
FILTER LINE OF SIGHT ESTIMATION ERROR (anglerate=4)
x 10^-4
.... true error; _____ filter estimated std-dev
angle rate in milliradians/second
2
1
0
-1
-2
0
1
2
3
4
5
6
7
time in seconds

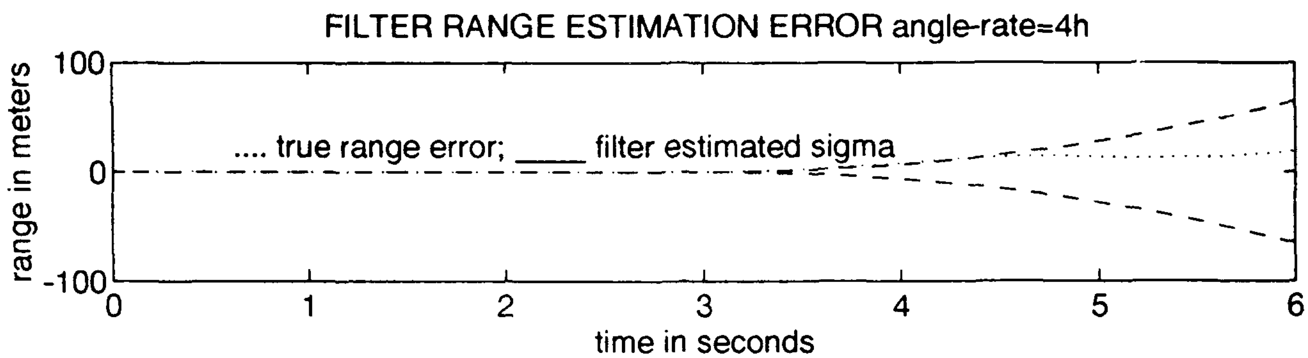
FILTER RANGE ESTIMATION ERROR angle-rate=4h
.... true range error; _____ filter estimated sigma
range in meters
100
0
-100
0
1
2
3
4
5
6
time in seconds

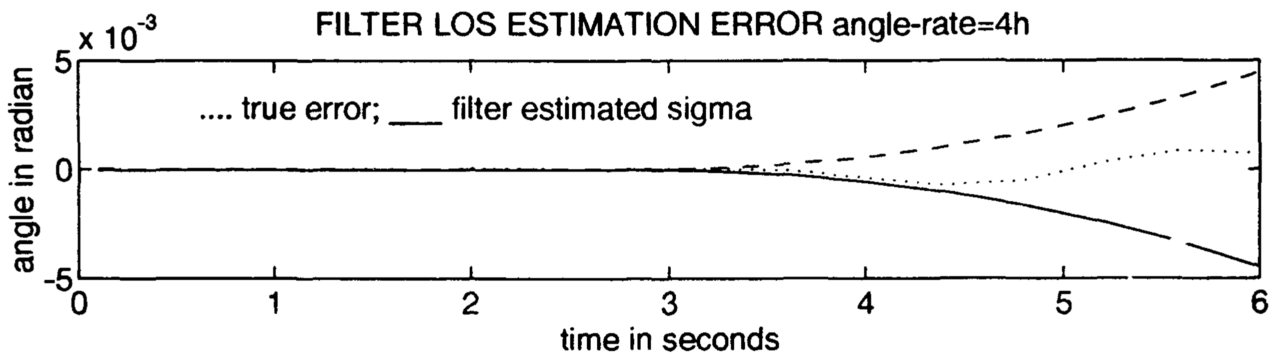
FILTER LOS ESTIMATION ERROR angle-rate=4h
x 10^-3
.... true error; ___ filter estimated sigma
angle in radian
5
0
-5
0
1
2
3
4
5
6
time in seconds

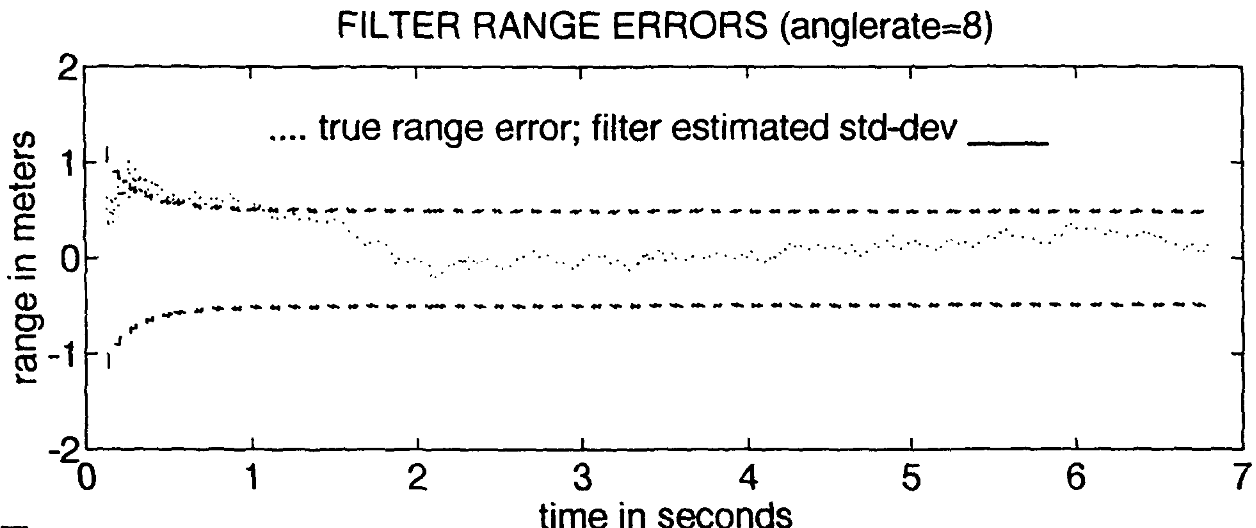
FILTER RANGE ERRORS (anglerate=8)
.... true range error; filter estimated std-dev _____
range in meters
2
1
0
-1
-2
0
1
2
3
4
5
6
7
time in seconds

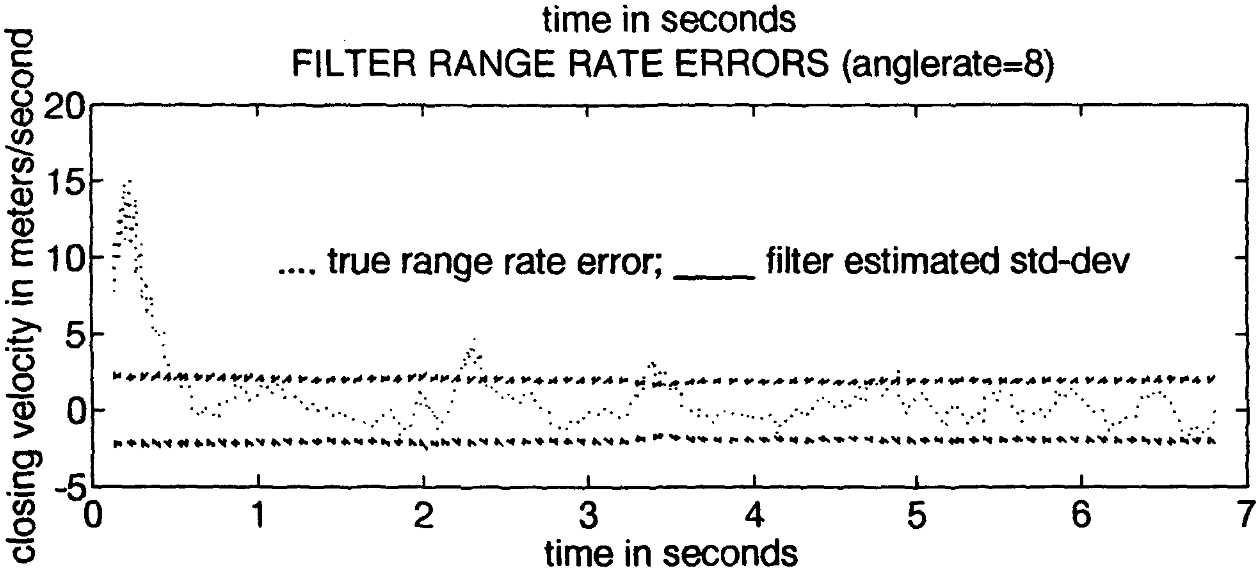
FILTER RANGE RATE ERRORS (anglerate=8)
.... true range rate error; _____ filter estimated std-dev
closing velocity in meters/second
20
15
10
5
0
-5
0
1
2
3
4
5
6
7
time in seconds

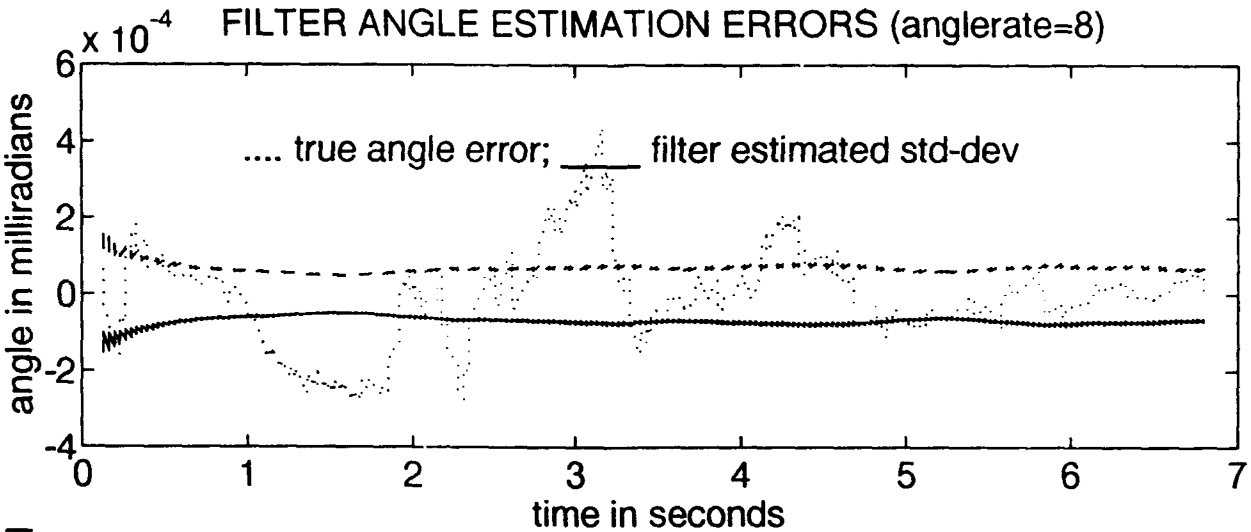
FILTER ANGLE ESTIMATION ERRORS (anglerate=8)
x 10^-4
.... true angle error; ____ filter estimated std-dev
angle in milliradians
time in seconds

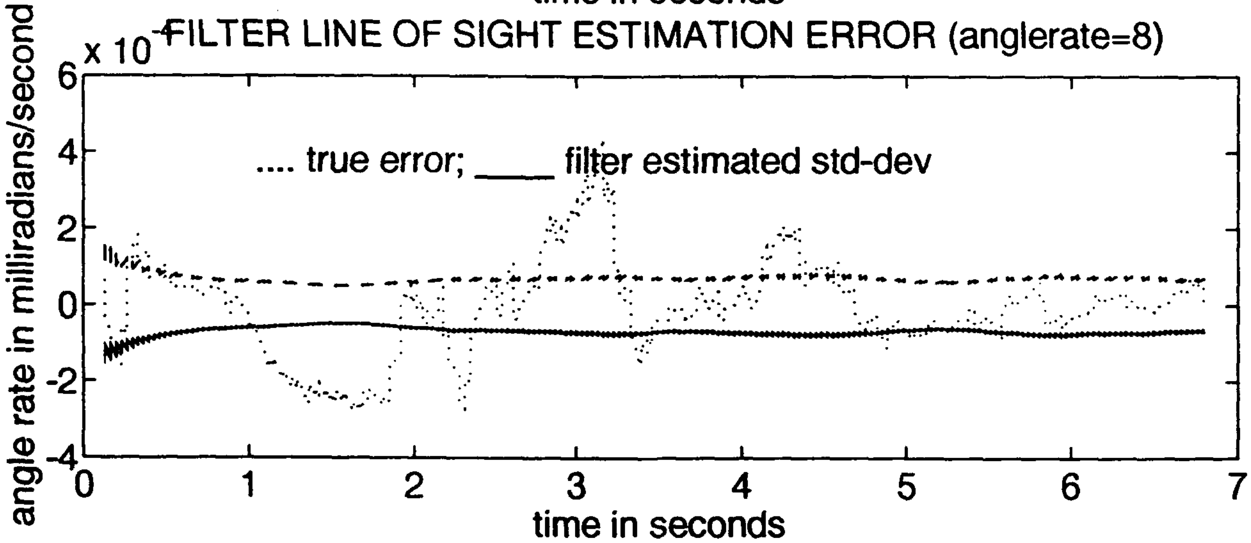
FILTER LINE OF SIGHT ESTIMATION ERROR (anglerate=8)
x 10^-4
.... true error; ____ filter estimated std-dev
angle rate in milliradians/second
time in seconds

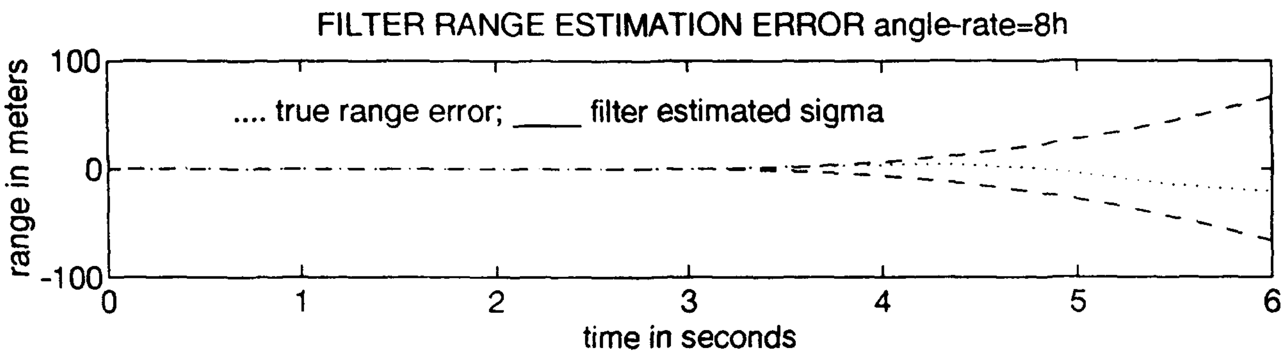
FILTER RANGE ESTIMATION ERROR angle-rate=8h
.... true range error; _____ filter estimated sigma
range in meters
100
0
-100
0
1
2
3
4
5
6
time in seconds

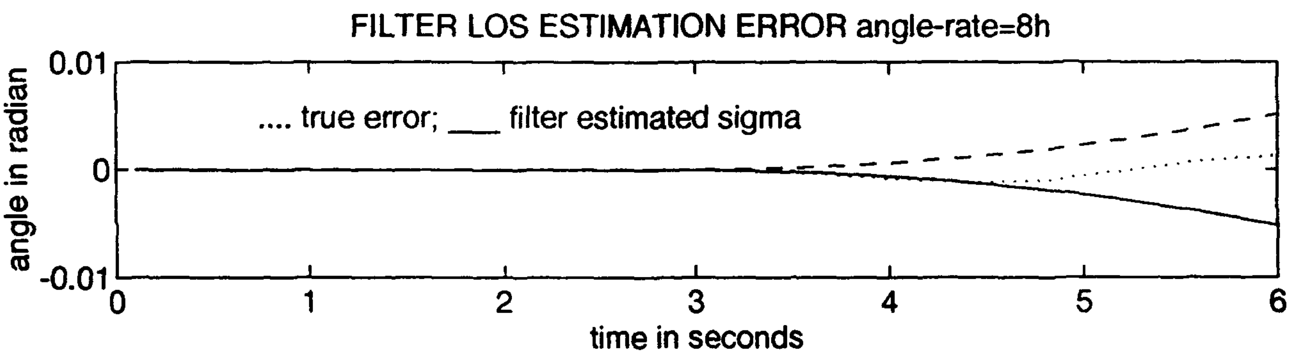
FILTER LOS ESTIMATION ERROR angle-rate=8h
.... true error; ___ filter estimated sigma
angle in radian
0.01
0
-0.01
0
1
2
3
4
5
6
time in seconds

FILTER RANGE ERRORS (angle-rate = 4.0E-3)

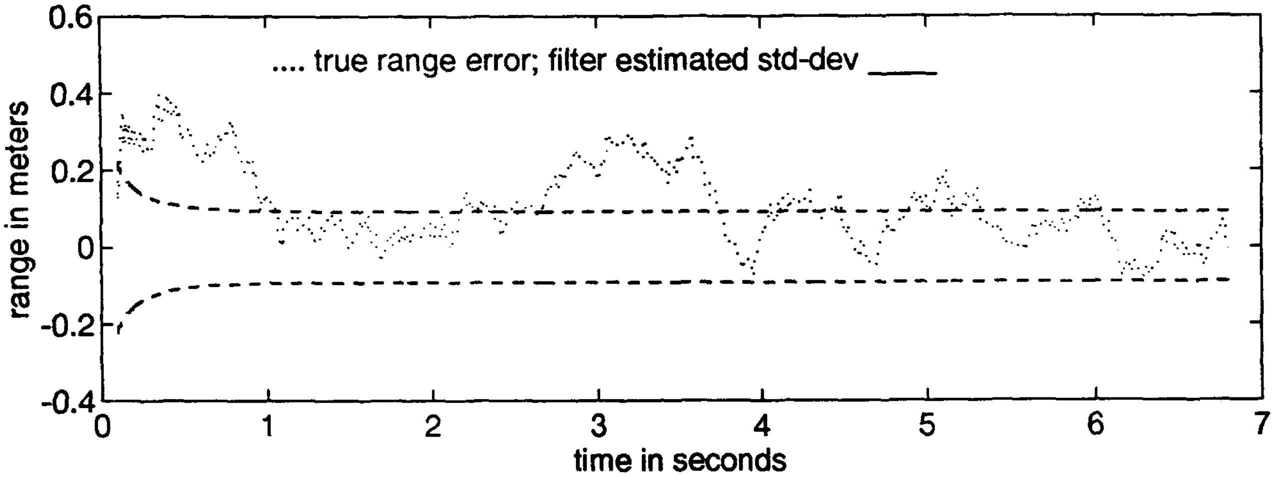

FILTER RANGE-RATE ERRORS (angle-rate = 4.0E-3)

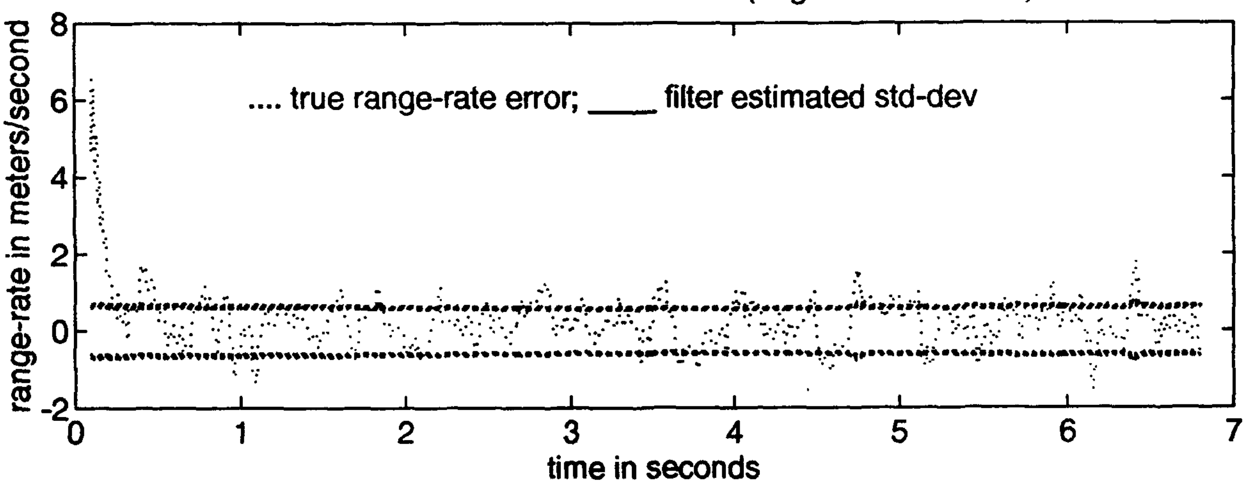

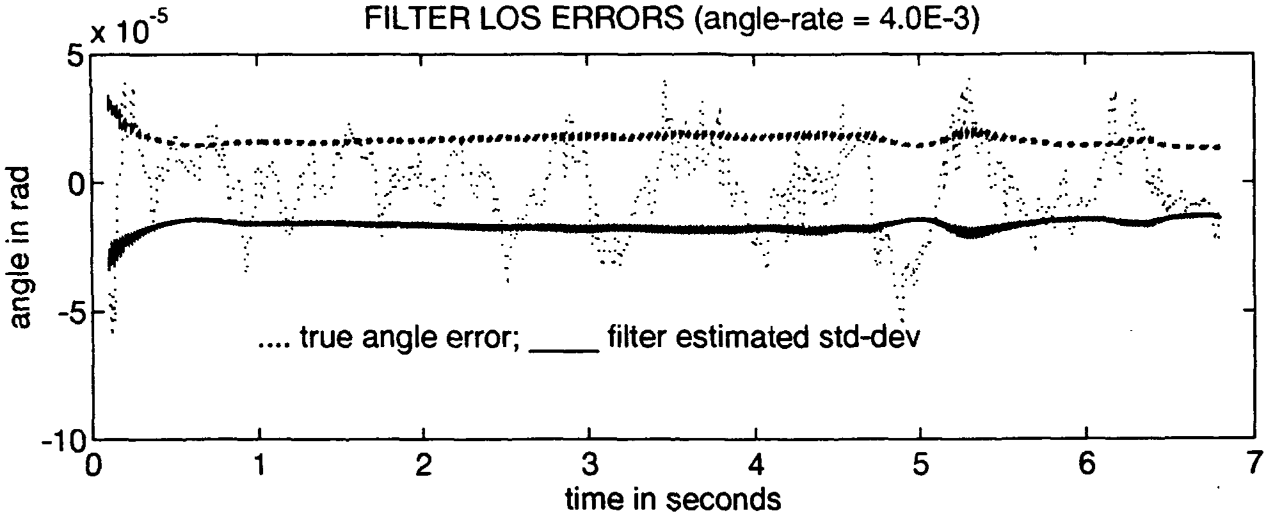
FILTER LOS ERRORS (angle-rate = 4.0E-3)
x 10^-5
angle in rad
.... true angle error; _____ filter estimated std-dev
time in seconds
5
0
-5
-10
0
1
2
3
4
5
6
7

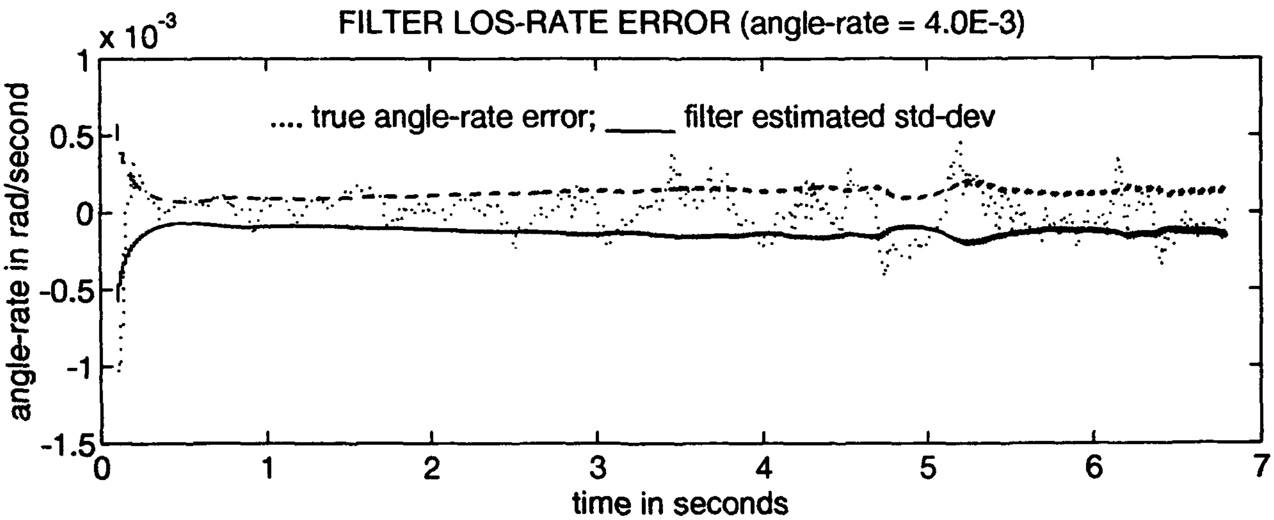
FILTER LOS-RATE ERROR (angle-rate = 4.0E-3)
x 10^-3
angle-rate in rad/second
.... true angle-rate error; _____ filter estimated std-dev
time in seconds
1
0.5
0
-0.5
-1
-1.5
0
1
2
3
4
5
6
7

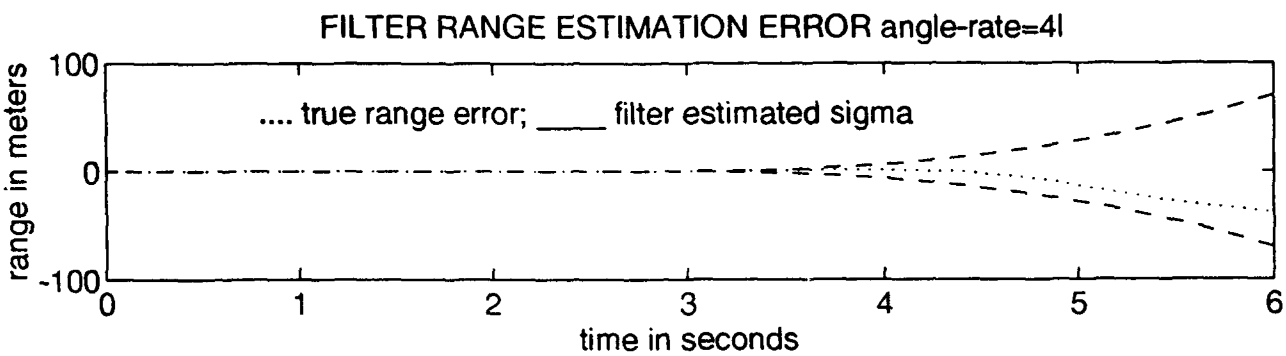
FILTER RANGE ESTIMATION ERROR angle-rate=4l
.... true range error; ____ filter estimated sigma
range in meters
100
0
-100
0
1
2
3
4
5
6
time in seconds

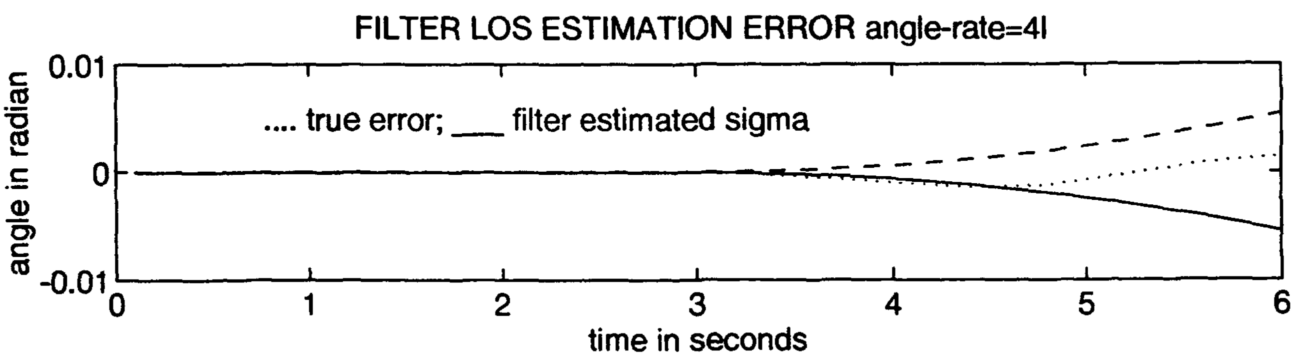
FILTER LOS ESTIMATION ERROR angle-rate=4l
.... true error; ___ filter estimated sigma
angle in radian
0.01
0
-0.01
0
1
2
3
4
5
6
time in seconds

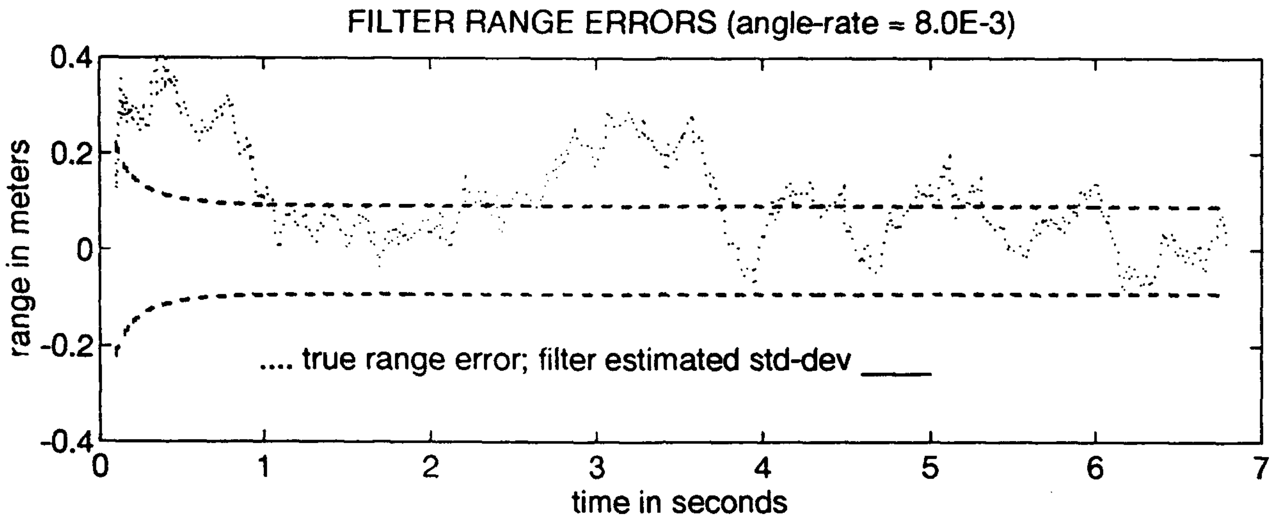
FILTER RANGE ERRORS (angle-rate = 8.0E-3)
range in meters
0.4
0.2
0
-0.2
-0.4
.... true range error; filter estimated std-dev ____
0
1
2
3
4
5
6
7
time in seconds

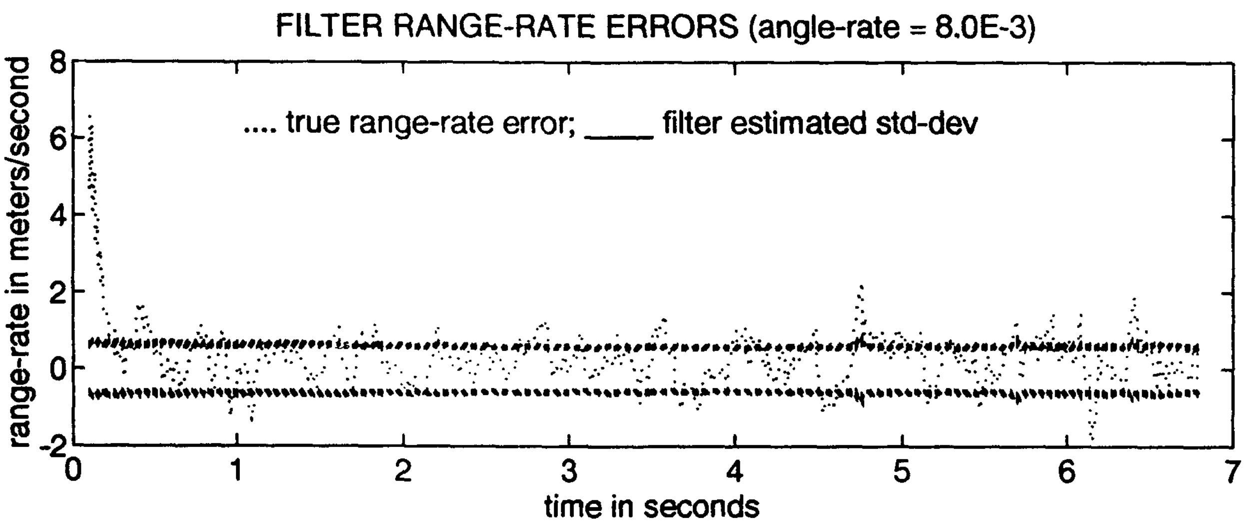
FILTER RANGE-RATE ERRORS (angle-rate = 8.0E-3)
range-rate in meters/second
8
6
4
2
0
-2
.... true range-rate error; ____ filter estimated std-dev
0
1
2
3
4
5
6
7
time in seconds

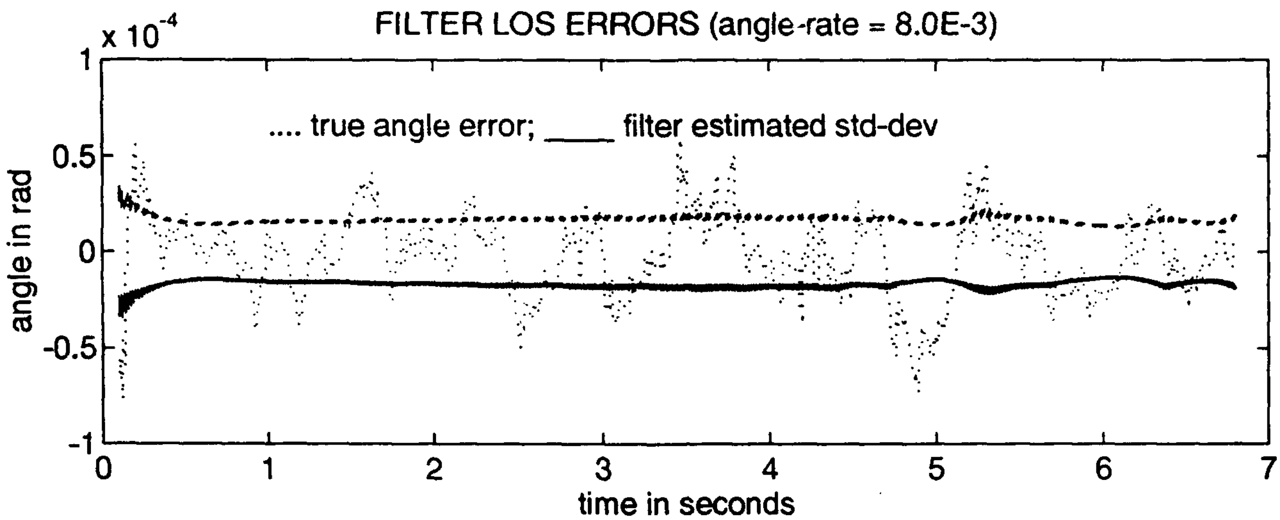

x 10^-4
FILTER LOS ERRORS (angle-rate = 8.0E-3)
.... true angle error; ____ filter estimated std-dev
angle in rad
1
0.5
0
-0.5
-1
0
1
2
3
4
5
6
7
time in seconds

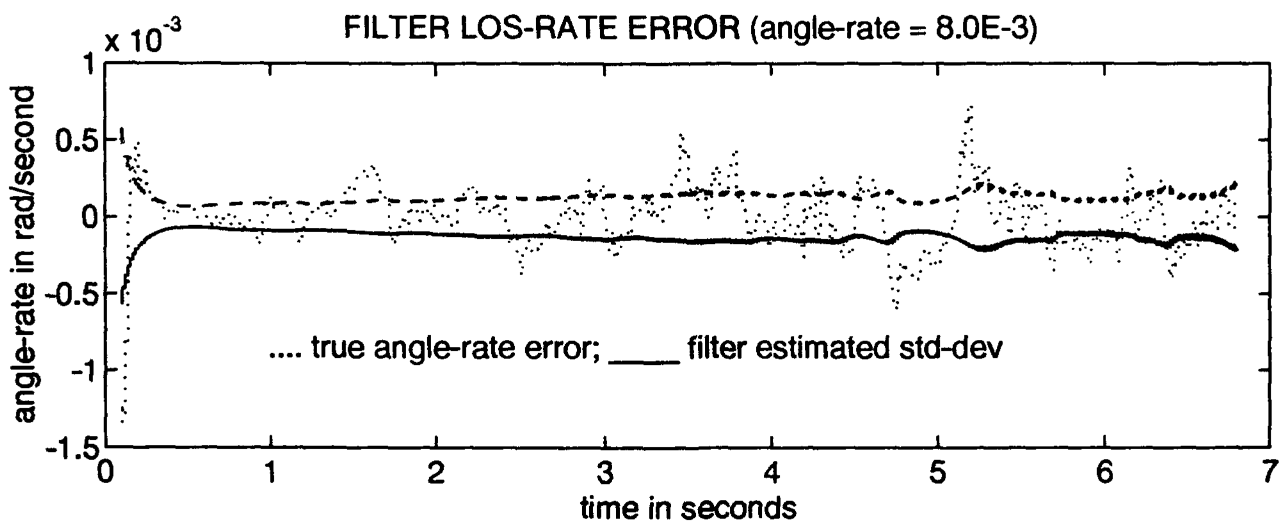

x 10^-3
FILTER LOS-RATE ERROR (angle-rate = 8.0E-3)
.... true angle-rate error; ____ filter estimated std-dev
angle-rate in rad/second
1
0.5
0
-0.5
-1
-1.5
0
1
2
3
4
5
6
7
time in seconds

FILTER RANGE ESTIMATION ERROR angle-rate=8l

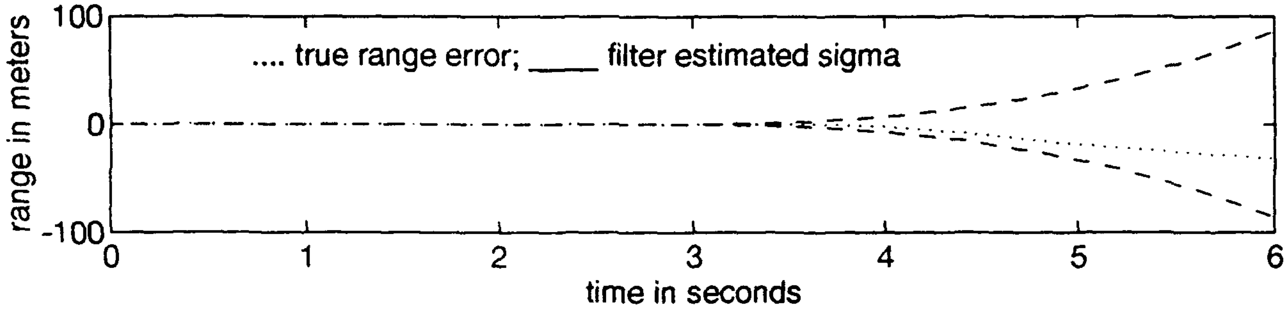

FILTER LOS ESTIMATION ERROR angle-rate=8l

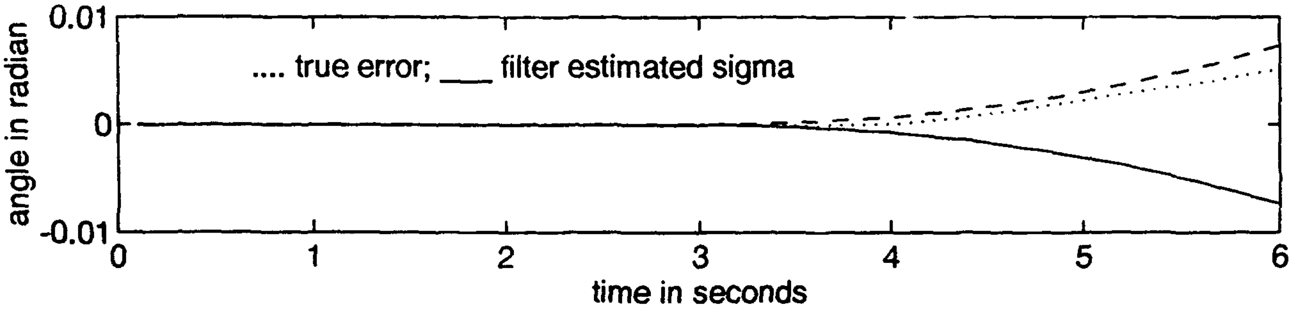

Appendix F

This appendix contains simulation plots for the ladar 60 Hz and 30 Hz pulse-rate noise run sets. The aircraft is initially heading east and beginning a 3 g turn to the north. All dynamic noise strengths are set at baseline values. All ladar measurements are varied together as presented in Table 3-2. The missile is launched from the $\pi/4$ approach angle. Each run has a trajectory plot, estimated range errors, range-rate errors, LOS errors and LOS-rate errors. Estimated range and LOS plots are found in the $\pi/4$ missile approach angle run plots in Appendix A. Each plot set contains filter divergence plots of range error and angle error for a three second divergence from three to six seconds. The divergence plots, which define the volume cross-section, are used for performance comparison versus the baseline. In Figures F-2 thru F-25 a 60 Hz pulse-rate is assumed. In Figures F-26 thru F-49 a 30 Hz pulse-rate is assumed.

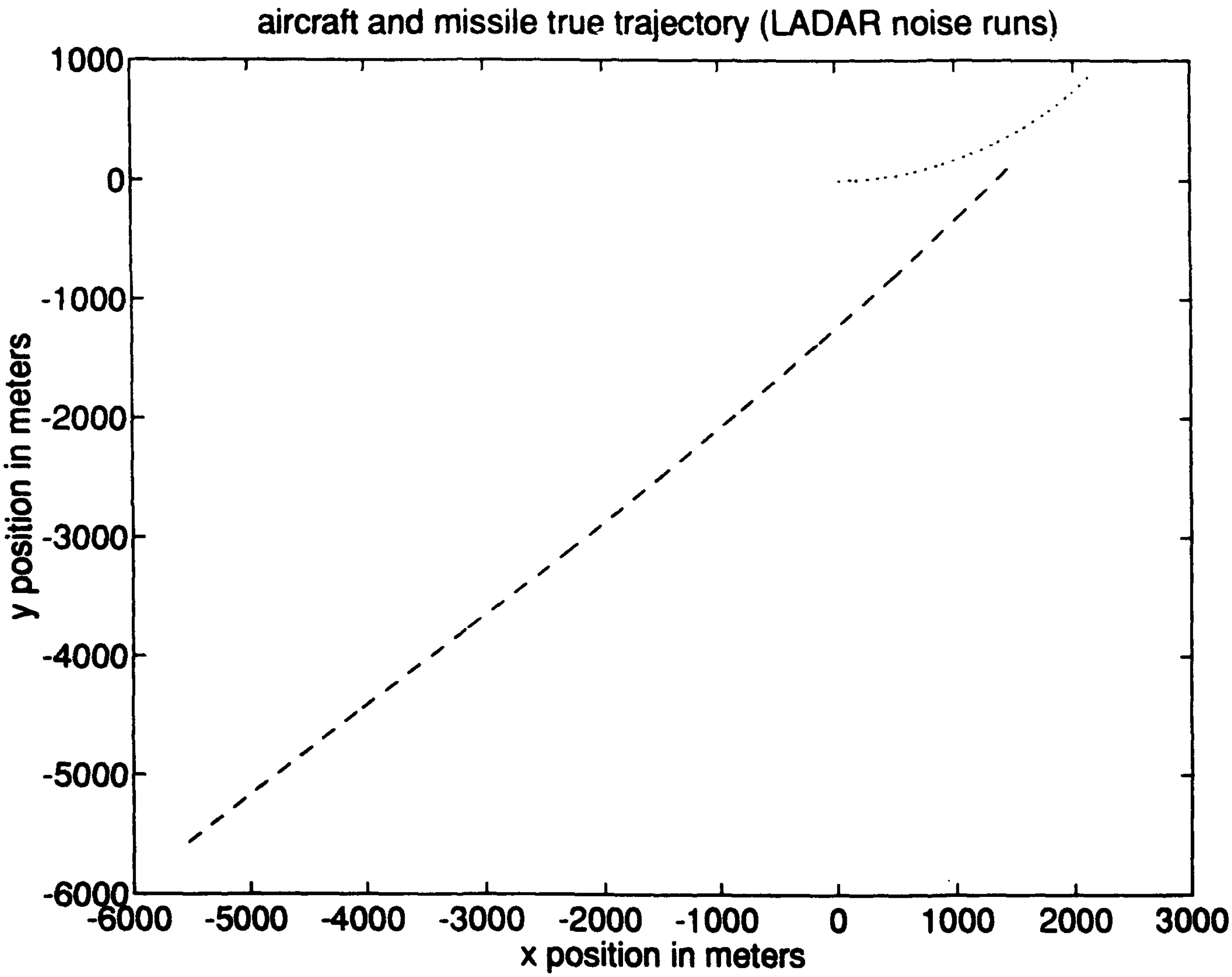
aircraft and missile true trajectory (LADAR noise runs)
1000
0
-1000
-2000
-3000
-4000
-5000
-6000
y position in meters
-6000
-5000
-4000
-3000
-2000
-1000
0
1000
2000
3000
x position in meters

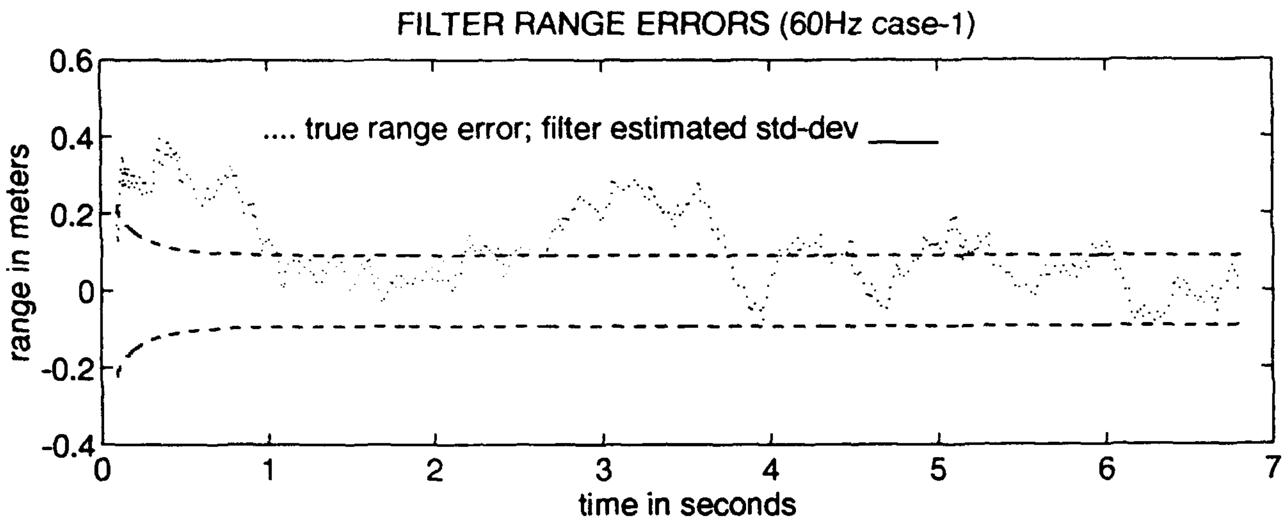
FILTER RANGE ERRORS (60Hz case-1)
.... true range error; filter estimated std-dev ____
range in meters
time in seconds
0.6
0.4
0.2
0
-0.2
-0.4
0
1
2
3
4
5
6
7

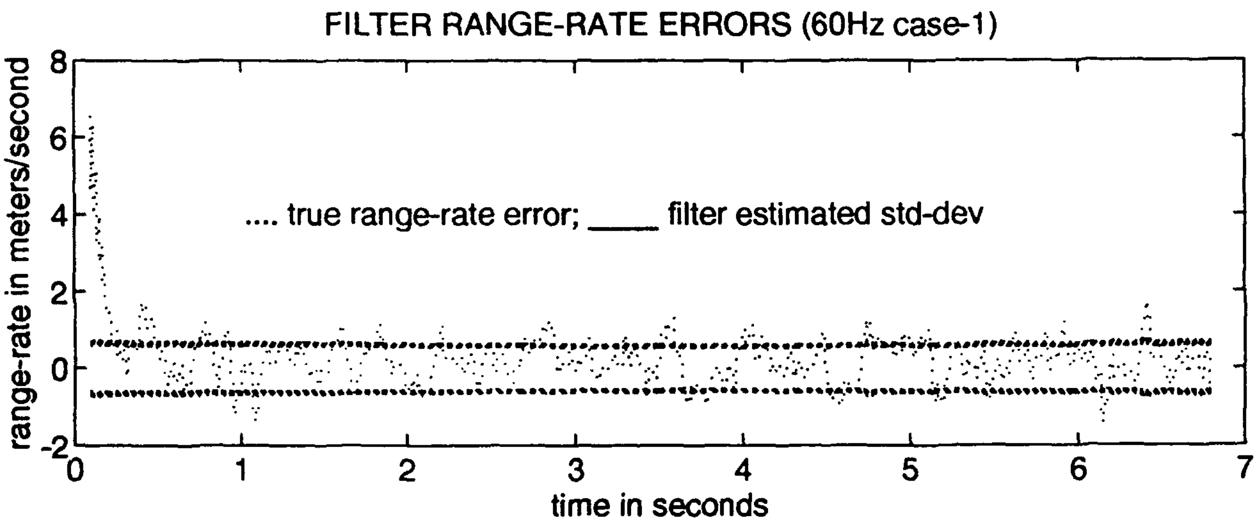
FILTER RANGE-RATE ERRORS (60Hz case-1)
.... true range-rate error; ____ filter estimated std-dev
range-rate in meters/second
time in seconds
8
6
4
2
0
-2
0
1
2
3
4
5
6
7

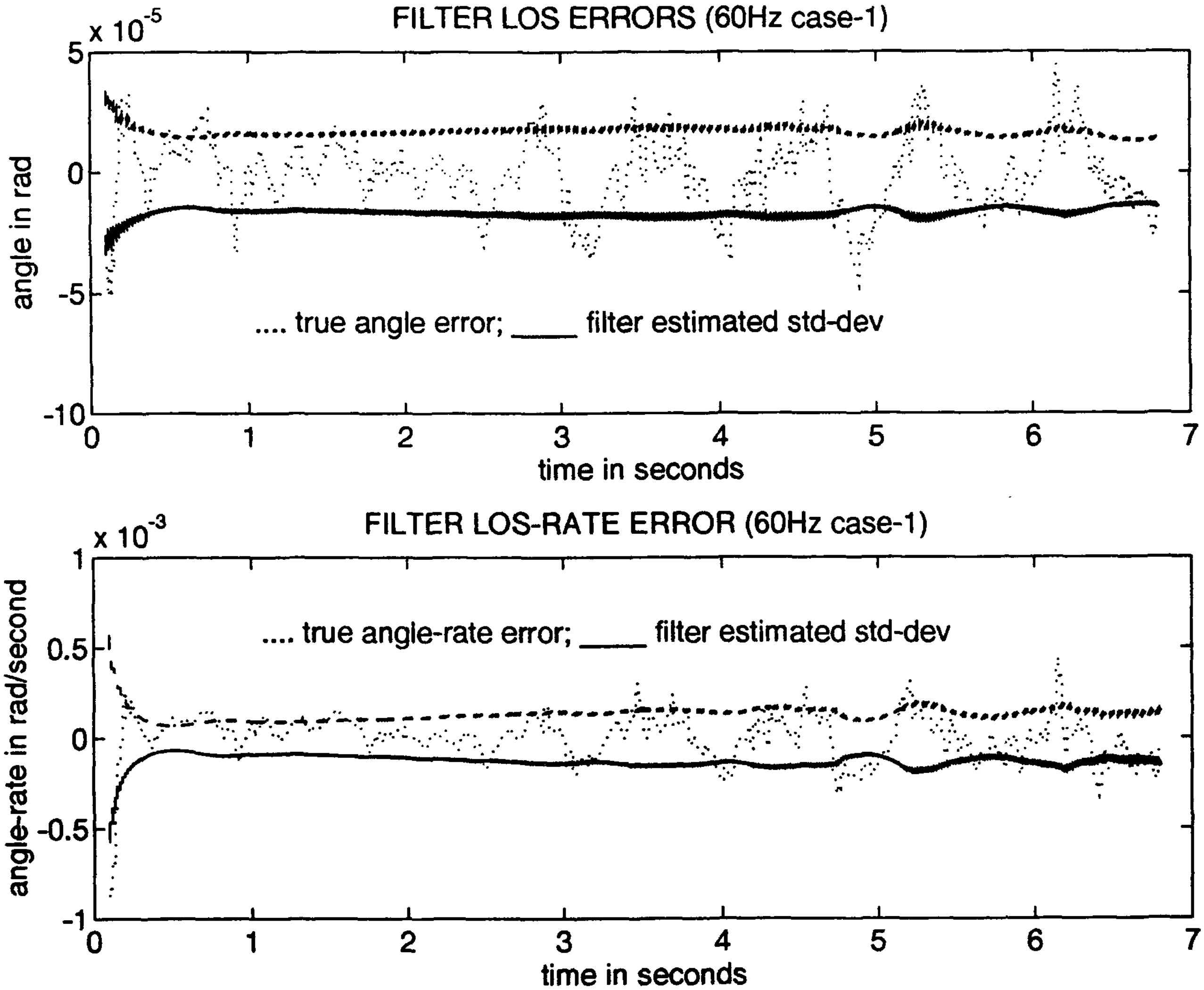
FILTER LOS ERRORS (60Hz case-1)
x 10^-5
angle in rad
.... true angle error; _____ filter estimated std-dev
time in seconds
FILTER LOS-RATE ERROR (60Hz case-1)
x 10^-3
angle-rate in rad/second
.... true angle-rate error; _____ filter estimated std-dev
time in seconds

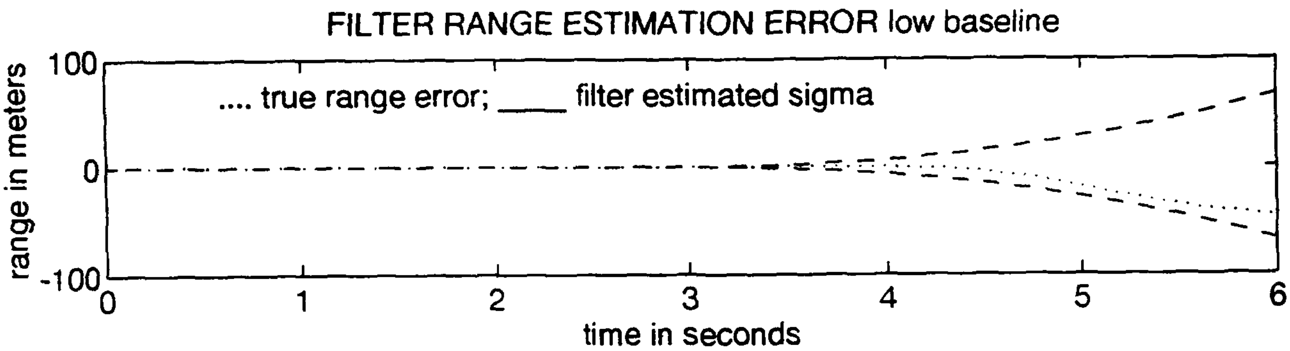
FILTER RANGE ESTIMATION ERROR low baseline
.... true range error; ____ filter estimated sigma
range in meters
100
0
-100
0
1
2
3
4
5
6
time in seconds

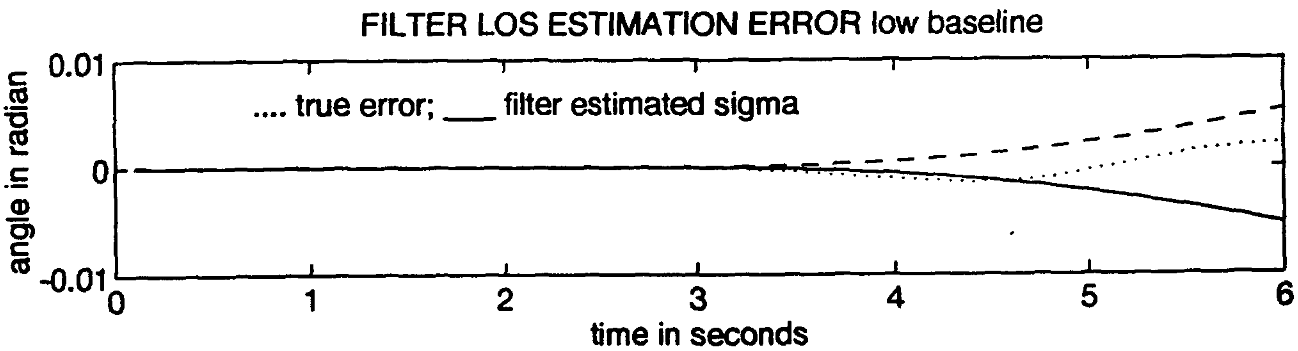
FILTER LOS ESTIMATION ERROR low baseline
.... true error; ___ filter estimated sigma
angle in radian
0.01
0
-0.01
0
1
2
3
4
5
6
time in seconds

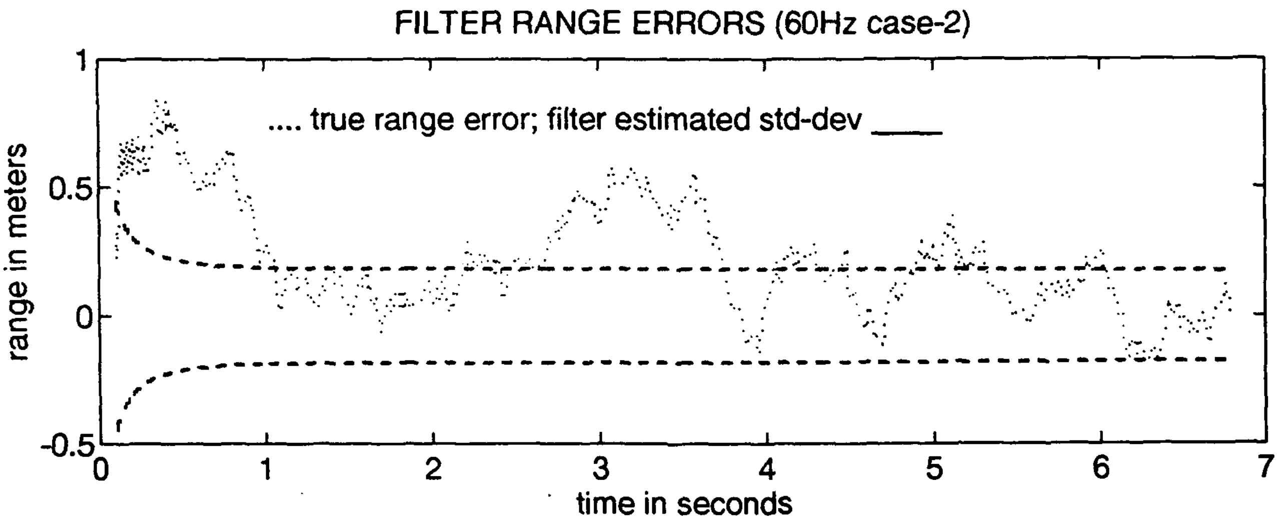
FILTER RANGE ERRORS (60Hz case-2)
.... true range error; filter estimated std-dev ____
range in meters
time in seconds
1
0.5
0
-0.5
0
1
2
3
4
5
6
7

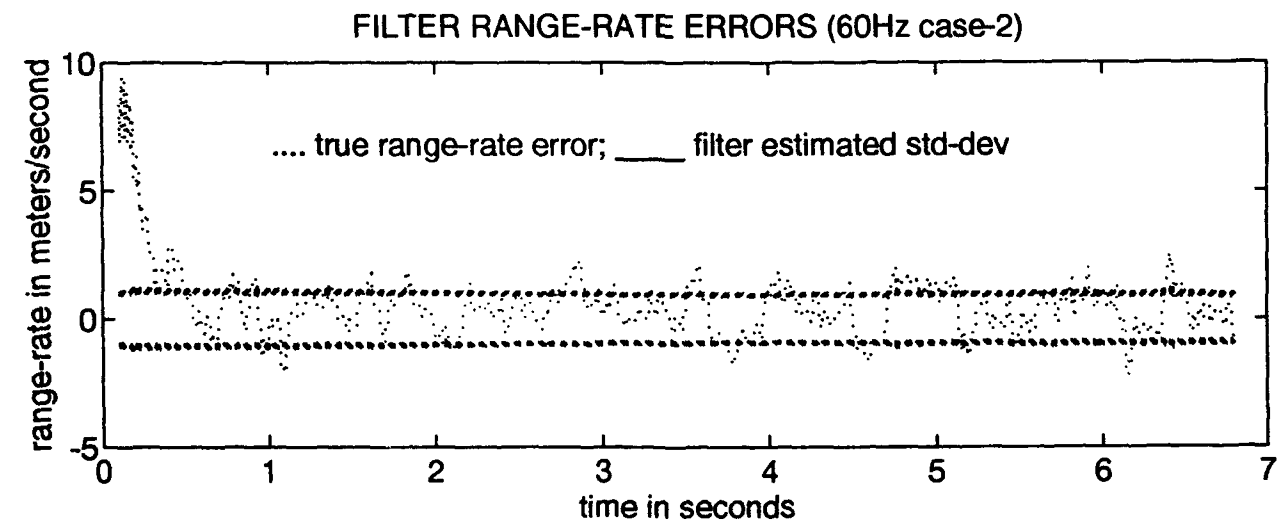
FILTER RANGE-RATE ERRORS (60Hz case-2)
.... true range-rate error; ____ filter estimated std-dev
range-rate in meters/second
time in seconds
10
5
0
-5
0
1
2
3
4
5
6
7

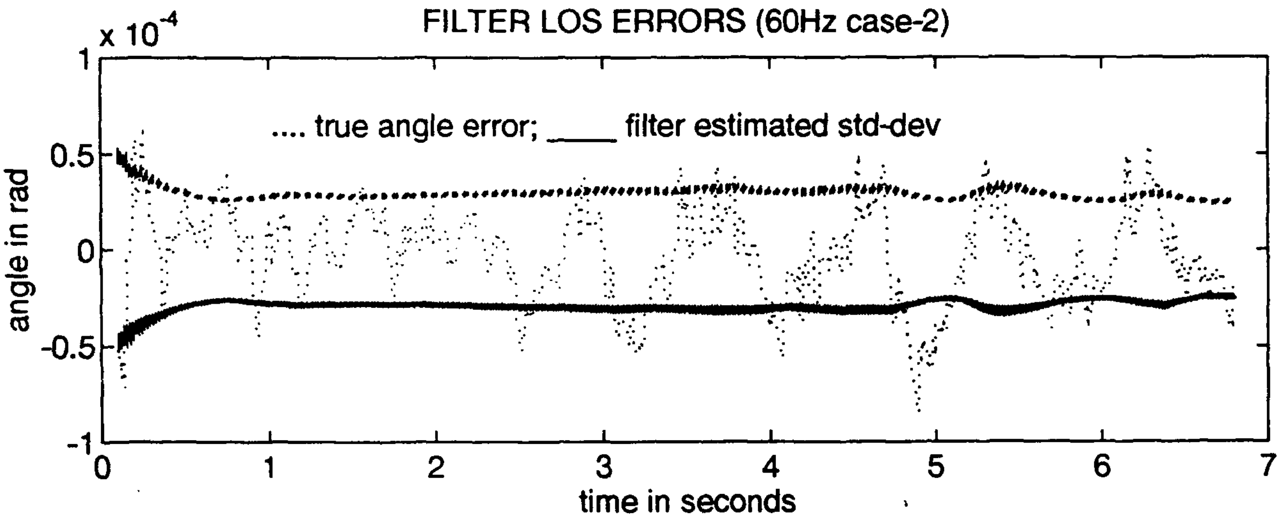

FILTER LOS ERRORS (60Hz case-2)
x 10^-4
.... true angle error; ____ filter estimated std-dev
angle in rad
time in seconds

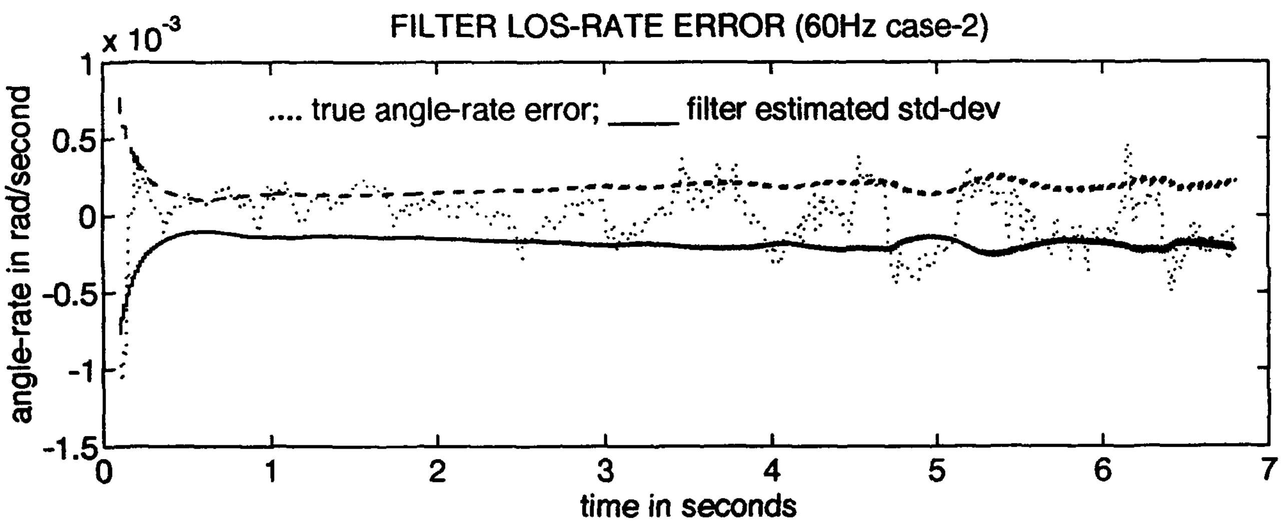

FILTER LOS-RATE ERROR (60Hz case-2)
x 10^-3
.... true angle-rate error; ____ filter estimated std-dev
angle-rate in rad/second
time in seconds

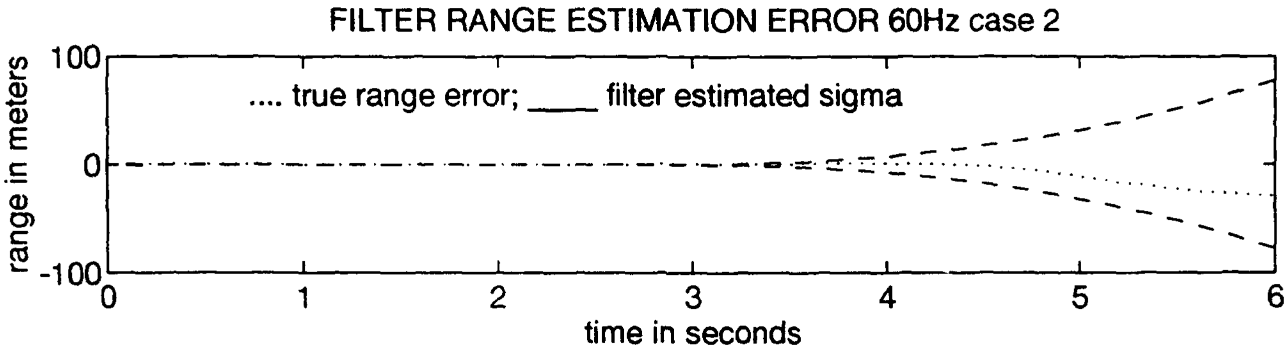
FILTER RANGE ESTIMATION ERROR 60Hz case 2
.... true range error; ____ filter estimated sigma
range in meters
100
0
-100
0
1
2
3
4
5
6
time in seconds

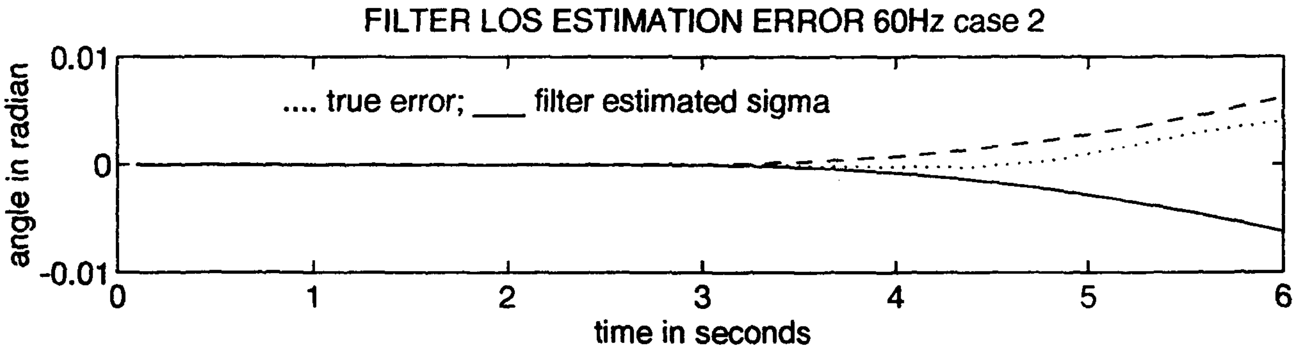
FILTER LOS ESTIMATION ERROR 60Hz case 2
.... true error; ___ filter estimated sigma
angle in radian
0.01
0
-0.01
0
1
2
3
4
5
6
time in seconds

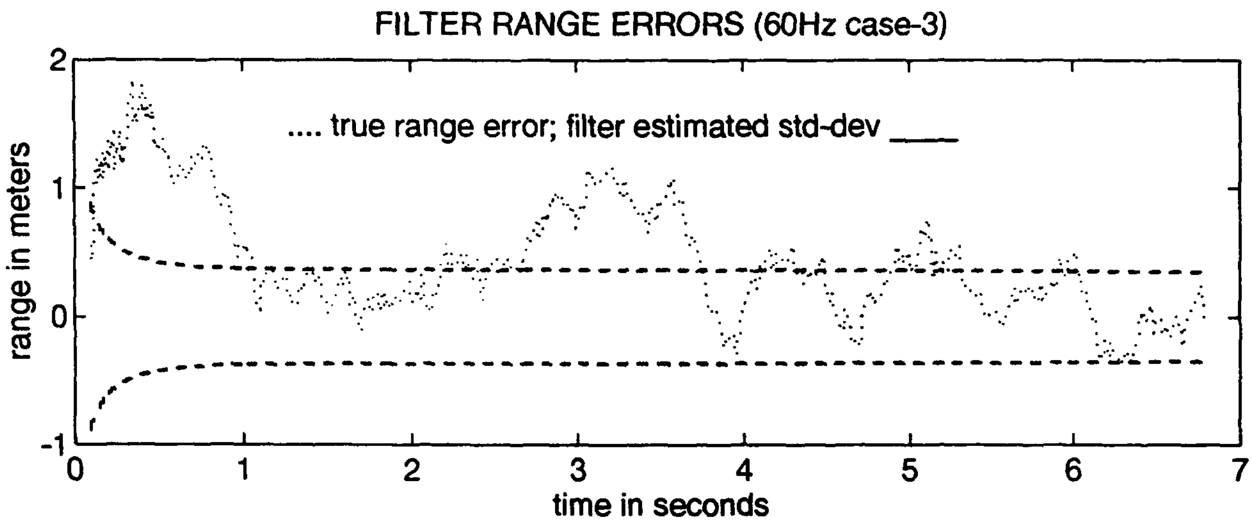
FILTER RANGE ERRORS (60Hz case-3)
.... true range error; filter estimated std-dev ____
range in meters
time in seconds
2
1
0
-1
0
1
2
3
4
5
6
7

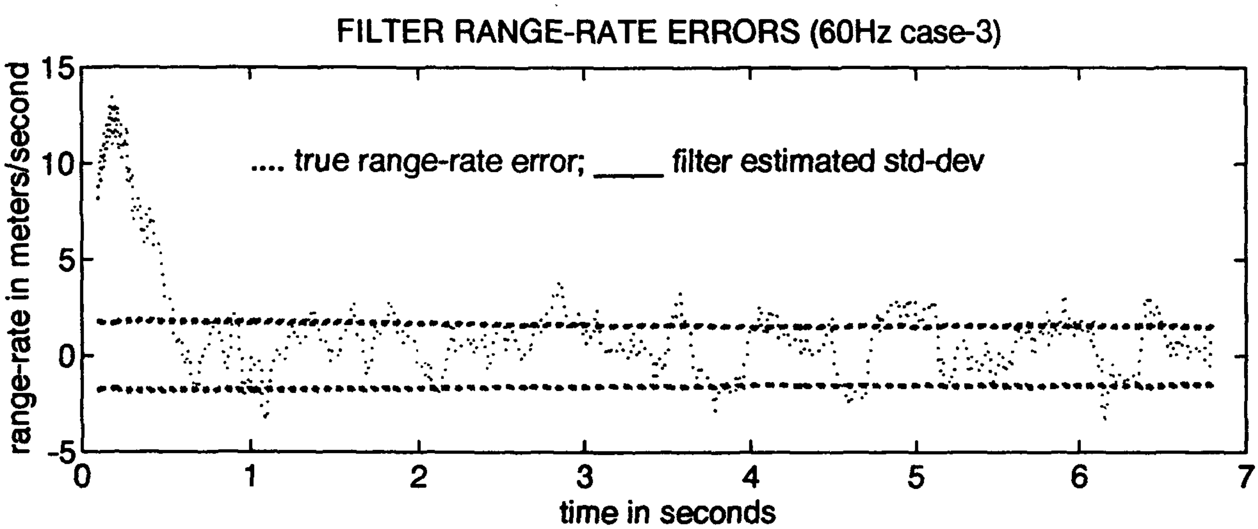
FILTER RANGE-RATE ERRORS (60Hz case-3)
.... true range-rate error; ____ filter estimated std-dev
range-rate in meters/second
time in seconds
15
10
5
0
-5
0
1
2
3
4
5
6
7

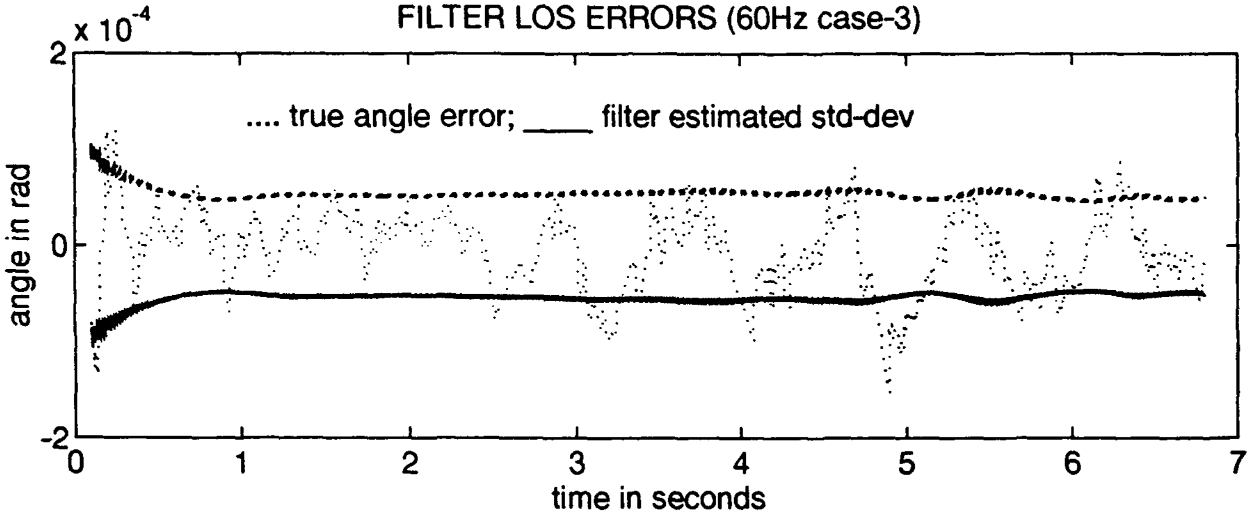
FILTER LOS ERRORS (60Hz case-3)
x 10^-4
2
0
-2
.... true angle error; ____ filter estimated std-dev
angle in rad
0
1
2
3
4
5
6
7
time in seconds

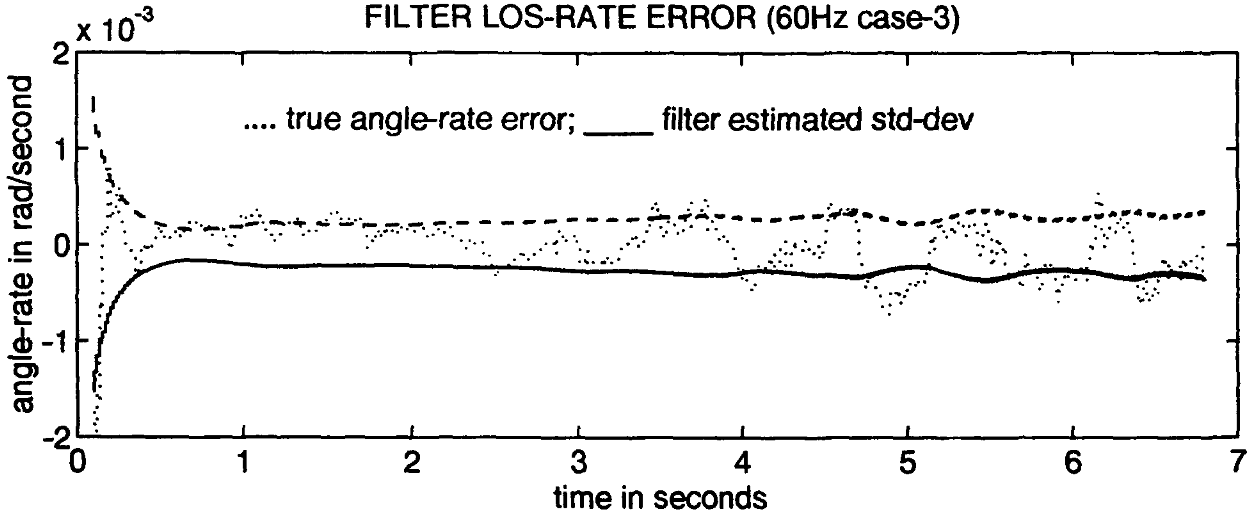
FILTER LOS-RATE ERROR (60Hz case-3)
x 10^-3
2
1
0
-1
-2
.... true angle-rate error; ____ filter estimated std-dev
angle-rate in rad/second
0
1
2
3
4
5
6
7
time in seconds

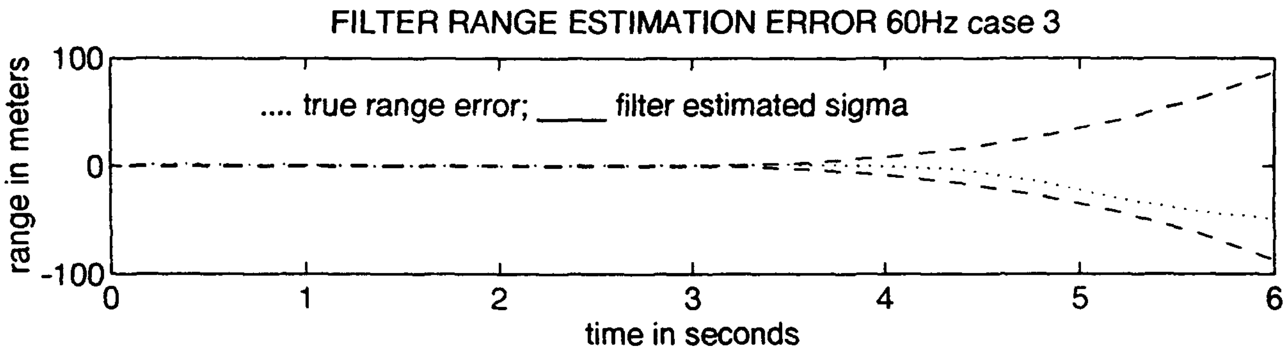
FILTER RANGE ESTIMATION ERROR 60Hz case 3
.... true range error; ____ filter estimated sigma
range in meters
100
0
-100
0
1
2
3
4
5
6
time in seconds

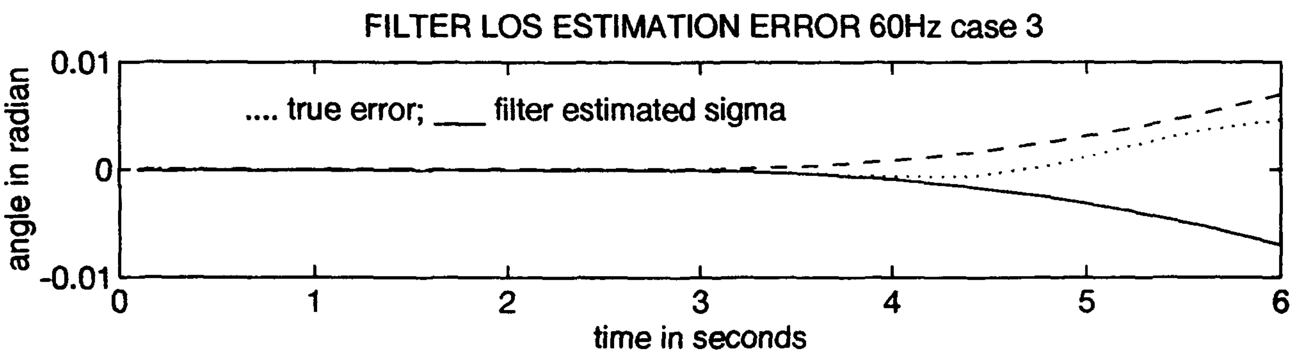
FILTER LOS ESTIMATION ERROR 60Hz case 3
.... true error; ___ filter estimated sigma
angle in radian
0.01
0
-0.01
0
1
2
3
4
5
6
time in seconds

FILTER RANGE ERRORS (60Hz case-4)

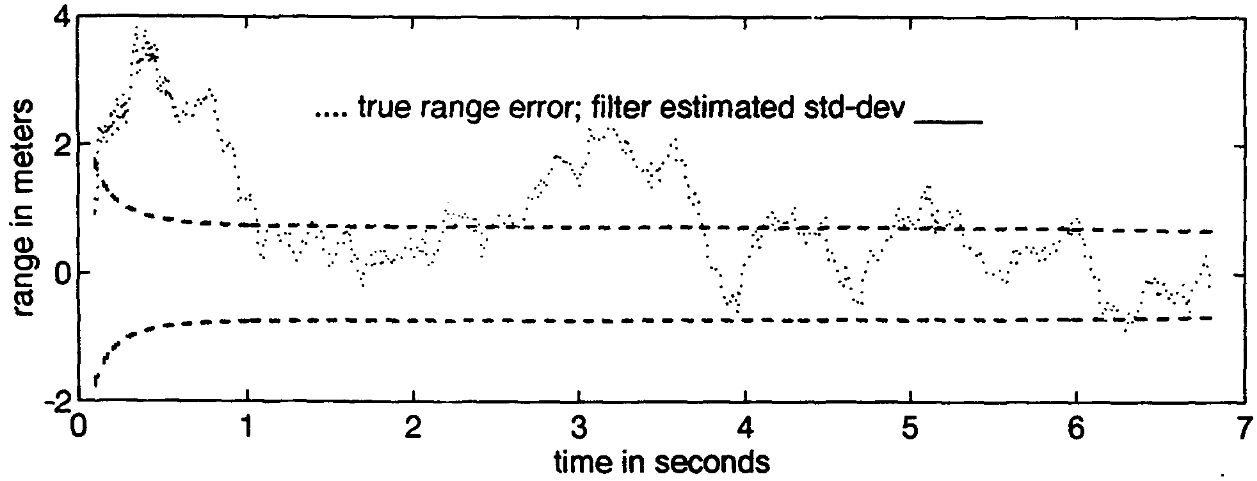

FILTER RANGE-RATE ERRORS (60Hz case-4)

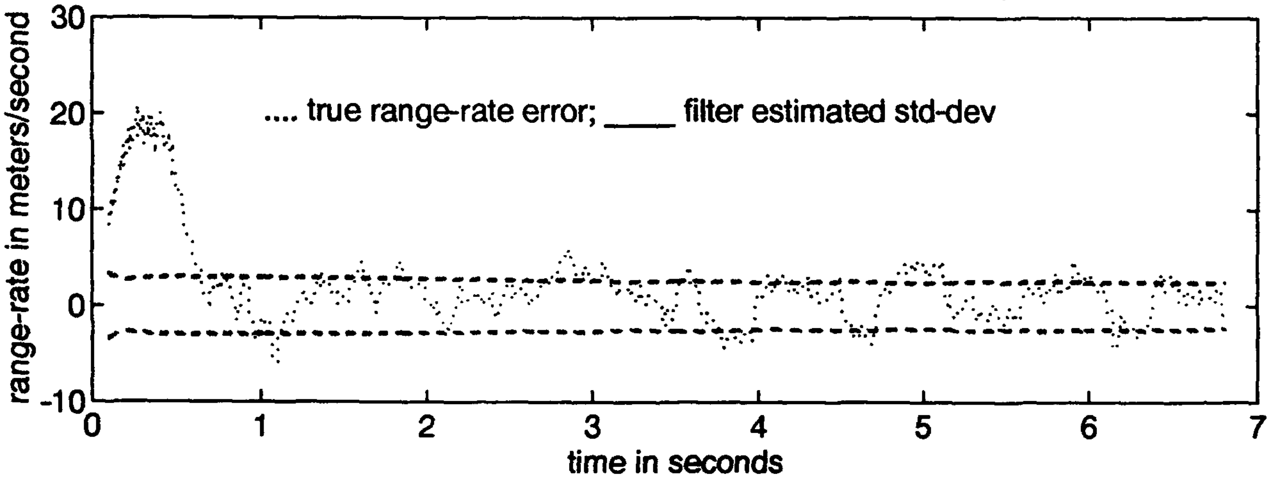

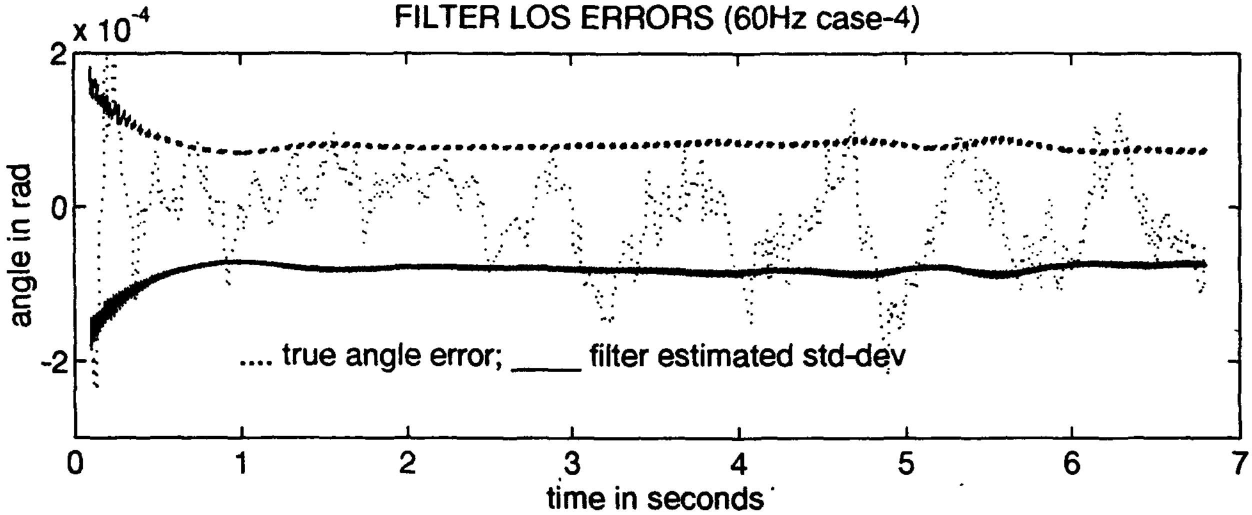
FILTER LOS ERRORS (60Hz case-4)
x 10^-4
2
0
-2
angle in rad
.... true angle error; ____ filter estimated std-dev
0
1
2
3
4
5
6
7
time in seconds

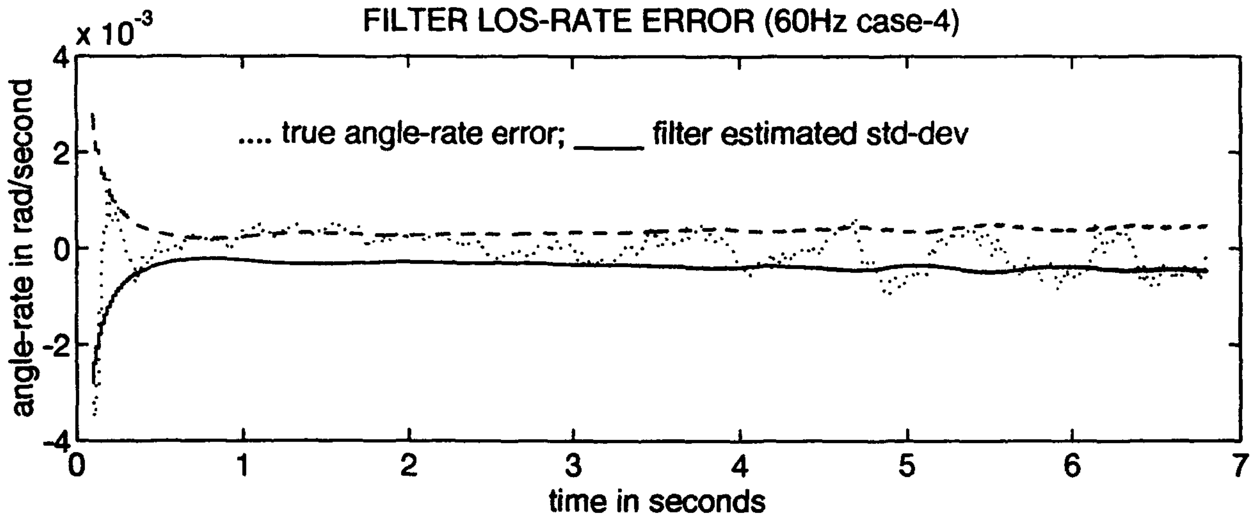
FILTER LOS-RATE ERROR (60Hz case-4)
x 10^-3
4
2
0
-2
-4
angle-rate in rad/second
.... true angle-rate error; ____ filter estimated std-dev
0
1
2
3
4
5
6
7
time in seconds

FILTER RANGE ESTIMATION ERROR 60Hz case 4

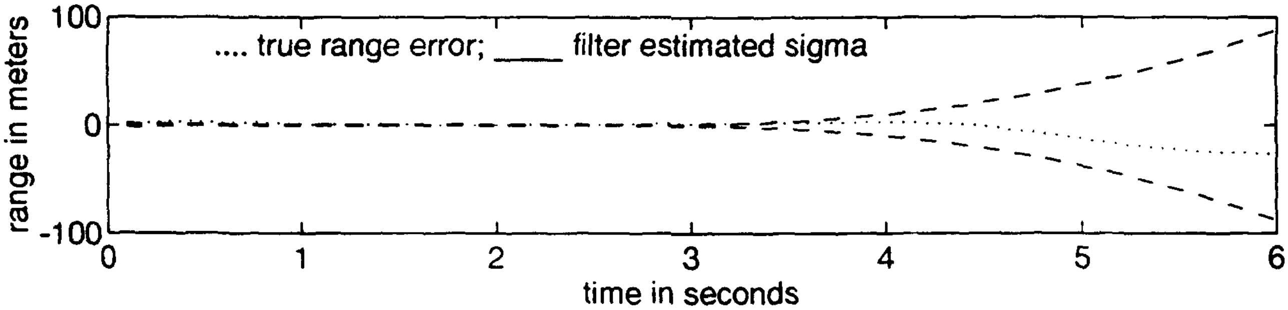

FILTER LOS ESTIMATION ERROR 60Hz case 4

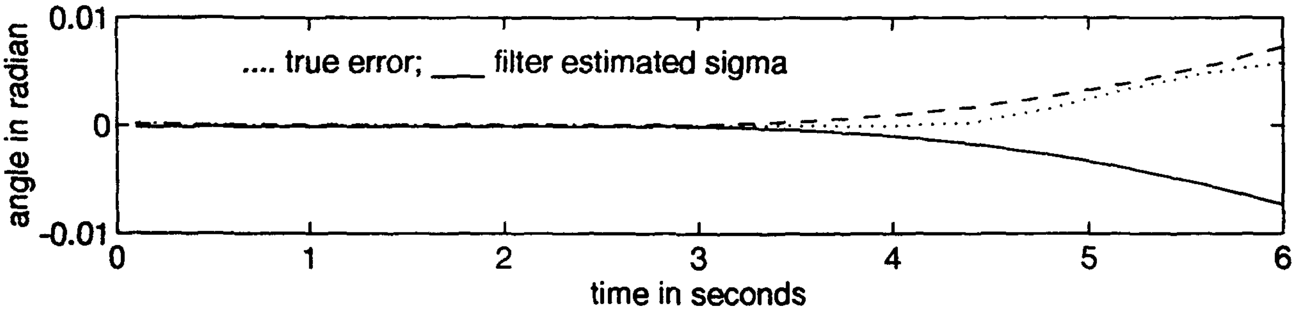

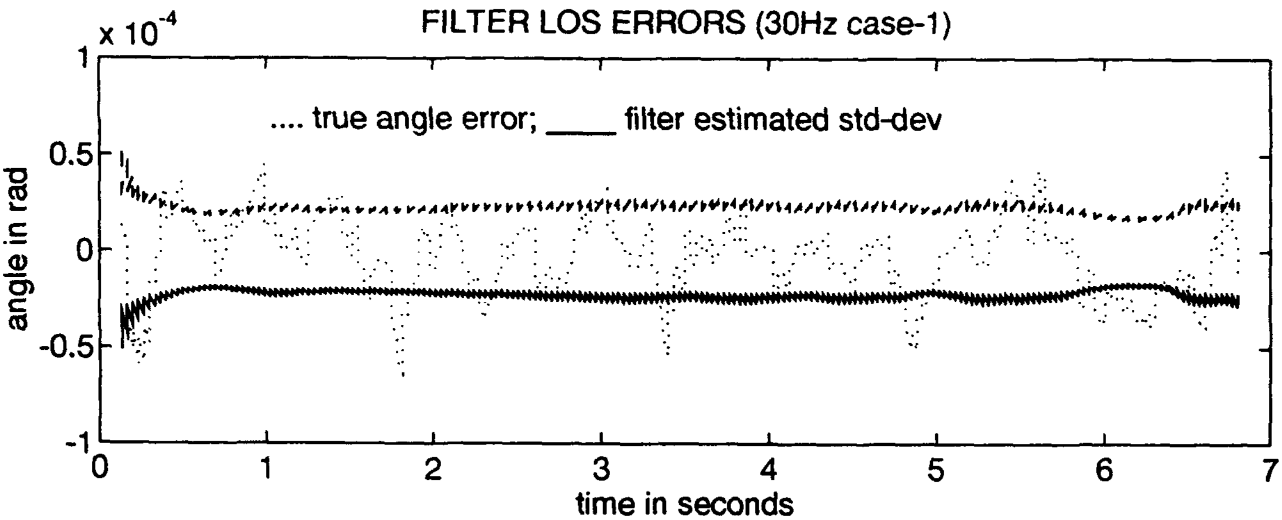

x 10^-4
FILTER LOS ERRORS (30Hz case-1)
.... true angle error; ____ filter estimated std-dev
angle in rad
1
0.5
0
-0.5
-1
0
1
2
3
4
5
6
7
time in seconds

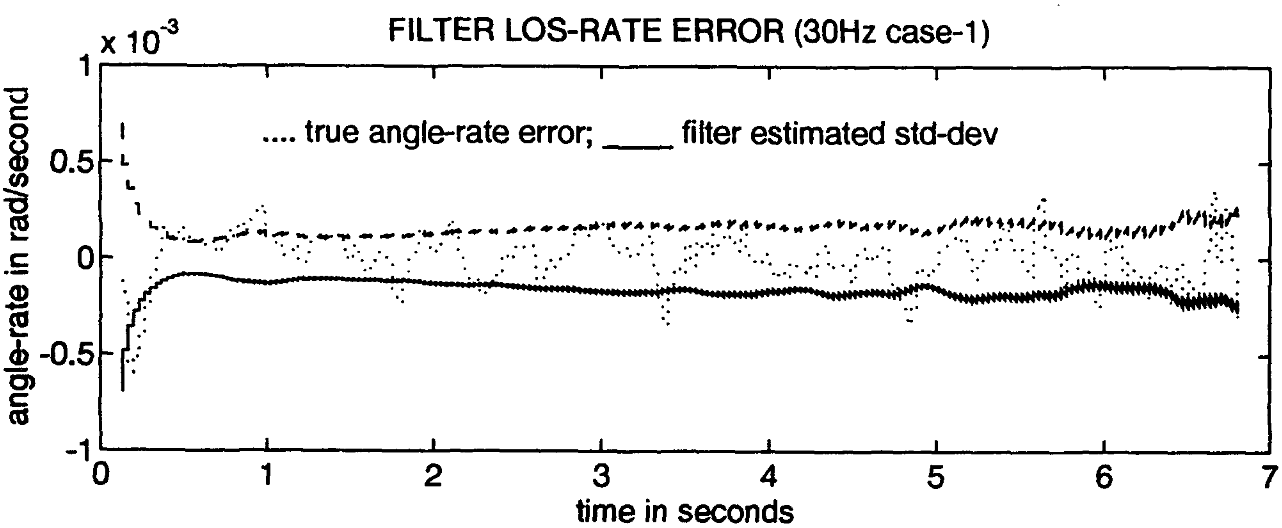

x 10^-3
FILTER LOS-RATE ERROR (30Hz case-1)
.... true angle-rate error; ____ filter estimated std-dev
angle-rate in rad/second
1
0.5
0
-0.5
-1
0
1
2
3
4
5
6
7
time in seconds

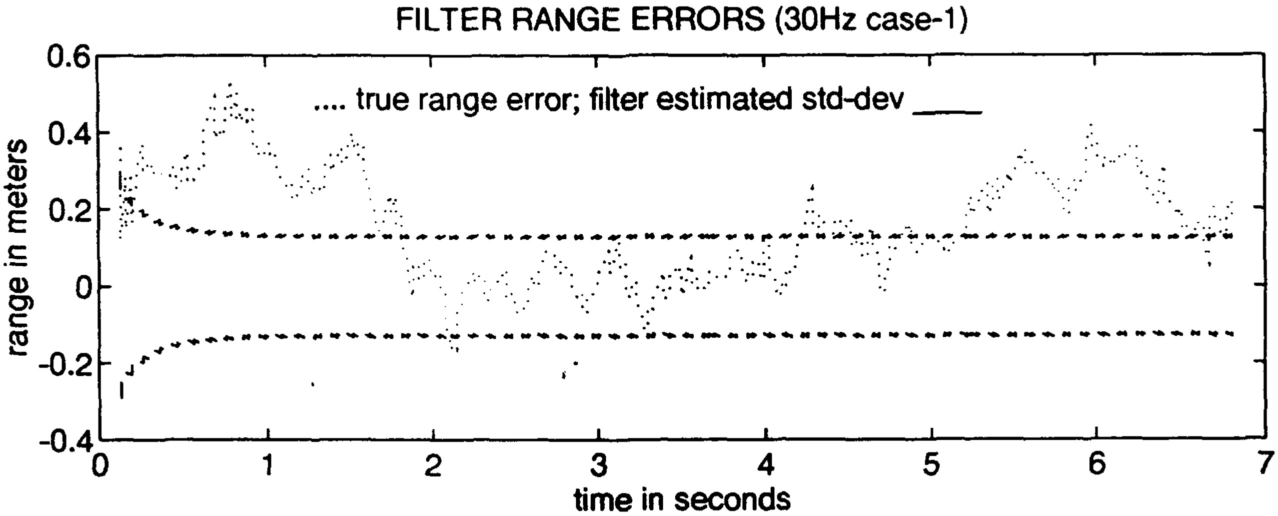
FILTER RANGE ERRORS (30Hz case-1)
.... true range error; filter estimated std-dev ____
range in meters
0.6
0.4
0.2
0
-0.2
-0.4
0
1
2
3
4
5
6
7
time in seconds

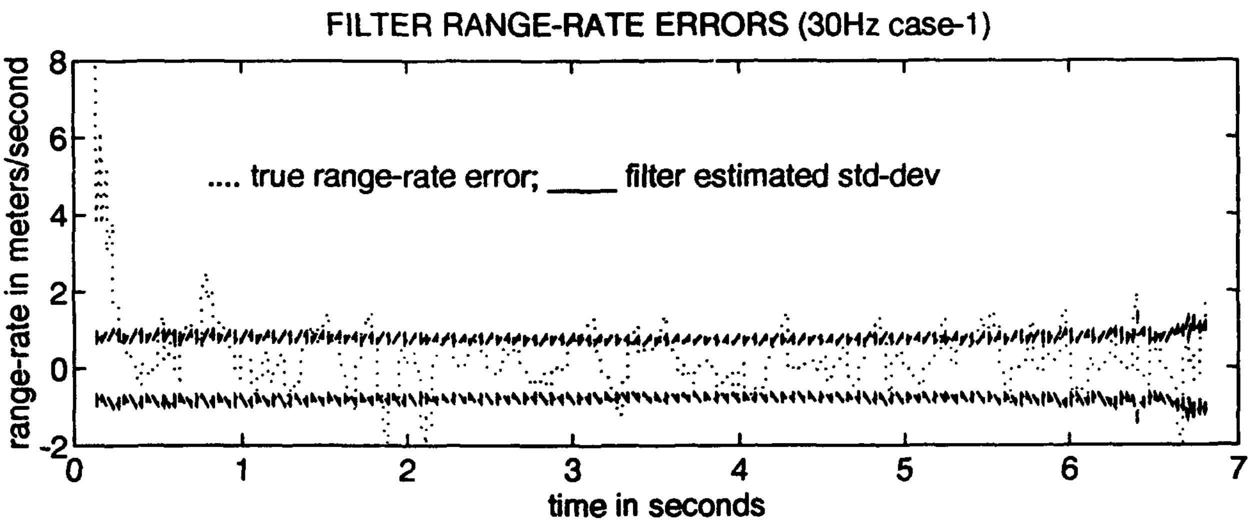
FILTER RANGE-RATE ERRORS (30Hz case-1)
.... true range-rate error; ____ filter estimated std-dev
range-rate in meters/second
8
6
4
2
0
-2
0
1
2
3
4
5
6
7
time in seconds

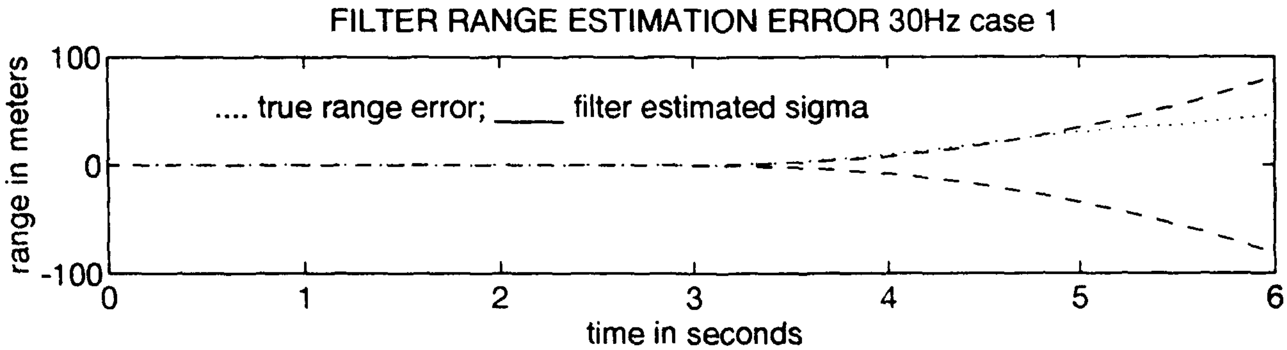
FILTER RANGE ESTIMATION ERROR 30Hz case 1
.... true range error; ____ filter estimated sigma
range in meters
100
0
-100
0
1
2
3
4
5
6
time in seconds

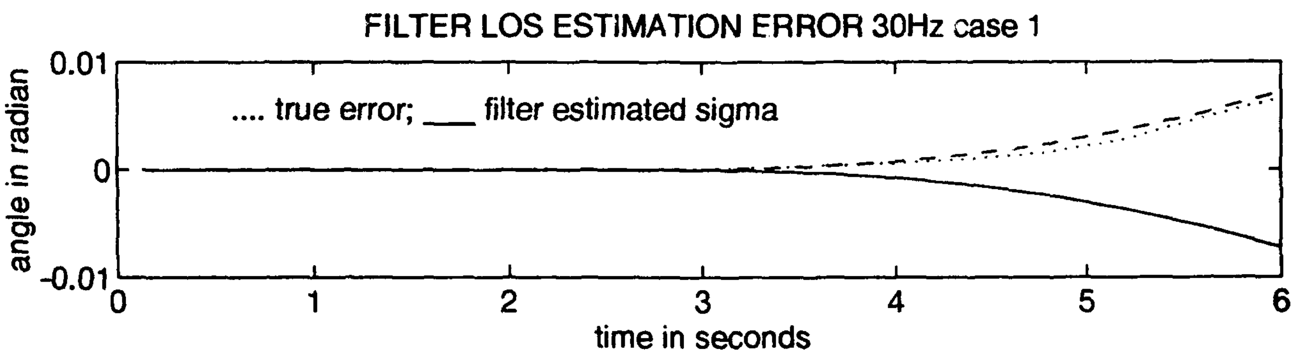
FILTER LOS ESTIMATION ERROR 30Hz case 1
.... true error; ___ filter estimated sigma
angle in radian
0.01
0
-0.01
0
1
2
3
4
5
6
time in seconds

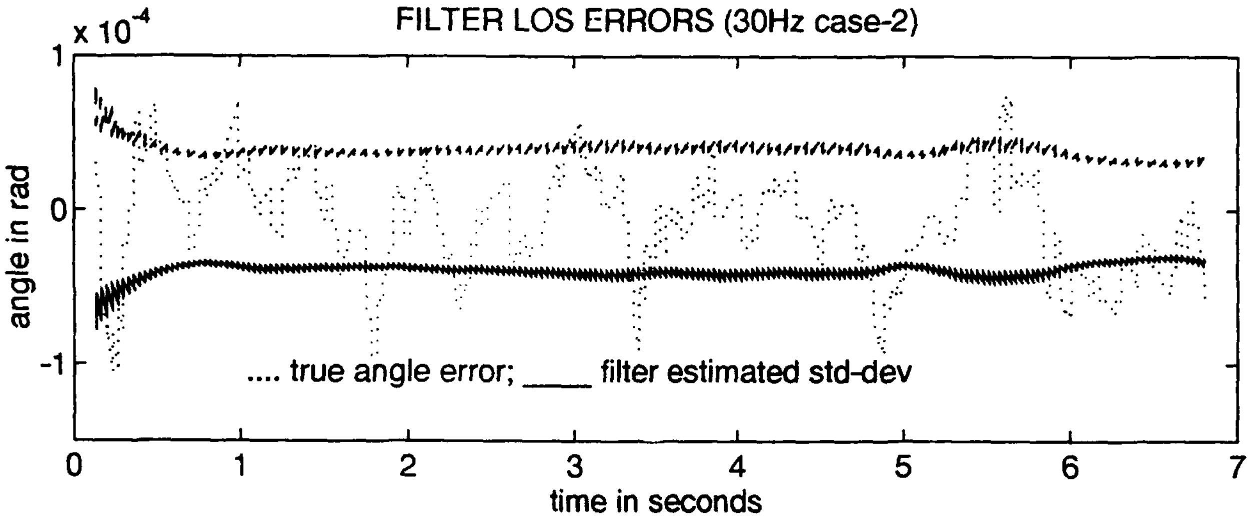
FILTER LOS ERRORS (30Hz case-2)
x 10^-4
angle in rad
.... true angle error; ____ filter estimated std-dev
time in seconds

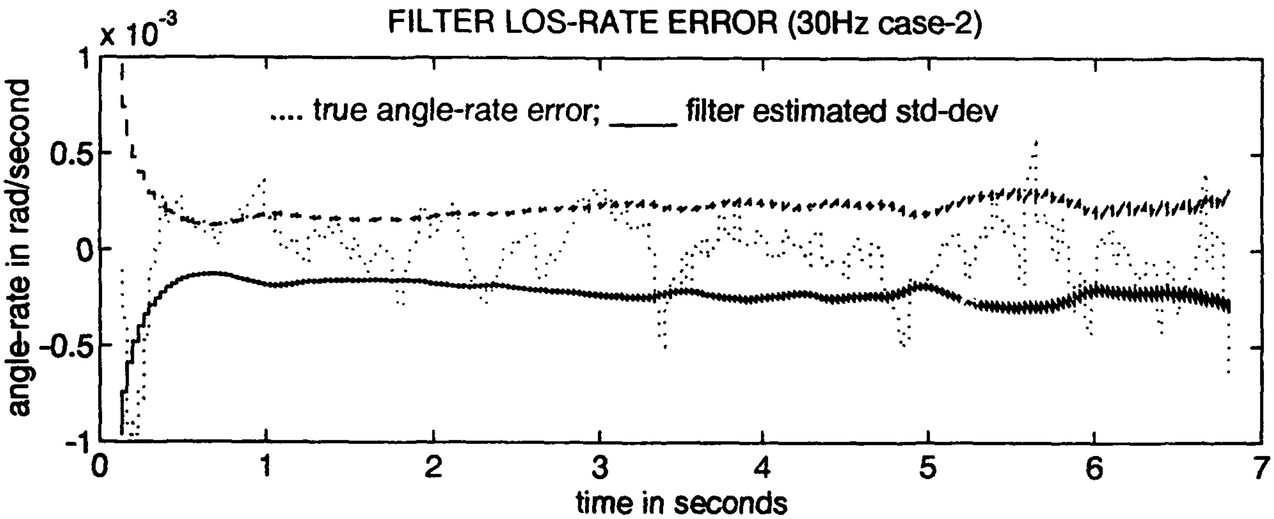
FILTER LOS-RATE ERROR (30Hz case-2)
x 10^-3
angle-rate in rad/second
.... true angle-rate error; ____ filter estimated std-dev
time in seconds

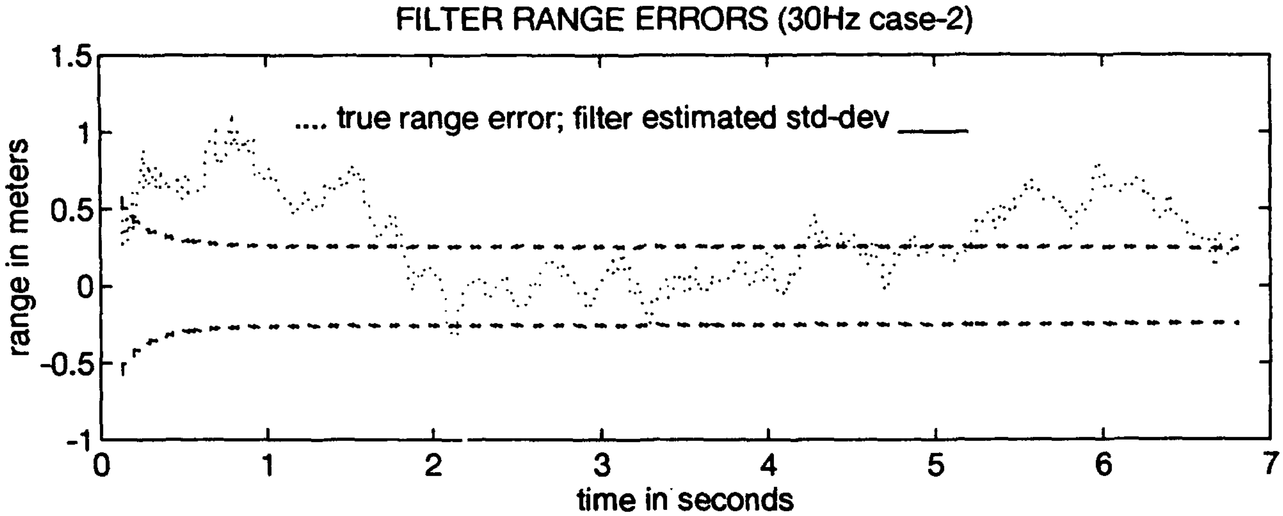

FILTER RANGE ERRORS (30Hz case-2)
.... true range error; filter estimated std-dev ____
range in meters
time in seconds

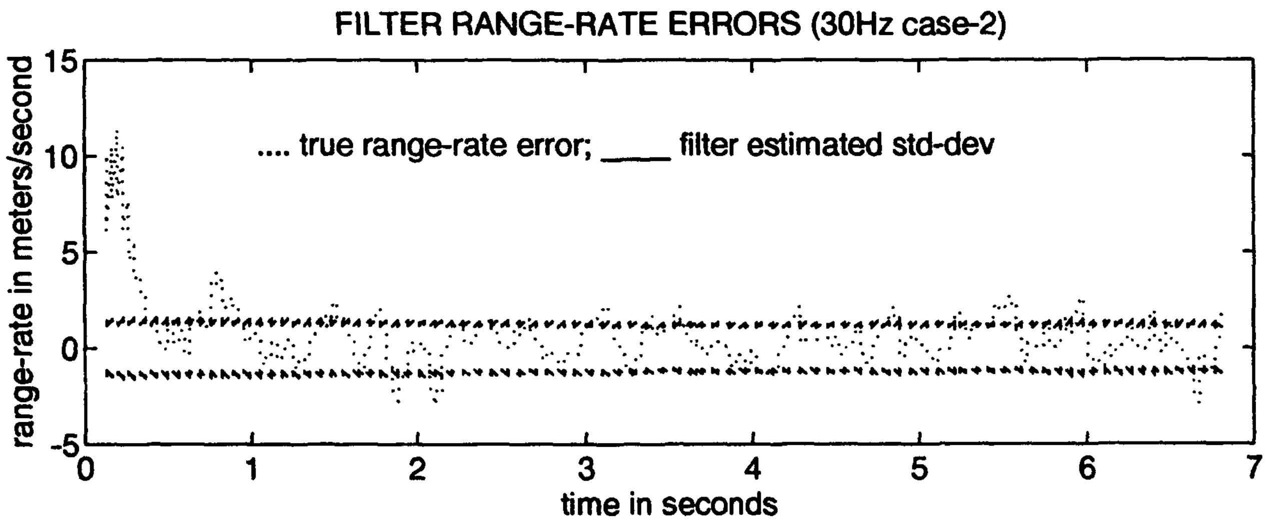

FILTER RANGE-RATE ERRORS (30Hz case-2)
.... true range-rate error; ____ filter estimated std-dev
range-rate in meters/second
time in seconds

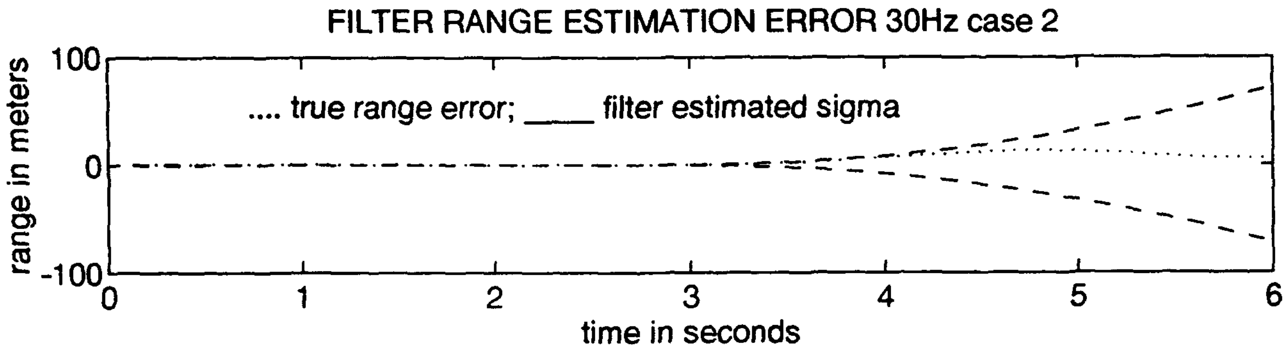
FILTER RANGE ESTIMATION ERROR 30Hz case 2
.... true range error; ____ filter estimated sigma
range in meters
100
0
-100
0
1
2
3
4
5
6
time in seconds

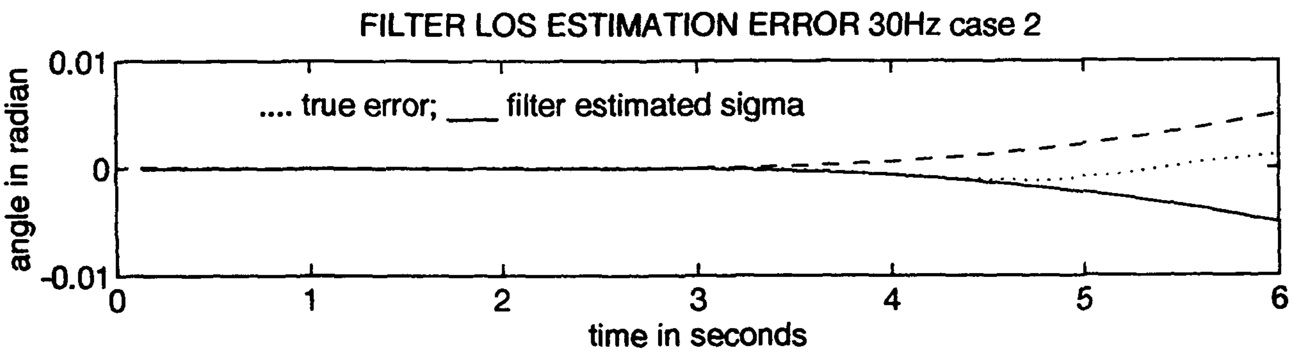
FILTER LOS ESTIMATION ERROR 30Hz case 2
.... true error; ___ filter estimated sigma
angle in radian
0.01
0
-0.01
0
1
2
3
4
5
6
time in seconds

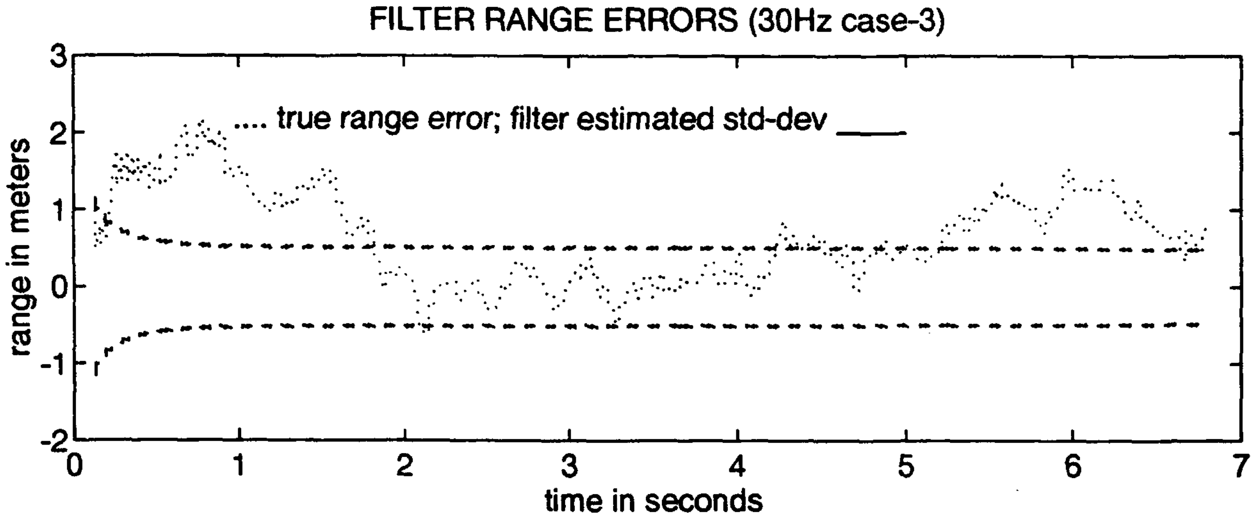
FILTER RANGE ERRORS (30Hz case-3)
.... true range error; filter estimated std-dev ____
range in meters
time in seconds
3
2
1
0
-1
-2
0
1
2
3
4
5
6
7

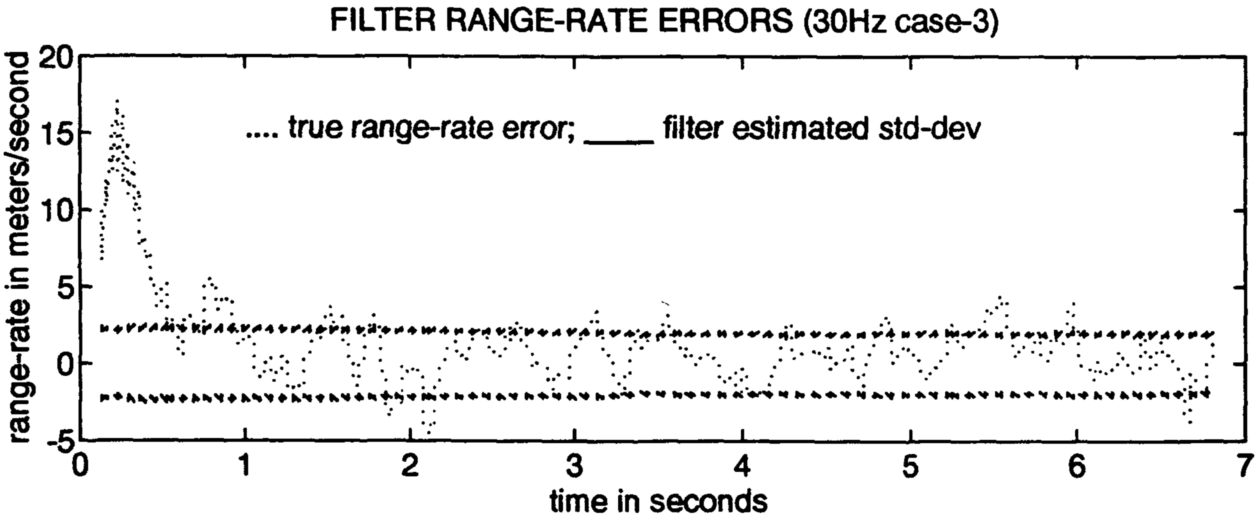
FILTER RANGE-RATE ERRORS (30Hz case-3)
.... true range-rate error; ____ filter estimated std-dev
range-rate in meters/second
time in seconds
20
15
10
5
0
-5
0
1
2
3
4
5
6
7

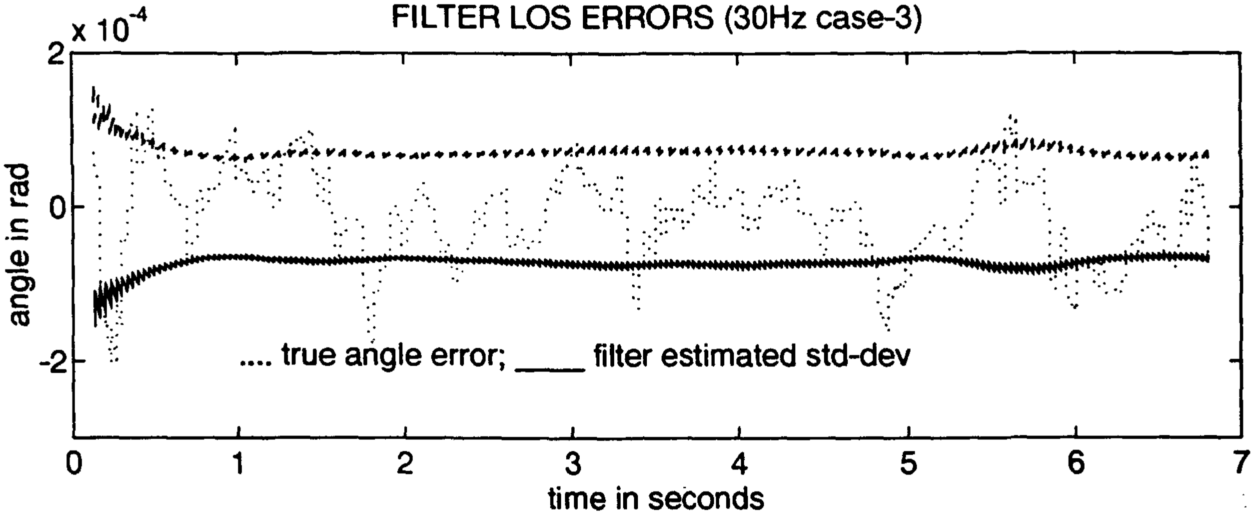
FILTER LOS ERRORS (30Hz case-3)
x 10^-4
2
0
-2
angle in rad
.... true angle error; ____ filter estimated std-dev
0
1
2
3
4
5
6
7
time in seconds

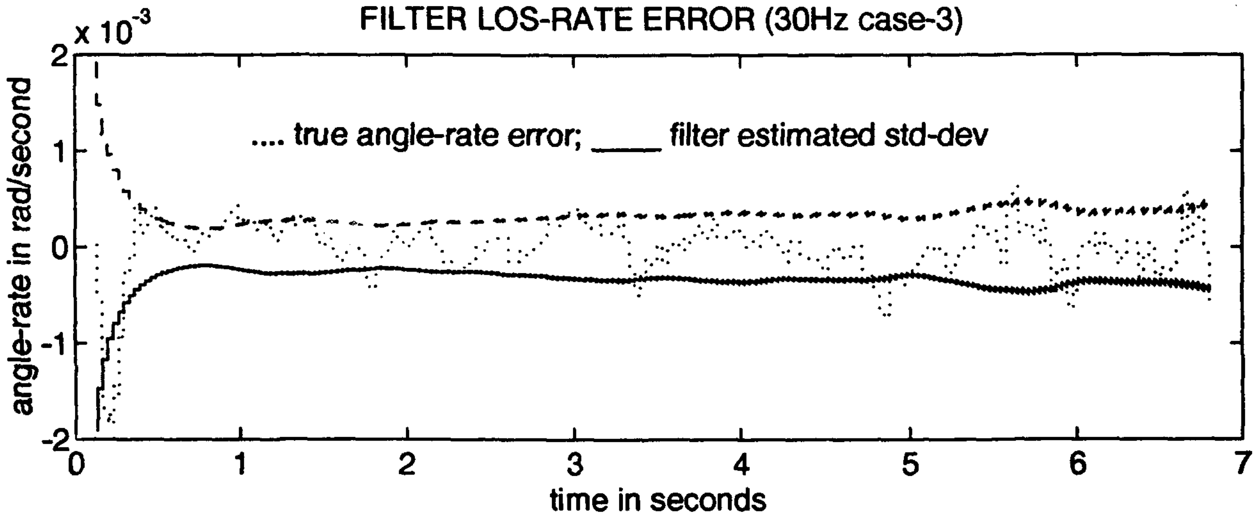
FILTER LOS-RATE ERROR (30Hz case-3)
x 10^-3
2
1
0
-1
-2
angle-rate in rad/second
.... true angle-rate error; ____ filter estimated std-dev
0
1
2
3
4
5
6
7
time in seconds

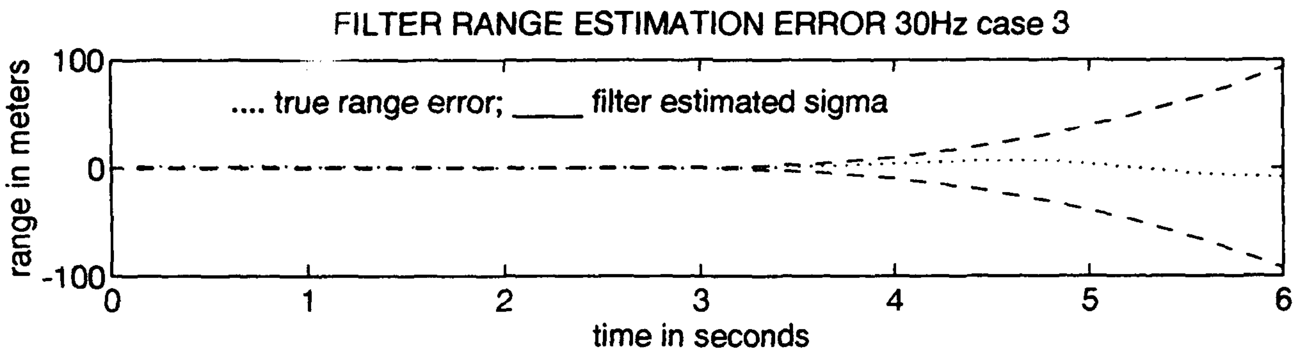
FILTER RANGE ESTIMATION ERROR 30Hz case 3
.... true range error; ____ filter estimated sigma
range in meters
100
0
-100
0
1
2
3
4
5
6
time in seconds

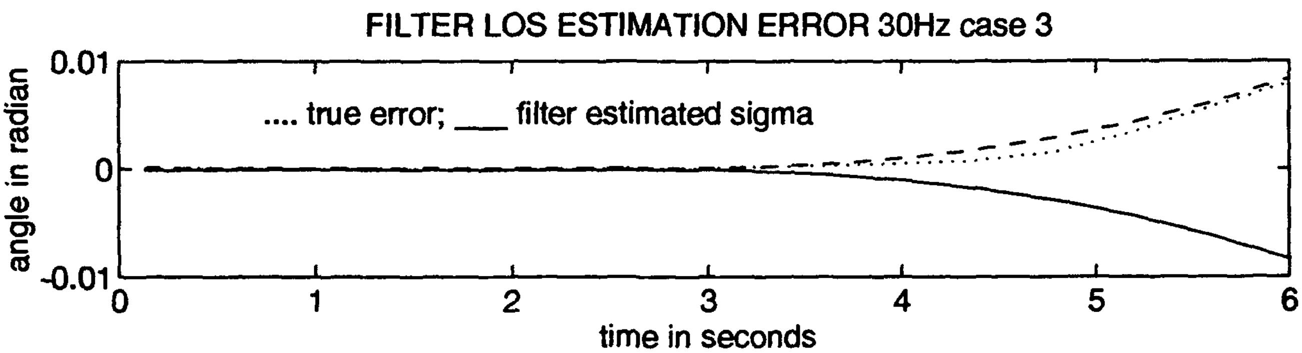
FILTER LOS ESTIMATION ERROR 30Hz case 3
.... true error; ___ filter estimated sigma
angle in radian
0.01
0
-0.01
0
1
2
3
4
5
6
time in seconds

FILTER RANGE ERRORS (30Hz case-4)

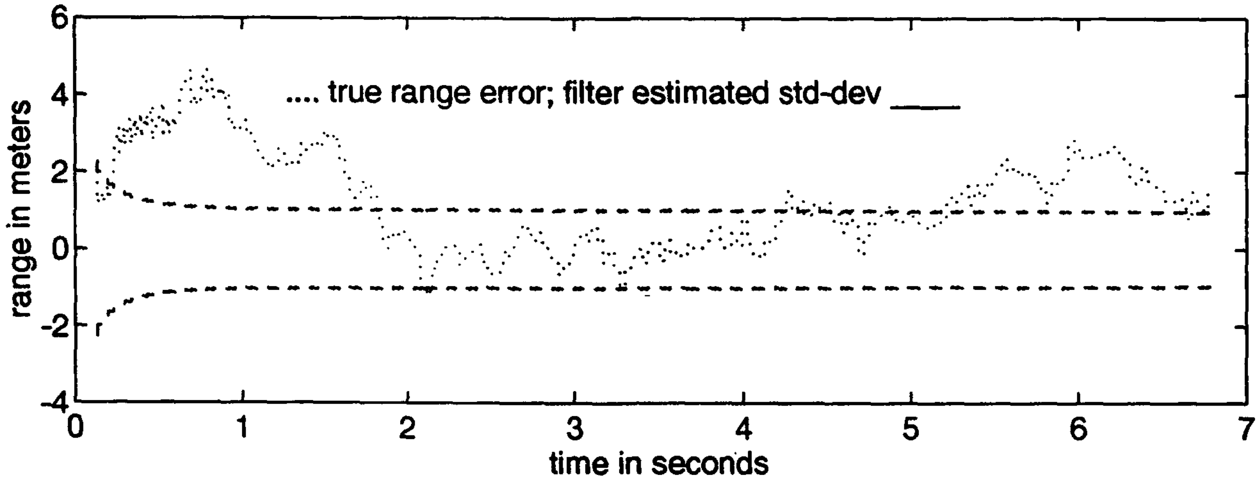

FILTER RANGE-RATE ERRORS (30Hz case-4)

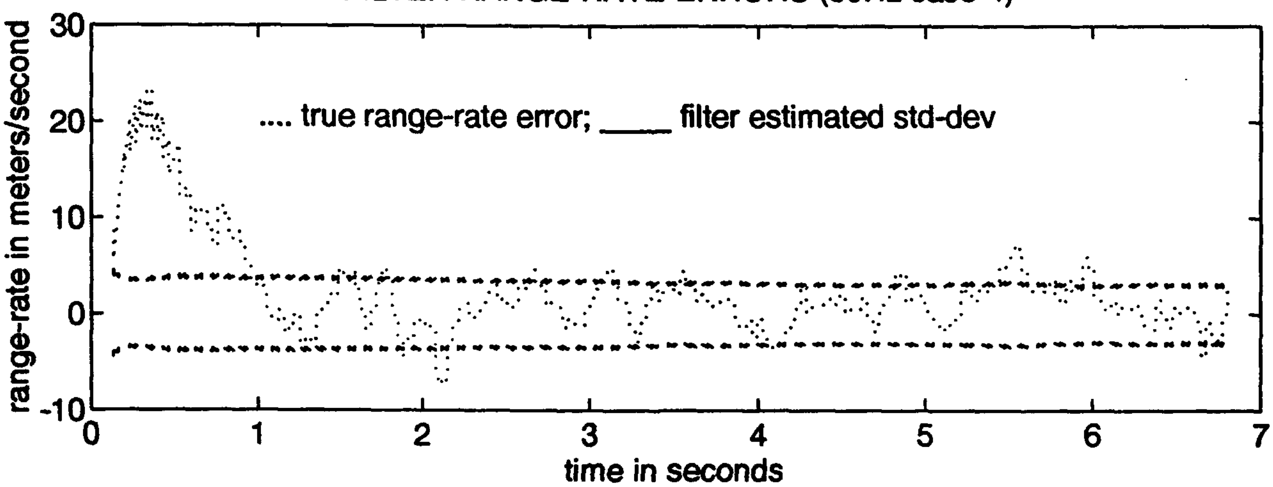

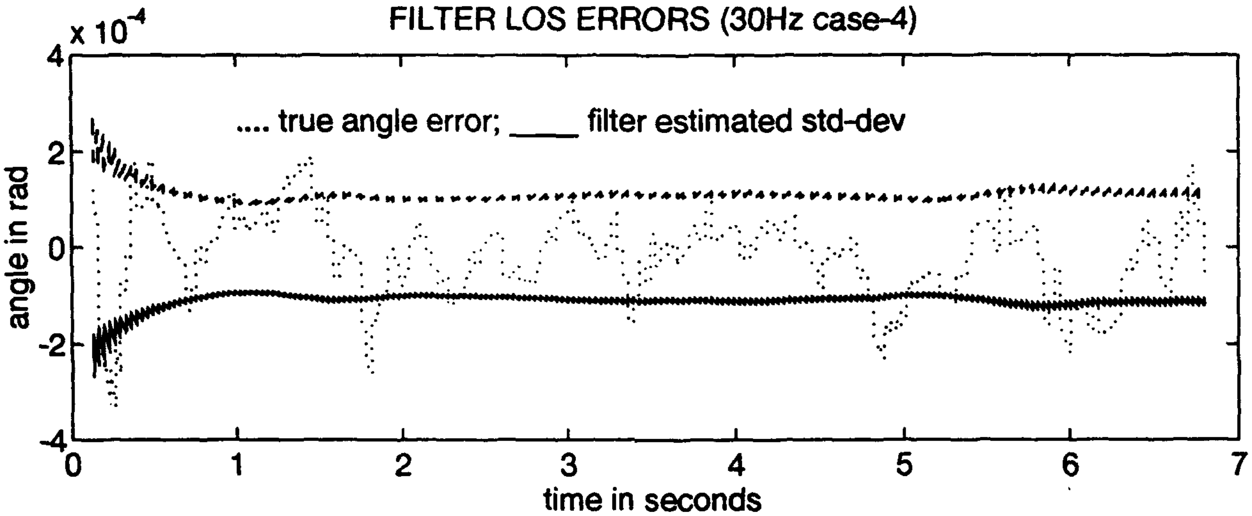

FILTER LOS ERRORS (30Hz case-4)
x 10^-4
.... true angle error; ____ filter estimated std-dev
angle in rad
time in seconds

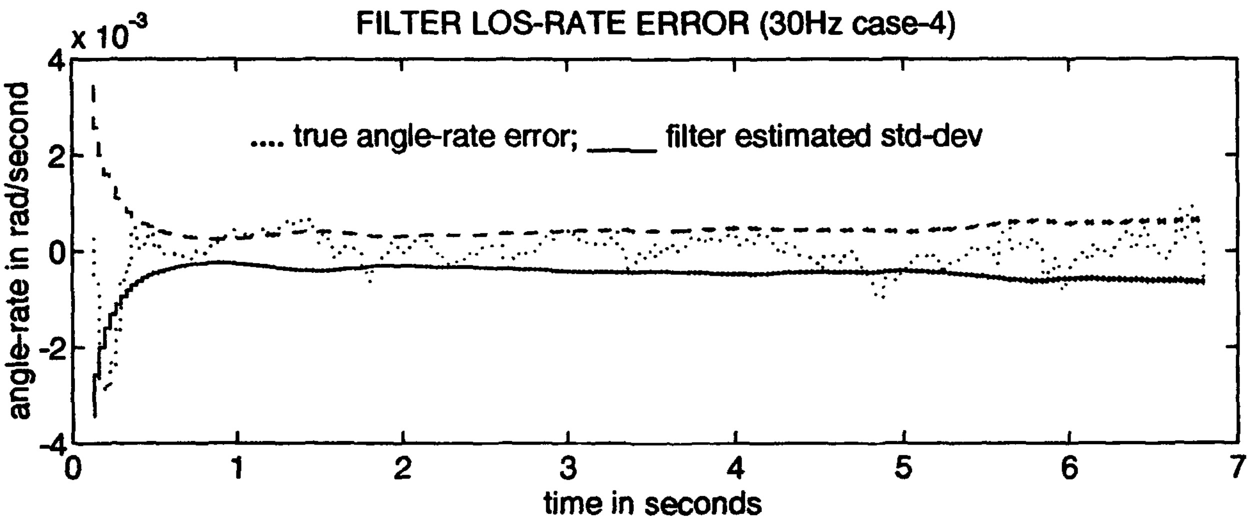

FILTER LOS-RATE ERROR (30Hz case-4)
x 10^-3
.... true angle-rate error; ____ filter estimated std-dev
angle-rate in rad/second
time in seconds

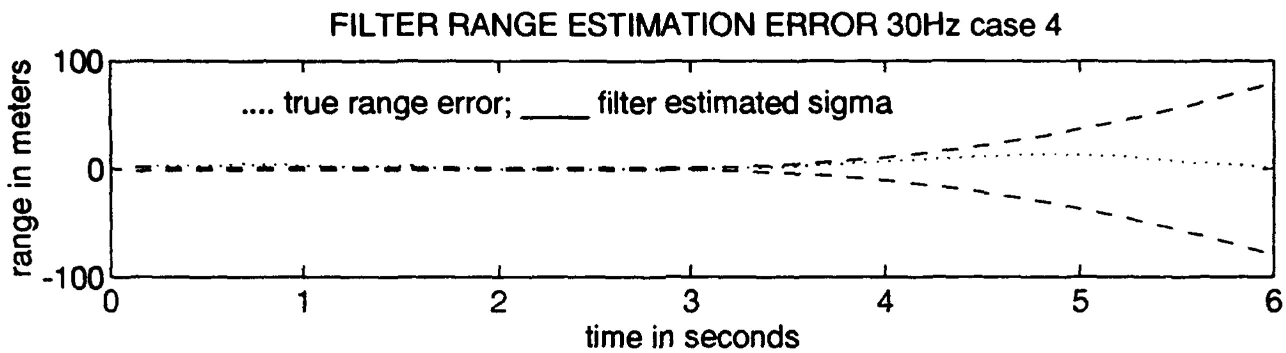
FILTER RANGE ESTIMATION ERROR 30Hz case 4
.... true range error; _____ filter estimated sigma
range in meters
100
0
-100
0
1
2
3
4
5
6
time in seconds

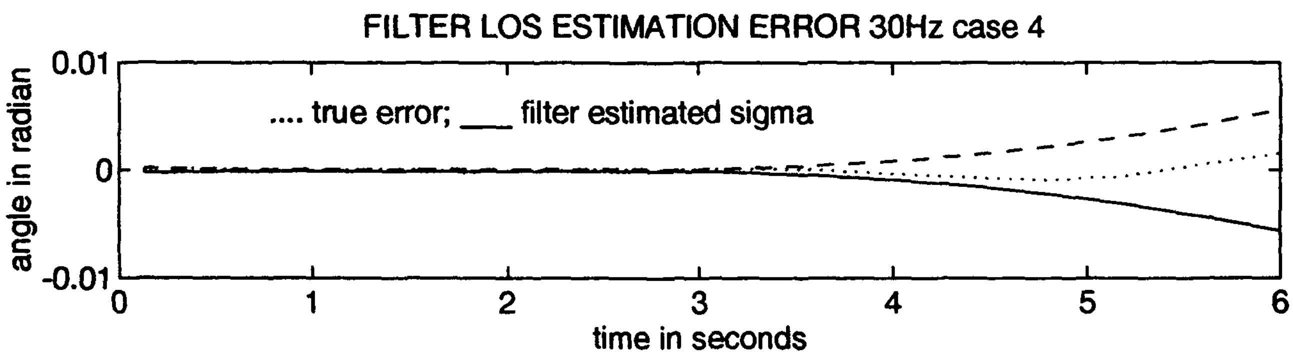
FILTER LOS ESTIMATION ERROR 30Hz case 4
.... true error; ___ filter estimated sigma
angle in radian
0.01
0
-0.01
0
1
2
3
4
5
6
time in seconds

Appendix G

This appendix contains simulation plots for the aircraft INS measurement noise run sets. The aircraft is initially heading east and beginning a 3 g turn to the north. All dynamic noise strengths and ladar measurement noises are set at baseline values. INS acceleration measurements are turned off. INS velocity measurements are varied as presented in Table 3-4. The missile is launched from the $\pi/4$ approach angle. Each run has a trajectory plot, estimated range errors, range-rate errors, LOS errors and LOS-rate errors. Estimated range and LOS plots are found in the $\pi/4$ missile approach angle run plots in Appendix A. Each plot set contains filter divergence plots of range error and angle error for a three second divergence from three to six seconds. The divergence plots, which define the volume cross-section, are used for performance comparison versus the baseline (Figure 4-4).

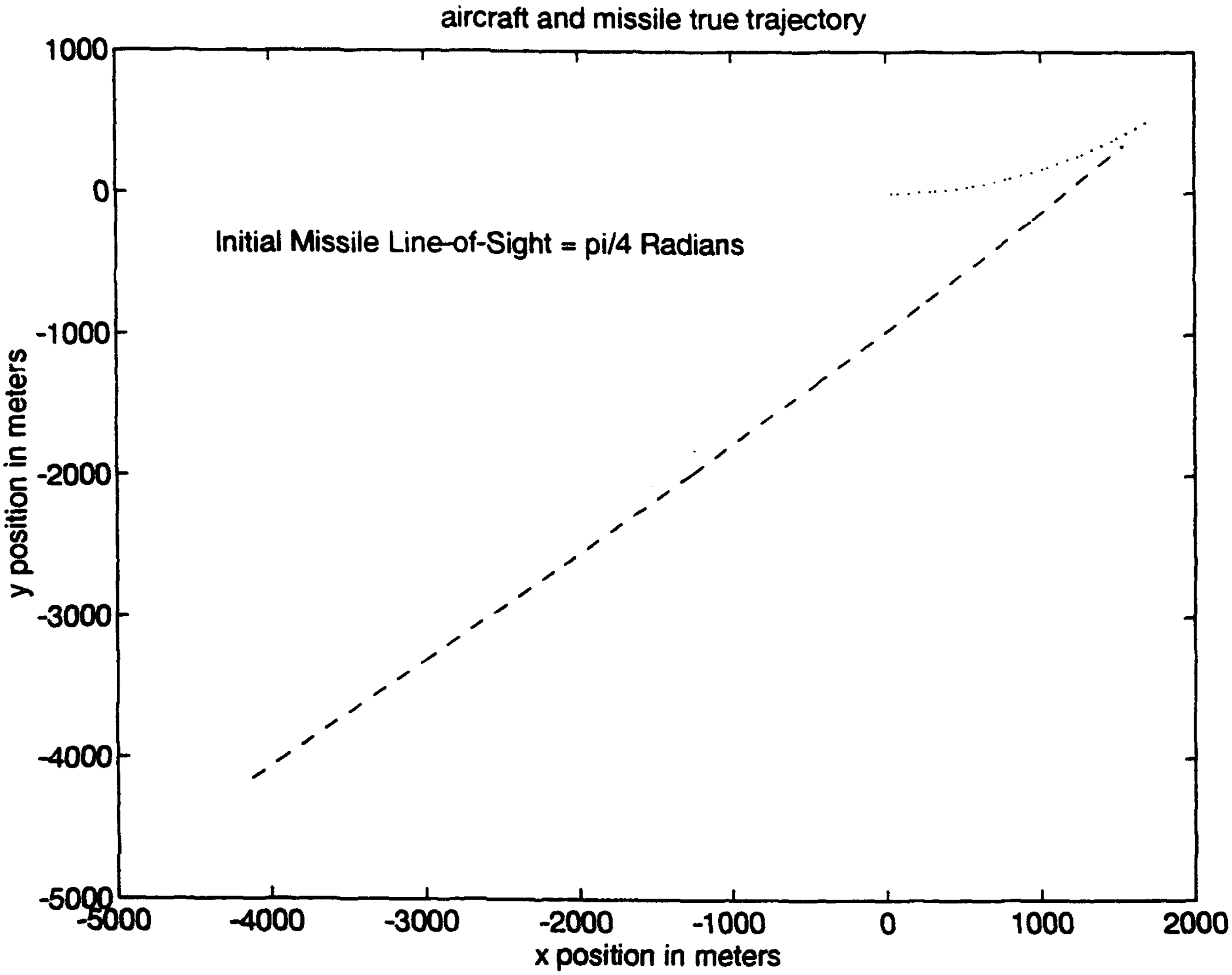
aircraft and missile true trajectory
1000
0
-1000
-2000
-3000
-4000
-5000
-5000
-4000
-3000
-2000
-1000
0
1000
2000
Initial Missile Line-of-Sight = pi/4 Radians
y position in meters
x position in meters

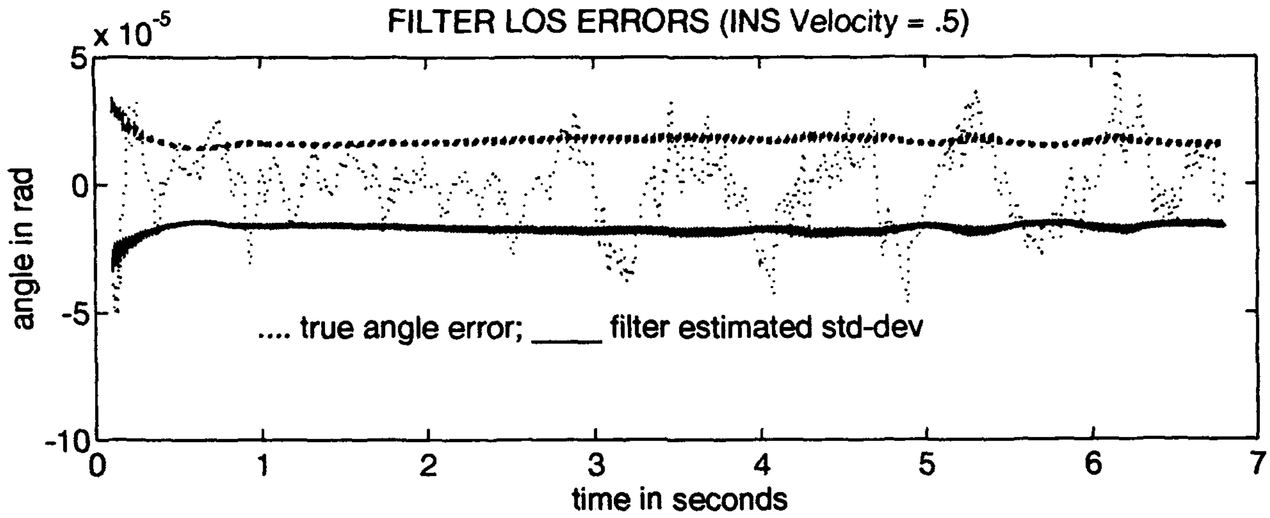
FILTER LOS ERRORS (INS Velocity = .5)
x 10^-5
5
0
-5
-10
angle in rad
.... true angle error; _____ filter estimated std-dev
0
1
2
3
4
5
6
7
time in seconds

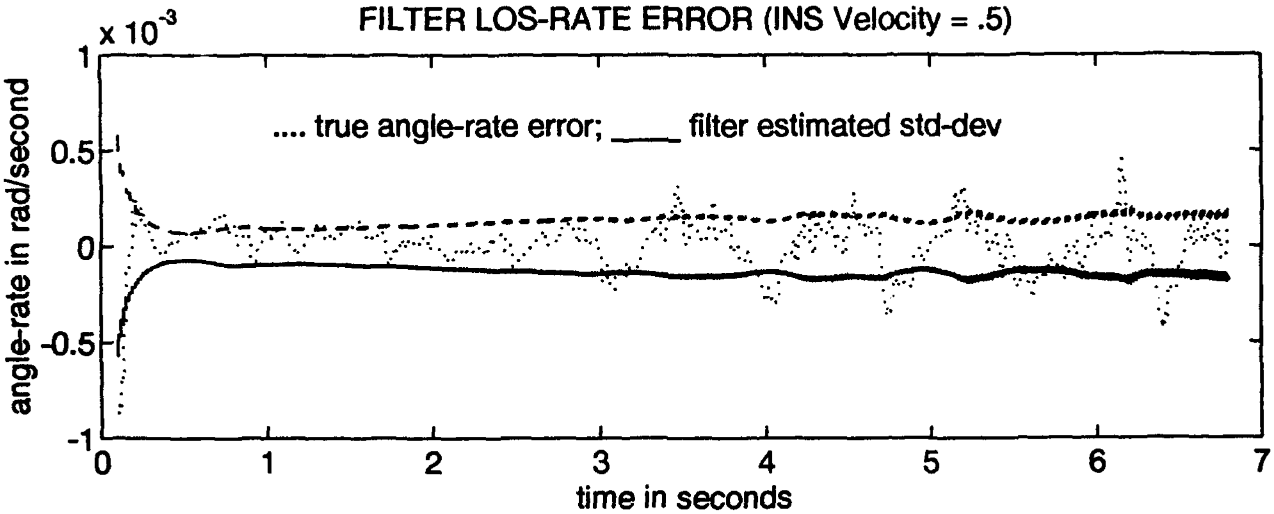
FILTER LOS-RATE ERROR (INS Velocity = .5)
x 10^-3
1
0.5
0
-0.5
-1
angle-rate in rad/second
.... true angle-rate error; _____ filter estimated std-dev
0
1
2
3
4
5
6
7
time in seconds

FILTER RANGE ERRORS (INS Velocity = .5)

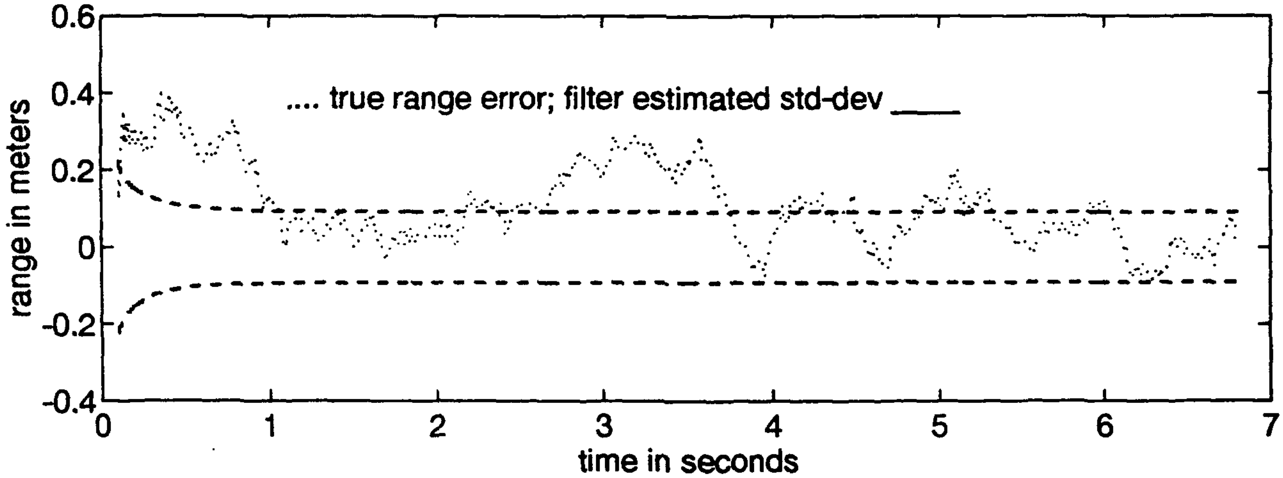

FILTER RANGE-RATE ERRORS (INS Velocity = .5)

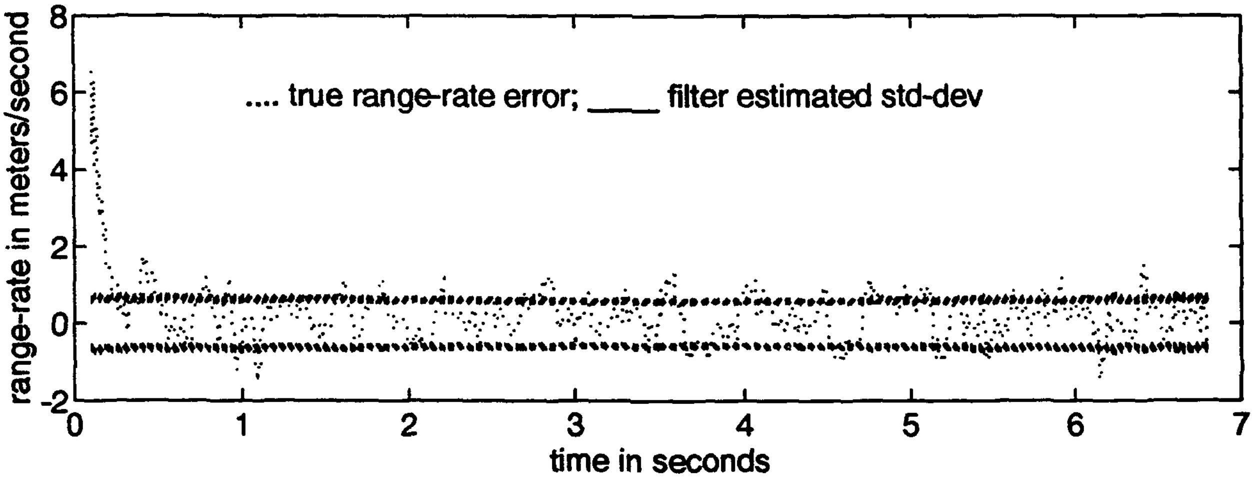

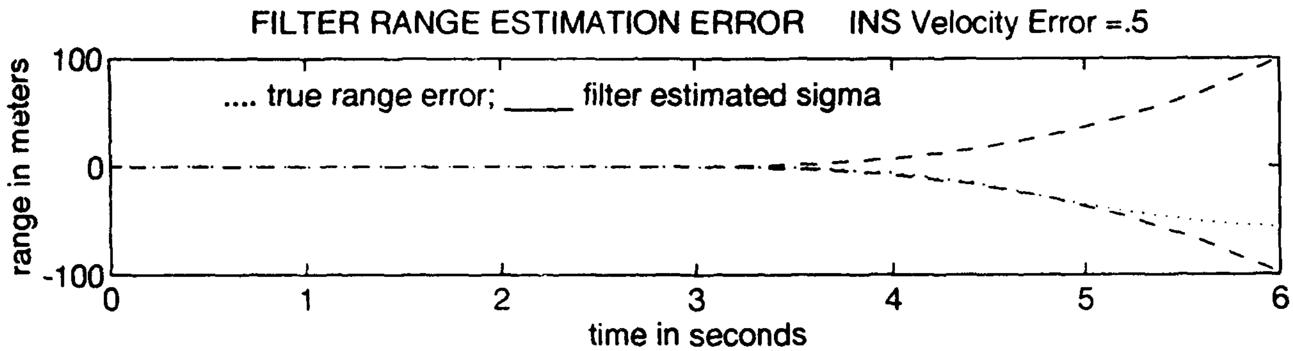
FILTER RANGE ESTIMATION ERROR INS Velocity Error =.5
.... true range error; ____ filter estimated sigma
range in meters
100
0
-100
0
1
2
3
4
5
6
time in seconds

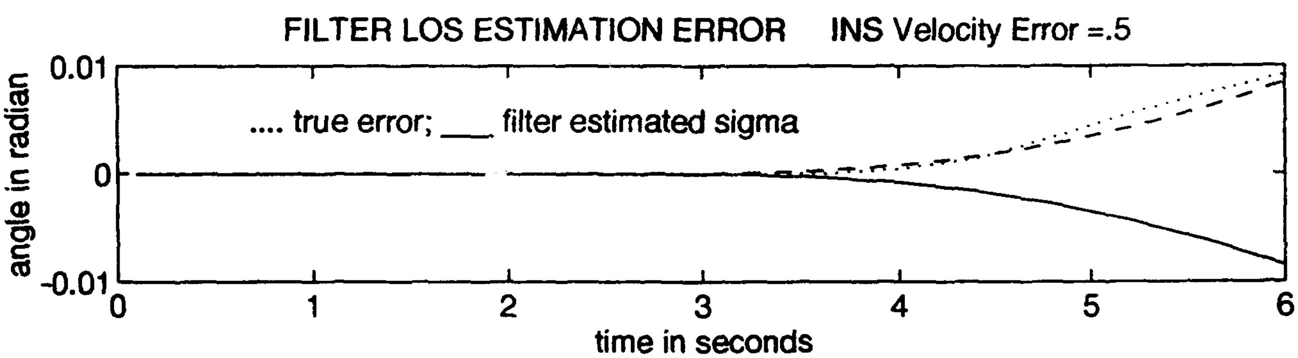
FILTER LOS ESTIMATION ERROR INS Velocity Error =.5
.... true error; ___ filter estimated sigma
angle in radian
0.01
0
-0.01
0
1
2
3
4
5
6
time in seconds

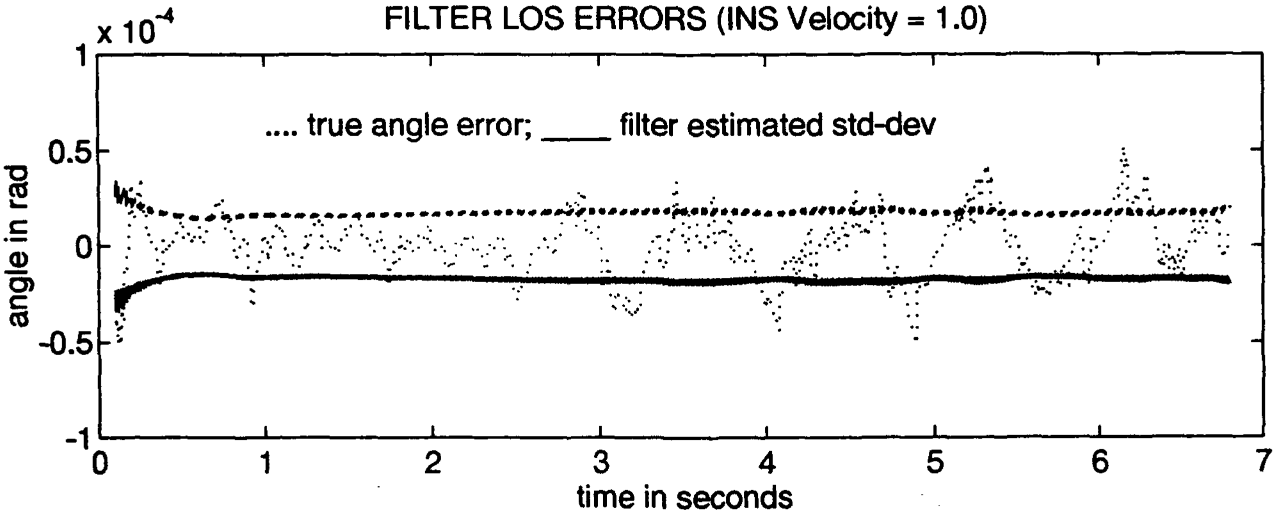
FILTER LOS ERRORS (INS Velocity = 1.0)
x 10^-4
.... true angle error; ____ filter estimated std-dev
angle in rad
time in seconds
1
0.5
0
-0.5
-1
0 1 2 3 4 5 6 7

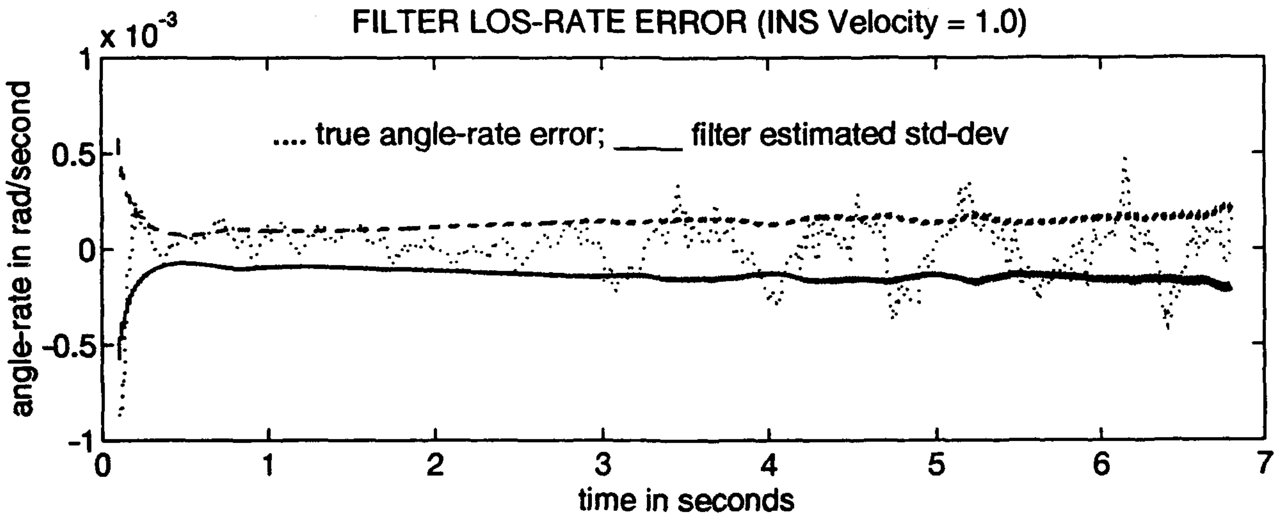
FILTER LOS-RATE ERROR (INS Velocity = 1.0)
x 10^-3
.... true angle-rate error; ____ filter estimated std-dev
angle-rate in rad/second
time in seconds
1
0.5
0
-0.5
-1
0 1 2 3 4 5 6 7

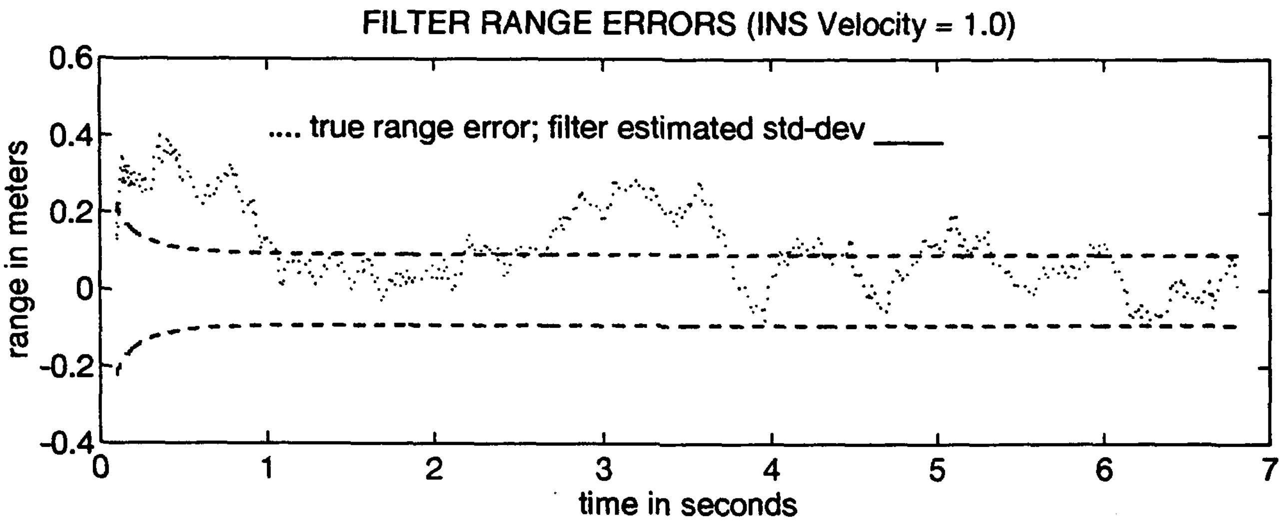
FILTER RANGE ERRORS (INS Velocity = 1.0)
.... true range error; filter estimated std-dev ____
range in meters
0.6
0.4
0.2
0
-0.2
-0.4
0
1
2
3
4
5
6
7
time in seconds

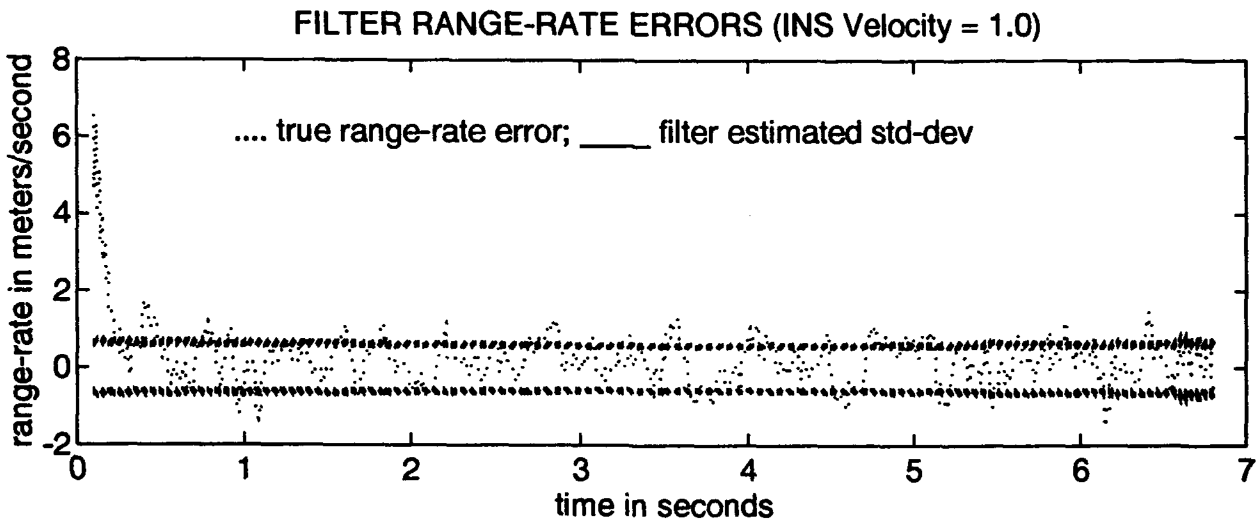
FILTER RANGE-RATE ERRORS (INS Velocity = 1.0)
.... true range-rate error; ____ filter estimated std-dev
range-rate in meters/second
8
6
4
2
0
-2
0
1
2
3
4
5
6
7
time in seconds

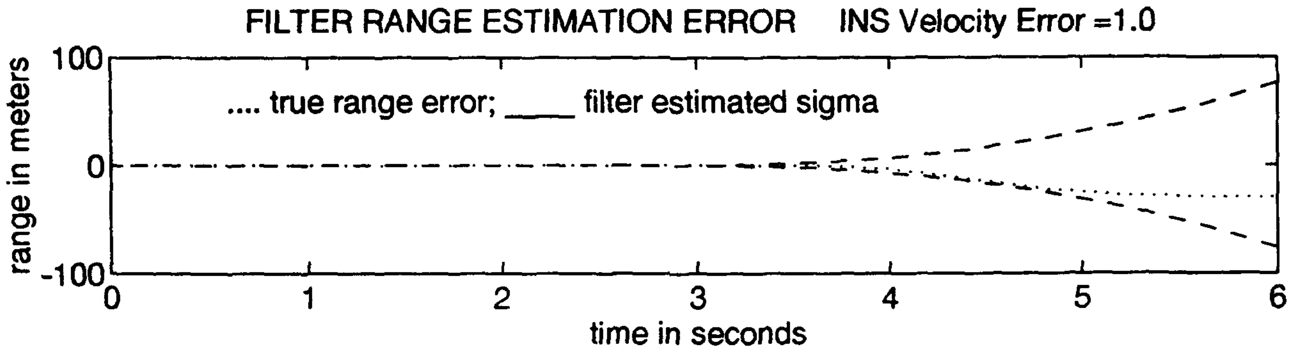
FILTER RANGE ESTIMATION ERROR INS Velocity Error =1.0
.... true range error; ____ filter estimated sigma
range in meters
100
0
-100
0
1
2
3
4
5
6
time in seconds

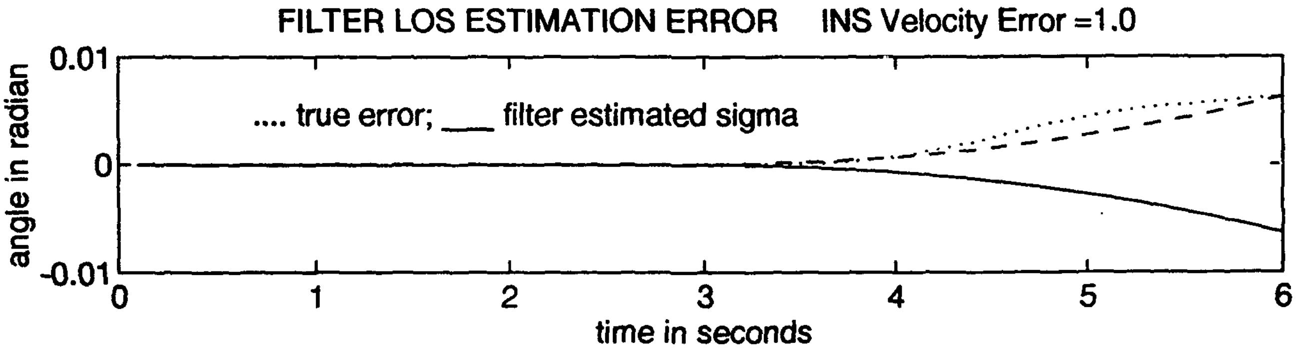
FILTER LOS ESTIMATION ERROR INS Velocity Error =1.0
.... true error; ___ filter estimated sigma
angle in radian
0.01
0
-0.01
0
1
2
3
4
5
6
time in seconds

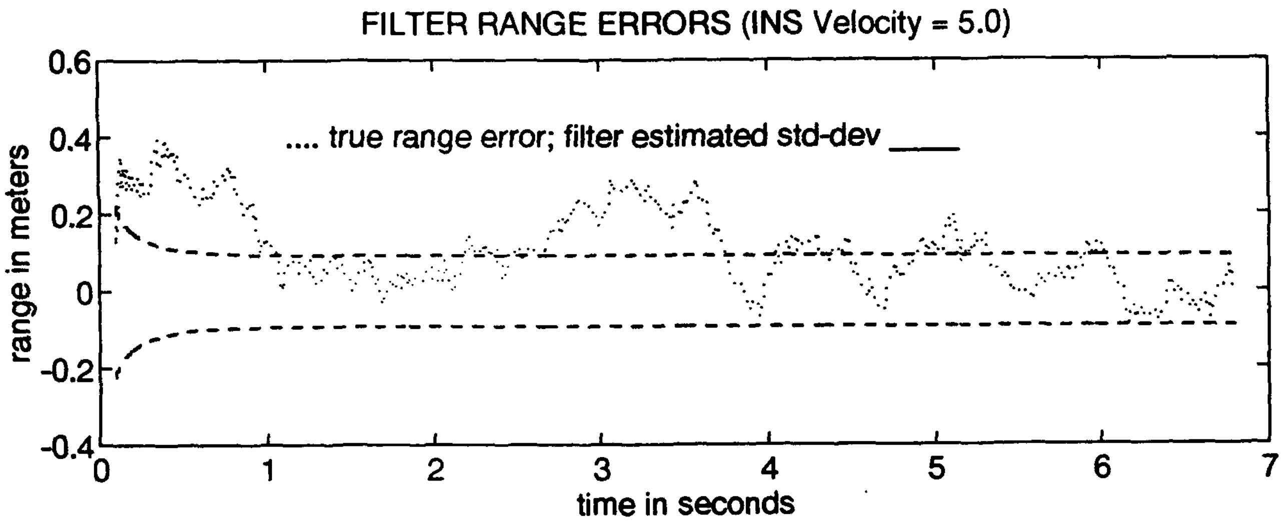
FILTER RANGE ERRORS (INS Velocity = 5.0)
.... true range error; filter estimated std-dev ____
range in meters
time in seconds
0.6
0.4
0.2
0
-0.2
-0.4
0
1
2
3
4
5
6
7

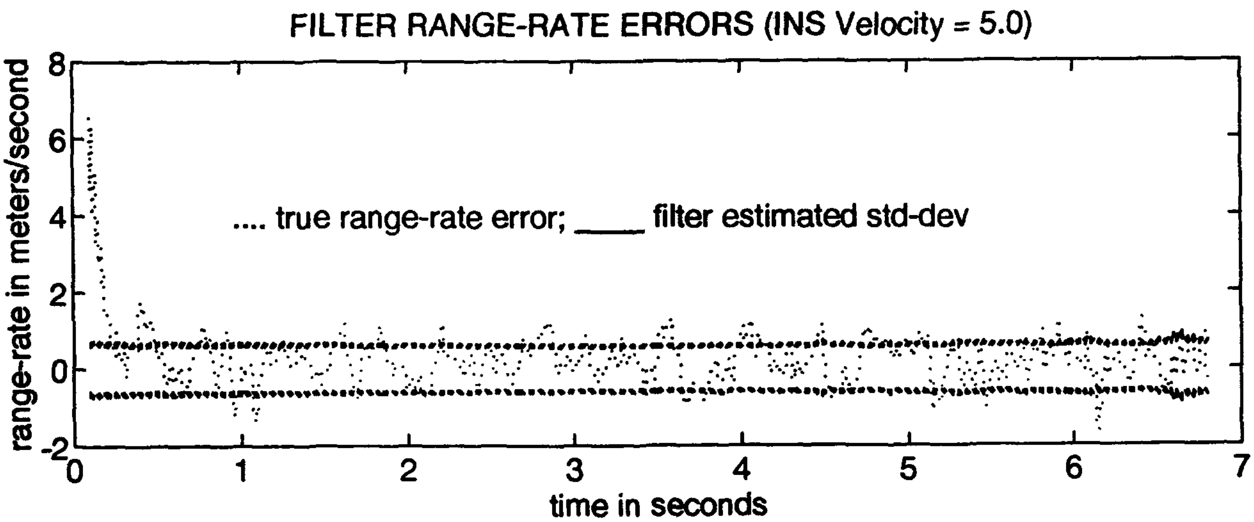
FILTER RANGE-RATE ERRORS (INS Velocity = 5.0)
.... true range-rate error; ____ filter estimated std-dev
range-rate in meters/second
time in seconds
8
6
4
2
0
-2
0
1
2
3
4
5
6
7

FILTER LOS ERRORS (INS Velocity = 5.0)

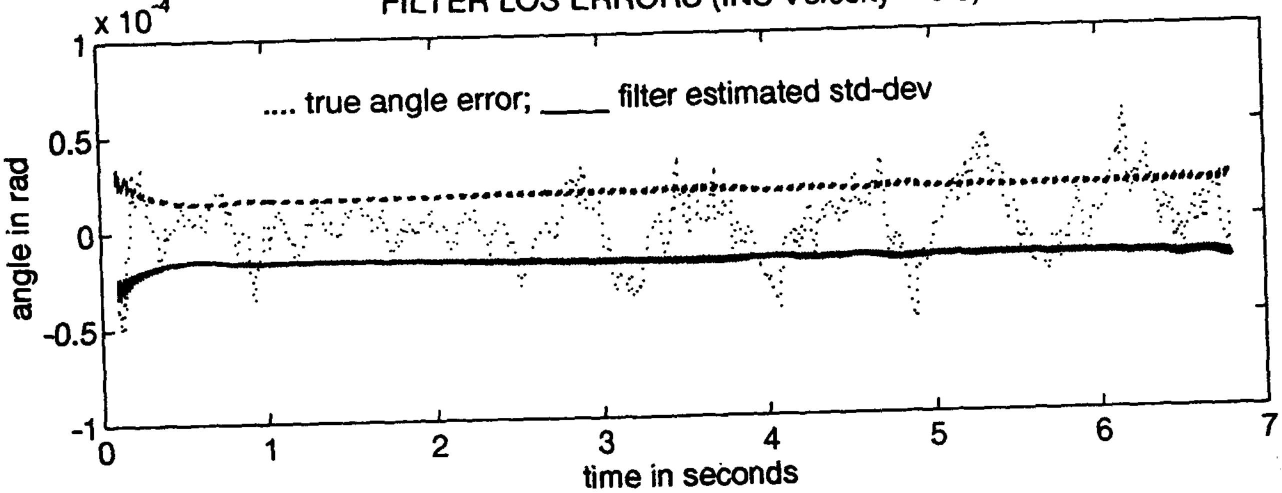

FILTER LOS-RATE ERROR (INS Velocity = 5.0)

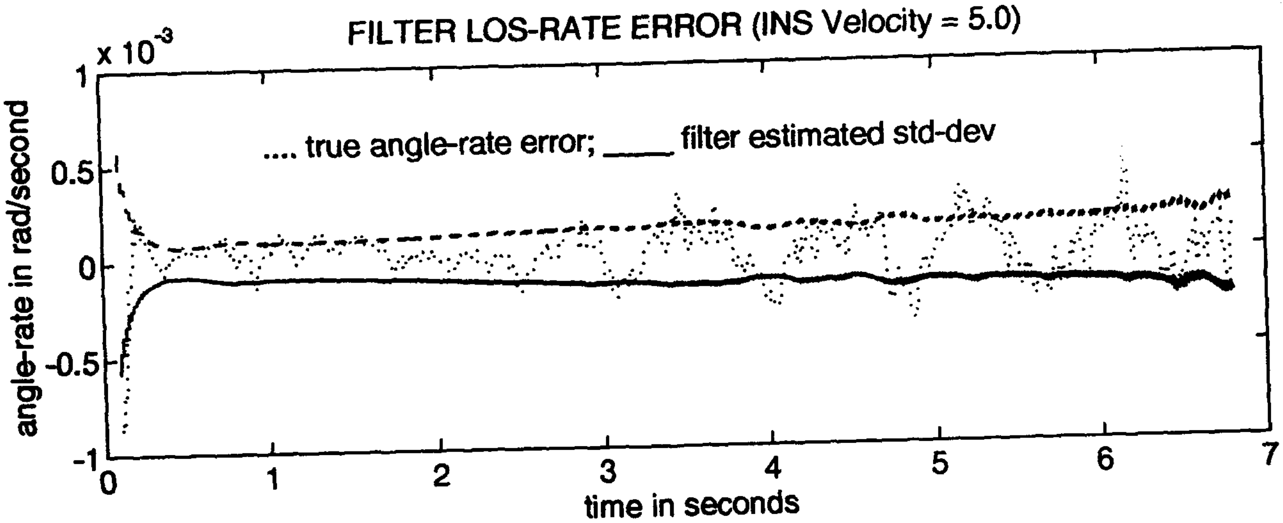

FILTER RANGE ESTIMATION ERROR   INS Velocity Error =5.0

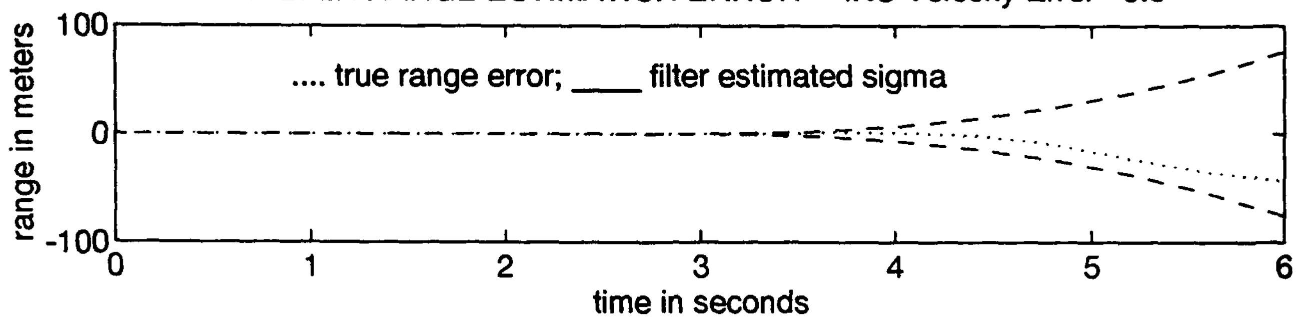

FILTER LOS ESTIMATION ERROR   INS Velocity Error =5.0

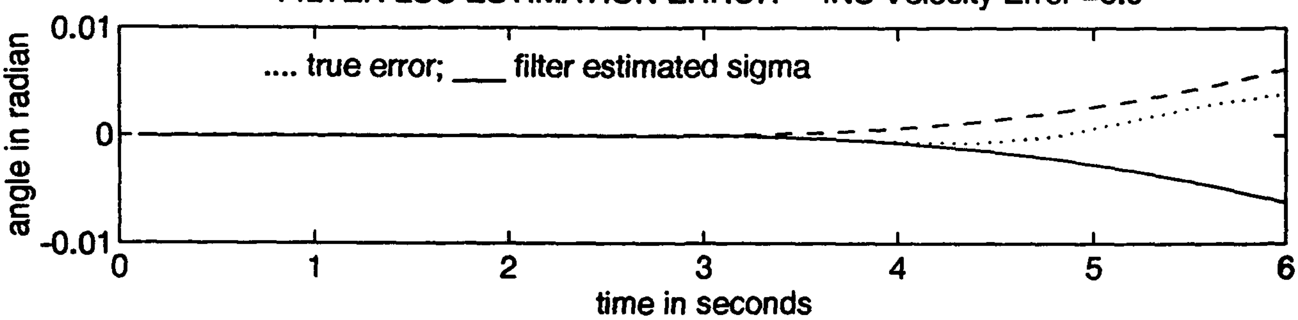

Appendix H

This appendix contains simulation plots for the pilot induced error run sets. The aircraft is initially heading east and beginning a 3 g turn to the north. All dynamic noise strengths and measurement noises (except pilot error) are set at baseline values. INS acceleration measurements are turned off. Noise diffussion strength representing pilot induced error is varied from the $(0.1g)^2$/sec baseline value to $(0.5g)^2$/sec in $(0.1g)^2$/sec increments. The missile is launched from the $\pi/4$ approach angle. Each run has a trajectory plot, estimated range errors, range-rate errors, LOS errors and LOS-rate errors. Estimated range and LOS plots are found in the $\pi/4$ missile approach angle run plots in Appendix A. Each plot set contains filter divergence plots of range error and angle error for a three second divergence from three to six seconds. The divergence plots, which define the volume cross-section, are used for performance comparison versus the baseline (Figure 4-4).

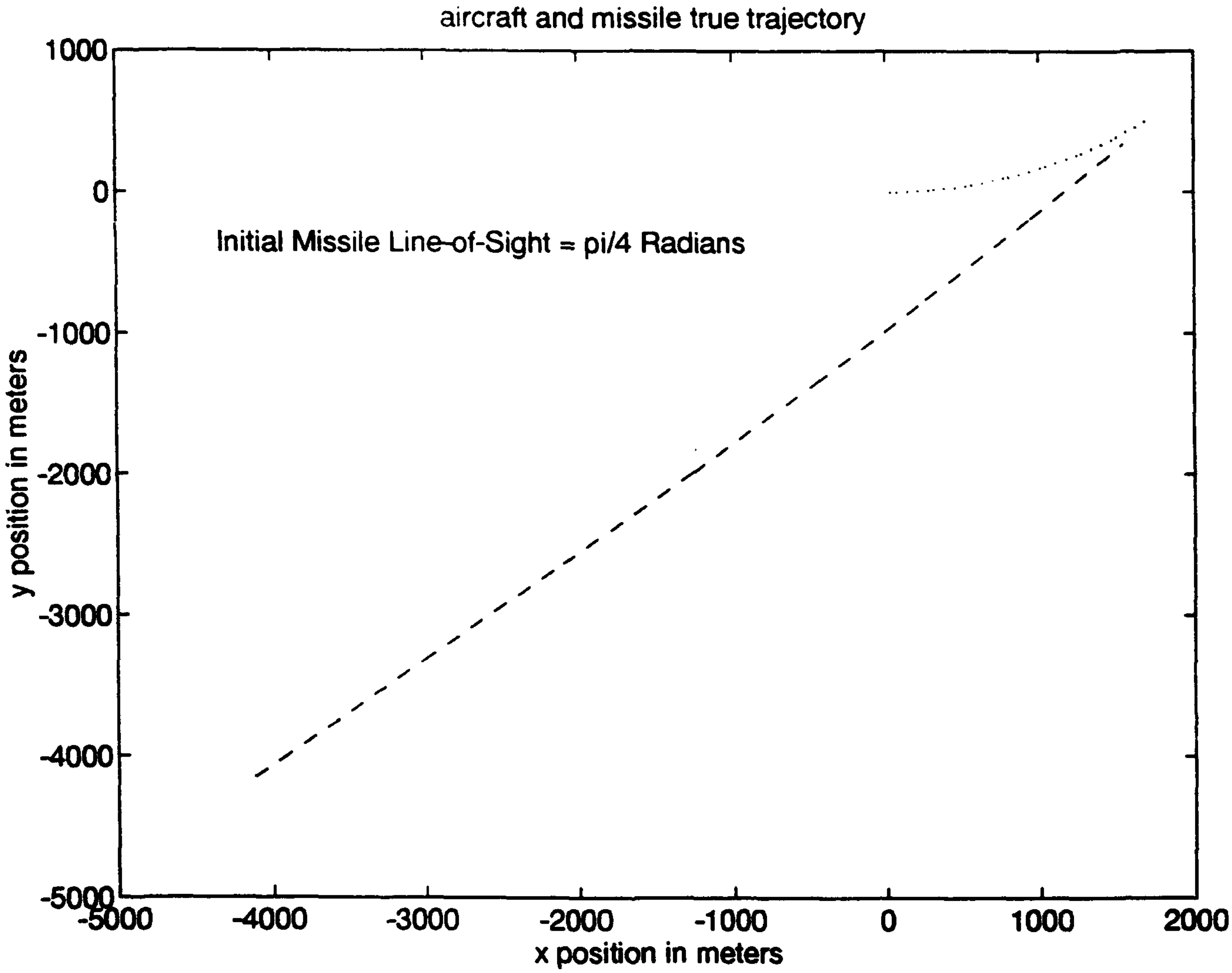
aircraft and missile true trajectory
1000
0
-1000
-2000
-3000
-4000
-5000
Initial Missile Line-of-Sight = pi/4 Radians
y position in meters
-5000
-4000
-3000
-2000
-1000
0
1000
2000
x position in meters

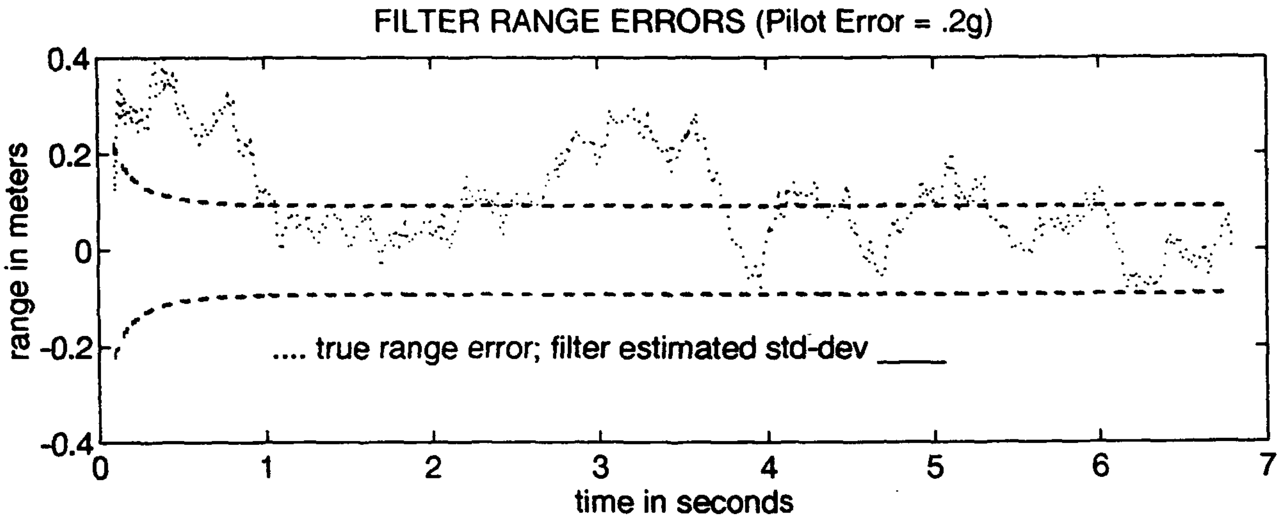
FILTER RANGE ERRORS (Pilot Error = .2g)
range in meters
.... true range error; filter estimated std-dev ____
time in seconds
0.4
0.2
0
-0.2
-0.4
0
1
2
3
4
5
6
7

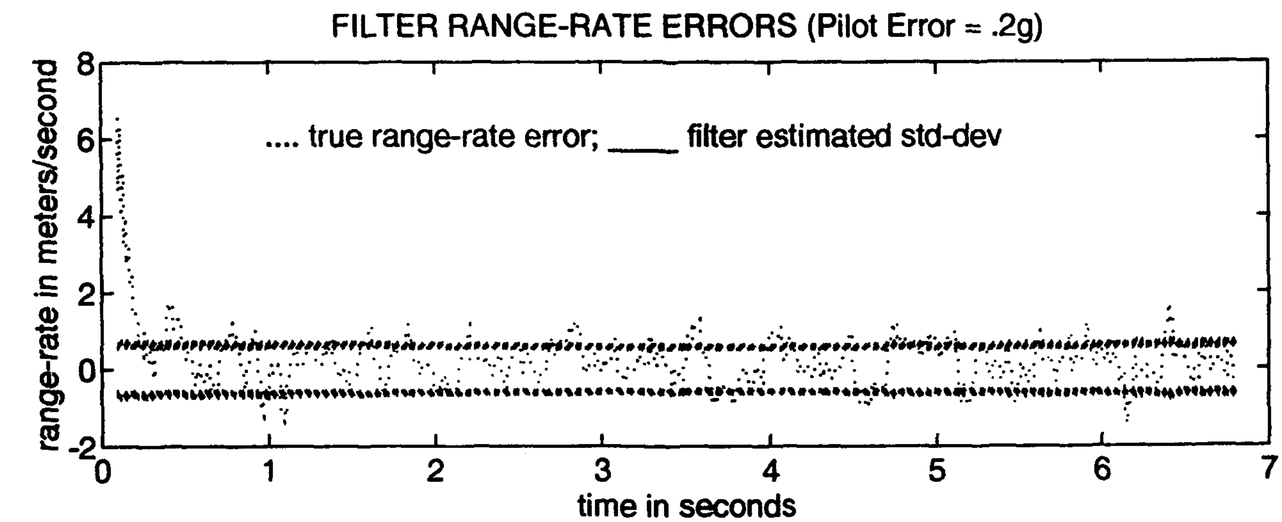
FILTER RANGE-RATE ERRORS (Pilot Error = .2g)
range-rate in meters/second
.... true range-rate error; ____ filter estimated std-dev
time in seconds
8
6
4
2
0
-2
0
1
2
3
4
5
6
7

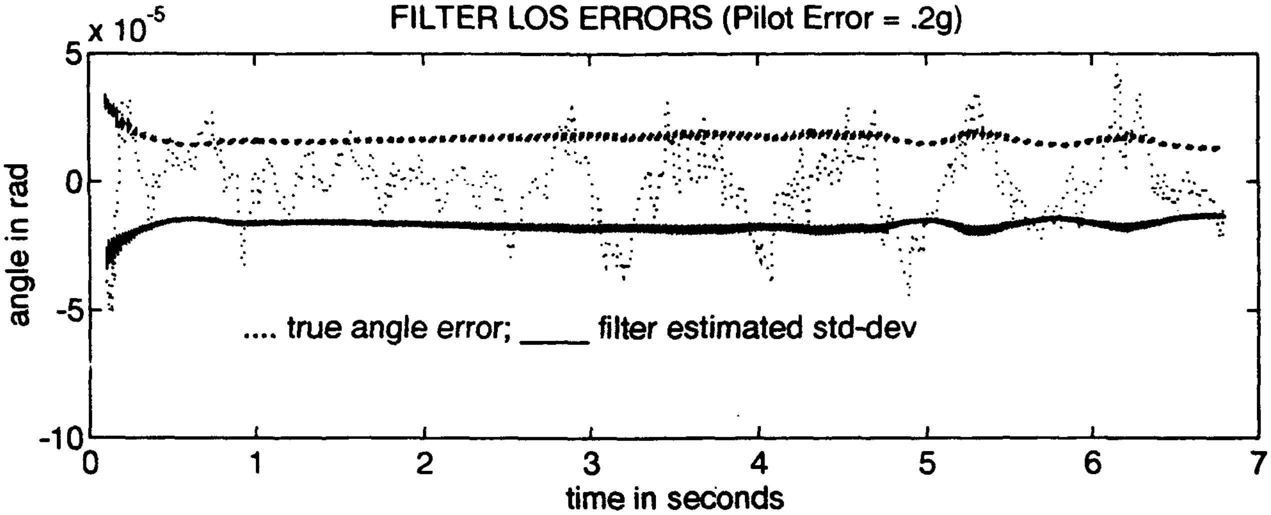
FILTER LOS ERRORS (Pilot Error = .2g)
x 10^-5
5
0
-5
-10
angle in rad
.... true angle error; ____ filter estimated std-dev
0
1
2
3
4
5
6
7
time in seconds

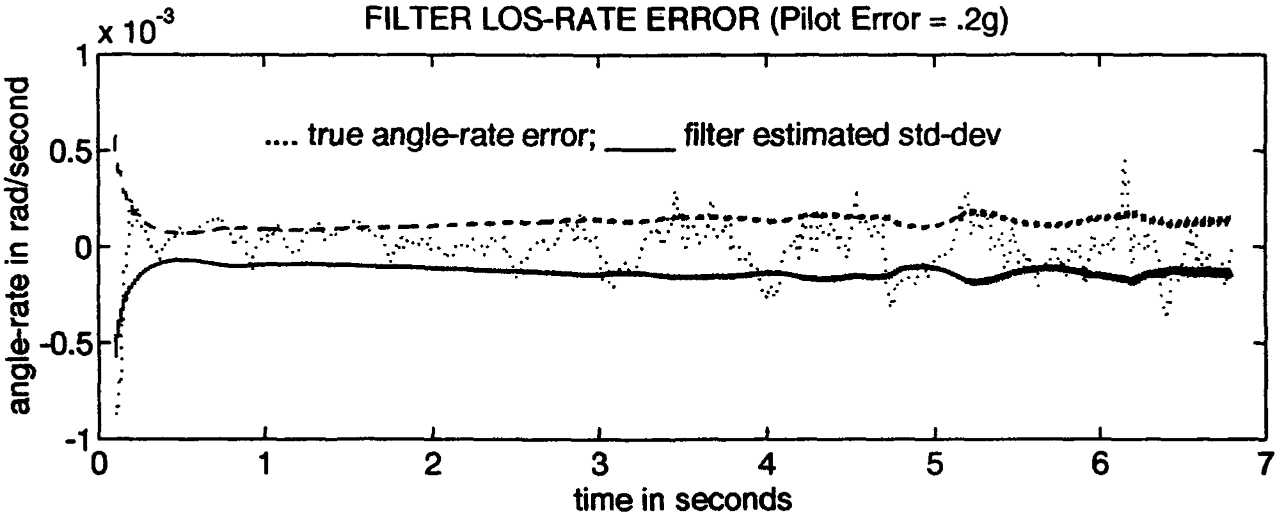
FILTER LOS-RATE ERROR (Pilot Error = .2g)
x 10^-3
1
0.5
0
-0.5
-1
angle-rate in rad/second
.... true angle-rate error; ____ filter estimated std-dev
0
1
2
3
4
5
6
7
time in seconds

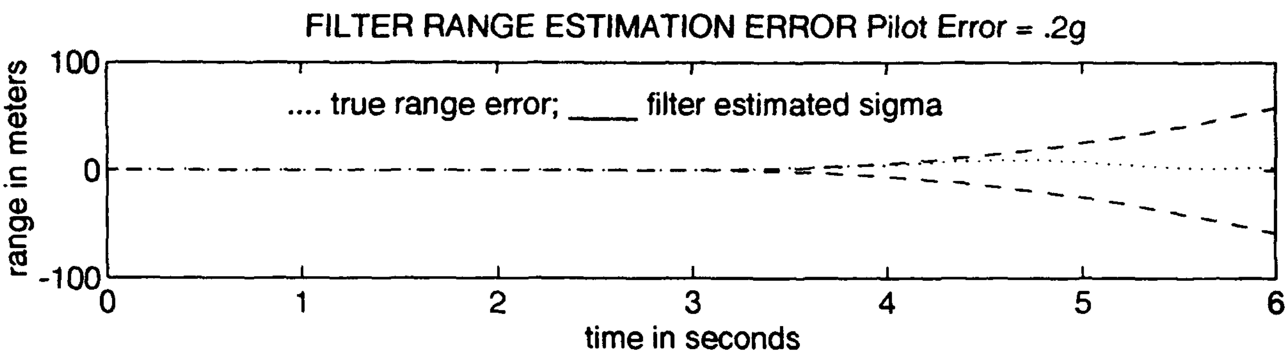
FILTER RANGE ESTIMATION ERROR Pilot Error = .2g
.... true range error; _____ filter estimated sigma
range in meters
100
0
-100
0
1
2
3
4
5
6
time in seconds

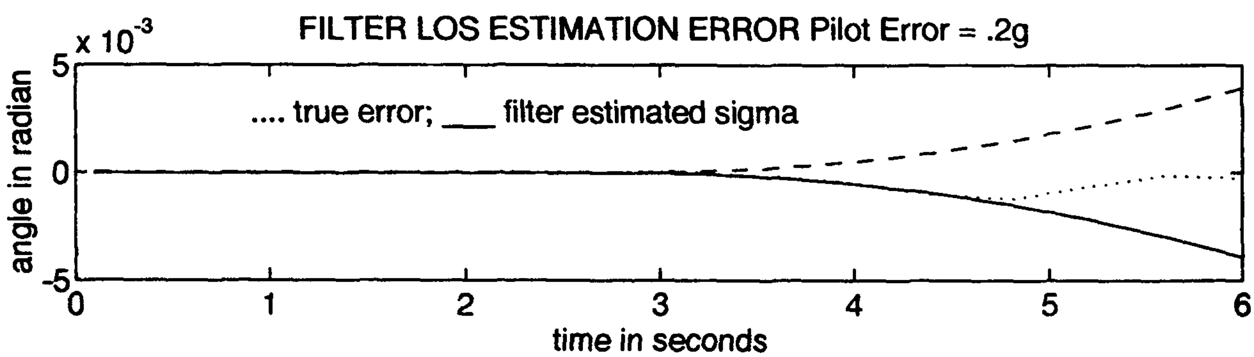
FILTER LOS ESTIMATION ERROR Pilot Error = .2g
x 10^-3
.... true error; ___ filter estimated sigma
angle in radian
5
0
-5
0
1
2
3
4
5
6
time in seconds

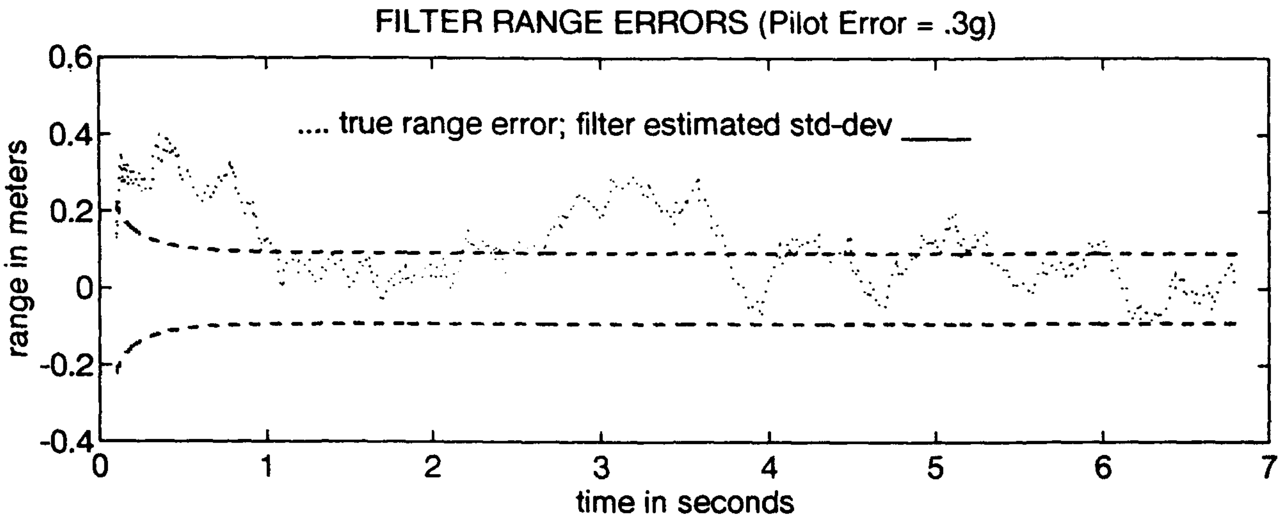

FILTER RANGE ERRORS (Pilot Error = .3g)
.... true range error; filter estimated std-dev ____
range in meters
0.6
0.4
0.2
0
-0.2
-0.4
0
1
2
3
4
5
6
7
time in seconds

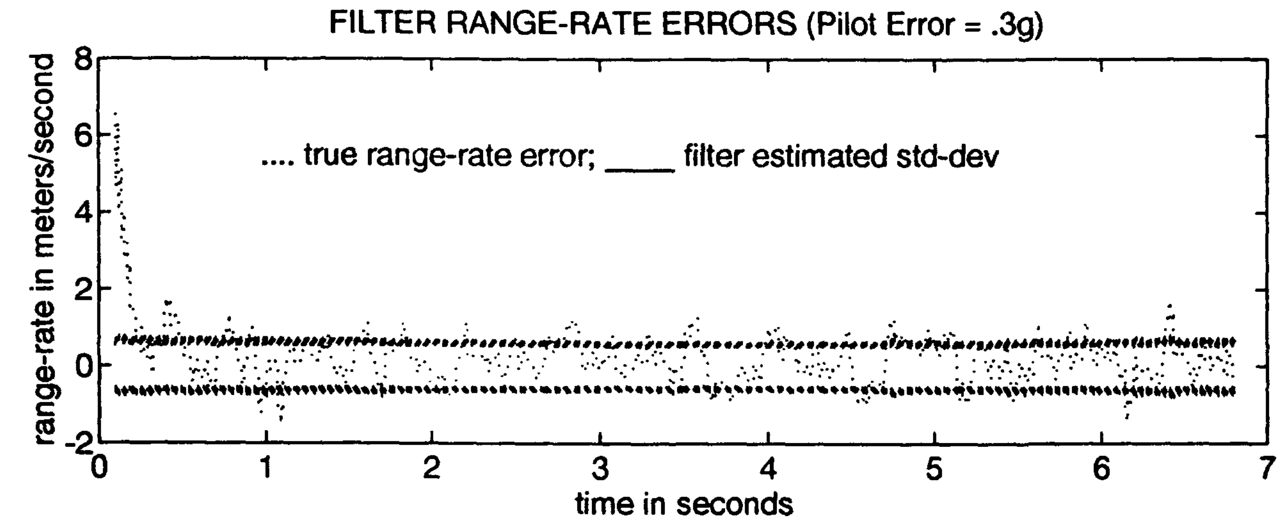

FILTER RANGE-RATE ERRORS (Pilot Error = .3g)
.... true range-rate error; ____ filter estimated std-dev
range-rate in meters/second
8
6
4
2
0
-2
0
1
2
3
4
5
6
7
time in seconds

FILTER LOS ERRORS (Pilot Error = .3g)

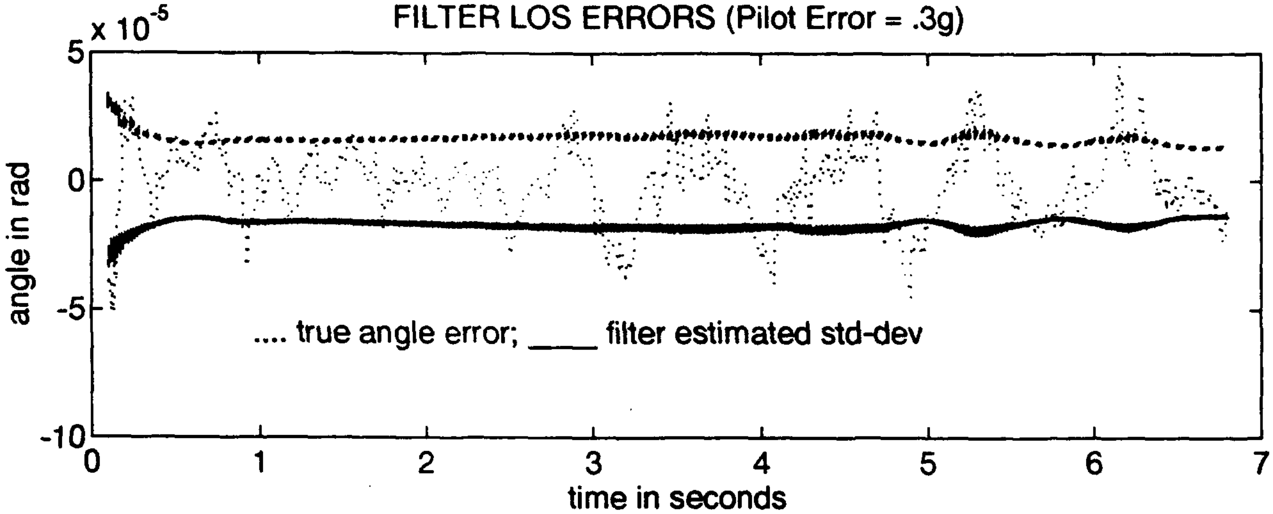

FILTER LOS-RATE ERROR (Pilot Error = .3g)

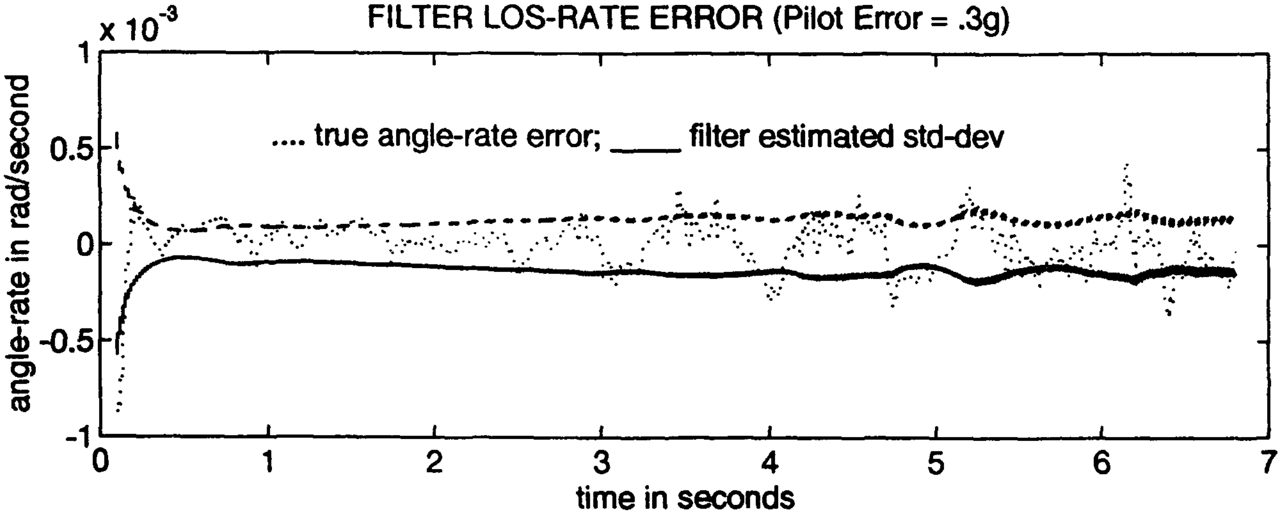

FILTER RANGE ESTIMATION ERROR Pilot Error = .3g

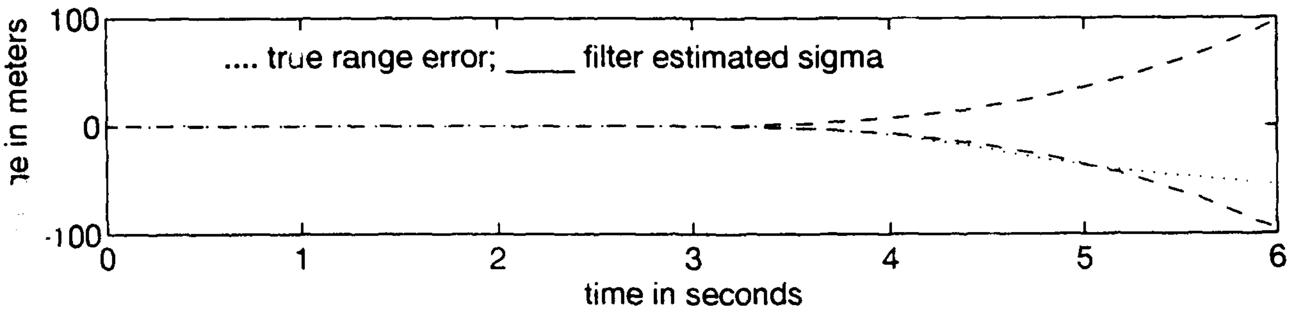

FILTER LOS ESTIMATION ERROR Pilot Error = .3g

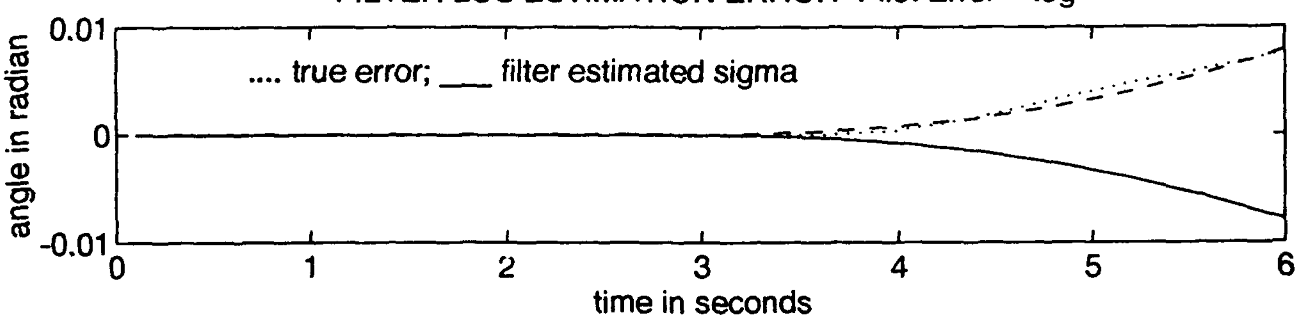

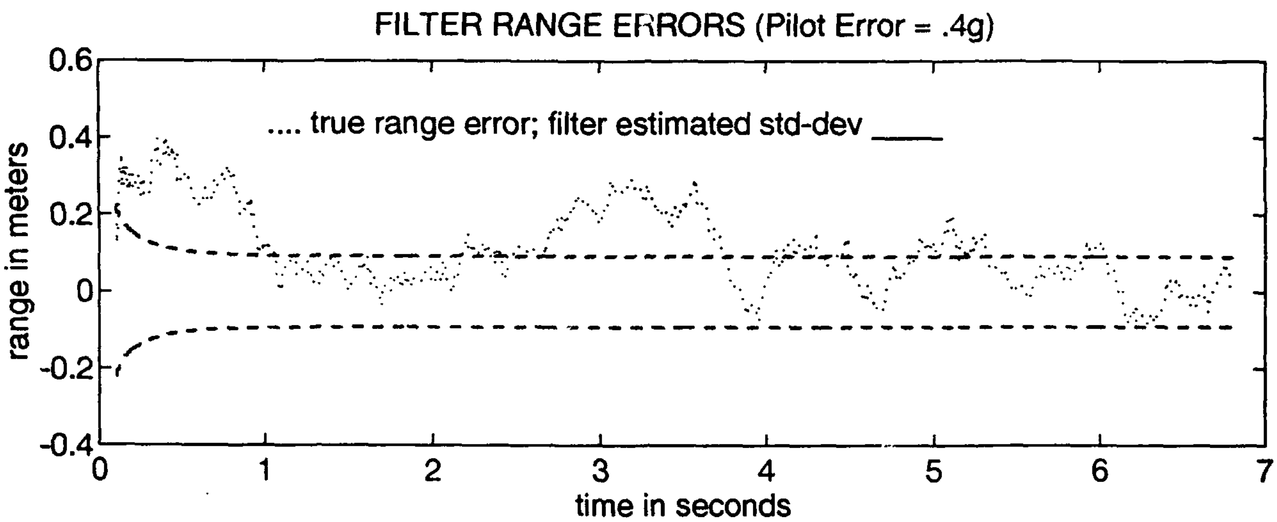
FILTER RANGE ERRORS (Pilot Error = .4g)
.... true range error; filter estimated std-dev ____
range in meters
time in seconds

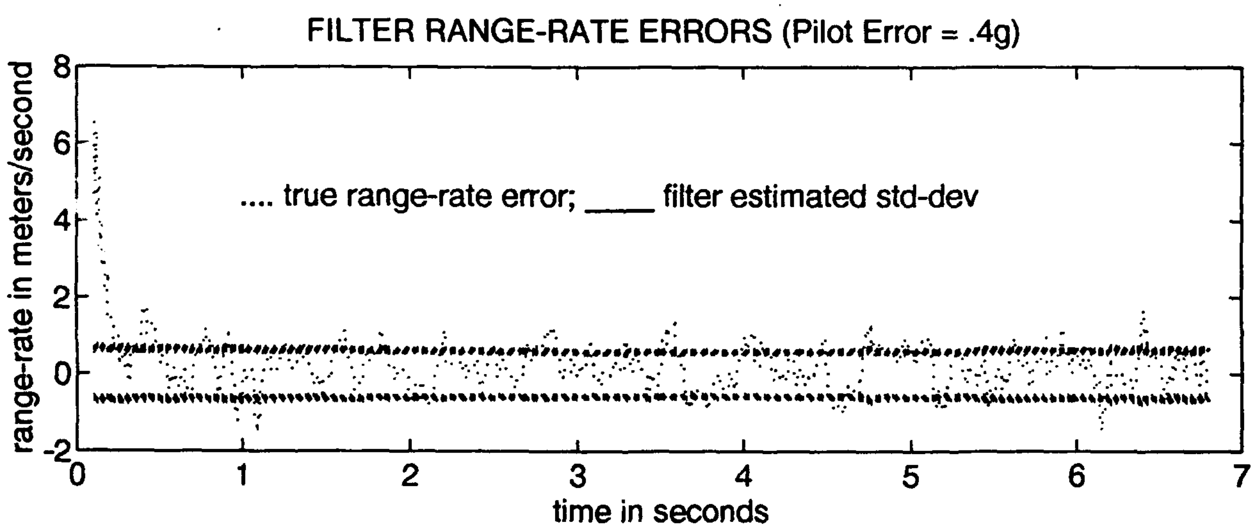
FILTER RANGE-RATE ERRORS (Pilot Error = .4g)
.... true range-rate error; ____ filter estimated std-dev
range-rate in meters/second
time in seconds

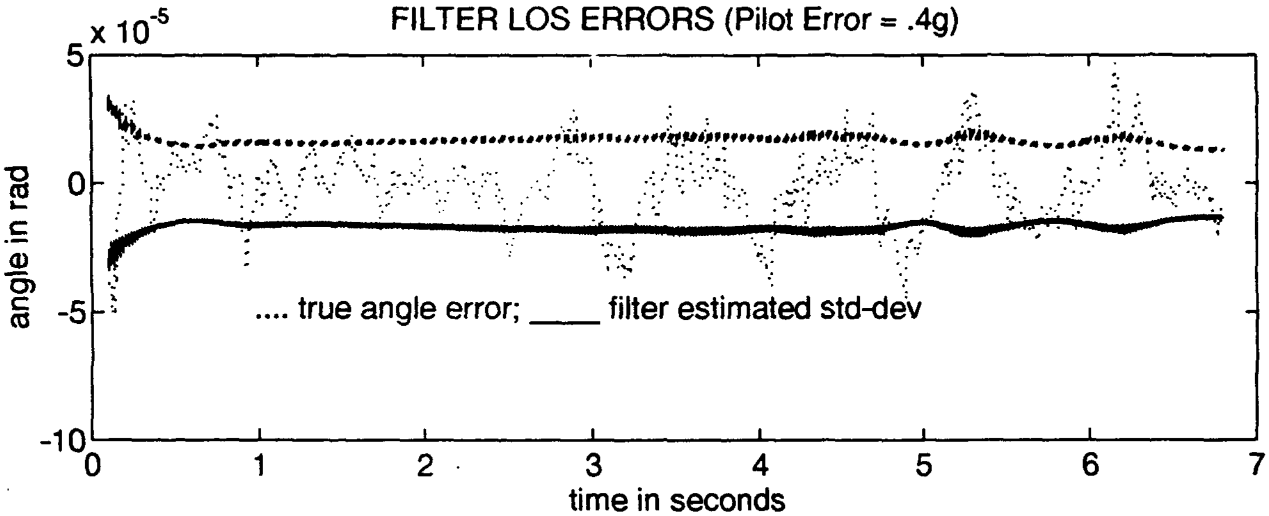

FILTER LOS ERRORS (Pilot Error = .4g)
x 10^-5
5
0
-5
-10
angle in rad
.... true angle error; ____ filter estimated std-dev
0
1
2
3
4
5
6
7
time in seconds

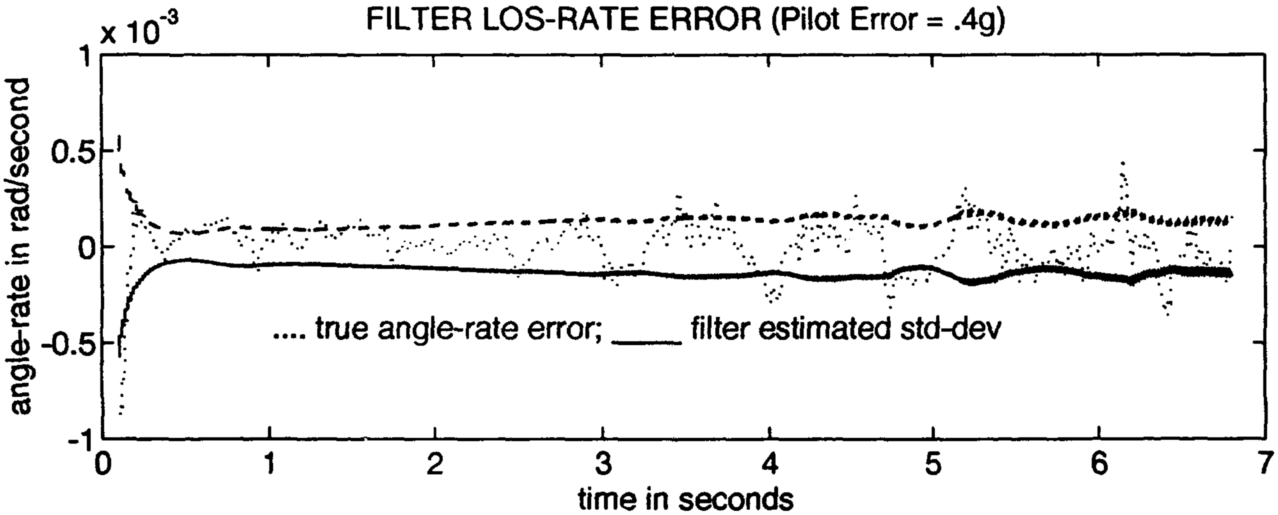

FILTER LOS-RATE ERROR (Pilot Error = .4g)
x 10^-3
1
0.5
0
-0.5
-1
angle-rate in rad/second
.... true angle-rate error; ____ filter estimated std-dev
0
1
2
3
4
5
6
7
time in seconds

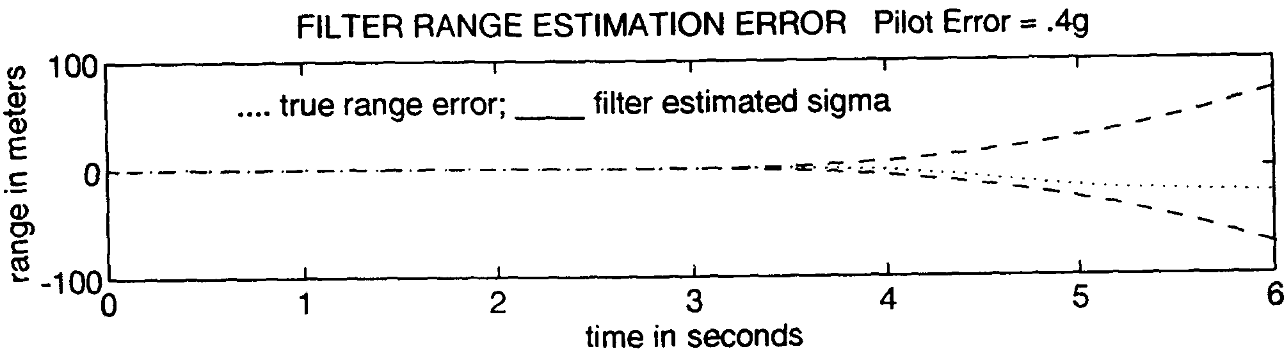
FILTER RANGE ESTIMATION ERROR Pilot Error = .4g
.... true range error; ____ filter estimated sigma
range in meters
100
0
-100
0
1
2
3
4
5
6
time in seconds

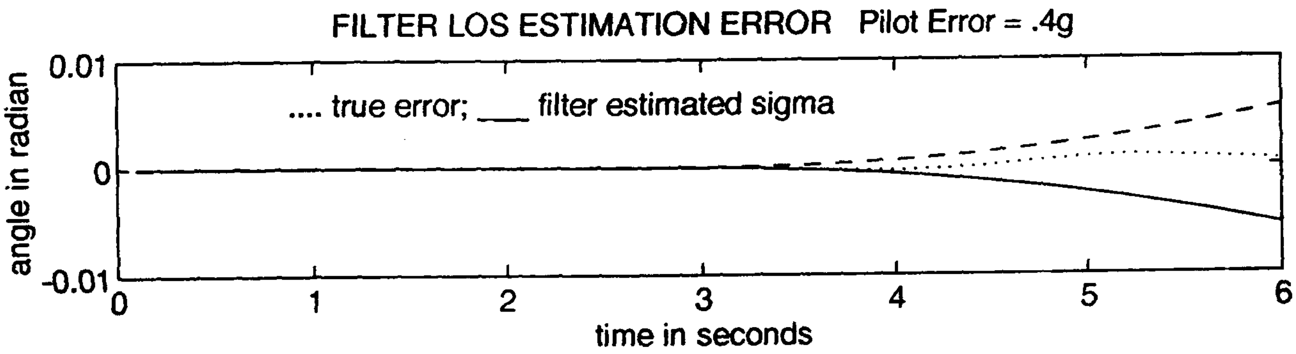
FILTER LOS ESTIMATION ERROR Pilot Error = .4g
.... true error; ___ filter estimated sigma
angle in radian
0.01
0
-0.01
0
1
2
3
4
5
6
time in seconds

FILTER RANGE ERRORS (Pilot Error = .5g)

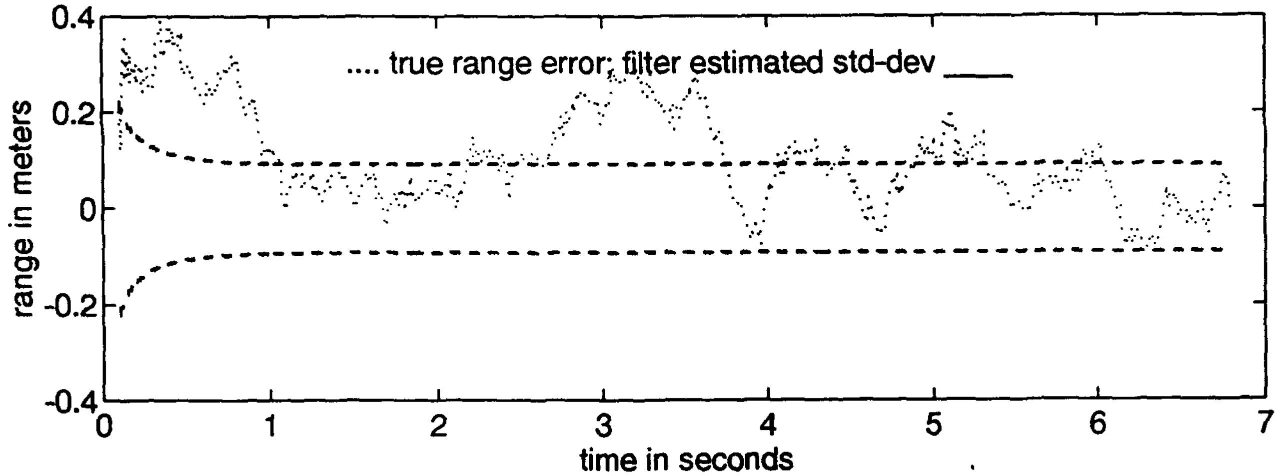

FILTER RANGE-RATE ERRORS (Pilot Error = .5g)

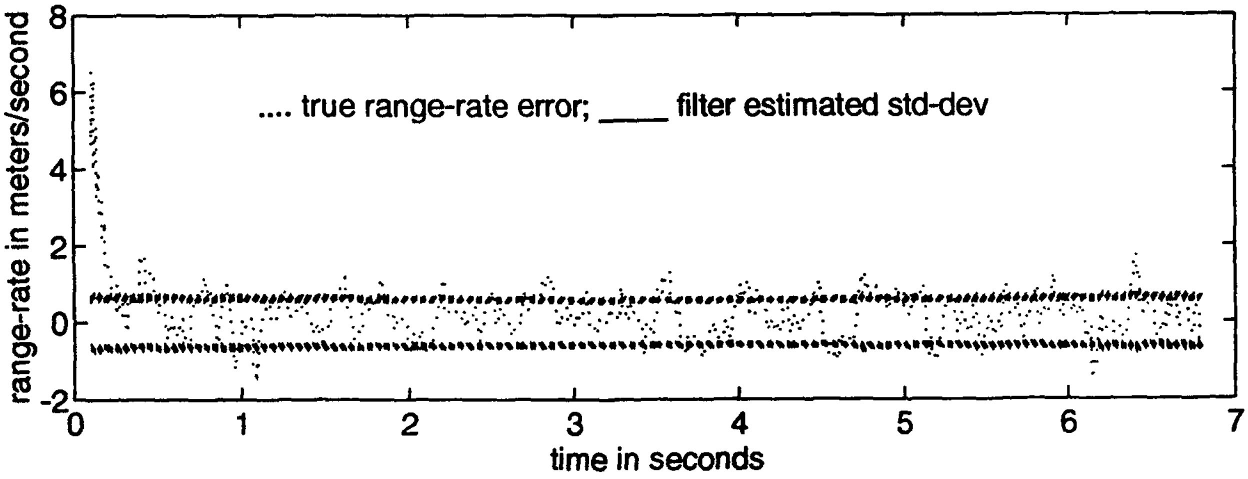

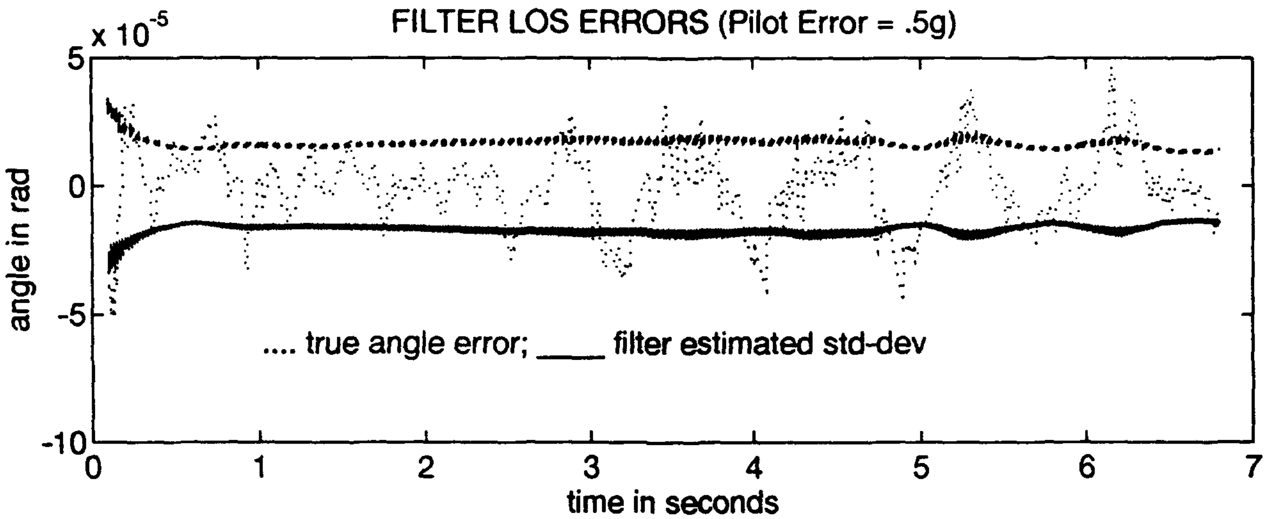

FILTER LOS ERRORS (Pilot Error = .5g)
x 10^-5
5
0
-5
-10
angle in rad
.... true angle error; ____ filter estimated std-dev
0
1
2
3
4
5
6
7
time in seconds

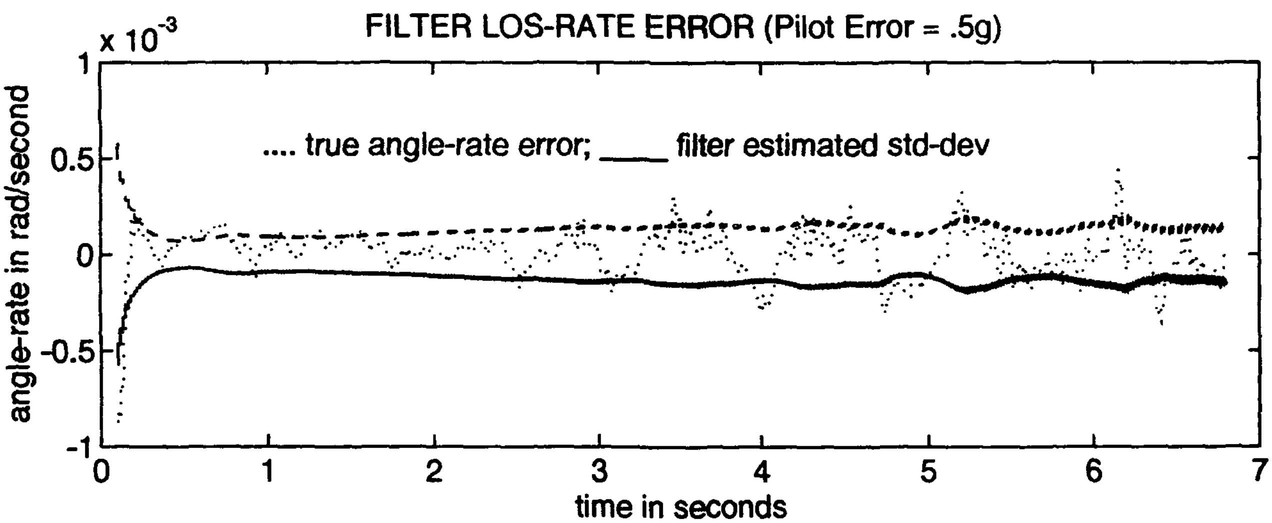

FILTER LOS-RATE ERROR (Pilot Error = .5g)
x 10^-3
1
0.5
0
-0.5
-1
angle-rate in rad/second
.... true angle-rate error; ____ filter estimated std-dev
0
1
2
3
4
5
6
7
time in seconds

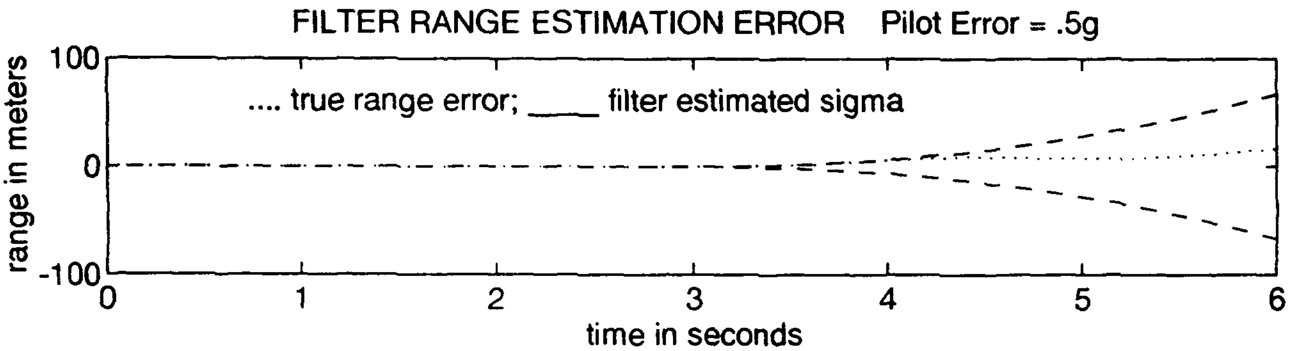
FILTER RANGE ESTIMATION ERROR Pilot Error = .5g
.... true range error; ____ filter estimated sigma
range in meters
100
0
-100
0
1
2
3
4
5
6
time in seconds

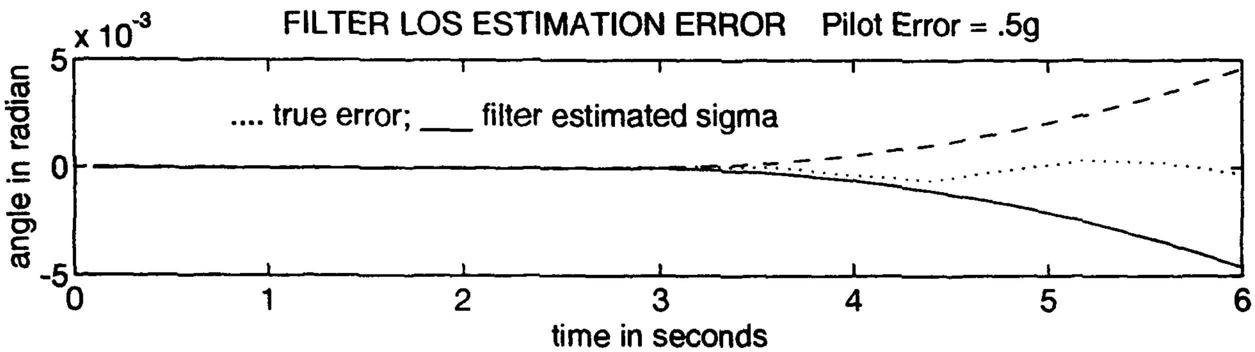
FILTER LOS ESTIMATION ERROR Pilot Error = .5g
x 10^-3
.... true error; ___ filter estimated sigma
angle in radian
5
0
-5
0
1
2
3
4
5
6
time in seconds

Appendix I

This appendix contains simulation plots for the aircraft turn-rate and n parameter run sets. The aircraft is initially heading east and beginning a turn to the north. The turn rate varies from 1.0 g to 5.0 g in 1.0 g increments. The n-parameter noise set at (0.25)/sec and 4.0/sec for each turn (except baseline which also includes an n parameter noise strength of (1.0)/sec). Baseline conditions are a 3g turn with n parameter noise strength set at (4.0)/sec All other dynamic noise strengths and measurement noises are set at baseline values. INS acceleration measurements are turned off. The missile is launched from the $\pi/4$ approach angle. Each turn set has a trajectory plot, estimated range errors, range-rate errors, LOS errors and LOS-rate errors. Each turn set contains filter divergence plots of range error and angle error for a three second divergence from three to six seconds for all values of n parameter noise. The divergence plots, which define the volume cross-section, are used for performance comparison versus the baseline (Figure 4-4).

aircraft and missile true trajectory (Aircraft 1g turn)

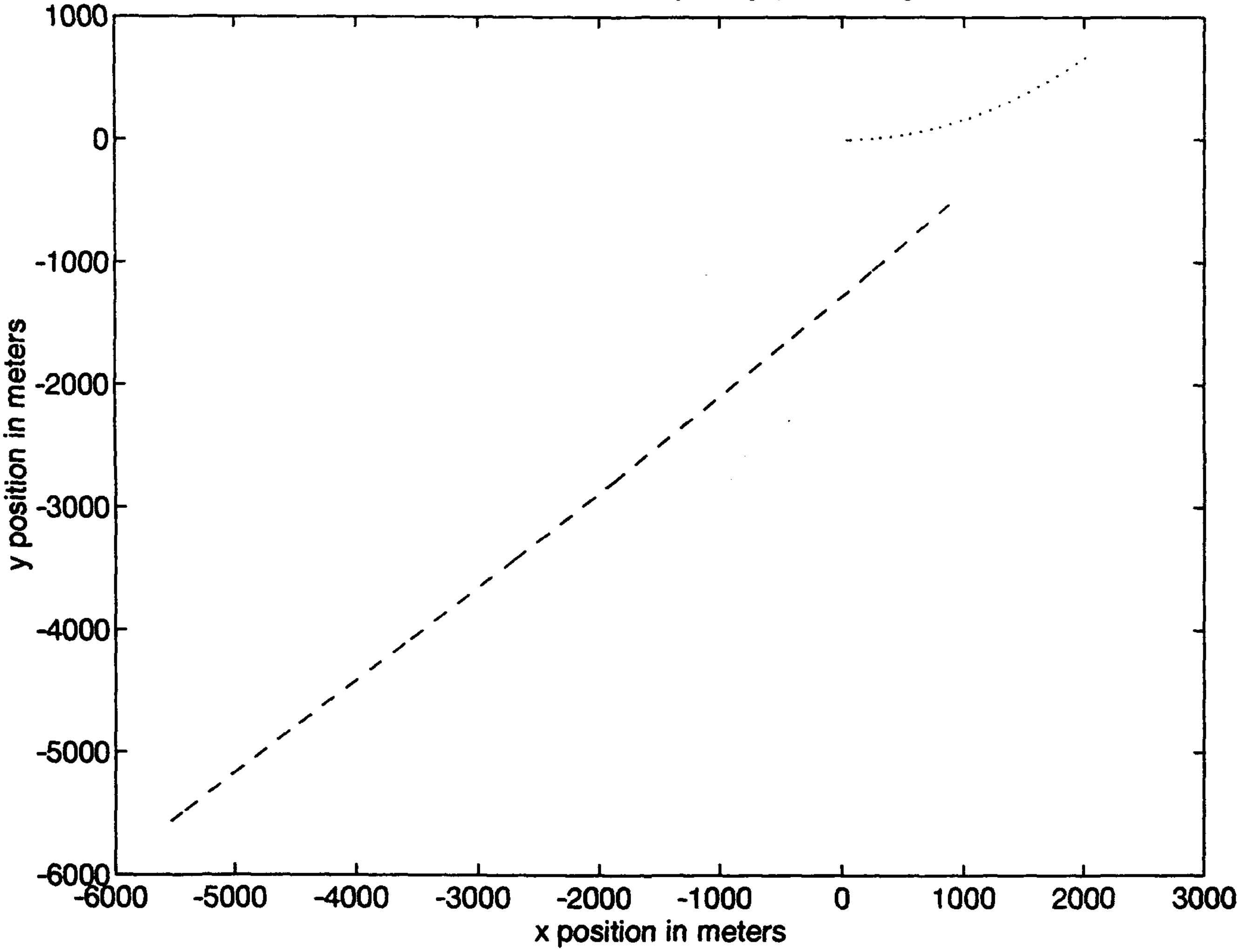

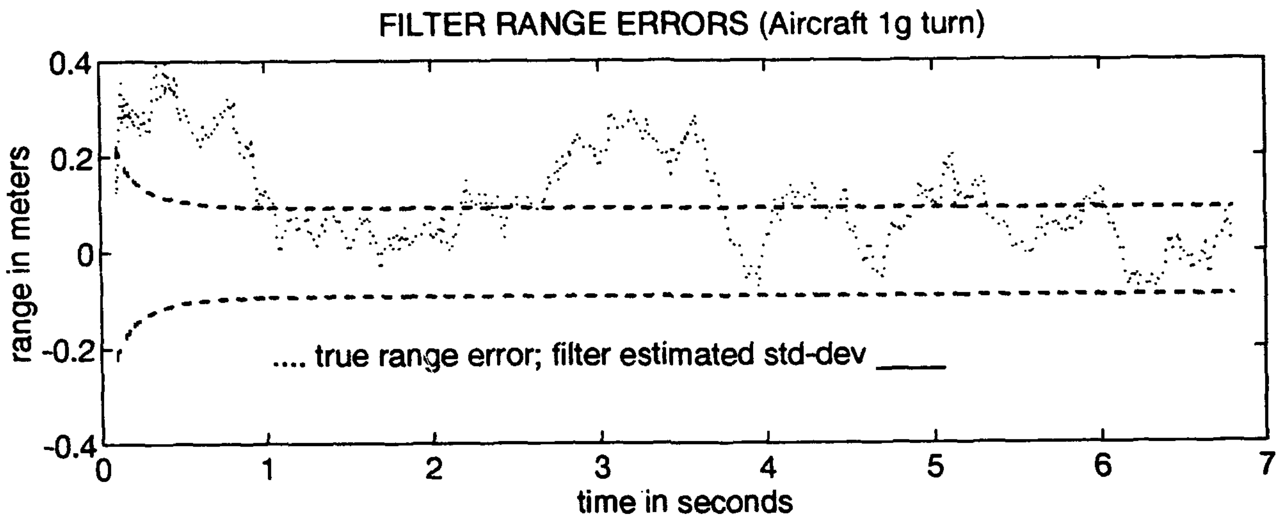
FILTER RANGE ERRORS (Aircraft 1g turn)
range in meters
0.4
0.2
0
-0.2
-0.4
0
1
2
3
4
5
6
7
time in seconds
.... true range error; filter estimated std-dev ____

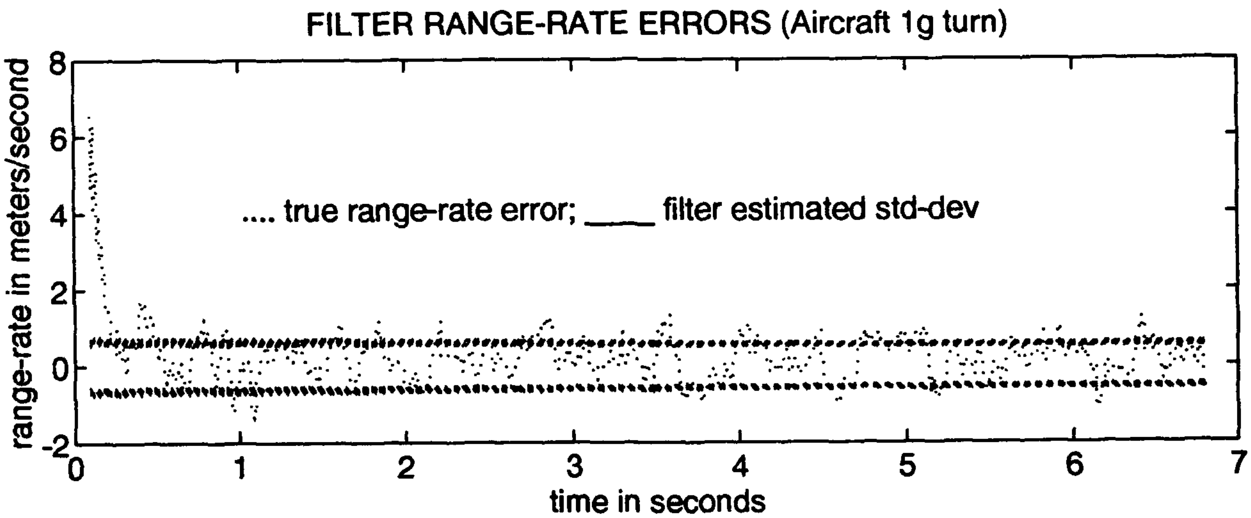
FILTER RANGE-RATE ERRORS (Aircraft 1g turn)
range-rate in meters/second
8
6
4
2
0
-2
0
1
2
3
4
5
6
7
time in seconds
.... true range-rate error; ____ filter estimated std-dev

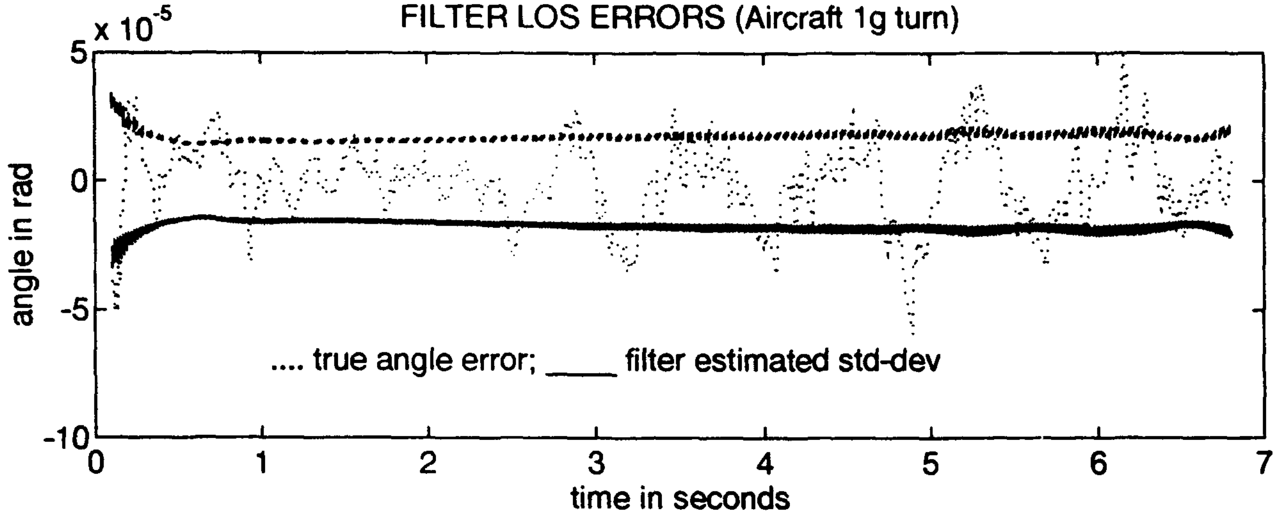
x 10^-5
FILTER LOS ERRORS (Aircraft 1g turn)
5
0
-5
-10
angle in rad
.... true angle error; ____ filter estimated std-dev
0
1
2
3
4
5
6
7
time in seconds

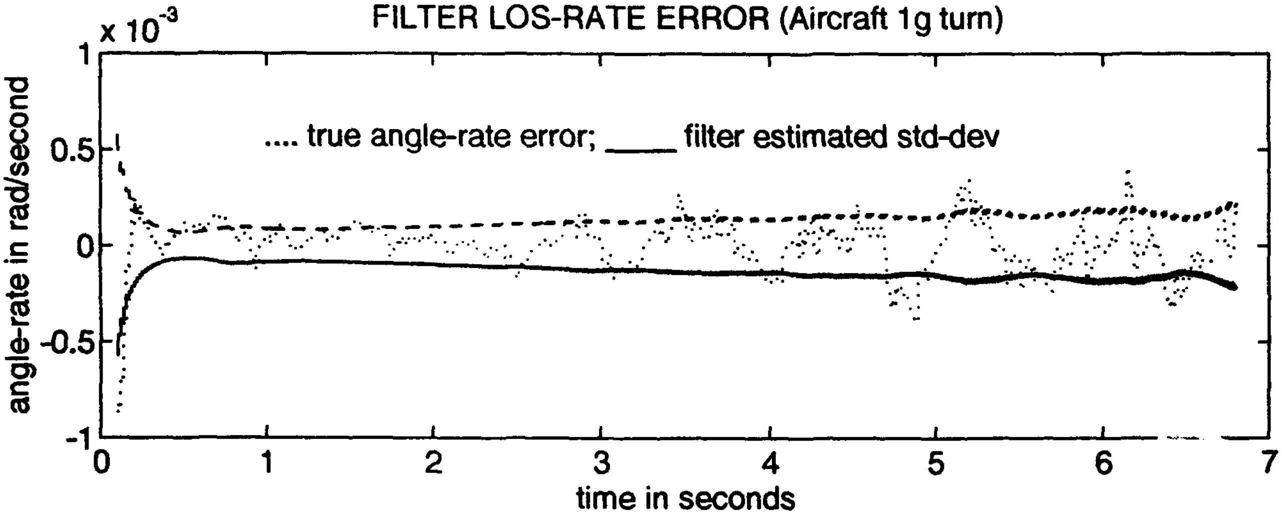
x 10^-3
FILTER LOS-RATE ERROR (Aircraft 1g turn)
1
0.5
0
-0.5
-1
angle-rate in rad/second
.... true angle-rate error; ____ filter estimated std-dev
0
1
2
3
4
5
6
7
time in seconds

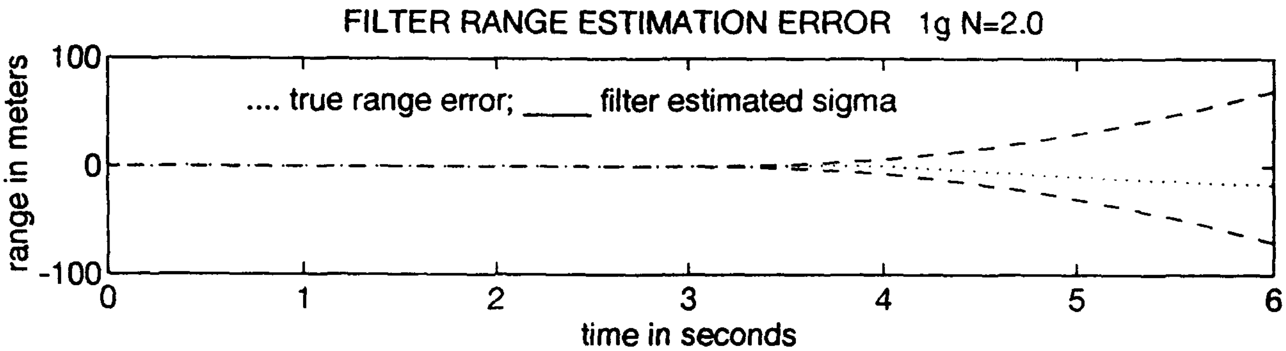
FILTER RANGE ESTIMATION ERROR 1g N=2.0
.... true range error; ____ filter estimated sigma
range in meters
100
0
-100
0
1
2
3
4
5
6
time in seconds

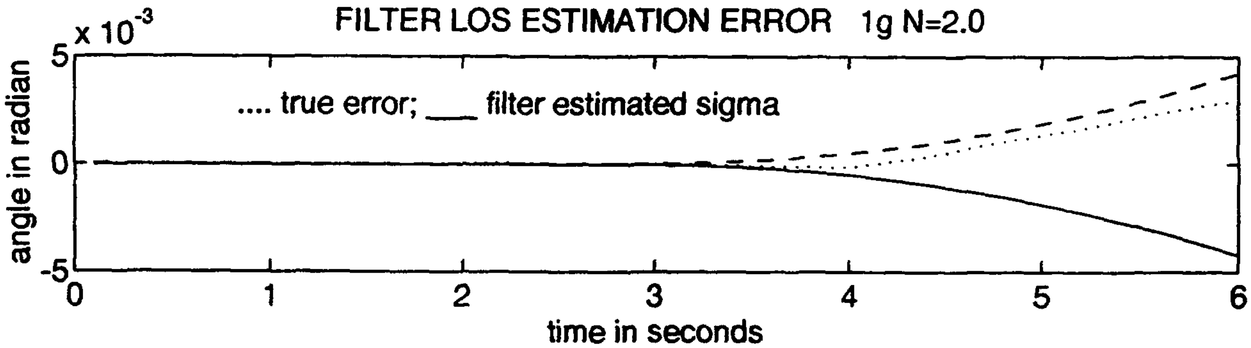
FILTER LOS ESTIMATION ERROR 1g N=2.0
x 10-3
.... true error; ___ filter estimated sigma
angle in radian
5
0
-5
0
1
2
3
4
5
6
time in seconds

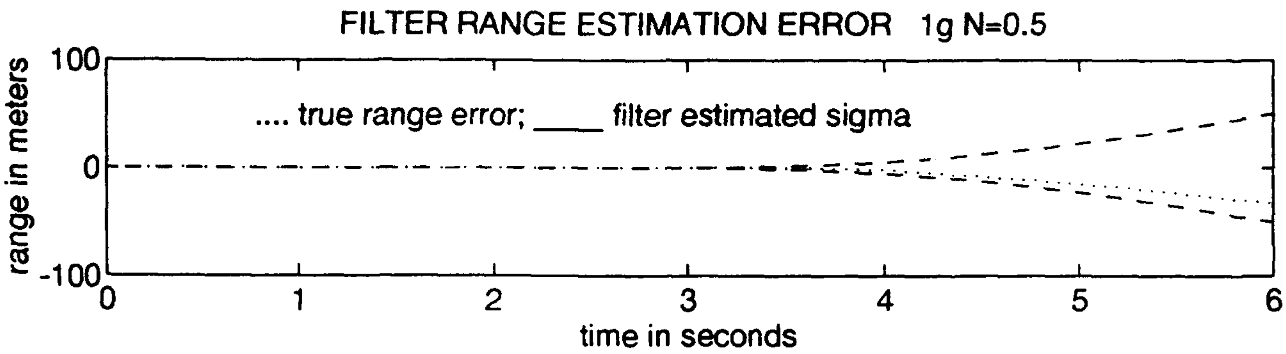
FILTER RANGE ESTIMATION ERROR 1g N=0.5
100
0
-100
range in meters
.... true range error; ____ filter estimated sigma
0
1
2
3
4
5
6
time in seconds

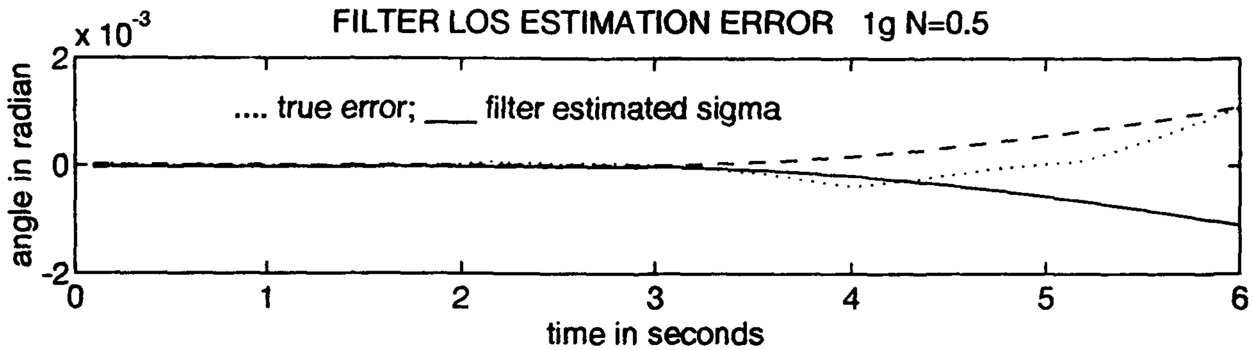
FILTER LOS ESTIMATION ERROR 1g N=0.5
x 10-3
2
0
-2
angle in radian
.... true error; ___ filter estimated sigma
0
1
2
3
4
5
6
time in seconds

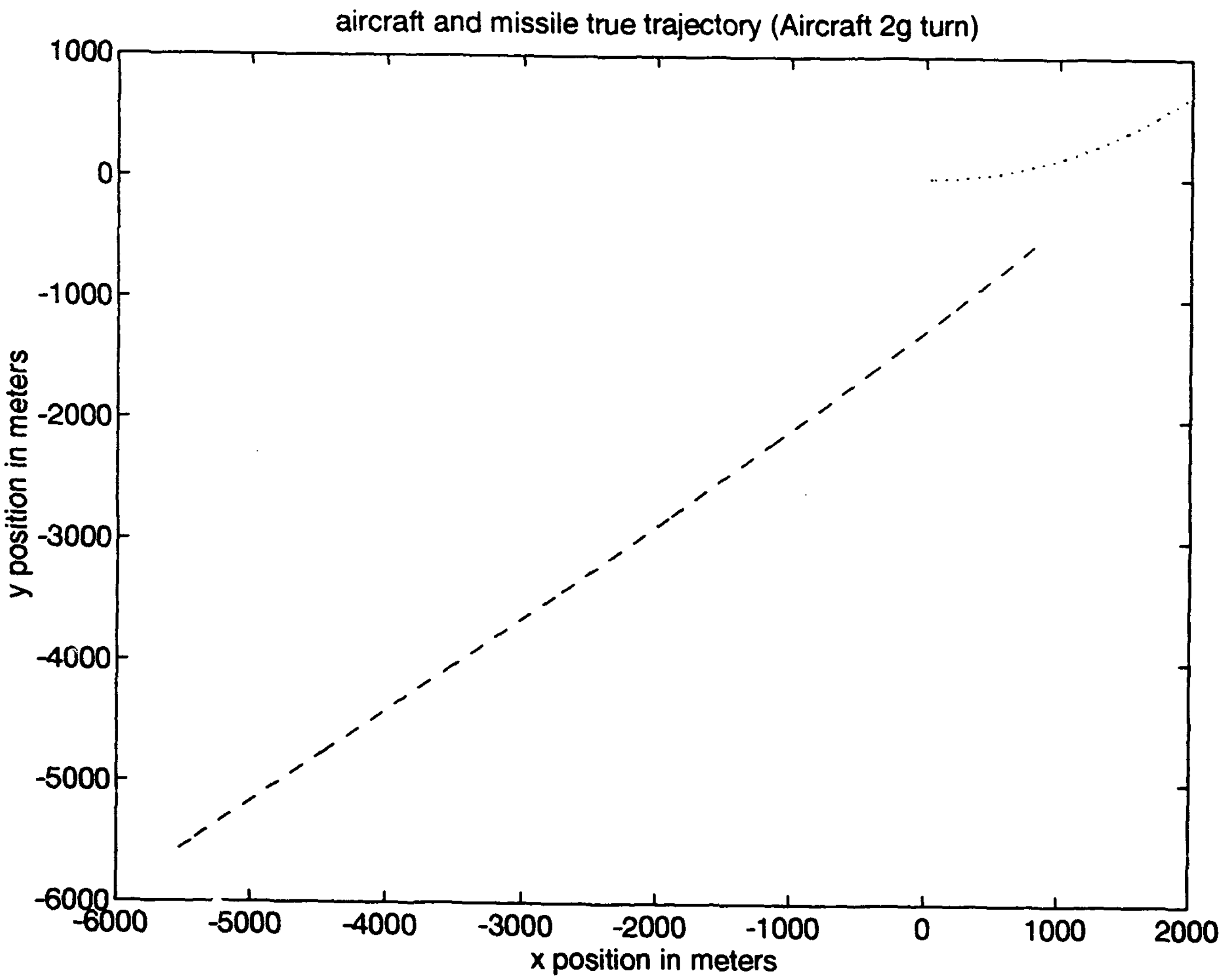
aircraft and missile true trajectory (Aircraft 2g turn)
1000
0
-1000
-2000
-3000
-4000
-5000
-6000
y position in meters
-6000
-5000
-4000
-3000
-2000
-1000
0
1000
2000
x position in meters

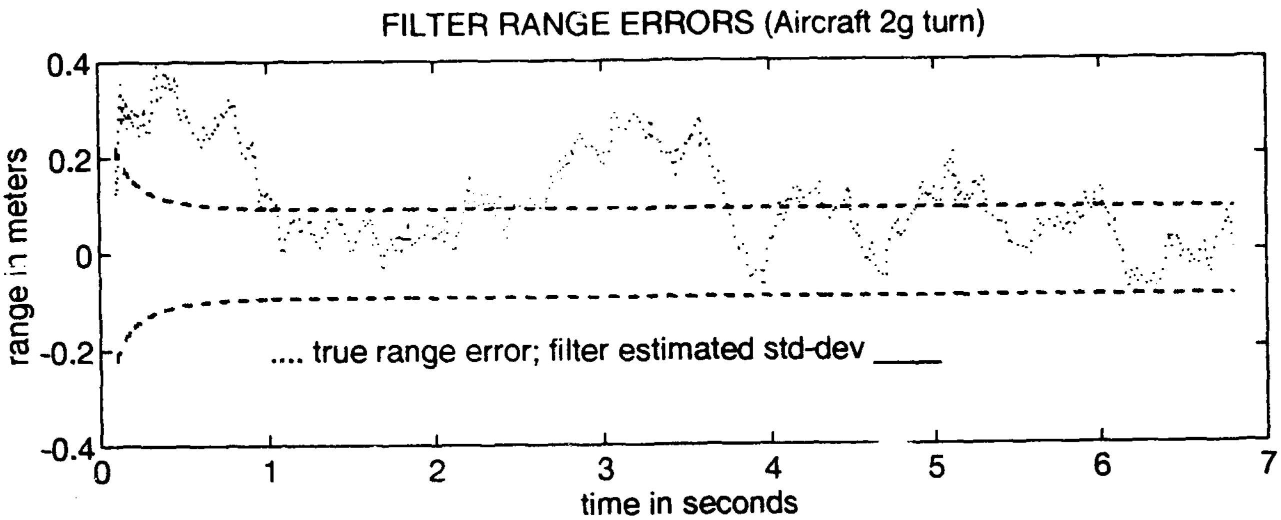

FILTER RANGE ERRORS (Aircraft 2g turn)
range in meters
time in seconds
.... true range error; filter estimated std-dev ____
0.4
0.2
0
-0.2
-0.4
0
1
2
3
4
5
6
7

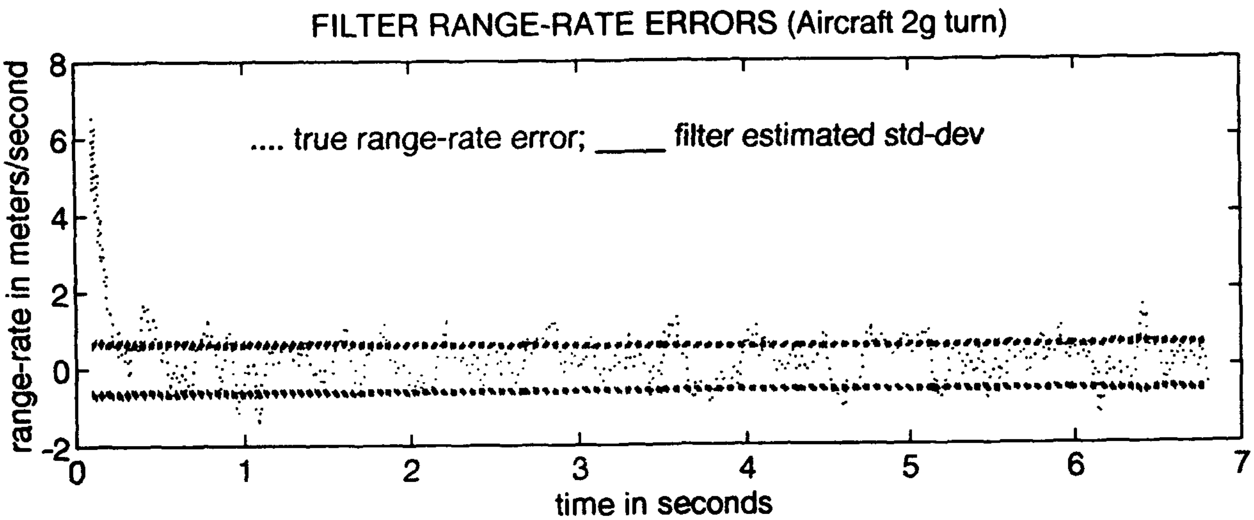

FILTER RANGE-RATE ERRORS (Aircraft 2g turn)
range-rate in meters/second
time in seconds
.... true range-rate error; ____ filter estimated std-dev
8
6
4
2
0
-2
0
1
2
3
4
5
6
7

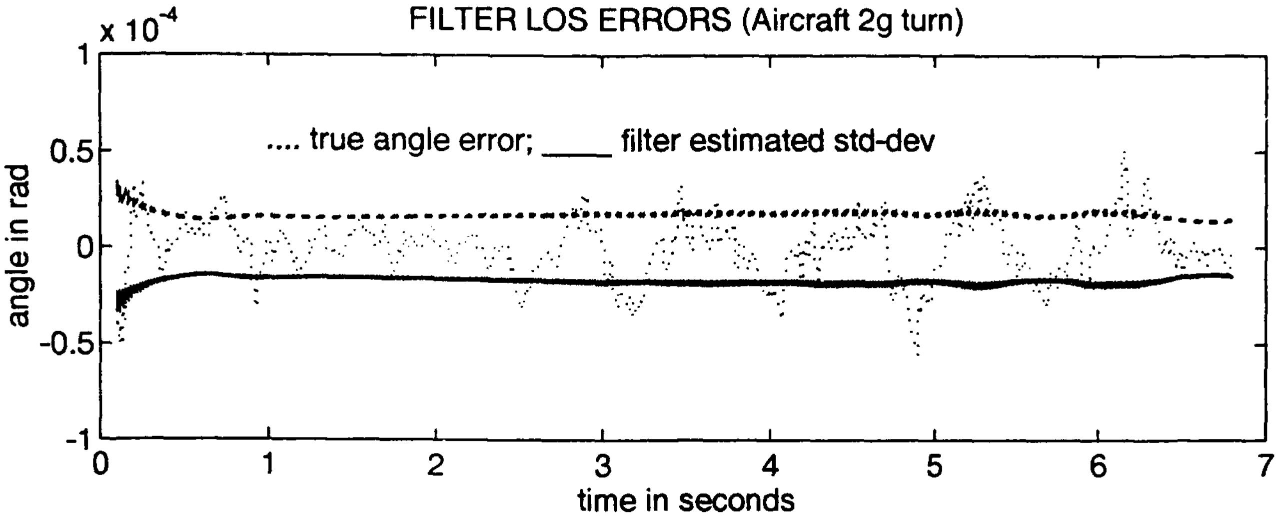
x 10^-4
FILTER LOS ERRORS (Aircraft 2g turn)
.... true angle error; _____ filter estimated std-dev
angle in rad
1
0.5
0
-0.5
-1
0
1
2
3
4
5
6
7
time in seconds

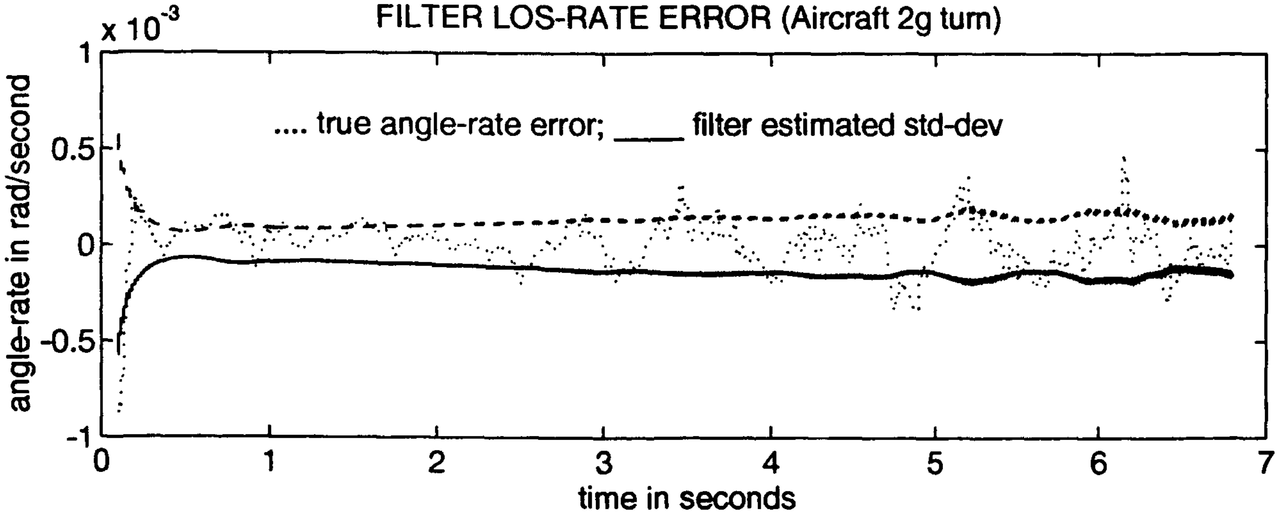
x 10^-3
FILTER LOS-RATE ERROR (Aircraft 2g turn)
.... true angle-rate error; _____ filter estimated std-dev
angle-rate in rad/second
1
0.5
0
-0.5
-1
0
1
2
3
4
5
6
7
time in seconds

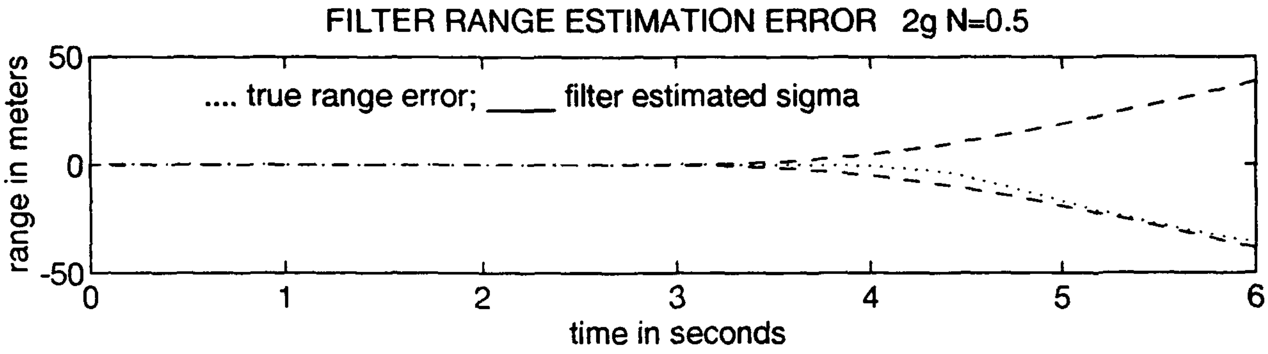
FILTER RANGE ESTIMATION ERROR 2g N=0.5
.... true range error; ____ filter estimated sigma
range in meters
50
0
-50
0
1
2
3
4
5
6
time in seconds

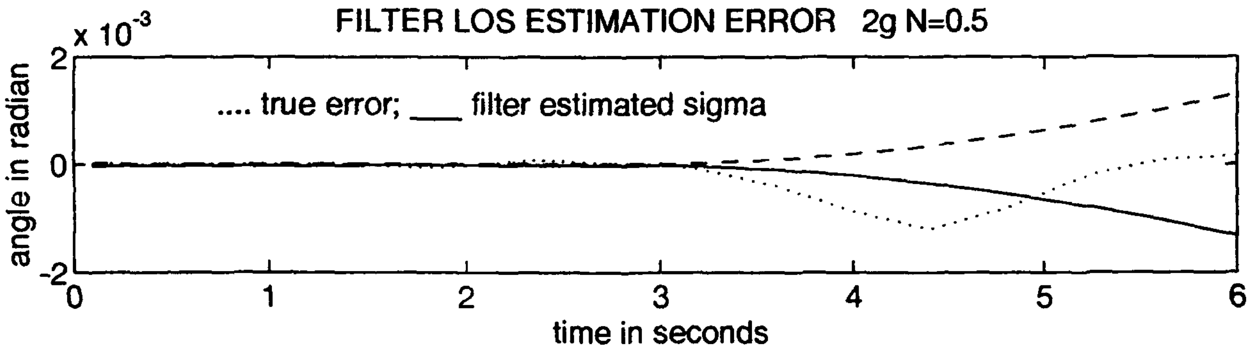
FILTER LOS ESTIMATION ERROR 2g N=0.5
x 10^-3
.... true error; ___ filter estimated sigma
angle in radian
2
0
-2
0
1
2
3
4
5
6
time in seconds

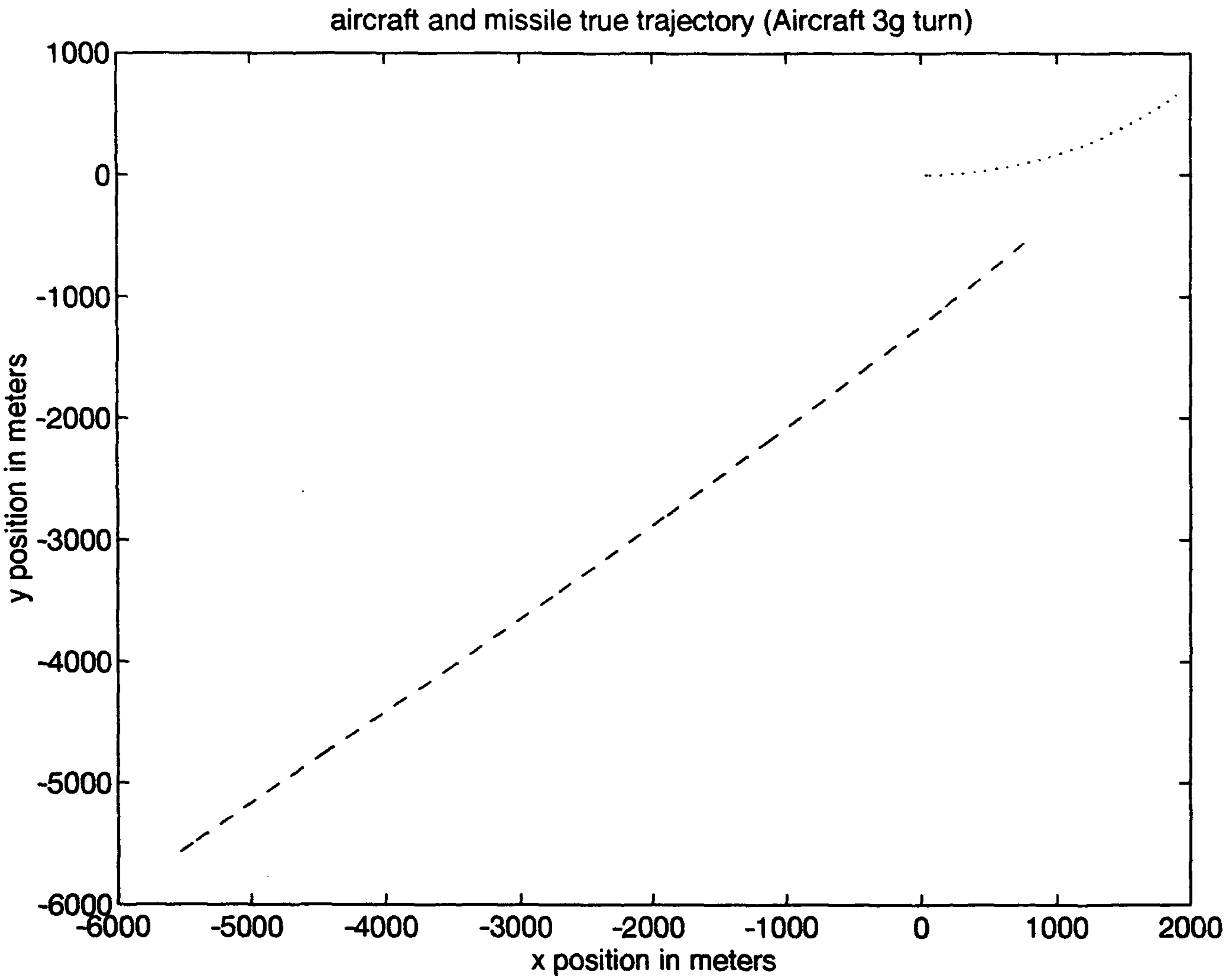
aircraft and missile true trajectory (Aircraft 3g turn)
y position in meters
x position in meters
1000
0
-1000
-2000
-3000
-4000
-5000
-6000
-6000
-5000
-4000
-3000
-2000
-1000
0
1000
2000

FILTER RANGE ERRORS (Aircraft 3g turn)

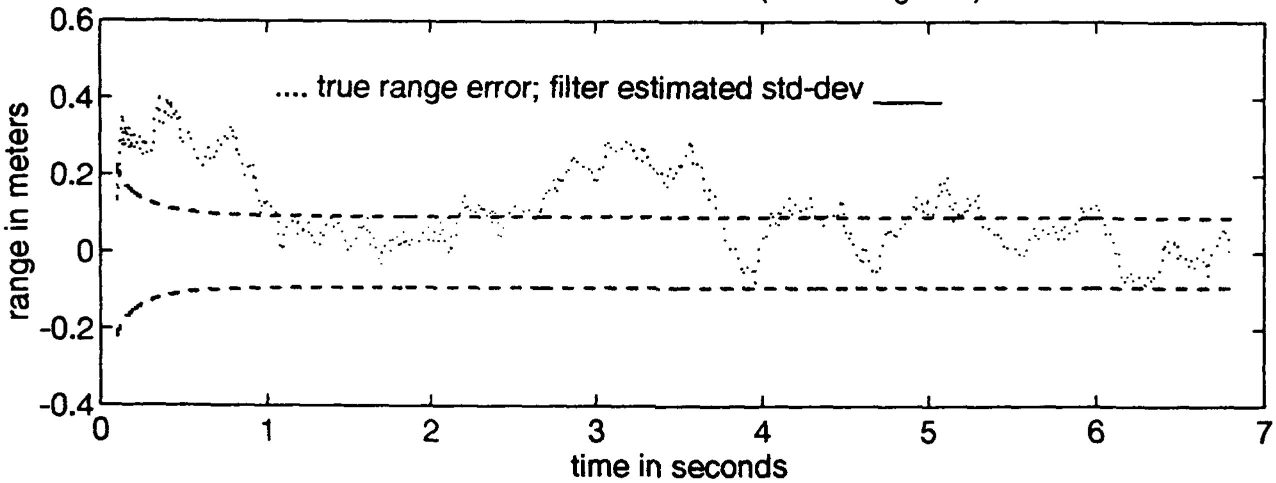

FILTER RANGE-RATE ERRORS (Aircraft 3g turn)

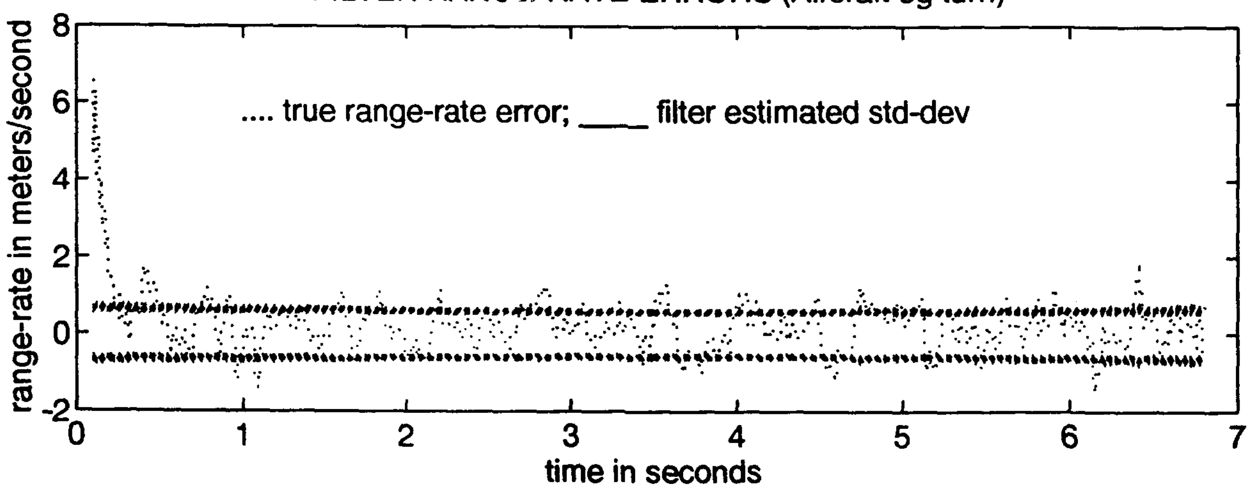

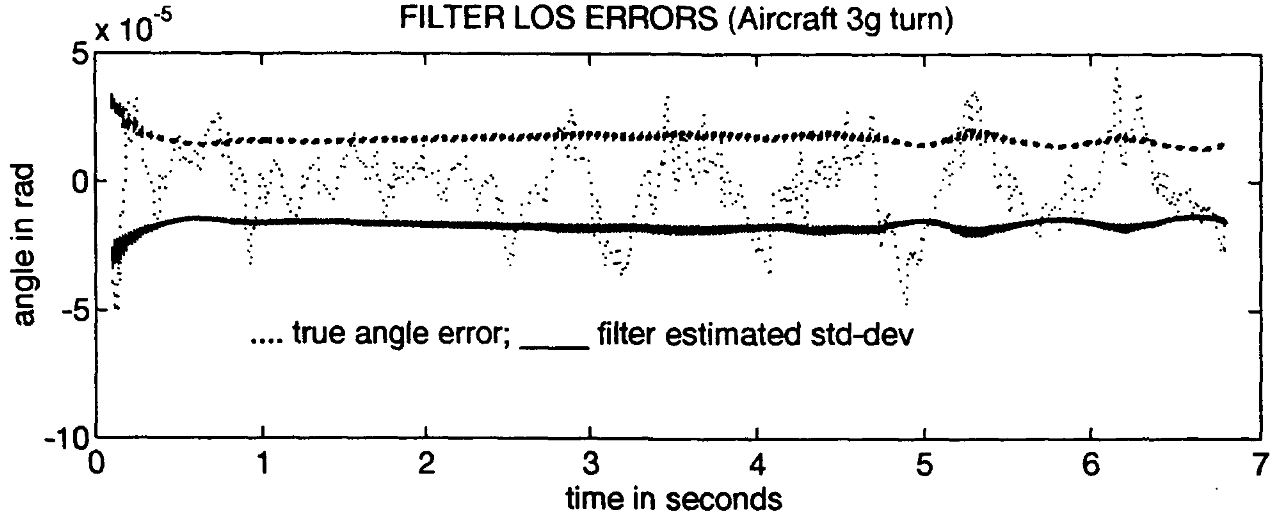
FILTER LOS ERRORS (Aircraft 3g turn)
x 10^-5
5
0
-5
-10
angle in rad
.... true angle error; ____ filter estimated std-dev
0
1
2
3
4
5
6
7
time in seconds

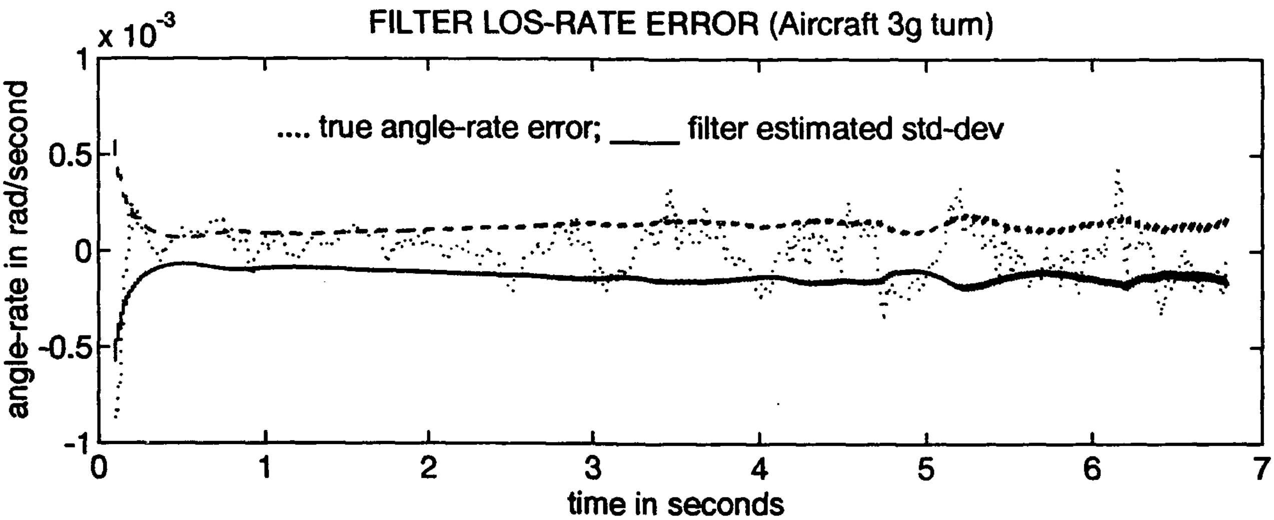
FILTER LOS-RATE ERROR (Aircraft 3g turn)
x 10^-3
1
0.5
0
-0.5
-1
angle-rate in rad/second
.... true angle-rate error; ____ filter estimated std-dev
0
1
2
3
4
5
6
7
time in seconds

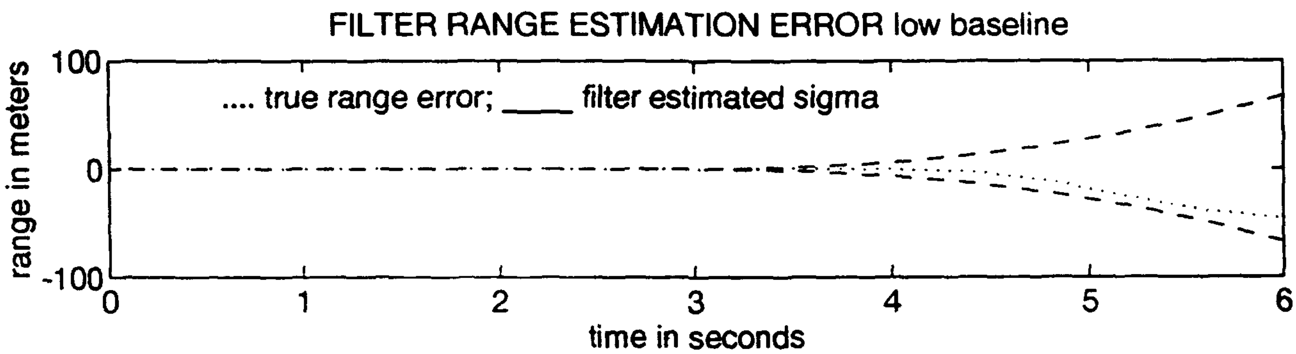
FILTER RANGE ESTIMATION ERROR low baseline
.... true range error; ____ filter estimated sigma
range in meters
100
0
-100
0
1
2
3
4
5
6
time in seconds

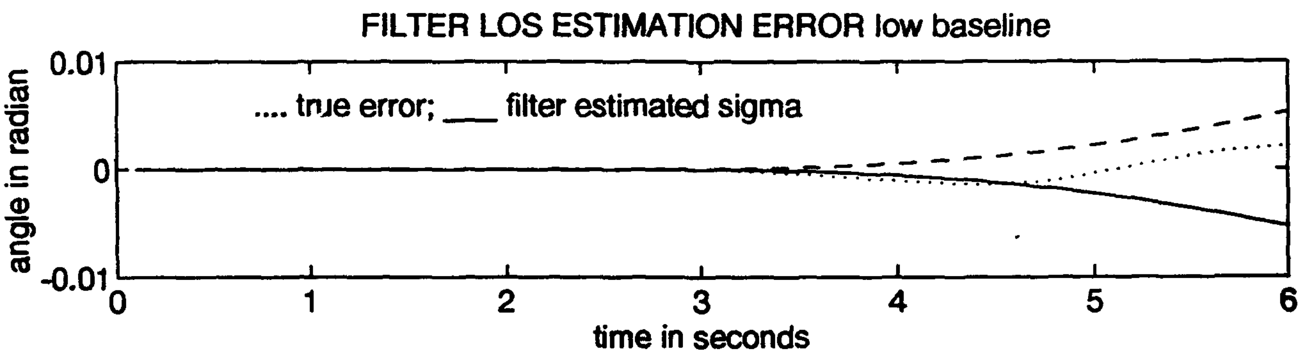
FILTER LOS ESTIMATION ERROR low baseline
.... true error; ___ filter estimated sigma
angle in radian
0.01
0
-0.01
0
1
2
3
4
5
6
time in seconds

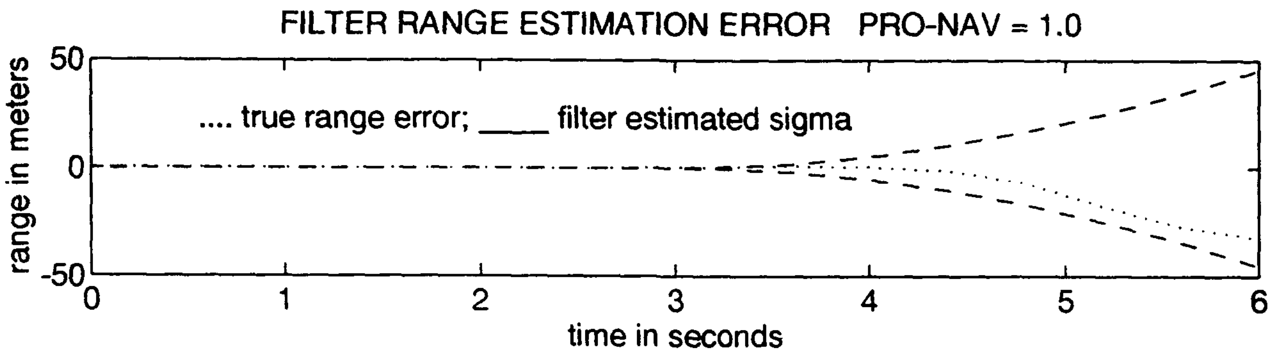

FILTER RANGE ESTIMATION ERROR PRO-NAV = 1.0
.... true range error; ____ filter estimated sigma
range in meters
50
0
-50
0
1
2
3
4
5
6
time in seconds

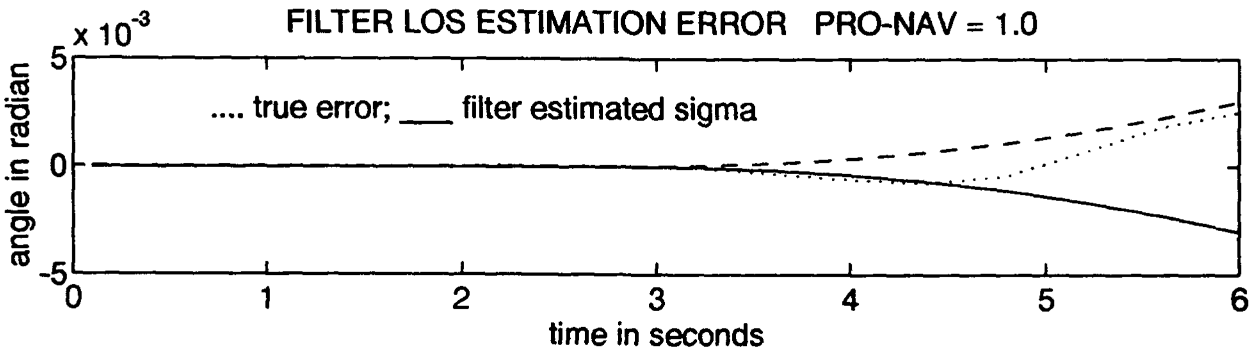

FILTER LOS ESTIMATION ERROR PRO-NAV = 1.0
x 10^-3
.... true error; ___ filter estimated sigma
angle in radian
5
0
-5
0
1
2
3
4
5
6
time in seconds

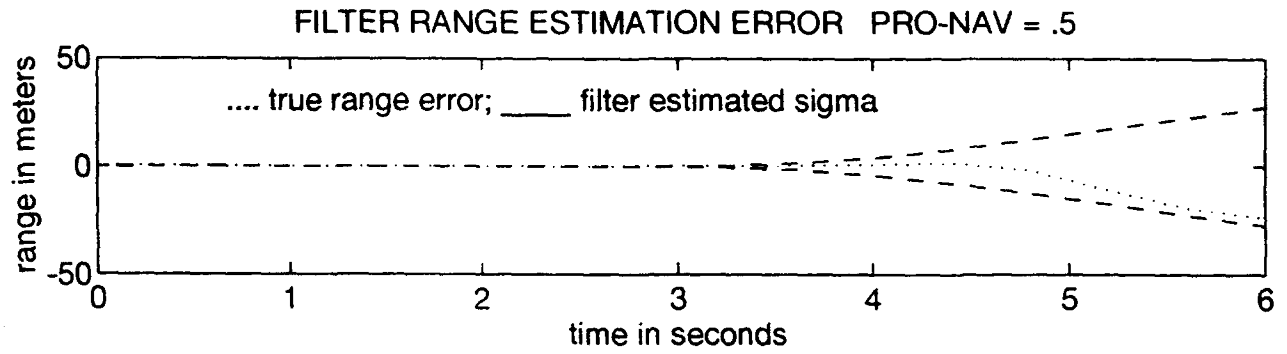
FILTER RANGE ESTIMATION ERROR PRO-NAV = .5
.... true range error; ____ filter estimated sigma
range in meters
50
0
-50
0
1
2
3
4
5
6
time in seconds

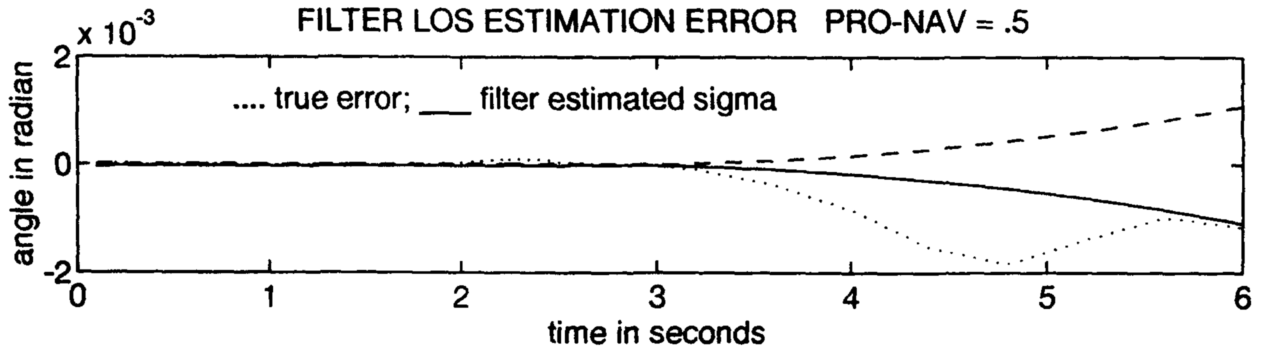
FILTER LOS ESTIMATION ERROR PRO-NAV = .5
x 10^-3
.... true error; ___ filter estimated sigma
angle in radian
2
0
-2
0
1
2
3
4
5
6
time in seconds

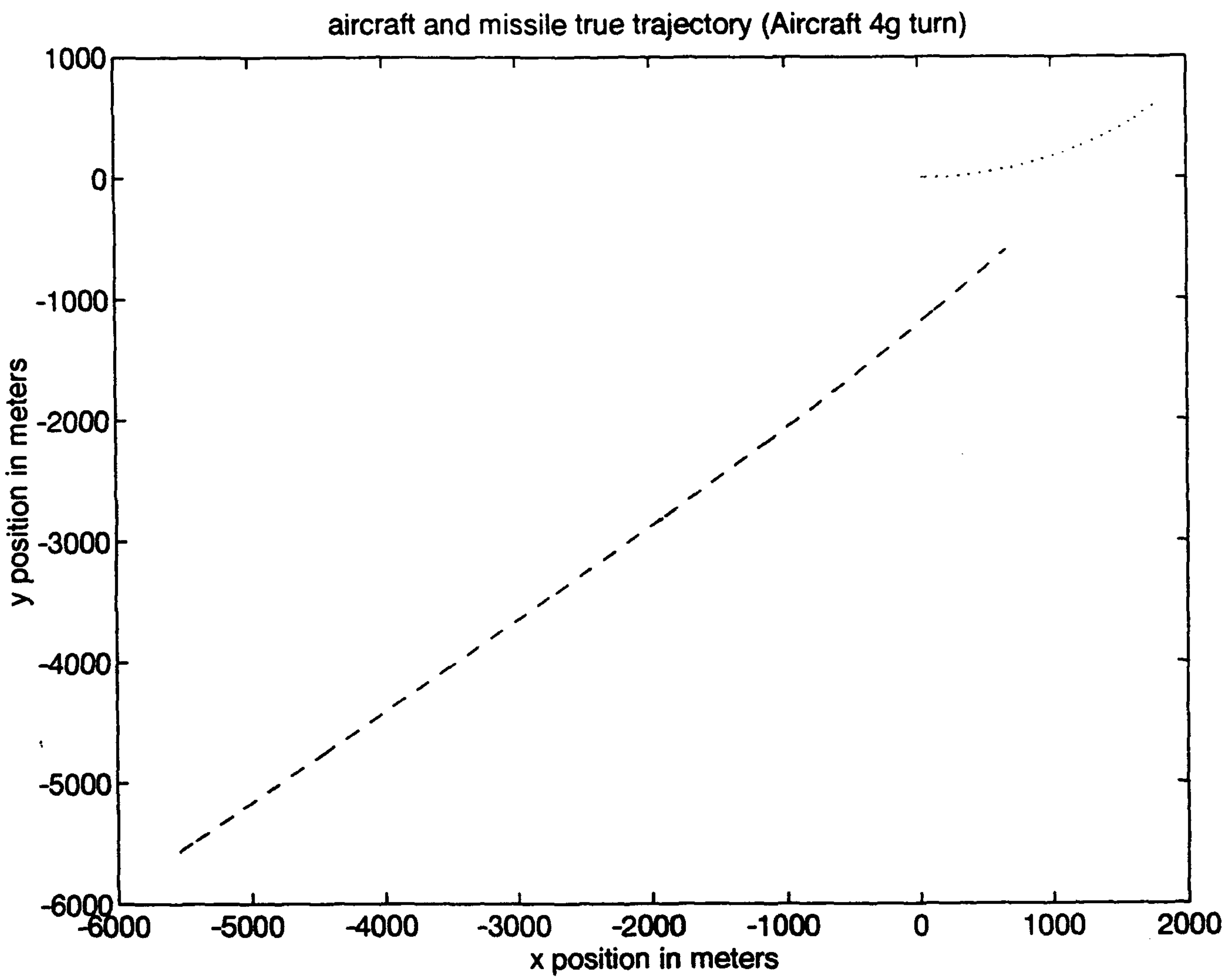
aircraft and missile true trajectory (Aircraft 4g turn)
1000
0
-1000
-2000
-3000
-4000
-5000
-6000
y position in meters
-6000
-5000
-4000
-3000
-2000
-1000
0
1000
2000
x position in meters

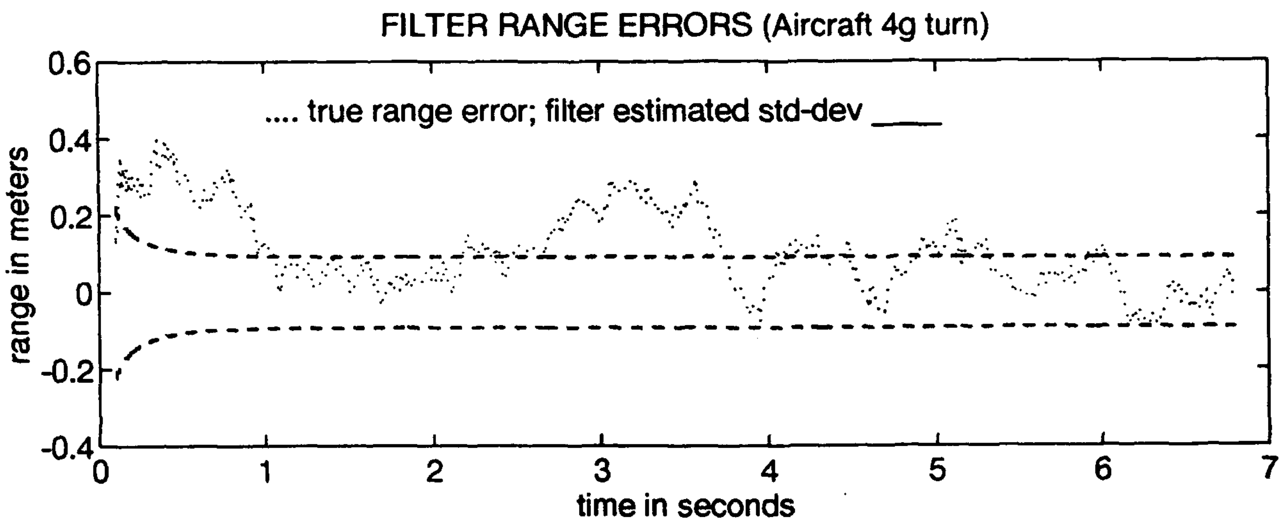
FILTER RANGE ERRORS (Aircraft 4g turn)
.... true range error; filter estimated std-dev ____
range in meters
0.6
0.4
0.2
0
-0.2
-0.4
0
1
2
3
4
5
6
7
time in seconds

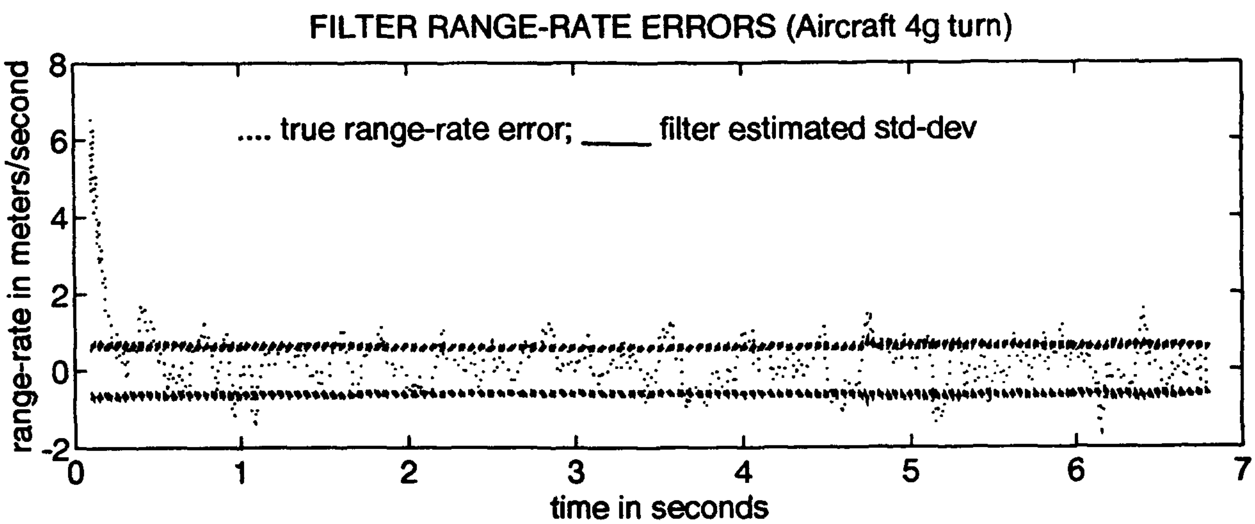
FILTER RANGE-RATE ERRORS (Aircraft 4g turn)
.... true range-rate error; ____ filter estimated std-dev
range-rate in meters/second
8
6
4
2
0
-2
0
1
2
3
4
5
6
7
time in seconds

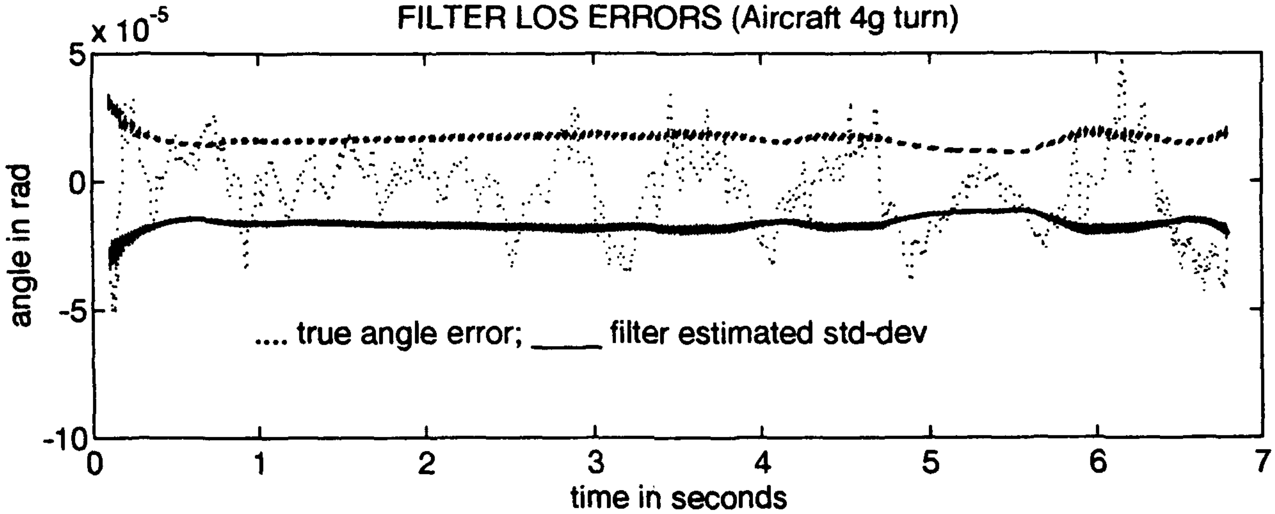
FILTER LOS ERRORS (Aircraft 4g turn)
x 10-5
5
0
-5
-10
angle in rad
.... true angle error; ____ filter estimated std-dev
0
1
2
3
4
5
6
7
time in seconds

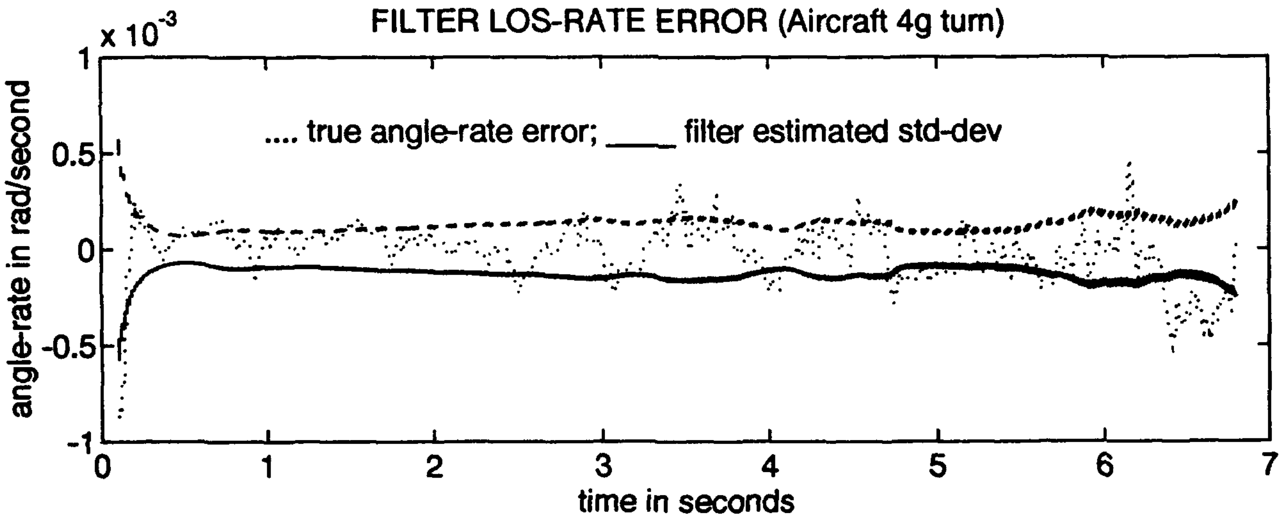
FILTER LOS-RATE ERROR (Aircraft 4g turn)
x 10-3
1
0.5
0
-0.5
-1
angle-rate in rad/second
.... true angle-rate error; ____ filter estimated std-dev
0
1
2
3
4
5
6
7
time in seconds

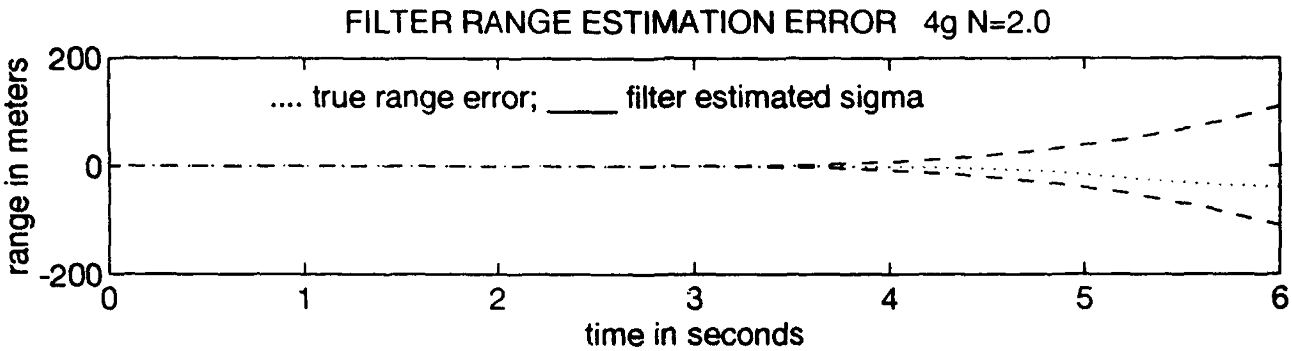
FILTER RANGE ESTIMATION ERROR 4g N=2.0
.... true range error; ____ filter estimated sigma
range in meters
200
0
-200
0
1
2
3
4
5
6
time in seconds

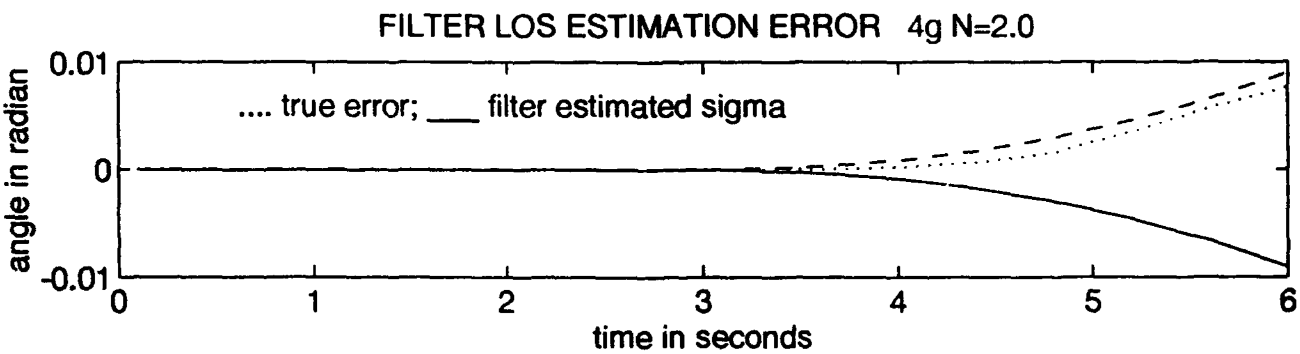
FILTER LOS ESTIMATION ERROR 4g N=2.0
.... true error; ___ filter estimated sigma
angle in radian
0.01
0
-0.01
0
1
2
3
4
5
6
time in seconds

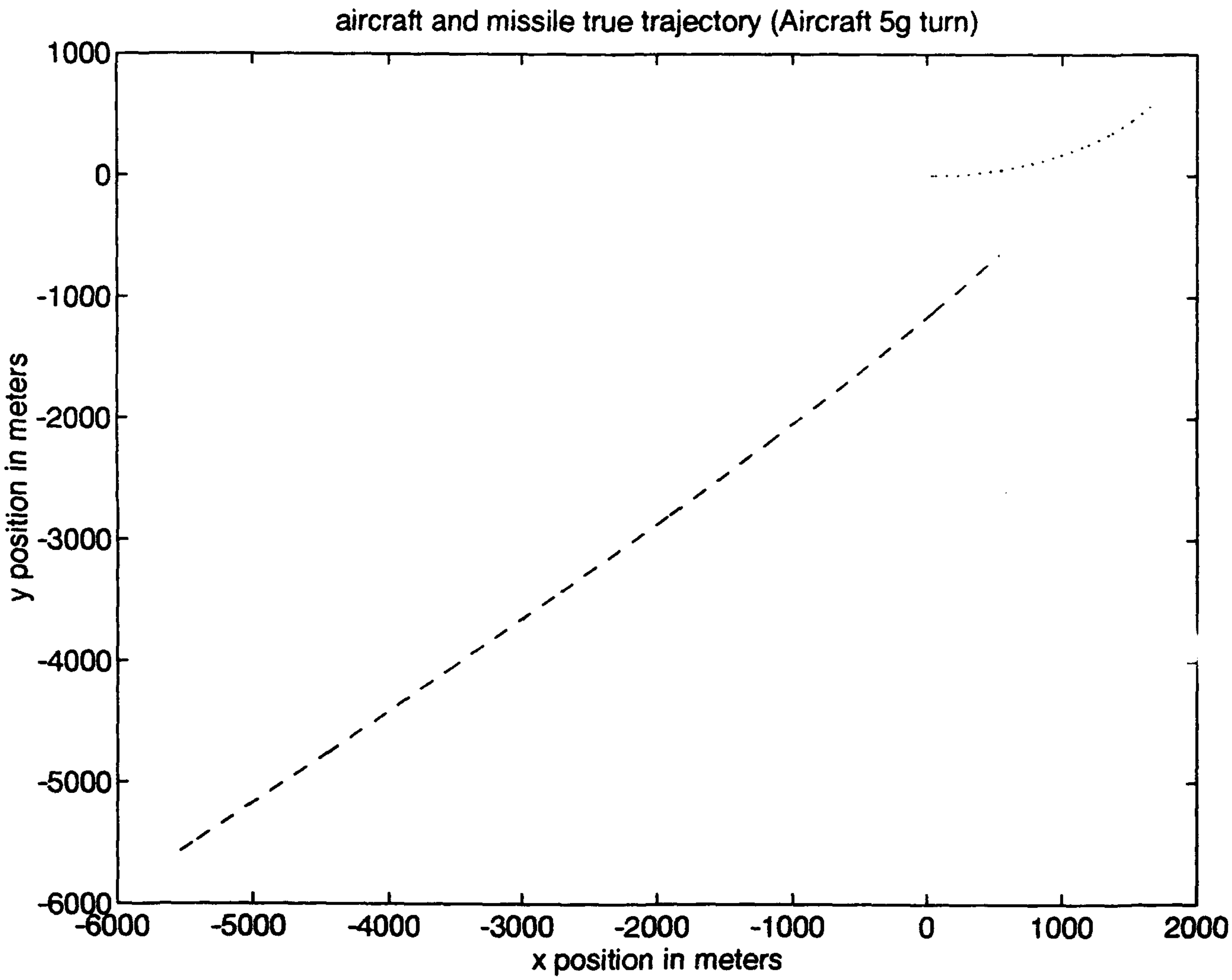
aircraft and missile true trajectory (Aircraft 5g turn)
1000
0
-1000
-2000
-3000
-4000
-5000
-6000
y position in meters
-6000
-5000
-4000
-3000
-2000
-1000
0
1000
2000
x position in meters

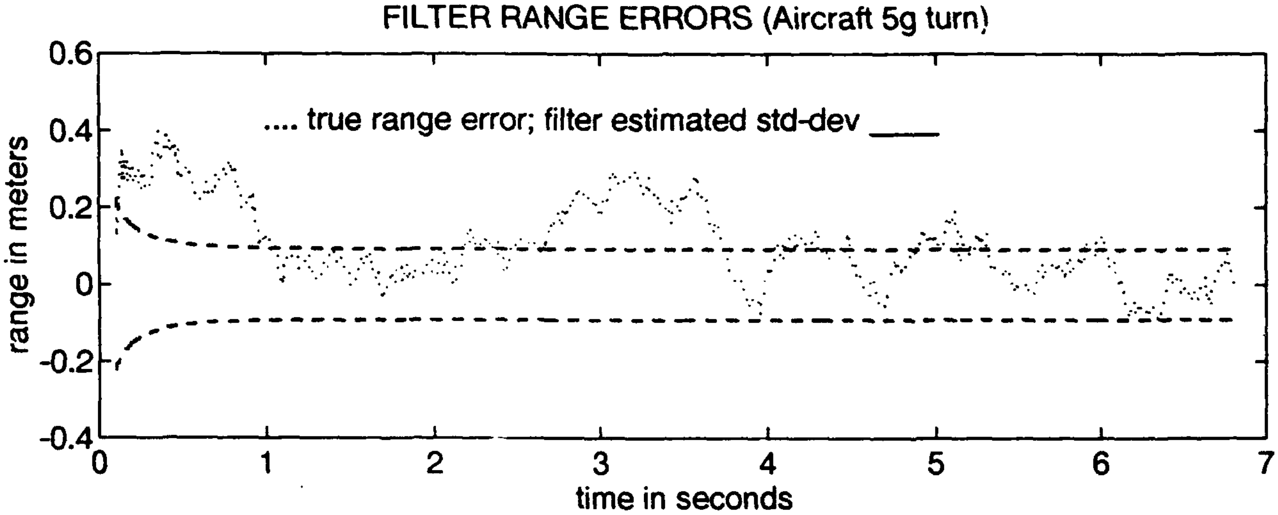
FILTER RANGE ERRORS (Aircraft 5g turn)
.... true range error; filter estimated std-dev ____
range in meters
0.6
0.4
0.2
0
-0.2
-0.4
0
1
2
3
4
5
6
7
time in seconds

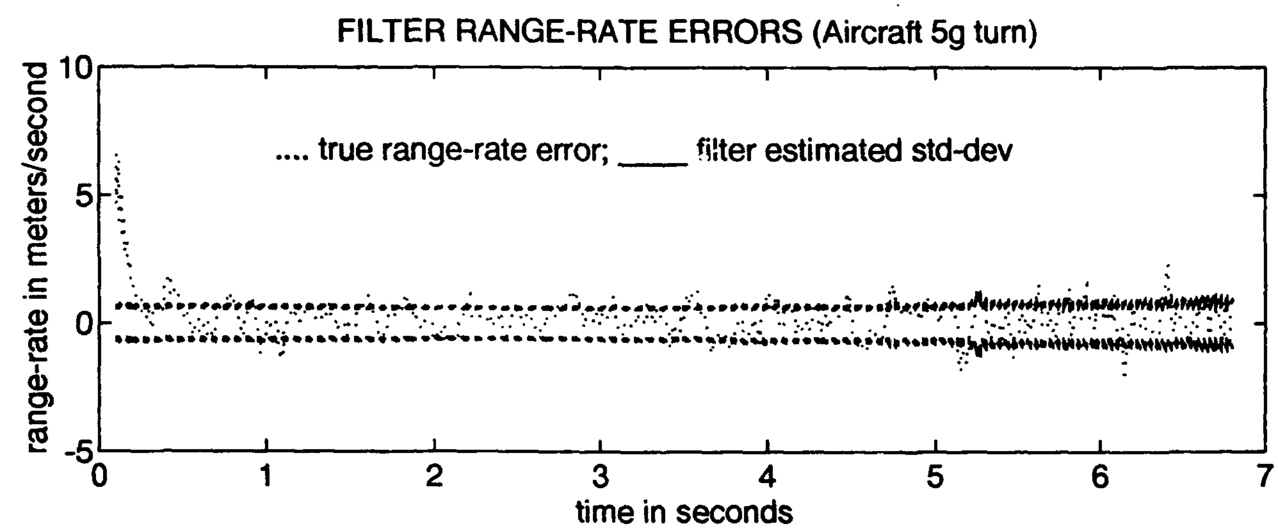
FILTER RANGE-RATE ERRORS (Aircraft 5g turn)
.... true range-rate error; ____ filter estimated std-dev
range-rate in meters/second
10
5
0
-5
0
1
2
3
4
5
6
7
time in seconds

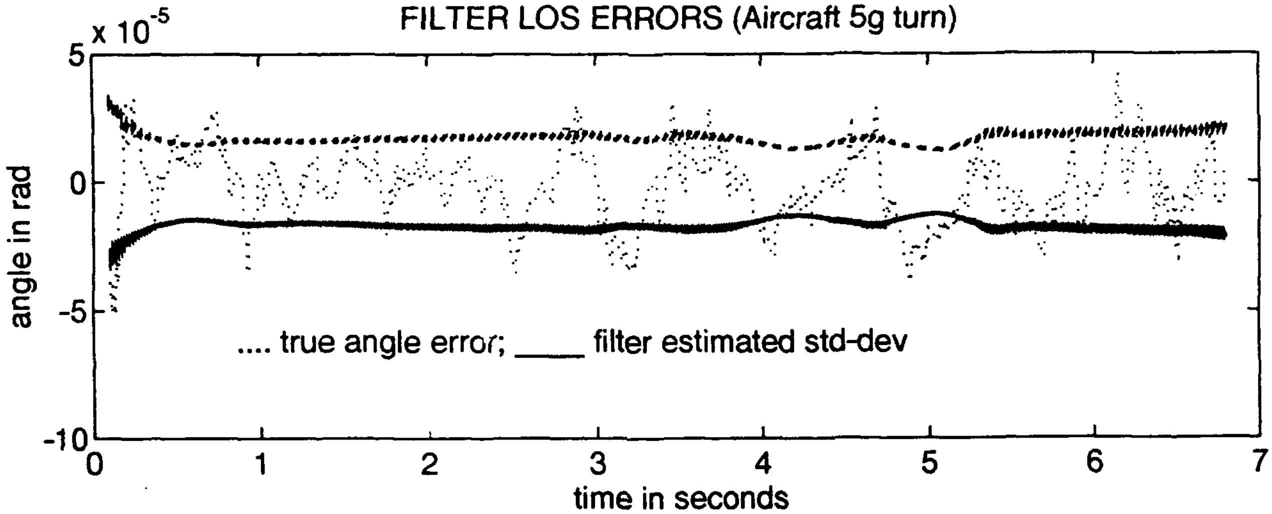
FILTER LOS ERRORS (Aircraft 5g turn)
x 10^-5
5
0
-5
-10
angle in rad
.... true angle error; ____ filter estimated std-dev
0
1
2
3
4
5
6
7
time in seconds

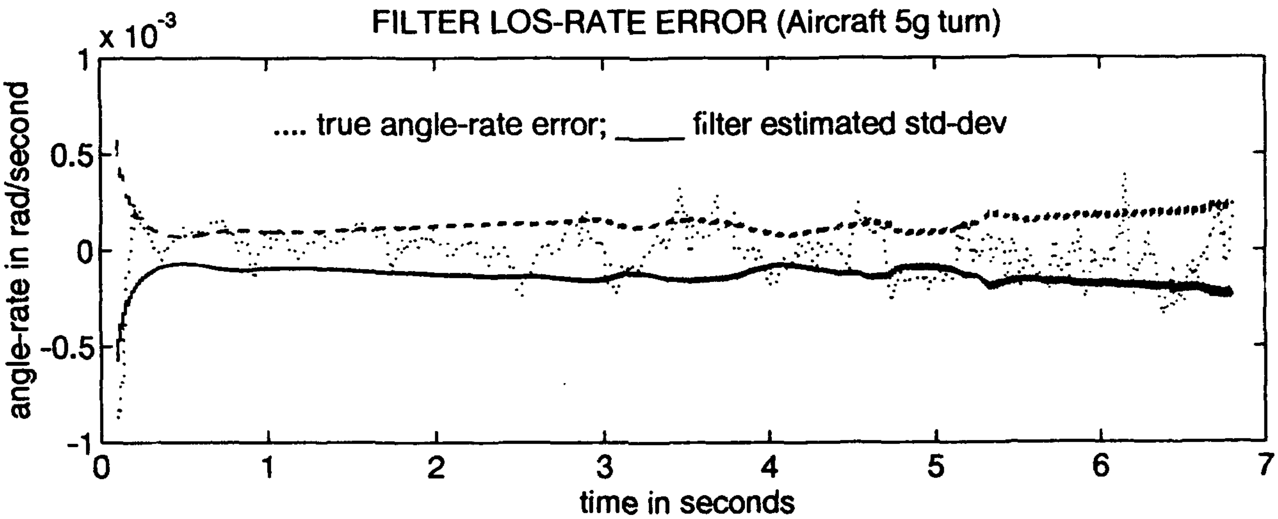
FILTER LOS-RATE ERROR (Aircraft 5g turn)
x 10^-3
1
0.5
0
-0.5
-1
angle-rate in rad/second
.... true angle-rate error; ____ filter estimated std-dev
0
1
2
3
4
5
6
7
time in seconds

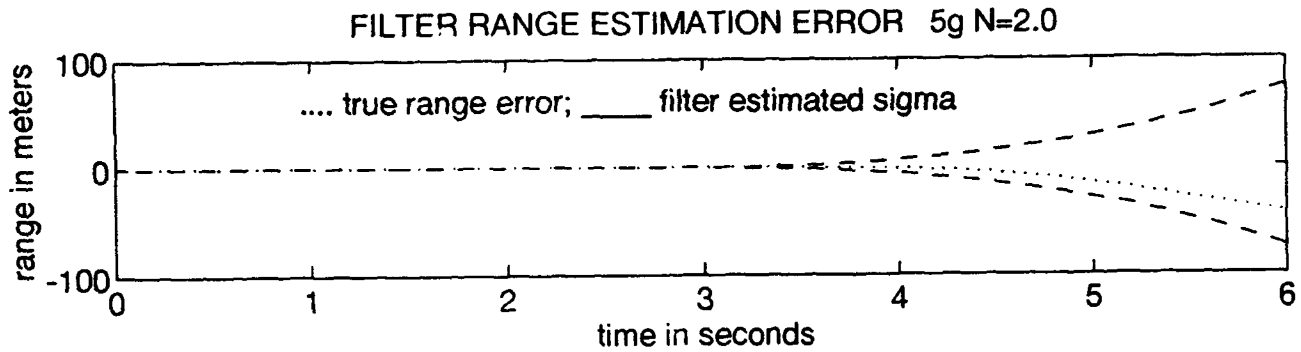
FILTER RANGE ESTIMATION ERROR 5g N=2.0
range in meters
100
0
-100
.... true range error; ____ filter estimated sigma
0
1
2
3
4
5
6
time in seconds

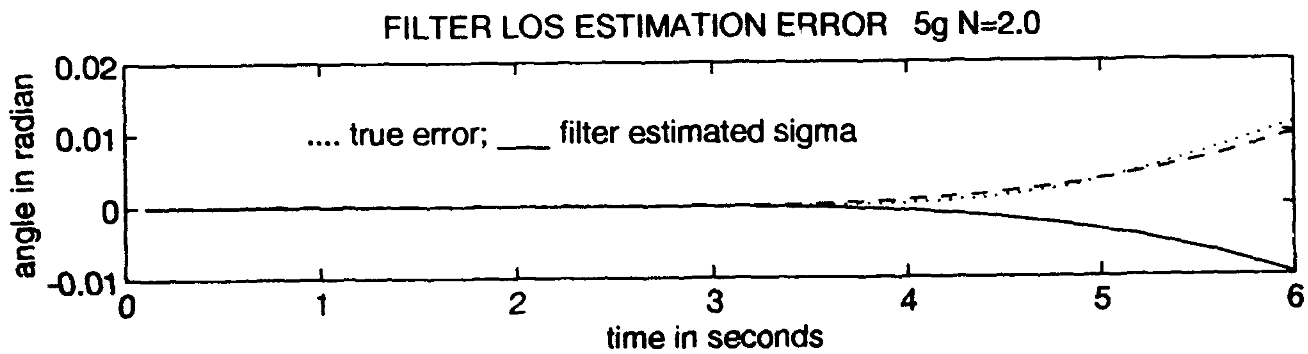
FILTER LOS ESTIMATION ERROR 5g N=2.0
angle in radian
0.02
0.01
0
-0.01
.... true error; ___ filter estimated sigma
0
1
2
3
4
5
6
time in seconds